EMID-702801

DEPARTMENT OF ENERGY
Environmental Management Los Alamos Field Office (EM-LA)
Los Alamos, New Mexico 87544

RECEIVED
JUN 29 2023
NMED Hazardous Waste Bureau

EMLA-23-BF251-2-1

June 29, 2023

Mr. Rick Shean
Designated Agency Manager
Hazardous Waste Bureau
New Mexico Environment Department
2905 Rodeo Park Drive East, Building 1
Santa Fe, NM 87505-6313

Subject: Submittal of the Annual Progress Report on Chromium Plume Control Interim Measure Performance, April 2022 through March 2023

Dear Mr. Shean:

Enclosed please find two hard copies with electronic files of the "Annual Progress Report on Chromium Plume Control Interim Measure Performance, April 2022 through March 2023." This progress report presents data and results from April 2022 through March 2023 and provides information on operations during the period, data from performance monitoring wells, and information pertaining to longer-term changes in the hydraulics and water-table structure in response to the chromium interim measure (IM). The report's appendices (on CD) include, in addition to data from April 2022 through March 2023, analytical data from monitoring of injected tracers from April 2021 through March 2022, which were inadvertently excluded from the previous report. Three supplemental technical reports (Enclosures 2, 3, and 4) are provided as references. This progress report is being submitted to fulfill fiscal year 2023 Milestone 2 in Appendix B of the 2016 Compliance Order on Consent.

If you have any questions, please contact Clark Short at (505) 551-2942 (clark.short@em-la.doe.gov) or Cheryl Rodriguez at (505) 414-0450 (cheryl.rodriguez@em.doe.gov).

Sincerely,

Digitally signed by BRIAN HARCEK
Date: 2023.06.29 08:50:03 -06'00'

Arturo Q. Duran For
Compliance and Permitting Manager
U.S. Department of Energy
Environmental Management
Los Alamos Field Office

Enclosure(s):
1. Two hard copies with electronic files – Annual Progress Report on Chromium Plume Control Interim Measure Performance, April 2022 through March 2023 (EM2023-0392)
2. Hydraulic Analysis of the Pajarito Plateau (EMID-702080)
3. Chromium Model: Calibrated with Uncertainty through 2022 (EMID-702081)
4. Chromium Interim Measure Capture Zone Analysis (EMID-702082)

cc (letter with CD/DVD enclosure[s]):
Laurie King, EPA Region 6, Dallas, TX
Raymond Martinez, San Ildefonso Pueblo, NM
Dino Chavarria, Santa Clara Pueblo, NM
Steve Yanicak, NMED-DOE-OB
Neelam Dhawan, NMED-HWB
Ricardo Maestas, NMED-HWB
Cheryl Rodriguez, EM-LA
emla.docs@em.doe.gov
n3brecords@em-la.doe.gov
Public Reading Room (EPRR)
PRS website

cc (letter emailed):
Jennifer Payne, LANL
Stephen Hoffman, NA-LA
William Alexander, N3B
Mei Ding, N3B
Robert Edwards, N3B
Michael Erickson, N3B
Cheryl Fountain, N3B
Vicky Freedman, N3B
Dana Lindsay, N3B
Robert Macfarlane, N3B
Christian Maupin, N3B
Patrick McGuire, N3B
Bruce Robinson, N3B
Vince Rodriguez, N3B
Clark Short, N3B
Bradley Smith, N3B
Troy Thomson, N3B
Amanda White, N3B
Brinson Willis, N3B
M. Lee Bishop, EM-LA
John Evans, EM-LA
Michael Mikolanis, EM-LA
Hai Shen, EM-LA
Susan Wacaster, EM-LA

Enclosure 1

Annual Progress Report on Chromium Plume Control
Interim Measure Performance, April 2022 through March 2023

June 2023
EM2023-0392

Annual Progress Report on Chromium Plume Control Interim Measure Performance, April 2022 through March 2023

EM2022-0392

Annual Progress Report on Chromium Plume Control Interim Measure Performance, April 2022 through March 2023

June 2023

Responsible N3B program director:

Printed Name	Signature	Title	Organization	Date
Michael Erickson		Program Director	Water Program	6/26/2023

Responsible N3B representative:

Printed Name	Signature	Title	Organization	Date
Troy Thomson		Program Manager	N3B Environmental Remediation Program	6/26/2023

Responsible DOE EM-LA representative:

Printed Name	Signature	Title	Organization	Date
Arturo Q. Duran	Digitally signed by BRIAN HARCEK Date: 2023.06.29 08:50:36 -06'00' For	Compliance and Permitting Manager	Office of Quality and Regulatory Compliance	

EXECUTIVE SUMMARY

This progress report on the chromium plume control interim measure (IM) performance builds upon previous IM performance progress reports by providing information on IM activities, as well as results from April 2022 through March 2023. IM operations during this reporting period included pumping from five chromium plume extraction wells, CrEX-1, CrEX-2, CrEX-3, CrEX-4, and CrEX-5; treatment with ion exchange to remove chromium; and injection of treated water into five injection wells, CrIN-1, CrIN-2, CrIN-3, CrIN-4, and CrIN-5.

The operational configuration varied during the reporting period because of maintenance downtimes and operational direction from the New Mexico Environment Department (NMED), and the recommendations offered in this report are based on data and observations during this period of partial operation. These recommendations include (1) eventual return to operation of the IM at full capacity, (2) selective partial operation in the interim, and (3) prioritized installation of regional aquifer groundwater monitoring wells R-79 and R-80.

This report includes four appendices including

- chromium IM extraction and injection flow data,
- analytical water quality data collected under the Interim Facility-Wide Groundwater Monitoring Plan,
- analytical water quality data collected from chromium treatment unit influent and effluent, and
- Los Alamos County well pumping data.

The following supporting references are provided with this report's submittal package:

- "Hydraulic Analysis of the Pajarito Plateau,"
- "Chromium Model: Calibrated with Uncertainty through 2022," and
- "Chromium Interim Measure Capture Zone Analysis."

CONTENTS

Figures

Tables

Appendices

Acronyms and Abbreviations

amsl	above mean sea level
bgs	below ground surface
Consent Order	2016 Compliance Order on Consent
CM	Chromium Model
CME	corrective measures evaluation
CTUA	Chromium Treatment Unit A
CTUC	Chromium Treatment Unit C
CZ	capture zone
DOE	Department of Energy (U.S.)
EIM	Environmental Information Management (database)
EMCA	essential mission critical activities
EM-LA	Environmental Management Los Alamos Field Office (DOE)
EPA	Environmental Protection Agency (U.S.)
FEHM	Finite Element Heat and Mass Transfer (computer model)
FTB	field trip blank
GELC	GEL Laboratories, LLC, Division of the GEL Group, Inc., Charleston, SC
GGRL	Geochemistry and Geomaterials Research Laboratories (LANL)
GWQB	Ground Water Quality Bureau (NMED)
gpm	gallons per minute
IM	interim measure
IFGMP	Interim Facility-Wide Groundwater Monitoring Plan
IX	ion exchange
LANL	Los Alamos National Laboratory
M-K	Mann-Kendall
MY	monitoring year
N3B	Newport News Nuclear BWXT-Los Alamos, LLC
NDS	naphthalene disulfonic acid
NMED	New Mexico Environment Department
NMWQCC	New Mexico Water Quality Control Commission
NTS	naphthalene trisulfonic acid

S1	screen 1
S2	screen 2
SOP	standard operating procedure
ZOI	zone of influence

INTRODUCTION

This progress report on the chromium plume control interim measure (IM) performance builds upon previous IM performance progress reports by providing information on IM activities, as well as results from April 2022 through March 2023. Also included is supporting documentation (four appendices and three references provided with this report's submittal package), described below. This progress report fulfills the reporting requirements in the April 2018 "Chromium Plume Control Interim Measure Performance Monitoring Work Plan" (LANL 2018, 603010). The monitoring and associated reporting are conducted to evaluate performance of the IM conducted under the May 2015 "Interim Measures Work Plan for Chromium Plume Control" (LANL 2015, 600458) and Appendix C of the June 2016 Compliance Order on Consent (Consent Order).

The primary objective of the IM is to achieve and maintain the downgradient chromium plume edge, as defined by the 50-µg/L New Mexico Water Quality Control Commission groundwater standard, within the Los Alamos National Laboratory (LANL or the Laboratory) boundary. The specific metric was met for reducing chromium concentrations at the IM monitoring well R-50 to concentrations of 50 µg/L or less over a period of approximately 3 yr. A secondary objective of the IM is to hydraulically control eastward migration of the plume. Results from eastern area operations have been evaluated in the February 2023 "Initial Five-Year Evaluation of the Interim Measures for Chromium Plume Control with an Assessment of Potential Modifications to Operations" (N3B 2022, 702597).

IM operations during this reporting period included pumping from five chromium plume extraction wells, CrEX-1, CrEX-2, CrEX-3, CrEX-4, and CrEX-5; treatment with ion exchange (IX) to remove chromium; and injection of treated water into five injection wells, CrIN-1, CrIN-2, CrIN-3, CrIN-4, and CrIN-5 (Figure 1.0-1). The operational configuration varied during the reporting period because of maintenance downtimes and operational direction from the New Mexico Environment Department (NMED) (see Section 2.1).

This progress report presents data from monitoring wells outlined in the "Chromium Plume Control Interim Measure Performance Monitoring Work Plan" (LANL 2018, 603010), as well as data from regional aquifer groundwater monitoring wells R-13, R-15, R-43 screens 1 and 2, R-62, R-70 screens 1 and 2, R-71 screens 1 and 2, and R-72 screens 1 and 2. The additional monitoring well R-73 had issues during drilling and well construction. On July 28, 2022, the 14-in. carbon steel drive casing separated as it was being pulled out of the borehole; the casing remained stuck downhole, and existing conditions did not allow the well to be completed in accordance with New Mexico Office of the State Engineer administrative code and the NMED-approved well design. R-73 is undergoing plugging and abandonment. Field pilot tests using amendments were conducted to assess the potential in situ remediation strategies using sodium dithionite at R-42 and molasses at R-28. In this report, R-42 serves as an example to represent pre-IM conditions. R-28 assists in making IM flow inferences from tracers; however, the geochemistry is not considered representative of the aquifer. Additional monitoring wells are planned to close data gaps associated with the chromium plume extents.

The following appendices are included on CD with this report:

- Appendix A provides chromium IM extraction and injection flow data for the period of record reported in this progress report (April 2022 through March 2023).
- Appendix B provides analytical water quality data for extraction well samples, as well as data for chromium performance monitoring well samples collected under the Interim Facility-Wide Groundwater Monitoring Plan for the period of record reported in this progress report (April 2022 through March 2023).

- Appendix C provides analytical water quality data collected from the chromium treatment units' influent and effluent streams for the period of record reported in this progress report (April 2022 through March 2023).
- Appendix D provides Los Alamos County well pumping data for the period of record reported in this progress report (April 2022 through March 2023).

Supporting references provided with this report's submittal package are the following:

- "Hydraulic Analysis of the Pajarito Plateau" (Neptune 2023, 702780) presents the analysis used to refine the conceptual understanding of groundwater hydraulics of the aquifer beneath the Pajarito Plateau, supporting fate and transport modeling of dissolved phase contaminants of concern in two distinct areas of the regional aquifer. This analysis of hydraulic gradients includes regional impacts of Los Alamos County well pumping on the chromium project area.
- "Chromium Model: Calibrated with Uncertainty through 2022" (Neptune 2023, 702781) documents the numerical model of the chromium project area used to support optimization of the existing IM network, improve understanding of the plume, and provide quantitative metrics for uncertainty, aiding in decision-making associated with chromium transport and IM operations.
- "Chromium Interim Measure Capture Zone Analysis" (Neptune 2023, 702782) documents an initial capture zone analysis of IM operations, used to determine IM system impact on the potentiometric surface and chromium plume capture.

2.0 INTERIM MEASURE OPERATIONS

2.1 Operations and Testing

Operations and testing are reported for April 2022 through March 2023. Table 2.1-1 presents significant operational and maintenance activities; Figure 2.1-1 provides flow rates for the CrEX wells; Figure 2.1-2 provides injection well flow rates and water levels; and Table 2.1-2 presents quarterly volumes of treated effluent injected into the aquifer.

2.1.1 System Operations

The treatment system and multiple infrastructure wells were operated for the majority of the second quarter and third quarter of 2022 and then went to partial operations during the fourth quarter of 2022 through the second quarter of 2023.

With minor exceptions, the IM system was operated continuously from April 1, 2022, to October 29, 2022. Operation of the IM ceased from May 9, 2022, to May 16, 2022, in preparation for potential evacuation of Los Alamos because of the Cerro Pelado fire.

The system was partially operated from October 2022 through March 2023. Operation of CrEX-3 ceased on October 27, 2022, because of identification of improper grounding on routine inspection. Operation of CrEX-1 and CrEX-2 ceased on October 28, 2022, because of subsequent inspection and identification of improper grounding at CrEX-1. Operation of CrIN-1, CrIN-2, and CrIN-3 ceased on October 28, 2022 to balance inflow and outflow to the system. During partial operation, CrEX-4 operated at approximately 65–70 gallons per minute (gpm); CrEX-5 at 75–80 gpm; CrIN-4 at 70 gpm; and CrIN-5 at 70 gpm. The IM system was shut down completely on March 31, 2023, at the direction of the NMED Groundwater Quality Bureau (NMED-GWQB) (NMED 2022, 702464).

Table 2.1-1 presents the specific operation of each extraction and injection well and chromium treatment unit (Chromium Treatment Unit A [CTUA] and Chromium Treatment Unit C [CTUC]), as well as shutdowns that may have occurred between April 2022 and March 2023.

2.2 Routine and Nonroutine Activities

Table 2.1-1 also describes additional activities, including major maintenance and IX vessel changeouts that occurred between April 2022 and March 2023.

2.3 Chromium Mass Removal

Although mass removal rates and efficiency are not directly related to IM performance, they may provide insights into observed plume response. Table 2.1-3 presents estimates for chromium mass removal for the IM to date. Estimates are based upon three types of analytical chromium measurements. The first is based upon field kit measurements of nonfiltered groundwater samples. The second is based upon an analytical laboratory measurement (typically at GEL Laboratories, LLC [GELC] via U.S. Environmental Protection Agency [EPA] Method SW-846:6020B) of nonfiltered groundwater samples. The third is a laboratory-based measurement of filtered groundwater samples using a 0.45-µm membrane. The frequency of the field-based measurements is once to twice per week, and the laboratory-based measurements are approximately weekly. Influent results from both CTUA and CTUC treatment units are incorporated in calculations. Values between the field measurement and nonfiltered laboratory results are compared in the final column of Table 2.1-3 as a percent difference. Quarterly differences range from approximately 1% to 10%. On average, field measurements values are approximately 7.5% higher than analytical laboratory measurements. Filtered laboratory values resemble nonfiltered groundwater samples.

3.0 PERFORMANCE MONITORING RESULTS

The "Interim Measures Work Plan for Chromium Plume Control" states that performance monitoring will be conducted to evaluate plume response associated with IM operations and to guide adjustments in operational strategies (LANL 2015, 600458). Water quality results and water-level data from April 2022 to March 2023 are presented in this section.

Additional performance monitoring results beyond the annual report can be found in the initial 5-year evaluation of the IM (N3B 2022, 702597).

3.1 Sampling

Figure 1.0-1 shows the locations of the performance monitoring wells, piezometers, and additional monitoring wells in the chromium project area.

Table 3.1-1 lists the frequency of analytical suites collected at performance monitoring locations, piezometers, and additional monitoring wells addressed in this report.

The following monitoring wells are scheduled for monthly sampling for performance monitoring of the IM:

- R-11
- R-35a and R-35b
- R-44 screens 1 and 2
- R-45 screens 1 and 2

- R-50 screens 1 and 2
- R-61 screen 1
- SIMR-2

On October 1, 2021, five piezometers located within the chromium plume project area (CrPZ-1, CrPZ-2a, CrPZ-3, CrPZ-4, and CrPZ-5) were incorporated into the "Interim Facility-Wide Groundwater Monitoring Plan for the 2022 Monitoring Year, October 2021–September 2022" (IFGMP) (N3B 2021, 701449). These piezometers were completed in coreholes that were drilled in 2016 to collect aquifer sediment samples for bench-scale studies. The piezometers were initially intended for collection of water-level data and screening-level geochemistry data because the piezometers had not undergone full development following installation. A review of the historical data from the piezometers indicated that they are likely producing representative groundwater samples, and the piezometers are sampled quarterly. CrPZ-2a was added to the 2023 IFGMP watch list because dissolved oxygen remains low (<1 mg/L) after three casing volumes have been purged. However, chemistry does not appear to be affected, and samples are collected after three casing volumes have been purged.

The following monitoring wells are addressed in this report as support for the performance wells and are scheduled for monthly sampling:

- R-70 screens 1 and 2
- R-71 screens 1 and 2
- R-72 screens 1 and 2

The following monitoring wells are addressed in this report as support for the performance wells and are sampled on a quarterly basis:

- R-13
- R-15
- R-43 screens 1 and 2
- R-62

Data gaps exist at the following locations:

- R-44 screen 1: in monitoring year (MY) 2023 Quarter 1, R-44 was undergoing maintenance and the well was not operational; therefore, no analytical data will be available for this site during this sampling event. The well maintenance has been completed and the well has returned to operation.
- R-44 screen 2: in MY 2023 Quarter 1, R-44 was undergoing maintenance and the well was not operational; therefore, no field or analytical data will be available for this site during this sampling event. The well maintenance has been completed and the well has returned to operation.
- R-70 screen 2: in MY 2023 Quarter 3, R-70 screen 1 was mistakenly sampled again for the R-70 screen 2 event; therefore, no analytical data will be available for R-70 screen 2 for this sampling event.

- R-71 screen 1: in MY 2023 Quarter 1 during the October monthly and November quarterly sampling events, due to upgrades on the control panel, the well was not operational and the sample was canceled; therefore, no analytical data will be available for these sampling events. The electrical work has been completed and the well has returned to operation.
- R-71 screen 2: in MY 2023 Quarter 1 during the October monthly and November quarterly sampling events, because of work being completed on the well pad, the well was not operational and the sampling was canceled; therefore, no analytical data will be available for these sampling events. The electrical work has been completed and the well has returned to operation.
- R-72 screen 1: in MY 2023 Quarter 1 during the November quarterly sampling event, because of work being completed on the well pad, the well was not operational and the sampling was canceled; therefore, no analytical data will be available for this sampling event. The electrical work has been completed and the well has returned to operation.
- R-72 screen 2: in MY 2023 Quarter 1 during the October monthly and November quarterly sampling events, because of work being completed on the well pad, the well was not operational and the sampling was canceled; therefore, no analytical data will be available for these sampling events. The electrical work has been completed and the well has returned to operation.

3.2 Monitoring Results

Time-series plots are provided for the performance monitoring wells, additional monitoring wells, and piezometers in Figures 3.2-1 through 3.2-28. Time-series plots for extraction wells are provided in Figures 3.2-29 through 3.2-33.

Time-series plots begin in January 2009, with the exception of more recent wells R-50 screen 1 and 2, R-61 screen 1, R-62, R-70 screen 1 and 2, R-71 screen 1 and 2, R-72 screen 1 and 2, SIMR-2, and piezometer wells. Two time-series plots are included for each location and provide a subset of key constituents. The first plot charts chromium, nitrate plus nitrite as nitrogen, and sulfate; the second plot charts chloride, perchlorate, and tritium. These constituents are found within the chromium plume and exhibit trends related to the area of the IM. Chromium is stable as chromate (CrO_4^{2-}) in the regional aquifer under oxic and circumneutral pH conditions and migrates at the same rate of average groundwater flow under static and operating IM scenarios. Regional groundwater elevations are displayed on the plots for context.

The time-series plots show the timelines for the approximate startups of eastern and southern portions of the IM system injection. The southern area IM initial phase in January 2017 is defined by significant startups of CrIN-4 and CrIN-5. The start of the eastern area IM in November 2019 is defined by significant startups of CrIN-1 and CrIN-2. The CrIN-3 startup in late 2017 is not portrayed in the plots. The essential mission critical activities (EMCA) work pause (due to COVID-19 restrictions) beginning on March 24, 2020, is shown on the plots.

The Mann-Kendall (M-K) test was employed to examine the IM influence on concentration trends of chromium, chloride, sulfate, nitrate plus nitrite as nitrogen, and perchlorate in groundwater collected from R-11, R-15, R-44, R-45, R-50, R-61, R-70, CrEX-1, CrEX-2, CrEX-3, CrEX-4, and CrEX-5. The M-K test is a nonparametric statistic that identifies whether or not there are increasing or decreasing trends for time-series data. This test offers a statistical confidence that a monotonic trend is or is not occurring (Gilbert 1987, 056179). The M-K test was employed using a 95% confidence level; therefore, trends were identified only when the calculated p-value (α) is ≤0.5. The M-K test statistic (S) is calculated using Equations 1 and 2 where each data point is compared with all previous data points and assigned a value [-1, 0, 1]. The resulting array is then summed (Gilbert 1987, 056179). Large positive numbers of the sum of the assigned values indicate that later recorded data are higher than previous data and an upward trend is occurring; and large negative numbers indicate a downward trend. When S is small, no trend is observed.

$$S = \sum_{k=1}^{n-1} \sum_{j=k+1}^{n} sgn(x_j - x_k) \qquad \textbf{Equation 1}$$

$$sgn(x_j - x_k) = \begin{cases} 1 \; if \; x_j - x_k > 0 \\ 0 \; if \; x_j - x_k = 0 \\ -1 \; if \; x_j - x_k > 0 \end{cases} \qquad \textbf{Equation 2}$$

To ease examination of the IM influence, monitoring wells have been grouped into three different regions as shown in Figure 3.2-34: (1) plume centroid, (2) southern plume area, and (3) northeastern plume area. In the sections that follow, concentration trends for chromium and other geochemical constituents are examined for statistically significant trends based on different phases of the IM. M-K values were calculated for three phases corresponding to key IM operations, which align with time-series plots:

- Phase 1: data collected before IM operations (January 2009–January 2017)
- Phase 2: initial operations in the southern plume area through beginning of eastern area IM operations (January 2017–November 2019)
- Phase 3: Eastern area IM operations through partial system pause (November 2019–November 2022). Note: M-K testing was not performed on most data collected after the partial system pause because the limited data are unlikely to yield meaningful results. Results were not included in phase 3 so as to not convolute the effect of the eastern area IM operations phase.

Results of the M-K analysis for the three plume zones are as follows: (1) plume centroid results are presented in Table 3.2-1, (2) southern plume area analysis is presented in Table 3.2-2, and (3) northeastern plume results are presented in Table 3.2-3.

Wells R-45 screen 2 and R-61 screen 1 were selected for additional M-K tests on data collected after the partial system pause was put in place. These wells were selected because there appears to be strong visual evidence of chromium trends after the partial system pause. The M-K tests from these data sets quantitatively indicate statistically significant chromium concentration trends decreasing at R-45 screen 2 and increasing at R-61. Results of the additional analyses are shown in Table 3.2-4.

M-K analysis was performed using ProUCL (https://www.epa.gov/land-research/proucl-software).

Appendix B (on CD included with this document) contains all data for this reporting period collected at IFGMP wells. Appendix B also includes injected tracer data that were inadvertently excluded from the 2022 chromium plume control IM performance annual progress report (N3B 2022, 702170).

3.2.1 Concentration Trends by Plume Area

Results of the M-K test at a 95% confidence level are provided in Tables 3.2-1 through 3.2-4. To simplify the presentation, monitoring and extraction wells chosen for analysis were locations potentially influenced by IM injection or extraction operations. On this basis, wells R-43 and R-62 were excluded—they exhibit concentration trends but are relatively distant from the IM infrastructure wells, and the trends predate the start of IM operations. Furthermore, piezometers CrPZ-1, CrPZ-2a, CrPZ-3, CrPZ-4, and CrPZ-5 are omitted because before October 2021, samples from the piezometers were not considered representative of the regional aquifer. Discussion of M-K results is limited to chromium concentrations. Additional information on geochemistry can be found in the Figures 3.2-1 through 3.2-33 for chloride, sulfate, perchlorate, and nitrate plus nitrite as nitrogen, and in Tables 3.2-1 through 3.2-4.

Natural tracers and co-contaminants include chloride and sulfate, which have significantly higher concentrations in extraction wells within or near the plume centroid than at the plume periphery. These anions largely pass through the selective anion exchange resin in the chromium treatment system with little or no change in concentration. Although the anion exchange resins exchange chloride for chromate, the chromate concentrations are low relative to chloride, so there is an insignificant effect on chloride concentrations in treated water streams. As a result, both chloride and sulfate serve as excellent geochemical markers to indicate where treated water injected into CrIN wells is appearing in monitoring wells near the plume periphery. Similarly, decreases in chromium concentrations can also be attributed to the appearance of treated water in monitoring wells. Because chloride has the least potential reactivity and cleanest signal, it is used in this analysis to indicate treated water arrivals.

3.2.2 Plume Centroid Concentration Trends

Chromium concentrations have not been considered representative at well R-28, as indicated by results from a pilot study using molasses and ethanol, which investigated the potential to immobilize chromium via biochemical amendment injection. The only wells located in the centroid area of the plume that represent pre-amendment chromium concentrations are R-42, CrEX-3, and CrEX-4 (Figure 3.2-34, Table 3.2-1). Both extraction wells exhibit decreasing chromium concentration trends in phase 3, and CrEX-3 shows no trend in phase 2. Chromium and nitrate plus nitrite as nitrogen concentrations have rebounded at R-42 since the addition of sodium dithionite in late August 2017.

3.2.3 Southern Plume Area Concentration Trends

Four monitoring wells (R-15, R-44 screen 1, R-50, and R-61 screen 1) and two extraction wells (CrEX-1 and CrEX-2) located in the southern plume area were included in the M-K test for trend analysis (Figure 3.2-34, Table 3.2-2). Before IM operations, chromium concentrations in three of the monitoring wells showed increasing trends (R-15, R-61 screen 1, and R-50 screen 1), but only R-50 screen 1 was above the 50-µg/L groundwater standard. Concentrations at well R-15, located near the southern Laboratory boundary on the western-southwestern boundary of the chromium plume, had measured approximately 1.5 times (~12 µg/L) background concentrations (7.48 µg/L) by the time sustained southern plume area operations had commenced, whereas wells R-44 screen 1 and R-61 screen 1 concentration trends peaked at approximately twice the background concentration.

After the IM operations commenced, southern plume area concentration trends were observed. R-50 screen 1 and R-40 screen 1 show decreasing chromium concentration trends, as well as an increase in chloride and sulfate because of the arrival of treated injection water. Chromium concentrations remain constant, and no trend is observed at R-50 screen 2. R-44 screen 2 shows an increasing chromium concentration trend in phase 3, likely due to the impact of eastern plume area injection activity. Chromium concentration trends decrease at CrEX-1, and CrEX-2, likely due to dilution effects. R-15 had no significant changes in chromium concentrations. And R-61 screen 1 shows increasing chromium concentration trends in three phases, which may be impacted by the nearby CrEX-2 extraction activity.

3.2.4 Northeastern Plume Area Concentration Trends

There are three monitoring wells (R-11, R-45, R-70) and one extraction well (CrEX-5) located in the northeastern plume area included in the M-K analysis (see Figure 3.2-34, Table 3.2-3). Monitoring well R-70 was not installed before IM operations.

R-11, with a depth to the top of the screen of 12 ft below the water table, shows increasing chromium concentration trends, which peaked around 32 µg/L in 2013 before declining to relatively stable concentrations between 5 µg/L and 15 µg/L in 2018 and continue to measure below the 50-µg/L groundwater standard (Figure 3.2-1). Monitoring well R-45 screens 1 and 2 both show increases in chromium concentration before IM operations. R-45 screen 1 shows a decreasing chromium trend after the onset of the IM. R-45 screen 2 shows variably increasing chromium concentration trends in every phase before October 29, 2022. After the partial system pause, a rapid decline in chromium concentrations has been observed. R-70 screens 1 and 2, as well as CrEX-5, show decreasing concentrations after the onset of the IM.

3.3 Water Table Maps

Regional potentiometric surface maps, also called water table maps, are presented as an additional line of evidence in evaluating IM performance and in interpreting potential changes in concentrations of key constituents in performance monitoring wells, additional wells, and piezometers. Long-term pumping and injection at IM infrastructure wells may affect the structure of the potentiometric surface over time in the form of drawdown around extraction wells and mounding around injection wells. The relationship between changes in the water table, chromium concentrations, and tracer breakthrough provides insight into overall IM performance.

Recharge to the regional water table occurs primarily at the mountain block (Jemez Mountains), and mountain front (Sierra de los Valles), resulting in large lateral and downward vertical gradients in western areas of perched-intermediate and regional aquifers. Smaller gradients are observed in the center of the Pajarito Plateau, where recharge is comparatively much less, and upward vertical gradients are evident from artesian wells along the Rio Grande, indicating groundwater discharges to the river along this segment. The regional water table is located 900–1000 ft below ground surface, and water table elevations range from 6300 ft above mean sea level (ft amsl) on the western edge of the Pajarito Plateau, to approximately 5300 ft amsl on the eastern edge of the plateau, near or west of the Rio Grande. Within the area of the IM wells, the water table is at elevations between 5831 and 5833 feet ft amsl. In general, the water table has been declining at a rate of approximately 0.33 ft per yr across the Pajarito Plateau. Rates of decline are higher in the center of the plateau where Los Alamos County supply wells are located.

The groundwater hydraulics analysis presented in detail in “Hydraulic Analysis of the Pajarito Plateau” (Neptune 2023, 702780) was executed to refine the conceptual understanding of groundwater hydraulics of the regional aquifer beneath the Pajarito Plateau in support of fate and transport modeling. Additionally, the analysis identified the influence of Los Alamos County water supply well pumping by examining spatial and temporal hydraulic gradients in the chromium project area. The analysis focused on four time periods which had semi-equilibrium responses to pumping stresses.

Spearman’s rank correlation, $\alpha < 0.001$, (Neptune 2023, 702780) indicates that supply well pumping has a measurable influence on nearby gradients; the range of direct pumping influence appears limited to approximately 2 km (~1.25 mi) or less. At the mountain block mountain front to the west, estimated magnitudes of vertical and lateral gradients in the regional aquifer are approximately 1 to 2 orders of magnitude (10–100) times larger than those observed in the vicinity of supply wells.

The PM-4 water supply well pumps at the highest rate (gpm) of all Los Alamos County supply wells and is located south of the chromium plume with measurable impacts on water levels in monitoring wells drilled in Mortandad Canyon. However, impacts from local extraction and injection from the IM system operation are shown to overwhelm impacts from PM-4. Results show that shifts in hydraulic gradients due to IM operations are substantially greater than those resulting from PM-4 pumping. Hence, for the purposes of fate and transport modeling to support chromium remediation in the short term (~5–20 yr), the influence of pumping supply wells is not needed to support IM operations decision-making.

This performance report provides four shallow regional and four deep regional water table maps. Figure 3.3-1 depicts a baseline shallow regional potentiometric surface map (May 1, 2020) during an extended IM pause, which began March 25, 2020. Figure 3.3-2 depicts a deep regional potentiometric surface map for the same date, May 1, 2020. Figures 3.3-3 through 3.3-8 depict potentiometric surface maps over the course of the annual reporting period. Figure 3.3-3 shows shallow regional potentiometric surfaces from April 2, 2022, which represents the beginning of the reporting period. Figure 3.3-4 shows the deep regional potentiometric surfaces from April 2, 2022. Figure 3.3-5 depicts a shallow regional potentiometric surface map from September 10, 2022, at full system operation, after the system was on for almost 6 months. Figure 3.3-6 shows a deep regional potentiometric surface map from September 10, 2022. Figure 3.3-7 depicts a potentiometric surface map from March 19, 2023, during partial system shutdown, when CrEX-1, CrEX-2, CrEX-3, CrIN-1, CrIN-2, and CrIN-3 were off for 5 months. Figure 3.3-8 shows a deep regional potentiometric surface map from March 19, 2023.

The potentiometric water-level contours are based on synoptic data sets (i.e., measurements taken as close as possible in time to one another). The water-level data used for each map is the first groundwater-level measurement taken on each day, which is typically at 1:00 or 1:01 a.m. For shallow regional potentiometric surface maps, only the upper-screen data are used, where multiple screens are present. The only shallow regional (water table) screen data point intentionally excluded from use in all the shallow regional data sets is R-36, given the uncertainty in its water-level measurements, which is anomalously high. Additionally, the synoptic shallow regional potentiometric surface map from March 19, 2023, shows a 3-ft head difference between R-71 screen 1 and R-62, although both locations are spatially close; R-71 water levels were excluded in favor of the established data set from R-62. However, accounting for R-71 water levels in the synoptic water table does not change the interpretation in the area around the IM wells. Deep regional potentiometric contours include data from deeper screens more than 50 ft below the regional water table surface. There are fewer deep screens than shallow regional screens (8 at depth compared with 21 shallow). A list of the screens used for shallow and deep potentiometric contours can be found in "Chromium Interim Measure Capture Zone Analysis" (Neptune 2023, 702782, Table 2).

The deep regional potentiometric surface maps all show a gradient that is generally towards the southeast, similar to the baseline shallow regional potentiometric surface map (Figure 3.3-1). Regional aquifer surface contours were drawn by hand using the three-point method as described by EPA guidance (https://cfpub.epa.gov/si/si_public_record_report.cfm? dirEntryId=287064&Lab=NRMRL). In this method, adjacent wells are grouped into triplets, and a gradient vector is calculated for each set of triplets using the method of Heath (https://pubs.usgs.gov/wsp/2220/report.pdf). This method assumes that

- the water table surface is planar,
- flow is mostly horizontal, and
- there is no pumping or injection within a triplet.

Since these assumptions are not always appropriate, some interpretation is necessary to produce a realistic potentiometric surface.

3.4 Quantitative Analyses

3.4.1 Numerical Chromium Model

A numerical model of the chromium plume area has been built using the Finite Element Heat and Mass Transfer (FEHM) code (https://fehm.lanl.gov/) with data collected through March 2022. FEHM can account for complexities associated with partially penetrating wells, aquifer heterogeneity, and complex boundary conditions and has been benchmarked against MODFLOW https://www.usgs.gov/mission-areas/wateR-resources/science/modflow-and-related-programs. This section provides a brief description of the IM Chromium Model (CM), and details of the model can be found in "Chromium Model: Calibrated with Uncertainty through 2022" (Neptune 2023, 702781).

The CM extends 137 mi^2 in length and 2000 to 3000 ft in depth, from the top of the water table to 3280 ft amsl. The model domain is discretized into an unstructured tetrahedral mesh. Variable grid sizes are used based on the distance from the chromium plume area and the proximity to injection and extraction wells, with the latter requiring a more refined grid.

Hydrologic and transport parameters include advective porosity, dispersivity, horizontal and vertical hydraulic conductivity, and specific storage. Some parameters are assigned to individual cells within the model grid following the pilot point approach (Doherty 2003, 700894), while others are homogeneous throughout the domain. Given the heterogeneity of the regional aquifer deposits, a unique value of hydraulic conductivity is assigned to each cell in the model domain. The final parameter values are based on model calibration, which is achieved by changing the values of model input parameters to match field data.

All boundary conditions, like other model parameters, use input distributions that limit parameters to plausible values. The hydraulic gradient in the model is set by assigning constant head conditions to the western (mountain block) and eastern (Rio Grande) boundaries. No-flow boundaries are set approximately parallel to regional flow (north and south model edges). The base of the model, which is sufficiently deep (1300–1970 ft) does not impact plume transport behavior at the top of the regional aquifer.

Hydraulic windows have been defined to represent sources of chromium and groundwater entering the regional aquifer from the vadose zone. Currently, five hydraulic windows are used to represent continuing sources to the regional aquifer. Their locations have been inferred from groundwater concentrations of chromium and other analytes, such as perchlorate, nitrate plus nitrite as nitrogen, and tritium [see "Chromium Model: Calibrated with Uncertainty through 2022" (Neptune 2023, 702781)].

3.4.2 Capture Zone Analysis

The combined extraction at CrEX-1, CrEX-2, CrEX-3, and CrEX-4 has resulted in an integrated area of groundwater capture. Capture and flood zone analyses have been performed using both analytical and numerical approaches using methodologies described in the EPA sentinel document, "A Systematic Approach for Evaluation of Capture Zones at Pump and Treat Systems" (https://cfpub.epa.gov/si/si_public_record_report.cfm?Lab=NRMRL&dirEntryId=187788).

Five methods, which consist of two analytical methods and three numerical methods, were executed to provide multiple lines of evidence for hydraulic capture, as recommended in the EPA guidance document cited above. Two analytical methods were executed to determine the lateral extent of integrated capture when all five extraction wells are operational. These approaches assume a homogeneous subsurface geology and a flow system that has achieved equilibrium (i.e., steady state). Three numerical methods were also executed to calculate the lateral and vertical extent of capture. Although the analytical and numerical approach both assume a steady state, i.e., the capture zones have achieved complete development and have reached a maximum reach, the numerical methods can account for geologic heterogeneity within the regional aquifer.

Capture zone estimates from each method are shown in Figure 3.4-1; these estimates are based on calculations with all extraction and injection wells operational and run to steady-state equilibrium conditions. The approximate chromium plume extent (defined by the 50-µg/L contour) is shown as a dashed grey line for context and is equivalent to the deep plume depicted in Figure 1.0-1.

Three numerical methods are also shown in Figure 3.4-1, including solute transport, potentiometric surface mapping, and particle-tracking approaches. All three methods used for capture zone analysis leverage the calibrated CM. These methods account for the heterogeneous spatial distribution of hydraulic conductivity within the regional aquifer and permit the exploration of parametric uncertainty. Although only one parametric simulation is presented in Figure 3.4-1 for simplicity, multiple simulations were executed to determine lateral and vertical capture in the modeling.

The lateral capture zone estimates from each method are depicted in a unique color in Figure 3.4-1. The orange line corresponds to an analytical potentiometric surface mapping method, which involves mapping the contours of a water table surface using temporal hydraulic head measurements. The capture zone estimate is generated by identifying two key synoptic periods, one when the IM is fully operational and one when the IM is shut down (after equilibrium is established), and comparing the resulting maps. The results are compared using closed contours and flow vectors to determine the capture zone.

The brown line corresponds to a solute transport method and is similar to the analytical potentiometric surface mapping described above, but modeling can explicitly account for geologic heterogeneity, resultant groundwater flow behavior, and both advective and dispersive processes. In this method, the release of a hypothetical conservative tracer occurs upgradient to determine the zone of capture at the extraction wells.

The green line corresponds to a particle-tracking method and is similar to the solute transport method; however, instead of simulating the release of a hypothetical conservative tracer upgradient, particles are released upgradient and traced to their exit points at extraction wells. Particles that terminate in extraction wells determine the zone of capture. The black line depicts an analytical flow solution estimating the width of capture used for screening a target capture zone (https://cfpub.epa.gov/si/si_public_record_report.cfm?Lab=NRMRL&dirEntryId=187788) but cannot be used to determine capture zone depth. A detailed description of the chromium IM capture zone analysis is provided in “Chromium Interim Measure Capture Zone Analysis” (Neptune 2023, 702782).

3.5 Injected Tracers and Geochemical Signature of Treated Water

Injected tracers have been deployed into each of the five injection wells to allow observations of tracer arrivals at monitoring wells and extraction wells. Naphthalene sulfonate tracers were used for all injection wells because they are highly soluble, generally nonbiodegrading, nontoxic, and nonadsorbing; have very low detection limits; and are relatively inexpensive for the large injection masses necessary for detection at monitoring and extraction wells (Rose et al. 2001, 232203). The following tracers were deployed into the injection wells:

- CrIN-1: 2,6-naphthalene disulfonic acid (2,6-NDS) was injected on March 31, 2021;
- CrIN-2: 1,3,5-naphthalene trisulfonic acid (1,3,5-NTS) was injected on March 30, 2021;

- CrIN-3: 1,3,6-NTS was injected on September 10, 2018;
- CrIN-4: 1,5-NDS was injected on May 17 and 18, 2017; and 2,6-NDS was injected on September 17, 2018.
- CrIN-5: 1,6-NDS was injected on May 18 and May 19, 2017; and 2,7-NDS was injected on September 18, 2018

Because concentrations of chloride and sulfate are unaffected by the treatment process, their concentrations in injection water are largely a continuous, flow-weighted average of extraction well concentrations. Therefore, treated water arrivals cannot be traced to a particular injection well. By contrast, naphthalene sulfonate tracers were introduced as a concentrated slug of short duration. Hence, injected tracers can indicate an unequivocal arrival of treated water from an injection to an extraction well. By combining tracer data with geochemical responses due to injection water signals, flow patterns and mixing associated with IM operation can be discerned.

3.5.1 CrIN-4 and CrIN-5 Tracers

NDS[1,5-] tracer injection into CrIN-4 occurred in May 2017, and 2,6-NDS tracer injection occurred in September 2018. NDS[1,6-] tracer injection into CrIN-5 occurred in May 2017, and 2,7-NDS tracer injection occurred in September 2018.

Figure 3.5-1 presents a time-series plot of chromium and tracers detected in R-50 screen 1, including 1,5-NDS, and 2,6-NDS. The screen is approximately 10 ft below the regional water table at R-50. NDS[1,5-] was detected in August 2018. Shortly after the 1,5-NDS arrival, the chloride concentration reached 20 mg/L, which is approximately the injection water concentration, suggesting that the regional aquifer water originally present in R-50 screen 1 was completely replaced by the injection water. NDS[2,6-] was detected once on January 15, 2019, at R-50 screen 1. The tracer appears to have biodegraded in the regional aquifer soon after it arrived at R-50 screen 1, an unexpected outcome given that naphthalene sulfonate tracers are known to have lifetimes of many years in geothermal reservoirs (Rose et al., 2001, 232203). As can be seen in Figure 3.5-1, R-50 screen 1 chromium concentrations rapidly declined as the injection water from CrIN-4 arrived.

Figure 3.5-2 shows the 1,5-NDS tracer arrival in CrEX-1 at a similar time to the arrival at R-50 screen 1, despite CrEX-1 being located twice as far from the CrIN-4 injection site. Unlike R-50 screen 1, the tracer concentration at CrEX-1 has not significantly decreased and remains relatively high to present day. Because CrEX-1 has been pumped, as opposed to just being a passive monitoring location like R-50 screen 1, it is possible to estimate the fraction of tracer recovered at this extraction well. Approximately 16.5% of the 1,5-NDS tracer mass has been recovered to date, implying that at least 16.5% of the water injected into CrIN-4 since the tracer was injected has been drawn into CrEX-1. Given the current trend shown in Figure 3.5-2, the tracer recovery is expected to increase, and the estimated fraction of water injected into CrIN-4 reaching CrEX-1 is also expected to continue to increase. As this occurs, a secondary but much weaker tracer signal may appear in the injection wells from water extracted at CrEX-1.

Although CrIN-4 is the major contributor of injected water to CrEX-1, with the apparent susceptibility of some of these tracers to biodegrade, it is possible that some contributions of injected water is from CrIN-5. However, CrIN-5 tracers have not been detected at CrEX-1 or at any monitoring well.

Finally, chloride, sulfate, and chromium concentration histories in R-50 screen 2, as well as lack of tracer arrivals, indicate that injection fluid has not arrived in the deeper screen (see Figure 3.2-14).

There has also been no evidence of tracer or injection water arrivals at SIMR-2, despite its relatively close proximity to CrIN-4 and CrIN-5, approximately 1100 and 2000 ft to the southeast, respectively.

3.5.2 CrIN-3 Tracers

NTS[1,3,6-] tracer injection into CrIN-3 occurred on September 12, 2018.

Figure 3.5-3 presents a time-series plot of chromium and tracers in R-44 screen 1, including 1,3,6-NTS. The screen is approximately 15 ft below the regional water table. NTS[1,3,6-] was first detected at R-44 screen 1 in December 2018 and has shown a definitive response to injection water and the 1,3,6-NTS tracer. Shortly after the 1,3,6-NTS arrival, the chloride concentration trends rapidly approach injection water concentrations. No tracer or injection water signal has been detected in R-44 screen 2, which is approximately 100 ft below the regional water table. Chloride concentration trends are similar for R-45 screen 1 (Figure 3.2-11).

Thus, the CrIN-3 injection water seems to remain relatively shallow, similarly to the injection water from CrIN-4. The CrIN-3 tracer and injection water signatures have not been detected at R-13 or SIMR-2.

3.5.3 CrIN-1 and CrIN-2 Tracers

NDS[2,6-] tracer injection into CrIN-1 occurred in March 2021. NTS[1,3,5-] tracer injection into CrIN-2 occurred in March 2021.

The 2,6-NDS tracer injected into CrIN-1 appears to have inexplicably biodegraded before it could be detected in any monitoring or extraction well. If the 2,6-NDS tracer had a longevity in the regional aquifer similar to the 2,6-NDS CrIN-4 injection, it should have been detected in R-45 screen 1 or CrEX-5. The reason the 2,6-NDS tracer had a shorter longevity in the regional aquifer (relative to CrIN-4) has not yet been determined.

Figure 3.5-4 shows that in December 2021, 1,3,5-NTS was first detected at CrEX-3. The total tracer mass recovery to date in CrEX-3 has been about 1% of the injection mass, but it is increasing with no indication of biodegradation. This result suggests that the injection water arriving in R-45 screen 1 came from CrIN-1 rather than CrIN-2.

Figure 3.2-33 shows the chloride, sulfate, and chromium concentration histories in CrEX-5, which, in lieu of a tracer response, can be used to look for evidence of treated water arrival from CrIN-1. While the trends in sulfate and chromium are consistent with the possibility of a treated water arrival, it is clear that the concentrations of all constituents have been decreasing since CrEX-5 began operations. Hence, the lower concentrations may be due to a concentration decrease in groundwater drawn into CrEX-5, treated water arrival, or both. Since chloride concentrations in CrEX-5 have dropped below the average concentration in injection water, then at least some of the observed decrease is from groundwater being treated at CrEX-5, presumably from locations within or at the edge of the plume where concentrations are lower.

Figure 3.2-18 shows chloride, sulfate, and chromium trends in R-70 screen 2, which has higher concentrations relative to R-70 screen 1 and appears to be better connected to the plume centroid than the upper screen at R-70. Chloride, sulfate, and chromium trends at R-70 screen 2 are similar to those at CrEX-5, although the chloride concentration at R-70 screen 2 has dropped to even lower levels than in CrEX-5. These results suggest that treated injection water has not yet arrived at R-70 screen 2, given the continuously declining concentrations of chloride and sulfate to levels lower than the injection fluid concentrations. Furthermore, there are no signs of injection water reaching R-70 screen 1.

Instead, a reasonable assumption is that CrEX-5 is, at least in part, pulling groundwater from R-70 preferentially from the depths of R-70 screen 2 and perhaps from R-70 screen 1 as well.

3.5.4 IM Flow Inferences from Tracers

A qualitative picture of injection footprints is shown in Figure 3.5-5, which not only integrates information provided in this report, but also draws on results from previous tracer studies documented in Reimus et al. (Reimus et al. 2021, 701331) and the absence of a cross-hole response with the R-28 amendment injection. Inferences from injection water tracers and geochemistry are as follows:

- Injection flow into CrIN-4 reached both R-50 screen 1 and CrEX-1, with about 17% of the injection flow (likely more) being drawn into CrEX-1. CrIN-4 injection water has not reached other observation locations, including R-50 screen 2 and SIMR-2. The injection water appears to remain shallow, at least in the vicinity of R-50.
- Injection flow into CrIN-5 has not been definitively observed at any location, possibly due to the biodegradation of the CrIN-5 tracer. Injection flow into CrIN-2 reached CrEX-3, with about a 1% tracer recovery at CrEX-3 to date. CrIN-2 injection water has not reached either R-45 screen 1 or R-45 screen 2 or any other locations.
- Injection flow into CrIN-1 reached R-45 screen 1 very rapidly, but the rapid degradation of the tracer injected into CrIN-1 has prevented a positive detection of arrival at CrEX-5. CrIN-1 injection flow does not appear to be reaching R-45 screen 2, R-70 screen 1, or R-70 screen 2.
- CrEX-3 is extracting groundwater from CrIN-2, with an exact percentage of the injected water currently unknown but likely to be significantly higher than the 1% of CrIN-2 tracer mass already recovered.

To date, tracers introduced in injection wells and the distinct geochemical signature of injection water are present only in the shallow upper 50 ft of the regional aquifer in only the upper screens at wells R-44, R-45, and R-50. There is no tracer evidence to date of injection water migration below depths of the upper screens.

3.5.5 Estimation of Flow Velocities

Tracer injections, which are observed at monitoring or extraction wells, aid in understanding the details of plume-scale groundwater flow dynamics under the influence of the IM extraction and injection. In addition to the tracer results, monitoring-well observations of various geochemical signatures in injection water provide insights into plume-scale groundwater flow dynamics, including estimates of flow porosity and how volumetric flow is distributed within the aquifer porosity over large interrogation volumes. These estimations are described in the Proceedings of the 2021 Waste Management Symposium (Reimus et al. 2021, 701331)

4.0 DISCUSSION

4.1 Notice of Violation

On June 6, 2022, NMED-GWQB issued "Notice of Violation, Los Alamos National Laboratory Underground Injection Control Wells, DP-1835" (NMED 2022, 702153) to the U.S. Department of Energy Environmental Management Los Alamos Field Office (EM-LA) based on measured concentrations of total dissolved chromium in the regional aquifer at well R-45 screen 2 that exceeded the 20.6.2.3103 New Mexico Administrative Code groundwater standard of 50 µg/L. EM-LA reported this exceedance to

NMED-GWQB on February 26, 2021, in the “Quarterly Report for the Discharge of Treated Groundwater to the Regional Aquifer Under Discharge Permit 1835, Calendar Year 2020 Quarter 4, Class V Underground Injection Control Wells,” (N3B 2021, 701249).

On September 30, 2022, EM-LA submitted the “Regional Aquifer Monitoring Well R-45 Action Plan,” (R-45 Action Plan) providing activities that EM-LA proposed for addressing chromium in the regional aquifer (N3B 2022, 702350). On December 12, 2022, NMED-GWQB provided a review of the R-45 Action Plan and direction to cease all injection of treated water authorized under Discharge Permit 1835 by April 1, 2023, “until the Permittees complete the proposed corrective actions and can definitively prove through qualitative and quantitative analyses, simulations, monitoring well installation, and continued monitoring that further migration is not occurring.” (NMED 2022, 702464).

To address NMED-GWQB concerns associated with the IM influence on the regional aquifer and chromium plume migration, EM-LA prepared an initial 5-year evaluation of the IM and submitted this assessment to NMED on February 28, 2023 (N3B 2023, 702597). This document presents an analysis of the IM influence on the regional aquifer system in the vicinity of the chromium plume, along with a predictive assessment of potential impacts associated with modifying IM operations. The analysis of the IM influence on the regional aquifer examined potentiometric surfaces, chromium concentrations, and concentrations of injected tracers and natural tracers resulting from groundwater treatment. In addition, a calibrated numerical model of the chromium plume area has been used to supplement the assessment of chromium plume migration, specifically by supporting the evaluation of extraction well capture and examining IM performance under different operational scenarios.

The results presented in this 2023 annual performance monitoring report align with results and conclusions from the initial 5-year evaluation (N3B, 2023, 702597), the hydraulic analyses presented in “Hydraulic Analysis of the Pajarito Plateau”(Neptune 2023, 702780), the IM Chromium Model (Neptune 2023, 702781), and the capture zone analysis presented in “Chromium Interim Measure Capture Zone Analysis” (Neptune 2023, 702782).

4.2 Decreasing Chromium Concentration at R-45 Screen 2

Chromium concentrations at R-45 screen 2 responded quickly to partial operation in October 2022, immediately beginning to decrease (Figure 3.2-12, Table 3.2-4). Concentrations peaked at 69.1 µg/L on October 25, 2022, and decreased below 50 µg/L to 49.1 µg/L by February 2, 2023. The R-45 chromium concentration has continued to decrease and is 41.7 µg/L as of April 12, 2023. The rapid response to partial operation suggests that continued partial operation is a viable option for maintaining hydraulic control along the Pueblo de San Ildefonso boundary through operation of CrIN-4 and CrIN-5 and extraction of chromium along the northeastern plume edge through operation of CrEX-5 while also addressing NMED’s concerns about chromium concentrations at R-45 screen 2.

4.3 Evaluation of the Efficacy of the IM

Multiple lines of evidence are used to evaluate the performance of the IM. The primary line of evidence for IM performance is chromium concentration trends in performance monitoring wells compared with the long-term trends before IM operations. M-K analyses have confirmed a decrease in chromium concentrations in all five extraction wells and in key monitoring well locations, most significantly in R-50 screen 1. The R-50 screen 1 results indicate that the primary objective of the IM has been met, namely to reduce chromium concentrations in R-50 screen 1 and maintain the 50-µg/L chromium concentration on the LANL boundary.

Additionally, a principal objective of the IM has been to hydraulically control the chromium plume (LANL 2015, 600458). To date, the IM has been successful in controlling the lateral extent of the plume in the south and southeastern regions of the plume. Although there is still uncertainty with respect to either vertical or lateral distribution of the chromium plume in the plume centroid and southeastern and northeastern regions of the plume, the hydraulic and geochemical data and information indicate that IM operations have generally contained the plume within the Laboratory boundary.

5.0 RECOMMENDATIONS

The following recommendations are based on the IM results, which continue to align with the initial 5-year evaluation:

- Data from multiple lines of evidence will continue to be used to inform adaptive management strategies, in particular, potential adjustments to the IM system operation going forward.
- In the future, the IM system should be restarted at full capacity to maximize the benefits of the IM, to confirm conclusions presented in the initial 5-year evaluation, and to provide information on plume behavior that will aid in final remedy design;
- EM-LA is advocating for resumption of partial operations, including operation of CrIN-3, CrIN-4, CrIN-5, CrEX-5, and a selection of other existing CrEX wells to maximize hydraulic control along the laboratory boundary with Pueblo de San Ildefonso and chromium extraction;
- Deep extraction does not appear to be necessary at this time to continue to achieve IM objectives but may emerge as a priority, pending analyses and associated zonal sampling that will become available when deeper monitoring wells (R-76 and R-77) are installed.
- Planned monitoring wells R-79 and R-80 are needed on a priority basis to reduce uncertainties in lateral and vertical extents of the chromium plume and to provide additional performance monitoring.

6.0 REFERENCES AND MAP DATA SOURCES

6.1 References

The following reference list includes documents cited in this report. Parenthetical information following each reference provides the author(s), publication date, and ERID, ESHID, or EMID. ERIDs were assigned by the Laboratory's Associate Directorate for Environmental Management (IDs through 599999); ESHIDs were assigned by the Laboratory's Associate Directorate for Environment, Safety, and Health (IDs 600000 through 699999); and EMIDs are assigned by Newport News Nuclear BWXT-Los Alamos, LLC (IDs 700000 and above).

Doherty, J., March-April 2003. "Ground Water Model Calibration Using Pilot Points and Regularization," *Ground Water,* Vol. 41, No. 2, pp. 170-177. (Doherty 2003, 700894)

Gilbert, R.O., 1987. *Statistical Methods for Environmental Pollution Monitoring*, Van Nostrand Reinhold, New York, New York. (Gilbert 1987, 056179)

LANL (Los Alamos National Laboratory), May 2015. "Interim Measures Work Plan for Chromium Plume Control," Los Alamos National Laboratory document LA-UR-15-23126, Los Alamos, New Mexico. (LANL 2015, 600458)

LANL (Los Alamos National Laboratory), April 2018. "Chromium Plume Control Interim Measure Performance Monitoring Work Plan," Los Alamos National Laboratory document LA-UR-18-23082, Los Alamos, New Mexico. (LANL 2018, 603010)

N3B (Newport News Nuclear BWXT-Los Alamos, LLC) (J. Murdock, A. Duran), February 26, 2021. "Quarterly Report for the Discharge of Treated Groundwater to the Regional Aquifer Under Discharge Permit 1835, Calendar Year 2020 Quarter 4, Class V Underground Injection Control Wells," Newport News Nuclear BWXT-Los Alamos, LLC, document EM2021-0056, Los Alamos, New Mexico. (N3B 2021, 701249)

N3B (Newport News Nuclear BWXT-Los Alamos, LLC), May 2021. "Interim Facility-Wide Groundwater Monitoring Plan for the 2022 Monitoring Year, October 2021–September 2022," Newport News Nuclear BWXT-Los Alamos, LLC, document EM2021-0131, Los Alamos, New Mexico. (N3B 2021, 701449)

N3B (Newport News Nuclear BWXT-Los Alamos, LLC), February 2023. "Initial Five-Year Evaluation of the Interim Measures for Chromium Plume Control with an Assessment of Potential Modifications to Operations," Newport News Nuclear BWXT-Los Alamos, LLC, document EM2023-0067, Los Alamos, New Mexico. (N3B 2022, 702597)

N3B (Newport News Nuclear BWXT-Los Alamos, LLC), June 2022. "Annual Progress Report on Chromium Plume Control Interim Measure Performance, July 2021 through March 2022," Newport News Nuclear BWXT-Los Alamos, LLC, document EM2022-0355, Los Alamos, New Mexico. (N3B 2022, 702170)

N3B (Newport News Nuclear BWXT-Los Alamos, LLC), September 2022. "Regional Aquifer Monitoring Well R-45 Action Plan," Newport News Nuclear BWXT-Los Alamos, LLC, document EM2022-0318, Los Alamos, New Mexico. (N3B 2022, 702350)

Neptune (Neptune and Company, Inc), April 28, 2023. "Hydraulic Analysis of the Pajarito Plateau," report prepared by Neptune and Company, Inc, for the U.S. Department of Energy Environmental Management Los Alamos Field Office, Los Alamos, New Mexico. (Neptune 2023, 702780)

Neptune (Neptune and Company, Inc), February 17, 2023. "Chromium Model: Calibrated with Uncertainty through 2022," report prepared by Neptune and Company, Inc, for the U.S. Department of Energy Environmental Management Los Alamos Field Office, Los Alamos, New Mexico. (Neptune 2023, 702781)

Neptune (Neptune and Company, Inc), January 31, 2023. "Chromium Interim Measure Capture Zone Analysis," report prepared by Neptune and Company, Inc, for the U.S. Department of Energy Environmental Management Los Alamos Field Office, Los Alamos, New Mexico. (Neptune 2023, 702782)

NMED (New Mexico Environment Department), December 12, 2022. "Corrective Action Plan Response and Further Action Required, Los Alamos National Laboratory Underground Injection Control Wells, DP-1835," New Mexico Environment Department Ground Water Quality Bureau letter to A. Duran (DOE-EM-LA) and R. Macfarlane (N3B) from J. Ball (NMED-GWQB), Santa Fe, New Mexico. (NMED 2022, 702464)

NMED (New Mexico Environment Department), June 6, 2022. “Notice of Violation, Los Alamos National Laboratory Underground Injection Control Wells, DP-1835,” New Mexico Environment Department letter to A.D.D.E.-L.a.J.M. (N3B) from J. Ball (NMED-GWQB), Santa Fe, New Mexico. (NMED 2022, 702153)

Reimus, P., D. Katzman, M. Ding, and B. Willis, March 8–12, 2021. “Using Tracers and Opportunistic Geochemical Signatures to Inform Modeling of Cr(VI) Migration at LANL,” Waste Management 2021 Conference, March 8–12, 2021, Phoenix, Arizona. (Reimus et al. 2021, 701331)

Rose, P.E., W.R. Benoit, and P.M. Kilbourn, December 2001. “The Application of the Polyaromatic Sulfonates as Tracers in Geothermal Reservoirs,” *Geothermics,* Vol. 30, No. 6, pp. 617–640. (Rose et al. 2001, 232203)

6.2 Map Data Sources

Hillshade; Los Alamos National Laboratory, ER-ES, As published; \\slip\gis\Data\HYP\LiDAR\2014\Bare_Earth\BareEarth_DEM_Mosaic.gdb; 2014.

Unpaved roads; Los Alamos National Laboratory, ER-ES, As published, GIS projects folder; \\slip\gis\GIS\Projects\14-Projects\14-0062\project_data.gdb\digitized_site_features\digitized_roads; 2017.

Drainage channel; Los Alamos National Laboratory, ER-ES, As published, GIS projects folder; \\slip\gis\GIS\Projects\15-Projects\15-0080\project_data.gdb\correct_drainage; 2017.

Structures; Los Alamos National Laboratory, KSL Site Support Services, Planning, Locating and Mapping Section; 06 January 2004; as published 29 November 2010.

Paved Road Arcs; Los Alamos National Laboratory, FWO Site Support Services, Planning, Locating and Mapping Section; 06 January 2004; as published 29 November 2010.

Chromium plume > 50 ppb; Los Alamos National Laboratory, ER-ES, As published; \\slip\gis\GIS\Projects\13-Projects\13-0065\shp\chromium_plume_2.shp; 2018.

Regional groundwater contour May 2017, 4-ft interval; Los Alamos National Laboratory, ER-ES, As published; \\slip\gis\GIS\Projects\16-Projects\16-0027\project_data.gdb\line\contour_wl2017may_2ft; 2017.

Regional groundwater contour November 2017, 2-ft interval; Los Alamos National Laboratory, ER-ES, As published; \\slip\gis\GIS\Projects\16-Projects\16-0027\project_data.gdb\line\contour_wl2017nov_2ft; 2017.

Point features; As published; EIM data pull; 2017.

Technical Area Boundaries; Los Alamos National Laboratory, Site Planning & Project Initiation Group, Infrastructure Planning Office; September 2007; as published 13 August 2010

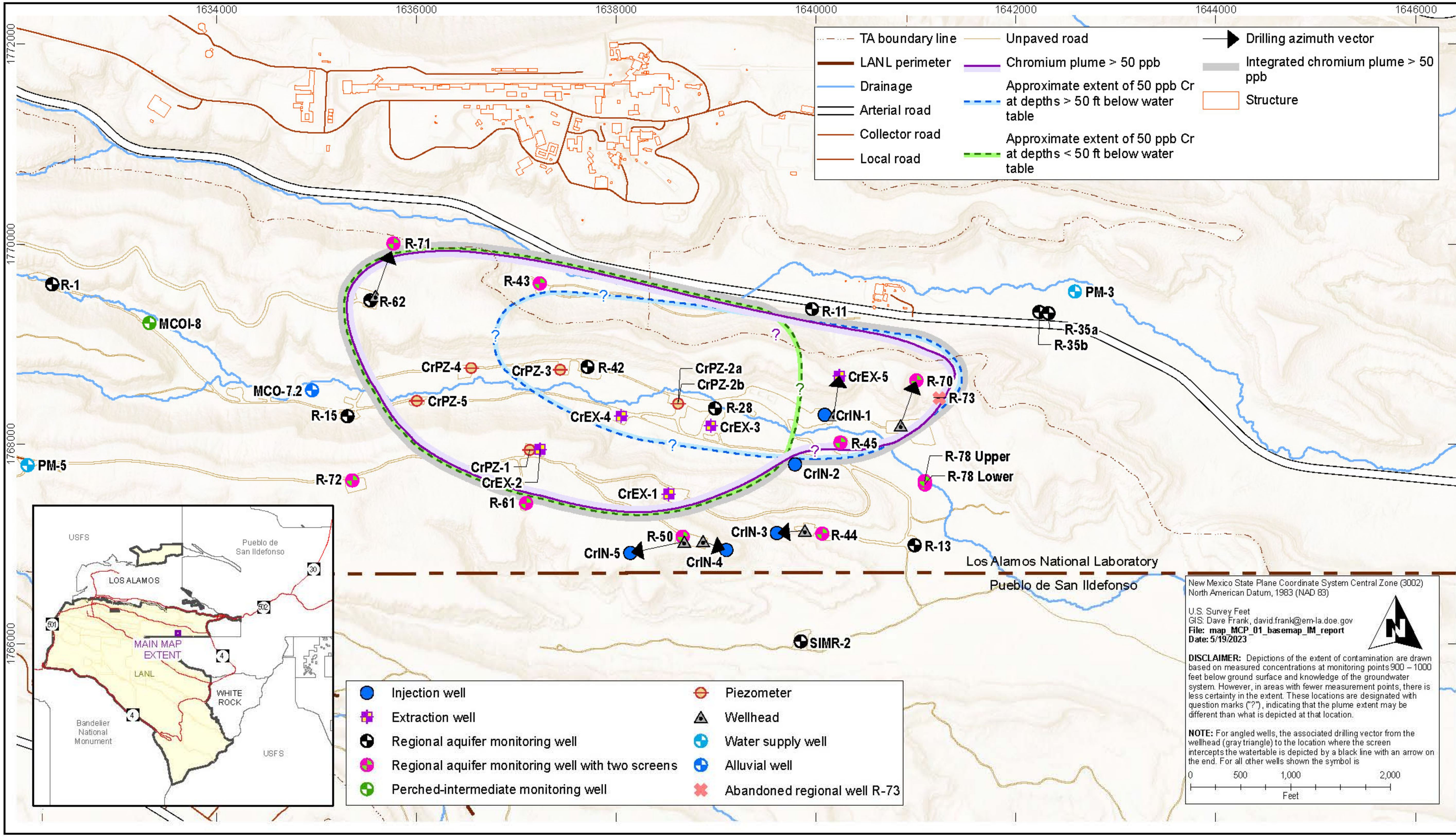

Figure 1.0-1 Chromium project area map

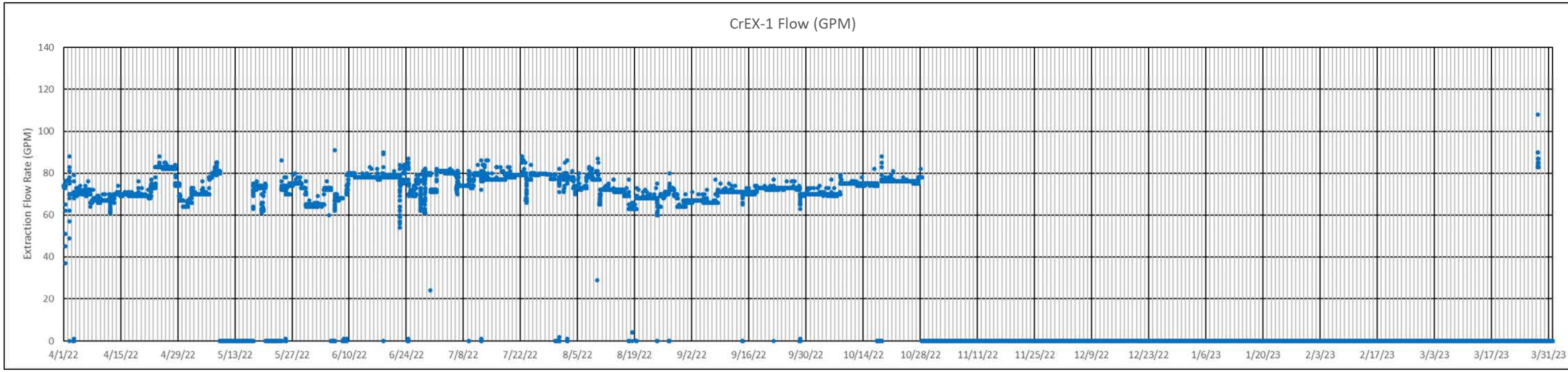

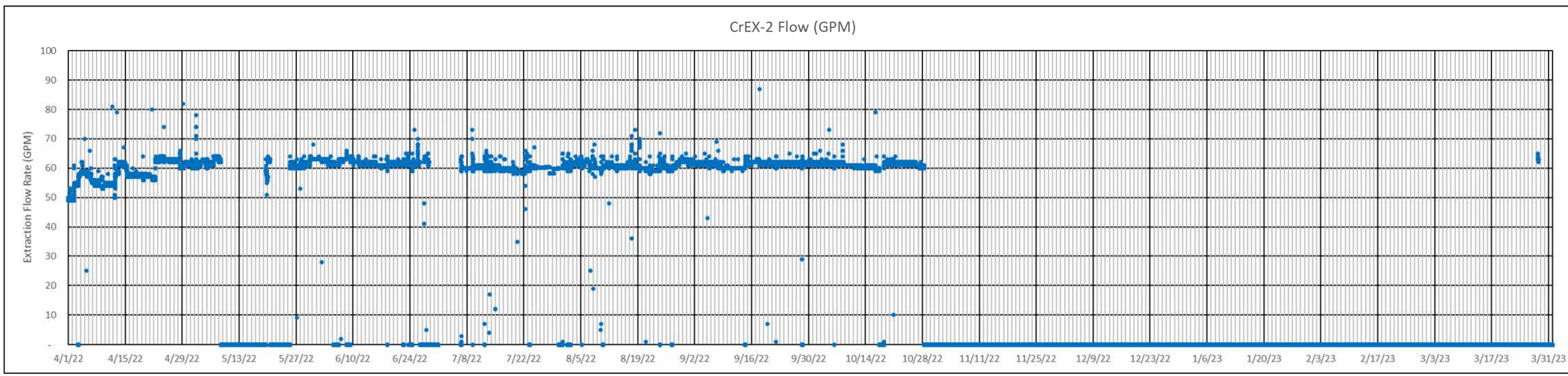

Figure 2.1-1 Extraction flow rates for CrEX wells for April 1, 2022, through March 31, 2023

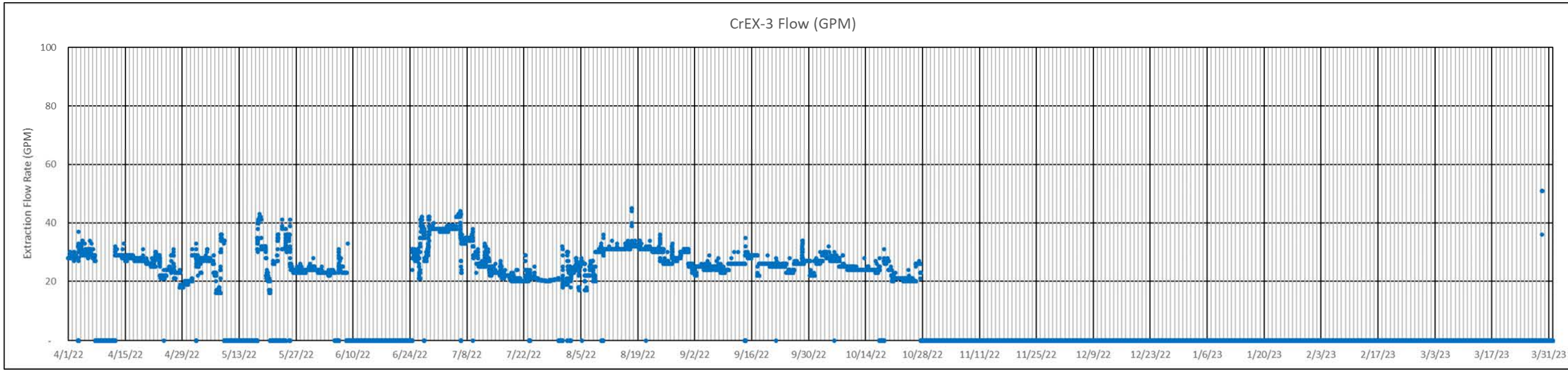

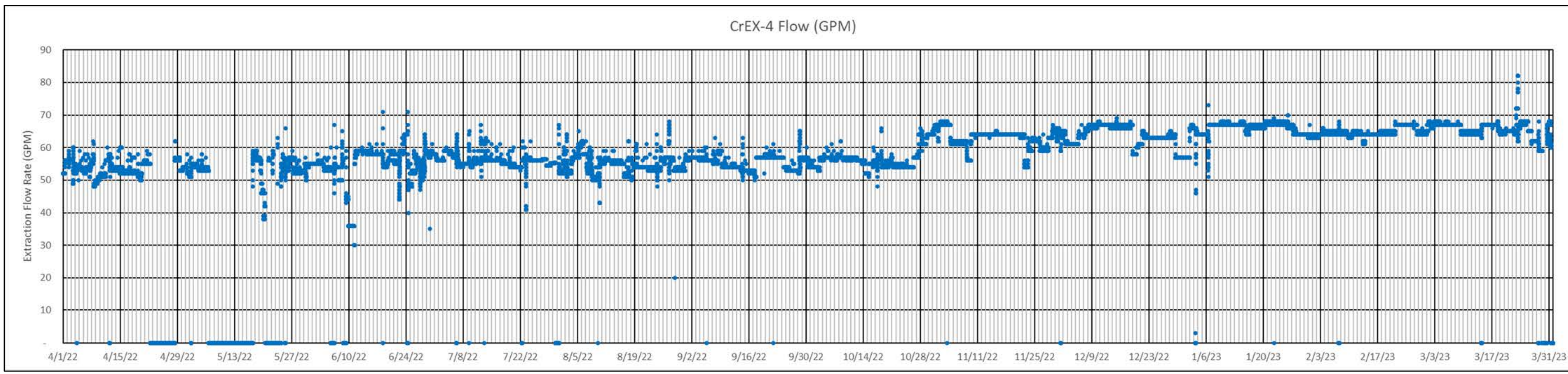

Figure 2.1-1 (continued) **Extraction flow rates for CrEX wells for April 1, 2022, through March 31, 2023**

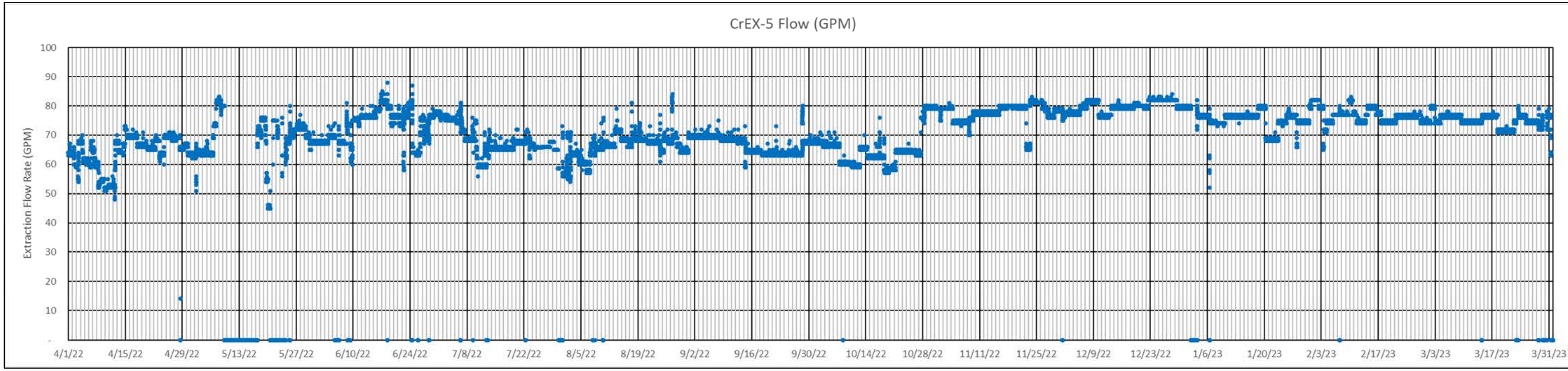

Figure 2.1-1 (continued) **Extraction flow rates for CrEX wells for April 1, 2022, through March 31, 2023**

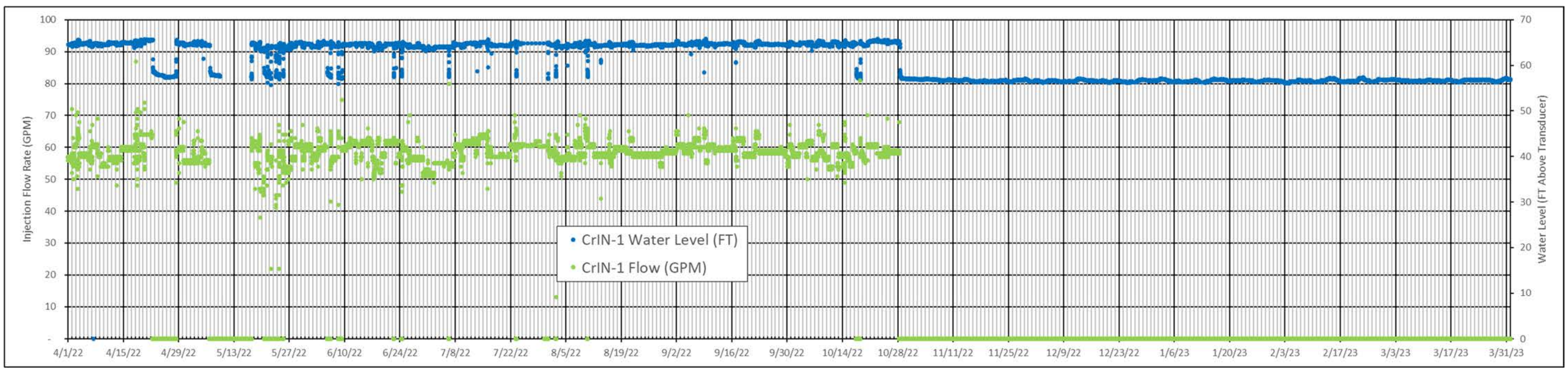

Figure 2.1-2 **Injection well flow rates and water levels for CrIN wells for April 1, 2022, through March 31, 2023**

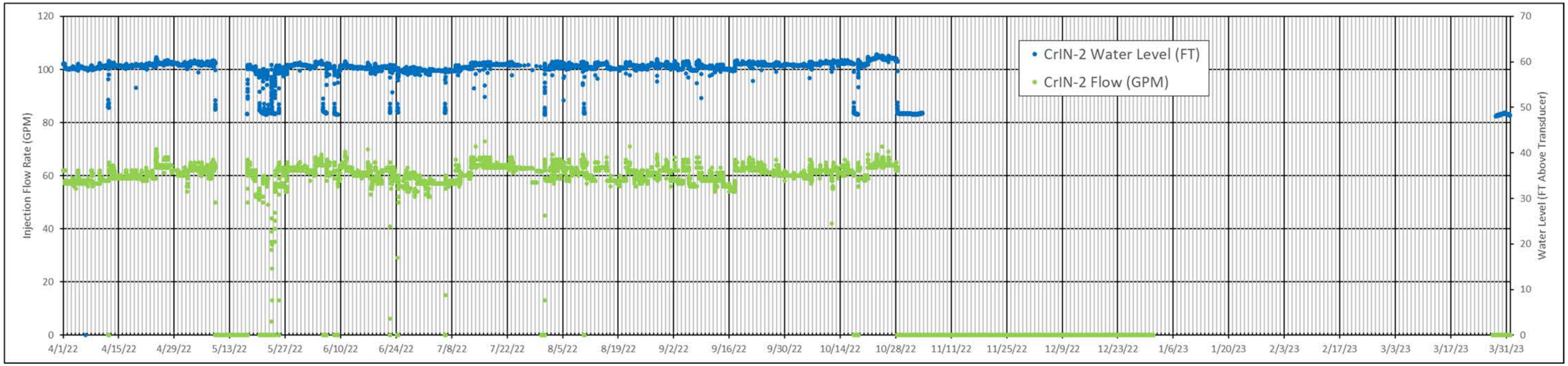

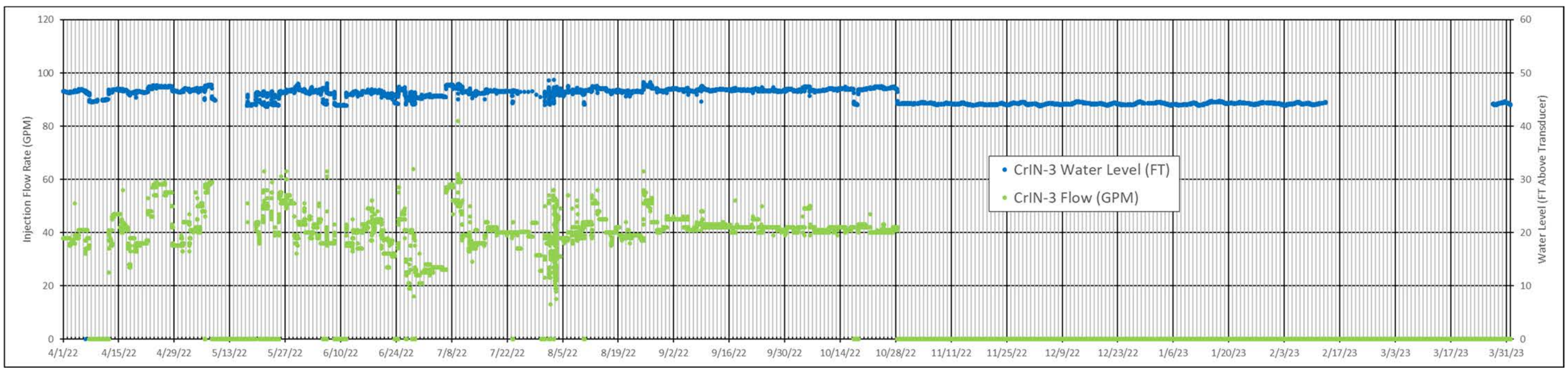

Figure 2.1-2 (continued) **Injection well flow rates and water levels for CrIN wells for April 1, 2022, through March 31, 2023**

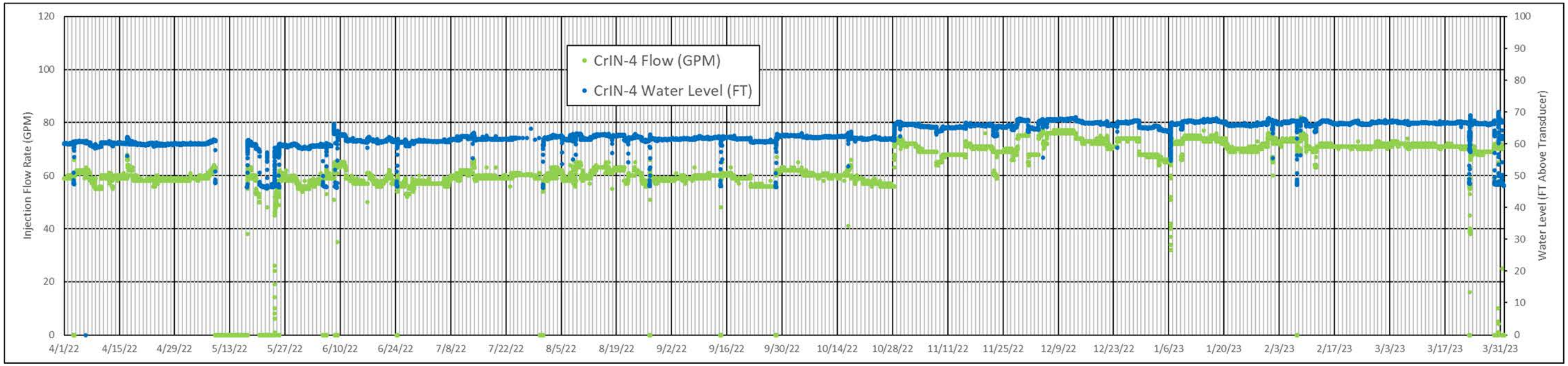

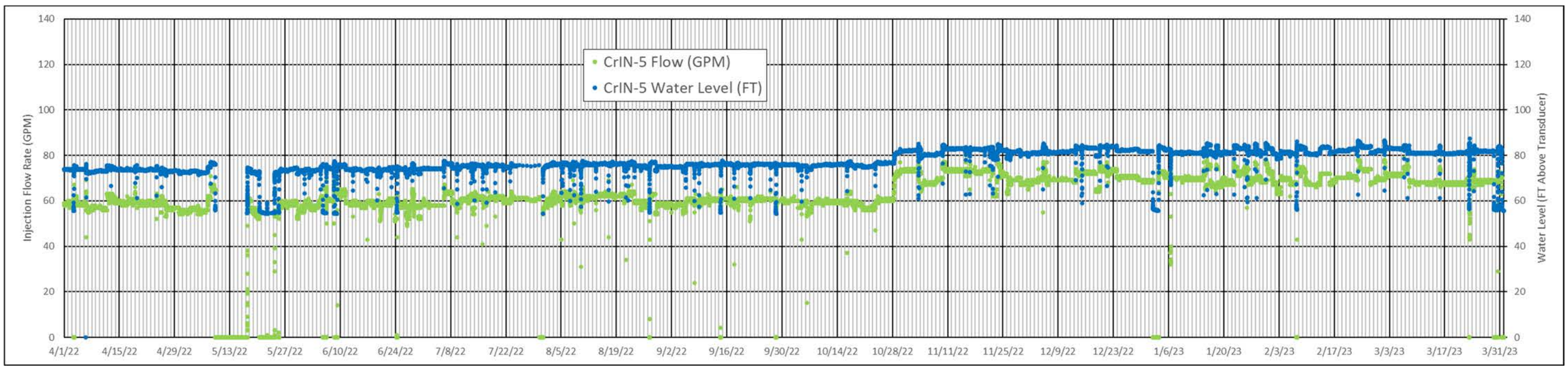

Figure 2.1-2 (continued) **Injection well flow rates and water levels for CrIN wells for April 1, 2022, through March 31, 2023**

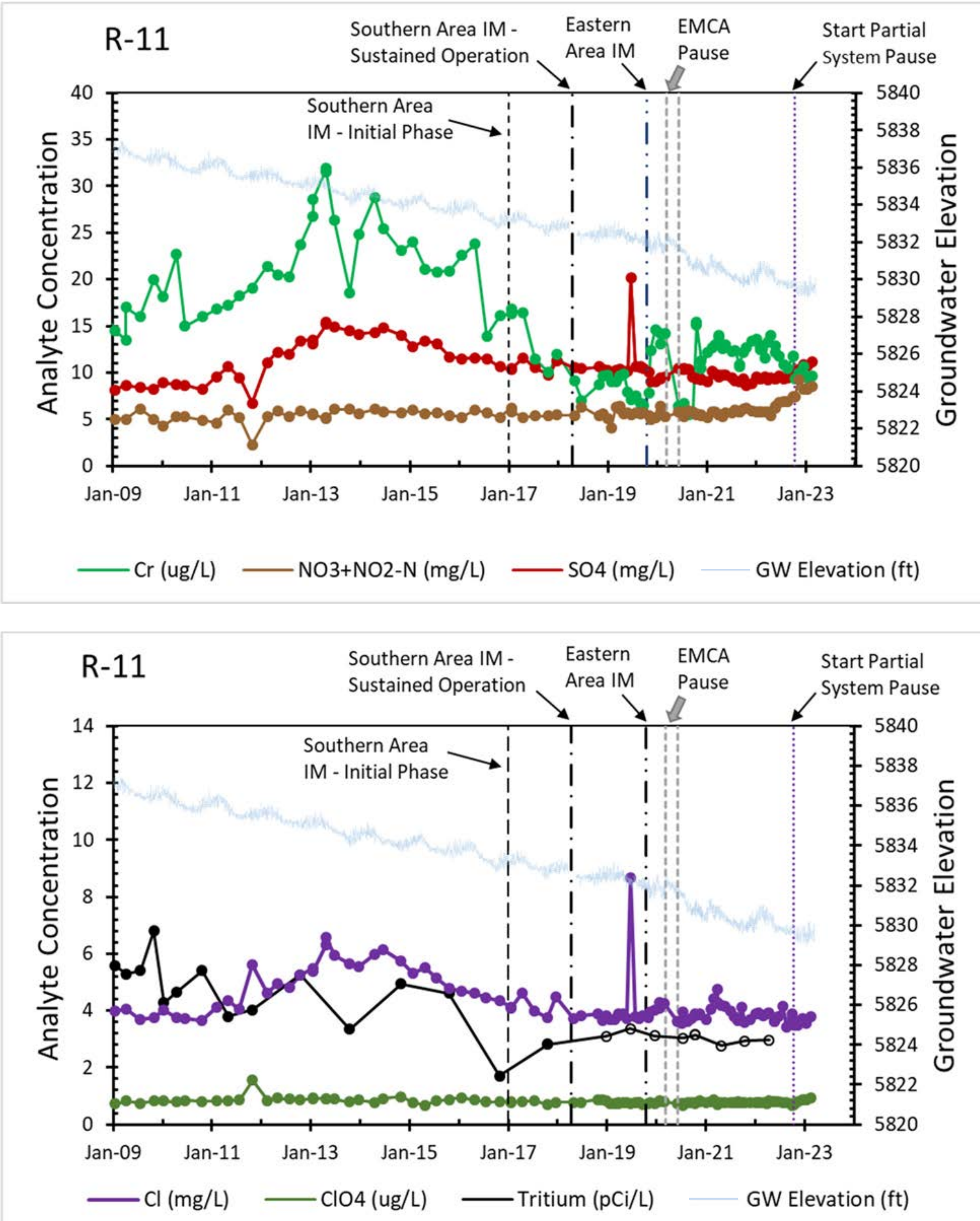

Notes: Open symbols represent nondetection results and solid symbols represent detection results at the plotted value. The background for chromium is 7.48 µg/L. Groundwater elevations represent raw data (without barometric adjustment).

Figure 3.2-1 Time-series plots for R-11

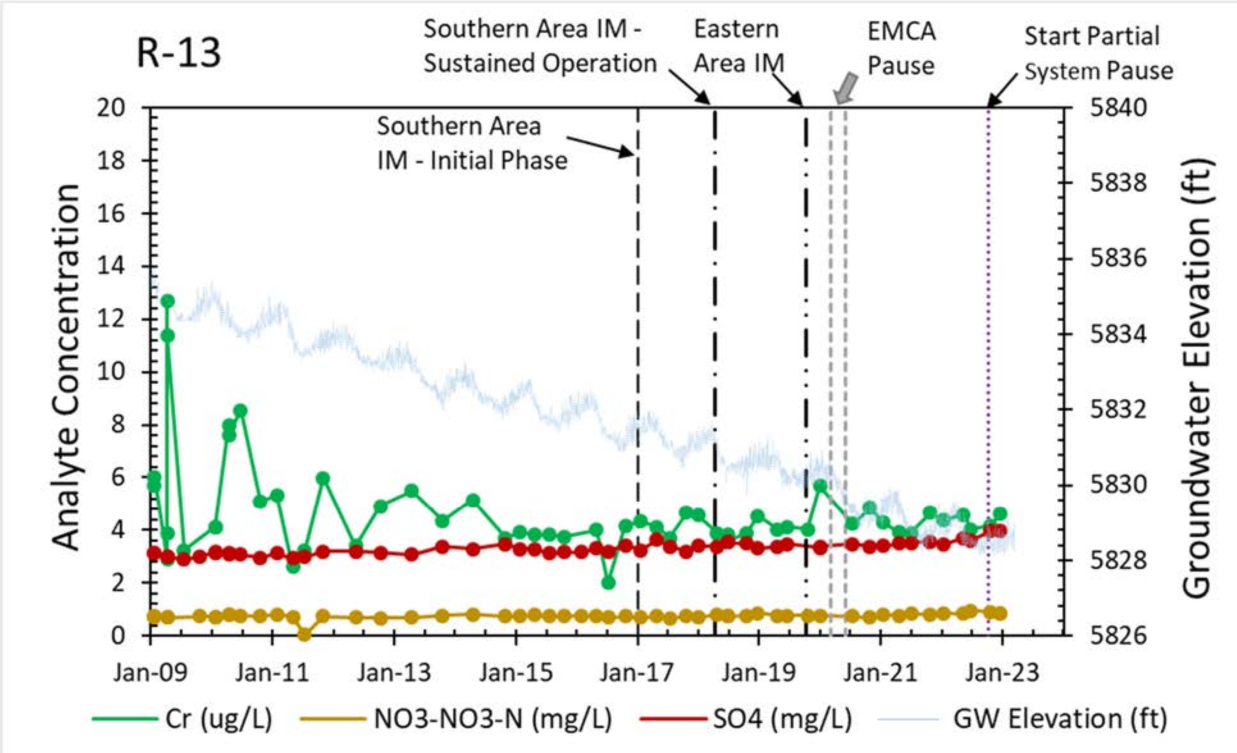

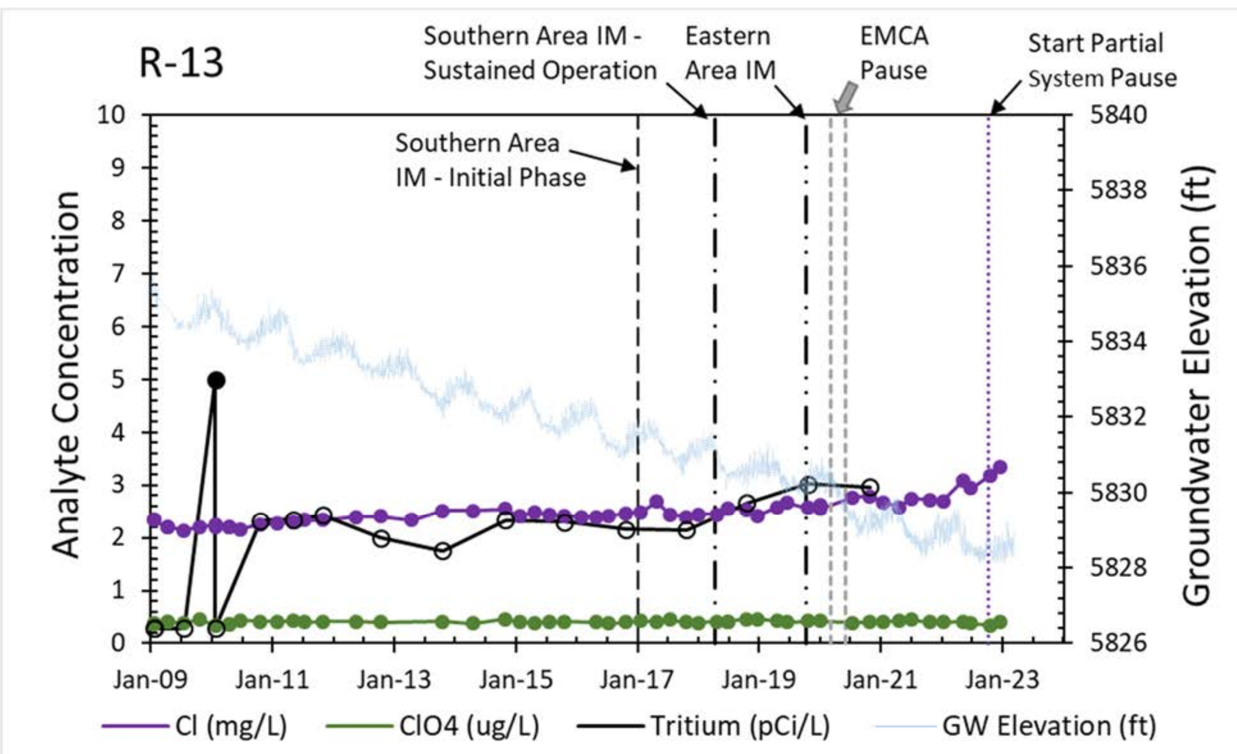

Notes: Open symbols represent nondetection results and solid symbols represent detection results at the plotted value. The background for chromium is 7.48 µg/L. Groundwater elevations represent raw data (without barometric adjustment).

Figure 3.2-2 Time-series plots for R-13

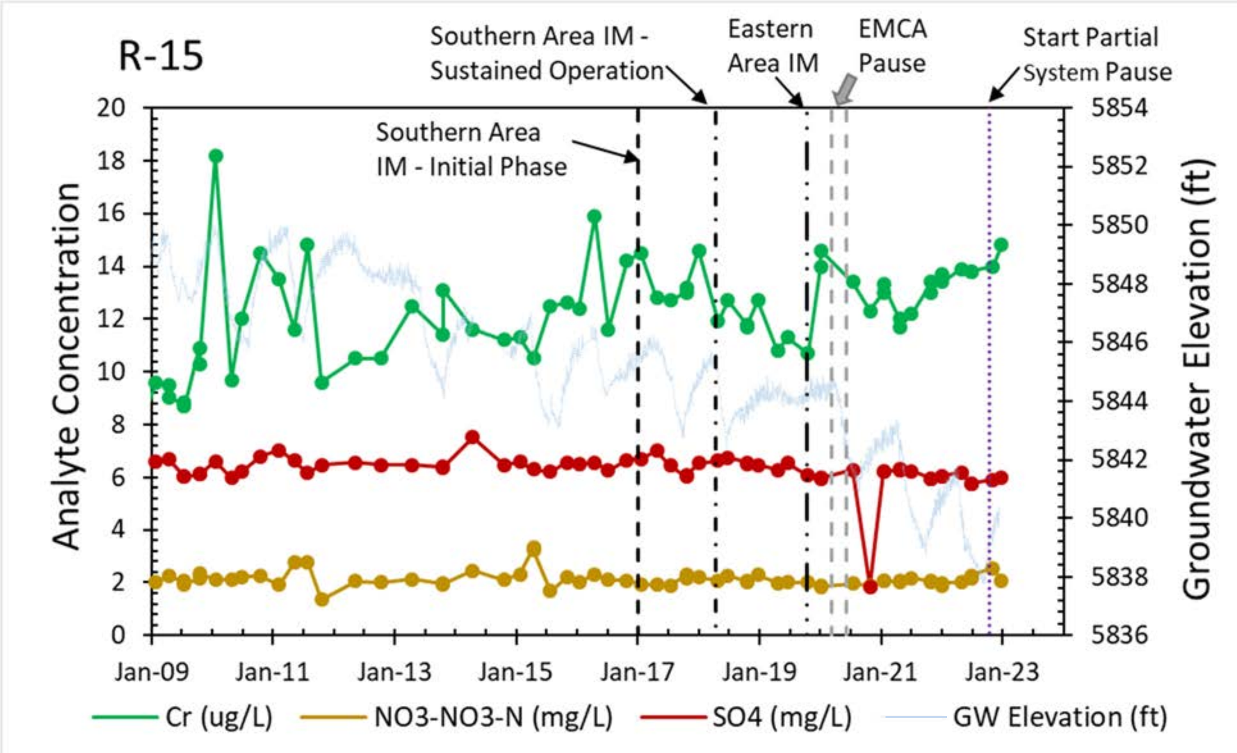

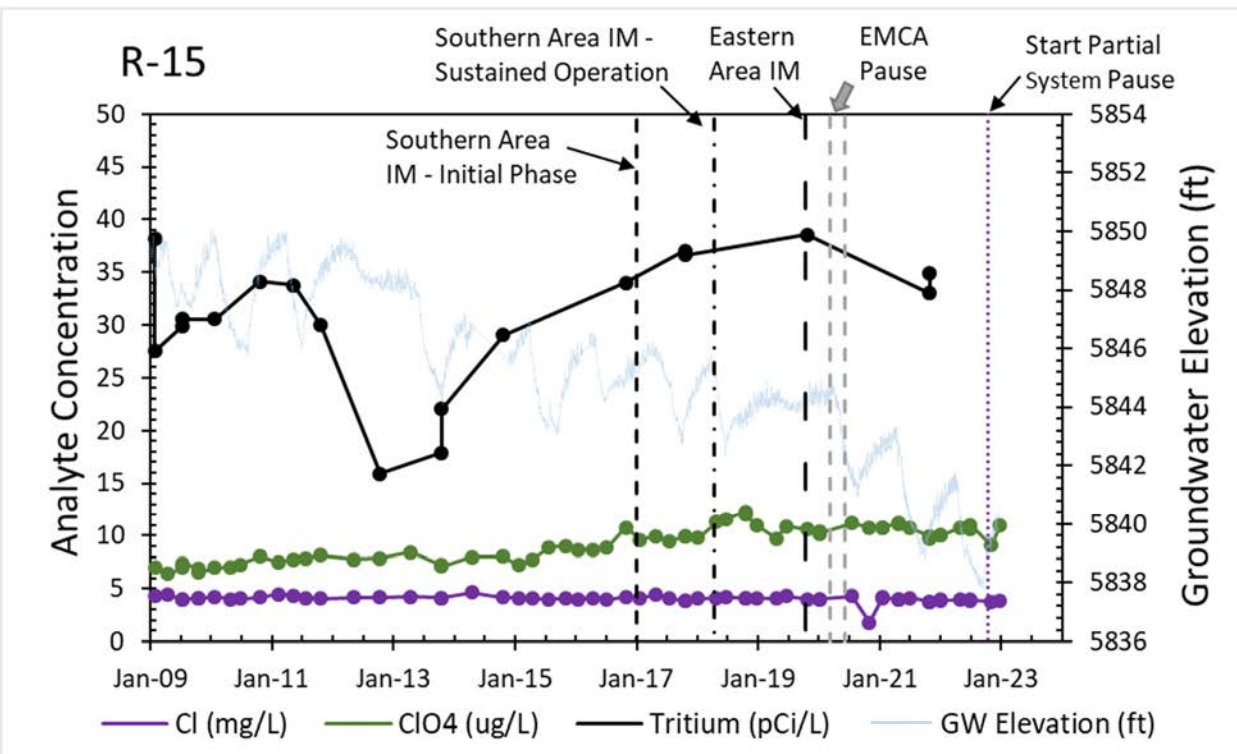

Notes: Open symbols represent nondetection results and solid symbols represent detection results at the plotted value. The background for chromium is 7.48 µg/L. Groundwater elevations represent raw data (without barometric adjustment).

Figure 3.2-3 Time-series plots for R-15

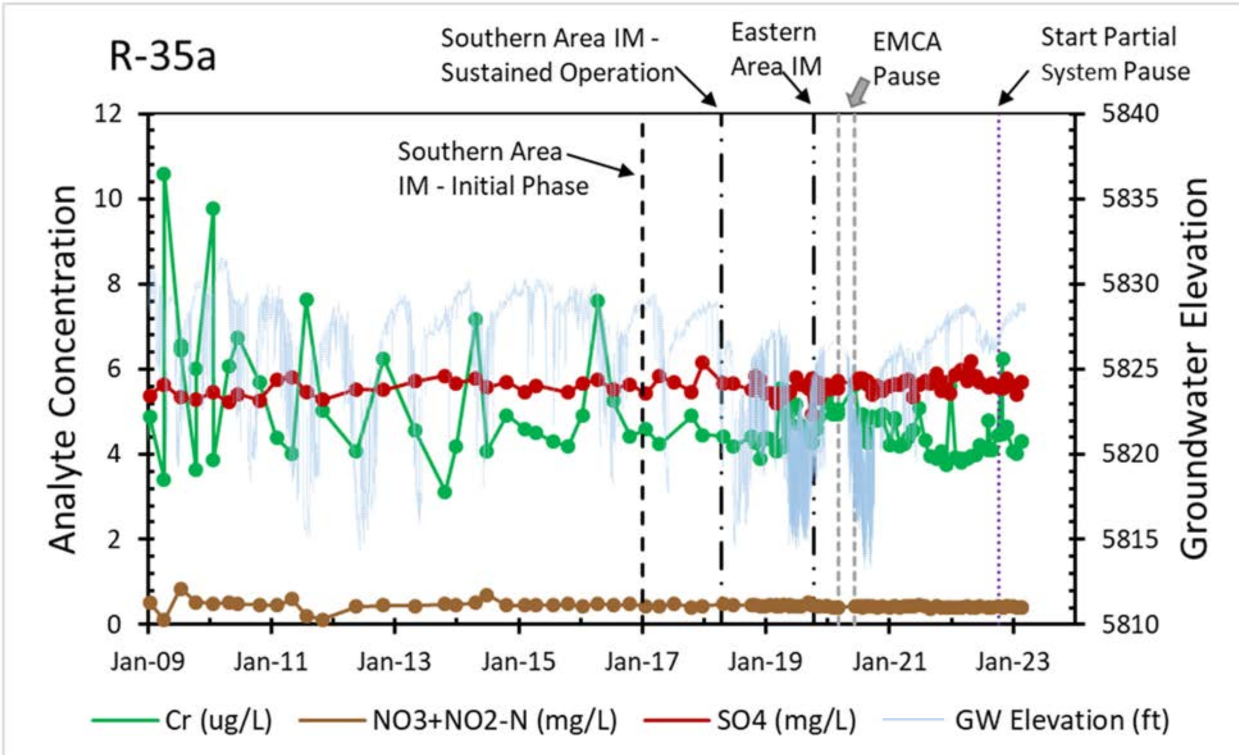

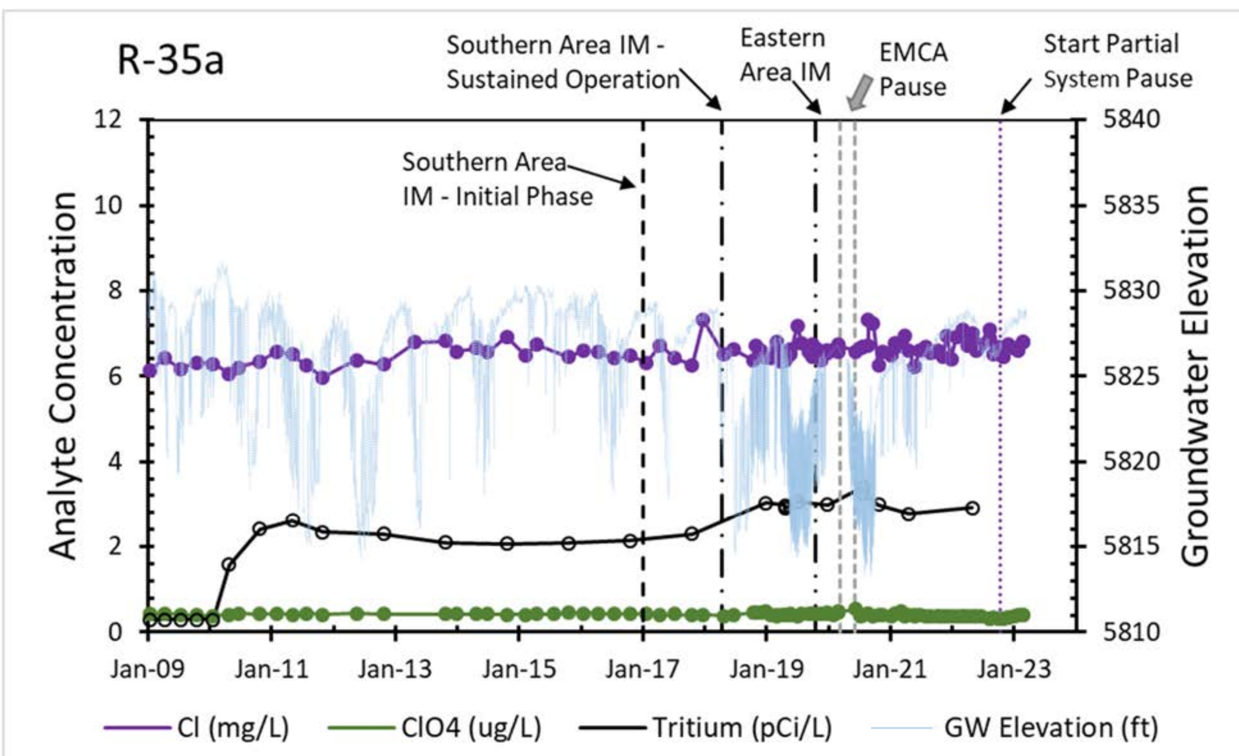

Notes: Open symbols represent nondetection results and solid symbols represent detection results at the plotted value. The background for chromium is 7.48 µg/L. Groundwater elevations represent raw data (without barometric adjustment).

Figure 3.2-4 Time-series plots for R-35a (deeper R-35 location)

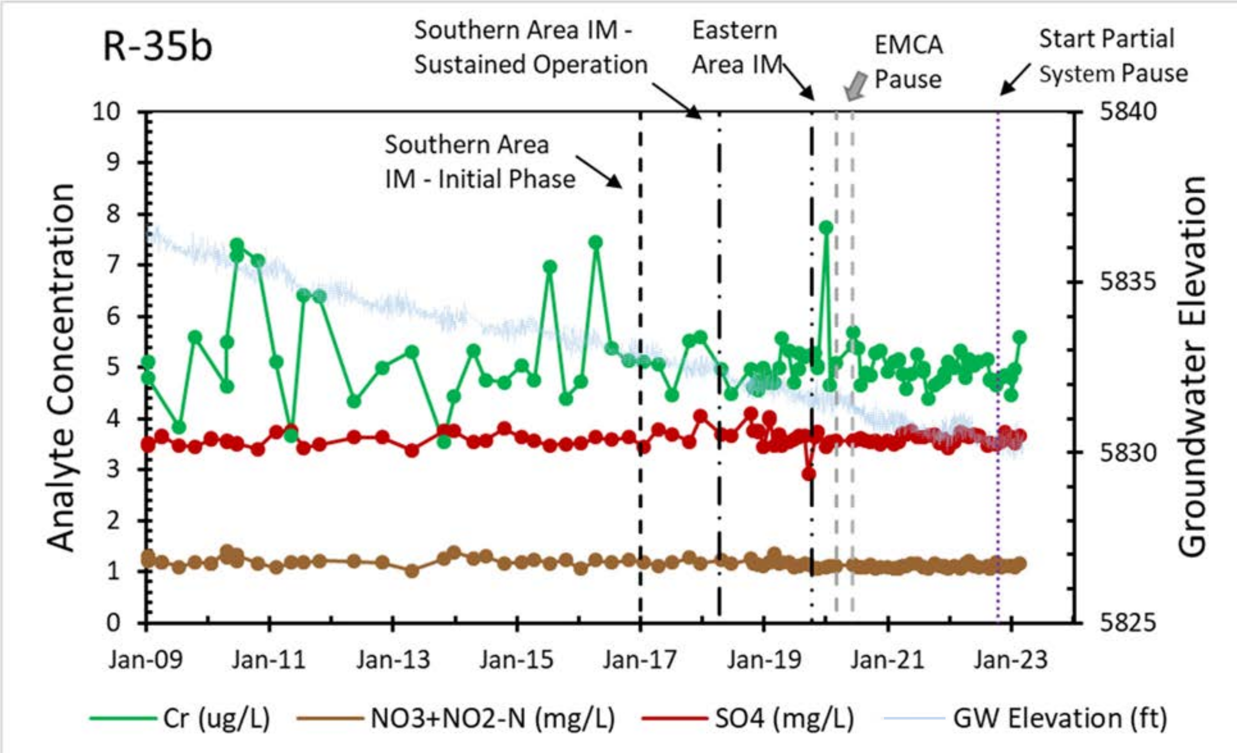

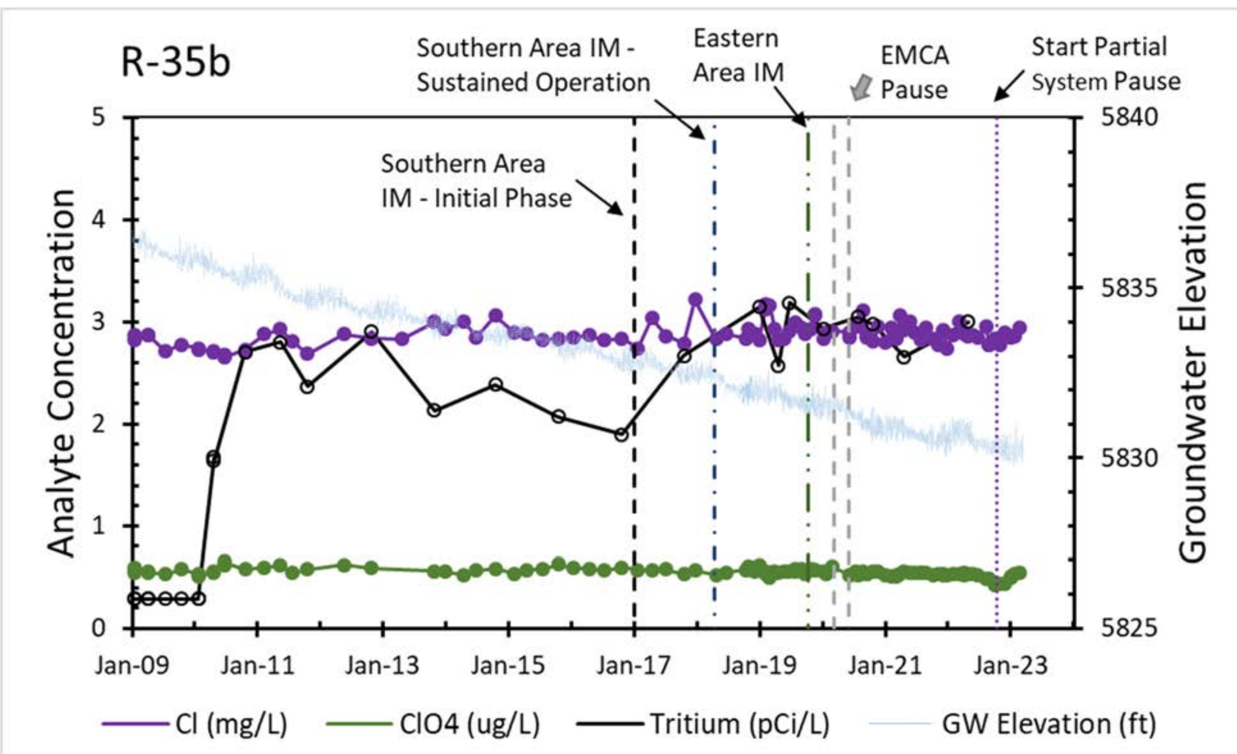

Notes: Open symbols represent nondetection results and solid symbols represent detection results at the plotted value. The background for chromium is 7.48 µg/L. Groundwater elevations represent raw data (without barometric adjustment).

Figure 3.2-5 Time-series plots for R-35b (shallower R-35 location)

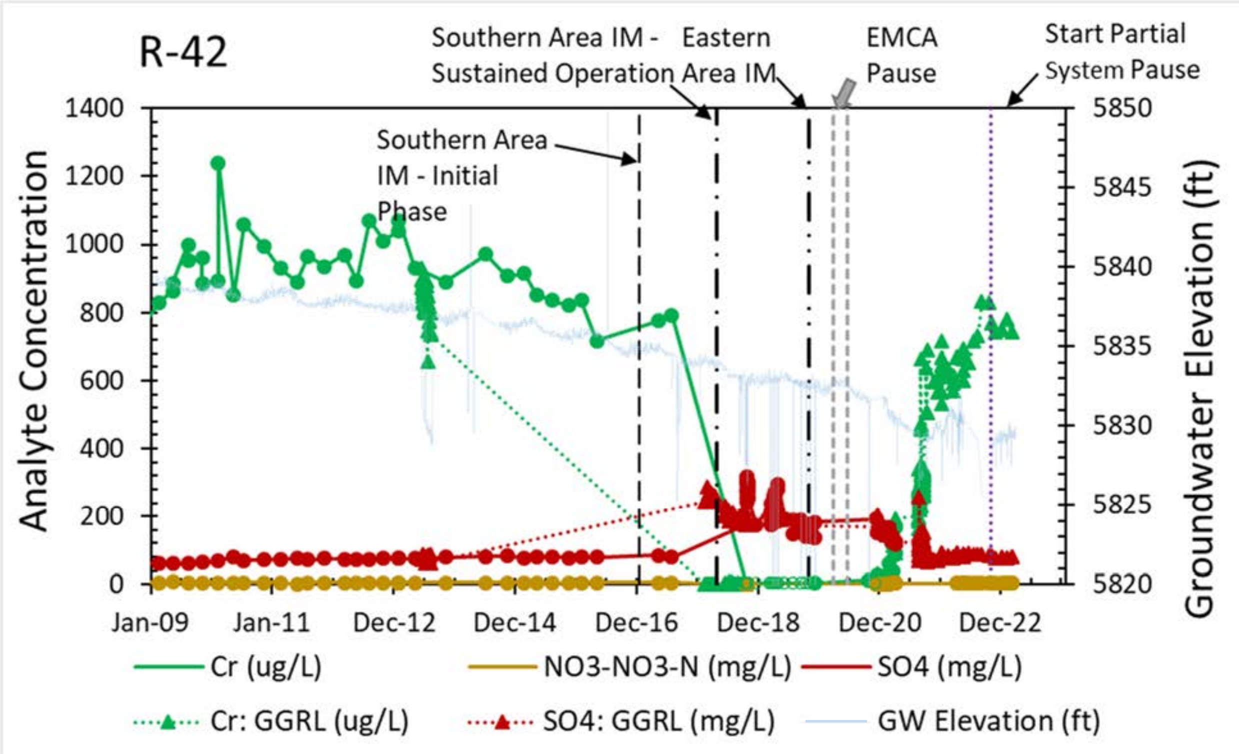

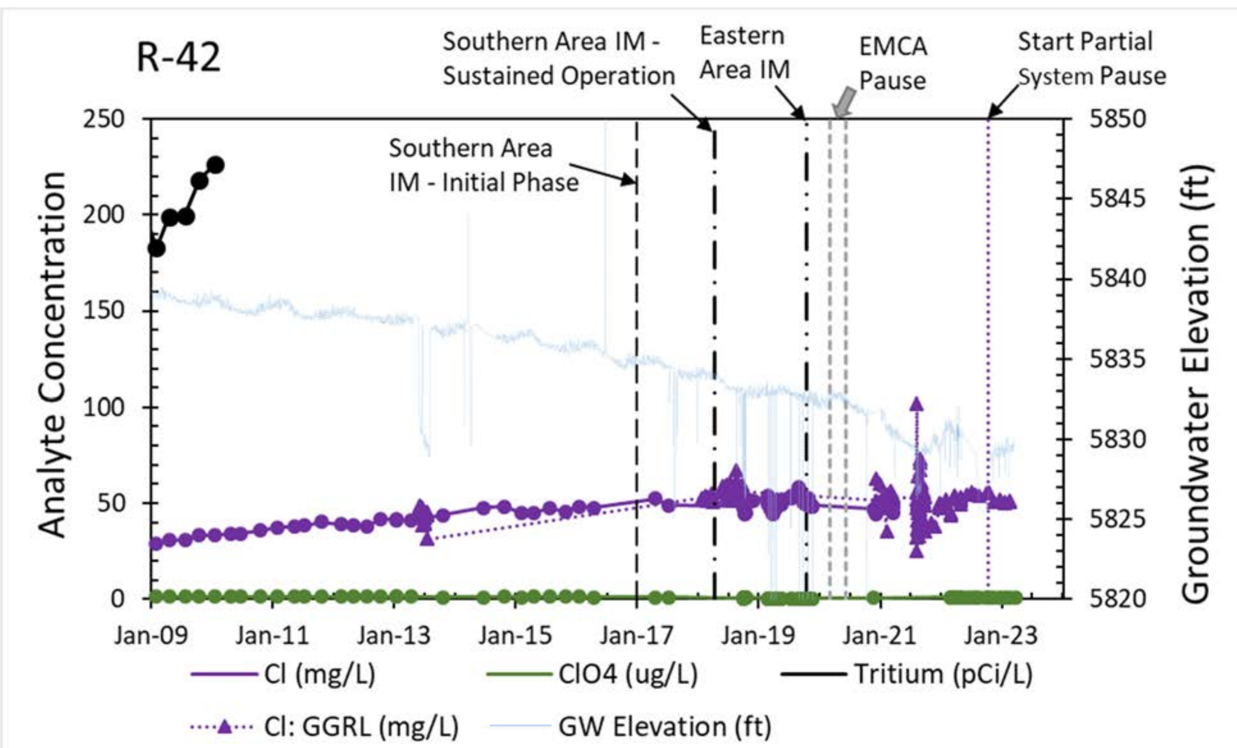

Notes: Open symbols represent nondetection results and solid symbols represent detection results at the plotted value. The background for chromium is 7.48 µg/L. Groundwater elevations represent raw data (without barometric adjustment).

Figure 3.2-6 Time-series plots for R-42

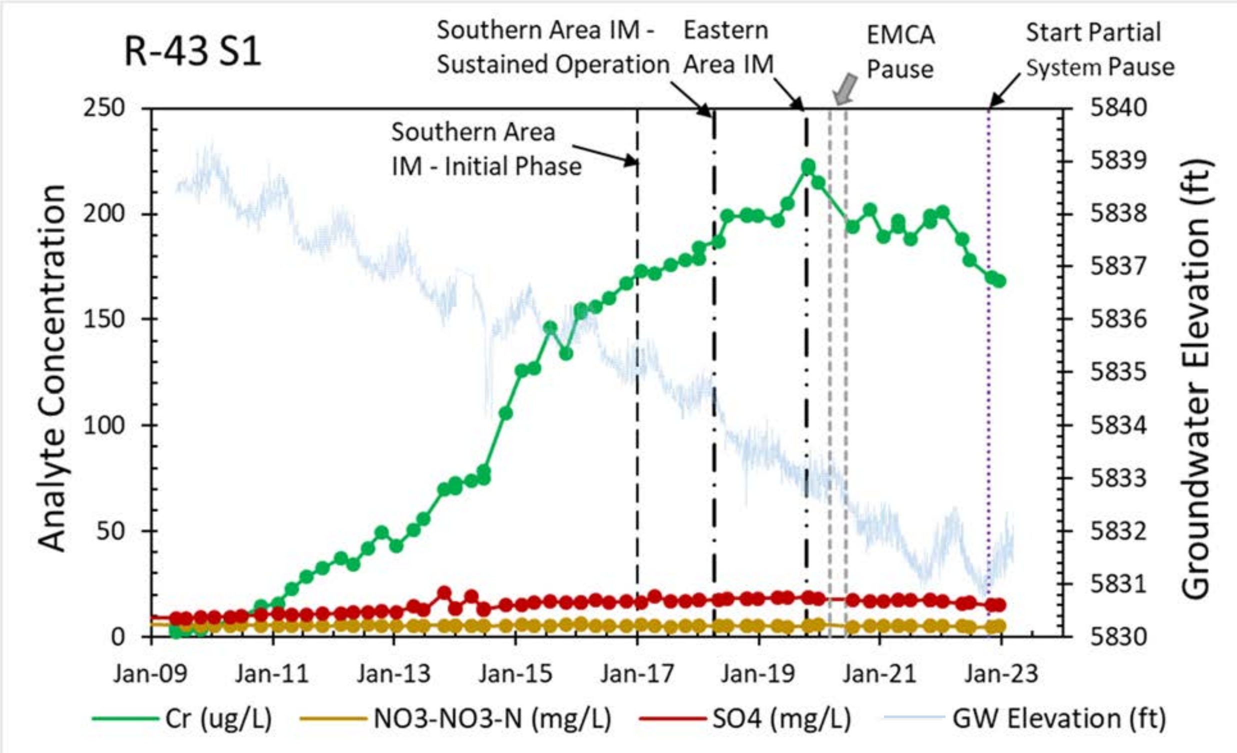

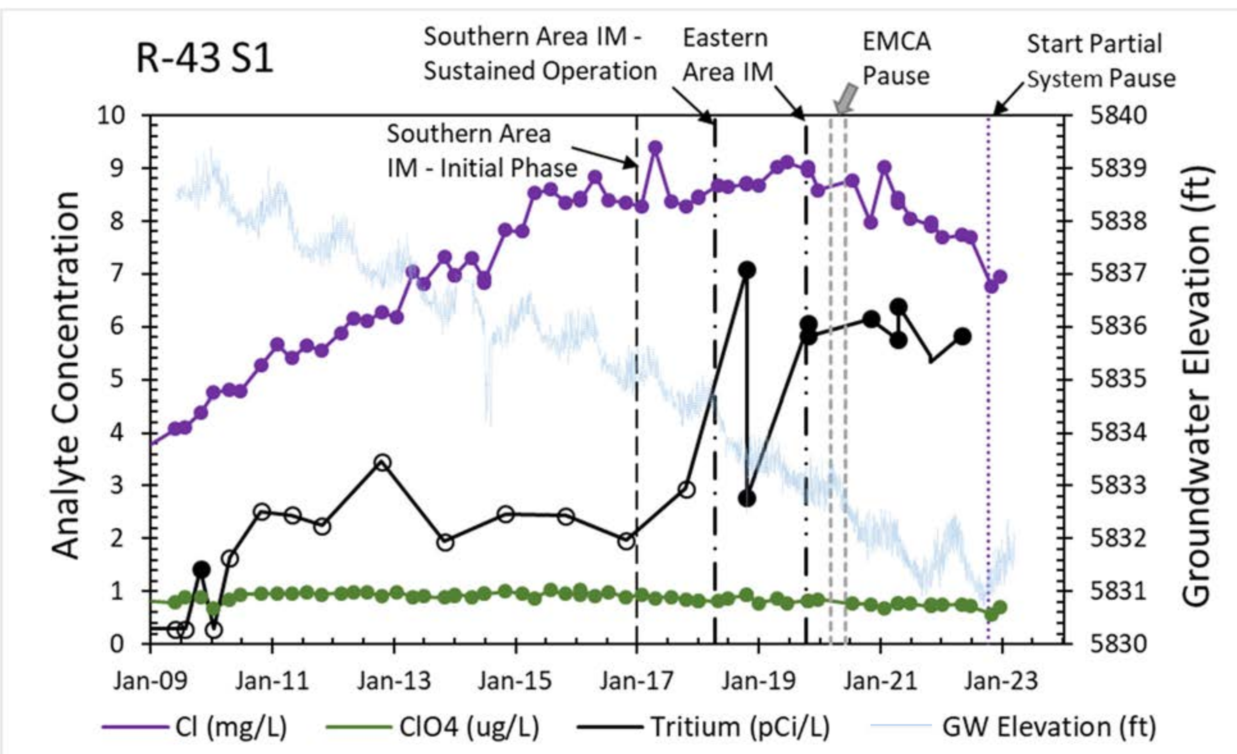

Notes: Open symbols represent nondetection results and solid symbols represent detection results at the plotted value. Background for chromium is 7.48 µg/L. Groundwater elevations represent raw data (without barometric adjustment). S1 = Screen 1.

Figure 3.2-7 Time-series plots for R-43 screen 1

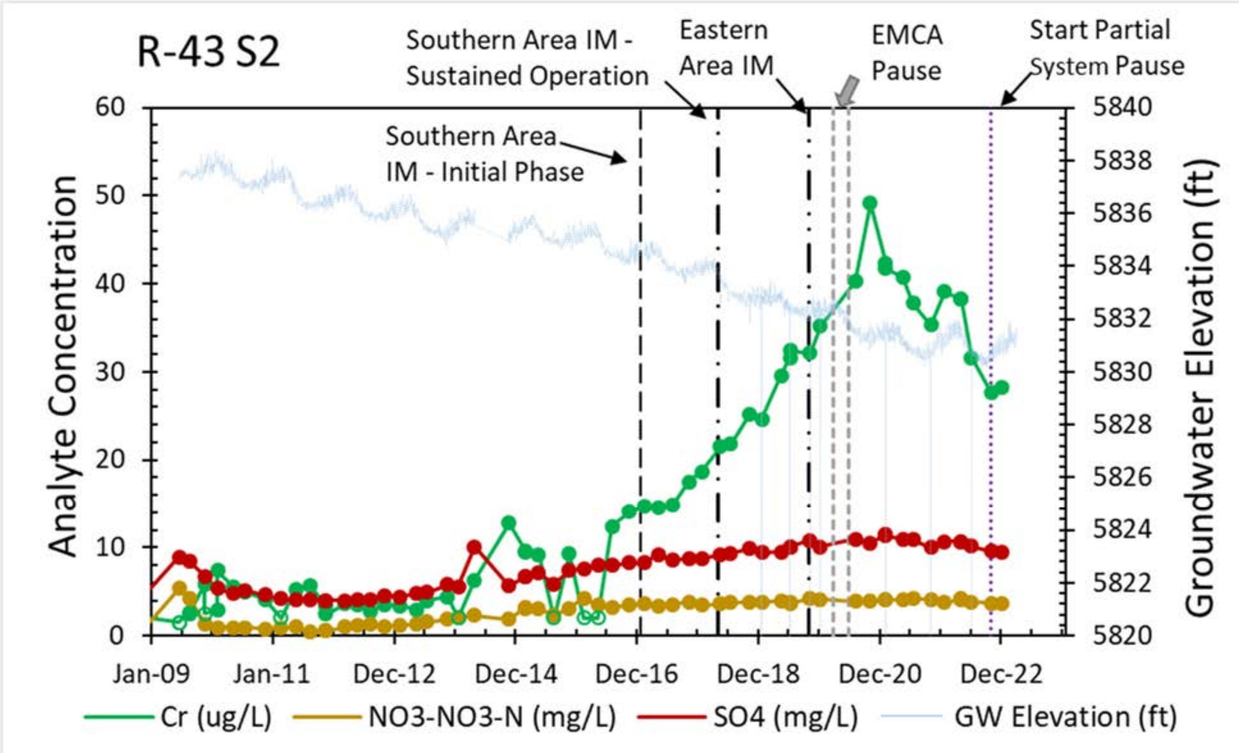

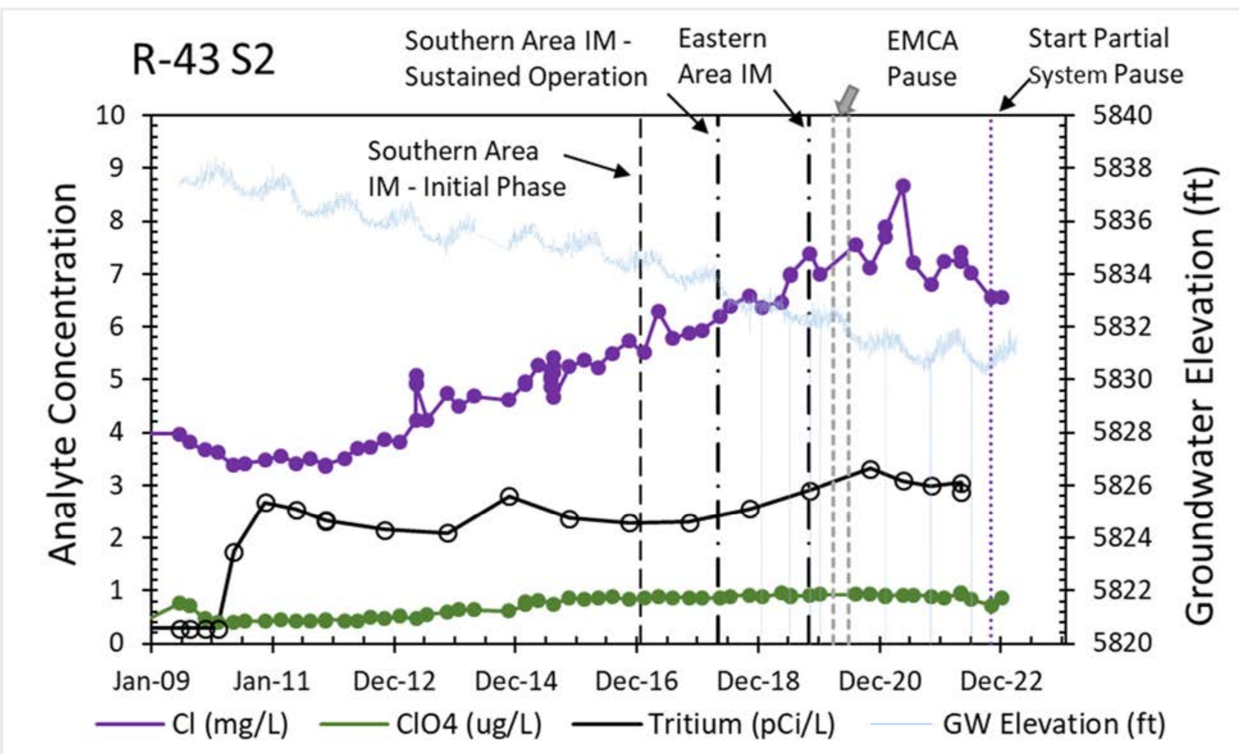

Notes: Open symbols represent nondetection results and solid symbols represent detection results at the plotted value. Background for chromium is 7.48 µg/L. Groundwater elevations represent raw data (without barometric adjustment). S2 = Screen 2.

Figure 3.2-8 Time-series plots for R-43 screen 2

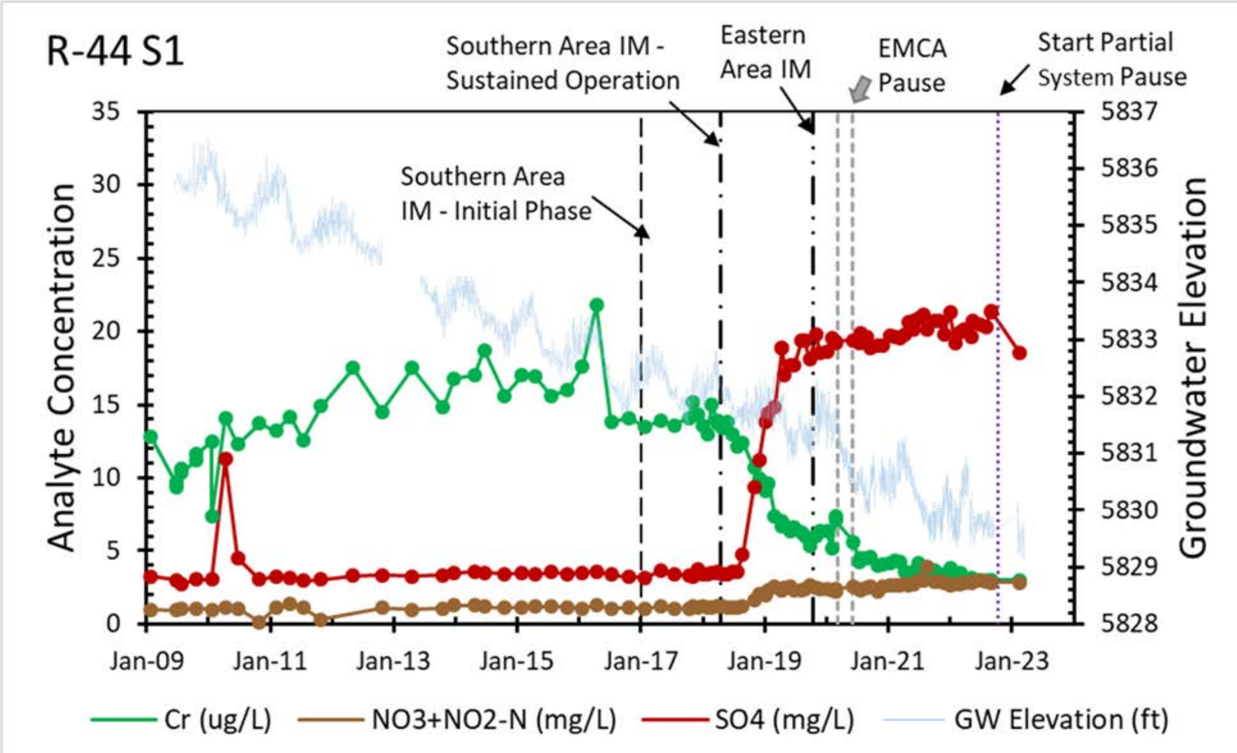

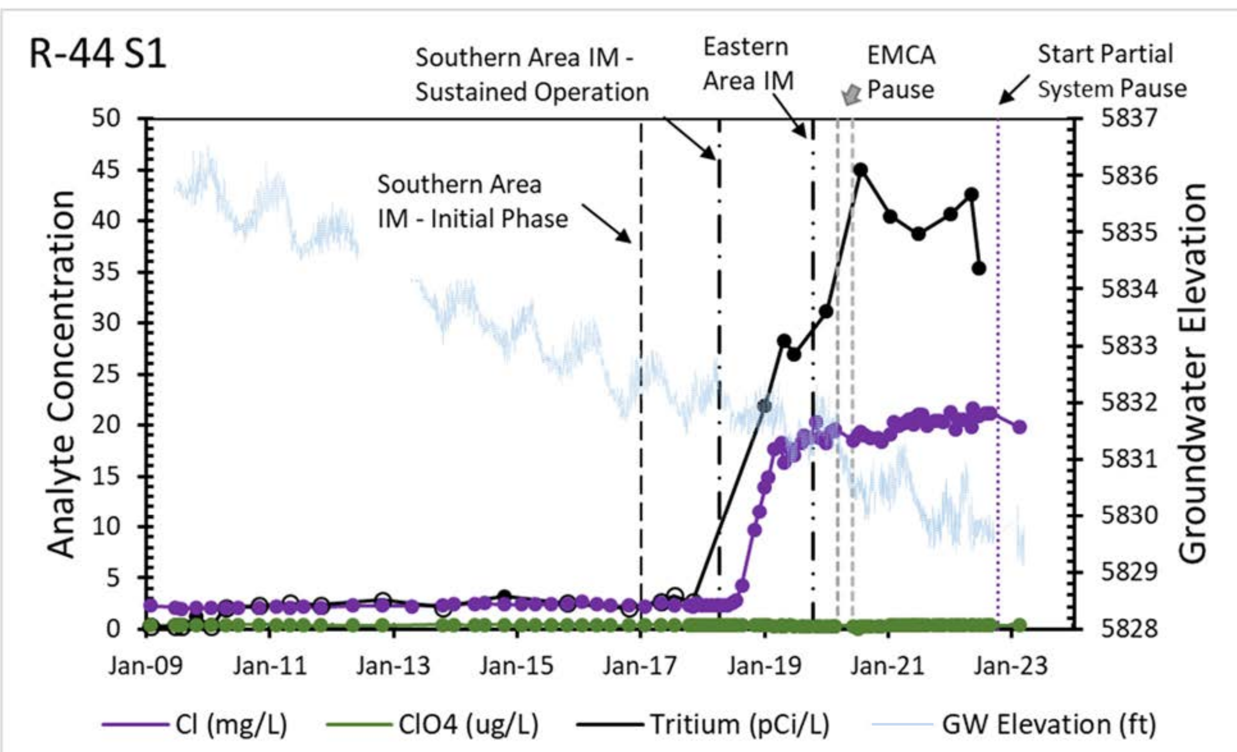

Notes: Open symbols represent nondetection results and solid symbols represent detection results at the plotted value. Background for chromium is 7.48 µg/L. Groundwater elevations represent raw data (without barometric adjustment). S1 = Screen 1.

Figure 3.2-9 Time-series plots for R-44 screen 1

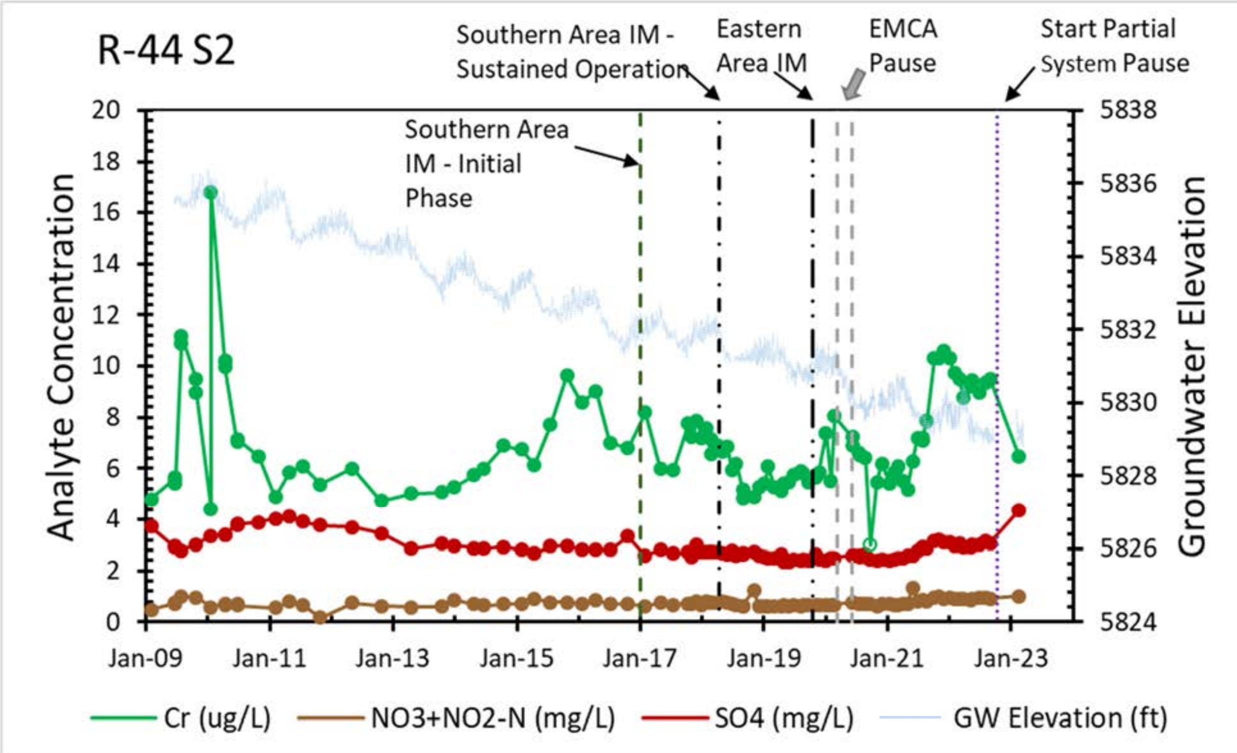

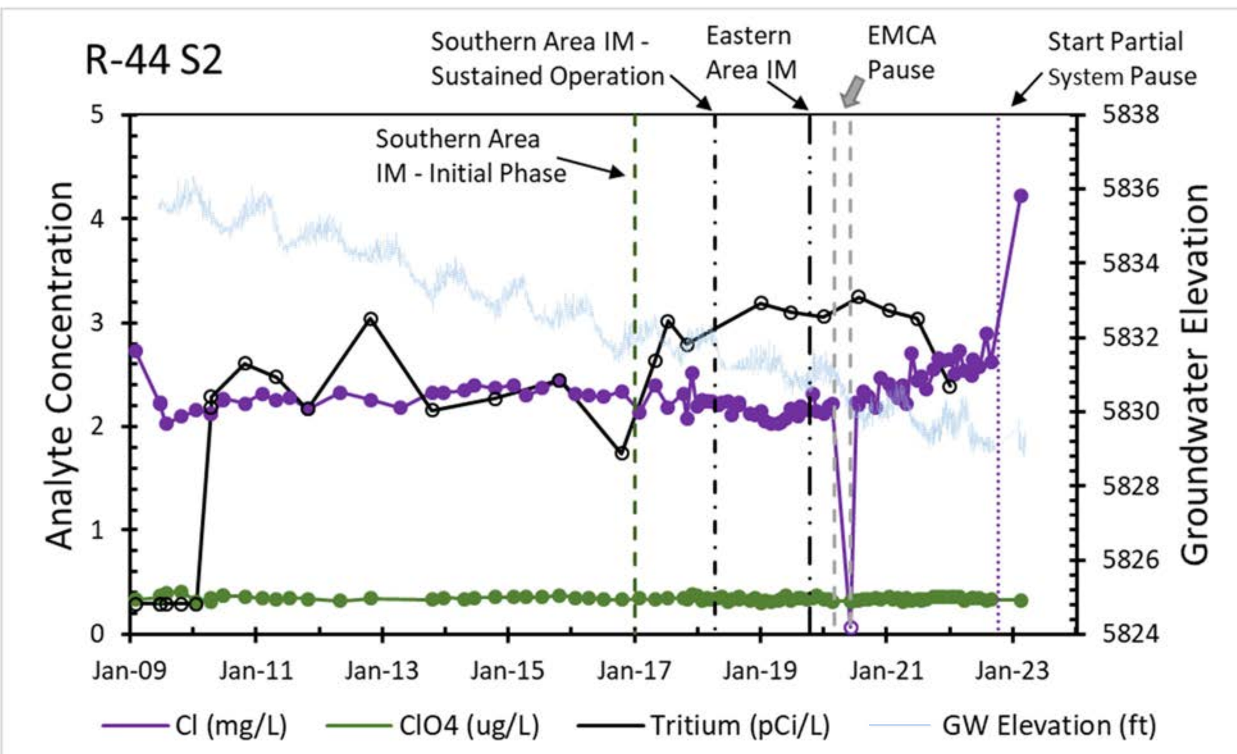

Notes: Open symbols represent nondetection results and solid symbols represent detection results at the plotted value. Background for chromium is 7.48 µg/L. Groundwater elevations represent raw data (without barometric adjustment). S2 = Screen 2

Figure 3.2-10 Time-series plots for R-44 screen 2

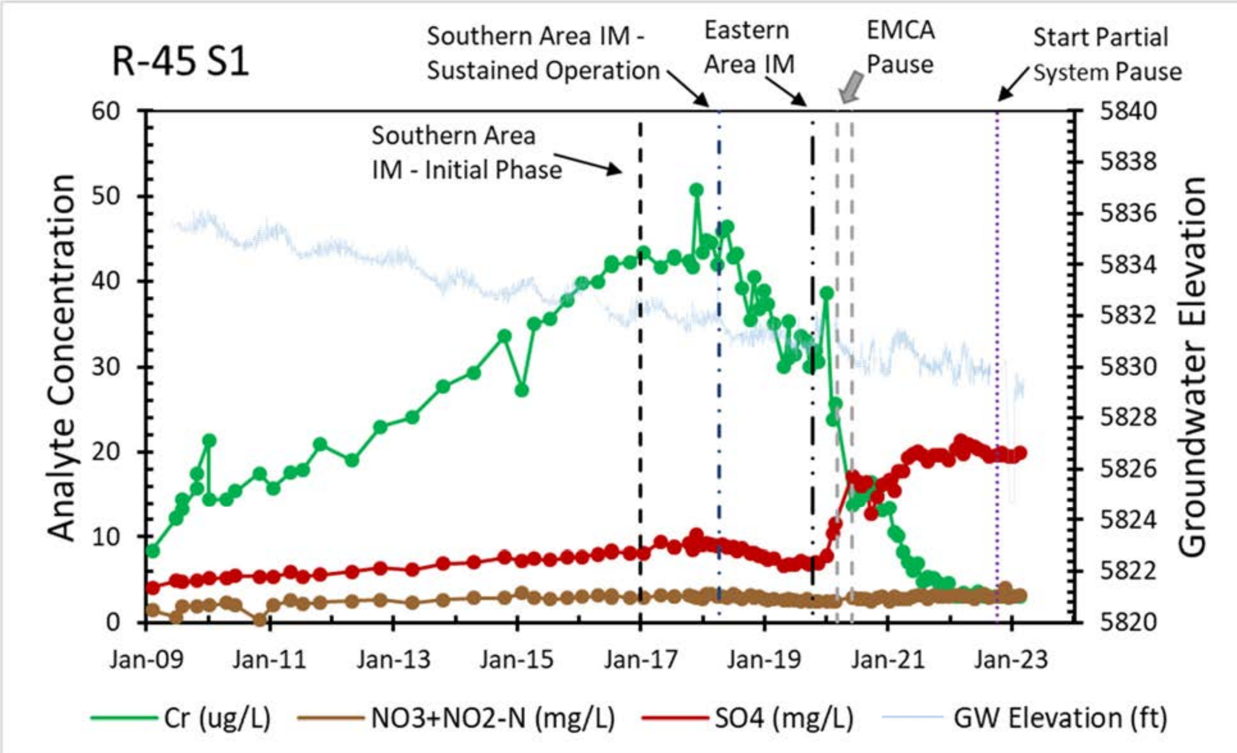

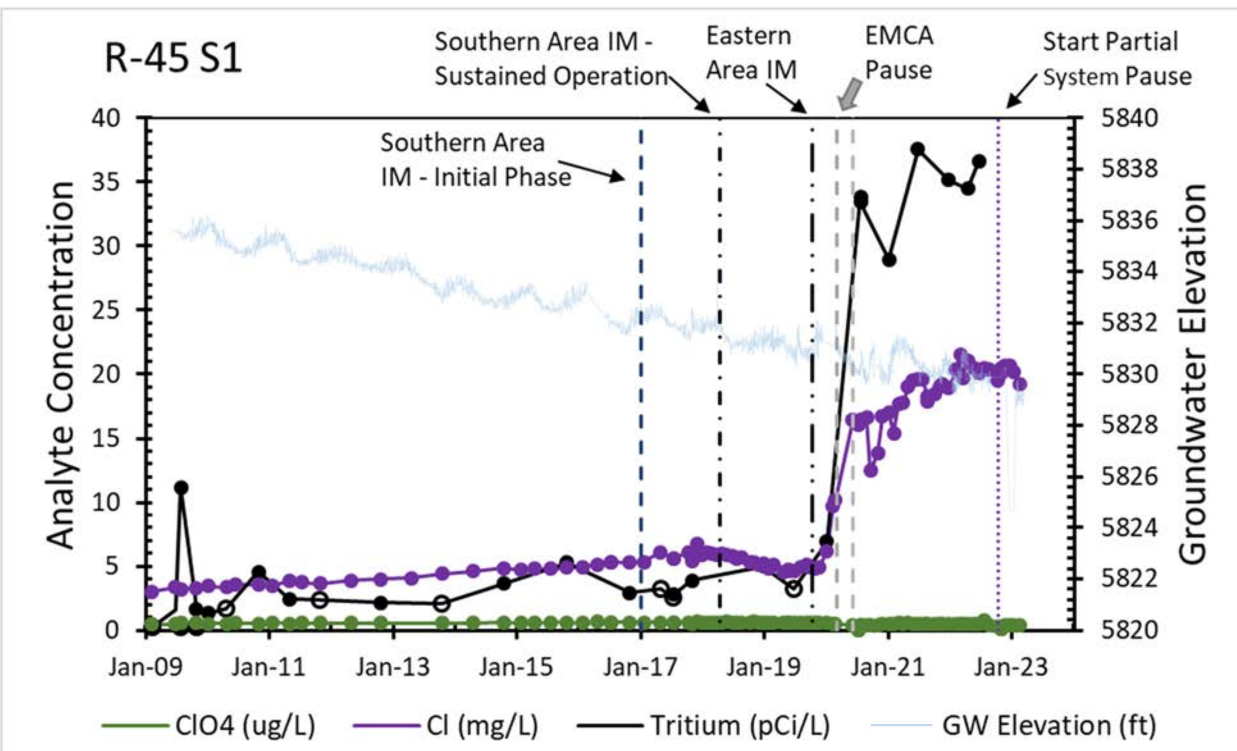

Notes: Open symbols represent nondetection results and solid symbols represent detection results at the plotted value. The background for chromium is 7.48 µg/L. Groundwater elevations represent raw data (without barometric adjustment). S1 = Screen 1.

Figure 3.2-11 Time-series plots for R-45 screen 1

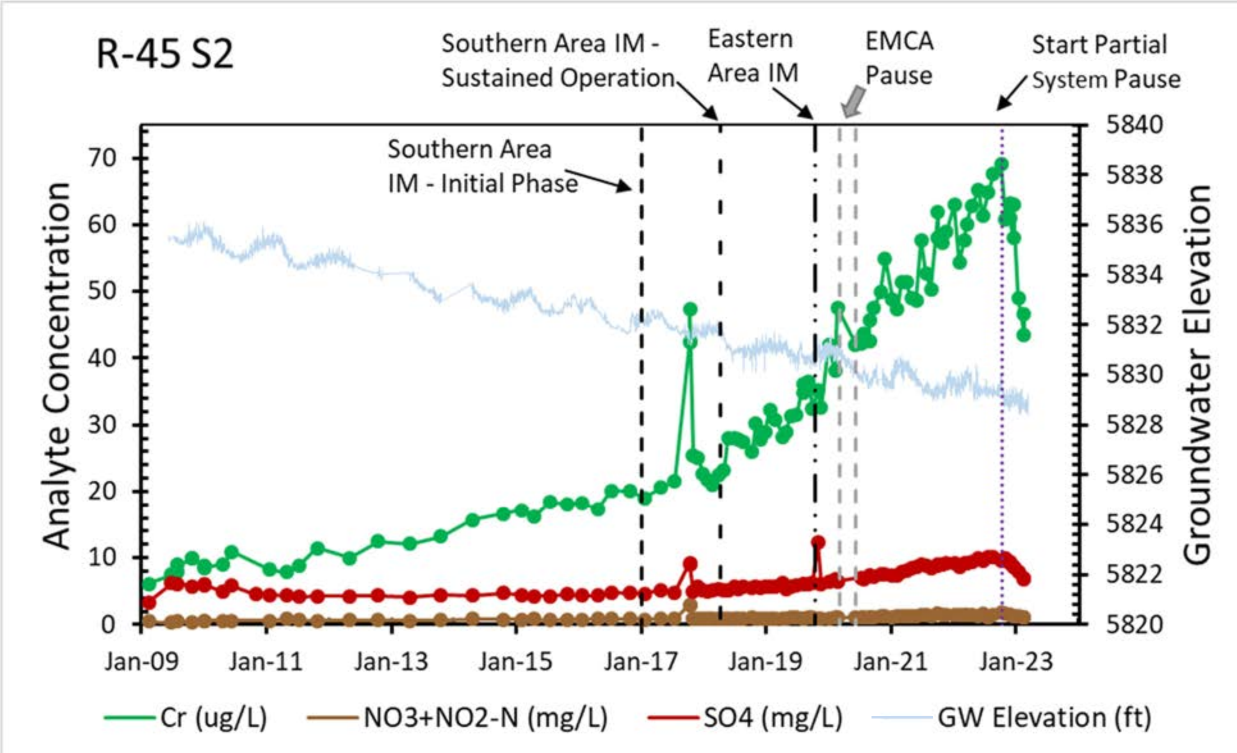

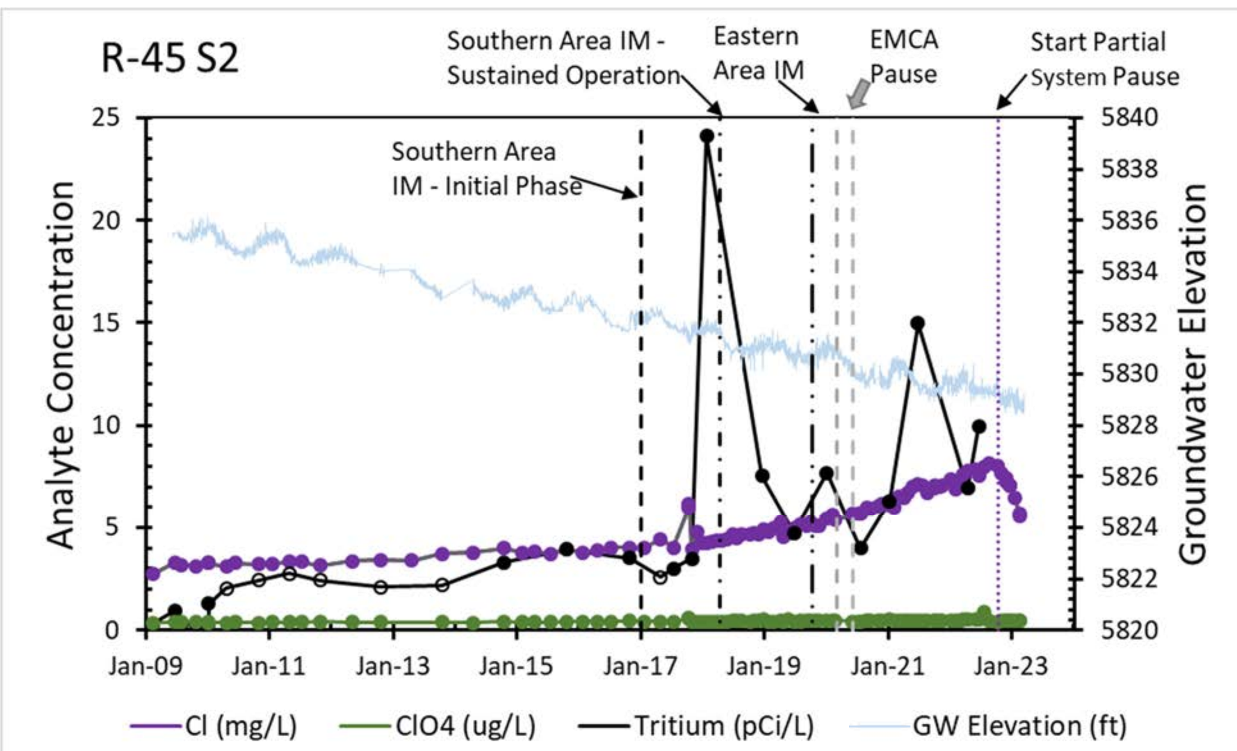

Notes: Open symbols represent nondetection results and solid symbols represent detection results at the plotted value. Background for chromium is 7.48 µg/L. Groundwater elevations represent raw data (without barometric adjustment). S2 = Screen 2.

Figure 3.2-12 Time-series plots for R-45 screen 2

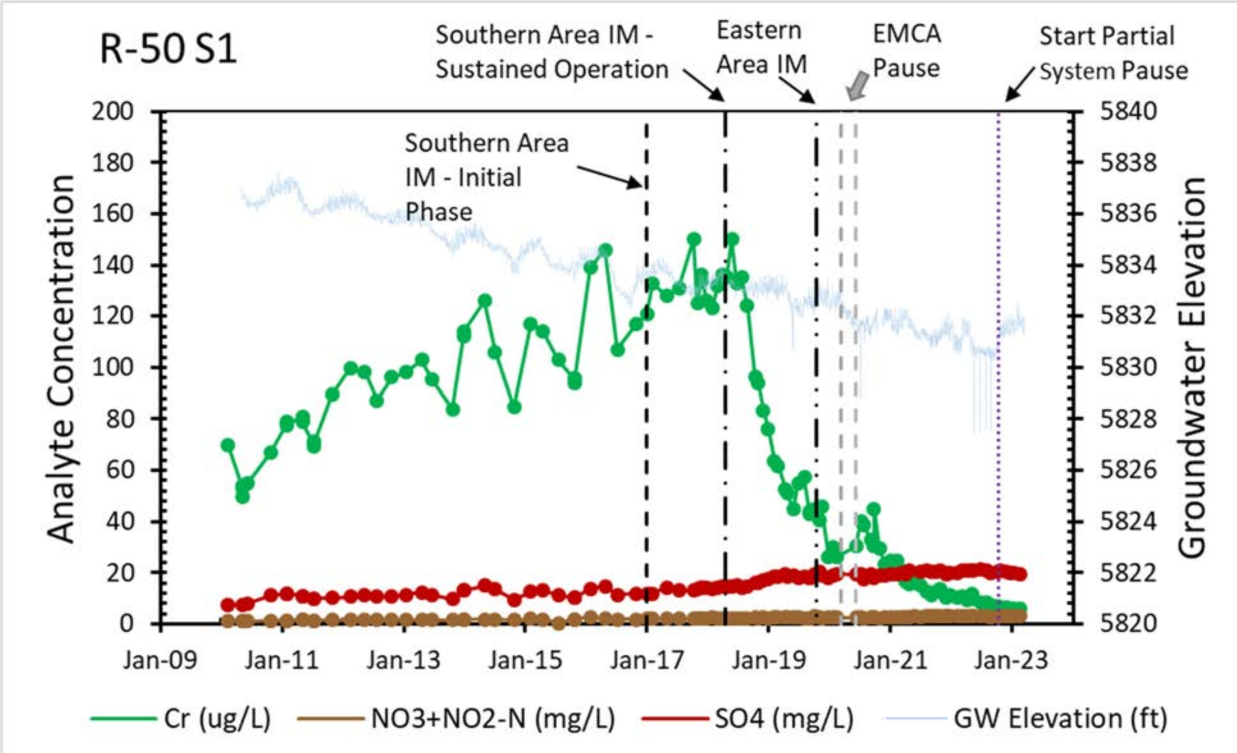

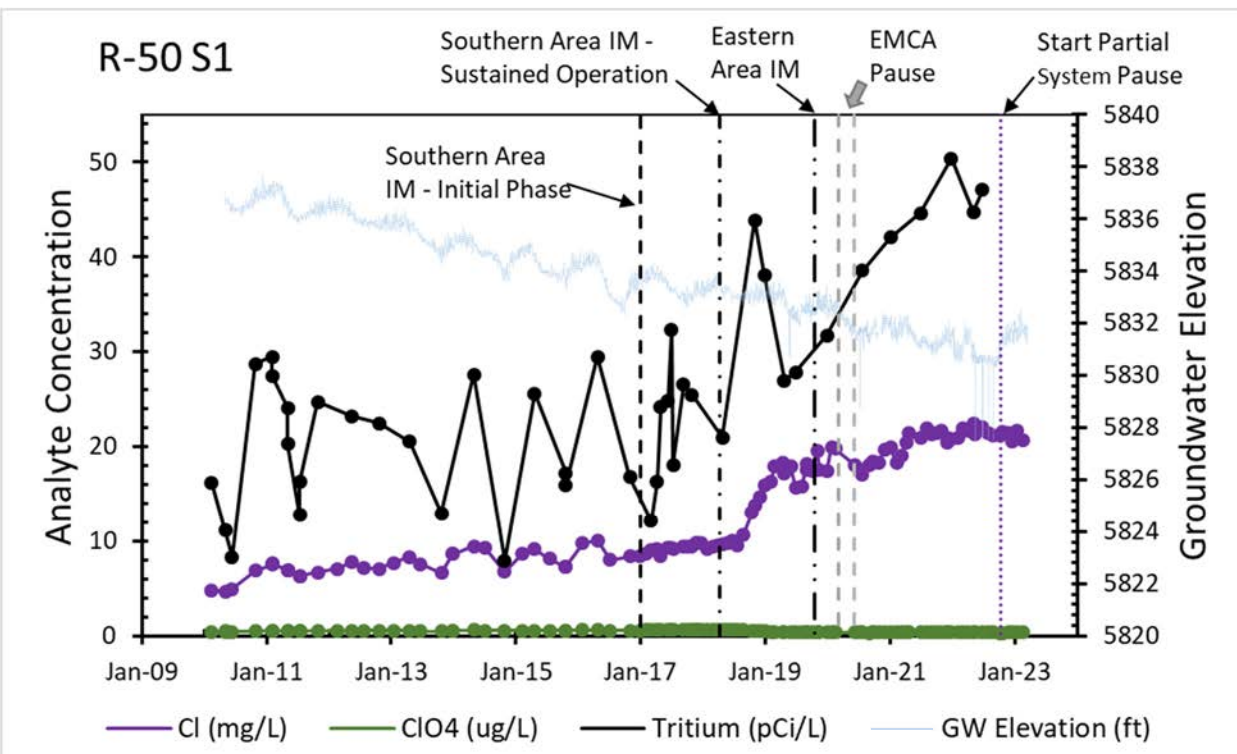

Notes: Solid symbols represent detection results at the plotted value. The background for chromium is 7.48 µg/L. Groundwater elevations represent raw data (without barometric adjustment). S1 = Screen 1.

Figure 3.2-13 Time-series plots for R-50 screen 1

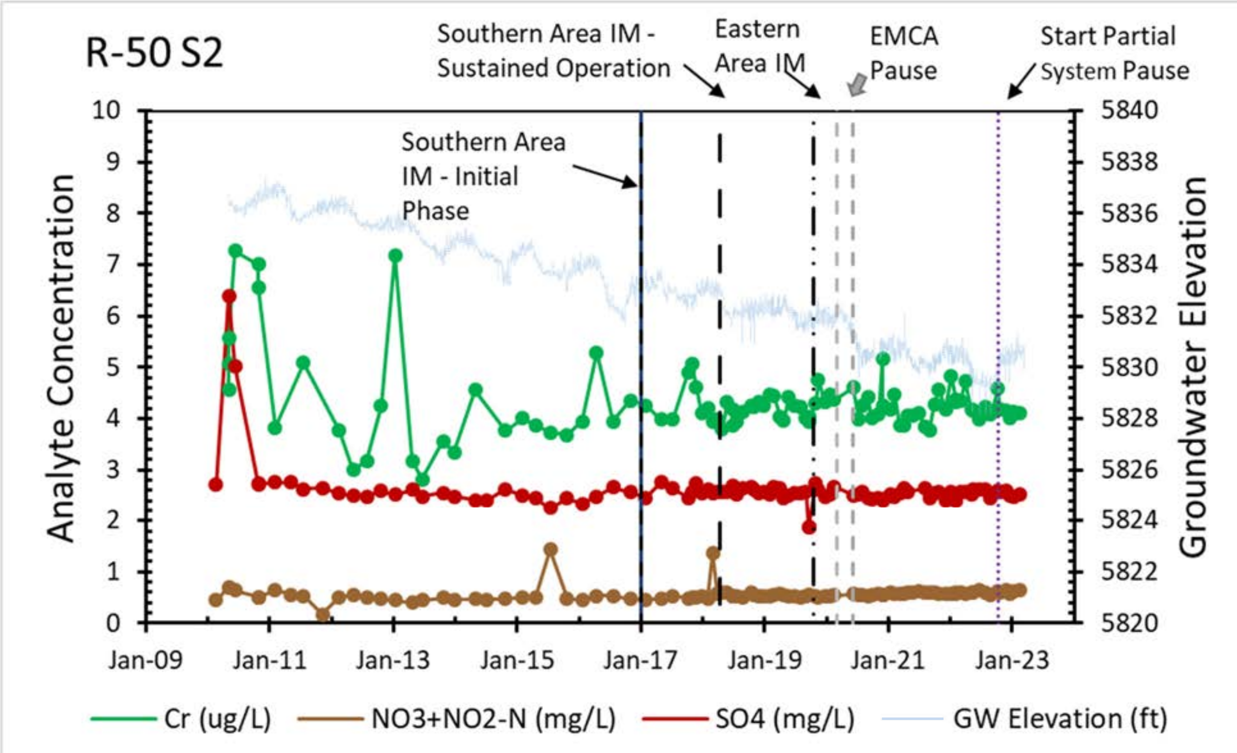

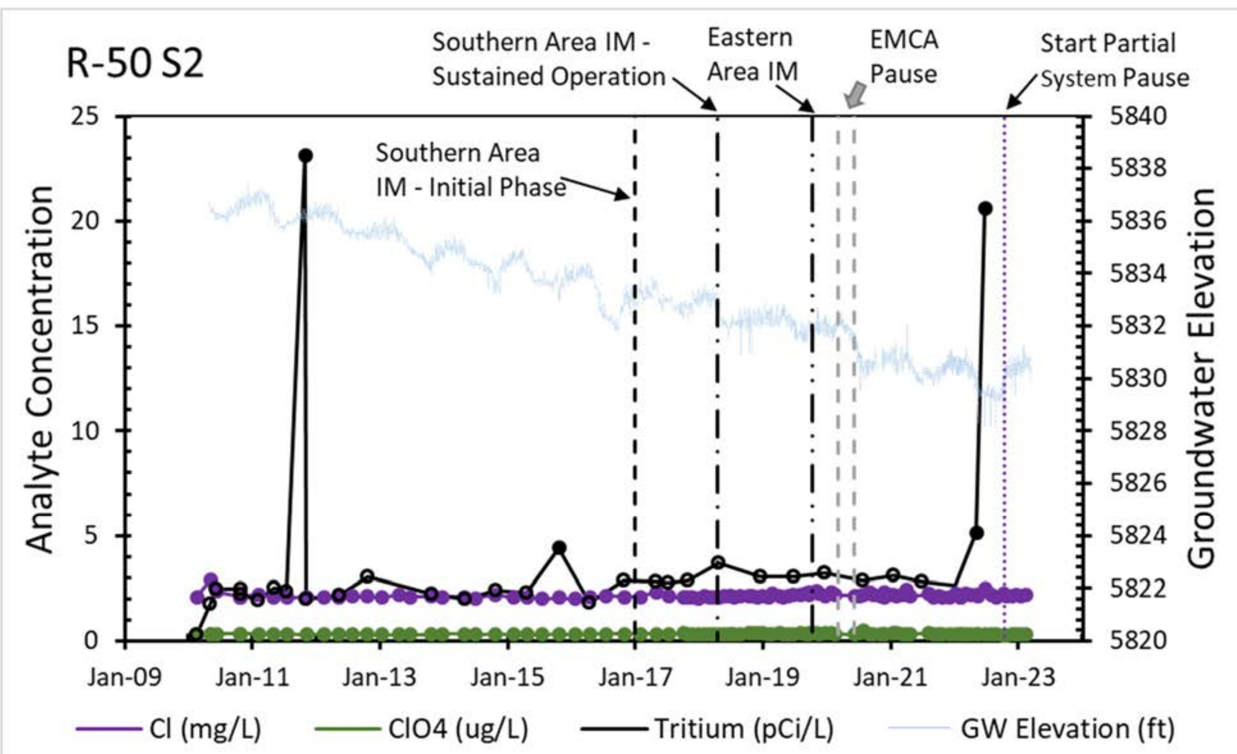

Notes: Open symbols represent nondetection results and solid symbols represent detection results at the plotted value. Background for chromium is 7.48 µg/L. Groundwater elevations represent raw data (without barometric adjustment). S2 = Screen 2.

Figure 3.2-14 Time-series plots for R-50 screen 2

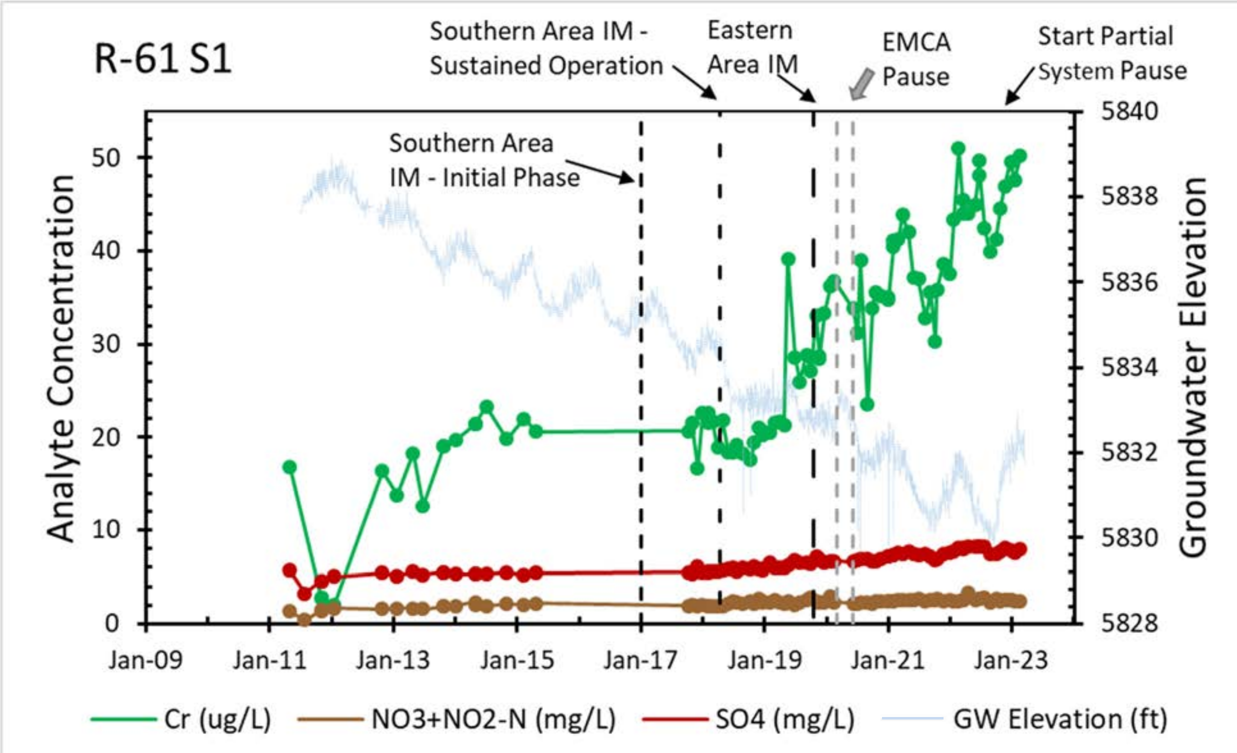

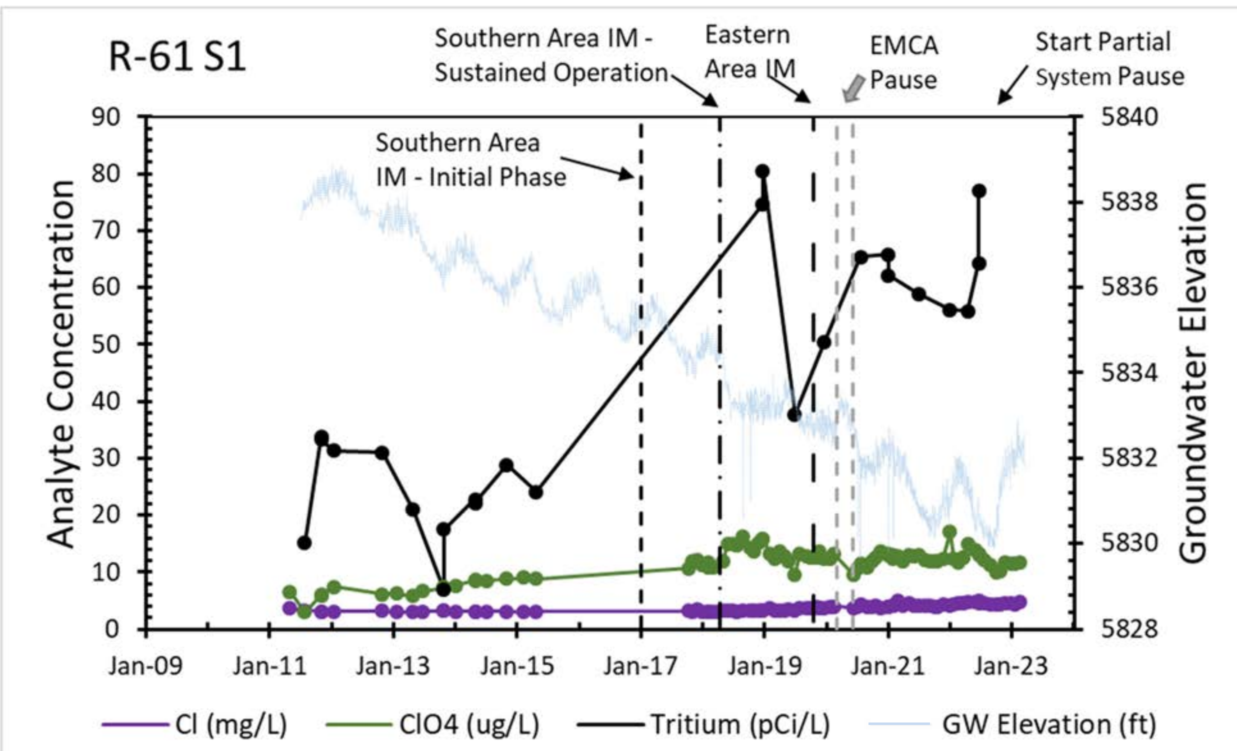

Notes: Solid symbols represent detection results at the plotted value. Background for chromium is 7.48 µg/L. Groundwater elevations represent raw data (without barometric adjustment). R-61 screen 1 (S1) is on the watch list because of locally reducing conditions around the well. Current data are considered useful for the purposes of this performance monitoring report.

Figure 3.2-15 Time-series plots for R-61 screen 1

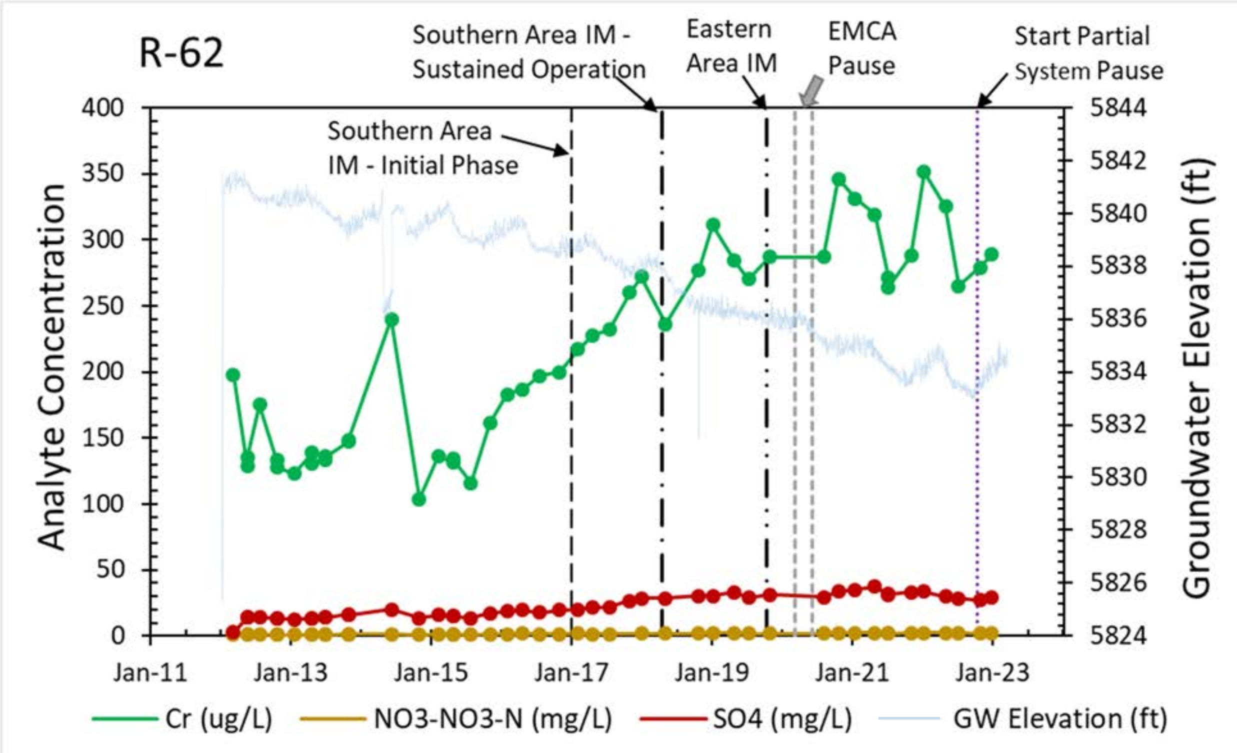

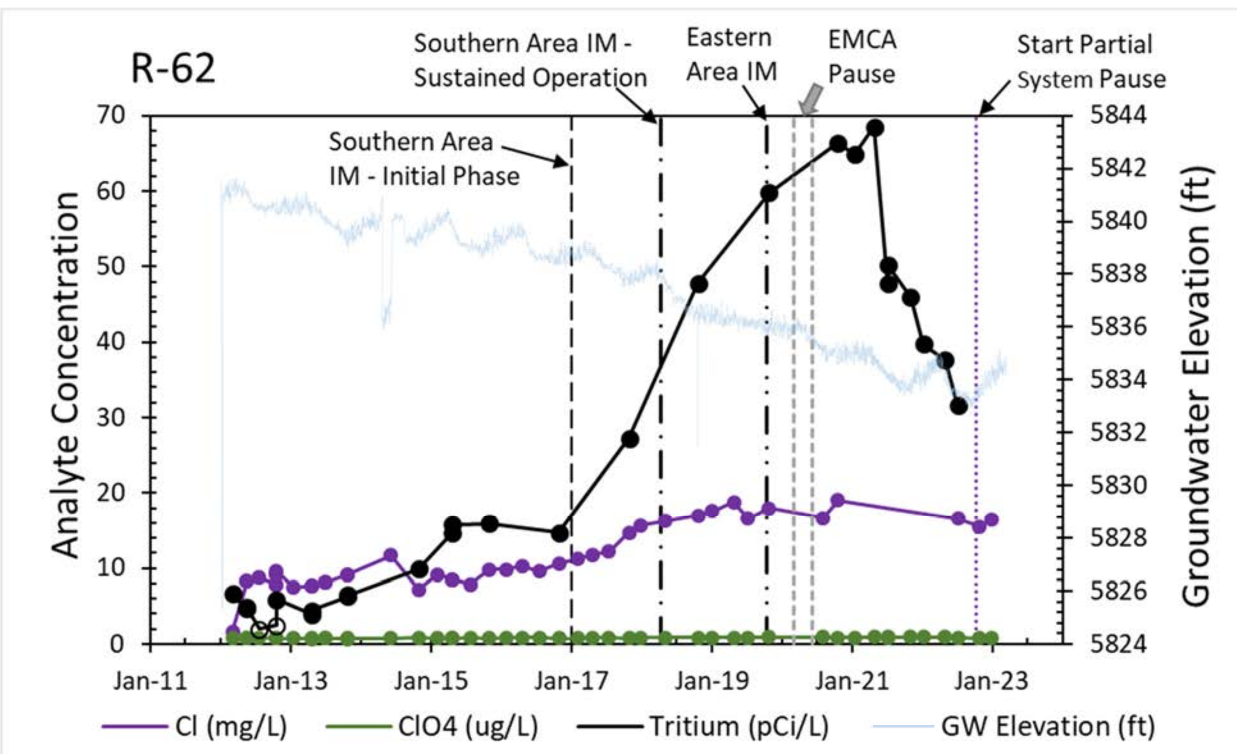

Notes: Open symbols represent nondetection results and solid symbols represent detection results at the plotted value. The background for chromium is 7.48 µg/L. Groundwater elevations represent raw data (without barometric adjustment).

Figure 3.2-16 Time-series plots for R-62

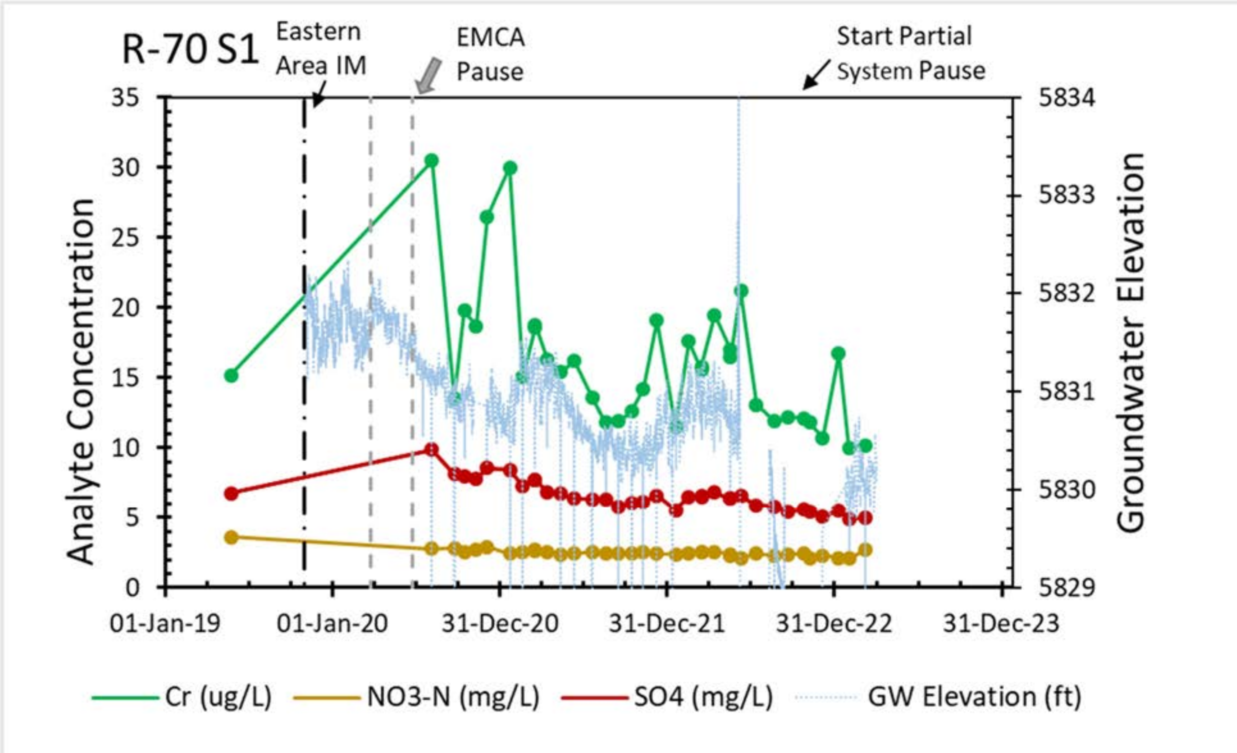

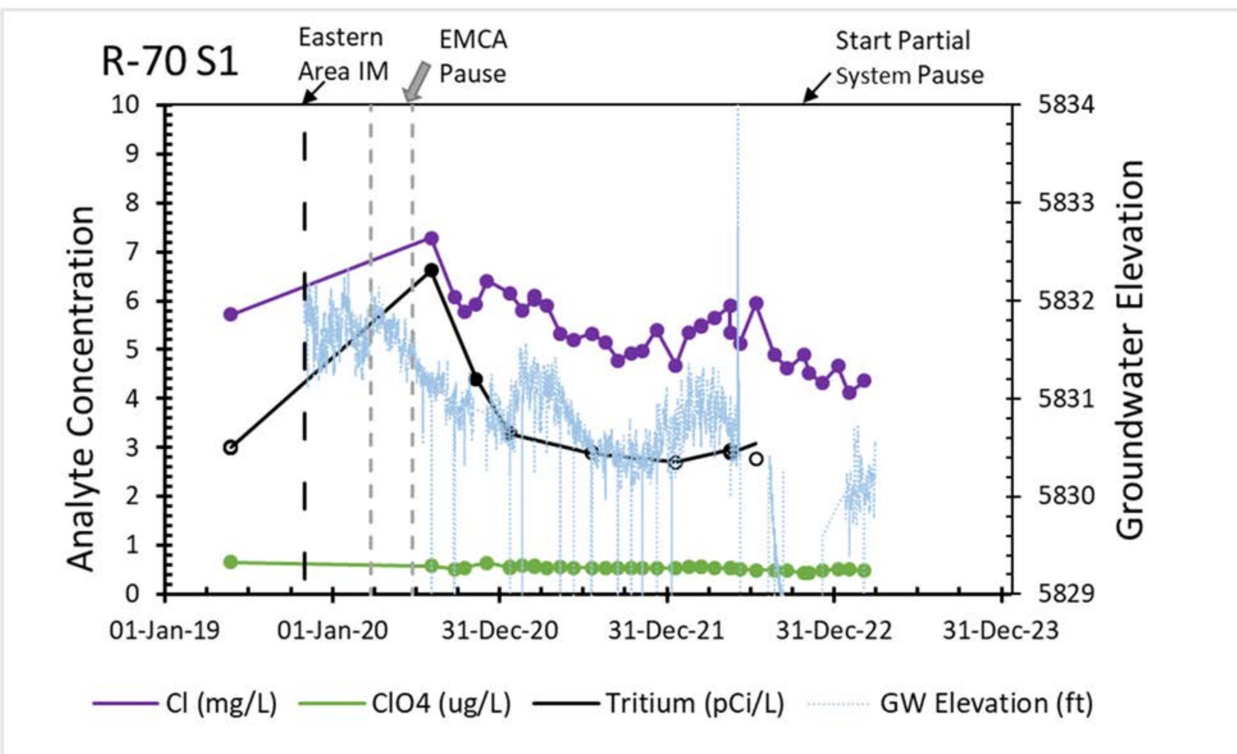

Notes: Open symbols represent nondetection results and solid symbols represent detection results at the plotted value. Background for chromium is 7.48 µg/L. Groundwater elevations represent raw data (without barometric adjustment). S1 = Screen 1.

Figure 3.2-17 Time-series plots for R-70 screen 1

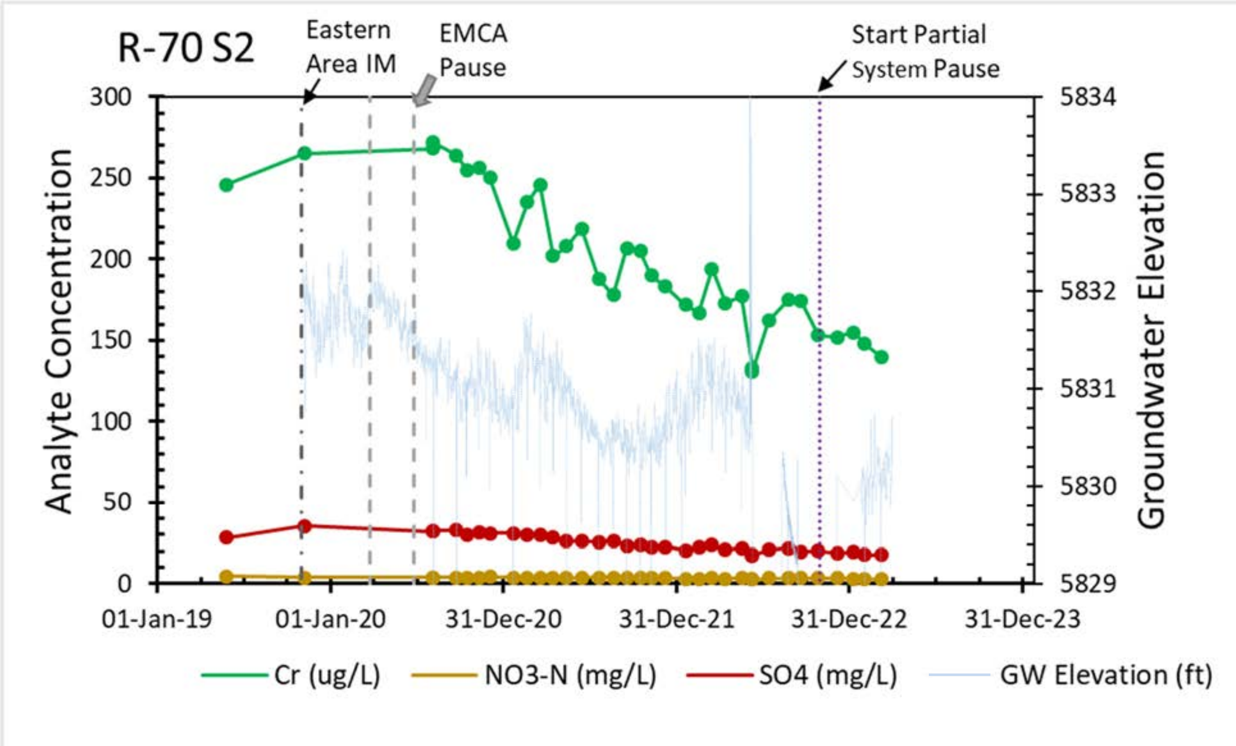

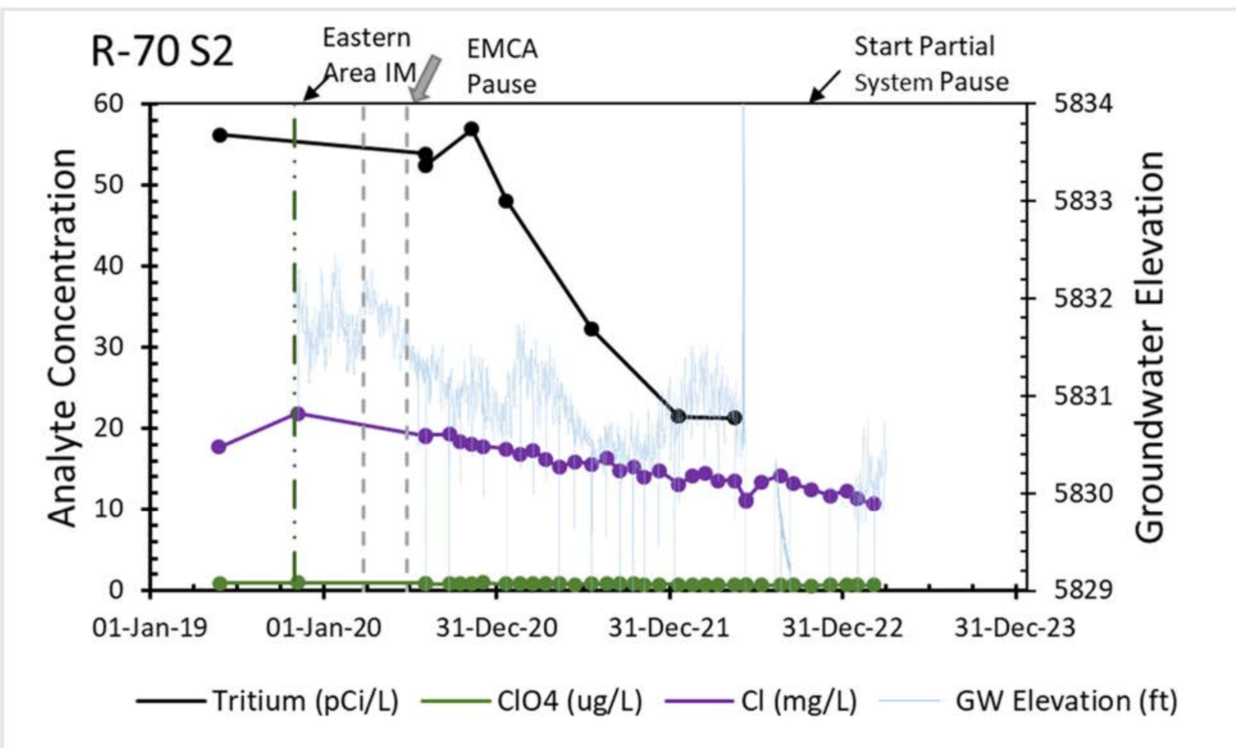

Notes: Solid symbols represent detection results at the plotted value. The background for chromium is 7.48 µg/L. Groundwater elevations represent raw data (without barometric adjustment). S2 = Screen 2.

Figure 3.2-18 Time-series plots for R-70 screen 2

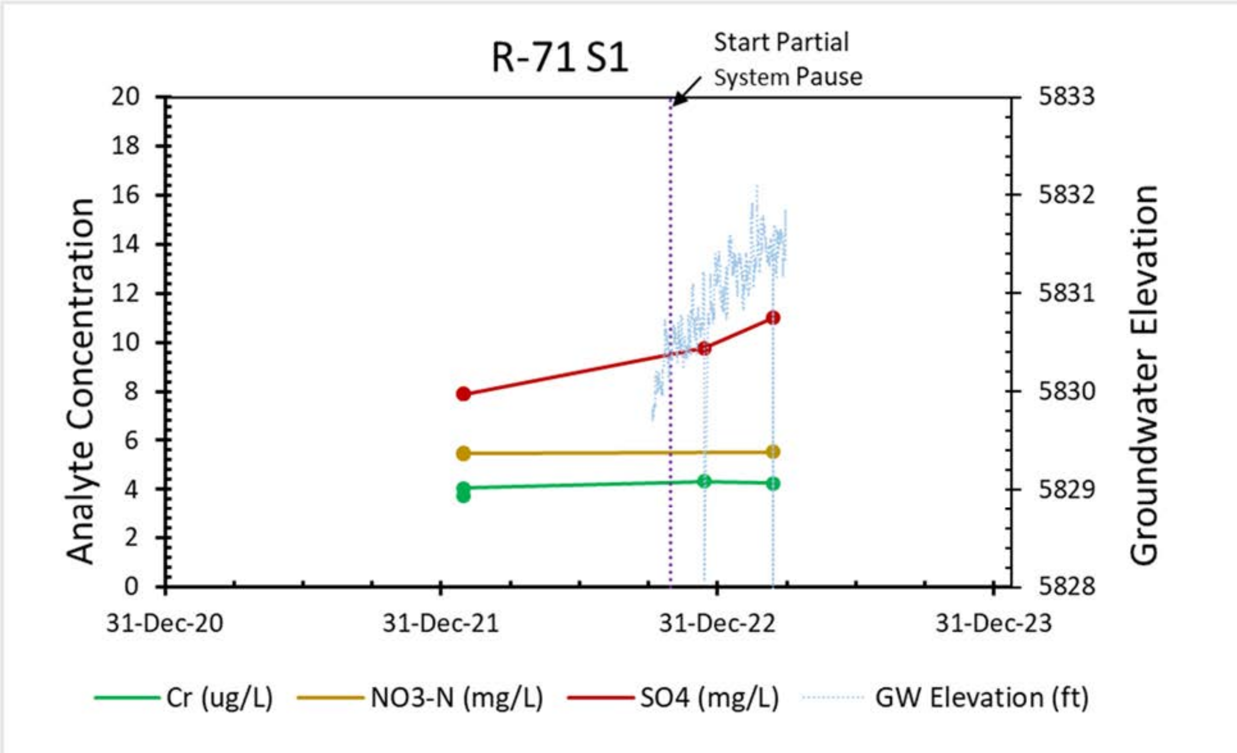

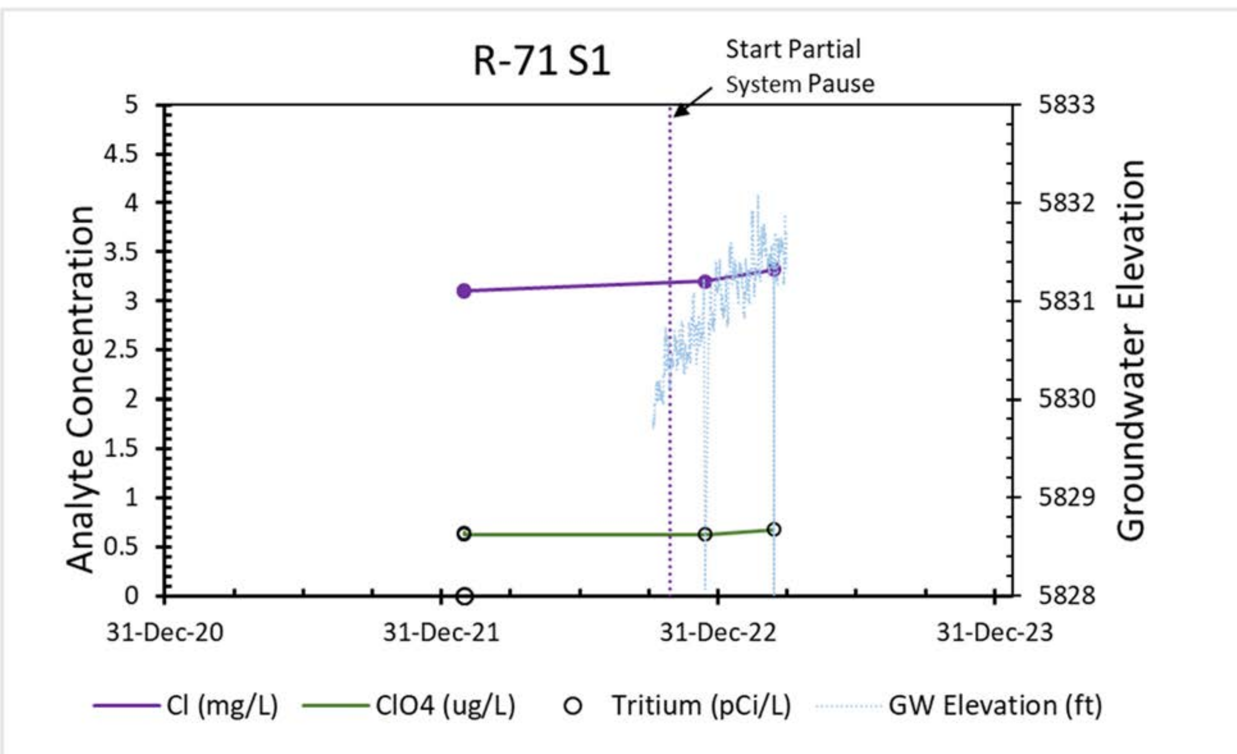

Notes: Solid symbols represent detection results at the plotted value. The background for chromium is 7.48 µg/L. Groundwater elevations represent raw data (without barometric adjustment). S1 = Screen 1.

Figure 3.2-19 Time-series plots for R-71 screen 1

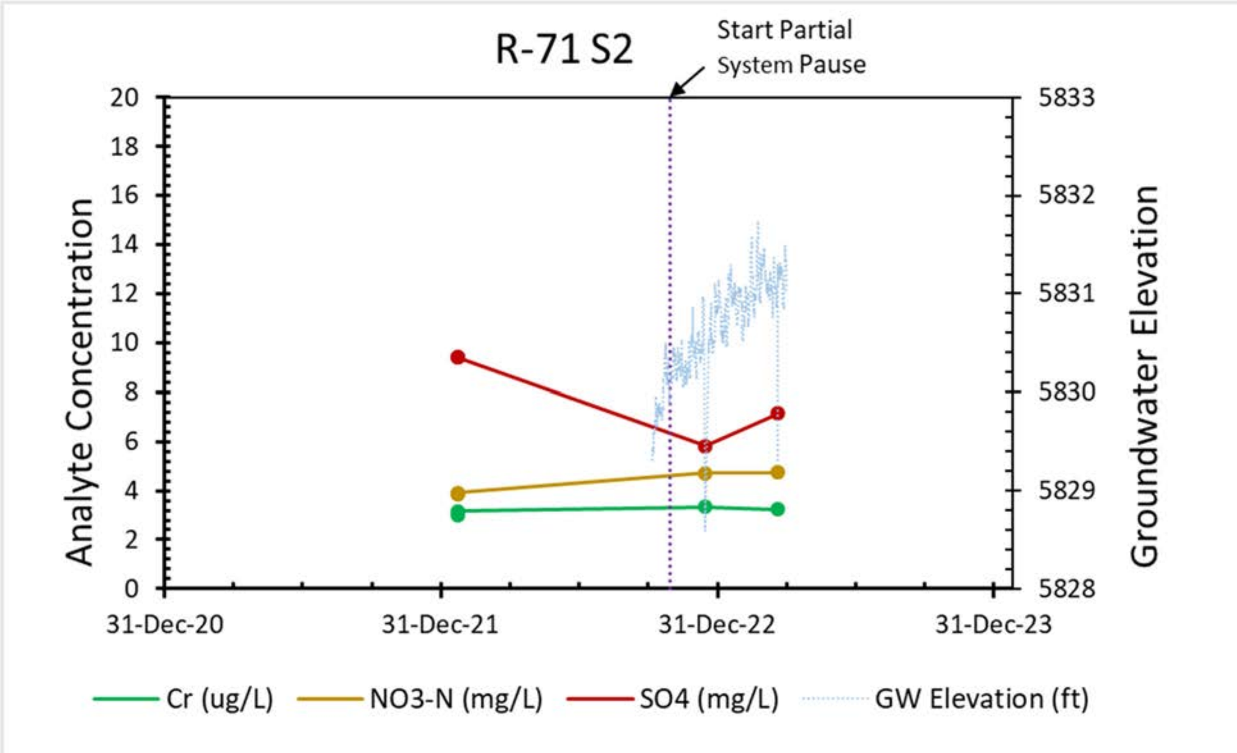

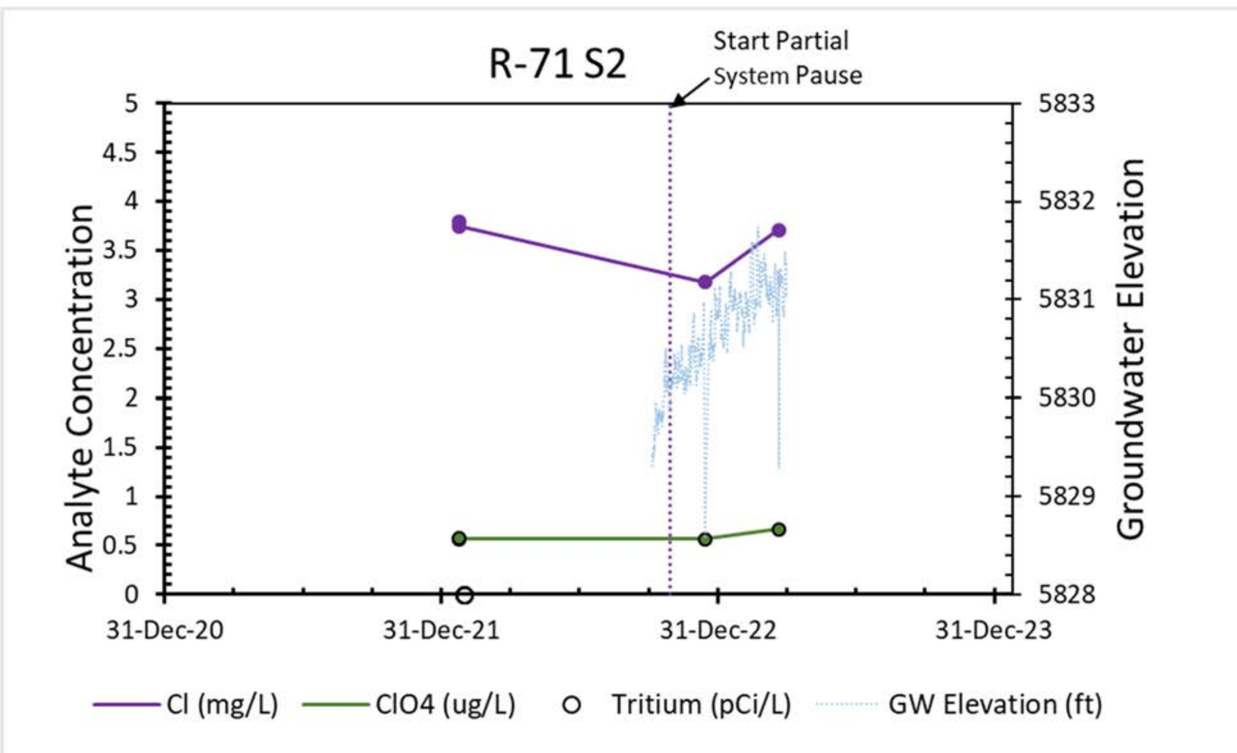

Notes: Solid symbols represent detection results at the plotted value. The background for chromium is 7.48 µg/L. Groundwater elevations represent raw data (without barometric adjustment). S2 = Screen 2.

Figure 3.2-20 Time-series plots for R-71 screen 2

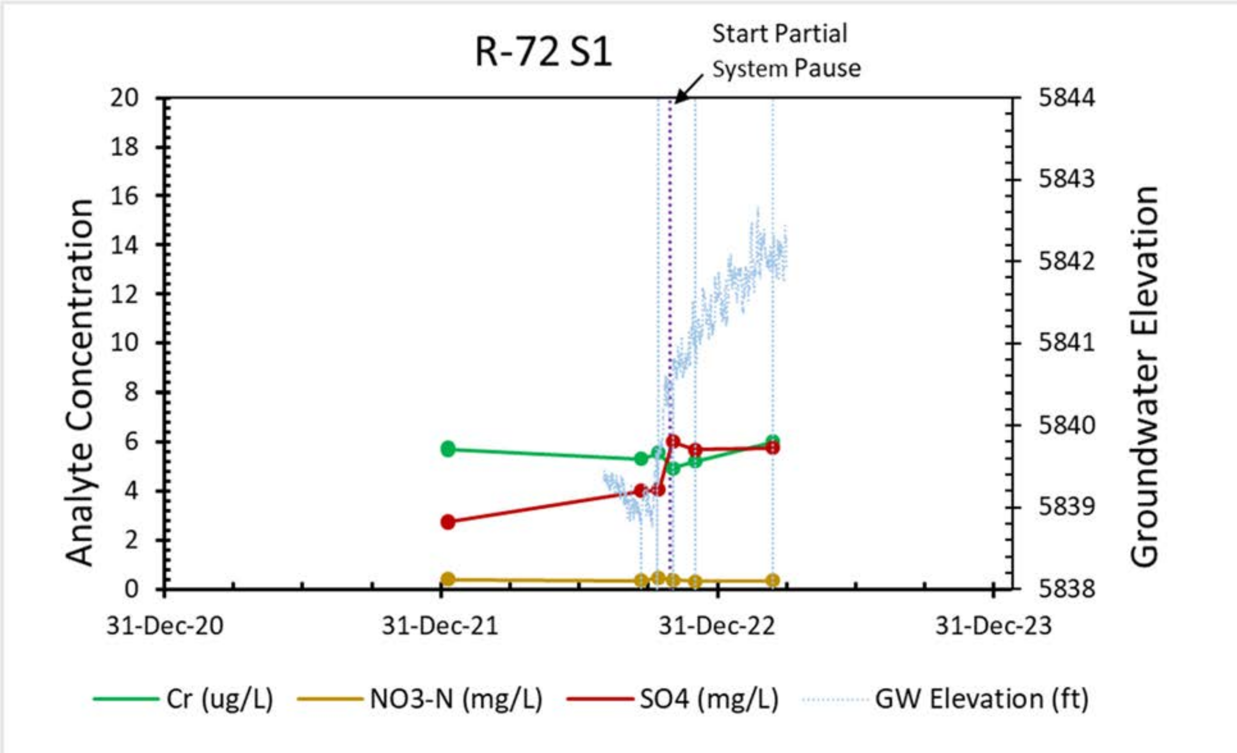

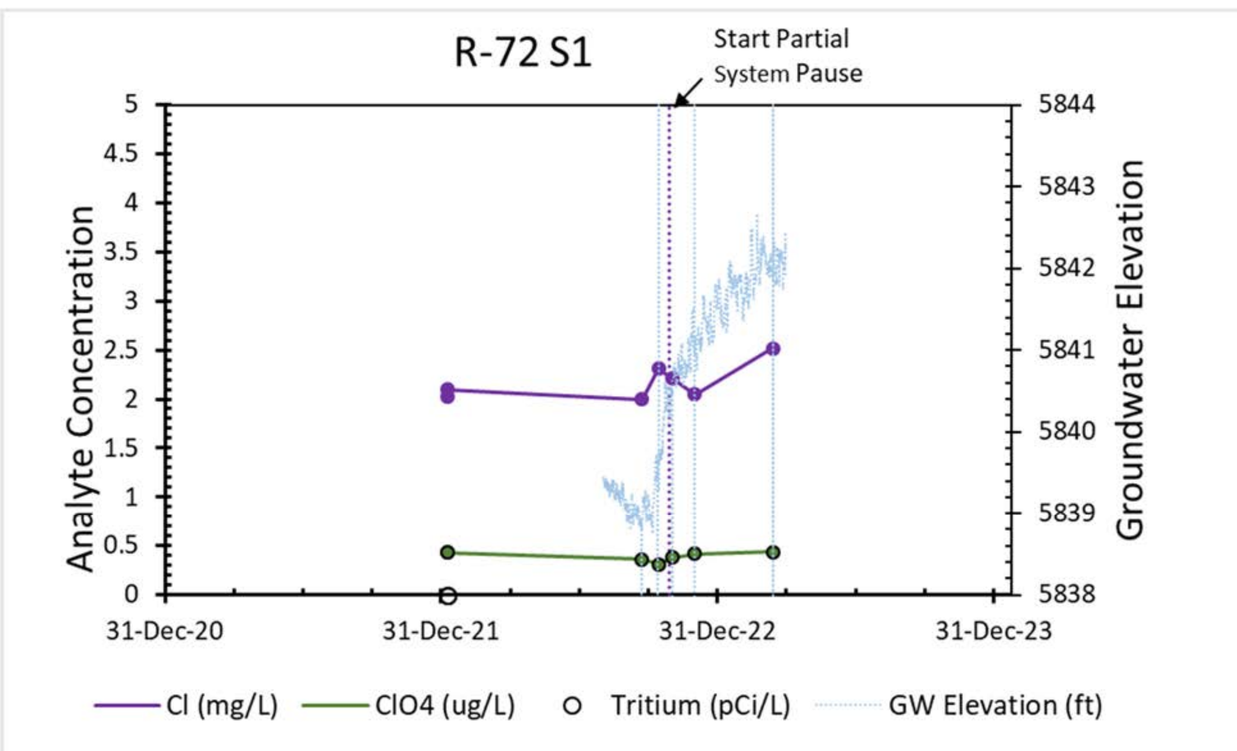

Notes: Solid symbols represent detection results at the plotted value. The background for chromium is 7.48 µg/L. Groundwater elevations represent raw data (without barometric adjustment). S1 = Screen 1.

Figure 3.2-21 Time-series plots for R-72 screen 1

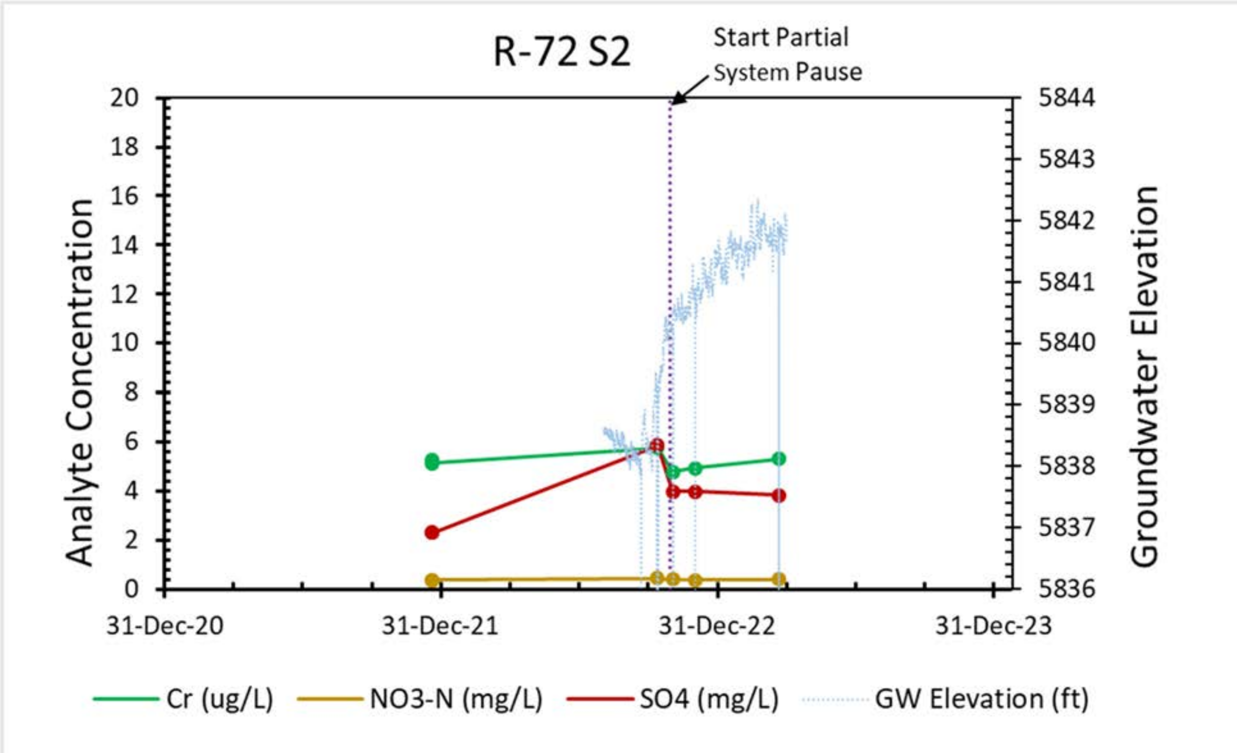

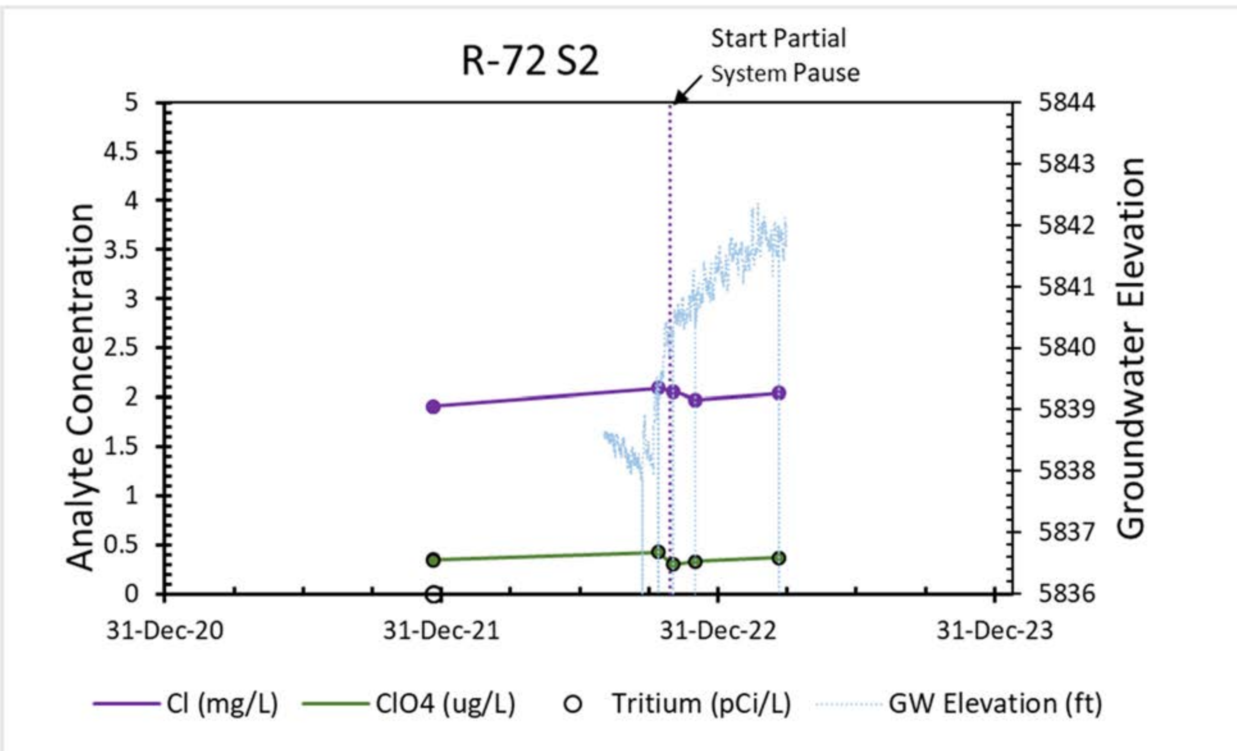

Notes: Solid symbols represent detection results at the plotted value. The background for chromium is 7.48 µg/L. Groundwater elevations represent raw data (without barometric adjustment). S2 = Screen 2.

Figure 3.2-22 Time-series plots for R-72 screen 2

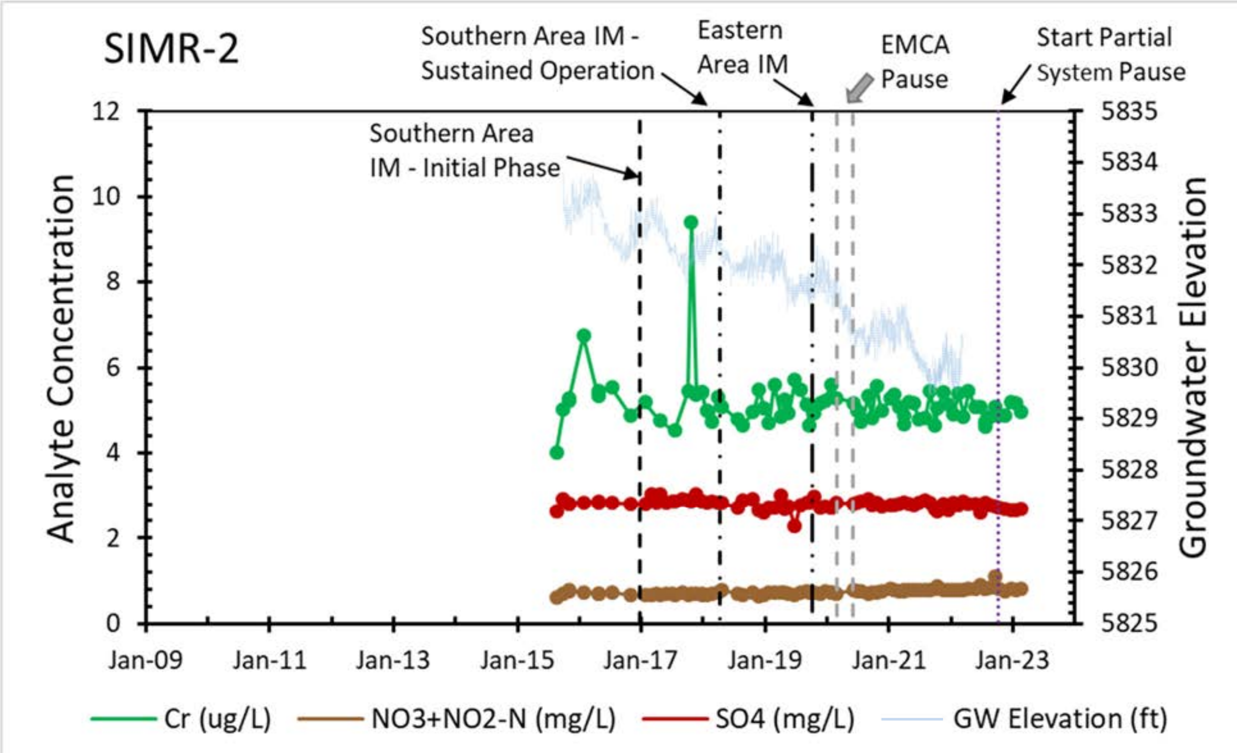

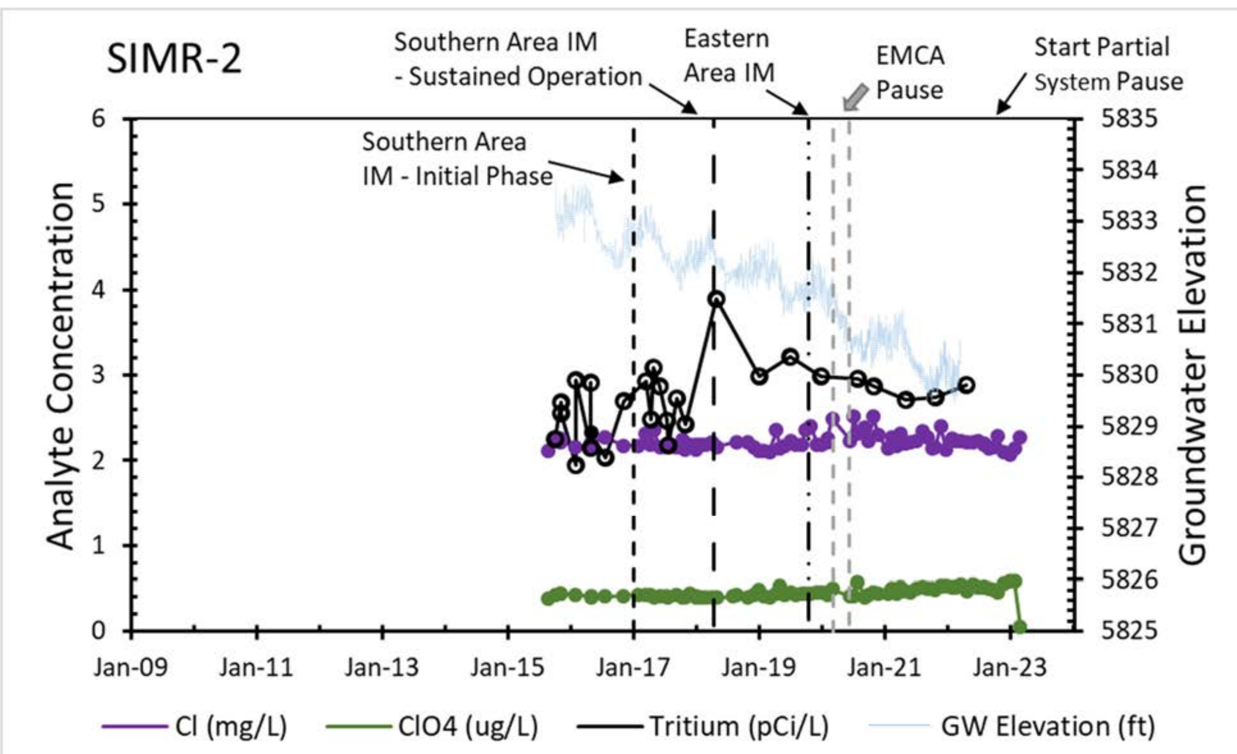

Notes: Open symbols represent nondetection results and solid symbols represent detection results at the plotted value. The background for chromium is 7.48 µg/L. Groundwater elevations represent raw data (without barometric adjustment).

Figure 3.2-23 Time-series plots for SIMR-2

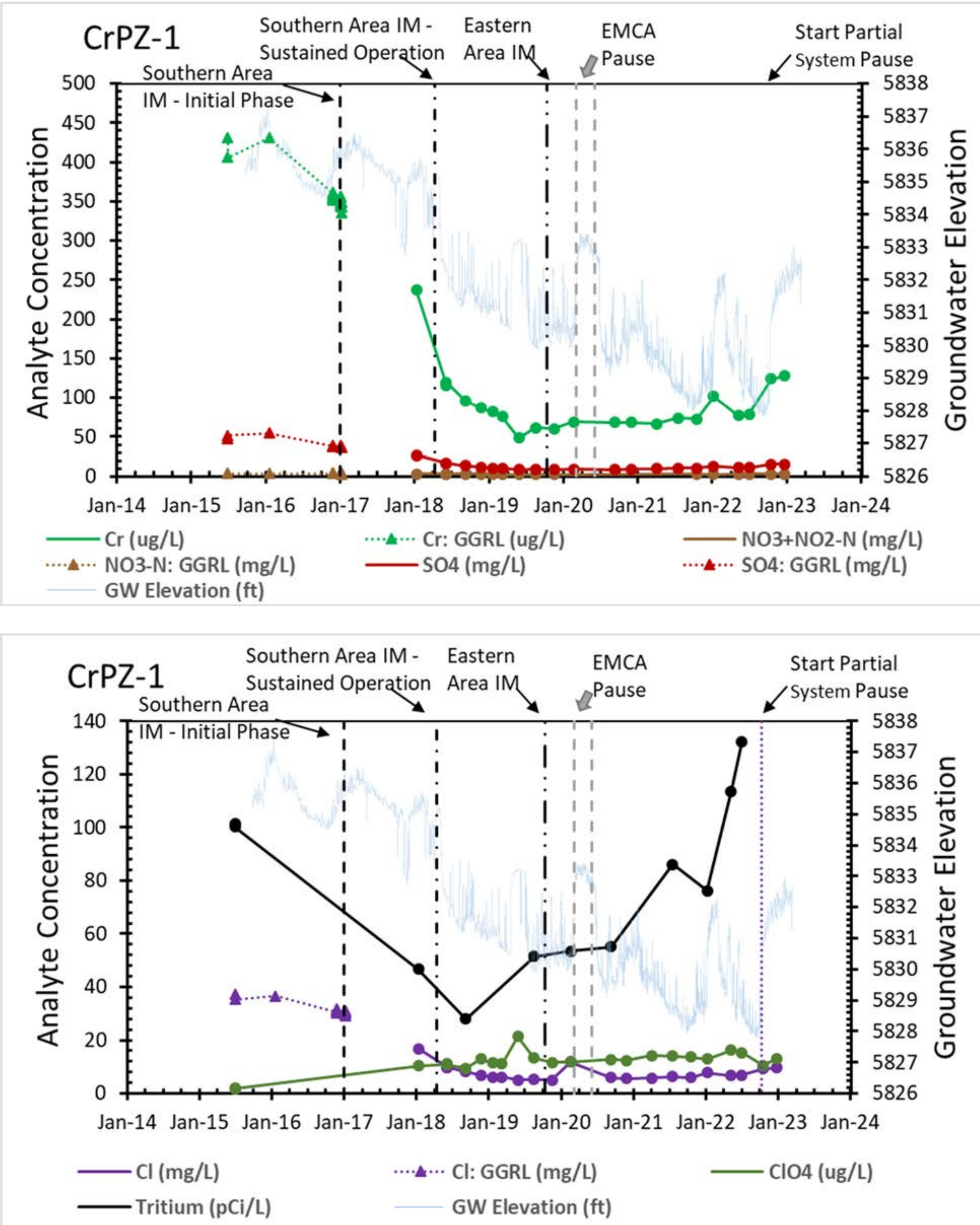

Notes: Solid symbols represent detection results at the plotted value. The background for chromium is 7.48 µg/L. Data represented by triangles and dashed lines indicate screening-level data analyzed at LANL's Geochemistry and Geomaterials Research Laboratories (GGRL). Groundwater elevations represent raw data (without barometric adjustment).

Figure 3.2-24 Time-series plots for CrPZ-1

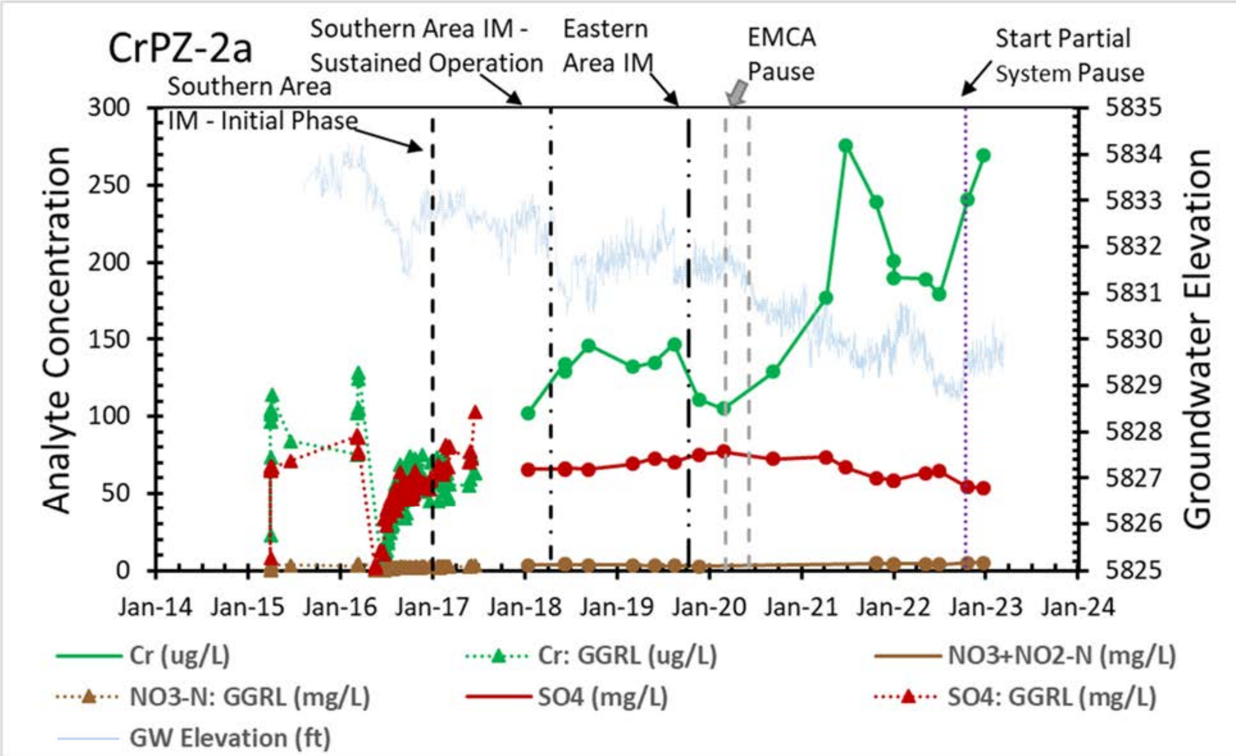

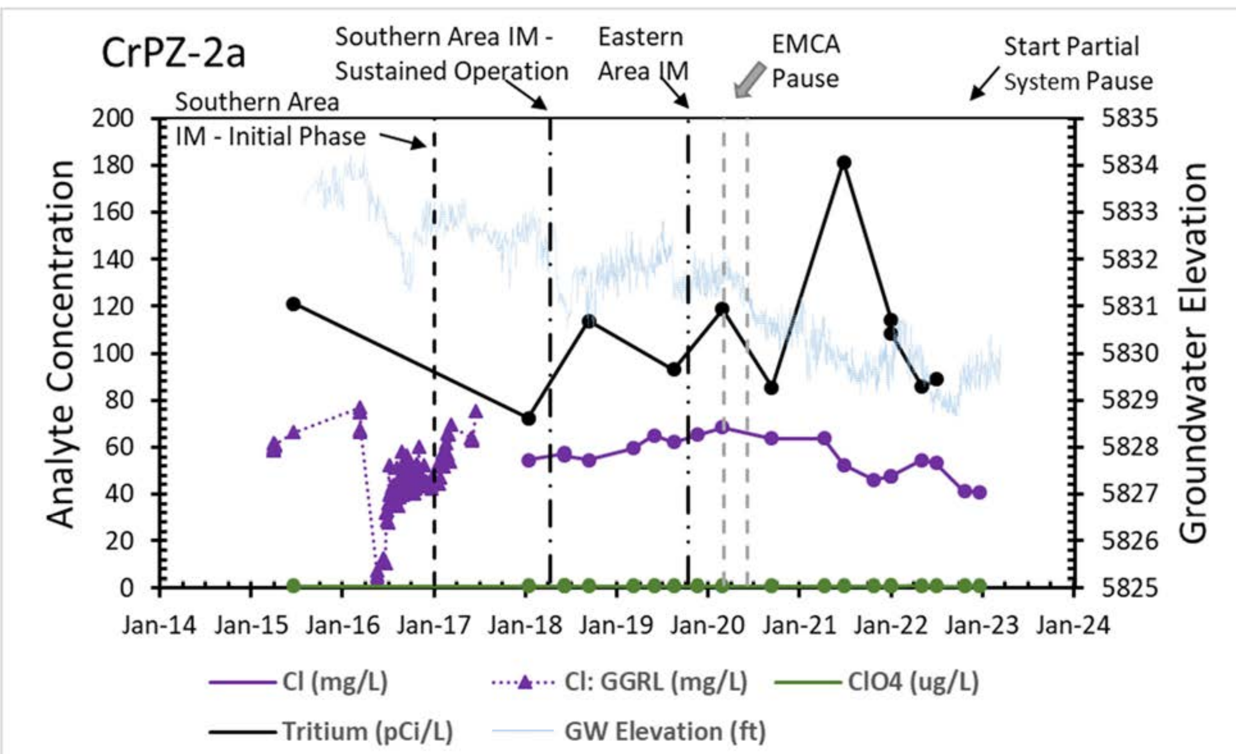

Notes: Solid symbols represent detection results at the plotted value. The background for chromium is 7.48 µg/L. Data represented by triangles and dashed lines indicate screening-level data analyzed at LANL's Geochemistry and Geomaterials Research Laboratories (GGRL). Groundwater elevations represent raw data (without barometric adjustment).

Figure 3.2-25 Time-series plots for CrPZ-2a

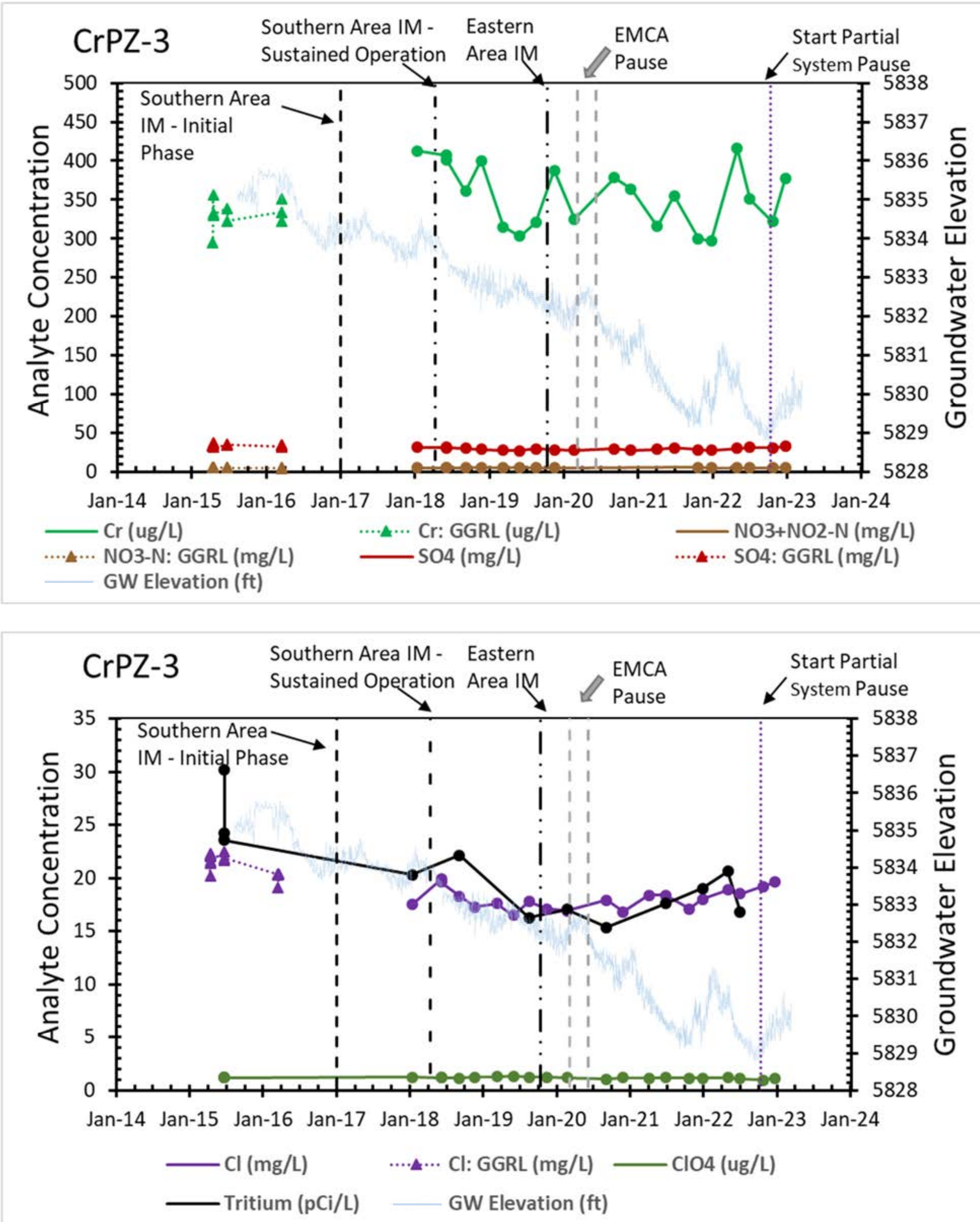

Notes: Solid symbols represent detection results at the plotted value. The background for chromium is 7.48 µg/L. Data represented by triangles and dashed lines indicate screening-level data analyzed at LANL's Geochemistry and Geomaterials Research Laboratories (GGRL). Groundwater elevations represent raw data (without barometric adjustment).

Figure 3.2-26 Time-series plots for CrPZ-3

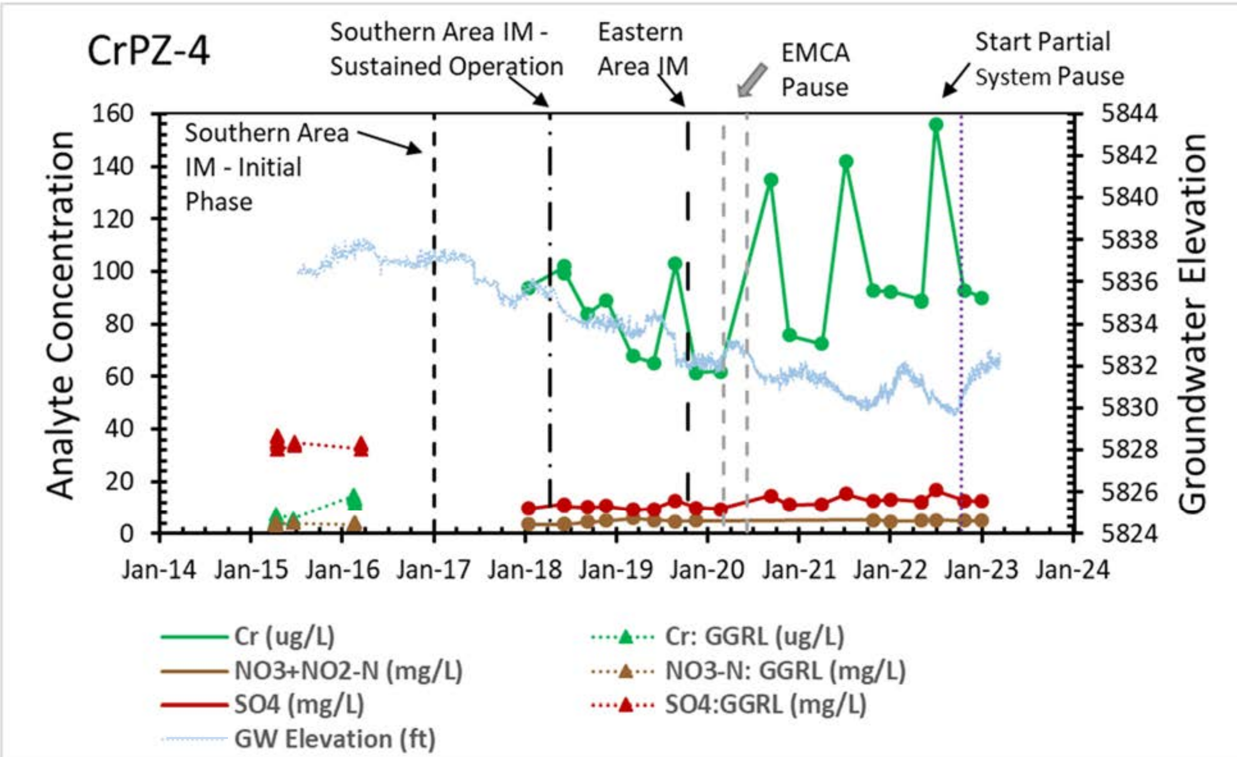

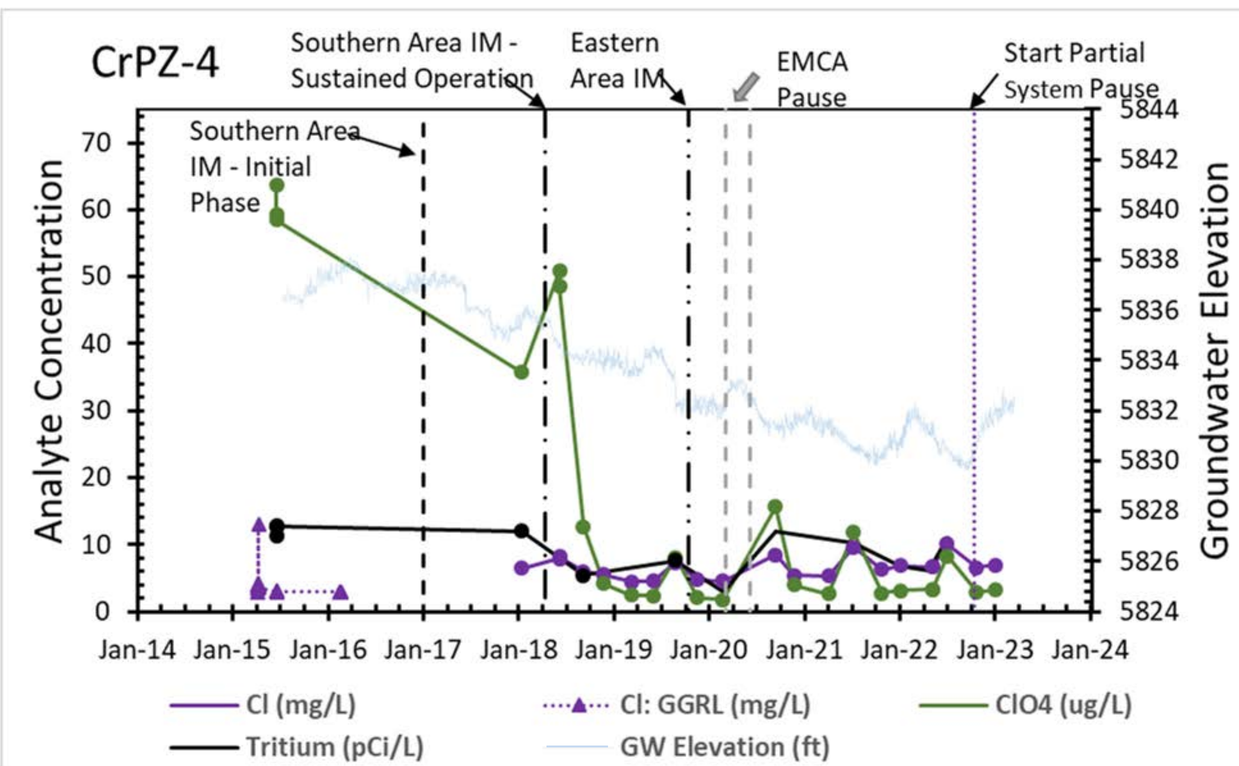

Notes: Solid symbols represent detection results at the plotted value. The background for chromium is 7.48 µg/L. Data represented by triangles and dashed lines indicate screening-level data analyzed at LANL's Geochemistry and Geomaterials Research Laboratories (GGRL). Groundwater elevations represent raw data (without barometric adjustment).

Figure 3.2-27 Time-series plots for CrPZ-4

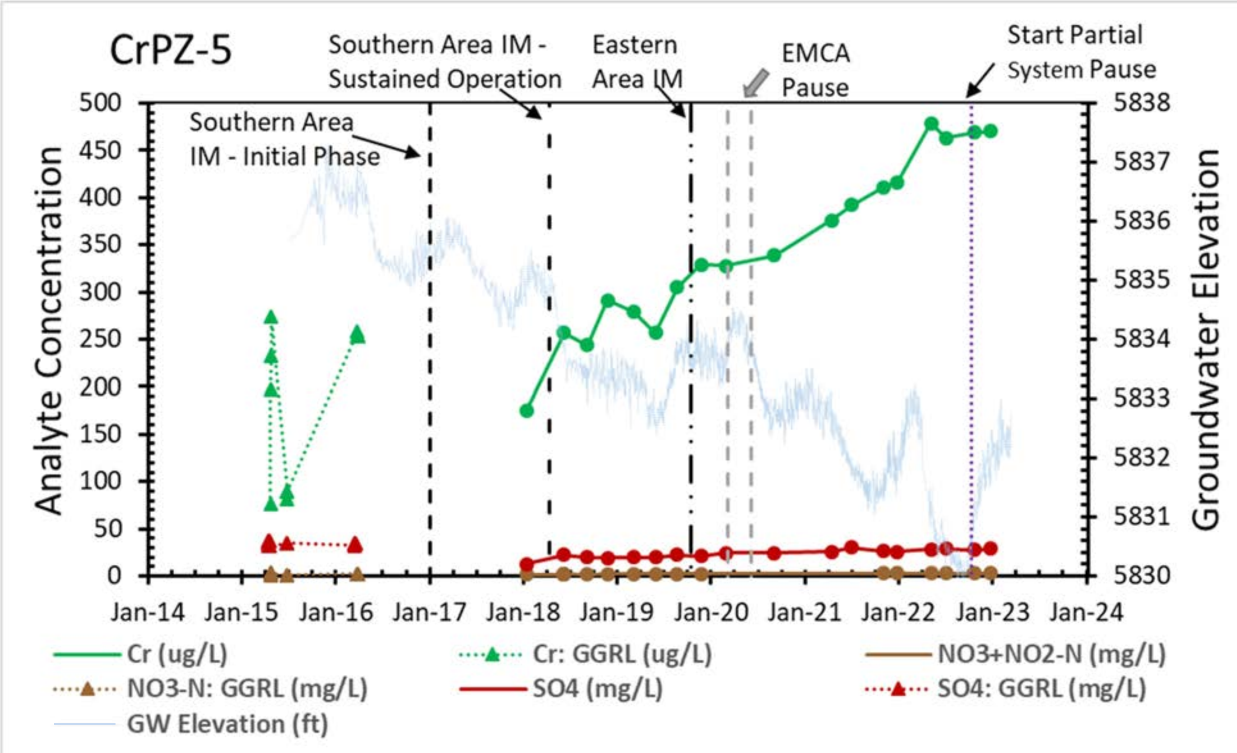

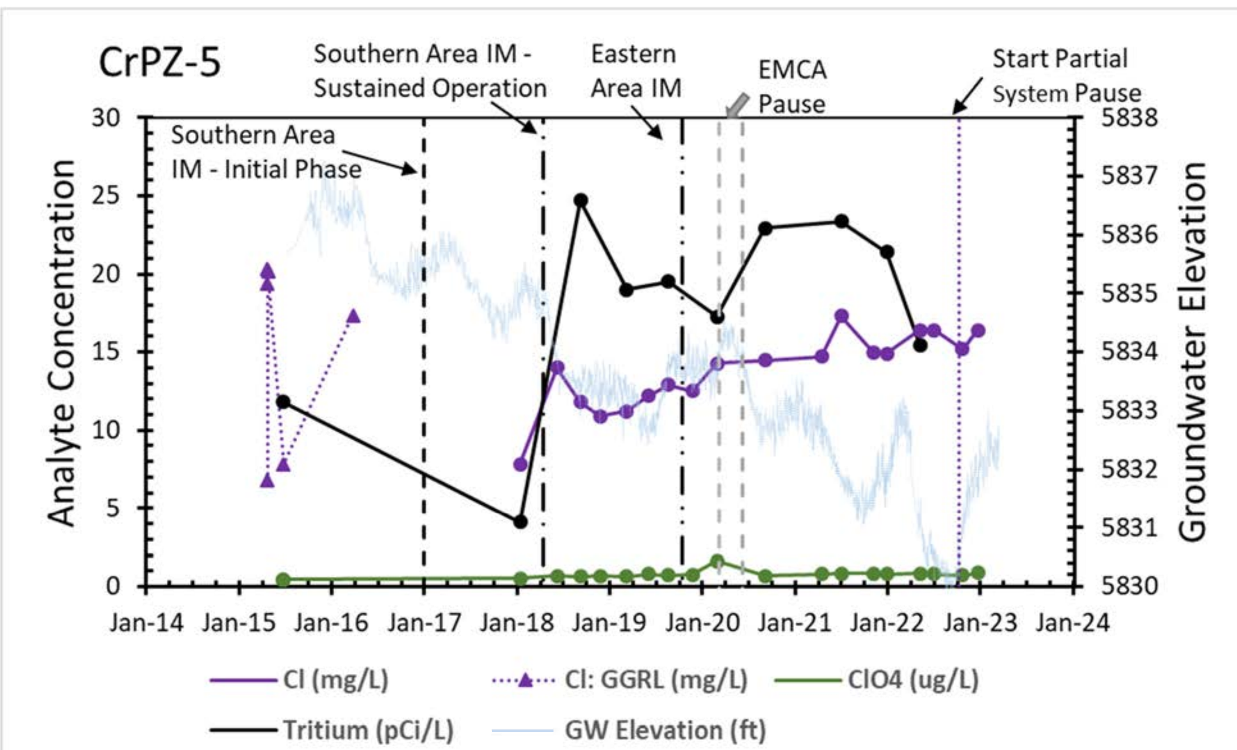

Notes: Solid symbols represent detection results at the plotted value. The background for chromium is 7.48 µg/L. Data represented by triangles and dashed lines indicate screening-level data analyzed at LANL's Geochemistry and Geomaterials Research Laboratories (GGRL). Groundwater elevations represent raw data (without barometric adjustment).

Figure 3.2-28 Time-series plots for CrPZ-5

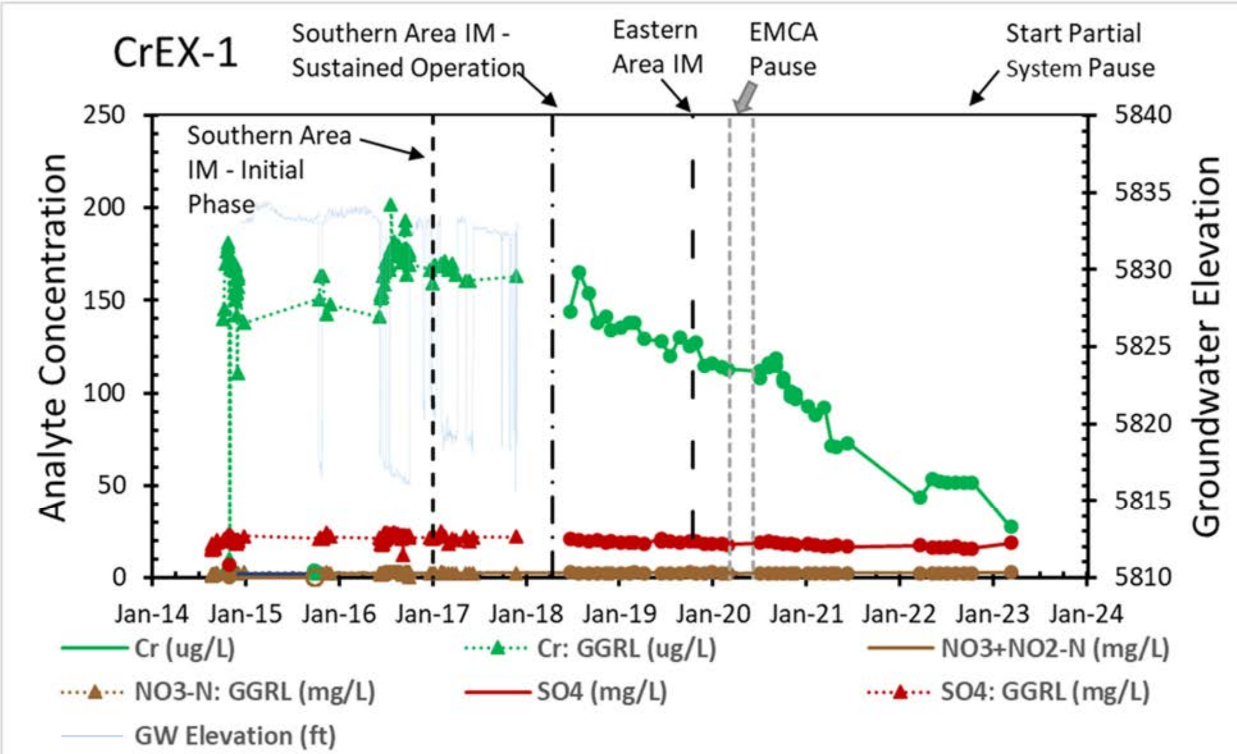

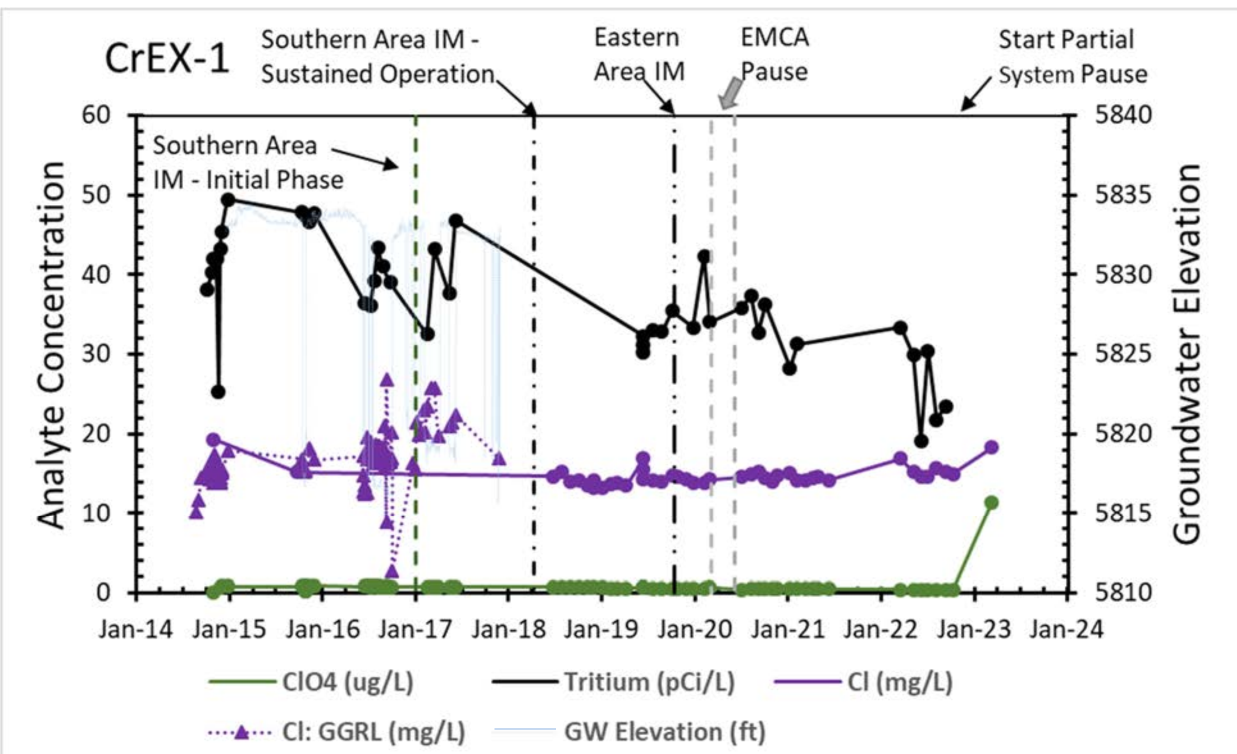

Notes: Open symbols represent nondetection results and solid symbols represent detection results at the plotted value. The background for chromium is 7.48 µg/L. Data represented by triangles and dashed lines indicate screening-level data analyzed at LANL's Geochemistry and Geomaterials Research Laboratories (GGRL). Groundwater elevations represent raw data (without barometric adjustment).

Figure 3.2-29 Time-series plots for CrEX-1

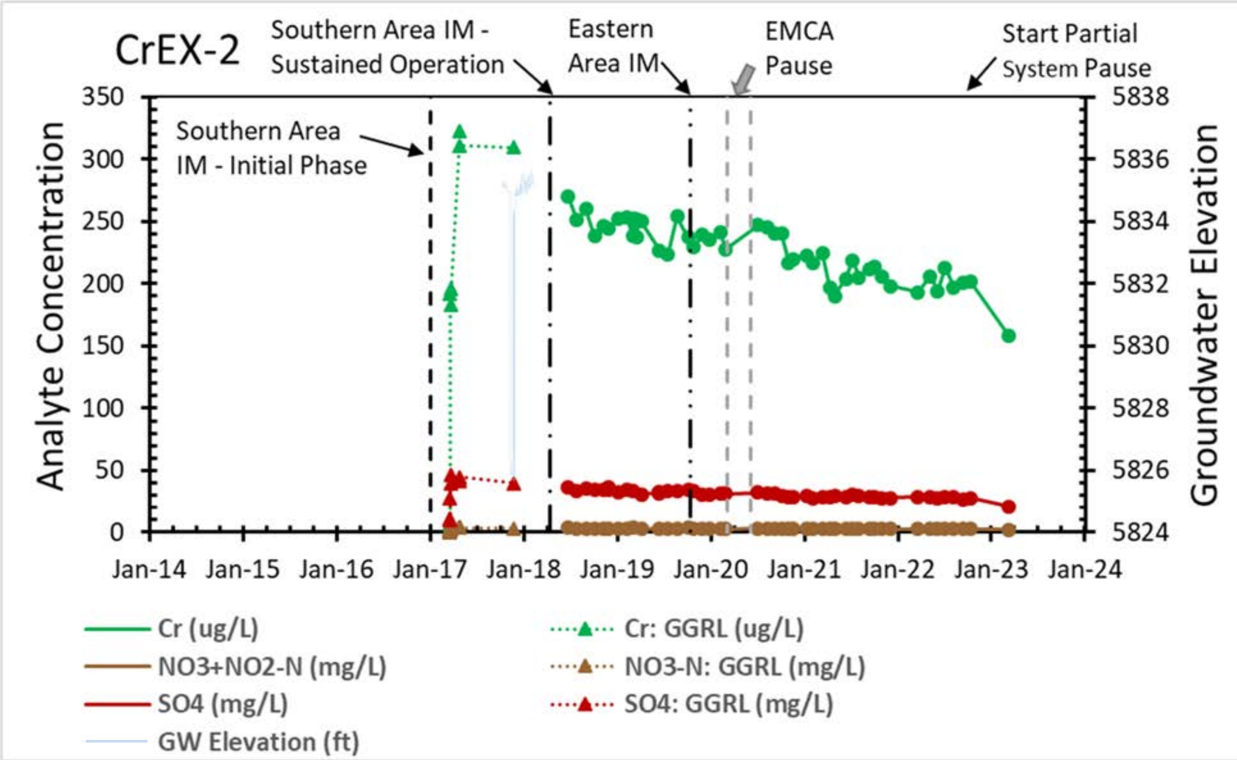

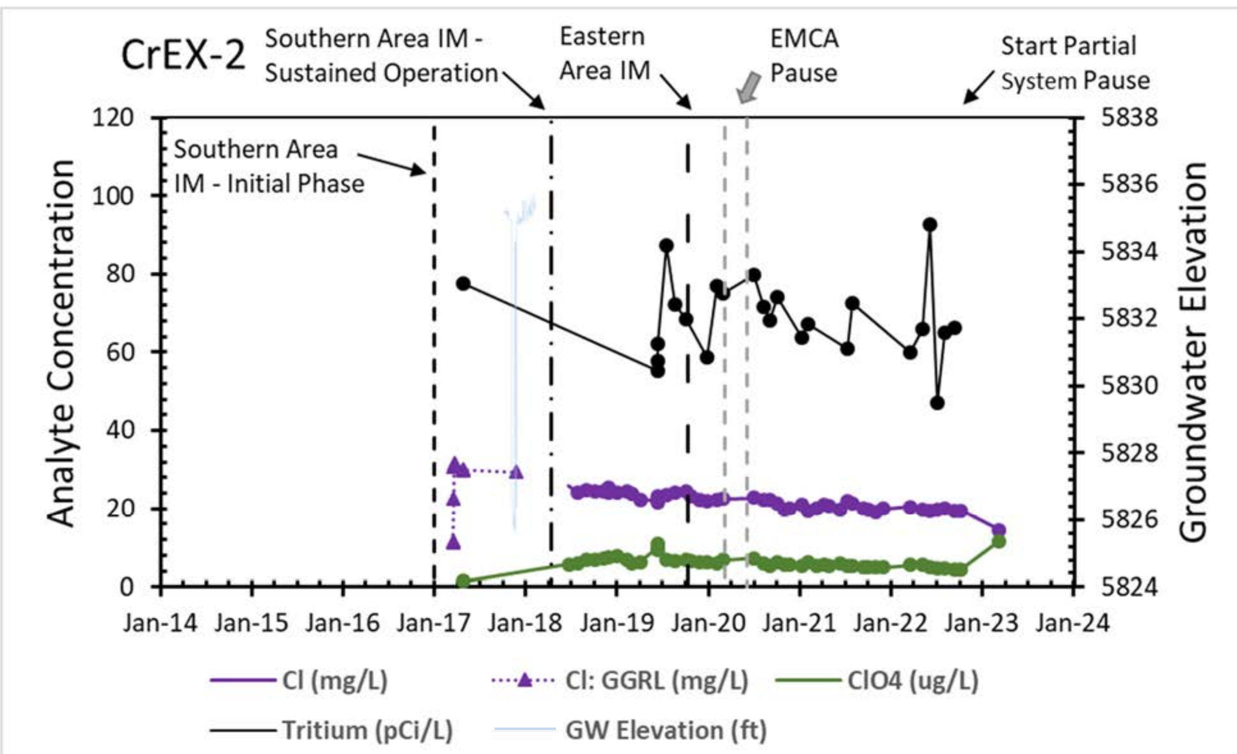

Notes: Solid symbols represent detection results at the plotted value. The background for chromium is 7.48 µg/L. Data represented by triangles and dashed lines indicate screening-level data analyzed at LANL's Geochemistry and Geomaterials Research Laboratories (GGRL). Groundwater elevations represent raw data (without barometric adjustment).

Figure 3.2-30 Time-series plots for CrEX-2

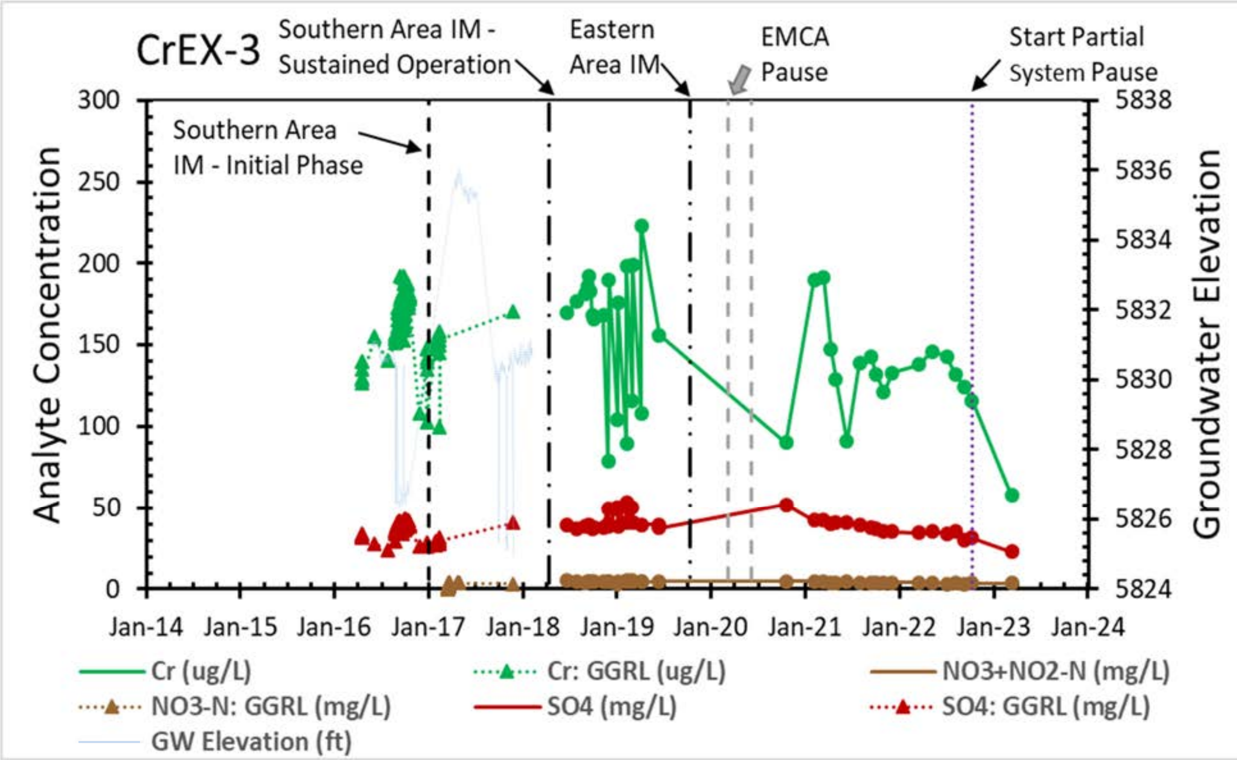

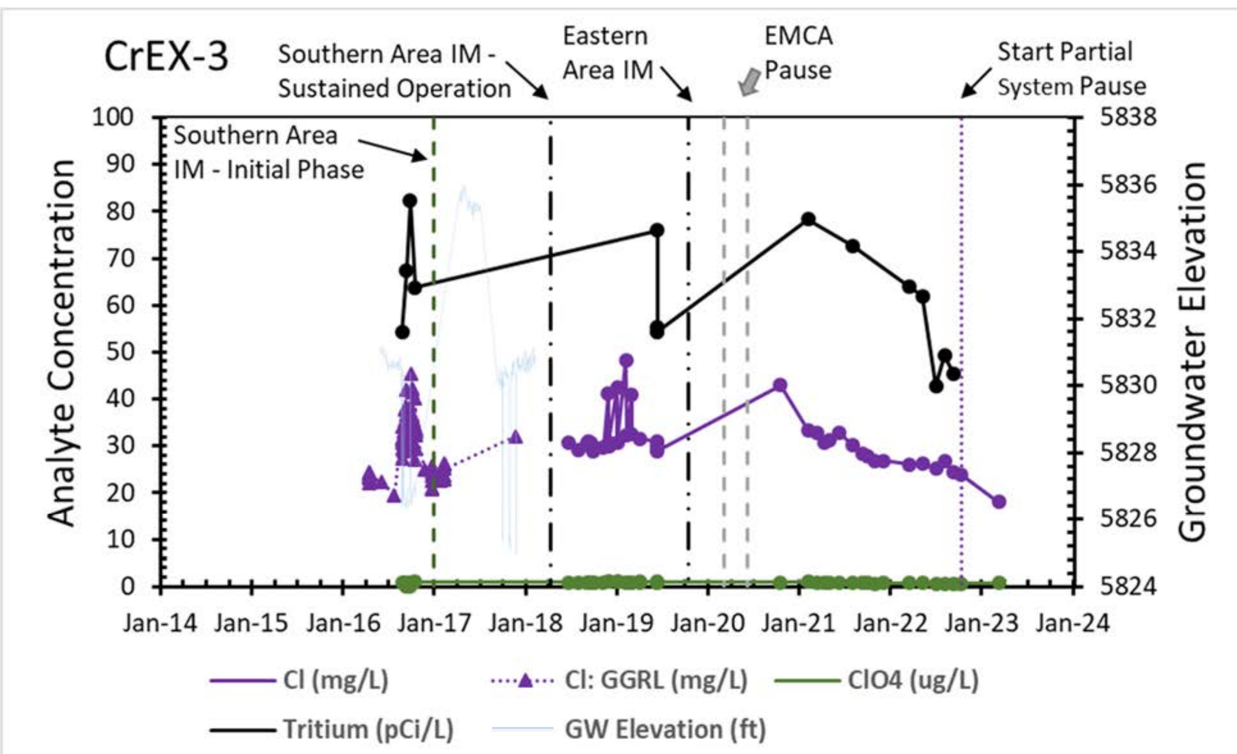

Notes: Solid symbols represent detection results at the plotted value. The background for chromium is 7.48 µg/L. Data represented by triangles and dashed lines indicate screening-level data analyzed at LANL's Geochemistry and Geomaterials Research Laboratories (GGRL). Groundwater elevations represent raw data (without barometric adjustment).

Figure 3.2-31 Time-series plots for CrEX-3

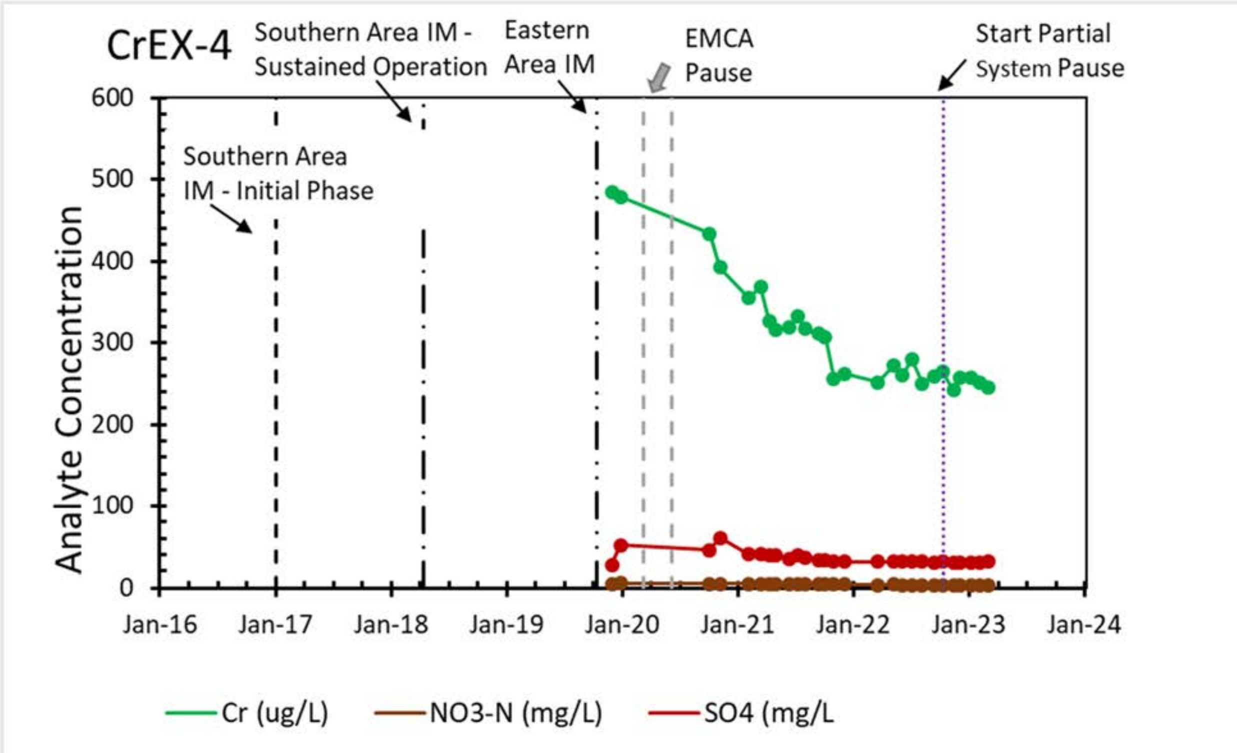

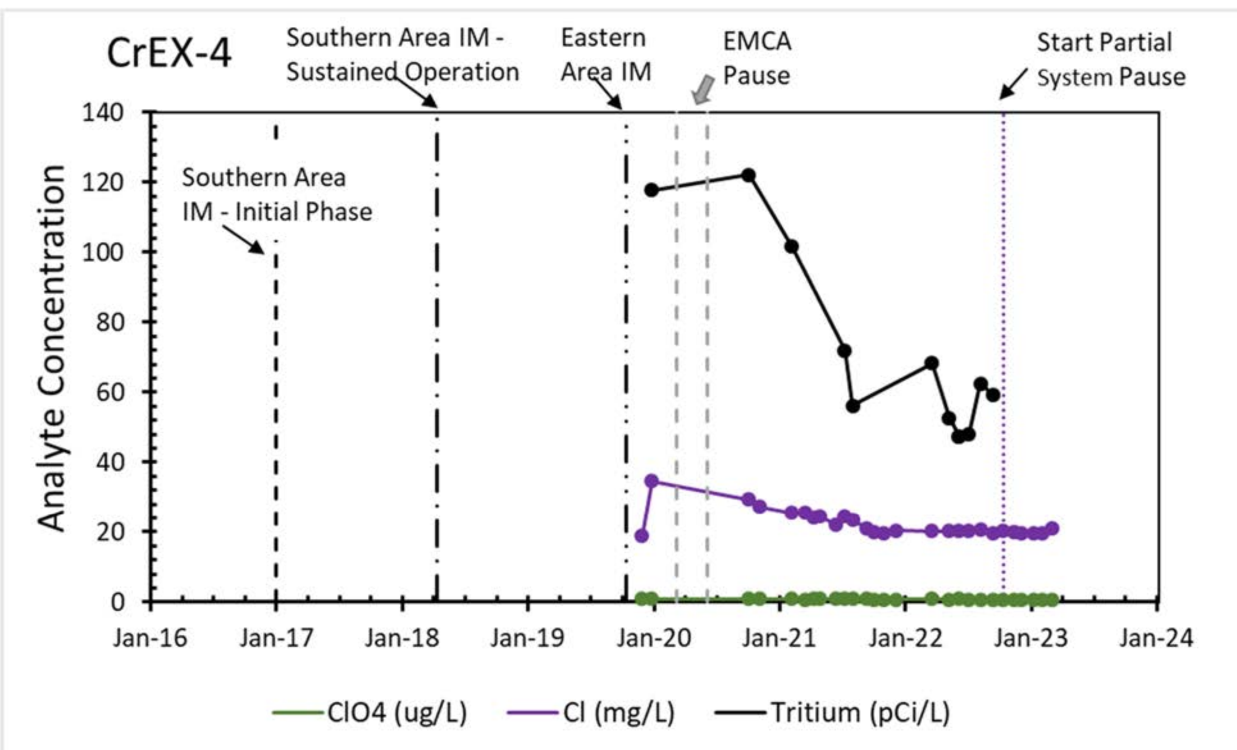

Notes: Solid symbols represent detection results at the plotted value. The background for chromium is 7.48 µg/L. Groundwater elevations represent raw data (without barometric adjustment).

Figure 3.2-32 Time-series plots for CrEX-4

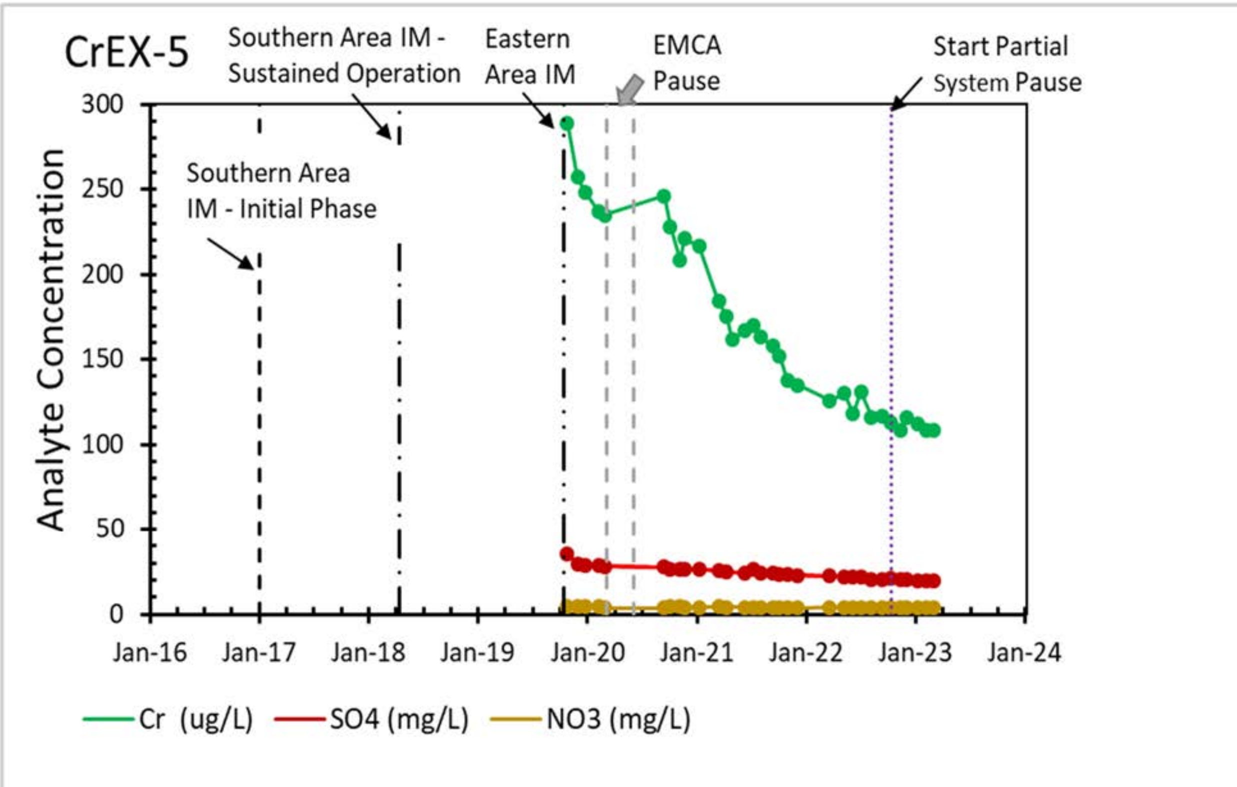

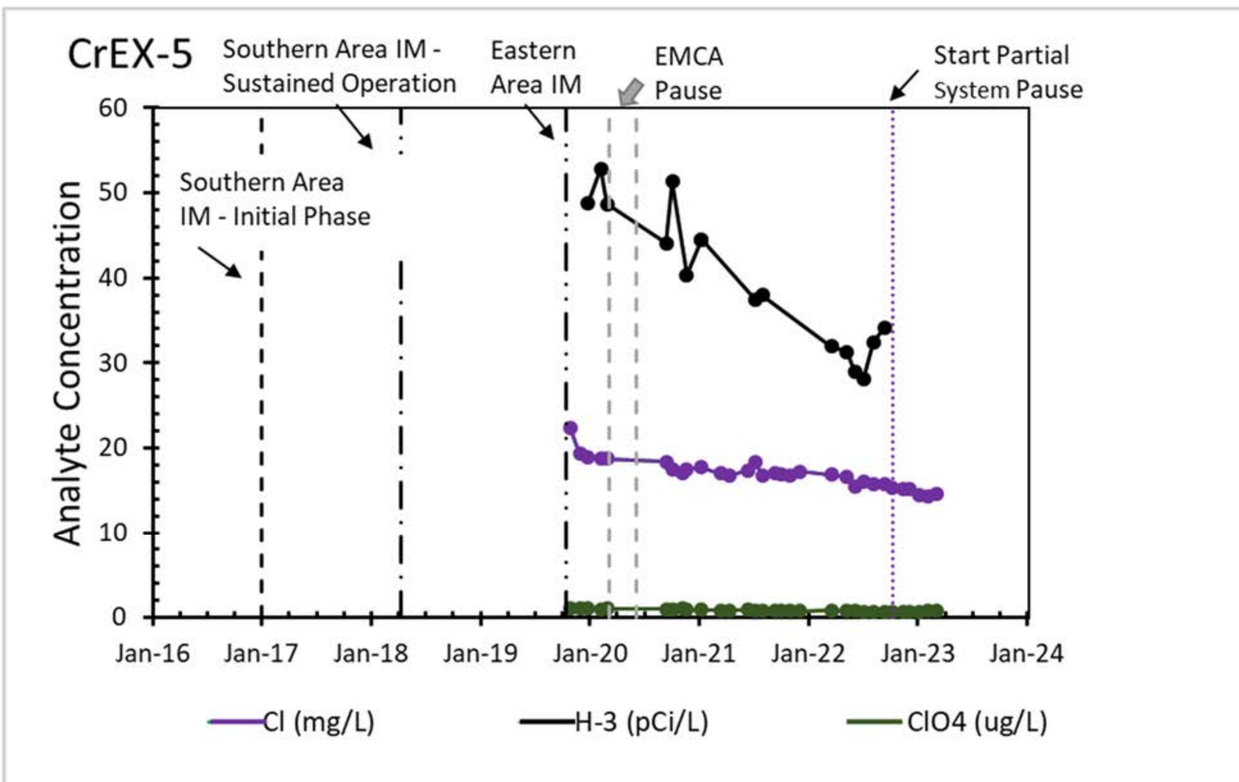

Notes: Solid symbols represent detection results at the plotted value. The background for chromium is 7.48 µg/L. Groundwater elevations represent raw data (without barometric adjustment).

Figure 3.2-33 Time-series plots for CrEX-5

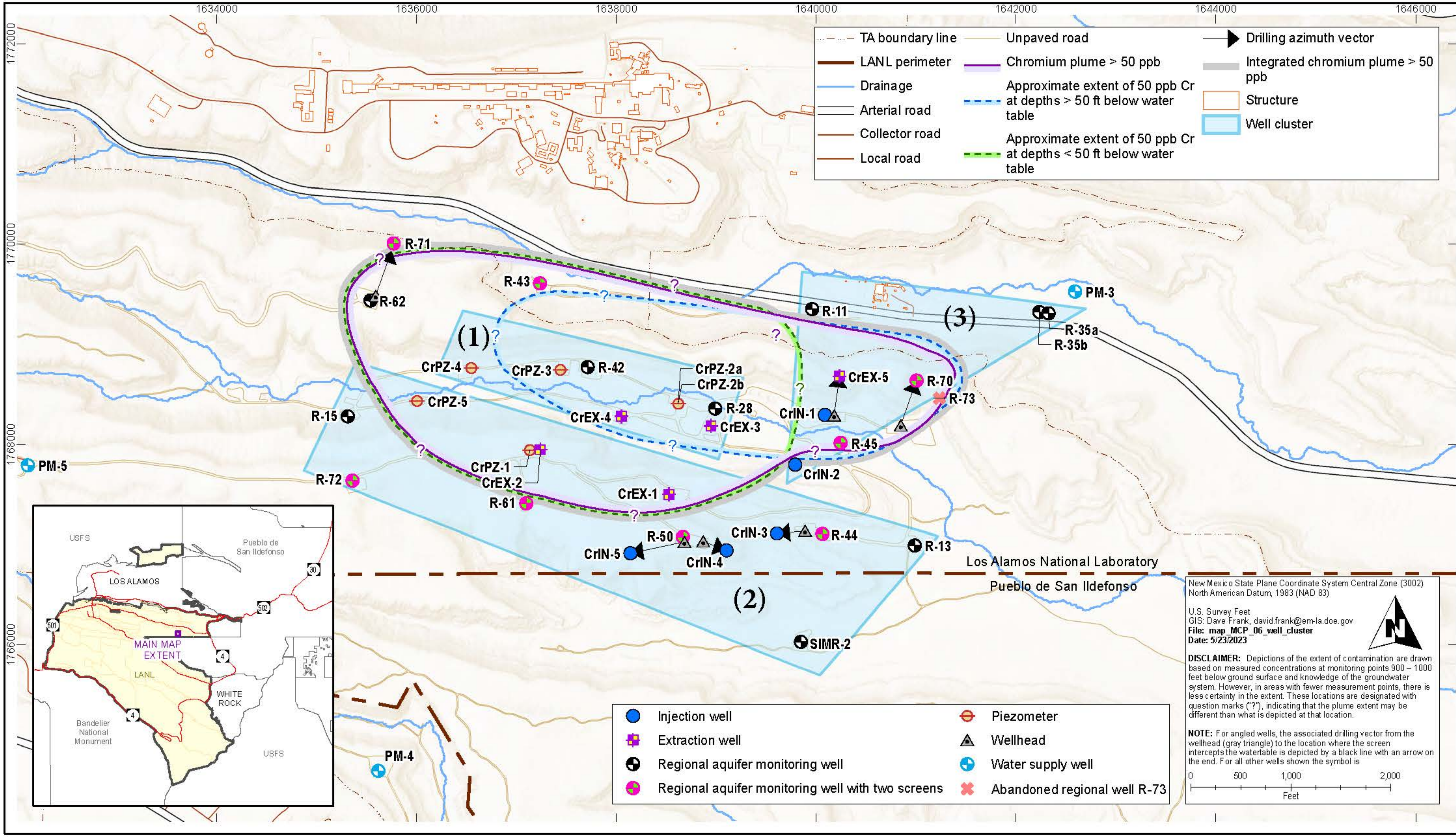

Notes: Groups of monitoring wells: (1) plume centroid, (2) southern area of the plume, and (3) northeastern area of the plume.
Source: "Initial Five-Year Evaluation of the Interim Measures for Chromium Plume Control with an Assessment of Potential Modifications to Operations" (N3B 2022, 702597).

Figure 3.2-34 Zones of the chromium plume

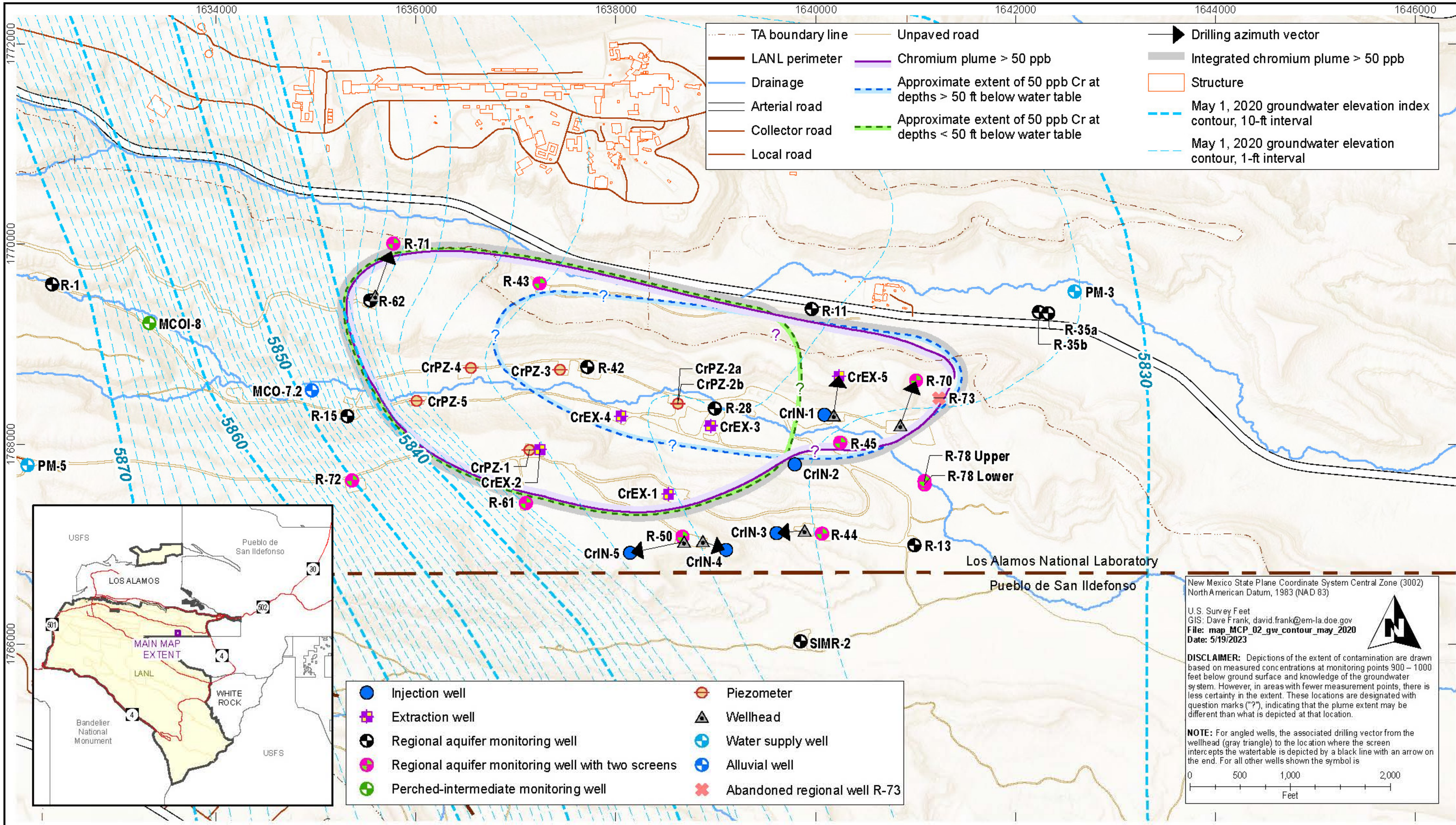

Figure 3.3-1 Baseline shallow regional potentiometric surface for May 1, 2020

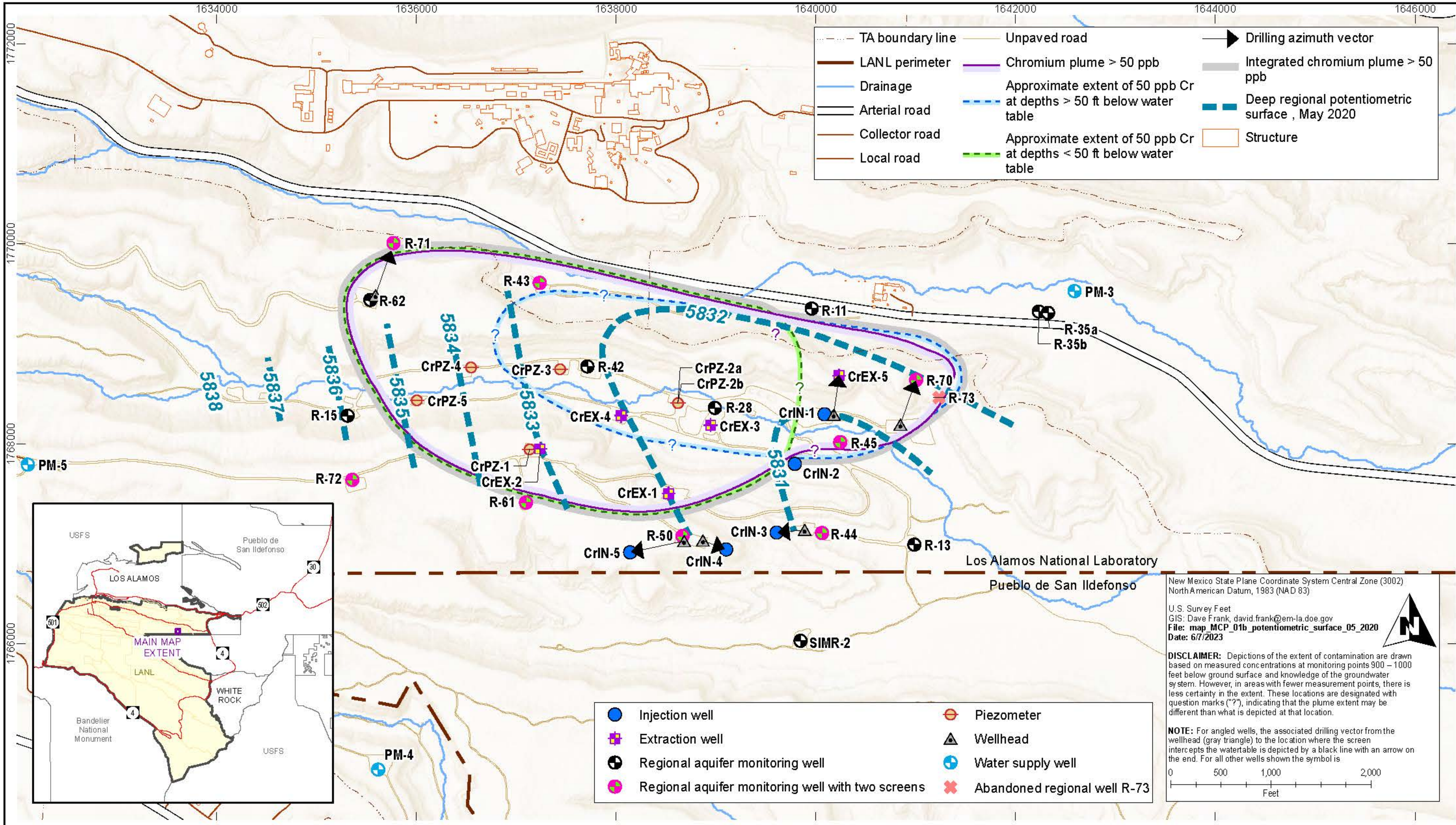

Figure 3.3-2 Baseline deep regional potentiometric surface for May 1, 2020

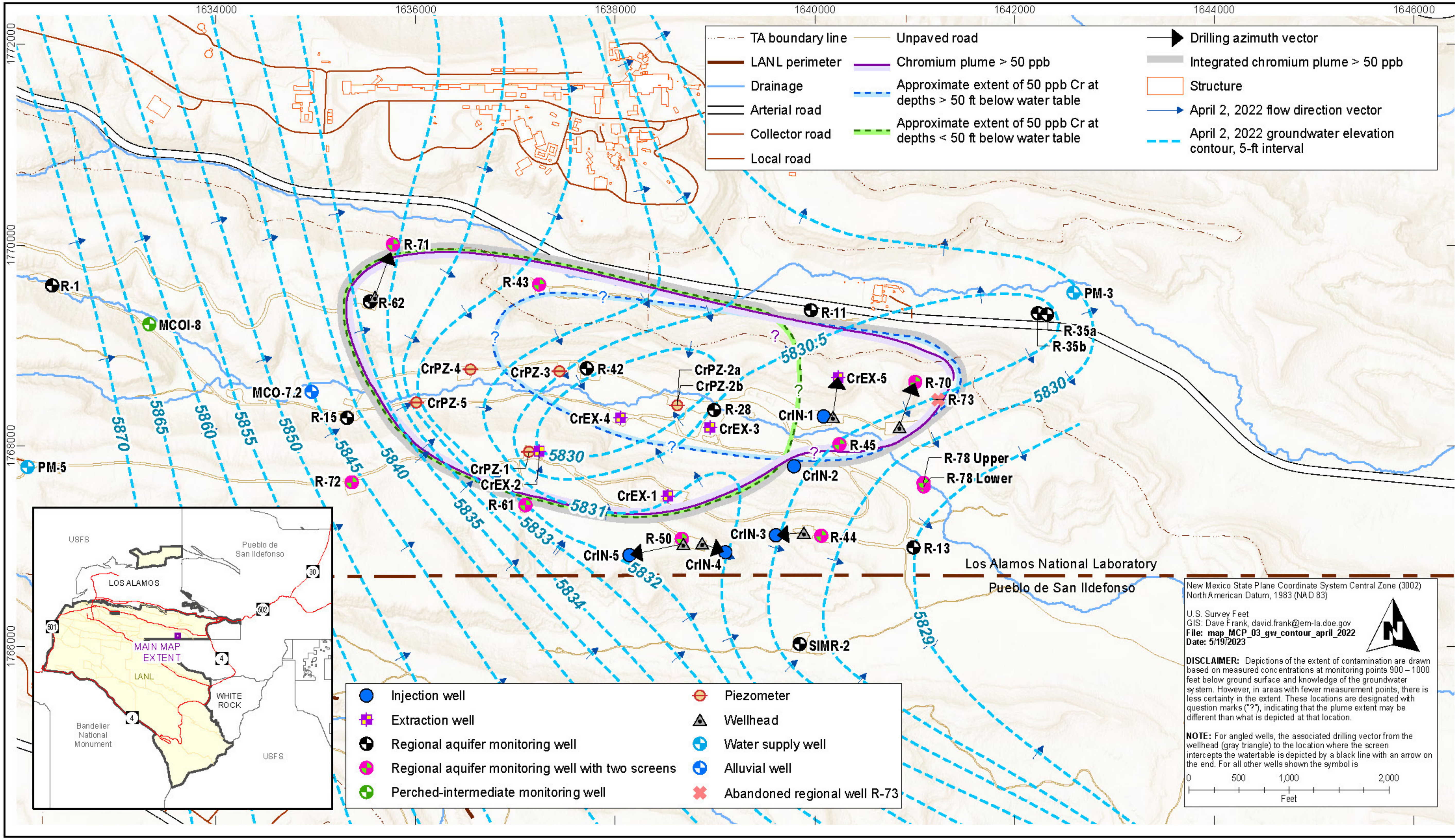

Figure 3.3-3 Shallow regional potentiometric surface for April 2, 2022

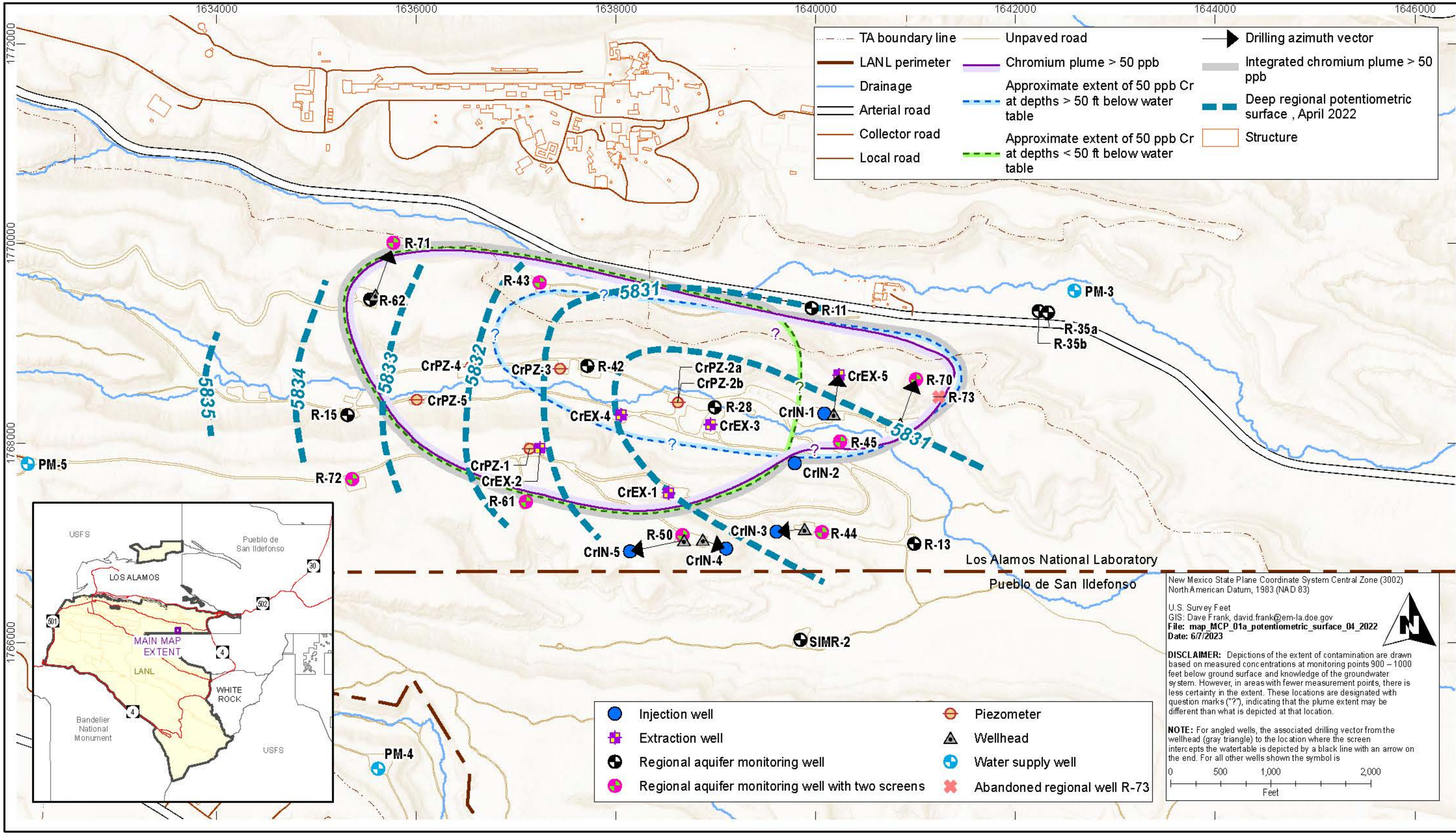

Figure 3.3-4 Deep regional potentiometric surface for April 2, 2022

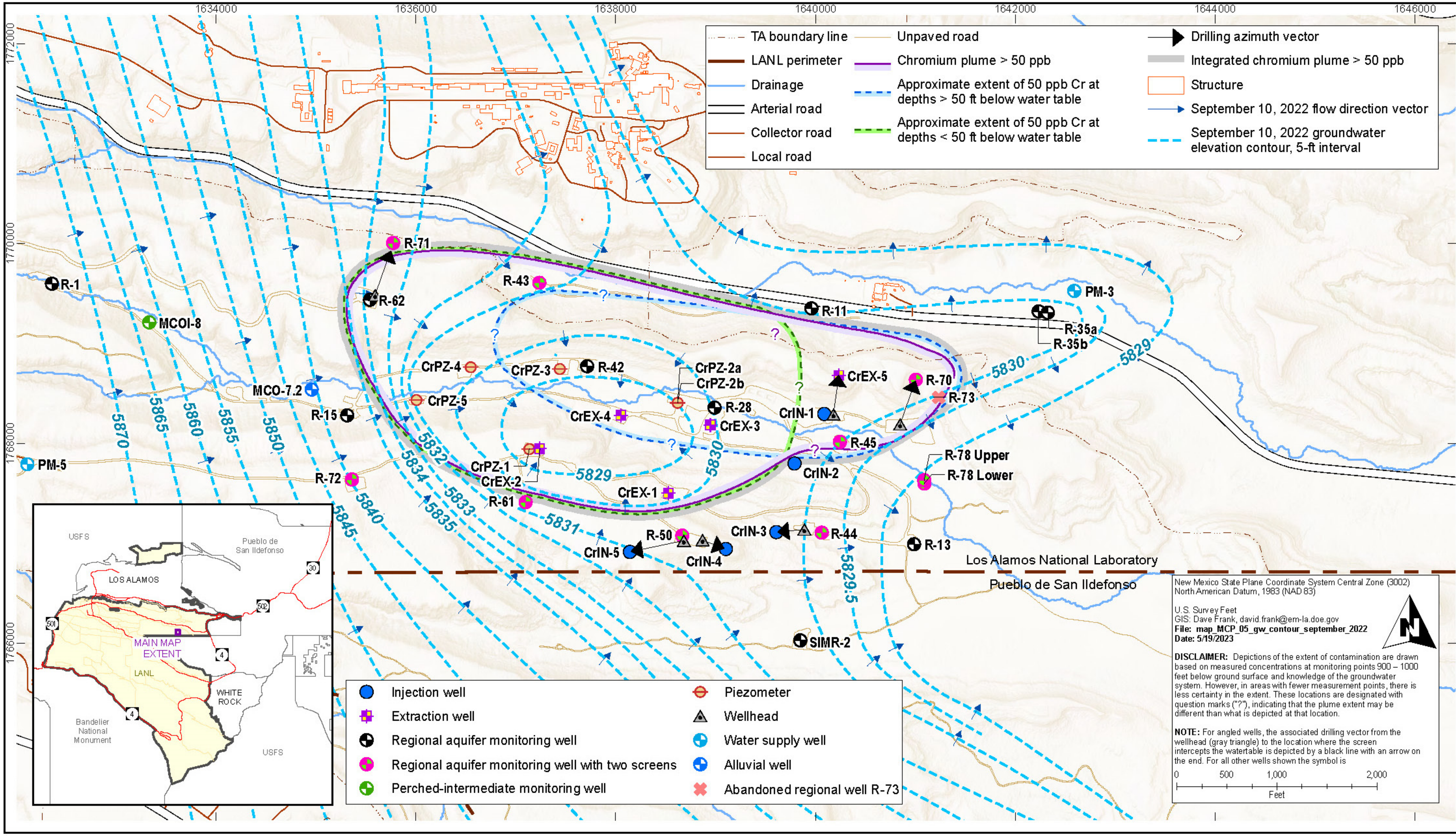

Figure 3.3-5 Shallow regional potentiometric surface for September 10, 2022

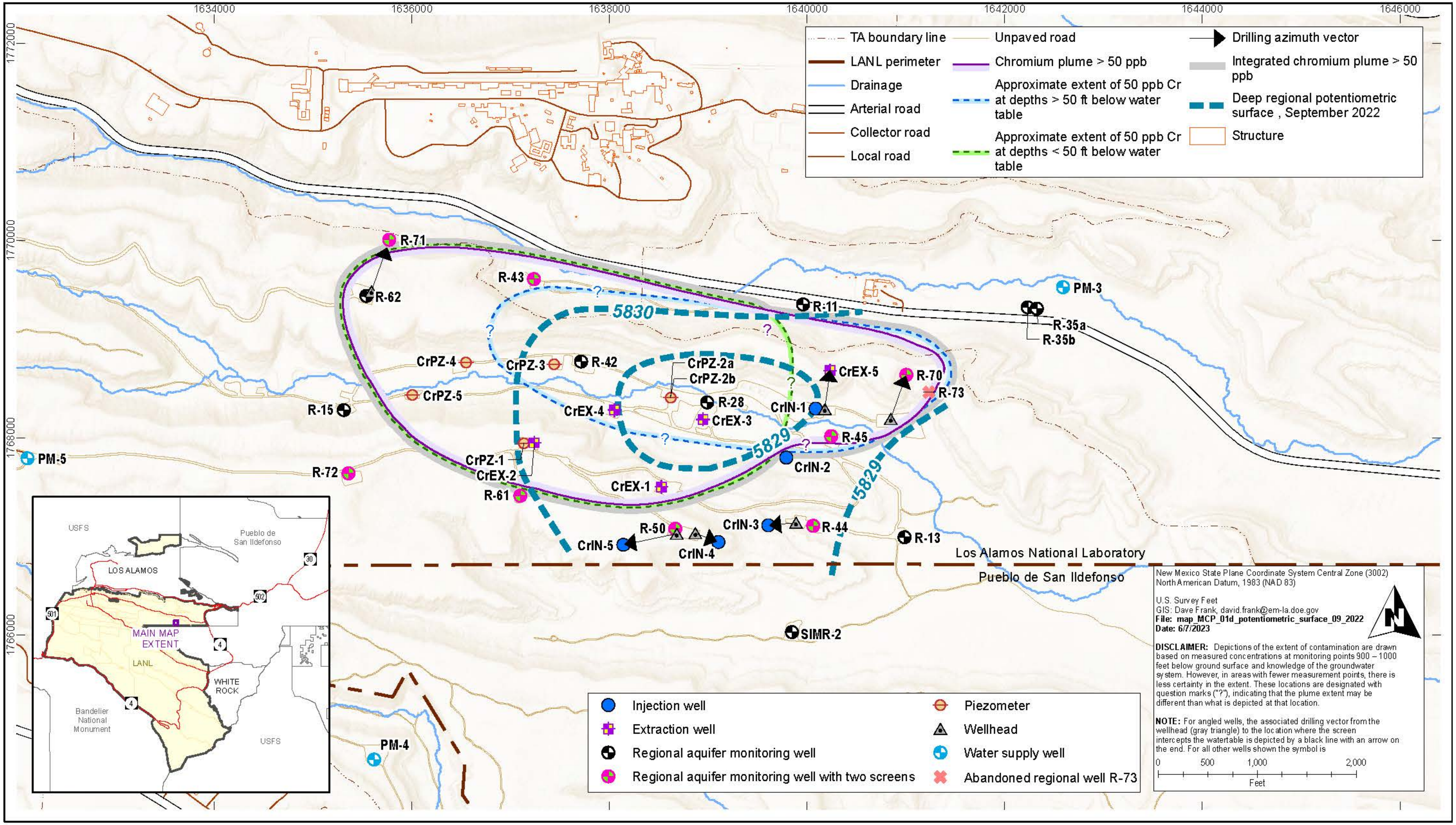

Figure 3.3-6 Deep regional potentiometric surface for September 10, 2022

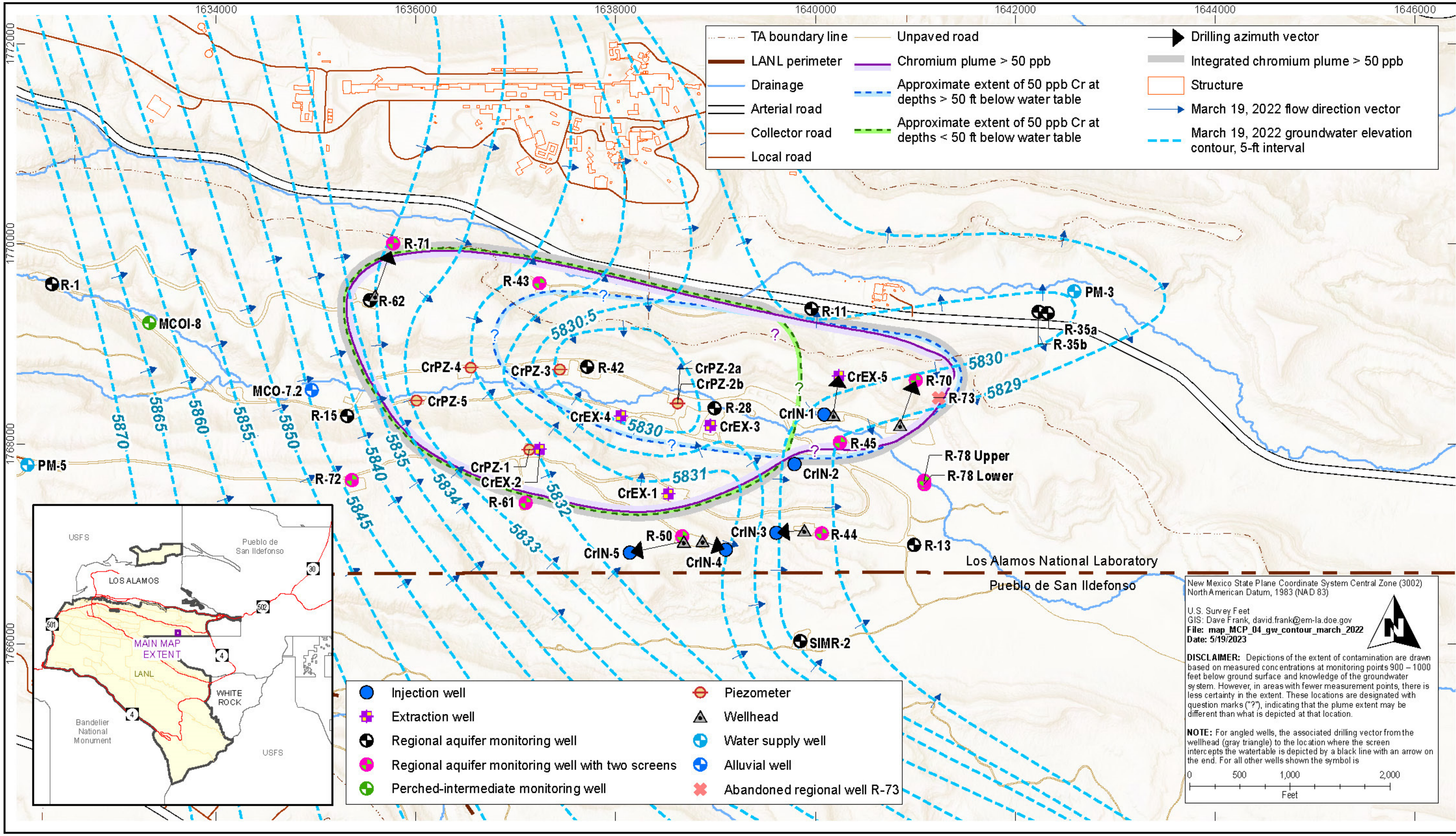

Figure 3.3-7 Shallow regional potentiometric surface for March 19, 2023

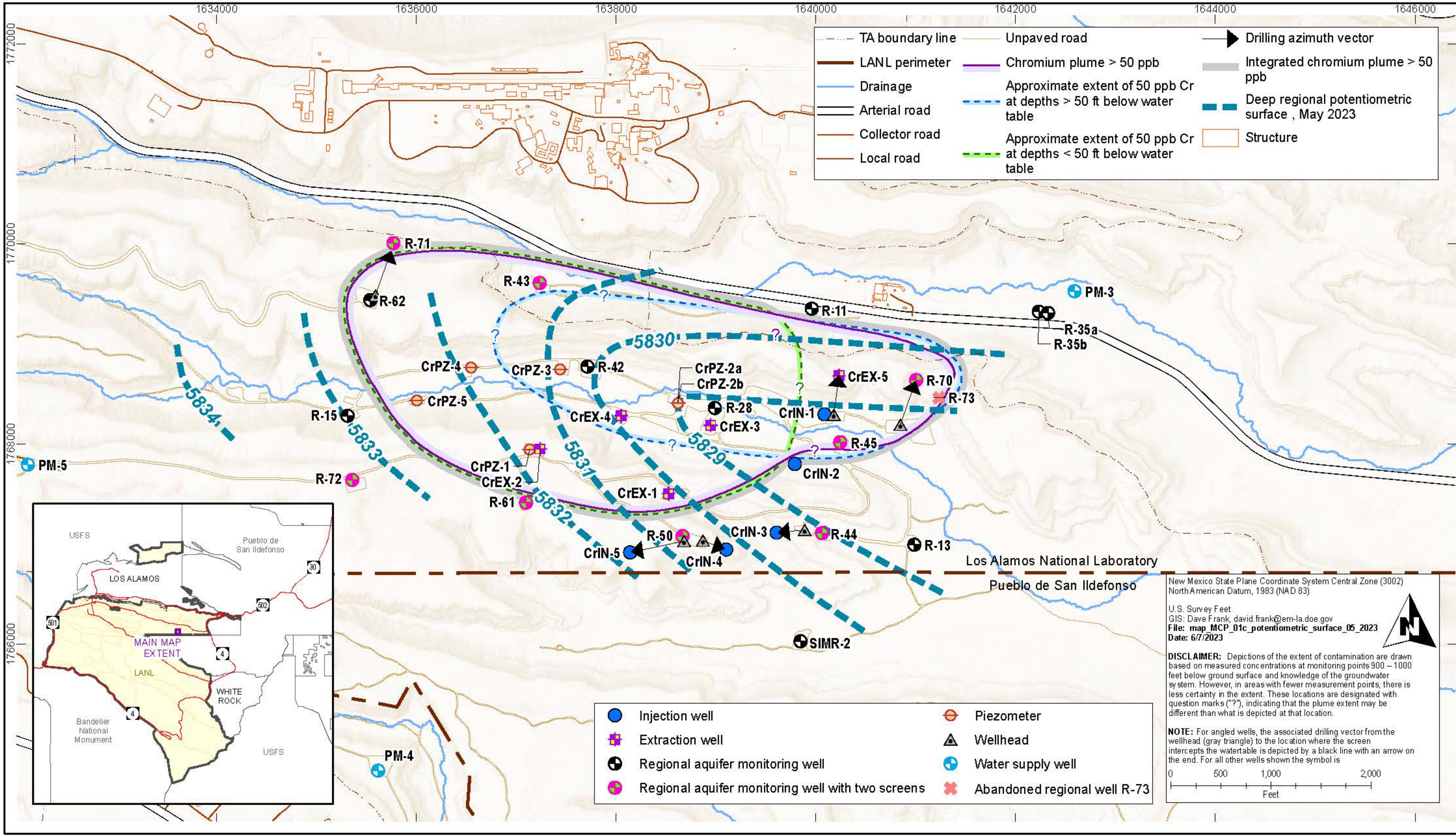

Figure 3.3-8 Deep regional potentiometric surface for March 19, 2023

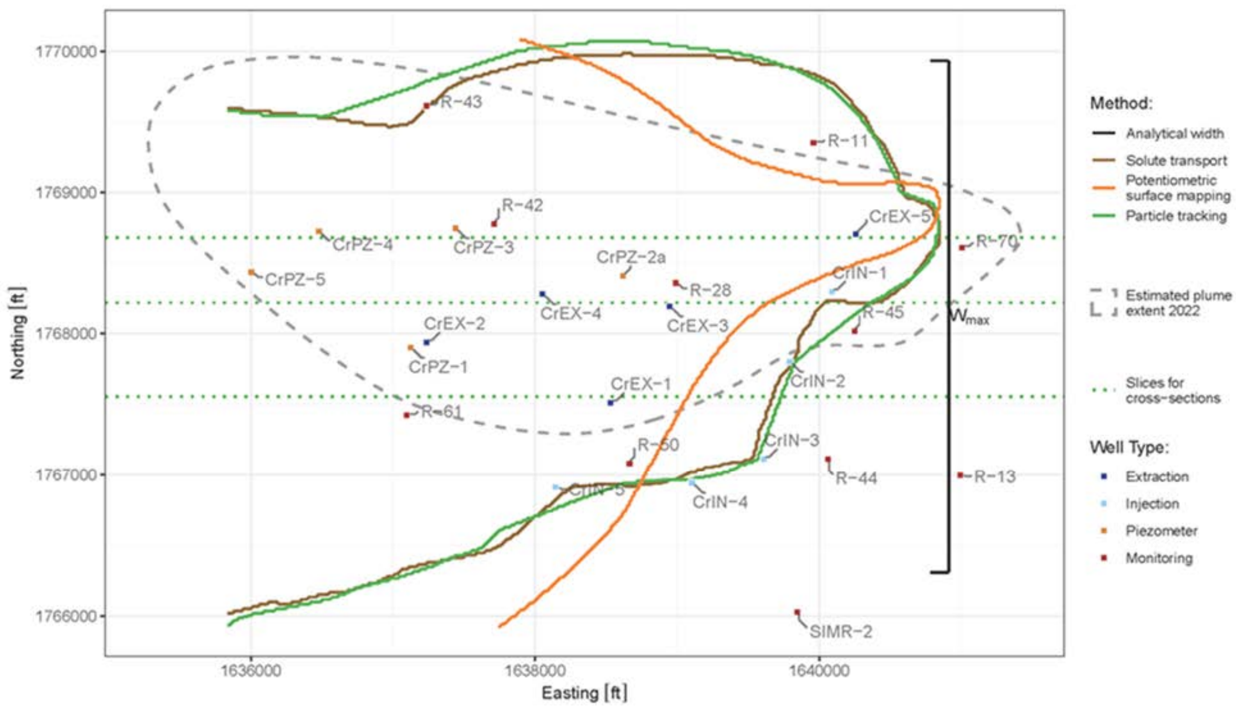

Notes: Estimated chromium plume extent is defined by 50-ppb.

Sources: "Initial Five-Year Evaluation of the Interim Measures for Chromium Plume Control with an Assessment of Potential Modifications to Operations" (N3B 2022, 702597); Enclosure 3, Chromium Interim Measure Capture Zone Analysis (Neptune 2023, 702782).

Figure 3.4-1 Capture zone of the IM during full operation, estimated by multiple methods

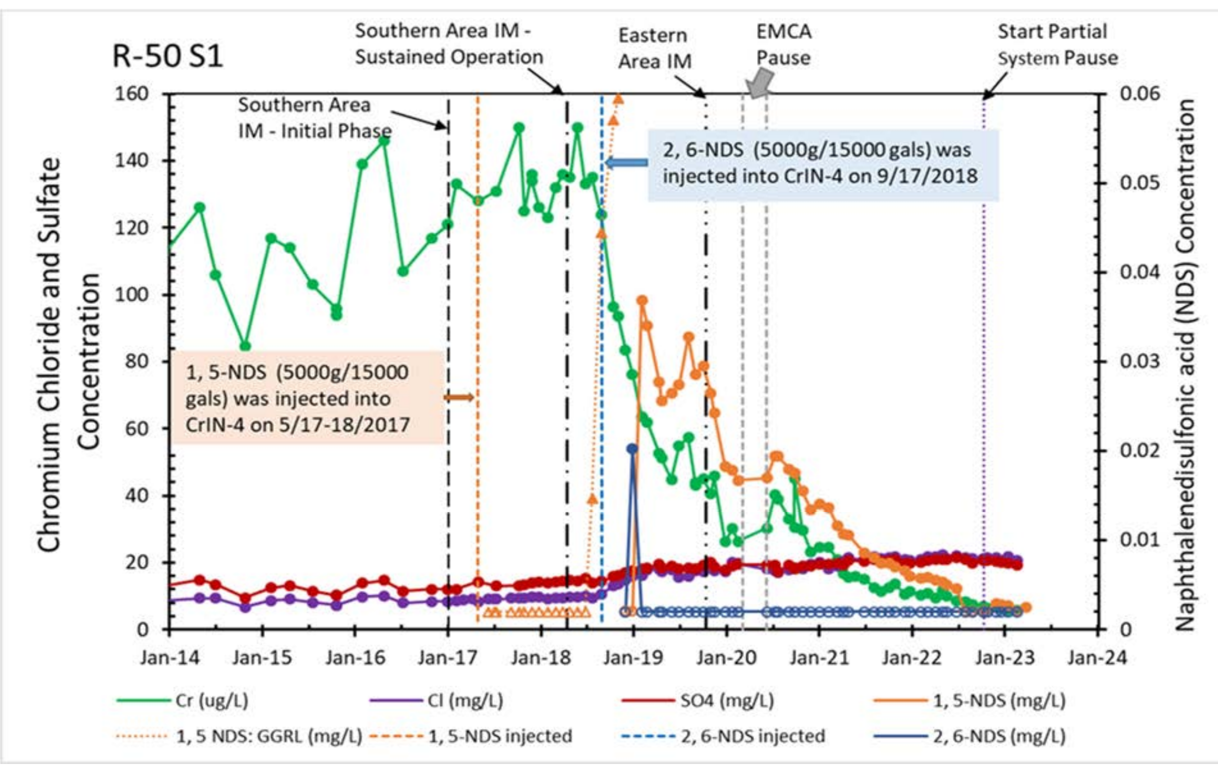

Notes: Open symbols represent nondetection results and solid symbols represent detection results at the plotted value. The background for chromium is 7.48 µg/L. S1 = Screen 1.

Figure 3.5-1 Time-series plots of tracer detections for R-50 screen 1

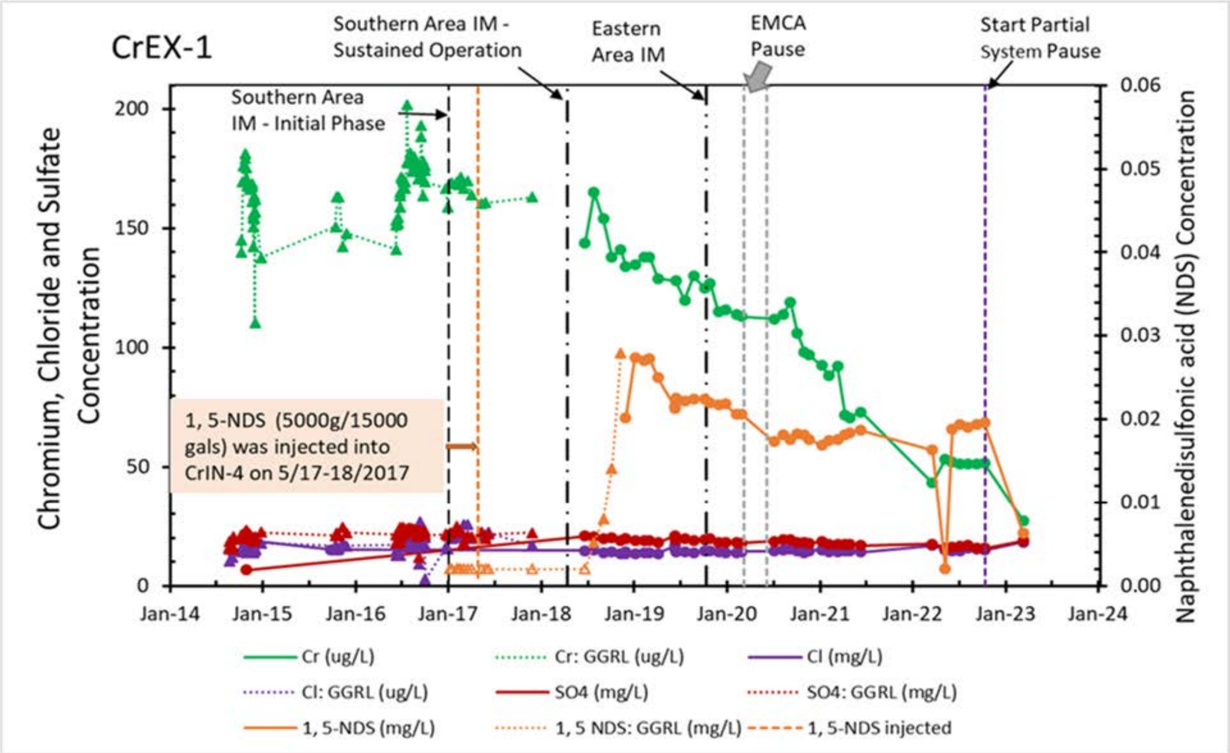

Notes: Open symbols represent nondetection results and solid symbols represent detection results at the plotted value. The background for chromium is 7.48 µg/L.

Figure 3.5-2 Time-series plots of tracer detections for CrEX-1

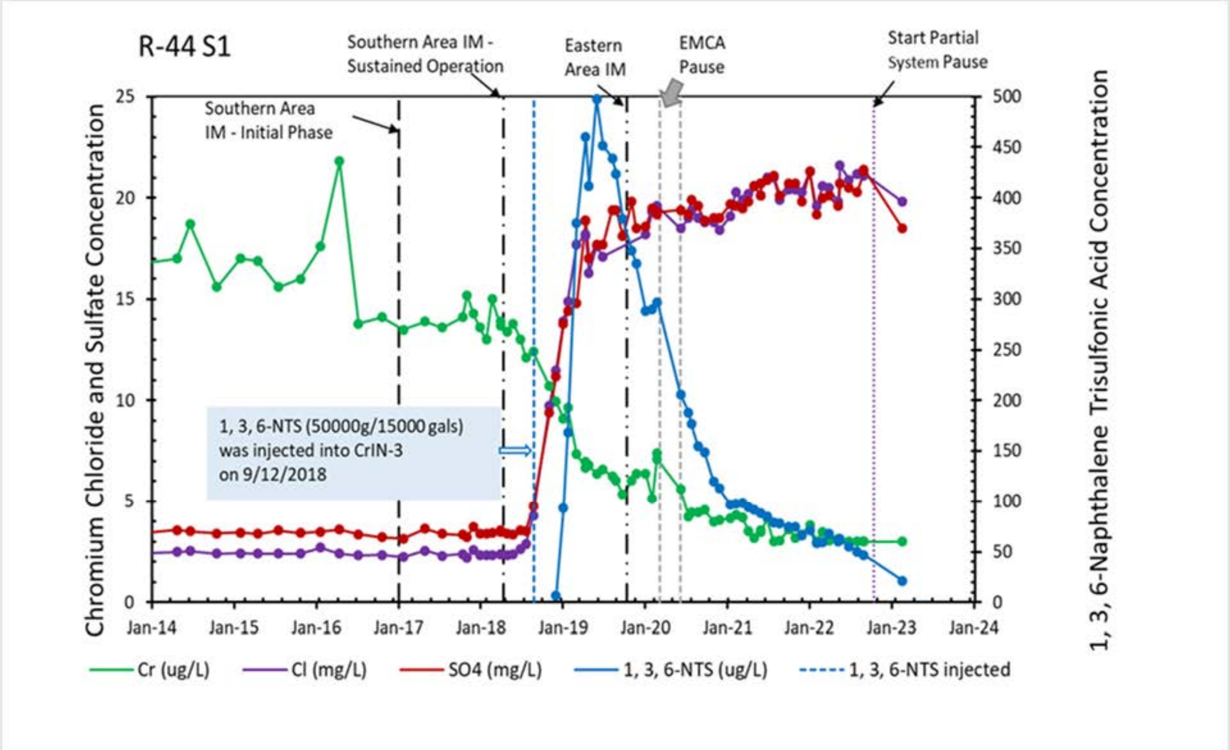

Notes: Open symbols represent nondetection results and solid symbols represent detection results at the plotted value. The background for chromium is 7.48 µg/L. S1 = Screen 1.

Figure 3.5-3 Time-series plots of tracer detections for R-44 screen 1

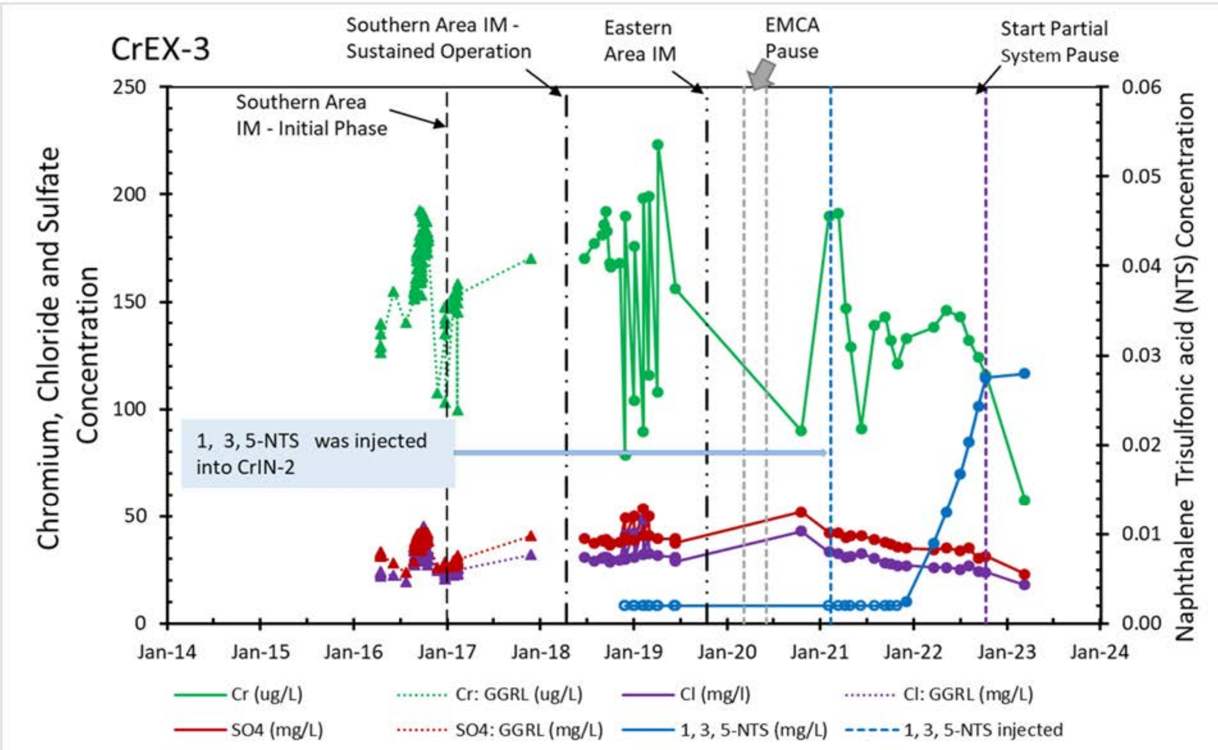

Notes: Open symbols represent nondetection results and solid symbols represent detection results at the plotted value. The background for chromium is 7.48 µg/L.

Figure 3.5-4 Time-series plots of tracer detections for CrEX-3

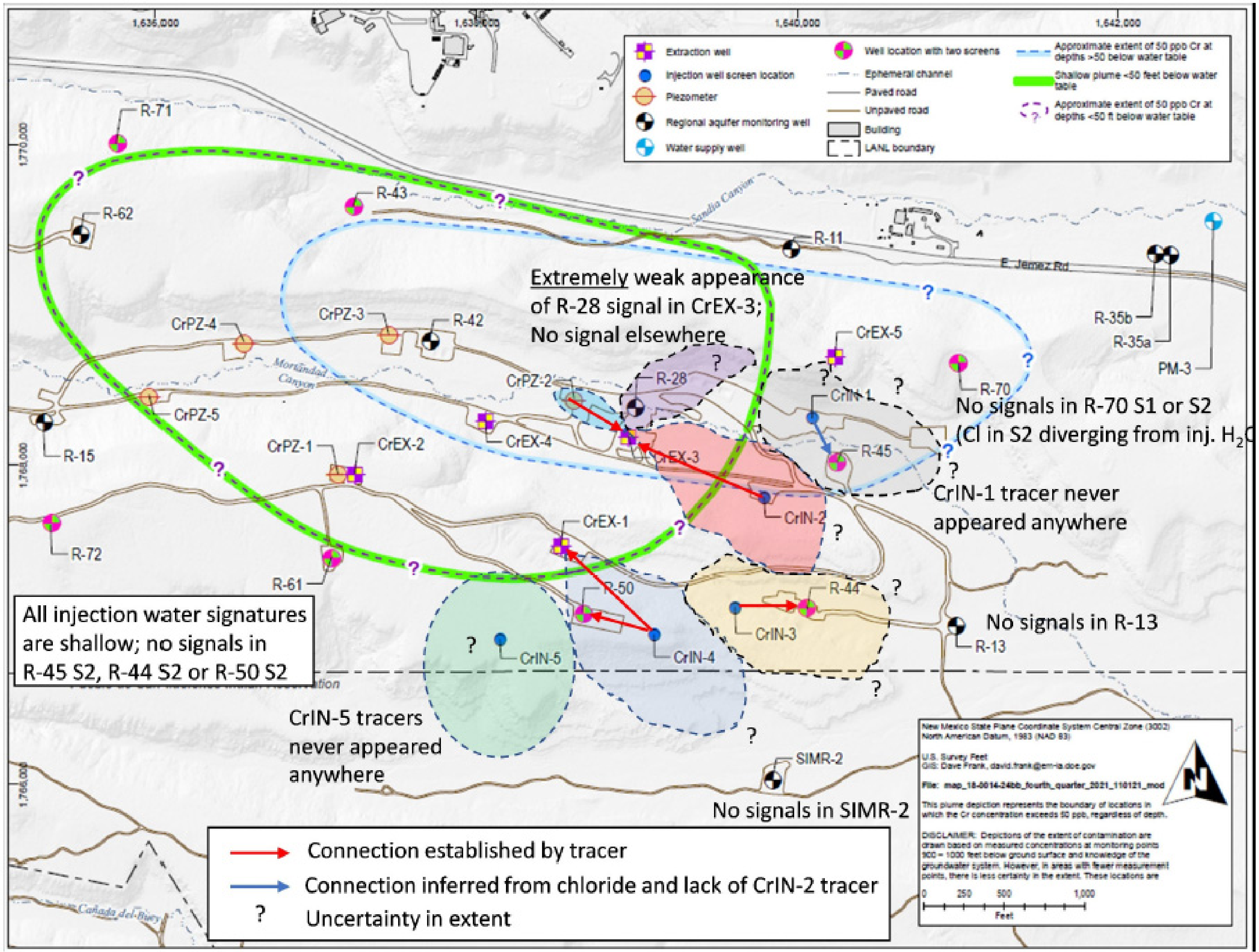

Notes: Depiction of IM injection flows and summary of other inferences from tracer and geochemical signatures. S1 = Screen 1; S2 = Screen 2.
Source: "Initial Five-Year Evaluation of the Interim Measures for Chromium Plume Control with an Assessment of Potential Modifications to Operations" (N3B 2022, 702597).

Figure 3.5-5 Tracer footprints

Table 2.1-1
Operations and Maintenance Activity Summary

Maintenance Date	Elements Involved	Operation/Maintenance Description
4/1/2022 through 4/3/2022	CrEX-1, CrEX-2, CrEX-3, CrEX-4, CrEX-5, CTUA, CTUC, CrIN-1, CrIN-2, CrIN-3, CrIN-4, CrIN-5	Extraction, treatment, and injection of treated groundwater occurred per operational plan.
4/3/2022	CTU-A	IX vessel exchanges were completed as follows because of an increase in the amount of hexavalent chromium at the primary IX vessel effluent as determined via field instrument analysis: • Treatment train A – replaced primary IX vessel with the secondary IX vessel; new secondary IX vessel installed. • Treatment train B – replaced primary IX vessel with the secondary IX vessel; new secondary IX vessel installed. • Treatment train C – replaced primary IX vessel with the secondary IX vessel; new secondary IX vessel installed. Both influent filter bags replaced.
4/3/2022 through 4/7/2022	CrEX-1, CrEX-2, CrEX-3, CrEX-4, CrEX-5, CTUA, CTUC, CrIN-1, CrIN-2, CrIN-3, CrIN-4, CrIN-5	Extraction, treatment, and injection of treated groundwater occurred per operational plan.
4/7/2022	CTUC CrEX-3, CrIN-3	CTUC Treatment train B turned off because of an increase in the amount of hexavalent chromium at the primary IX vessel effluent as determined via field instrument analysis. CrEX-3 and CrIN-3 turned off to balance flow.
4/8/2022 through 4/12/2022	CrEX-1, CrEX-2, CrEX-4, CrEX-5, CTUA, CTUC, CrIN-1, CrIN-2, CrIN-4, CrIN-5	Extraction, treatment, and injection of treated groundwater occurred per operational plan.
4/12/2022	CTUC CrEX-3, CrIN-3	IX vessel exchanges were completed as follows because of an increase in the amount of hexavalent chromium at the primary IX vessel effluent as determined via field instrument analysis: • Treatment train A – replaced primary IX vessel with the secondary IX vessel; new secondary IX vessel installed. • Treatment train B – replaced primary IX vessel with the secondary IX vessel; new secondary IX vessel installed. CrEX-3 and CrIN-3 turned on to balance flow.
4/12/2022 through 4/22/2022	CrEX-1, CrEX-2, CrEX-3, CrEX-4, CrEX-5, CTUA, CTUC, CrIN-1, CrIN-2, CrIN-3, CrIN-4, CrIN-5	Extraction, treatment, and injection of treated groundwater occurred per operational plan.
4/22/2022	CrEX-4, CrIN-1	CrEX-4 turned off in preparation for tracer test at R-42. CrIN-1 also turned off to balance flow.
4/22/2022 through 4/28/2022	CrEX-1, CrEX-2, CrEX-3, CrEX-5, CTUA, CTUC, CrIN-2, CrIN-3, CrIN-4, CrIN-5	Extraction, treatment, and injection of treated groundwater occurred per operational plan.

Table 2.1-1 (continued)

Maintenance Date	Elements Involved	Operation/Maintenance Description
4/28/2022	CrEX-4, CrIN-1	CrEX-4 turned on after tracer test at R-42. CrIN-1 also turned on to balance flow.
4/28/2022 through 5/6/2022	CrEX-1, CrEX-2, CrEX-3, CrEX-4, CrEX-5, CTUA, CTUC, CrIN-1, CrIN-2, CrIN-3, CrIN-4, CrIN-5	Extraction, treatment, and injection of treated groundwater occurred per operational plan.
5/6/2022	CrEX-4, CrIN-1	CrEX-4 turned off to monitor data from tracer test at R-42. CrIN-1 also turned off to balance flow.
5/6/2022 through 5/8/2022	CrEX-1, CrEX-2, CrEX-3, CrEX-5, CTUA, CTUC, CrIN-2, CrIN-3, CrIN-4, CrIN-5	Extraction, treatment, and injection of treated groundwater occurred per operational plan.
5/8/2022	CrEX-2, CrIN-3	CrEX-2 turned off because of wellhead air relief valve (ARV) issues. CrIN-3 also turned off to balance flow.
5/9/2022	CrEX-1, CrEX-3, CrEX-5, CTUA, CTUC, CrIN-2, CrIN-4, CrIN-5	Extraction, treatment, and injection of treated groundwater occurred per operational plan.
5/9/2022 through 5/16/2022	Entire system	Turned off all extraction wells, injection wells, and treatment units because of Cerro Pelado wildfire.
5/17/2022 through 5/19/2022	CrEX-1, CrEX-3, CrEX-4, CrEX-5, CTUA, CTUC, CrIN-1, CrIN-2, CrIN-4, CrIN-5	Extraction, treatment, and injection of treated groundwater occurred per operational plan.
5/19/2022	CrEX-2, CrIN-3	CrEX-2 turned on after ARV repaired. CrIN-3 also turned on to balance flow.
5/20/2022	Entire system	Turned off all extraction wells, injection wells, and treatment units because of remote access issues.
5/21/2022 through 5/22/2022	CrEX-3, CrEX-4, CrEX-5, CTUA, CTUC, CrIN-1, CrIN-2, CrIN-3	Extraction, treatment, and injection of treated groundwater occurred per operational plan.
5/23/2022	Entire system	System off because of an uninterruptible power supply unit issue at booster station.
5/24/2022	CrEX-1, CrEX-3, CrEX-4, CrEX-5, CTUA, CTUC, CrIN-1, CrIN-2, CrIN-4, CrIN-5	Extraction, treatment, and injection of treated groundwater occurred per operational plan.
5/25/2022	CTUA	IX vessel exchanges were completed as follows because of an increase in the amount of hexavalent chromium at the primary IX vessel effluent as determined via field instrument analysis: • Treatment train A – replaced primary IX vessel with the secondary IX vessel; new secondary IX vessel installed. • Treatment train B – replaced primary IX vessel with the secondary IX vessel; new secondary IX vessel installed. • Treatment train C – replaced primary IX vessel with the secondary IX vessel; new secondary IX vessel installed. Both influent filter bags replaced.

Table 2.1-1 (continued)

Maintenance Date	Elements Involved	Operation/Maintenance Description
5/25/2022 (continued)	CTUC	IX vessel exchanges were completed as follows because of an increase in the amount of hexavalent chromium at the primary IX vessel effluent as determined via field instrument analysis: • Treatment train A – replaced primary IX vessel with the secondary IX vessel; new secondary IX vessel installed. • Treatment train B – replaced primary IX vessel with the secondary IX vessel; new secondary IX vessel installed. Both influent bags replaced.
5/25/2022 through 6/8/2022	CrEX-1, CrEX-2, CrEX-3, CrEX-4, CrEX-5, CTUA, CTUC, CrIN-1, CrIN-2, CrIN-3, CrIN-4, CrIN-5	Extraction, treatment, and injection of treated groundwater occurred per operational plan.
6/8/2022	Entire system	Turned off all extraction wells, injection wells, and treatment units to replace uninterruptible power supply unit at the booster station.
6/9/2022 through 6/11/2022	CrEX-1, CrEX-2, CrEX-4, CrEX-5, CTUA, CTUC, CrIN-1, CrIN-2, CrIN-4, CrIN-5 CrEX-3, CrIN-3	Extraction, treatment, and injection of treated groundwater occurred per operational plan. CrEX-3 turned off because of transmitter issues. CrIN-3 also turned off to balance flow.
6/11/2022 through 6/22/2022	CrEX-1, CrEX-2, CrEX-4, CrEX-5, CTUA, CTUC, CrIN-1, CrIN-2, CrIN-3, CrIN-4, CrIN-5	Extraction, treatment, and injection of treated groundwater occurred per operational plan. CrIN-3 turned on to balance flow.
6/22/2022	CTUC	IX vessel exchanges were completed as follows because of an increase in the amount of hexavalent chromium at the primary IX vessel effluent as determined via field instrument analysis: • Treatment train A – replaced primary IX vessel with the secondary IX vessel; new secondary IX vessel installed. • Treatment train B – replaced primary IX vessel with the secondary IX vessel; new secondary IX vessel installed. Both influent bags replaced.
6/23/2022	CrEX-1, CrEX-2, CrEX-4, CrEX-5, CTUA, CTUC, CrIN-1, CrIN-2, CrIN-3, CrIN-4, CrIN-5	Extraction, treatment, and injection of treated groundwater occurred per operational plan.
6/24/2022	CrEX-3	CrEX-3 turned on after replacing transmitter.
6/24/2022 through 6/29/2022	CrEX-1, CrEX-2, CrEX-3, CrEX-4, CrEX-5, CTUA, CTUC, CrIN-1, CrIN-2, CrIN-3, CrIN-4, CrIN-5	Extraction, treatment, and injection of treated groundwater occurred per operational plan.
6/29/2022	CrEX-2	CrEX-2 turned off because of power failure.
6/29/2022 through 6/30/2022	CrEX-1, CrEX-3, CrEX-4, CrEX-5, CTUA, CTUC, CrIN-1, CrIN-2, CrIN-3, CrIN-4, CrIN-5	Extraction, treatment, and injection of treated groundwater occurred per operational plan.

Table 2.1-1 (continued)

Maintenance Date	Elements Involved	Operation/Maintenance Description
7/1/2022 through 7/6/2022	CrEX-1, CrEX-3, CrEX-4, CrEX-5, CTUA, CTUC, CrIN-1, CrIN-2, CrIN-3, CrIN-4, CrIN-5	Extraction, treatment, and injection of treated groundwater occurred per operational plan.
7/6/2022	CTUA CrEX-2	IX vessel exchanges were completed as follows because of an increase in the amount of hexavalent chromium at the primary IX vessel effluent as determined via field instrument analysis: • Treatment train A – replaced primary IX vessel with the secondary IX vessel; new secondary IX vessel installed. • Treatment train B – replaced primary IX vessel with the secondary IX vessel; new secondary IX vessel installed. • Treatment train C – replaced primary IX vessel with the secondary IX vessel; new secondary IX vessel installed. Both influent filter bags replaced. CrEX-2 turned on after uninterruptible power supply unit was replaced.
7/6/2022 through 7/23/2022	CrEX-1, CrEX-2, CrEX-3, CrEX-4, CrEX-5, CTUA, CTUC, CrIN-1, CrIN-2, CrIN-3, CrIN-4, CrIN-5	Extraction, treatment, and injection of treated groundwater occurred per operational plan.
7/23/2022	CTU-C	IX vessel exchanges were completed as follows because of an increase in the amount of hexavalent chromium at the primary IX vessel effluent as determined via field instrument analysis: • Treatment train A – replaced primary IX vessel with the secondary IX vessel; new secondary IX vessel installed. • Treatment train B – replaced primary IX vessel with the secondary IX vessel; new secondary IX vessel installed. Both influent filter bags replaced.
7/23/2022 through 7/30/2022	CrEX-1, CrEX-2, CrEX-3, CrEX-4, CrEX-5, CTUA, CTUC, CrIN-1, CrIN-2, CrIN-3, CrIN-4, CrIN-5	Extraction, treatment, and injection of treated groundwater occurred per operational plan.
7/30/2022	Entire system	All extraction wells, injection wells, and treatment units shut off because of power outage caused by thunderstorms.
7/31/2022	Entire system	All extraction wells, injection wells, and treatment units turned on.
7/31/2022 through 8/2/2022	CrEX-1, CrEX-2, CrEX-3, CrEX-4, CrEX-5, CTUA, CTUC, CrIN-1, CrIN-2, CrIN-3, CrIN-4, CrIN-5	Extraction, treatment, and injection of treated groundwater occurred per operational plan.
8/2/2022	CTUA	IX vessel exchanges were completed as follows because of an increase in the amount of hexavalent chromium at the primary IX vessel effluent as determined via field instrument analysis: • Treatment train A – replaced primary IX vessel with the secondary IX vessel; new secondary IX vessel installed. Both influent and all three effluent filter bags replaced.

Table 2.1-1 (continued)

Maintenance Date	Elements Involved	Operation/Maintenance Description
8/2/2022 through 8/10/2022	CrEX-1, CrEX-2, CrEX-3, CrEX-4, CrEX-5, CTUA, CTUC, CrIN-1, CrIN-2, CrIN-3, CrIN-4, CrIN-5	Extraction, treatment, and injection of treated groundwater occurred per operational plan.
8/10/2022	CTUA	IX vessel exchanges were completed as follows because of an increase in the amount of hexavalent chromium at the primary IX vessel effluent as determined via field instrument analysis: • Treatment train A – replaced primary IX vessel with the secondary IX vessel; new secondary IX vessel installed. • Treatment train B – replaced primary IX vessel with the secondary IX vessel; new secondary IX vessel installed. • Treatment train C – replaced primary IX vessel with the secondary IX vessel; new secondary IX vessel installed. Both influent filter bags replaced.
8/10/2022 through 8/27/2022	CrEX-1, CrEX-2, CrEX-3, CrEX-4, CrEX-5, CTUA, CTUC, CrIN-1, CrIN-2, CrIN-3, CrIN-4, CrIN-5	Extraction, treatment, and injection of treated groundwater occurred per operational plan.
8/27/2022	CTUC	IX vessel exchanges were completed as follows because of an increase in the amount of hexavalent chromium at the primary IX vessel effluent as determined via field instrument analysis: • Treatment train A – replaced primary IX vessel with the secondary IX vessel; new secondary IX vessel installed. • Treatment train B – replaced primary IX vessel with the secondary IX vessel; new secondary IX vessel installed.
8/27/2022 through 9/14/2022	CrEX-1, CrEX-2, CrEX-3, CrEX-4, CrEX-5, CTUA, CTUC, CrIN-1, CrIN-2, CrIN-3, CrIN-4, CrIN-5	Extraction, treatment, and injection of treated groundwater occurred per operational plan.
9/14/2022	CTUA	IX vessel exchanges were completed as follows because of an increase in the amount of hexavalent chromium at the primary IX vessel effluent as determined via field instrument analysis: • Treatment train A – replaced primary IX vessel with the secondary IX vessel; new secondary IX vessel installed. • Treatment train B – replaced primary IX vessel with the secondary IX vessel; new secondary IX vessel installed. • Treatment train C – replaced primary IX vessel with the secondary IX vessel; new secondary IX vessel installed. Both influent filter bags replaced.
9/14/2022 through 9/28/2022	CrEX-1, CrEX-2, CrEX-3, CrEX-4, CrEX-5, CTUA, CTUC, CrIN-1, CrIN-2, CrIN-3, CrIN-4, CrIN-5	Extraction, treatment, and injection of treated groundwater occurred per operational plan.
9/28/2022	CTU-C	IX vessel exchanges were completed as follows because of an increase in the amount of hexavalent chromium at the primary IX vessel effluent as determined via field instrument analysis: • Treatment train A – replaced primary IX vessel with the secondary IX vessel; new secondary IX vessel installed. • Treatment train B – replaced primary IX vessel with the secondary IX vessel; new secondary IX vessel installed. Both influent filter bags replaced.

Table 2.1-1 (continued)

Maintenance Date	Elements Involved	Operation/Maintenance Description
9/28/2022 through 9/30/2022	CrEX-1, CrEX-2, CrEX-3, CrEX-4, CrEX-5, CTUA, CTUC, CrIN-1, CrIN-2, CrIN-3, CrIN-4, CrIN-5	Extraction, treatment, and injection of treated groundwater occurred per operational plan.
10/1/2022 through 10/18/2022	CrEX-1, CrEX-2, CrEX-3, CrEX-4, CrEX-5, CTUA, CTUC, CrIN-1, CrIN-2, CrIN-3, CrIN-4, CrIN-5	Extraction, treatment, and injection of treated groundwater occurred per operational plan.
10/18/2022	CTUA	IX vessel exchanges were completed as follows because of an increase in the amount of hexavalent chromium at the primary IX vessel effluent as determined via field instrument analysis: • Treatment train A – replaced primary IX vessel with the secondary IX vessel; new secondary IX vessel installed. • Treatment train B – replaced primary IX vessel with the secondary IX vessel; new secondary IX vessel installed. • Treatment train C – replaced primary IX vessel with the secondary IX vessel; new secondary IX vessel installed. Both influent and all three effluent filter bags replaced.
10/18/2022 through 10/27/2022	CrEX-1, CrEX-2, CrEX-3, CrEX-4, CrEX-5, CTUA, CTUC, CrIN-1, CrIN-2, CrIN-3, CrIN-4, CrIN-5	Extraction, treatment, and injection of treated groundwater occurred per operational plan.
10/27/2022	CrEX-3	CrEX-3 turned off because of improper grounding observed during inspection.
10/28/2022	CrEX-1, CrEX-2, CrIN-1, CrIN-2, CrIN-3	CrEX-1 and CrEX-2 turned off because of improper grounding observed during inspection at CrEX-1. CrIN-1, CrIN-2, and CrIN-3 turned off to balance flow.
10/28/2022 through 11/2/2022	CrEX-4, CrEX-5, CTUA, CTUC, CrIN-4, CrIN-5	Extraction, treatment, and injection of treated groundwater occurred per operational plan.
11/2/2022	CTUC	IX vessel exchanges were completed as follows because of an increase in the amount of hexavalent chromium at the primary IX vessel effluent as determined via field instrument analysis: • Treatment train A – replaced primary IX vessel with the secondary IX vessel; new secondary IX vessel installed. • Treatment train B – replaced primary IX vessel with the secondary IX vessel; new secondary IX vessel installed. Both influent filter bags replaced.
11/2/2022 through 11/8/2022	CrEX-4, CrEX-5, CTUA, CTUC, CrIN-4, CrIN-5	Extraction, treatment, and injection of treated groundwater occurred per operational plan.
11/8/2022	CTUC	CTUC turned off because of reduced flow rates with CrEX-1, CrEX-2, and CrEX-3 turned off.
11/8/2022 through 11/23/2022	CrEX-4, CrEX-5, CTUA, CrIN-4, CrIN-5	Extraction, treatment, and injection of treated groundwater occurred per operational plan.
11/23/2022	CTUA	IX vessel exchanges were completed as follows because of an increase in the amount of hexavalent chromium at the primary IX vessel effluent as determined via field instrument analysis: • Treatment train A – replaced primary IX vessel with the secondary IX vessel; new secondary IX vessel installed.

Table 2.1-1 (continued)

Maintenance Date	Elements Involved	Operation/Maintenance Description
11/23/2022 through 12/1/2022	CrEX-4, CrEX-5, CTUA, CrIN-4, CrIN-5	Extraction, treatment, and injection of treated groundwater occurred per operational plan.
12/1/2022	CTUA	IX vessel exchanges were completed as follows because of an increase in the amount of hexavalent chromium at the primary IX vessel effluent as determined via field instrument analysis: • Treatment train B – replaced primary IX vessel with the secondary IX vessel; new secondary IX vessel installed. • Treatment train C – replaced primary IX vessel with the secondary IX vessel; new secondary IX vessel installed. Both influent and all three effluent filter bags replaced.
12/1/2022 through 12/31/2022	CrEX-4, CrEX-5, CTUA, CrIN-4, CrIN-5	Extraction, treatment, and injection of treated groundwater occurred per operational plan.
1/1/2023 through 1/3/2023	CrEX-4, CrEX-5, CTUA, CrIN-4, CrIN-5	Extraction, treatment, and injection of treated groundwater occurred per operational plan.
1/3/2023	CTUA	IX vessel exchanges were completed as follows because of an increase in the amount of hexavalent chromium at the primary IX vessel effluent as determined via field instrument analysis: • Treatment train A – replaced primary IX vessel with the secondary IX vessel; new secondary IX vessel installed. • Treatment train B – replaced primary IX vessel with the secondary IX vessel; new secondary IX vessel installed. • Treatment train C – replaced primary IX vessel with the secondary IX vessel; new secondary IX vessel installed. Both influent filter bags replaced.
1/3/2023 through 2/7/2023	CrEX-4, CrEX-5, CTUA, CrIN-4, CrIN-5	Extraction, treatment, and injection of treated groundwater occurred per operational plan.
2/7/2023	CTUA	IX vessel exchanges were completed as follows because of an increase in the amount of hexavalent chromium at the primary IX vessel effluent as determined via field instrument analysis: • Treatment train A – replaced primary IX vessel with the secondary IX vessel; new secondary IX vessel installed. • Treatment train B – replaced primary IX vessel with the secondary IX vessel; new secondary IX vessel installed. • Treatment train C – replaced primary IX vessel with the secondary IX vessel; new secondary IX vessel installed. Both influent filter bags replaced.
2/7/2023 through 3/14/2023	CrEX-4, CrEX-5, CTUA, CrIN-4, CrIN-5	Extraction, treatment, and injection of treated groundwater occurred per operational plan.
3/14/2023	CTUA	IX vessel exchanges were completed as follows because of an increase in the amount of hexavalent chromium at the primary IX vessel effluent as determined via field instrument analysis: • Treatment train A – replaced primary IX vessel with the secondary IX vessel; new secondary IX vessel installed. • Treatment train B – replaced primary IX vessel with the secondary IX vessel; new secondary IX vessel installed. • Treatment train C – replaced primary IX vessel with the secondary IX vessel; new secondary IX vessel installed. Both influent filter bags replaced.

Table 2.1-1 (continued)

Maintenance Date	Elements Involved	Operation/Maintenance Description
3/14/2023 through 3/31/2023	CrEX-4, CrEX-5, CTUA, CrIN-4, CrIN-5	Extraction, treatment, and injection of treated groundwater occurred per operational plan.
3/31/2023	CrEX-4, CrEX-5, CTUA, CrIN-4, CrIN-5	Extraction, treatment, and injection of treated groundwater suspended per NMED direction.

Table 2.1-2
Quarterly Volumes of Treated Effluent Injected

Period	CrIN-1 (gal.)	CrIN-2 (gal.)	CrIN-3 (gal.)	CrIN-4 (gal.)	CrIN-5 (gal.)
2nd Quarter 2022	5,771,600	6,703,736	3,906,744	6,502,612	6,472,477
3rd Quarter 2022	7,694,466	7,921,306	5,339,771	7,775,805	7,893,427
4th Quarter 2022	2,208,402	2,335,420	1,581,093	8,983,244	8,912,522
1st Quarter 2023	0	0	0	9,051,245	8,709,160

Table 2.1-3
Interim Measure Chromium Mass Removal Estimates

Quarter	Average Field Hexavalent Chromium (ppb)	Volume Extracted and Treated (gal.)	Chromium Removed				Difference between Field and Lab-based Values (%)
			Unfiltered, Field-based (lb)[a]	Unfiltered, Field-based (kg)	Unfiltered, Lab-based (kg)	Filtered, Lab-based (kg)	
Q4[b] 2016	180	665,267	1.0	0.5	—[c]	—	—
Q1[d] 2017	181	6,226,097	9.4	4.3	—	—	—
Q2[e] 2017	184	4,952,226	7.6	3.4	—	—	—
Q3[f] 2017	284	95,471	0.2	0.1	—	—	—
Q4 2017	237	5,599,138	11.1	5.0	—	—	—
Q1 2018	237	3,045,820	6.0	2.7	—	—	—
Q2 2018	227	13,360,000	25.3	11.5	—	—	—
Q3 2018	223	20,776,913	38.7	17.5	—	—	—
Q4 2018	206	20,442,977	35.1	15.9	—	—	—
Q1 2019	204	19,553,753	33.3	15.1	15.0	14.5	0.96%
Q2 2019	193	8,434,861	13.6	6.2	6.2	6.1	−0.69%
Q3 2019	190	15,574,060	24.7	11.2	10.4	10.5	6.98%
Q4 2019	208	24,066,243	41.8	18.9	17.5	17.8	7.76%
Q1 2020	215	27,198,274	48.8	22.1	21.7	21.8	2.02%
Q2 2020	0	0	0.0	0.0	0.0	0.0	n/a[g]
Q3 2020	183	14,980,866	22.9	10.4	9.5	9.4	9.37%
Q4 2020	223	24,336,996	45.3	20.5	18.4	18.1	10.9%
Q1 2021	201	25,836,790	43.3	19.7	18.2	18.1	7.84%
Q2 2021	217	35,220,210	63.8	28.9	26.3	26.6	9.36%
Q3 2021	223	29,251,727	54.4	24.7	22.2	22.3	10.4%
Q4 2021	214	26,523,831	47.4	21.5	19.5	19.4	10.0%
Q1 2022	212	12,133,616	21.5	9.7	8.9	8.7	8.06%
Q2 2022	159	28,975,770	38.4	17.4	16.2	16.1	7.10%
Q3 2022	164	35,911,739	49.1	22.3	20.3	20.2	9.62%
Q4 2022	183	23,861,852	36.4	16.5	14.6	14.8	12.3%
Q1 2023	193	17,988,049	29.0	13.1	Not available at time of calculation	Not available at time of calculation	Not available at time of calculation
Total	**n/a**	**445,012,546**	**748.1**	**339.3**	**n/a**	**n/a**	**7.47% (Q averages)**

[a] Kilogram-to-pound conversions are subject to rounding errors due to the number of significant figures used.

[b] Q4 = Quarter 4.

[c] — = Data not available.

[d] Q1 = Quarter 1.

[e] Q2 = Quarter 2.

[f] Q3 = Quarter 3.

[g] n/a = Not applicable.

Table 3.1-1
Frequency of Analytical Suites Collected at Performance Monitoring Locations, Piezometers, and Additional Monitoring Wells Addressed in this Report

Location	Metals	Low-Level Tritium	General Inorganics[a]	Naphthalene Sulfonate Tracers	Sodium Bromide Tracer	Sodium Perrhenate Tracer	Deuterated Water Tracer
Performance Monitoring Locations							
R-11	M[b]	S[c]	M	M	M	M	M
R-35a	M	S	M	M	M	M	M
R-35b	M	S	M	M	M	M	M
R-44 S1[d]	M	Q[e]	M	M	M	M	—[f]
R-44 S2[g]	M	Q	M	M	M	M	—
R-45 S1	M	Q	M	M	M	M	M
R-45 S2	M	Q	M	M	M	M	M
R-50 S1	M	Q	M	M	M	—	—
R-50 S2	M	Q	M	M	M	—	—
R-61 S1	M	Q	M	—	M	—	—
SIMR-2	M	S	M	M	M	—	—
Piezometers							
CrPZ-1	Q	Q	Q	—	Q	—	—
CrPZ-2a	Q	Q	Q	—	Q	—	—
CrPZ-3	Q	Q	Q	—	Q	—	—
CrPZ-4	Q	Q	Q	—	Q	—	—
CrPZ-5	Q	Q	Q	—	Q	—	—
Additional Wells							
R-42[h]	M	—	M	M[i]	M	M[i]	—
R-43 S1	Q	S	Q	—	Q	—	—
R-43 S2	Q	S	Q	—	Q	—	—
R-62	Q	Q	Q	—	Q	—	—
R-70 S1	M	Q	M	M	M	M	M
R-70 S2	M	Q	M	M	M	M	M
R-71 S1	M	Q	M	—	M	—	—
R-71 S2	M	Q	M	—	M	—	—
R-72 S1	M	Q	M	—	M	—	—
R-72 S2	M	Q	M	—	M	—	—

Note: R-28 geochemistry results are not considered as representative of the aquifer and are not included in this table or in Appendix B.

[a] Includes nitrate plus nitrite as nitrogen, sulfate, and perchlorate.

[b] M = Monthly.

[c] S = Semiannually.

[d] S1= Screen 1.

[e] Q = Quarterly.

[f] — = Not analyzed.

[g] S2 = Screen 2.

[h] Monthly pilot amendment testing at R-42 began in November 2021 under the NMED-approved work plan. Upon evaluation of the hydrogeochemical results, R-42 will be included as part of IFGMP sampling for MY 2024, pending MY 2024 IFGMP approval.

[I] Sampling occurred April through May 2022.

Table 3.2-1
Mann-Kendall Test Results for Chromium Plume Centroid Wells

CrEX-3 Mann-Kendall Test Results						
Test	Phase 1		Phase 2		Phase 3	
	Screen 1	Screen 2	Screen 1	Screen 2	Screen 1	Screen 2
Chromium Concentration at CrEX-3 Mann-Kendall Test						
M-K Test Value (S)	n/a*	n/a	−9	n/a	−24	n/a
Critical Value (0.05)	n/a	n/a	0.411	n/a	0.174	n/a
Standard Deviation of S	n/a	n/a	30.81	n/a	24.23	n/a
Standardized Value of S	n/a	n/a	−0.26	n/a	−0.949	n/a
Approximate p-value	n/a	n/a	0.398	n/a	0.171	n/a
Concentration Trend	n/a	n/a	None	n/a	Decreasing	n/a
Chloride Concentration at CrEX-3 Mann-Kendall Test						
M-K Test Value (S)	n/a	n/a	38	n/a	−120	n/a
Critical Value (0.05)	n/a	n/a	0.144	n/a	0	n/a
Standard Deviation of S	n/a	n/a	35.38	n/a	24.23	n/a
Standardized Value of S	n/a	n/a	1.046	n/a	−4.91	n/a
Approximate p-value	n/a	n/a	0.148	n/a	4.55E−07	n/a
Concentration Trend	n/a	n/a	None	n/a	Decreasing	n/a
Sulfate Concentration at CrEX-3 Mann-Kendall Test						
M-K Test Value (S)	n/a	n/a	33	n/a	−120	n/a
Critical Value (0.05)	n/a	n/a	0.177	n/a	0	n/a
Standard Deviation of S	n/a	n/a	33.07	n/a	24.23	n/a
Standardized Value of S	n/a	n/a	0.968	n/a	−4.91	n/a
Approximate p-value	n/a	n/a	0.167	n/a	4.55E−07	n/a
Concentration Trend	n/a	n/a	None	n/a	Decreasing	n/a
Perchlorate Concentration at CrEX-3 Mann-Kendall Test						
M-K Test Value (S)	0	n/a	26	n/a	−95	n/a
Critical Value (0.05)	0.54	n/a	0.234	n/a	0	n/a
Standard Deviation of S	9.592	n/a	35.45	n/a	24.26	n/a
Standardized Value of S	n/a	n/a	0.705	n/a	−3.875	n/a
Approximate p-value	n/a	n/a	0.24	n/a	5.32E−05	n/a
Concentration Trend	None	n/a	None	n/a	Decreasing	n/a
Nitrate Concentration at CrEX-3 Mann-Kendall Test						
M-K Test Value (S)	n/a	n/a	24	n/a	−83	n/a
Critical Value (0.05)	n/a	n/a	0.23	n/a	0	n/a
Standard Deviation of S	n/a	n/a	30.82	n/a	24.26	n/a
Standardized Value of S	n/a	n/a	0.746	n/a	−3.381	n/a
Approximate p-value	n/a	n/a	0.228	n/a	3.62E−04	n/a
Concentration Trend	n/a	n/a	None	n/a	Decreasing	n/a

Table 3.2-1 (continued)

CrEX-4 Mann-Kendall Test Results						
Test	Phase 1		Phase 2		Phase 3	
	Screen 1	Screen 2	Screen 1	Screen 2	Screen 1	Screen 2
Chromium Concentration at CrEX-4 Mann-Kendall Test						
M-K Test Value (S)	n/a	n/a	n/a	n/a	−179	n/a
Critical Value (0.05)	n/a	n/a	n/a	n/a	0	n/a
Standard Deviation of S	n/a	n/a	n/a	n/a	35.46	n/a
Standardized Value of S	n/a	n/a	n/a	n/a	−5.019	n/a
Approximate p-value	n/a	n/a	n/a	n/a	2.59E−07	n/a
Concentration Trend	n/a	n/a	n/a	n/a	Decreasing	n/a
Chloride Concentration at CrEX-4 Mann-Kendall Test						
M-K Test Value (S)	n/a	n/a	n/a	n/a	−116	n/a
Critical Value (0.05)	n/a	n/a	n/a	n/a	0	n/a
Standard Deviation of S	n/a	n/a	n/a	n/a	35.38	n/a
Standardized Value of S	n/a	n/a	n/a	n/a	−3.25	n/a
Approximate p-value	n/a	n/a	n/a	n/a	5.77E−04	n/a
Concentration Trend	n/a	n/a	n/a	n/a	Decreasing	n/a
Sulfate Concentration at CrEX-4 Mann-Kendall Test						
M-K Test Value (S)	n/a	n/a	n/a	n/a	−148	n/a
Critical Value (0.05)	n/a	n/a	n/a	n/a	0	n/a
Standard Deviation of S	n/a	n/a	n/a	n/a	35.45	n/a
Standardized Value of S	n/a	n/a	n/a	n/a	−4.147	n/a
Approximate p-value	n/a	n/a	n/a	n/a	1.69E−05	n/a
Concentration Trend	n/a	n/a	n/a	n/a	Decreasing	n/a
Perchlorate Concentration at CrEX-4 Mann-Kendall Test						
M-K Test Value (S)	n/a	n/a	n/a	n/a	−143	n/a
Critical Value (0.05)	n/a	n/a	n/a	n/a	0	n/a
Standard Deviation of S	n/a	n/a	n/a	n/a	35.44	n/a
Standardized Value of S	n/a	n/a	n/a	n/a	−4.007	n/a
Approximate p-value	n/a	n/a	n/a	n/a	3.07E−05	n/a
Concentration Trend	n/a	n/a	n/a	n/a	Decreasing	n/a
Nitrate Concentration at CrEX-4 Mann-Kendall Test						
M-K Test Value (S)	n/a	n/a	n/a	n/a	−187	n/a
Critical Value (0.05)	n/a	n/a	n/a	n/a	0	n/a
Standard Deviation of S	n/a	n/a	n/a	n/a	35.46	n/a
Standardized Value of S	n/a	n/a	n/a	n/a	−5.245	n/a
Approximate p-value	n/a	n/a	n/a	n/a	7.82E−08	n/a
Concentration Trend	n/a	n/a	n/a	n/a	Decreasing	n/a

* n/a = Not applicable.

Table 3.2-2
Mann-Kendall Test Results for Chromium Plume Southern Wells

R-15 Mann-Kendall Test Results						
Test	Phase 1		Phase 2		Phase 3	
	Screen 1	Screen 2	Screen 1	Screen 2	Screen 1	Screen 2
Chromium Concentration at R-15 Mann-Kendall Test						
M-K Test Value (S)	156	n/a*	−56	n/a	31	n/a
Critical Value (0.05)	1.645	n/a	n/a	n/a	0.118	n/a
Standard Deviation of S	55.98	n/a	18.17	n/a	24.16	n/a
Standardized Value of S	2.769	n/a	−3.028	n/a	1.242	n/a
Approximate p-value	2.81E−03	n/a	1.23E−03	n/a	0.107	n/a
Concentration Trend	Increasing	n/a	Decreasing	n/a	None	n/a
Chloride Concentration at R-15 Mann-Kendall Test						
M-K Test Value (S)	−38	n/a	3	n/a	−34	n/a
Critical Value (0.05)	−1.645	n/a	n/a	n/a	0.088	n/a
Standard Deviation of S	53.21	n/a	18.27	n/a	24.23	n/a
Standardized Value of S	−0.695	n/a	0.109	n/a	−1.362	n/a
Approximate p-value	0.243	n/a	4.56E−01	n/a	0.0867	n/a
Concentration Trend	None	n/a	None	n/a	None	n/a
Sulfate Concentration at R-15 Mann-Kendall Test						
M-K Test Value (S)	52	n/a	−20	n/a	−28	n/a
Critical Value (0.05)	1.645	n/a	n/a	n/a	0.135	n/a
Standard Deviation of S	53.25	n/a	18.24	n/a	24.18	n/a
Standardized Value of S	0.958	n/a	−1.042	n/a	−1.117	n/a
Approximate p-value	0.169	n/a	1.49E−01	n/a	0.132	n/a
Concentration Trend	None	n/a	None	n/a	None	n/a
Perchlorate Concentration at R-15 Mann-Kendall Test						
M-K Test Value (S)	250	n/a	26	n/a	−10	n/a
Critical Value (0.05)	1.645	n/a	0.064	n/a	0.358	n/a
Standard Deviation of S	53.29	n/a	16.39	n/a	24.14	n/a
Standardized Value of S	4.672	n/a	1.525	n/a	−0.373	n/a
Approximate p-value	1.49E−06	n/a	0.0636	n/a	0.355	n/a
Concentration Trend	Increasing	n/a	None	n/a	None	n/a
Nitrate Concentration at R-15 Mann-Kendall Test						
M-K Test Value (S)	25	n/a	7	n/a	49	n/a
Critical Value (0.05)	1.645	n/a	0.383	n/a	0.023	n/a
Standard Deviation of S	56.03	n/a	16.36	n/a	24.08	n/a
Standardized Value of S	0.428	n/a	0.367	n/a	1.994	n/a
Approximate p-value	0.334	n/a	0.357	n/a	0.0231	n/a
Concentration Trend	None	n/a	None	n/a	Increasing	n/a

Table 3.2-2 (continued)

R-44 Mann-Kendall Test Results						
Test	Phase 1		Phase 2		Phase 3	
	Screen 1	Screen 2	Screen 1	Screen 2	Screen 1	Screen 2
Chromium Concentration at R-44 Mann-Kendall Test						
M-K Test Value (S)	302	33	−319	−194	−472	243
Critical Value (0.05)	1.645	1.645	−1.645	−1.645	−1.645	1.645
Standard Deviation of S	61.63	70.42	53.28	53.31	73.29	70.38
Standardized Value of S	4.884	0.454	−5.968	−3.62	−6.427	3.438
Approximate p-value	5.21E−07	0.352	1.20E−09	1.47E−04	6.53E−11	2.93E−04
Concentration Trend	Increasing	None	Decreasing	Decreasing	Decreasing	Increasing
Chloride Concentration at R-44 Mann-Kendall Test						
M-K Test Value (S)	212	213	320	−168	349	390
Critical Value (0.05)	1.645	1.645	1.645	−1.645	1.645	1.645
Standard Deviation of S	50.55	58.76	53.27	53.17	73.32	70.38
Standardized Value of S	4.174	3.608	5.988	−3.141	4.746	5.527
Approximate p-value	1.50E−05	1.54E−04	1.06E−09	8.43E−04	1.04E−06	1.63E−08
Concentration Trend	Increasing	Increasing	Increasing	Decreasing	Increasing	Increasing
Sulfate Concentration at R-44 Mann-Kendall Test						
M-K Test Value (S)	152	−130	309	−244	329	342
Critical Value (0.05)	1.645	−1.645	1.645	−1.645	1.645	1.645
Standard Deviation of S	50.6	58.81	53.26	55.99	73.24	70.36
Standardized Value of S	2.984	−2.193	5.783	−4.34	4.479	4.846
Approximate p-value	0.00142	0.0141	3.68E−09	7.12E−06	3.76E−06	6.28E−07
Concentration Trend	Increasing	Decreasing	Increasing	Decreasing	Increasing	Increasing
Perchlorate Concentration at R-44 Mann-Kendall Test						
M-K Test Value (S)	108	−32	−210	−70	327	120
Critical Value (0.05)	1.645	−1.645	−1.645	−1.645	1.645	1.645
Standard Deviation of S	47.92	55.98	53.29	53.25	73.38	70.24
Standardized Value of S	2.233	−0.554	−3.922	−1.296	4.442	1.694
Approximate p-value	0.0128	0.29	4.39E−05	0.0975	4.45E−06	0.0451
Concentration Trend	Increasing	None	Decreasing	None	Increasing	Increasing
Nitrate Concentration at R-44 Mann-Kendall Test						
M-K Test Value (S)	100	52	294	−98	396	337
Critical Value (0.05)	1.645	1.645	1.645	−-1.645	1.645	1.645
Standard Deviation of S	47.89	56.04	53.25	53.29	73.39	70.4
Standardized Value of S	2.067	0.91	5.503	−1.82	5.382	4.773
Approximate p-value	0.0194	0.181	1.87E−08	0.0344	3.68E−08	9.09E−07
Concentration Trend	Increasing	None	Increasing	Decreasing	Increasing	Increasing

Table 3.2-2 (continued)

R-44 Mann-Kendall Test Results						
Test	Phase 1		Phase 2		Phase 3	
	Screen 1	Screen 2	Screen 1	Screen 2	Screen 1	Screen 2
Chromium Concentration at R-50 Mann-Kendall Test						
M-K Test Value (S)	433	−57	−285	−21	−522	−53
Critical Value (0.05)	1.645	−1.645	−1.645	−1.645	−1.645	−1.645
Standard Deviation of S	73.4	56.01	56.01	55.99	73.42	73.37
Standardized Value of S	5.886	−1.168	−5.07	−0.357	−7.096	−0.709
Approximate p-value	1.98E−09	0.121	1.99E−07	0.36	6.40E−13	0.239
Concentration Trend	Increasing	None	Decreasing	None	Decreasing	None
Chloride Concentration at R-50 Mann-Kendall Test						
M-K Test Value (S)	299	−112	478	174	357	−74
Critical Value (0.05)	1.645	−1.645	1.645	1.645	1.645	−1.645
Standard Deviation of S	67.46	52.92	70.38	55.77	70.32	67.28
Standardized Value of S	4.418	−2.097	6.778	3.102	5.063	−1.085
Approximate p-value	4.99E−06	0.018	6.09E−12	9.62E−04	2.07E−07	0.139
Concentration Trend	Increasing	Decreasing	Increasing	Increasing	Increasing	None
Sulfate Concentration at R-50 Mann-Kendall Test						
M-K Test Value (S)	212	−216	334	−100	332	34
Critical Value (0.05)	1.645	−1.645	1.645	−1.645	1.645	1.645
Standard Deviation of S	67.3	53.19	55.98	55.81	70.18	67.33
Standardized Value of S	3.135	−4.042	5.948	−1.774	4.716	0.49
Approximate p-value	8.58E−04	2.65E−05	1.35E−09	0.038	1.20E−06	0.312
Concentration Trend	Increasing	Decreasing	Increasing	Decreasing	Increasing	None
Perchlorate Concentration at R-50 Mann-Kendall Test						
M-K Test Value (S)	344	−81	−349	74	137	−113
Critical Value (0.05)	1.645	−1.645	−1.645	1.645	1.645	−1.645
Standard Deviation of S	70.36	56	70.4	56.02	70.37	67.41
Standardized Value of S	4.875	−1.429	−4.943	1.303	1.933	−1.662
Approximate p-value	5.44E−07	0.0766	3.84E−07	0.0963	0.0266	0.0483
Concentration Trend	Increasing	None	Decreasing	None	Increasing	Decreasing
Nitrate Concentration at R-50 Mann-Kendall Test						
M-K Test Value (S)	388	−82	232	103	458	391
Critical Value (0.05)	1.645	−1.645	1.645	1.645	1.645	1.645
Standard Deviation of S	70.35	56.02	55.96	55.96	73.36	73.35
Standardized Value of S	5.501	−1.446	4.128	1.823	6.229	5.317
Approximate p-value	1.88E−08	0.0741	1.83E−05	0.0342	2.34E−10	5.27E−08
Concentration Trend	Increasing	None	Increasing	Increasing	Increasing	Increasing

Table 3.2-2 (continued)

R-44 Mann-Kendall Test Results						
Test	Phase 1		Phase 2		Phase 3	
	Screen 1	Screen 2	Screen 1	Screen 2	Screen 1	Screen 2
Chromium Concentration at R-61 Mann-Kendall Test						
M-K Test Value (S)	94	n/a	116	n/a	403	n/a
Critical Value (0.05)	n/a	n/a	1.645	n/a	1.645	n/a
Standard Deviation of S	24.23	n/a	50.55	n/a	82.65	n/a
Standardized Value of S	3.755	n/a	2.275	n/a	4.864	n/a
Approximate p-value	8.67E−05	n/a	0.0115	n/a	5.76E−07	n/a
Concentration Trend	Increasing	n/a	Increasing	n/a	Increasing	n/a
Chloride Concentration at R-61 Mann-Kendall Test						
M-K Test Value (S)	−13	n/a	212	n/a	426	n/a
Critical Value (0.05)	0.327	n/a	1.645	n/a	1.645	n/a
Standard Deviation of S	26.22	n/a	50.5	n/a	82.64	n/a
Standardized Value of S	−0.458	n/a	4.178	n/a	5.143	n/a
Approximate p-value	0.324	n/a	1.47E−05	n/a	1.35E−07	n/a
Concentration Trend	None	n/a	Increasing	n/a	Increasing	n/a
Sulfate Concentration at R-61 Mann-Kendall Test						
M-K Test Value (S)	43	n/a	240	n/a	467	n/a
Critical Value (0.05)	0.056	n/a	1.645	n/a	1.645	n/a
Standard Deviation of S	26.36	n/a	50.6	n/a	82.64	n/a
Standardized Value of S	1.593	n/a	4.724	n/a	5.639	n/a
Approximate p-value	0.0556	n/a	1.16E−08	n/a	8.56E−09	n/a
Concentration Trend	None	n/a	Increasing	n/a	Increasing	n/a
Perchlorate Concentration at R-61 Mann-Kendall Test						
M-K Test Value (S)	115	n/a	39	n/a	−10	n/a
Critical Value (0.05)	0	n/a	1.645	n/a	−1.645	n/a
Standard Deviation of S	26.4	n/a	47.93	n/a	82.48	n/a
Standardized Value of S	4.318	n/a	0.793	n/a	−0.109	n/a
Approximate p-value	7.87E−06	n/a	0.214	n/a	0.457	n/a
Concentration Trend	Increasing	n/a	None	n/a	None	n/a
Nitrate Concentration at R-61 Mann-Kendall Test						
M-K Test Value (S)	122	n/a	204	n/a	403	n/a
Critical Value (0.05)	0	n/a	1.645	n/a	1.645	n/a
Standard Deviation of S	26.38	n/a	50.55	n/a	82.59	n/a
Standardized Value of S	4.586	n/a	4.016	n/a	4.867	n/a
Approximate p-value	2.25E−06	n/a	2.96E−05	n/a	5.65E−07	n/a
Concentration Trend	Increasing	n/a	Increasing	n/a	Increasing	n/a

Table 3.2-2 (continued)

R-44 Mann-Kendall Test Results						
Test	Phase 1		Phase 2		Phase 3	
	Screen 1	Screen 2	Screen 1	Screen 2	Screen 1	Screen 2
Chromium Concentration at CrEX-1 Mann-Kendall Test						
M-K Test Value (S)	27	n/a	−64	n/a	−348	n/a
Critical Value (0.05)	0.234	n/a	0	n/a	−1.645	n/a
Standard Deviation of S	33.04	n/a	18.17	n/a	56.01	n/a
Standardized Value of S	0.787	n/a	−3.468	n/a	−6.196	n/a
Approximate p-value	0.216	n/a	2.62E−04	n/a	2.90E−10	n/a
Concentration Trend	None	n/a	Decreasing	n/a	Decreasing	n/a
Chloride Concentration at CrEX-1 Mann-Kendall Test						
M-K Test Value (S)	n/a	n/a	9	n/a	97	n/a
Critical Value (0.05)	n/a	n/a	0.388	n/a	1.645	n/a
Standard Deviation of S	n/a	n/a	24.21	n/a	40.15	n/a
Standardized Value of S	n/a	n/a	0.33	n/a	2.391	n/a
Approximate p-value	n/a	n/a	0.371	n/a	0.00839	n/a
Concentration Trend	n/a	n/a	None	n/a	Increasing	n/a
Sulfate Concentration at CrEX-1 Mann-Kendall Test						
M-K Test Value (S)	n/a	n/a	−46	n/a	−195	n/a
Critical Value (0.05)	n/a	n/a	0.032	n/a	−1.645	n/a
Standard Deviation of S	n/a	n/a	24.19	n/a	40.22	n/a
Standardized Value of S	n/a	n/a	−1.86	n/a	−4.823	n/a
Approximate p-value	n/a	n/a	0.0314	n/a	7.06E−07	n/a
Concentration Trend	n/a	n/a	Decreasing	n/a	Decreasing	n/a
Perchlorate Concentration at CrEX-1 Mann-Kendall Test						
M-K Test Value (S)	−29	n/a	−181	n/a	−173	n/a
Critical Value (0.05)	−1.645	n/a	−1.645	n/a	−1.645	n/a
Standard Deviation of S	50.61	n/a	37.86	n/a	40.3	n/a
Standardized Value of S	−0.553	n/a	−4.754	n/a	−4.268	n/a
Approximate p-value	0.29	n/a	9.98E−07	n/a	9.88E−06	n/a
Concentration Trend	None	n/a	Decreasing	n/a	Decreasing	n/a
Nitrate Concentration at CrEX-1 Mann-Kendall Test						
M-K Test Value (S)	37	n/a	12	n/a	−27	n/a
Critical Value (0.05)	0.13	n/a	0.259	n/a	−1.645	n/a
Standard Deviation of S	15.91	n/a	18.24	n/a	40.3	n/a
Standardized Value of S	2.263	n/a	0.603	n/a	−0.645	n/a
Approximate p-value	0.0118	n/a	0.273	n/a	0.259	n/a
Concentration Trend	None	n/a	None	n/a	None	n/a

Table 3.2-2 (continued)

R-44 Mann-Kendall Test Results						
Test	Phase 1		Phase 2		Phase 3	
	Screen 1	Screen 2	Screen 1	Screen 2	Screen 1	Screen 2
Chromium Concentration at CrEX-2 Mann-Kendall Test						
M-K Test Value (S)	n/a	n/a	−48	n/a	−251	n/a
Critical Value (0.05)	n/a	n/a	0.023	n/a	−1.645	n/a
Standard Deviation of S	n/a	n/a	24.19	n/a	56.01	n/a
Standardized Value of S	n/a	n/a	−1.943	n/a	−4.463	n/a
Approximate p-value	n/a	n/a	0.026	n/a	4.04E−06	n/a
Concentration Trend	n/a	n/a	Decreasing	n/a	Decreasing	n/a
Chloride Concentration at CrEX-2 Mann-Kendall Test						
M-K Test Value (S)	n/a	n/a	−46	n/a	−262	n/a
Critical Value (0.05)	n/a	n/a	0.021	n/a	−1.645	n/a
Standard Deviation of S	n/a	n/a	22.17	n/a	55.98	n/a
Standardized Value of S	n/a	n/a	−2.03	n/a	−4.662	n/a
Approximate p-value	n/a	n/a	0.0212	n/a	1.56E−06	n/a
Concentration Trend	n/a	n/a	Decreasing	n/a	Decreasing	n/a
Sulfate Concentration at CrEX-2 Mann-Kendall Test						
M-K Test Value (S)	n/a	n/a	−55	n/a	−278	n/a
Critical Value (0.05)	n/a	n/a	0.014	n/a	−1.645	n/a
Standard Deviation of S	n/a	n/a	24.26	n/a	55.93	n/a
Standardized Value of S	n/a	n/a	−2.226	n/a	−4.953	n/a
Approximate p-value	n/a	n/a	0.013	n/a	3.66E−07	n/a
Concentration Trend	n/a	n/a	Decreasing	n/a	Decreasing	n/a
Perchlorate Concentration at CrEX-2 Mann-Kendall Test						
M-K Test Value (S)	n/a	n/a	44	n/a	−309	n/a
Critical Value (0.05)	n/a	n/a	0.038	n/a	−1.645	n/a
Standard Deviation of S	n/a	n/a	24.28	n/a	56.03	n/a
Standardized Value of S	n/a	n/a	1.771	n/a	−5.497	n/a
Approximate p-value	n/a	n/a	0.0383	n/a	1.93E−08	n/a
Concentration Trend	n/a	n/a	Increasing	n/a	Decreasing	n/a
Nitrate Concentration at CrEX-2 Mann-Kendall Test						
M-K Test Value (S)	n/a	n/a	−11	n/a	−155	n/a
Critical Value (0.05)	n/a	n/a	0.295	n/a	−1.645	n/a
Standard Deviation of S	n/a	n/a	18.27	n/a	55.97	n/a
Standardized Value of S	n/a	n/a	−0.547	n/a	−2.751	n/a
Approximate p-value	n/a	n/a	0.292	n/a	0.00297	n/a
Concentration Trend	n/a	n/a	None	n/a	Decreasing	n/a

* n/a = Not applicable.

Table 3.2-3
Mann-Kendall Test Results for Chromium Plume Northeastern Wells

R-11 Mann-Kendall Test Results						
Test	Phase 1		Phase 2		Phase 3	
	Screen 1	Screen 2	Screen 1	Screen 2	Screen 1	Screen 2
Chromium Concentration at R-11 Mann-Kendall Test						
M-K Test Value (S)	200	n/a*	−143	n/a	−36	n/a
Critical Value (0.05)	1.645	n/a	n/a	n/a	−1.645	n/a
Standard Deviation of S	70.41	n/a	35.46	n/a	92.18	n/a
Standardized Value of S	2.826	n/a	−4.004	n/a	−0.38	n/a
Approximate p-value	2.35E−03	n/a	3.11E−05	n/a	0.352	n/a
Concentration Trend	Increasing	n/a	Decreasing	n/a	None	n/a
Chloride Concentration at R-11 Mann-Kendall Test						
M-K Test Value (S)	200	n/a	−58	n/a	−126	n/a
Critical Value (0.05)	1.645	n/a	n/a	n/a	−1.645	n/a
Standard Deviation of S	67.43	n/a	35.42	n/a	92.2	n/a
Standardized Value of S	2.951	n/a	−1.609	n/a	−1.356	n/a
Approximate p-value	0.00158	n/a	5.38E−02	n/a	0.0876	n/a
Concentration Trend	Increasing	n/a	None	n/a	None	n/a
Sulfate Concentration at R-11 Mann-Kendall Test						
M-K Test Value (S)	215	n/a	−4	n/a	−79	n/a
Critical Value (0.05)	1.645	n/a	0.456	n/a	−1.645	n/a
Standard Deviation of S	67.43	n/a	35.16	n/a	92.22	n/a
Standardized Value of S	3.174	n/a	−0.0853	n/a	−0.846	n/a
Approximate p-value	7.52E−04	n/a	0.466	n/a	0.199	n/a
Concentration Trend	Increasing	n/a	None	n/a	None	n/a
Perchlorate Concentration at R-11 Mann-Kendall Test						
M-K Test Value (S)	86	n/a	−75	n/a	−9	n/a
Critical Value (0.05)	1.645	n/a	0.018	n/a	−1.645	n/a
Standard Deviation of S	67.45	n/a	35.46	n/a	92.25	n/a
Standardized Value of S	1.26	n/a	−2.087	n/a	−0.0867	n/a
Approximate p-value	0.104	n/a	0.0185	n/a	0.465	n/a
Concentration Trend	None	n/a	Decreasing	n/a	None	n/a
Nitrate Concentration at R-11 Mann-Kendall Test						
M-K Test Value (S)	138	n/a	30	n/a	447	n/a
Critical Value (0.05)	1.645	n/a	0.201	n/a	1.645	n/a
Standard Deviation of S	64.51	n/a	35.45	n/a	92.2	n/a
Standardized Value of S	2.124	n/a	0.818	n/a	4.837	n/a
Approximate p-value	0.0168	n/a	0.207	n/a	6.59E−07	n/a
Concentration Trend	Increasing	n/a	None	n/a	Increasing	n/a

Table 3.2-3 (continued)

R-45 Mann-Kendall Test Results						
Test	Phase 1		Phase 2		Phase 3	
	Screen 1	Screen 2	Screen 1	Screen 2	Screen 1	Screen 2
Chromium Concentration at R-45 Mann-Kendall Test						
M-K Test Value (S)	418	339	−237	228	−549	477
Critical Value (0.05)	1.645	1.645	−1.645	1.645	1.645	−1.645
Standard Deviation of S	58.79	56.05	53.28	58.81	73.41	70.4
Standardized Value of S	7.093	6.173	−4.429	3.86	−7.465	6.761
Approximate p-value	6.58E−13	3.35E−10	4.73E−06	5.67E−06	4.17E−14	6.84E−12
Concentration Trend	Increasing	Increasing	Decreasing	Increasing	Decreasing	Increasing
Chloride Concentration at R-45 Mann-Kendall Test						
M-K Test Value (S)	320	262	−242	232	490	518
Critical Value (0.05)	1.645	1.645	−1.645	1.645	1.645	1.645
Standard Deviation of S	47.96	47.94	53.31	56.04	73.38	70.41
Standardized Value of S	6.652	5.445	−4.521	4.122	6.664	7.343
Approximate p-value	1.45E−11	2.60E−08	3.08E−06	1.88E−05	1.329E−11	1.045E−13
Concentration Trend	Increasing	Increasing	Decreasing	Increasing	Increasing	Increasing
Sulfate Concentration at R-45 Mann-Kendall Test						
M-K Test Value (S)	321	−80	−271	214	439	457
Critical Value (0.05)	1.645	−1.645	−1.645	1.645	1.645	1.645
Standard Deviation of S	47.95	47.96	53.28	56.04	73.32	70.4
Standardized Value of S	6.674	−1.647	−5.067	3.801	5.974	6.477
Approximate p-value	1.25E−11	0.0498	2.02E−07	7.21E−05	1.1582E−09	4.673E−11
Concentration Trend	Increasing	Decreasing	Decreasing	Increasing	Increasing	Increasing
Perchlorate Concentration at R-45 Mann-Kendall Test						
M-K Test Value (S)	207	166	−102	88	27	193
Critical Value (0.05)	1.645	1.645	−1.645	1.645	1.645	1.645
Standard Deviation of S	45.35	45.31	53.27	56.02	73.4	73.36
Standardized Value of S	4.543	3.642	−1.896	1.553	0.354	2.617
Approximate p-value	2.78E−06	1.35E−04	0.029	0.0602	0.362	0.00443
Concentration Trend	Increasing	Increasing	Decreasing	None	None	Increasing
Nitrate Concentration at R-45 Mann-Kendall Test						
M-K Test Value (S)	266	204	−195	157	368	430
Critical Value (0.05)	1.645	1.645	−1.645	1.645	1.645	1.645
Standard Deviation of S	47.94	45.31	53.26	56.03	73.36	73.39
Standardized Value of S	5.528	4.481	−3.642	2.784	5.003	5.846
Approximate p-value	1.62E−08	3.72E−06	1.35E−04	0.00268	2.83E−07	2.52E−09
Concentration Trend	Increasing	Increasing	Decreasing	Increasing	Increasing	Increasing

Table 3.2-3 (continued)

R-45 Mann-Kendall Test Results						
Test	Phase 1		Phase 2		Phase 3	
	Screen 1	Screen 2	Screen 1	Screen 2	Screen 1	Screen 2
Chromium Concentration at R-70 Mann-Kendall Test						
M-K Test Value (S)	n/a	n/a	n/a	n/a	−107	−341
Critical Value (0.05)	n/a	n/a	n/a	n/a	−1.645	−1.645
Standard Deviation of S	n/a	n/a	n/a	n/a	50.61	56.05
Standardized Value of S	n/a	n/a	n/a	n/a	−2.095	−6.066
Approximate p-value	n/a	n/a	n/a	n/a	0.0181	6.56E−10
Concentration Trend	n/a	n/a	n/a	n/a	Decreasing	Decreasing
Chloride Concentration at R-70 Mann-Kendall Test						
M-K Test Value (S)	n/a	n/a	n/a	n/a	−138	−333
Critical Value (0.05)	n/a	n/a	n/a	n/a	−1.645	−1.645
Standard Deviation of S	n/a	n/a	n/a	n/a	50.62	53.28
Standardized Value of S	n/a	n/a	n/a	n/a	−2.707	−6.231
Approximate p-value	n/a	n/a	n/a	n/a	3.40E−03	2.32E−10
Concentration Trend	n/a	n/a	n/a	n/a	Decreasing	Decreasing
Sulfate Concentration at R-70 Mann-Kendall Test						
M-K Test Value (S)	n/a	n/a	n/a	n/a	−189	−333
Critical Value (0.05)	n/a	n/a	n/a	n/a	−1.645	−1.645
Standard Deviation of S	n/a	n/a	n/a	n/a	47.95	53.3
Standardized Value of S	n/a	n/a	n/a	n/a	−3.921	−6.229
Approximate p-value	n/a	n/a	n/a	n/a	4.41E−05	2.35E−10
Concentration Trend	n/a	n/a	n/a	n/a	Decreasing	Decreasing
Perchlorate Concentration at R-70 Mann-Kendall Test						
M-K Test Value (S)	n/a	n/a	n/a	n/a	−168	−300
Critical Value (0.05)	n/a	n/a	n/a	n/a	−1.645	−1.645
Standard Deviation of S	n/a	n/a	n/a	n/a	47.86	53.31
Standardized Value of S	n/a	n/a	n/a	n/a	−3.489	−5.609
Approximate p-value	n/a	n/a	n/a	n/a	2.42E−04	1.02E−08
Concentration Trend	n/a	n/a	n/a	n/a	Decreasing	Decreasing
Nitrate Concentration at R-70 Mann-Kendall Test						
M-K Test Value (S)	n/a	n/a	n/a	n/a	−150	−281
Critical Value (0.05)	n/a	n/a	n/a	n/a	−1.645	−1.645
Standard Deviation of S	n/a	n/a	n/a	n/a	47.86	53.26
Standardized Value of S	n/a	n/a	n/a	n/a	−3.113	−5.258
Approximate p-value	n/a	n/a	n/a	n/a	9.25E−04	7.30E−08
Concentration Trend	n/a	n/a	n/a	n/a	Decreasing	Decreasing

Table 3.2-3 (continued)

R-45 Mann-Kendall Test Results						
Test	Phase 1		Phase 2		Phase 3	
	Screen 1	Screen 2	Screen 1	Screen 2	Screen 1	Screen 2
Chromium Concentration at CrEX-5 Mann-Kendall Test						
M-K Test Value (S)	n/a	n/a	6	n/a	−270	n/a
Critical Value (0.05)	n/a	n/a	0.374	n/a	−1.645	n/a
Standard Deviation of S	n/a	n/a	18.24	n/a	53.31	n/a
Standardized Value of S	n/a	n/a	0.274	n/a	−5.046	n/a
Approximate p-value	n/a	n/a	0.392	n/a	2.26E−07	n/a
Concentration Trend	n/a	n/a	None	n/a	Decreasing	n/a
Chloride Concentration at CrEX-5 Mann-Kendall Test						
M-K Test Value (S)	n/a	n/a	−60	n/a	−201	n/a
Critical Value (0.05)	n/a	n/a	0.001	n/a	−1.645	n/a
Standard Deviation of S	n/a	n/a	20.02	n/a	50.51	n/a
Standardized Value of S	n/a	n/a	−2.948	n/a	−3.959	n/a
Approximate p-value	n/a	n/a	0.0016	n/a	3.76E−05	n/a
Concentration Trend	n/a	n/a	Decreasing	n/a	Decreasing	n/a
Sulfate Concentration at CrEX-5 Mann-Kendall Test						
M-K Test Value (S)	n/a	n/a	−53	n/a	−245	n/a
Critical Value (0.05)	n/a	n/a	0.004	n/a	−1.645	n/a
Standard Deviation of S	n/a	n/a	20.11	n/a	50.59	n/a
Standardized Value of S	n/a	n/a	−2.586	n/a	−4.823	n/a
Approximate p-value	n/a	n/a	0.00485	n/a	7.06E−07	n/a
Concentration Trend	n/a	n/a	Decreasing	n/a	Decreasing	n/a
Perchlorate Concentration at CrEX-5 Mann-Kendall Test						
M-K Test Value (S)	n/a	n/a	n/a	n/a	−271	n/a
Critical Value (0.05)	n/a	n/a	n/a	n/a	−1.645	n/a
Standard Deviation of S	n/a	n/a	n/a	n/a	47.95	n/a
Standardized Value of S	n/a	n/a	n/a	n/a	−5.631	n/a
Approximate p-value	n/a	n/a	n/a	n/a	8.95E−09	n/a
Concentration Trend	n/a	n/a	n/a	n/a	Decreasing	n/a
Nitrate Concentration at CrEX-5 Mann-Kendall Test						
M-K Test Value (S)	n/a	n/a	n/a	n/a	−154	n/a
Critical Value (0.05)	n/a	n/a	n/a	n/a	−1.645	n/a
Standard Deviation of S	n/a	n/a	n/a	n/a	47.94	n/a
Standardized Value of S	n/a	n/a	n/a	n/a	−3.192	n/a
Approximate p-value	n/a	n/a	n/a	n/a	7.07E−04	n/a
Concentration Trend	n/a	n/a	n/a	n/a	Decreasing	n/a

* n/a = Not applicable.

Table 3.2-4
Mann-Kendall Test Results after IM Partial System Pause

M-K Test for R-45 screen 2 and R-61 after IM partial system pause		
Test	R-45 Screen 2	R-61
Chromium Concentration Mann-Kendall Test		
M-K Test Value (S)	−16	8
Critical Value (0.05)	0.031	0.042
Standard Deviation of S	8.083	4.082
Standardized Value of S	−1.856	1.715
Approximate p-value	0.0317	0.0432
Concentration Trend	**Decreasing**	**Increasing**

Appendix A

Chromium Interim Measure Extraction and Injection Flow Data
(on CD included with this document)

N3B RECORDS	
Media Information Page	
This is a placeholder page for a record that cannot be uploaded or would lose meaning or content if uploaded. The record can be requested through regdocs@em-la.doe.gov	
Document Date: 6/29/2023	**EM ID number:** 702801-01
Document Title: Appendix A Submittal of the Annual Progress Report on Chromium Plume Control Interim Measure Performance, April 2022 through March 2023	☒ **No restrictions** ☐ **UCNI** ☐ **Copyrighted**
Media type and quantity: 1 CD	**Software and version required to read media:** Adobe Acrobat 9.0
Other document numbers or notes: Files are too numerous and large to upload.	

Appendix B

Analytical Water Quality Data Collected under the Interim Facility-Wide Groundwater Monitoring Plan (on CD included with this document)

N3B RECORDS	
Media Information Page	
This is a placeholder page for a record that cannot be uploaded or would lose meaning or content if uploaded. The record can be requested through regdocs@em-la.doe.gov	
Document Date: 6/29/2023	**EM ID number:** 702801-02
Document Title: Appendix B Submittal of the Annual Progress Report on Chromium Plume Control Interim Measure Performance, April 2022 through March 2023	☒ **No restrictions** ☐ **UCNI** ☐ **Copyrighted**
Media type and quantity: 1 CD	**Software and version required to read media:** Adobe Acrobat 9.0
Other document numbers or notes: Files are too numerous and large to upload.	

Appendix C

Analytical Water Quality Data Collected from Chromium Treatment Unit Influent and Effluent (on CD included with this document)

N3B RECORDS	
Media Information Page	
This is a placeholder page for a record that cannot be uploaded or would lose meaning or content if uploaded. The record can be requested through regdocs@em-la.doe.gov	
Document Date: 6/29/2023	**EM ID number:** 702801-03
Document Title: Appendix C Submittal of the Annual Progress Report on Chromium Plume Control Interim Measure Performance, April 2022 through March 2023	☒ **No restrictions** ☐ **UCNI** ☐ **Copyrighted**
Media type and quantity: 1 CD	**Software and version required to read media:** Adobe Acrobat 9.0
Other document numbers or notes: Files are too numerous and large to upload.	

Appendix D

Los Alamos County Well Pumping Data
(on CD included with this document)

N3B RECORDS	
Media Information Page	
This is a placeholder page for a record that cannot be uploaded or would lose meaning or content if uploaded. The record can be requested through regdocs@em-la.doe.gov	
Document Date: 6/29/2023	**EM ID number:** 702801-04
Document Title: Appendix D Submittal of the Annual Progress Report on Chromium Plume Control Interim Measure Performance, April 2022 through March 2023	☒ **No restrictions** ☐ **UCNI** ☐ **Copyrighted**
Media type and quantity: 1 CD	**Software and version required to read media:** Adobe Acrobat 9.0
Other document numbers or notes: Files are too numerous and large to upload.	

Enclosure 2

Hydraulic Analysis of the Pajarito Plateau

EMID-702780

Neptune and Company, Inc.
1505 15th St.
Suite B
Los Alamos, New Mexico 87544
720-746-1803
www.neptuneinc.org

16 June 2023

To: Cheryl L. Rodriguez
DOE EM-LA

Please find attached to this letter a copy of the *Hydraulic Analysis of the Pajarito Plateau* report for enclosure to the *Annual Progress Report on Chromium Plume Control Interim Measure Performance, April 2022 through March 2023*.

Sincerely,
Lauren Foster

Neptune and Company

Hydraulic Analysis of the Pajarito Plateau

16 June 2023

NEPTUNE AND COMPANY, INC.
1505 15th St. Suite B, Los Alamos, NM 87544

CONTENTS

FIGURES

TABLES

ACRONYMS AND ABBREVIATIONS

CM	chromium model
Cr	chromium (assumed to be Cr^{+6} unless otherwise specified)
CSM	conceptual site model
EIM	Environmental Information Management (System)
EPA	U.S. Environmental Protection Agency
IM	interim measures
LAC	Los Alamos County
LANL	Los Alamos National Laboratory
MK	Mann-Kendall
RDX	Royal Demolition Explosive
RM	RDX model
SD	standard deviation
TA	technical area
VZ	vadose zone

1.0 Executive Summary

The regional groundwater aquifer below the Pajarito Plateau, where Los Alamos National Laboratory and the county of Los Alamos, New Mexico are located, is a large, heterogeneous system that supports multiple county water supply wells. Long-term decline of water levels in the regional aquifer has been observed for decades (Birdsell et al. 2005; Collins et al. 2005; DBS&A 2006; Koch and Schmeer 2010; Vesselinov 2005).

The goal of this white paper is to refine conceptual understanding of groundwater hydraulics of the aquifer beneath the Pajarito Plateau, in support of fate and transport modeling of dissolved-phase contaminants located in two distinct areas of the regional aquifer. Hydraulic gradients in the regional aquifer are characterized using simplifying assumptions to make numerical models computationally tractable and efficient. This study focuses on determining the spatial extent where supply-well pumping has a meaningful impact on hydraulic gradients in the regional aquifer.

The first set of analyses concentrate on the western portion of the regional aquifer where a plume of dissolved-phase hexahydro-1,3,5-trinitro-1,3,5-triazine (Royal Demolition Explosive [RDX]) exists. Temporal analysis of lateral and vertical hydraulic gradients across three depth horizons is used to answer the following two questions related to the RDX plume:

(1) Are regional aquifer gradients in the RDX plume and the downgradient portion of the regional aquifer expected to change enough to substantially affect flow and transport over a multi-decadal timeframe?
(2) Where are systematic changes in gradients observed because of county supply-well pumping?

The second set of hydraulic analyses are concentrated on a comparatively smaller portion of the regional aquifer in the central portion of the Pajarito Plateau where a plume of dissolved-phase hexavalent chromium (Cr^{+6} [Cr]) is located. This portion of the regional aquifer is located closer to supply wells, and the potential exists for influence on hydraulic gradients within the vicinity of the Cr plume. In contrast to the RDX plume, an interim measures (IM) system consisting of extraction wells, treatment with ion exchange, and injection wells has been installed with the intention of hydraulically controlling the plume. In this set of hydraulic analyses, four time periods are identified that represent different states of the aquifer in quasi-equilibrium in response to pumping stresses. Lateral and vertical hydraulic gradients are estimated and the periods are quantitatively compared to answer the following two questions related to the Cr plume:

(1) Does supply pumping meaningfully impact the hydraulic gradients in the Cr plume in the context of fate and transport modeling?
(2) How do the impacts from supply pumping on ambient gradients compare to impacts from IM operations?

Results of the first set of analyses show that hydraulic gradients across the site conform to a traditional hydrogeological conceptual model. Recharge occurs primarily at the mountain block

(Sierra de los Valles), resulting in large lateral and downward vertical gradients in western areas of the aquifer. Smaller gradients are observed in the center of the Pajarito Plateau, where recharge rates are comparatively much lower, and upward vertical gradients are evident from artesian wells along the Rio Grande, indicating groundwater discharges to the river along this segment.

Trend analysis demonstrates that, on average, water table decline across the Pajarito Plateau has been occurring at a rate of approximately 0.35 ft per year. Several potential mechanisms could contribute to the observed decline, including reductions in recharge due to climate change, reductions in surface infiltration due to impacts from recent wildfires, and supply-well pumping; impacts from the latter mechanism are the focus of this analysis. While McLin (McLin 2005) concluded that "the present regional piezometric surface is approximately parallel to, but lower than, the ancestral piezometric surface of 60 years ago (i.e., before any groundwater development)," spatial analysis presented herein suggests that rates of decline are higher in the center of the plateau where supply wells are concentrated. Correlation tests also suggest that supply-well pumping has a measurable influence on nearby gradients; the range of direct pumping influence appears limited to approximately 1.25 miles (2 km) or less. At the mountain block to the west, estimated magnitudes of vertical and lateral gradients in the regional aquifer are approximately 1 to 2 orders of magnitude (10-100 times) larger than those observed near supply wells. While changes in hydraulic gradients within approximately 1.25 miles (2 km) of supply wells are measurable and show some correlation to downgradient supply-well pumping, the observed rates of change are small enough to be negligible for the purposes of fate and transport modeling, for at least a few hundred years. Within these timeframes, uncertainty in other critical parameters that define groundwater flow and transport in a hydrologic model (e.g., hydraulic conductivity, advective porosity, and dispersion) likely outweigh the very small changes in hydraulic gradients through time.

The second analysis quantifies and compares the direct impacts that pumping from nearby supply well PM-04 has on water levels in the Cr plume. PM-04 is located within a 2-km radius of the Cr plume, and is typically only operated seasonally (summer months), providing a systematic opportunity to compare periods of sustained pumping with periods of prolonged shutoff. PM-04 also pumps at the highest rate of all supply wells, and is the supply well closest to the Cr plume that has measurable impacts on water levels in Cr plume monitoring wells. During periods of sustained PM-04 operations, the direction and magnitude of ambient gradients at most wells within the Cr plume are measurably shifted from ambient by changes in water levels. However, results show that shifts in hydraulic gradients due to the IM are substantially greater than those induced from sustained PM-04 pumping in the vicinity of the plume. Therefore, the influence of nearby supply wells is likely negligible for the purposes of fate and transport modeling of Cr plume migration and remediation on short time scales (~5-20 years), compared with the strong influence that local extraction and injection imposes on hydraulic gradients.

2.0 RDX Plume-Related Hydraulic Analyses

The goal of this part of the study is to refine the conceptual understanding of groundwater hydraulics on the Pajarito Plateau in support of fate and transport modeling of a dissolved-phase hexahydro-1,3,5-trinitro-1,3,5-triazine (RDX) plume, located in the western portion of the regional aquifer.

2.1 Introduction

Regional groundwater flow beneath the Pajarito Plateau is highly complex, as is typical in mountainous environments (Broxton and Vaniman 2005; Vesselinov 2005). Groundwater flow originates at points of recharge in upland elevations and flows to points of discharge at lower elevations. At larger scales (>3280 ft), simplified conceptualizations of flow patterns are valid to understand regional flow patterns; however, these approaches require many limiting and simplifying assumptions about the aquifer system, including:

- The aquifer system is relatively homogeneous and isotropic, or at most has a simple layered configuration.
- The water table approximately follows the topography of the land.
- Ground-surface slopes are small compared to density of flow lines and equipotential lines used to characterize flow.
- Under these ideal conditions, simple algebraic functions are valid to approximate flow (Freeze and Cherry 1979, 088742).

In most environments, these simplifying assumptions do not hold true at smaller scales (<1 mi) due to the heterogeneity of aquifer materials, geologic contacts between dissimilar units, the presence of faults, and/or localized recharge. After a broad pattern of groundwater flow is conceptualized at a site, water level observations can be used to test whether the conceptual site model (CSM) accurately reflects the observed data. If observations do not match the CSM, the CSM must be updated and refined to reflect the observations.

Figure 1, taken from Freeze and Cherry (1979) and annotated, shows the basic concepts of aquifer hydraulic-head distributions in a site with upland recharge and lowland discharge to a river, such as the case on the Pajarito Plateau. The diagram depicts downward flow and the production of downward (negative) vertical gradients near the upland plateau on the right-hand side of the figure (region 1). Dashed lines on Figure 1 are groundwater head contours, and arrows indicate direction of groundwater flow.

At depth, bedrock prevents continued downward flow, so groundwater flow is deflected horizontally (region 2), and no vertical gradients are observed. As groundwater flow approaches the discharge zone, flow turns upward, and groundwater discharges to the valley stream on the left-hand side of the figure (region 3). In this region, equipotential contours are expected to increase with depth, indicating that upward (positive) vertical gradients result in groundwater discharge to the stream. This example is a mirror image of the Pajarito Plateau, which has upland recharge to the west, and discharge to a river to the east.

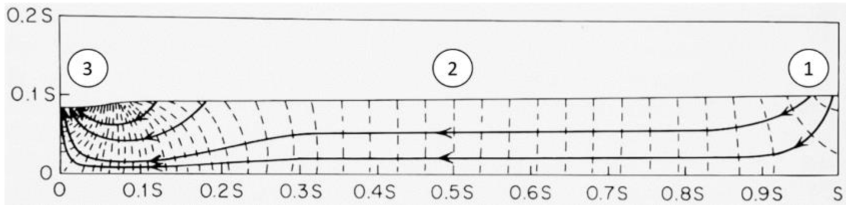

Figure 1. Figure from Freeze and Cherry (1979). The basic concepts of aquifer hydraulic head distributions in a site with upland recharge and lowland discharge to a river are shown. This example is a mirror image of the Pajarito Plateau, which has upland recharge to the west, and discharge to a river to the east.

The focus of the study here is the western portion of the Pajarito Plateau, where an RDX plume resides in the regional aquifer close to the mountain front. Figure 2 (modified from N3B (2019)) shows the locations of monitoring wells in the RDX plume area (in the orange box in the west), and supply wells (red stars) within the LANL boundary, along with contours representing regional aquifer water table conditions as of February 2014.

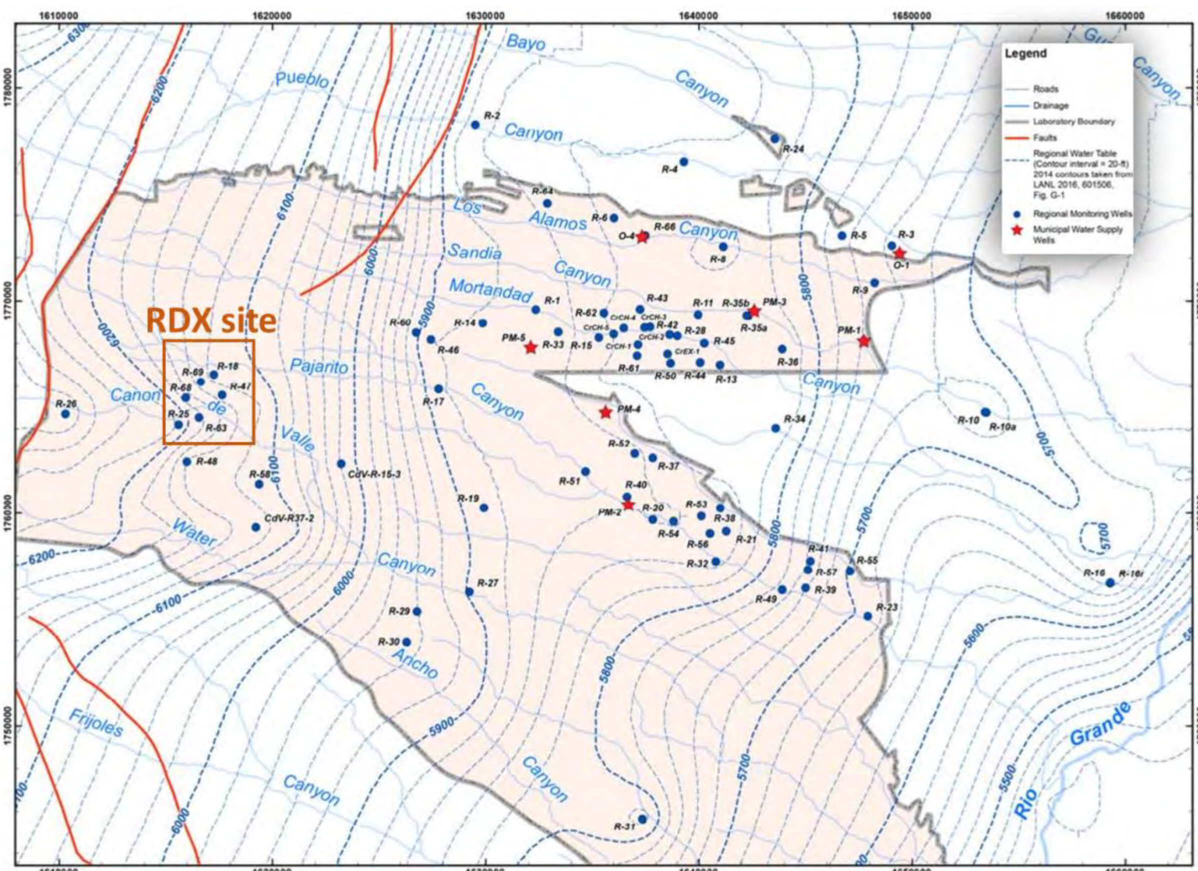

Figure 2. Location of RDX plume monitoring wells and supply wells within the LANL boundary. Figure modified from N3B (2019).

The RDX plume was formed by contaminated discharges at the 260 Outfall to Canon de Valle, and subsequent stream loss and recharge to the subsurface. In this area of the plateau, the regional aquifer lies up to 1000 feet below the surface. The large distance between the ground surface and the regional aquifer system means that topography likely has little to no impact on the regional aquifer water table. However, close to the mountain front, mountain block (deep, direct flow from the mountain block) and mountain front recharge (surface infiltration) occur.

According to the basic flow concepts as represented in Figure 1, this recharge produces downward vertical gradients in the regional aquifer near the mountain front (roughly the western third of Figure 2). Strong vertical gradients have been observed close to the mountain front at multi screened wells (e.g., R-25 and R-69) (N3B 2019). Further east along the Pajarito plateau, surface flows and recharge are diminished due to the semi-arid climate at the surface; regional groundwater flow is expected to transition to largely horizontal flow in this region (middle third of Figure 2), with little to no vertical gradients. In the eastern third of Figure 2, lateral and vertical gradients increase again as the surface topography and elevation drop almost 1000 feet to the Rio Grande along White Rock Canyon. Groundwater from the regional aquifer discharges to surface springs along White Rock Canyon (Purtymun et al. 1980), and upward vertical gradients in the regional aquifer are evident from artesian wells along the Rio Grande, indicating that groundwater also discharges to the river along this stretch (Purtymun 1995).

The following hydraulic analyses are used to test and refine the conceptual model of regional groundwater flow. While any aquifer model of a complex site must make simplifications to be numerically tractable, it is important to vet the simplifications with thorough analyses of site data. In particular, the answers to the following two questions influence how the RDX model (RM) is simplified and structured:

(1) Are regional aquifer gradients expected to change in the RDX plume and downgradient portion of the regional aquifer enough to meaningfully affect flow and transport?
(2) Where can systematic changes in gradients be correlated to county supply-well pumping?

To answer these questions, lateral and vertical hydraulic gradients are calculated at various depths across the aquifer system through time. The time series of hydraulic gradient magnitude and direction are assessed for potential trends and correlation with groundwater pumping from county supply wells.

2.1.1 Geologic Context

The water table at the RDX site lies entirely within the Puye Formation (Puye), which is characterized by coarse and highly heterogeneous alluvial fan sediments, whose origin and source of material were to the west. The Puye is over a thousand feet thick in some locations (LANL 2018, 602963). However, near the plume, the Puye is intersected by dacite flows from volcanic activity, collectively known as the Tschicoma Formation, with origins to the west. Few wells have been constructed in this unit due to it being poorly conductive overall. However, contacts between the highly conductive sands and gravels of the alluvial and fluvial Puye sediments, and the poorly conductive Tschicoma volcanic formations, have potential to alter local flow patterns in the regional aquifer.

Figure 3, a composite of figures from (LANL 2018), is a plan view of structural contours of the top of the Tschicoma Formation (also known as the dacite of Cerro Grande).

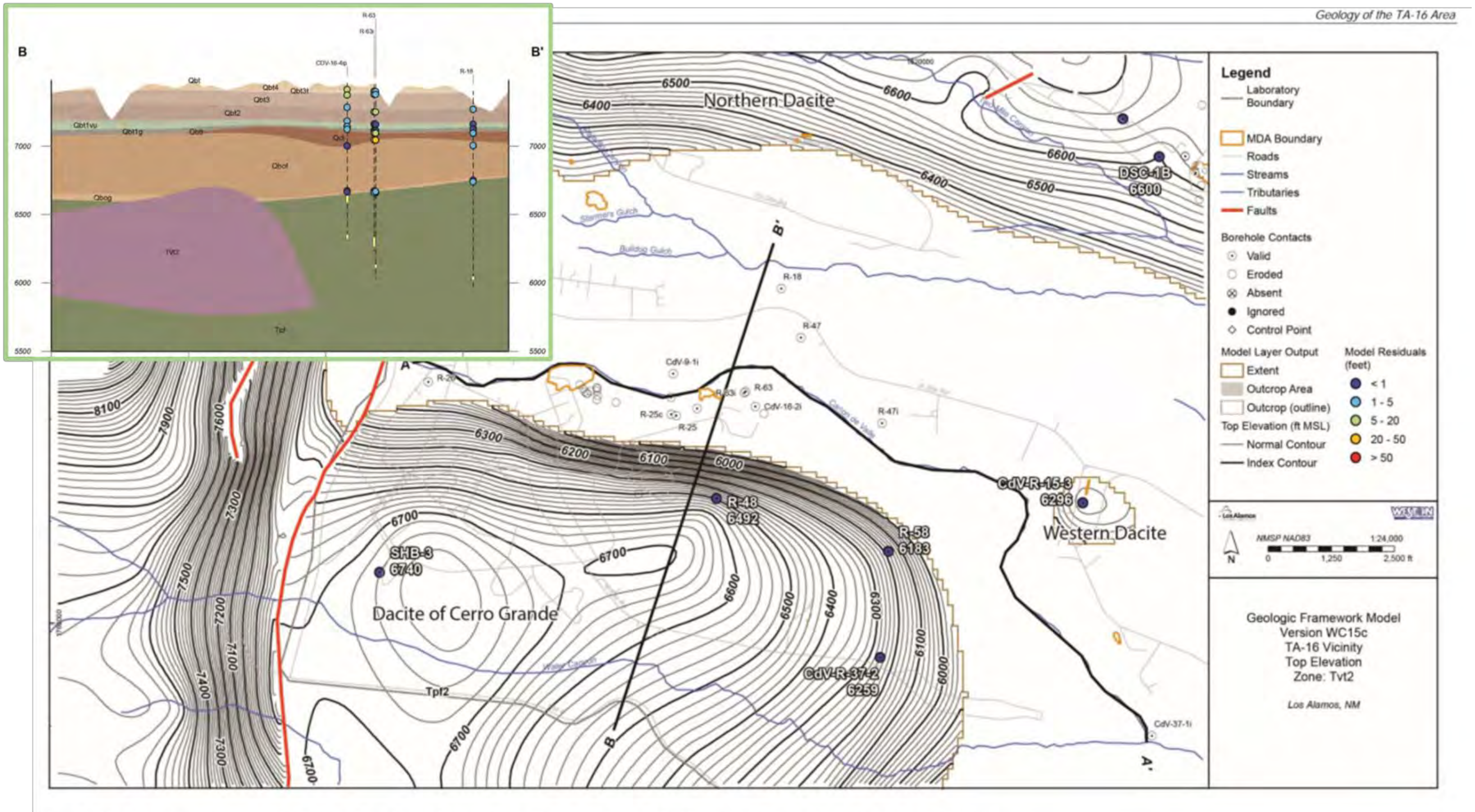

Figure C-11 Structure contour map for the top of the dacite of Cerro Grande (Tvt2) based on the WC15c version of the Laboratory's site geologic model

Figure 3. Structural contour and B-B' cross section (green inset) map of the Tschicoma Formation (tvt2), also known as the dacite of Cerro Grande. Composite of figures from LANL (2018).

Figure 3 includes a cross section showing the relative position of the Tschicoma (Tvt2, shown in purple) and Puye (Tpf, shown in green). Regional aquifer wells R-48, R-58, and CdV-R-37-2 are completed in the more permeable brecciated portions of the Tschicoma Formation.

Erosion and faulting have modified the geologic structure and topography of the Pajarito Plateau. Erosion of the Bandelier Tuff has created fingerlike mesas divided by deep canyons that extend west to east. Technical Area 16 (TA-16), where the RDX site is located (Figure 2), sits on one of these mesas, located south of, and adjacent to, Cañon de Valle. Extensive faulting has also been observed at the western edge of the Pajarito Plateau, known as the Pajarito Fault System, a narrow band of normal faults that trend to the north/northeast. Vertical faults of the Pajarito Fault System are shown as red lines in Figure 2 and Figure 3.

2.1.2 Hydrologic Context

Steep canyons between mesas on the Pajarito Plateau channelize and concentrate flow into the canyon bottoms, resulting in focused infiltration to the subsurface. Near the RDX plume, large stream losses in Cañon de Valle have been observed along the streambed, resulting in perched zones of saturation within the vadose zone (VZ), and water table mounding in the regional aquifer (N3B 2019). The TA-16 260 Outfall discharged directly into the Ca on de Valle canyon bottom, upstream of the region of observed stream loss.

RDX-contaminated water initially entered the hydrologic system at the land surface and was transported down to the regional aquifer. Discharge water containing RDX from the 260 Outfall mixed with surface water and shallow alluvial groundwater in Cañon de Valle. Subsequent recharge to the subsurface moved the soluble contaminant down into the perched zones of the upper and lower VZ. Infiltration into these perched zones is mainly thought to occur through fast pathways such as Pajarito fault-related faulting and fractures. Significant amounts of RDX have been observed in these perched zones, indicating contaminated recharge is expected to continue well into the future. The stored inventory in the VZ is one of the drivers for running the RM for 10s to 100s of years into the future to assess risk.

The shape of the regional water table is predominantly controlled by hydrologic recharge at the western boundary and discharge to the east. At the western boundary of the regional aquifer, recharge from the Sierra de los Valles mountain block provides higher hydraulic heads that force an overall west-to-east gradient. At the eastern boundary, the regional aquifer contributes to gaining stream conditions below the Rio Grande (Purtymun 1995) and is also expressed at the surface as discharges from springs in White Rock Canyon (Purtymun et al. 1980). Aside from the overall west-to-east hydraulic gradient within the aquifer, regional flows may also be influenced by local areas of infiltration (beneath canyons), heterogeneous lithology, and anisotropic aquifer properties. Pumping tests performed at supply wells PM-02 and PM-4 (McLin 2005, 2006) have shown a higher degree of lateral connectivity than vertical connectivity within the aquifer, suggesting hydraulic conductivities are generally higher laterally than vertically. Vertical differences in hydraulic heads and a lack of vertical propagation of pumping drawdown indicate some level of hydraulic stratification. This vertical anisotropy within the aquifer is likely caused by the depositional layering of the stratigraphic units that contain the regional aquifer.

2.2 Methods

2.2.1 Water-Level Data

Water levels are used in this study to estimate hydraulic gradients present in the regional aquifer beneath the Pajarito Plateau. A hydraulic gradient is the rate of change in hydraulic head (pressure head + elevation head) per distance (Fetter 1994). Hydraulic gradients are the mechanism that drive water through porous media; the magnitude and direction of the gradient indicates the direction of groundwater flow (in the absence of strong anisotropy, fractures, or large discontinuities).

Water level data from monitoring wells across the Pajarito Plateau are publicly available on IntellusNM, the public version of LANL's Environmental Information Management (EIM) database (https://intellusnm.com). Initially, water levels are not filtered or corrected as part of an exploratory data analysis presented to briefly look at long-term water table decline across the Pajarito Plateau. For this initial analysis, water levels for each well screen in the regional aquifer are aggregated to a monthly scale, first taking the mean at the 2-hour interval, then the mean of the 2-hour means for each calendar day, and lastly the mean of the daily means for each month. A Cook's distance (a statistical method for determining outliers) greater than or equal to 0.1 is used to identify and exclude outliers (Cook 1977).

For calculating lateral and vertical hydraulic gradients, a more robust treatment of the water level data is performed compared to that used for the exploratory data analysis. Additionally, the temporal resolution is increased; water levels are aggregated to a weekly scale. Water level observations are filtered based on measurement method and data quality. Bad data and observation jumps (e.g., transducer slips) are removed and corrected for, respectively, based on manual review of the data. Anomalous records are detected and removed using the anomalize R package (Dancho and Vaughan, 2020, https://github.com/business-science/anomalize). In some instances, visual inspection of the time series indicated that anomalous observations still existed, and such instances are manually removed. Water levels are barometrically corrected by regression deconvolution (Toll and Rasmussen 2007) using publicly available tidal data and barometric pressures from LANL's TA54 weather station (https://weathermachine.lanl.gov/ta54.asp).

The focus of this study is to identify long-term sustained trends and shifts in lateral and vertical hydraulic gradients in the aquifer that reflect more permanent shifts in hydraulic gradients. This is in contrast to immediate aquifer responses (e.g., drawdown during pumping), which cause a temporary drop in water levels, typically followed by full recovery. For the gradient analyses, water levels for each screen port are aggregated using the median value of all head values within a calendar week.

For lateral gradients, well triplets are constructed using well screens at the same approximate depth below the water table. Well screens in the Cr plume vicinity and downgradient region of the aquifer allow three depths to be investigated within the regional aquifer:

- the first depth, at the water table, represented by the first regional aquifer screen in multi-screened wells;
- the second depth, referred to as "mid-depth," represented by the second regional aquifer screen in multi-screened wells; and
- the third depth, referred to as "deep," represented by the third regional aquifer screen in multi-screened wells.

2.2.2 Lateral Gradients - Three-point method

The three-point method detailed in Heath (1983) is used to calculate the magnitude and direction (azimuth) of lateral hydraulic gradients in the aquifer system, using water levels at wells. This method requires a set of three wells, each with known water level and geographic location. The steps to compute the hydraulic gradient are:

1. Rank wells based on water level: high, intermediate, low.
2. Draw a line between the high and low wells. Calculate location on this line where the water level is equal to the intermediate well's water level.
3. Draw a line (contour) from the intermediate well through the location computed in step 2.
4. Draw a line perpendicular to the contour in step 3 through the low well's location.
5. Magnitude is equal to the difference in head between the intermediate and low wells, divided by the distance between the low well and the contour. Direction is equal to the azimuth of the line from step 4.

Figure 4 illustrates this process for wells R-68, R-69 screen 1, and R-47.

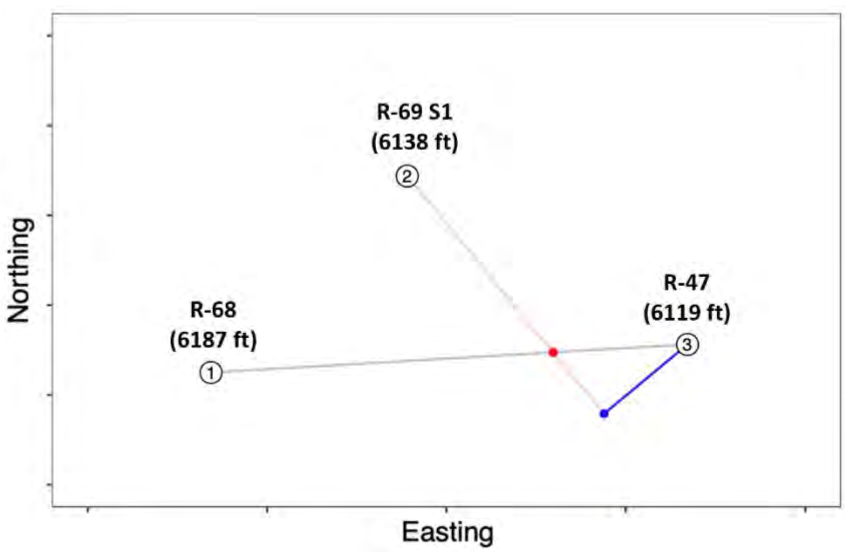

Figure 4. Diagram of gradient computation for wells R-68, R-69 screen 1, and R-47. Lines referenced in steps 3 and 4 are plotted in red and blue, respectively.

2.2.3 Vertical Gradients

The presence of vertical gradients in the regional aquifer can be assessed using wells with multiple screens, along with single-screened wells near to one another that are screened in different depths in the aquifer.

Vertical hydraulic gradients are calculated by taking the difference in observed water levels between the two screens (lower screen minus upper screen), divided by the absolute vertical distance between the midpoint elevation of the screened intervals. (The calculation of the vertical distance is illustrated in Figure 5) Positive vertical gradients indicate that the lower screen has a higher measured water level compared to the upper screen, indicating upward flow in the aquifer. Negative vertical gradients indicate that the lower screen has a lower measured water level compared to the upper screen, indicating downward flow in the aquifer. Few multi-screened wells, that have a long period of record for water levels, exist near the RDX plume. Since vertical gradients are of particular importance for understanding RDX fate and transport, R-18 and R-47 are also used to estimate the vertical hydraulic gradient in the RDX plume. R-18 and R-47's screens are at different depths within the aquifer, relatively close to one another, and are located approximately parallel to groundwater flow. Therefore, in this context, the difference in head between the two screens is assumed to represent a vertical gradient.

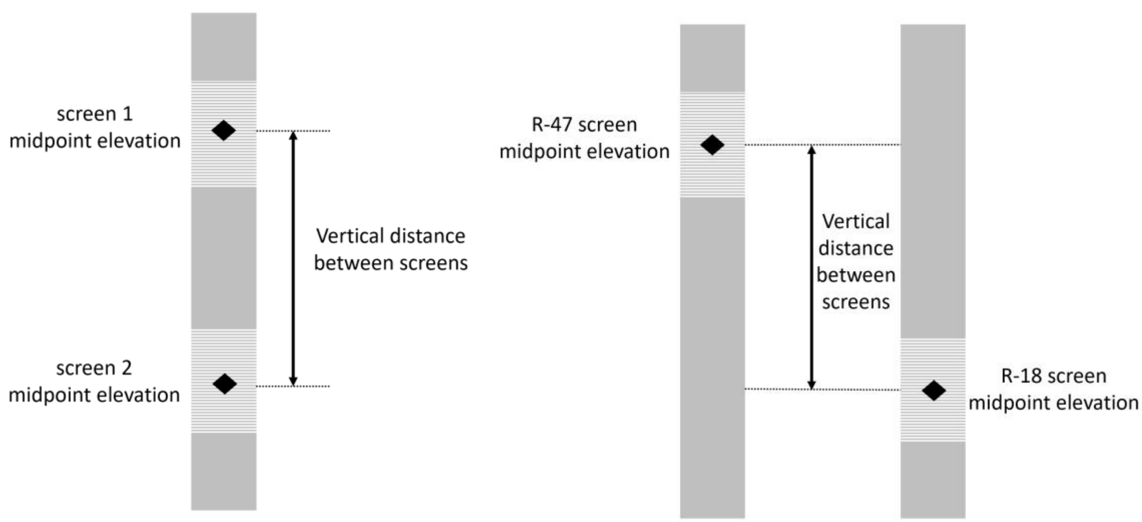

Figure 5. The vertical distance between pairs of well screens is calculated as the distance between the midpoint elevation of the screened intervals.

2.2.4 Trends and Estimated Linear Changes

The Mann-Kendall (MK) test for trend (Mann 1945; Kendall 1975; Gilbert 1987, 056179) is utilized to quantify whether hydraulic gradients monotonically increase or decrease over time. Positive (negative) values of the test statistic indicates that the magnitude/direction tends to consistently increase (decrease) over time, but the trend may or may not be linear. Each MK statistic result is accompanied by a calculated p-value. If the p-value is below the alpha-level (0.001), there is evidence of a monotonic trend in gradient magnitude/direction over time. Sen's method (Sen, 1968) is used to estimate the linear rate of change in gradient magnitude/direction over the period of interest. A 95% confidence interval for the Sen's slope parameter is also provided.

To condense the results section, Appendix A, where time-series plots of gradient magnitude and direction, and supply-well pumping (sum: PM-02 + PM-04 + PM-05) for all well screen triplets and vertical well screen pairs, are provided, along with tabulated results for statistical tests for trend, is included at the end of this paper. Each table associated with a set of triplets consists of the statistical analyses for hydraulic gradient magnitude (top table) and azimuth (bottom table).

2.2.5 Correlation to Supply-Well Pumping

The sum of the reported weekly gallons pumped for the closest three supply wells, PM-02, PM-04, and PM-05, is computed to look for a relationship between pumping at these three wells and changes in hydraulic gradient in the regional aquifer to the west. Spearman rank correlation, a statistical method for determining the relationship between two variables (Daniel, 1990), is used to quantify the strength and direction of a monotonic relationship (i.e., linear, or non-linear) between the total pumping at PM-02/04/05, and hydraulic gradient magnitudes and directions. Positive values of the Spearman rank correlation coefficient indicate that gradient magnitudes/directions tend to increase with increased total supply-well pumping, and negative values indicate that gradient magnitudes/directions tend to decrease with increased total supply-well pumping. A value of zero indicates no tendency of the gradient magnitudes/directions to increase or decrease with changes in total supply-well pumping. Values increase towards 1.0 as the relationship between gradient magnitude/direction and supply-well pumping approaches a perfect monotone function.

Each Spearman rank correlation statistical test result is accompanied by a p-value from the test. A p-value below the alpha-level (0.001) is evidence of a monotonic association between the hydraulic gradient magnitude/direction and total supply-well pumping. To condense the results section, Appendix A, where time-series plots of gradient magnitude and direction, and supply-well pumping (sum: PM-02 + PM-04 + PM-05) for all well screen triplets and vertical well screen pairs are provided, along with tabulated results for statistical tests for correlation, is included at the end of this paper.

2.3 Results

2.3.1 Long-Term Water Table Decline

Long-term decline of water levels in the regional aquifer across the Pajarito Plateau has been observed for decades (Birdsell et al. 2005; Koch and Schmeer 2010). Previous work has largely assumed that supply-well pumping is responsible for long-term decline. However, additional factors, such as reduced overall recharge due to higher evapotranspiration from an evolving climate at the surface, or reduced infiltration from precipitation due to extreme landscape changes from the Cero Grande and Las Conchas wildfires (in 2000 and 2011, respectively) could influence long-term water balance in the regional aquifer. Nevertheless, if water levels are declining at substantially greater rates towards the center of the aquifer system, compared to regions close to the mountain block (where heads are sustained from mountain recharge), this could result in an increase in overall hydraulic gradient magnitudes across the plateau, especially within the RDX plume and areas immediate downgradient in the regional aquifer.

Figure 6 consists of two plots that include estimated linear rates of change for regional aquifer screens completed near the water table of the regional aquifer. Figure 6 (top) is a spatial plot of the estimated rates of change at each well. Figure 6 (bottom) is a plot of estimated rate of change versus the weighted sum distance to county wells. The weights used to compute a weighted distance in Figure 6 (bottom) are based on the total annual average total pumping from each well; weights as assigned as the fraction of total annual supply well pumping between the supply wells. Regional wells in TA-16 with detected RDX concentrations are indicated with an orange box to the west. The left plot shows the estimated linear decline of water levels for well screens completed near the water table of the regional aquifer, using monthly aggregated values.

Estimated linear rates of change over the entire period of record for each screen range from just above zero (suggesting increasing water levels) to over -0.7 ft/yr, with a mean of -0.354 ft/yr and median of -0.375 ft/yr (Figure 7). Both plots in Figure 6 suggest that the regional aquifer near supply-well pumping shows greater rates of water table decline. However, in the RDX plume and downgradient area of the regional aquifer, the relationship appears to diminish somewhere west of R-17/R-19, and east of CdV-R-15-3. This suggests that hydraulic gradients west of R-17 and R-19 are not directly affected by county supply pumping. The decline in water levels seen at these wells may be related to other systematic losses of water not correlated to distance from supply wells, such as reduced recharge from the mountain front or reduced infiltration at the surface.

Figure 7 is a histogram showing the estimated aquifer water table decline. Estimated linear rates of change over the entire period of record for each screen range from just above zero (suggesting increasing water levels) to less than -0.7 ft/yr, with a mean of -0.354 ft/yr and median of -0.375 ft/yr).

The goal of the analyses in the following sections is to quantify the impacts on differential rates of decline observed across the regional aquifer and to understand changes in hydraulic gradients in the RDX and downgradient region. The spatial extent of water supply pumping is assessed by testing for correlation between supply well pumping and changes in observed lateral and vertical hydraulic gradients.

The estimated rates are plotted against a weighted sum distance from supply wells (Figure 6, right plot), where the weights are based on the annual average total pumping from each well.

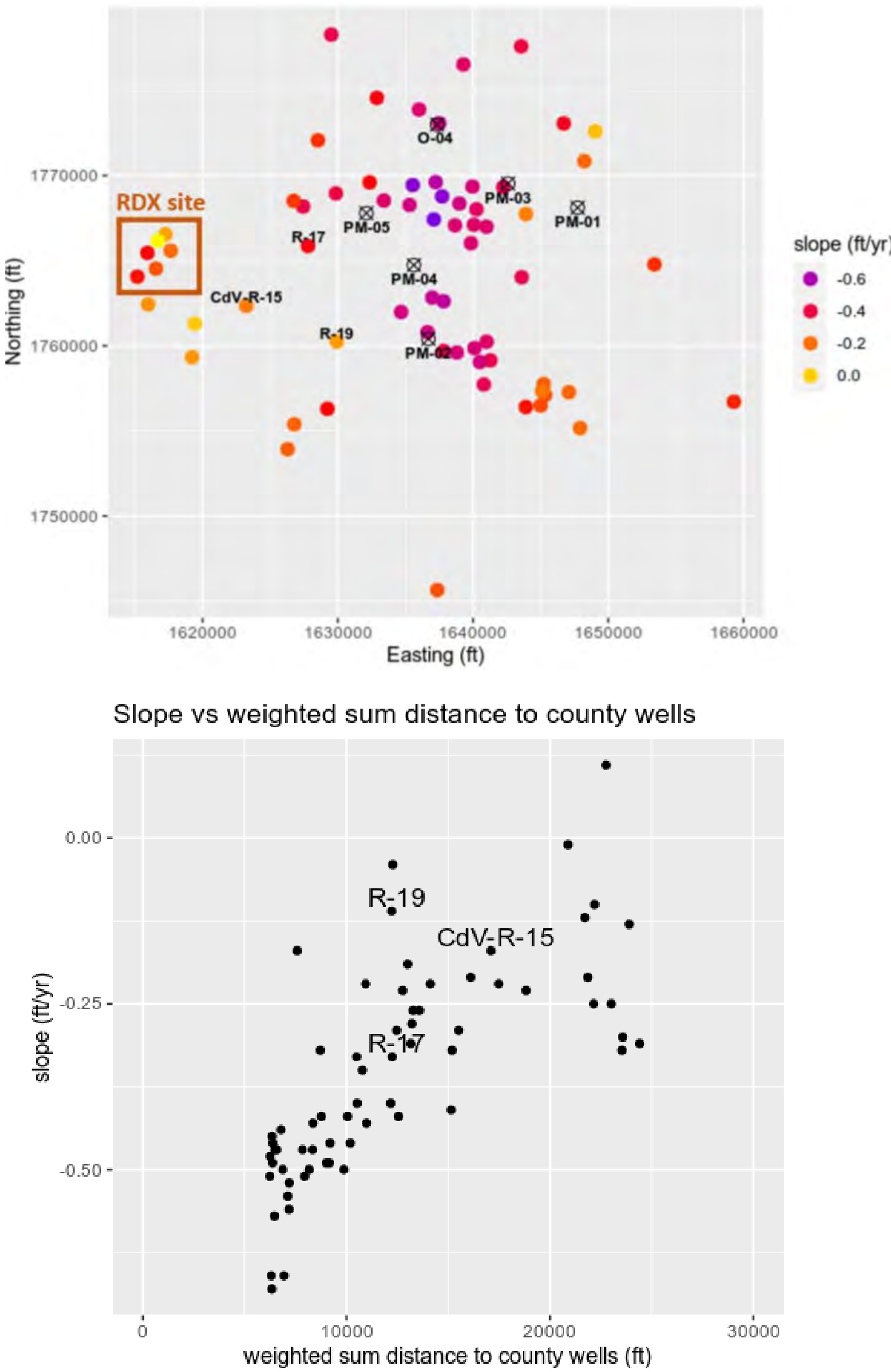

Figure 6. Spatial plot of estimated linear rates of change for regional aquifer water table screens (top). Regional wells in TA-16 with detected RDX concentrations are indicated with an orange box to the west. The estimated linear slope versus the weighted sum distance to county wells (bottom).

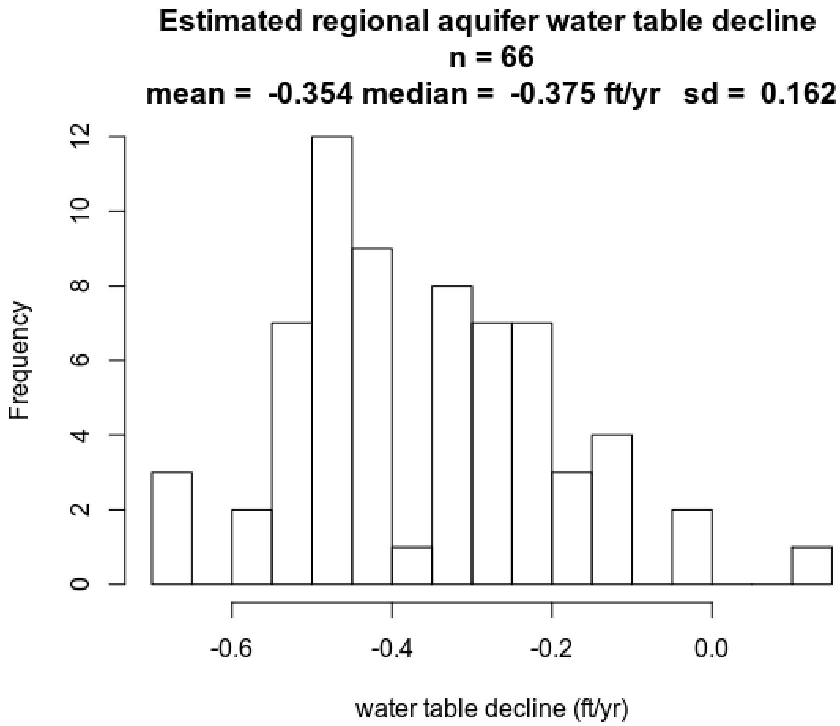

Figure 7. Histrogram of estimated linear rates of change of for regional aquifer water table screens.

2.3.2 Lateral Gradients

Lateral gradients estimated from weekly aggregated water level data are shown in Figure 8 (time--series plots for each triplet are available in Appendix A, Figures 1 through 6). On each plot in Figure 8 the PM wells are shown for geographical reference, but are not included in the lateral gradient analysis. Figure 8a shows the median lateral gradient magnitude for each triplet, colored by category. The horizontal extent of the lines indicates the horizontal extent (min/max of the well coordinates) for the well triplet. The plots in Figure 8b through Figure 8e include every gradient calculated for every triplet, plotted on top of one another, colored by time; RM calibration targets within the RDX plume area have a separate color bar for year in Figure 8b, due to their limited data. The length of the arrow indicates the magnitude of the gradient, with gradients shown proportionally in each plot (i.e., the triplets can be compared within but not between the different depth frames). The difficulty discerning week-to-week differences in the plots indicates that hydraulic gradients in the regional aquifer are regular over the period of record.

Figure 8b shows well triplets used as model calibration targets in the RM. Estimated hydraulic gradient magnitudes for the RM target triplets range from 0.028 to 0.048 ft/ft between the well triplets. The strongest lateral gradients measured in the regional aquifer occur in the RDX plume area (Figure 8a). Estimated azimuths generally point northeast and range from 50.25 to 64.5 degrees.

The water-table triplets, represented by the first/highest elevation regional aquifer screen in multi-screened wells and single-screened regional aquifer wells, are shown in Figure 8c. Similar to the reduction in water table decline observed west of at approximately R-17 and R-19 (Figure 6, right plot), water table gradients are higher in triplets located west of a roughly vertical line made by wells R-2, R-60, R-17, R-19, and R-27 (approximately 1628500 ft easting), compared to triplets located to the east of these wells. The triplets west of this line are immediately downgradient of the RDX plume and range in magnitude from 0.022 to 0.025 ft/ft Figure 8a), less than those measured upgradient in the RDX plume. Hydraulic gradient azimuths range from 43 to 104 degrees between well triplets in the west, most generally pointing east-northeast. To the east of this line, water table hydraulic gradients are estimated to be about an order of magnitude less compared to those to the west, ranging from <0.001 to 0.01 ft/ft with most falling between 0.001 and 0.006 ft/ft. Estimated hydraulic gradient azimuths range from -5 to 165 degrees, with most generally pointing east-northeast. The overall trend in gradient magnitude decline from west to east across the regional aquifer water table is apparent.

Mid-depth triplets (Figure 8d) include screens from wells that have at least a second screen in the regional aquifer, including the lower elevation regional aquifer screen in dual-screened wells, and the second regional aquifer screen for wells that have multiple screens. The spatial pattern of estimated hydraulic gradient magnitudes at mid-depth is similar to the water table screens, i.e., higher in triplets located to the west of R-17/R-19 (approximately 1628500 ft easting) compared to triplets located to the east of these wells (Figure 8a), though the available mid-depth screen data is limited to wells largely to the south of the RDX plume, versus directly downgradient. Nevertheless, estimated hydraulic gradient magnitudes range only from 0.024 to 0.026 ft/ft, consistent with water table gradients at the same approximate distance from the mountain front. Hydraulic gradient azimuths at this depth are very similar, ranging only from 73 to 76 degrees between all well triplets.

To the east of R-17 and R-19, hydraulic gradients are about an order of magnitude less compared to the west, ranging from 0.002 to 0.009 ft/ft, with most falling between 0.002 and 0.006 ft/ft. Hydraulic gradient azimuths range from 5 to 110 degrees. The results from the triplet to the north that includes R-69 is likely inaccurate due to the narrow geometry of the triplet. It is shown here for completeness, but may not be reliable given the geometry and contradictions to nearby triplets. A triplet cannot be completed with R-69 and R-25 since water level records do not overlap between these two wells.

Deep triplets include screens from wells that have a third screen in the regional aquifer. However, spatial data are extremely limited for this depth (Figure 8e). Between the RDX plume and the supply wells, only four wells contain a third screen in the regional aquifer. The estimated hydraulic gradient magnitudes are very similar between the two triplets (0.0305 and 0.0307 ft/ft). Magnitudes are slightly higher than the estimated gradients at the water table and mid-depth at the same approximate distance from the mountain front. The hydraulic gradient azimuth for triplet {CdV-R-37-2 screen 3, R-19 screen 4, CdV-R-15-3 S5} is approximately 47 degrees, and for {CdV-R-37-2 screen 3, R-25 S6, CdV-R-15-3 S5}, it is approximately 58 degrees.

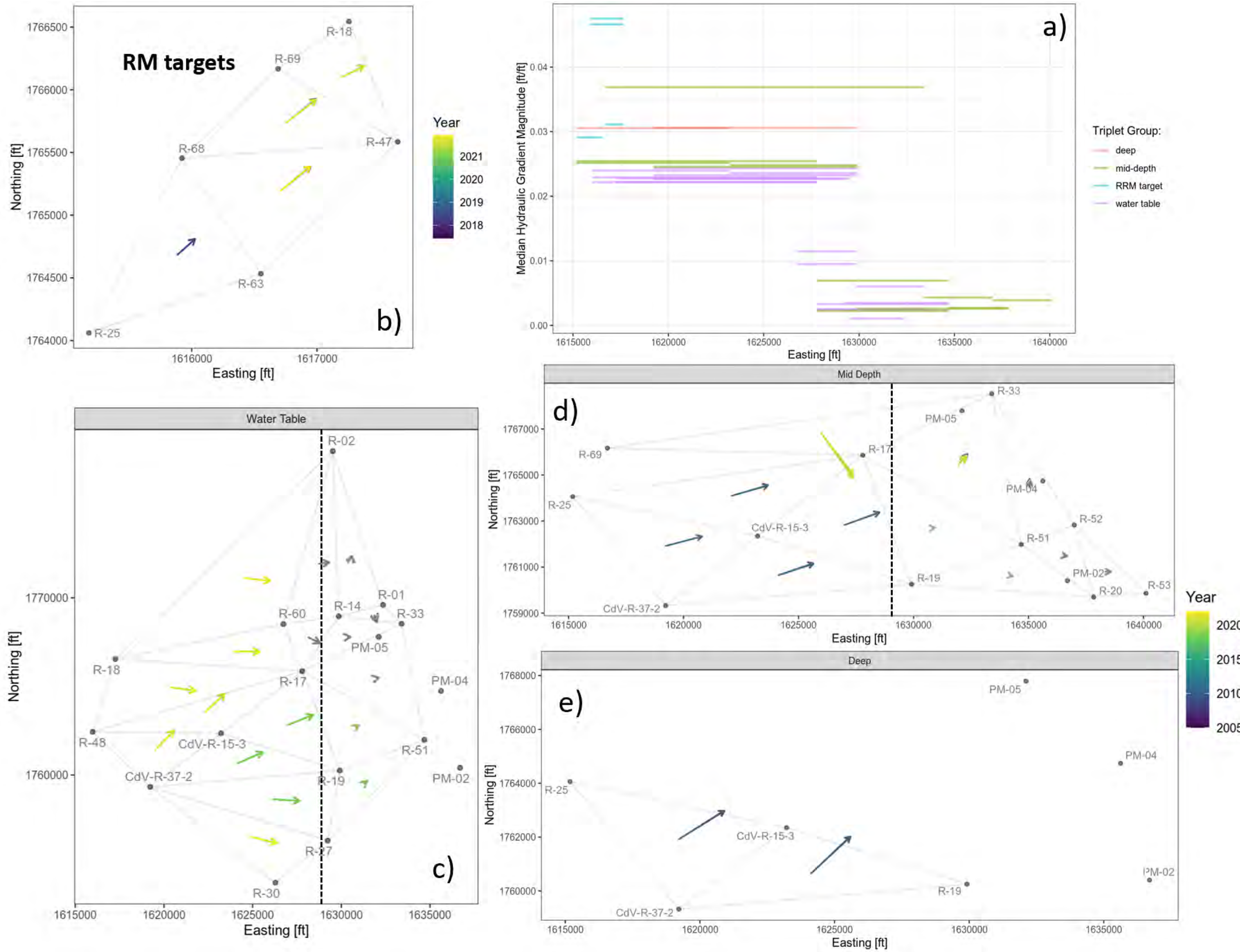

Figure 8. Median lateral gradient for each triplet, colored by group (a) and all weekly lateral hydraulic gradient results for each triplet plotted on top of one another, colored by time (b-e). The RM targets (b) have a separate color bar for time due to their short record. In (c) and (d), the vertical dashed line represents approximately 1628500 ft easting.

2.3.3 Trends over Time

Trend analysis results are described here with results provided in Appendix A. Time series for each triplet are provided in Figure 1 through Figure 6 in Appendix A, and trend results (Sen's Slope and Mann-Kendall analysis) are provided in Table 1 through Table 4. Gradient magnitude and azimuth results are based on weekly averaged water levels described in Section 2.2.1. Appendix A contains time series plots of gradient magnitude and azimuth and trend analysis results for:

- Figure 1 and Table 1 show results for the RM targets triplets.
- Figures 2 and 3, and Table 2, show results for the water-table triplets.
- Figures 4 and 5, and Table 3, show results for mid-depth triplets.
- Figure 6 and Table 4 show results for the deep triplets.

The limited data available for the RM target triplets means that the trend results presented (Figure 1 and Table 1 of Appendix A) should be considered preliminary, uncertain, and subject to change with time as more data are collected for these triplets. Nevertheless, RM target triples appear highly regular over the period of record available; the estimated magnitudes change roughly 1-3% over time and azimuths change about 1 degree over the same period of record.

Hydraulic gradients for the water-table triplets also appear highly regular, though long-term time series indicate small steady increases in magnitude over time for most areas of the regional aquifer between the RDX plume and the supply wells. The results from the Sen's Slope analysis (Appendix A Table 2) of trends in hydraulic gradient magnitude for all water-table triplets show statistically significant, increasing magnitudes at rates on the order of 10^{-6} and 10^{-7} yr^{-1} (i.e., four to five orders of magnitude less than the average gradient of 10^{-2} yr^{-1}).

Trends in azimuth at the water table indicate that some areas are trending slightly more northward (decreasing azimuth), and some areas are trending more southward (increasing azimuth), but overall, the direction of flow for each triplet over time is highly regular. For triplets west of wells R-2, R-60, R-17, R-19 and R-27, azimuths fluctuate only 1-2 degrees over the period of record (10 or more years) available. To the east of these wells, estimated azimuth vary by several degrees, with triplet {R-2, R-1, R-14} varying up to 20 degrees, and {R-33 screen 1, R-17 screen 1, R-14} varying up to 10 degrees. Both triplets are far downgradient of the RDX plume and include wells near PM-05, suggesting that supply-well pumping is affecting water levels at these triplets.

Gradient magnitudes at mid depth are extremely consistent in triplets to the west of R-17 and R-19. In triplet {R-17 screen 2, R-19 screen 4, CdV-R-15-3 screen 5}, gradient magnitude fluctuates between 0.0247 and 0.0250 ft/ft (about 1% difference) over the 5-year record, and triplets further to the west fluctuate approximately half as much in magnitude through time. Like the water-table triplets, hydraulic gradient magnitudes to the east of R-17 and R-19 appear much lower and more variable in time. For example, {R-20 screen 2, R-19 screen 4, R-51 screen 2} is one of the more regular triplets to the east of R-17 and R-19, but gradients at that triplet fluctuate between 0.0024 and 0.0028 ft/ft (about 16% difference). Well triplet {R-17 screen 2, R-33 screen 2, R-51 screen 2} appears the most variable, with gradient magnitude changing up to 50% over time, between 0.006 and 0.009 ft/ft. The Mann-Kendall test suggests that roughly a third of the triplets have no trend in magnitude or azimuth, including {R-17 screen 2, R-33 screen 2, R-51 screen 2}. The remaining triplets include both increasing and decreasing trends, suggesting that no clear trend in magnitude or azimuth is present. Estimated linear changes across mid-depth triplets are roughly 10^{-7} to 10^{-8} yr^{-1}, indicating that any trends over time are miniscule, although some triplets have relatively large fluctuations in magnitude. Azimuths fluctuate less than 1 degree in all mid-depth triplets west of R-17 and R-19; east of these wells, triplets fluctuate up to 5 to 10 degrees over time.

For deep triplets, neither strong trends nor substantial changes in magnitude or azimuth are apparent over the period of record. The Mann-Kendall test for triplet {CdV-R-37-2 screen 3, R-19 screen 4, CdV-R-15-3 S5} indicates a lack of significant trend in magnitude over time, though the estimated azimuth trend suggests an overall small rate of decline, approximately 1 degree over 6 years. The Mann-Kendall test and linear estimates for triplet {CdV-R-37-2 screen 3, R-25 S6, CdV-R-15-3 S5} both suggest slightly decreasing gradient magnitudes over time. Estimates of azimuth are also decreasing, at very low magnitudes. In both triplets, the estimated hydraulic gradient magnitude and azimuth are extremely regular over time, with the magnitude varying less than 1% over the period of record, and azimuth changing less than 1 degree.

2.3.4 Correlation to Supply-Well Pumping RM

Tables 1 through 4 in Appendix A present the results of tests for correlation with supply-well pumping:

- Table 1 provides the results for RM targets.
- Table 2 provides the results for water-table triplets.
- Table 3 provides the results for mid-depth triplets.
- Table 4 provides the results for deep triplets.

In the main text below, Figure 9 plots the correlation results for all triplets. The color indicates the strength of correlation (blue symbolizing positive correlation, and red symbolizing negative correlation); solid circles indicate correlation results with a p-value of less than 0.001. As described in Section 2.2.5, supply-well pumping is defined as the sum total of pumping from PM-02, PM-04, and PM-05.

The limited data available for RDX plume hydraulic gradient triplets (Appendix A, Figure 1) precludes a confident assessment of correlation with supply-well pumping. As with the trend results, the correlation results presented here (Figure 9a and Figure 9b) should be considered preliminary, uncertain, and subject to change as more data are collected.

Gradient magnitudes for triplets{R-18, R-47, R-69 screen 1} and {R-47, R-63, R-68} have high p-values, suggesting no correlation (Appendix A, Table 3). Triplet {R-47, R-68, R-69 screen 1} shows a small negative correlation with supply-well pumping, indicating that increases in supply-well pumping correlate with decreasing lateral hydraulic gradient magnitude; such a correlation is counterintuitive, and the mechanism is unclear. Therefore, this result is likely erroneous due to the limited period of record, and may serve as a reminder of the uncertainty resulting from limited periods of record and/or small sample sizes. The triplet {R-25 S5, R-63, R-68} shows positive correlation with supply-well pumping but has less than a year of available data. Since R-25 screen 5 has been abandoned, no further data will be available for this triplet in the future.

The results of tests for correlation between changes in hydraulic gradient magnitude and azimuth, and total supply-well pumping (PM-02/04/05) at the water table, are shown on Figure 9c and Figure 9d. Statistically-significant positive correlation (p-value < 0.001), represented by solid circles in the figures, is generally observed in hydraulic gradient magnitudes and changes in azimuth in the north and east. This indicates that increases in supply-well pumping are correlated to increases in observed hydraulic gradient magnitudes and changes in the direction of hydraulic gradients. In contrast, significant correlation with magnitude and azimuth is generally not seen in southwest triplets that include well screens in R-48, CdV-R-37-2, and CdV-R-15-3. While hydraulic gradient magnitudes for triplets that include these wells are increasing, changes over time are not correlated to supply-well pumping. The majority of well screens in Figure 9c and Figure 9d are completed in the Puye Formation, with the exceptions of R-48 and CdV-R-37-2 in the south, which are completed in the Tschicoma formation (Figure 3). Local, low-conductivity volcanic geology may influence how temporal impacts from supply-well pumping are propagated through the regional aquifer in this region.

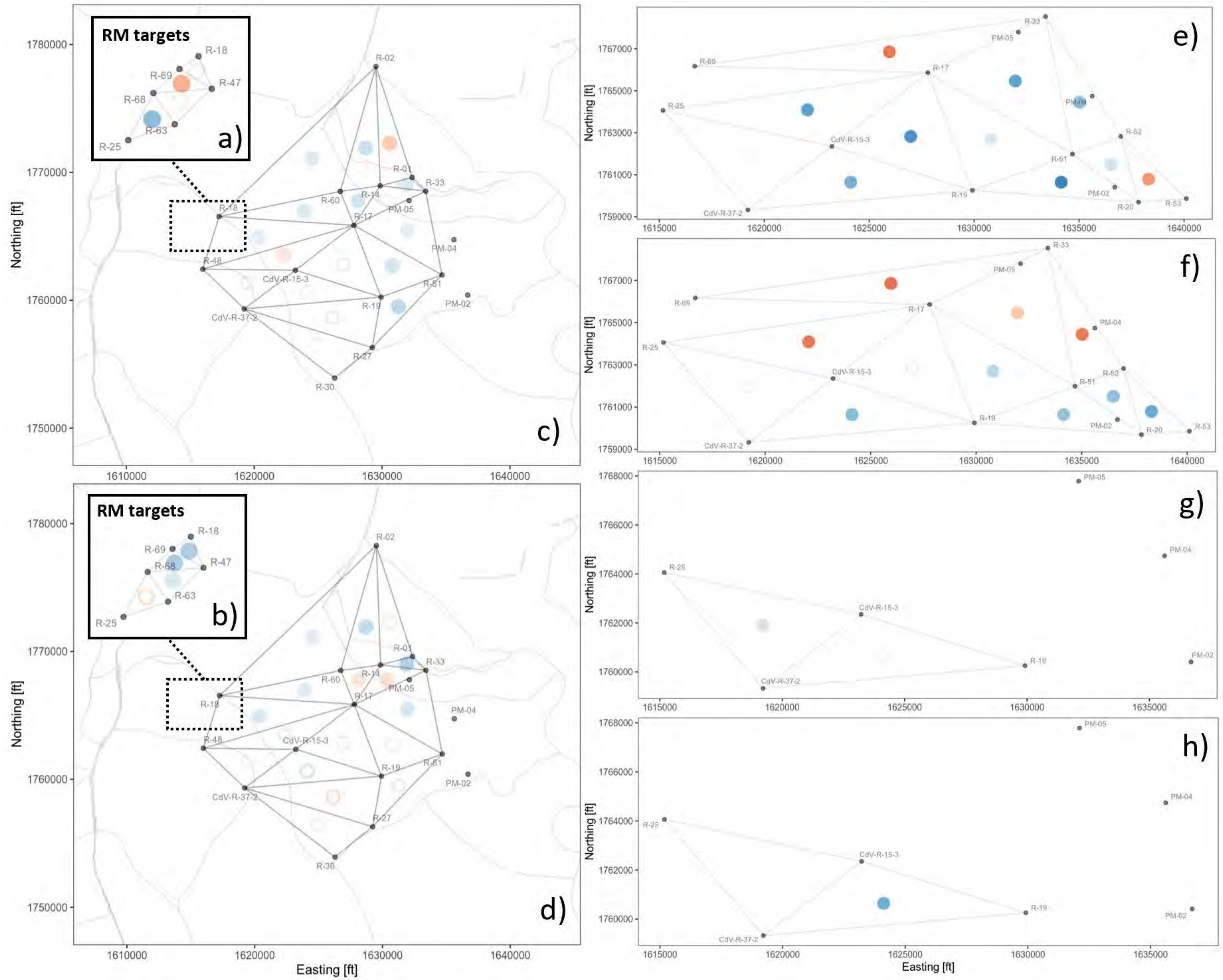

Figure 9. Correlation results for gradient magnitude and total supply-well pumping (above), and gradient azimuth and total supply-well pumping (below) for lateral gradients. Solid circles indicate correlation results with a p-value of less than 0.001.

While trends in time are not apparent in magnitude and azimuth, supply-well pumping shows high correlation to changes; thus, variable pumping rates through time appear to have a stronger influence on gradients at this depth (Figure 9e and Figure 9f). Statistically-significant positive correlation (p-value < 0.001) of hydraulic gradient magnitude with supply-well pumping is observed in nearly all mid-depth well triplets. The exception is the well triplet containing R-69 screen 2, which, due to its limited data in time, should not be considered conclusive. Well triplet {R-20 screen 2, R-52 screen 2, R-53 screen 3}, to the east of the PM wells, shows a negative correlation, corroborating the supply well impacts to the west with an inverse trend. Significant correlation is also generally seen with changes in azimuth in nearly all mid-depth well triplets. In the north, supply-well pumping is correlated to decreasing (more northerly) changes in direction of hydraulic gradients, and in the south increasing (more southerly) changes in direction. Overall, correlation between magnitude/azimuth and supply-well pumping is greater in mid-depth triplets compared to the water-table triplets. Despite CdV-R-37-2 being in the Tschicoma formation (Figure 3), supply-well pumping has a greater influence on hydraulic gradients in the regional aquifer at mid-depth compared to the water table.

For the deep triplets (Figure 9g and Figure 9h), statistically-significant positive correlation (p-value < 0.001) with supply-well pumping and hydraulic gradient magnitude is observed only in triplet {CdV-R-37-2 screen 3, R-25 S6, CdV-R-15-3 S5}, and significant correlation with azimuth is observed only in triplet {CdV-R-37-2 screen 3, R-19 screen 4, CdV-R-15-3 S5}. While some changes in magnitude and azimuth appear to be correlated to supply-well pumping at this depth, deep triplets show very little change in gradient magnitude and azimuth through time, indicating any impacts are likely quite small in magnitude.

2.3.5 Vertical Gradients

Vertical gradients are calculated using vertical screen pairs from multi-screen wells in the regional aquifer. Between the RDX plume and the supply wells, several multi-screened wells are available for analysis; data availability spans from 2000 to 2022. Not all well-screen pairs have water level records over this entire period; however, most pairs have at least 10 years of data (Appendix A, Figure 7). Figure 10a is a cross-section plot showing the median computed vertical gradient and the well's easting. The estimated vertical gradients are highest in the west, decreasing rapidly to the east. R-25 is the closest well to the mountain front with reliable data. Well R-26, shown in Figure 2, does not have reliable data due to issues with well construction (Kleinfelder 2005), and screens 5 and 6 have the largest measured vertical gradient; magnitudes decline rapidly with distance from the mountain front.

While spatial patterns are evident in vertical gradients, magnitudes are much more variable over time compared to the variability in lateral gradients. This could be due to different barometric influences (e.g., well barometric efficiency), especially when deep screens are involved. In other portions of the regional aquifer, where more recent wells are located with high barometric efficiency, changes in water level due to shifts in barometric pressure tend to occur rapidly and similarly across wells. However, in the RDX and downgradient region, older wells (such as R-25, CdV-R-15-3, and CdV-R-37-2) often have different barometric responses. While barometric correction is performed on the water level data here, it is an inexact correction.

Despite large changes in magnitude, and water-level records that span more than ten years, long-term trends in vertical gradient are very small or absent. While the Mann-Kendall test indicates significant trends in magnitude for some triplets over time, overall the estimated linear changes are on the order of 10^{-5} to 10^{-7} yr^{-1}. The variability in vertical gradients appears to overwhelm any small temporal trends.

Tests for correlation between changes in vertical gradient magnitude and supply-well pumping at PM-02/04/05 (Figure 10b) show that statistically-significant positive correlation (p-value < 0.001) of supply-well pumping with hydraulic gradient magnitude is observed in wells near the supply wells. As distance increases, little to no correlation is observed. In the RDX plume and immediate downgradient region, changes in vertical gradients are not correlated to downgradient supply-well pumping.

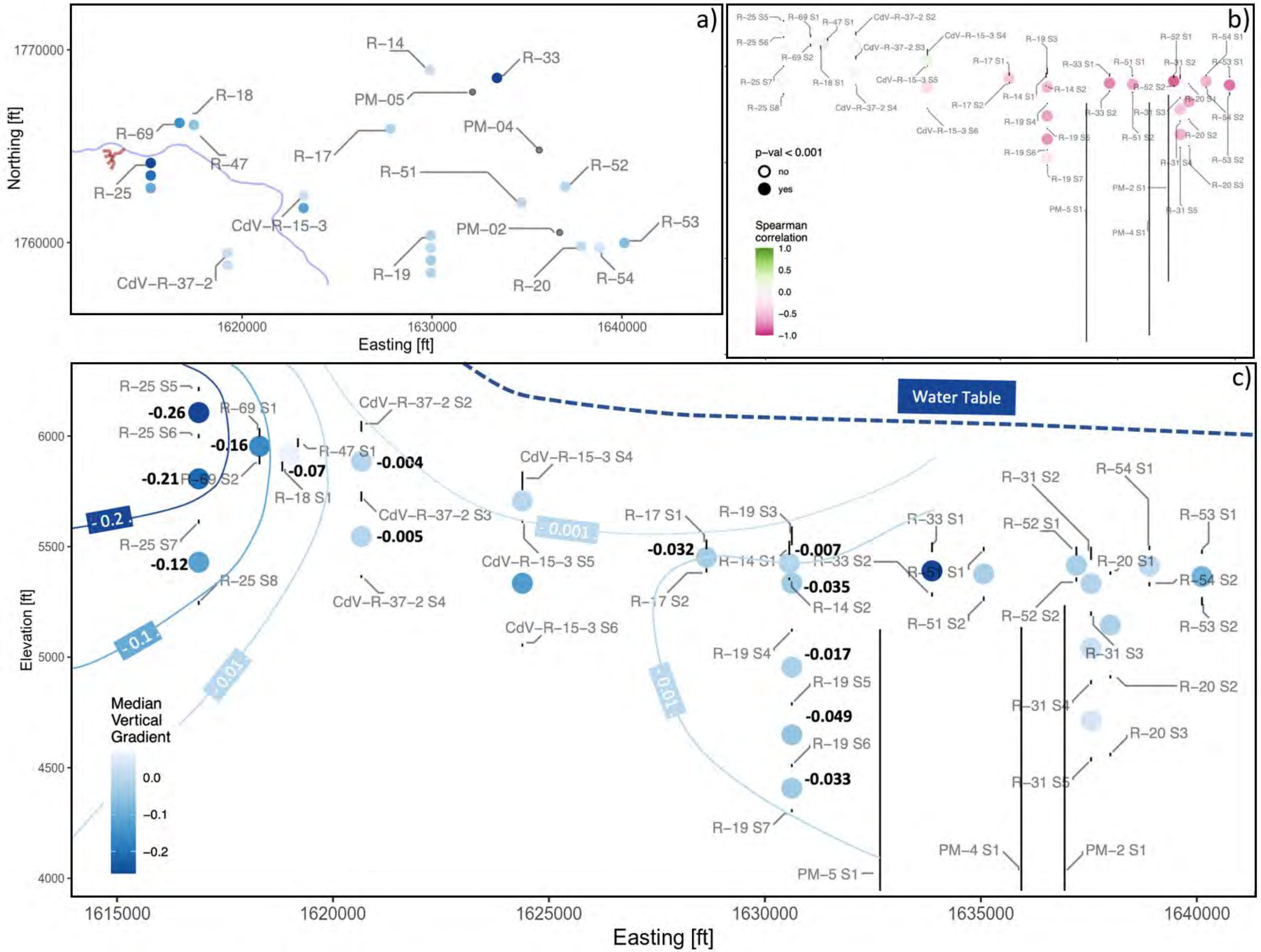

Figure 10. Calculated median vertical gradient for wells in the RDX region shown in plan view (a), and cross section view (c) with gradient contours added. The upper right plot (b) shows correlation between vertical gradients and total (PM-02 + PM-04 + PM-05) supply well pumping.

2.4 Discussion and Conclusions

The hydraulic analysis results show that strong lateral gradients are present in the western portion of the regional aquifer, close to the mountain block where the RDX plume is located, and that lateral gradient magnitudes dissipate quickly with distance from the mountain front. Combining all lateral gradients at all depth horizons into a single plot (Figure 8a), the strong decline in lateral magnitude from west to east is evident. A similar pattern is observed spatially with vertical gradients in the regional aquifer (Figure 10c). The largest vertical gradients are observed in R-25, the closest multi-screened well to the mountain block, and drop rapidly with distance from the mountain block. Further to the east, vertical gradients are small. At R-17 and R-19, the vertical gradients are approximately an order of magnitude less than those observed in the RDX plume area.

The presence of strong lateral and downward vertical gradients in the RDX plume region corroborates the conceptual model of regional groundwater flow and expected structure of equipotential contours from recharge in mountainous environments. In this type of environment, recharge from the mountain front is expected to produce strong local lateral and vertical gradients that quickly dissipate with distance away from the mountain block. While flow is generally expected to occur from west to east, local to the RDX plume and immediately downgradient, flow appears to be deflected to the northeast. This is likely a combination of spatially-variable recharge and the heterogeneous geology of the regional aquifer; the large low-permeability Tschicoma dacite unit to the south likely affects local flow patterns in the regional aquifer.

Tests for correlation between supply-well pumping and changes in lateral gradients indicate that supply-well pumping does have some degree of influence on gradients across the site. However, the influence diminishes with distance.

At the water table, statistically-significant positive correlation (p-value < 0.001) is observed in hydraulic gradient magnitudes and azimuths to the north and east. Significant correlation with gradient and azimuth is generally not seen in triplets to the southwest that include well screens from R-48, CdV-R-37-2, and CdV-R-15-3. Again, the large low permeability Tschicoma dacite unit to the south likely impacts how drawdown from supply-well pumping is propagated through the regional aquifer in this region.

Results for mid-depth triplets generally show higher correlation with supply-well pumping compared to the water-table triplets, including triplets with wells screens from R-48, CdV-R-37-2, and CdV-R-15-3. This is consistent with previous observations in the regional aquifer, where lower screens show greater response to supply-well pumping compared to screens at the water table (McLin 2005, 2006). While gradients appear more correlated to supply-well pumping at this depth, long-term trends are less apparent.

The two deep triplets show very weak or no correlation with supply-well pumping with magnitude; however, the triplet closer to the supply wells {CdV-R-37-2 screen 3, R-19 screen 4, CdV-R-15-3 screen 5} shows relatively high correlation between azimuth and supply-well pumping. Estimates of gradient magnitude and azimuth from triplets in the east show a high sensitivity to supply-well pumping. Triplets that include a supply well are probably inaccurate during periods of pumping. Nevertheless, the results show that water levels in the region show responses to pumping, and estimates of hydraulic gradient are likely impacted. The estimated gradients and azimuth for these triplets are probably only accurate within order of magnitude.

Despite the high correlation with supply-well pumping, and the fact that, in some cases, supply wells are included within a triplet, the variability in computed azimuth is extremely low, ranging less than 1 degree over the 6-year period of record. Therefore, while water levels appear sensitive to changes in supply-well pumping, the change in estimated hydraulic gradient and azimuth between periods when pumping is on, and when it is off, appears to be very small.

Testing for correlation with supply-well pumping and vertical gradients in the RDX plume and immediate downgradient region show no correlation with supply-well pumping. However, vertical gradients in wells near supply wells show higher correlation to supply-well pumping. Wells in very close proximity to the supply wells, such as R-20 screens 2 and 3, show very high correlation (0.926) to supply-well pumping.

Though small long-term trends are evident, the regularity of hydraulic gradients in the regional aquifer suggests that impacts from supply-well pumping in the RDX plume and downgradient area of the regional aquifer are minimal. Additionally, the observed lateral and vertical gradients in the RDX plume region are roughly 1 to 2 orders of magnitude higher than those downgradient and near the supply wells. This indicates that recharge mechanisms at the mountain front are far more likely to control the magnitude and direction of groundwater flow in this region of the aquifer compared to supply-well pumping. The results indicate that supply-well pumping has a measurable impact on hydraulic gradients in the regional aquifer, but their impact diminishes quickly with distance from their location. For most triplets in the RDX plume and downgradient, linear estimates of gradient magnitude indicate changes on the order of 10^{-6} to 10^{-8} ft/ft per year across all depth horizons. In the RDX plume and downgradient area of the regional aquifer, this equates to changes in magnitude and azimuth of 1 to 3% over the period of record. In the context of contaminant fate and transport modeling, a difference of this magnitude in modeled hydraulic gradient is negligible.

Overall, the two questions posed in introducing the reason for this data-based study of hydraulic gradients have been answered in these hydraulic analyses:

(1) Regional aquifer gradients are not expected to change in the RDX plume and downgradient portion of the regional aquifer enough to significantly affect flow and transport.
(2) Systematic changes in gradients due to county supply-well pumping appear to be limited to approximately 1.25 miles (2 km) radius from supply wells. Outside of this radius, hydraulic gradients are very regular.

3.0 Chromium Plume-Related Hydraulic Analyses

This section presents an investigation into hydraulic gradients of the regional aquifer within the vicinity of the chromium plume located in the regional aquifer below LANL.

3.1 Introduction

The purpose of installing the Interim Measures (IM) extraction, treatment, and injection system was to establish hydraulic control of the Cr plume (LANL 2015). Hydraulic analyses are performed in this section to quantify hydraulic gradients within the Cr plume site, and compare the shifts in magnitude and direction attributable to IM operations to those resulting from pumping from nearby Los Alamos County (LAC) supply wells (i.e., PM wells). In the current Cr model (CM), supply wells are not included as pumping stresses, because they are assumed to have a negligible impact. This section tests that assumption: the impact that supply wells have on vertical and lateral hydraulic gradients near the Cr plume is quantitatively compared to the impacts from the IM extraction and injection system.

While some PM wells have been shown to impact water levels in some monitoring wells within the Cr plume (McLin 2005, 2006; N3B 2021), the prevailing hypothesis has been that local extraction and injection from the IM overwhelms any potential impacts from the deeper and more distant (but longer-screened) supply wells that pump at much higher rates. Recent concerns that the fate and transport of Cr in the regional aquifer would not be accurately simulated without these stressors in the model have been raised, and this data-based study of hydraulic gradients was performed to interrogate this directly by answering the following two questions:

(1) Are estimated hydraulic gradients in the Cr plume expected to be impacted by PM-04 pumping enough to meaningfully affect contaminant fate and transport?
(2) How do the impacts from PM-04 pumping on hydraulic gradients compare to impacts from IM operations?

Section 3.2.2 provides additional detail regarding why PM-04 is the supply well of focus, and why PM-03, while much closer to the plume, is not considered in this analysis.

Gradient control points are described in “A Systematic Approach for Evaluation of Capture Zones at Pump and Treat Systems” (EPA 2008) as a way to demonstrate inward flow relative to a boundary, such as a property boundary or a target capture zone. The gradients are typically calculated between pairs of wells on either side of the boundary, or, in a more complex example in EPA (2008), as triplets calculated using the three-point method (Heath (1983), as described in Section 2.2.2. The density of wells in the Cr plume does not permit the types of well pair analyses suggested by EPA (2008), as wells are typically sparse in number and located several hundred feet apart (e.g., the cluster of wells between PM-02, PM-04, and PM-05 in Figure 2; also refer to Section 3.3 for spatial plots of Cr plume wells). The three-point method is used here to estimate lateral hydraulic gradients, which are used to quantitatively explore the impacts of IM operations versus supply well pumping on lateral gradients; well-screen pairs at dual-screened wells are used to look at pumping impacts on vertical gradients.

Four periods are identified:

- a baseline period when neither the IM nor PM-04 was pumping for an extended period,
- aquifer conditions when the IM had sustained operations in the absence of PM-04 pumping,
- aquifer conditions during extended periods when PM-04 had sustained operations while the IM was off, and
- aquifer conditions during extended periods when PM-04 and the IM were both operating simultaneously.

Periods are defined as times when pumping, IM operations, or both, had been occurring continuously for several weeks prior to data collection, and aquifer conditions are assumed to be in quasi-equilibrium with the pumping stresses and little further drawdown is occurring. Statistical tests are used to determine where significant differences in magnitude and direction exist between operational and baseline conditions. This enables the impacts of PM-04 to be quantitatively compared to the impacts of the IM. A ratio representing the magnitude of change in gradient and direction between the two periods is provided, where appropriate, to identify which portions of the aquifer are dominated by IM extraction and injection operations, and where supply wells have a greater impact.

3.1.1 Geologic Context

This section builds on the site descriptions provided in 2.1.

The shallow portion of the regional aquifer at the Cr plume lies mostly within the Puye Formation (Puye). However, a few monitoring wells penetrate below the Puye and into the upper portion of the underlying Miocene sediments (also known as the upper Santa Fe sediments, or Tcar). Figure 11 shows a cross-sectional view of the local geology in relation to the approximate regional water table (modified from N3B 2021). Supply well screens for PM-04 and PM-03 extend deep into the Tcar, including though several sequences of Miocene basalt. Regional aquifer well screens R-35, R-45, R-50, and R-70 are also shown.

While the Puye is over a thousand feet thick in the western portion of the aquifer (LANL 2018, 602963), near the Cr plume it is only a few hundred feet thick, in part due to the presence of a large sequence of basalt layers in the unsaturated zone, known as the Cerros del Rio basalt, that intersect the Puye. As indicated, small thin sequences of Puye sediments are sometimes encountered above the Cerros del Rio basalts. The remainder of the unsaturated zone to the ground surface is comprised of the Bandelier Tuff. Below the water table, Miocene basalts intersect the Tcar.

Few wells have been constructed into the Tcar, due to Cr contamination being largely restricted to the first 100-150 ft of the water table surface, and generally within the Puye. Additionally, the poorly consolidated sediments of the Tcar make drilling and completing monitoring wells challenging in these formations.

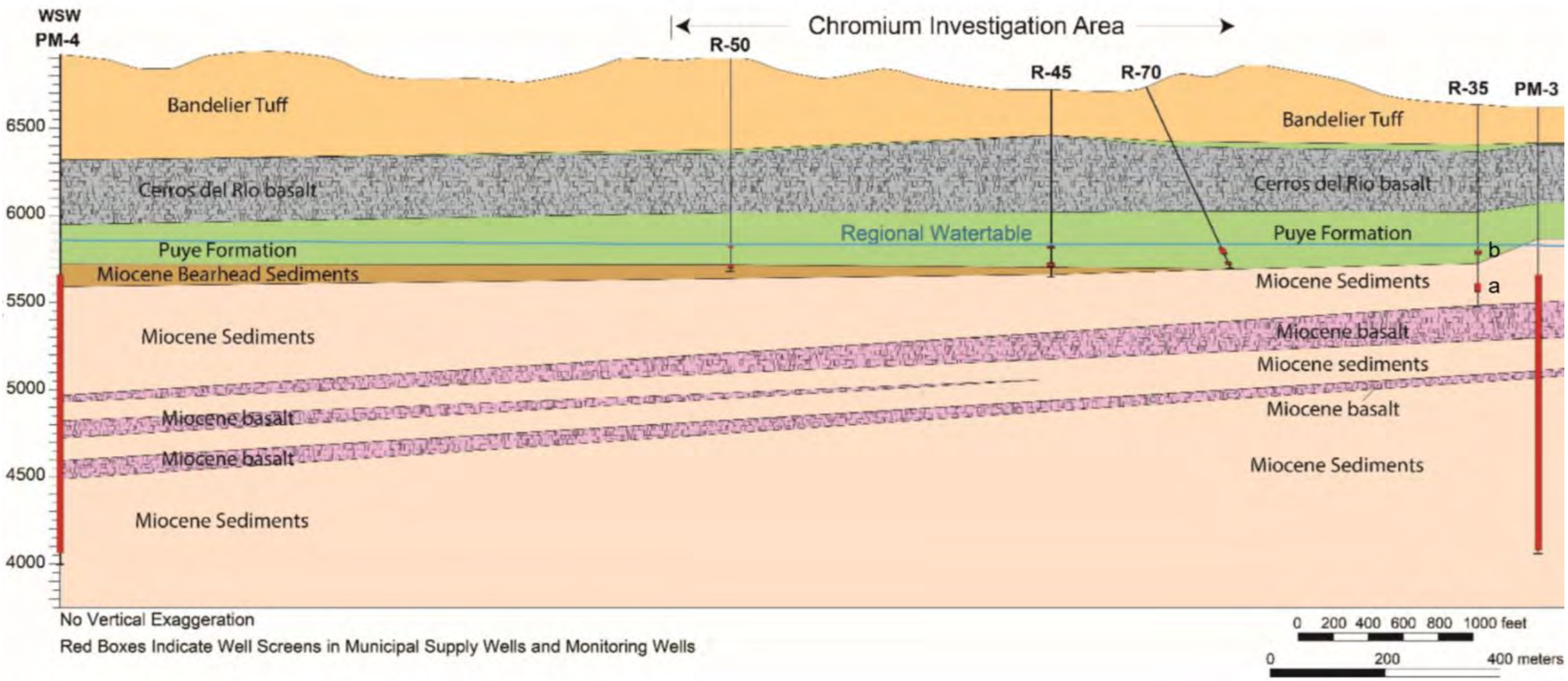

Figure 11. Cross-section of geology below the Cr plume. Supply wells are shown in red, and shallow Cr plume monitoring wells are shown in black (figure modified from (N3B 2021)).

3.1.2 Hydrologic Context

The regional water table in the Cr plume region is comparatively flat (Figure 2). At the western boundary of the regional aquifer, recharge from the Sierra de los Valles mountain block provides higher hydraulic heads, producing vertical and lateral gradients that are 1 to 2 orders of magnitude higher than those observed upgradient of the Cr plume (Section 2.3). This forces an overall west-to-east gradient in the regional aquifer, which is maintained through the Cr plume, though gradients are comparatively small. In the Cr plume, the flat water table results in small calculated differences in water-level elevation between monitoring locations. Thus, in this portion of the regional aquifer, estimates of hydraulic gradient magnitude and direction are more sensitive to small changes in water levels from pumping stresses. Pumping tests have shown a higher degree of lateral connectivity compared to vertical connectivity within the aquifer, suggesting that hydraulic conductivities are generally higher laterally than vertically (McLin 2005, 2006). This vertical anisotropy within the aquifer is probably caused by the depositional layering of the stratigraphic units of the regional aquifer; overall aquifer behavior is described as semi-confined or leaky. Additional discussion on aquifer characteristics is provided in Section 3.2.2.

At the land surface, steep canyons between mesas on the Pajarito Plateau have the ability to channelize and concentrate flow into the canyon bottoms, resulting in focused infiltration to the subsurface (Purtymun 1975). Most recharge, however, is thought to occur close to the mountain block. Surface expressions are rare on the Pajarito Plateau; most streamflow occurs only during heavy precipitation events, and rapidly infiltrates through highly permeable alluvial streambed sediments. Perennial flow is seen in a few streams on the steep slopes of the Sierra de los Valles. However, most surface water infiltrates to the subsurface by the time it reaches the western boundary of LANL (Figure 2); surface flows within the LANL boundary are typically ephemeral and do not regularly flow offsite.

Near the Cr plume, large amounts of stream loss in Sandia Canyon (fed largely by treated waste, cooling tower blowdown, and other lab discharges) have been observed along the streambed, resulting in perched zones of saturation within the VZ. However, the lack of mounding, and the presence of an extremely flat water table in this region, suggest that rates of total recharge from the VZ are relatively low and diffuse. Perched zones in the VZ coincide with Cerros del Rio basalt layers; these zones are thought to have the ability to collect and divert the flow of recharge laterally to some extent.

Because recharge is considered minimal and does not substantially impact flow in this portion of the regional aquifer, estimated hydraulic gradients are sensitive to small changes in water levels from groundwater pumping. In the next sections, the impacts to hydraulic gradients from pumping stresses in the vicinity of the Cr plume are quantified and compared.

3.2 Methods

3.2.1 Water-Level Data

Water level data from monitoring wells across the Pajarito Plateau are publicly available on IntellusNM, the public version of LANL's EIM database (https://intellusnm.com). In contrast to the RDX study, which focused on quantifying trends over time and correlating observed changes to downgradient supply-well pumping. For the Cr plume, periods are identified in the record where minimal transience in water levels are expected under certain pumping conditions, and are compared quantitatively. Each period is identified to reflect a semi-steady state where all active well pumping has been relatively constant for several weeks, and drawdown responses and estimated gradients are changing minimally.

Temporal averaging is not used in this series of analyses, and no barometric corrections are performed. Water-level data for monitoring wells is provided on an hourly basis during all four periods, though none of the wells have water levels for every hour within a period. During these periods (periods are defined in Section 3.2.3), each calculated lateral and vertical gradient is considered to be an independent sample/assessment of quasi-steady-state aquifer conditions. The mean and standard deviations of baseline water levels used in these analyses are shown in the pink columns of Table 1, indicating that, for most wells, the standard deviation within a period is very small, and is at least an order of magnitude less than the magnitude of change observed between periods. To condense the results section, histogram plots of water levels for each well screen are provided in Appendix B, Figures 1 through 29.

For lateral gradients, well triplets are defined using well screens at the same approximate depth below the water table. Well screens in the Cr plume vicinity allow two depths to be investigated within the regional aquifer:

- the first depth, near the top of the water table (with one exception, noted below), referred to here as "shallow," is represented by wells with only a single screen or the upper screen (typically screen 1 or "S1") in multi-screened wells; and
- the second depth, referred to here as "deep," is represented by the lower screen in dual-screened wells (typically screen 2 or "S2").

The exception noted above is R-13, which is a single-screened well that is completed about 150 ft below the water table, roughly equivalent to other deep screens in dual-screened wells. It is used in both shallow and deep triplets to provide estimates of impacts to lateral gradients in the region east of R-44 and R-45. Additionally, R-35a is purposely excluded from the deep analyses because it is known to be connected with PM-03 (which is not controlled for in this analysis), and any impacts from PM-04 or the IM are extremely minor in comparison. R-35a is the only Cr plume well that shows any connection to PM-03 pumping; the Cr plume does not exist at the R-35a location, and therefore R-35a is not the focus of this analysis.

Table 1. Mean water level elevation (in feet), standard deviation (SD), and change from baseline for the three pumping periods.

	PM-04 off + IM off (baseline)		PM-04 on + IM off			PM-04 off + IM on			PM-04 on + IM on		
Well	Mean	SD	Change	Mean	SD	Change	Mean	SD	Change	Mean	SD
CrPZ-1	5,833.24	0.09	-0.52	5,832.72	0.14	-3.59	5,829.64	0.18	-4.1	5,829.14	0.06
CrPZ-2a	5,831.58	0.09	-0.43	5,831.14	0.13	-1.46	5,830.12	0.16	-1.89	5,829.69	0.06
CrPZ-2b	5,831.41	0.09	-0.45	5,830.97	0.13	-1.93	5,829.48	0.16	-2.38	5,829.04	0.06
CrPZ-3	5,832.57	0.1	-0.48	5,832.09	0.15	-2.04	5,830.53	0.21	-2.61	5,829.96	0.06
CrPZ-4	5,833.08	0.09	-0.55	5,832.52	0.14	-1.71	5,831.37	0.17	-2.25	5,830.82	0.06
CrPZ-5	5,834.29	0.09	-0.57	5,833.72	0.14	-1.54	5,832.75	0.17	-2.15	5,832.15	0.06
R-01	5,874.46	0.12	-0.14	5,874.32	0.11	-0.37	5,874.09	0.19	-0.66	5,873.80	0.06
R-11	5,832.03	0.09	-0.34	5,831.69	0.12	-1.36	5,830.67	0.18	-1.79	5,830.25	0.07
R-13	5,830.04	0.08	-0.5	5,829.55	0.13	-0.47	5,829.58	0.17	-1.11	5,828.94	0.05
R-15	5,844.12	0.12	-1.83	5,842.29	0.2	-1.19	5,842.93	0.17	-3.05	5,841.07	0.09
R-33 S1	5,866.14	0.1	-0.23	5,865.91	0.12	-0.62	5,865.51	0.19	-1	5,865.13	0.06
R-33 S2	5,834.97	3.56	-3.01	5,831.96	0.5	3.77	5,838.74	2.51	-3.41	5,831.56	0.21
R-35a	5,825.55	1.35	-5.84	5,819.70	2.08	0.04	5,825.58	0.94	-0.89	5,824.65	0.64
R-35b	5,831.54	0.09	-0.21	5,831.34	0.11	-0.64	5,830.90	0.18	-0.88	5,830.66	0.06
R-42	5,832.79	0.1	-0.34	5,832.44	0.13	-2.39	5,830.39	0.28	-2.98	5,829.80	0.06
R-43 S1	5,833.03	0.09	-0.39	5,832.64	0.13	-0.97	5,832.06	0.18	-1.47	5,831.56	0.06
R-43 S2	5,832.33	0.09	-0.51	5,831.82	0.14	-0.87	5,831.46	0.18	-1.48	5,830.84	0.06
R-44 S1	5,830.96	0.08	-0.47	5,830.48	0.12	-0.03	5,830.93	0.18	-0.59	5,830.37	0.06
R-44 S2	5,830.62	0.09	-0.54	5,830.07	0.14	-0.19	5,830.43	0.18	-0.9	5,829.72	0.05
R-45 S1	5,830.70	0.09	-0.43	5,830.27	0.13	0.42	5,831.11	0.18	-0.06	5,830.63	0.09
R-45 S2	5,830.54	0.09	-0.46	5,830.08	0.13	-0.27	5,830.27	0.18	-0.84	5,829.70	0.1
R-50 S1	5,832.10	0.08	-0.5	5,831.60	0.12	-0.15	5,831.95	0.18	-0.79	5,831.31	0.06
R-50 S2	5,831.95	0.09	-0.6	5,831.36	0.13	-1.22	5,830.73	0.18	-1.96	5,829.99	0.06
R-61 S1	5,833.20	0.09	-0.55	5,832.64	0.12	-1.38	5,831.81	0.18	-2.09	5,831.11	0.06
R-61 S2	5,833.27	0.09	-0.61	5,832.66	0.13	-1.6	5,831.67	0.18	-2.38	5,830.89	0.06
R-62	5,835.98	0.08	-0.43	5,835.55	0.13	-1.02	5,834.96	0.18	-1.56	5,834.42	0.06
R-70 S1	5,831.70	0.08	-0.37	5,831.33	0.12	-0.63	5,831.07	0.18	-1.08	5,830.62	0.06
R-70 S2	5,831.83	0.08	-0.39	5,831.44	0.12	-0.75	5,831.09	0.19	-1.23	5,830.60	0.1
SIMR-2	5,831.09	0.09	-0.45	5,830.64	0.14	-0.2	5,830.89	0.18	-0.79	5,830.31	0.06

3.2.2 Supply Well PM-04

The focus of this analysis is to compare the impact from supply-well pumping to that from the operation of the IM. County supply well PM-04 was selected to represent the maximum impact that an existing and operating supply well can have on gradients within the Cr plume. Figure 12 shows average active pumping rates for Los Alamos County water supply wells. PM-04 (represented by blue dots on Figure 12) extracts at the highest average rate of all supply wells, and is not turned off daily as the other supply wells typically are. When wells pump at variable rates, for various lengths of time, and are shut off daily, the transience in the pumping signal makes it difficult to quantify the magnitude and extent to which a well may affect hydraulic gradients in the surrounding aquifer.

To determine the extent to which a well can influence water levels spatially in an aquifer, wells are pumped continuously for several days to weeks, allowing a cone of depression to expand into the surrounding aquifer. In large expansive aquifers without substantial lateral flow barriers, such as the regional aquifer below the Pajarito Plateau, a well's cone of depression expansion will slow down with time as the pumping stresses come into semi-equilibrium with sources of recharge to the aquifer (e.g., losing streams). If a cone of depression in a perfectly confined aquifer of infinite extent does not reach a source of recharge, it will continue to expand with time. At any monitoring location, drawdown will continue to increase with time and will never reach a steady state, though the rate of decline will diminish through time as the cone of depression expands further into the aquifer.

In a semi-confined or "leaky" aquifer like the regional aquifer below the Pajarito Plateau, a cone of depression initially develops around a well, and observed drawdown responses at nearby monitoring locations are similar to those of a confined aquifer. However, in leaky aquifers, the observed rate of decline in monitoring wells tends to abate much more quickly (or stop declining altogether), compared to what would be predicted in a perfectly confined system. The lower rates of displacement indicate that the stresses from pumping are being offset by recharge somewhere in the system, and further (steady) pumping does not result in declines in hydraulic head. In the case of leaky aquifers, a drop in hydraulic head below an overlying semi-confining layer can produce vertical gradients within this leaky layer, causing downward vertical flow and recharge to the productive portion of the aquifer below.

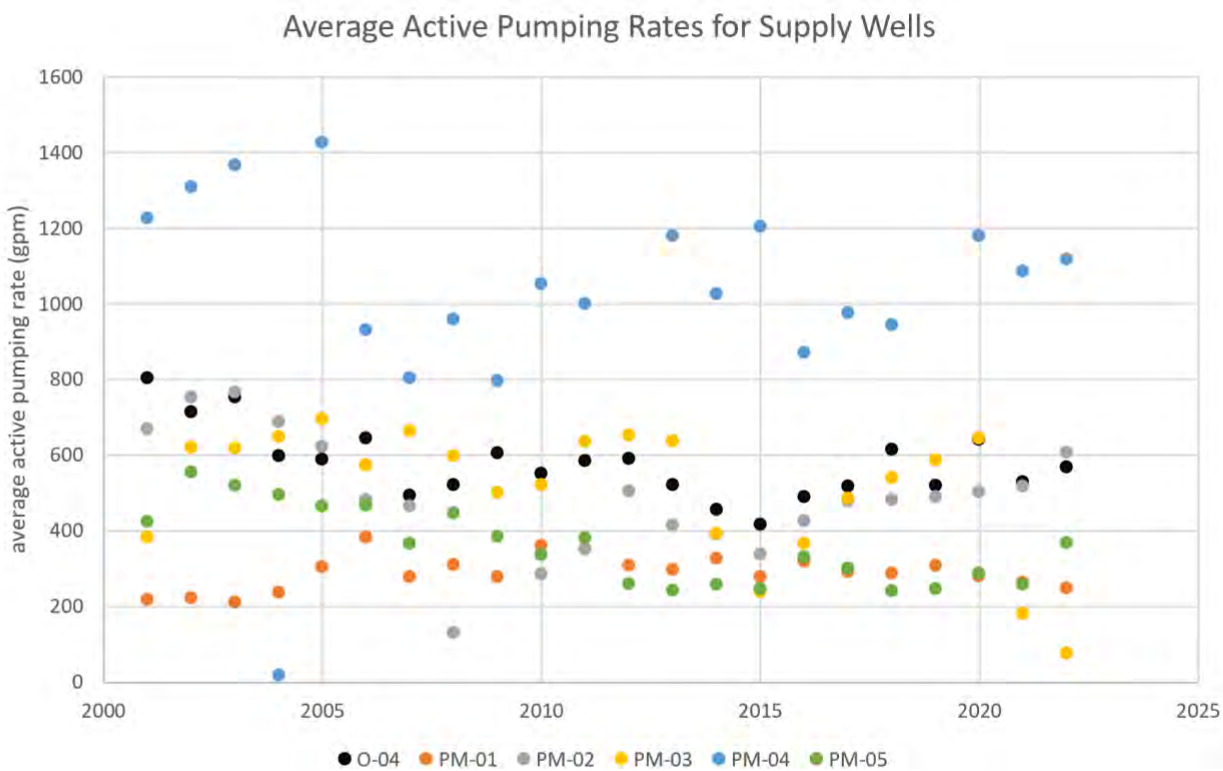

Figure 12. Average active pumping rates for Los Alamos County water supply wells. Only the reported rates for days of active pumping are used to calculate averages, days without pumping (0 gpm) are removed before averaging.

Reponses observed in monitoring wells from multiple-week aquifer tests show a clear reduction in water level displacement after one to two weeks of steady pumping. Supply wells are typically completed deeper in the aquifer; the screens in those wells start a few hundred feet below the water table and extend more than 1,000 feet. This "leaky-aquifer" behavior condition during long periods of sustained pumping is evident in Figure 13, which represents data collected from aquifer tests at PM-02 and PM-04, which lasted 25 and 21 days, respectively.

In both aquifer tests, the observed water-level displacement at the other supply well (PM-02 when PM-04 is in operation, and vice versa) diminishes after two to three weeks of sustained operation. The top two charts in Figure 13 show the aquifer test drawdown data fit to a confined aquifer Theis solution (blue curve), and the bottom two charts show the data fit to the Hantush-Jacob leaky aquifer solution. As described earlier, the confined aquifer Theis solution provides a good fit to early time data, but departs substantially from the observed data after only a few days. In contrast, the leaking aquifer solutions, which accounts for recharge from an overlying leaky layer, shows a much better overall fit to both early *and* late-time data. The range of estimated values of transmissivity (3,000 to 4,235 ft^2/day) for the regional aquifer reflect the uncertainty in parameter estimates obtained from aquifer tests.

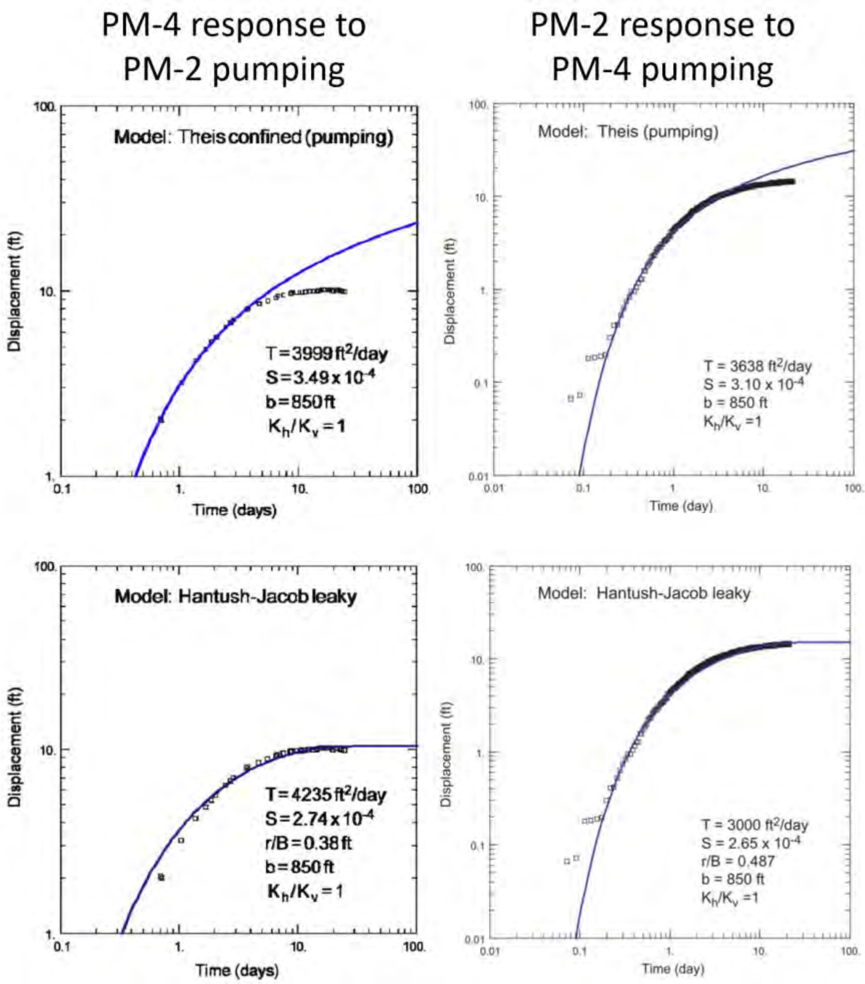

Figure 13. The top two charts show aquifer test drawdown data fit to a confined aquifer Theis solution (blue curve); the bottom two charts show the data fit to the Hantush-Jacob leaky aquifer solution. The confined aquifer Theis solution provides a good fit to early time data, but departs from the observed data after a few days. In contrast, the leaking aquifer solutions, which accounts for recharge from an overlying leaky layer, shows a much better overall fit to both early and late-time data.

The PM-02 and PM-04 pump tests are examples of ways to estimate the maximum impact a well has in an aquifer. However, they are logistically difficult to plan (ideally all surrounding wells are turned off) and therefore these types of tests occur at most a few times in a well's lifetime, and often only once following completion of the well. The PM-02 and PM-04 pump tests occurred in 2005 and 2006 (McLin 2005, 2006), respectively, when few monitoring wells existed in the Cr plume. Fortunately, when PM-02's 25-day aquifer test was conducted, R-13 and R-15 along the Cr plume's southern and western boundary, and PM-03 to the northeast of the Cr plume, were already installed. No water-level changes were observed at any of the three wells; they are thought to be too shallow and do not penetrate into the water-bearing units that yield water to PM-02 (R-13 and R-15) and/or the distance too great (PM-03, despite it being completed in similar water-bearing unit). Therefore, the impacts from pumping at PM-02 are ignored in this analysis.

Impacts from pumping at PM-03 are also neglected; R-35a is "the only monitoring well in the chromium investigation that shows a response to PM-03" (N3B 2021), despite its close proximity to the Cr plume (see Figure 11). It is theorized that strong vertical anisotropy is present throughout the regional aquifer, which may in part explain this behavior. Additionally, the Miocene basalt layers intersect PM-03's upper screen, potentially providing a hydraulically limiting barrier to shallower elevations in the aquifer (though R-35a is located above the basalt, which contradicts this). R-35b, located higher in the aquifer near the water table, shows no response to PM-03 pumping (N3B 2021).

During PM-04's aquifer test, water level decline was observed in PM-05, R-15, R-13, and R-14. The test results (McLin 2006) concluded that "in all probability, both PM-04 and PM-05 are in hydraulic communication with numerous other wells in Mortandad Canyon, including wells R-1, R-33, TW-8, R-28, and R-34." The theoretical extent of PM-04's influence was depicted extending to Otowi-4 (O-4) to the northwest of the Cr plume.

While extended pumping from PM-05 and O-4, such as that from multi-week aquifer tests, could produce a cone of depression that would likely extend to regions of the Cr plume (and thus impact hydraulic gradients), their pumping schedules are such that they only operate a fraction of the day. Like most supply wells, PM-05 and O-4 are typically only operated at night, and are shut off during the day. The lack of sustained operation does not permit the development of large cones of depression, like those during aquifer tests described previously. The daily on/off operation of PM-05 and O-4 allows the aquifer to recover from their pumping stresses; direct impacts on regional hydraulic gradients are likely much more localized compared to those from PM-04.

In contrast, PM-04 normally operates relatively constantly for long periods, similar to a pump test. Continuous pumping allows the cone of depression to extend much further into the aquifer, resulting in sustained shifts in hydraulic gradient. Historically, PM-04 has operated primarily in the summer months to accommodate the increase in water demand. Once turned on, it is typically operated continuously for weeks to months at a time. This operational schedule allows several opportunities to identify sustained periods of operations in the historical record, in contrast to the limited data available during the PM-02 and PM-04 pump tests in 2005 and 2006.

In summary, this analysis focuses on PM-04 because it is the supply well that:

- is closest to the Cr plume (other than PM-03, which shows little impact);
- pumps at the highest flow rate of all supply wells;
- has the most observed hydraulic connections to wells within the Cr plume;
- creates the largest cone of depression compared to other supply wells from operations; and
- provides multiple opportunities to look at sustained pumping events.

3.2.3 Time Periods

Three time periods are selected to bracket ideal times when PM-04 was pumping steadily and/or the IM was operating continuously for a few consecutive weeks, allowing the aquifer to come into quasi-equilibrium with the pumping stresses. The dates defining each period are included in Table 2, and shown graphically in Figure 14 where periods are highlighted on timeseries water levels from representative well screens within the Cr plume. These pumping periods are compared to a baseline period when neither the IM nor PM-04 were operating for several months. Each period that includes either pumping (PM-04) or operation (the IM) (or both) is selected such that it follows an initial 2-to-4-week period during which pumping and/or operation was relatively steady. After this initial period, the aquifer system is assumed to be in quasi-equilibrium with the pumping stresses and hydraulic gradients are not changing.

Baseline conditions (PM-04 off + IM off) are defined by a period roughly midway through the period in 2020 when all extraction and injection was ceased for roughly four months due to Covid-19 restrictions. The impacts of PM-04 pumping (PM-04 on + IM off) are captured at the end of the 2020 shutdown period when PM-04 began sustained operation while the IM remained off. The impacts of the IM (PM-04 off + IM on) are defined by a period of pumping in April/May, after the IM had been turned back on for several months and was operating at near capacity (including CrEX-3), but PM-04 had been off for several months.

To look at the combined impacts of PM-04 and the IM (PM-04 on + IM on), a one-week period is selected where the IM had been operating for several months at relatively steady rates (including CrEX-3), and PM-04 had been operating at near capacity for several weeks. While water levels appear to decline slightly after the defined period of PM-04 on + IM on (Figure 14), this period was selected to include all wells pumping (including CrEX-3, which was turned off on July 13, 2021).

Histogram plots of well screen 2-hr hydraulic head data within each of the four periods are provided in Appendix B Figure 1 through Figure 29.

Table 2. Dates for the four time periods used in the Cr hydraulic analyses.

Time period	IM status	PM-04	Start time	End time	Duration
1	Off	Off	May 1, 2020	May 21, 2020	21 days
2	Off	On	June 25, 2020	July 13, 2020	18 days
3	On	Off	March 19, 2021 April 2, 2021 April 11, 2021 April 28, 2021	March 23, 2021 April 7, 2021 April 16, 2021 May 2, 2021	17 days
4	On	On	June 12, 2021	June 18, 2021	6 days

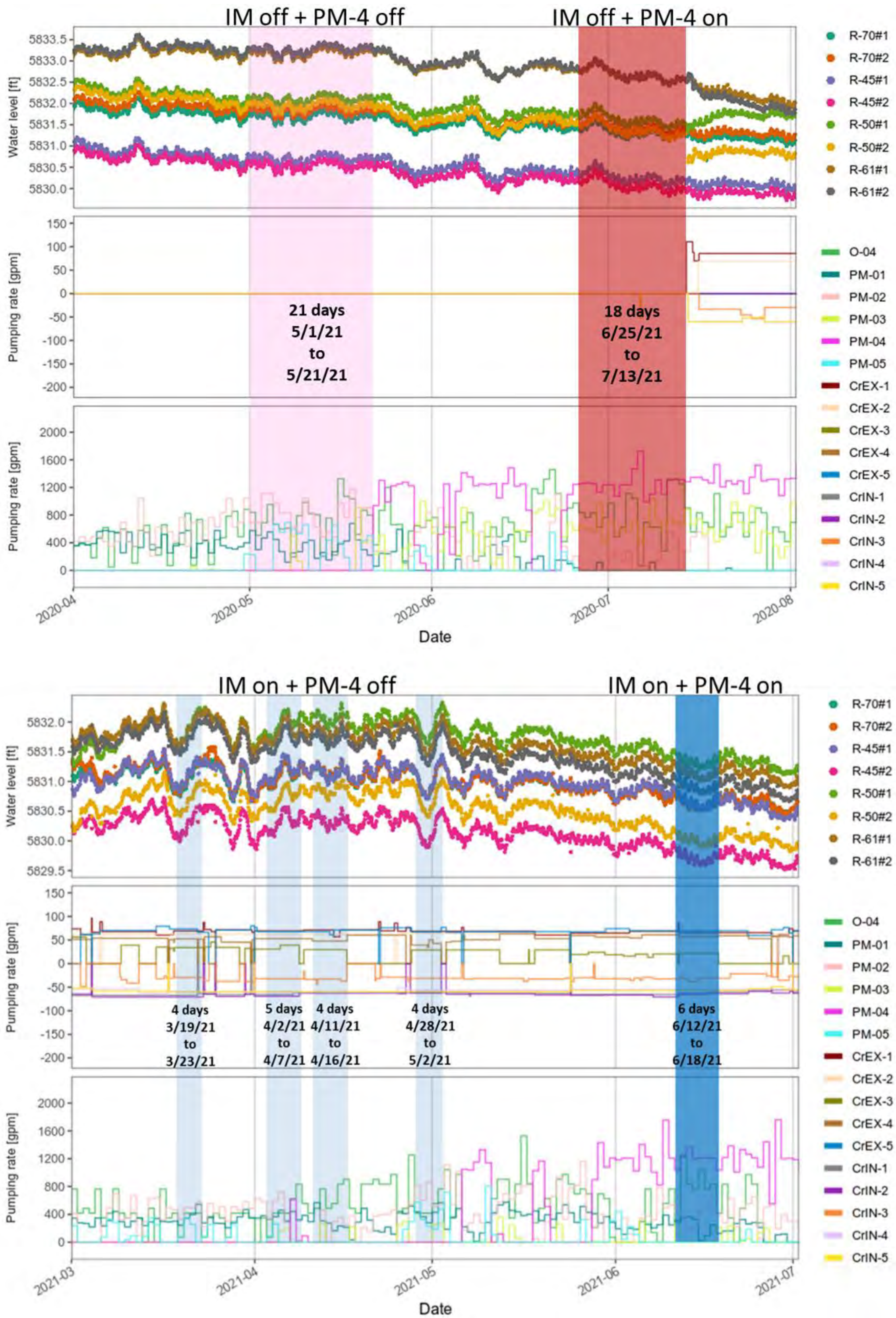

Figure 14. Time periods used in the Cr hydraulic analyses.

3.2.4 Calculating IM versus PM-04 Ratios

This section quantitatively compares the impact of IM operation on vertical and lateral gradients to the impact from pumping at PM-04.

The three-point method (Heath 1983), described in detail in section 2.2.2, is used to estimate lateral gradients. Vertical gradients are calculated as the difference in water level measured in vertical pairs of well screens, divided by the vertical distance between the midpoint of each screen.

Density plots of vertical gradients are used to visualize distributions of gradient values where the values across the full dataset are shown on the y-axis as rug plots and as a density curve, whose height reflects the integral of the area under the curve (Figure 15 provides an example). For lateral gradients, histogram plots are used to show the distribution of estimated gradient magnitudes and direction between the four periods (Figure 16 provides an example). To condense the results section, histogram plots of lateral gradient magnitude and direction for all well triplets are included in .

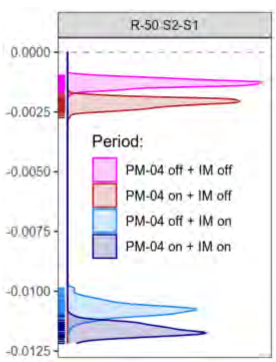

Figure 15. Example of a density plot showing distribution of estimated vertical gradients for R-50 for the four time periods.

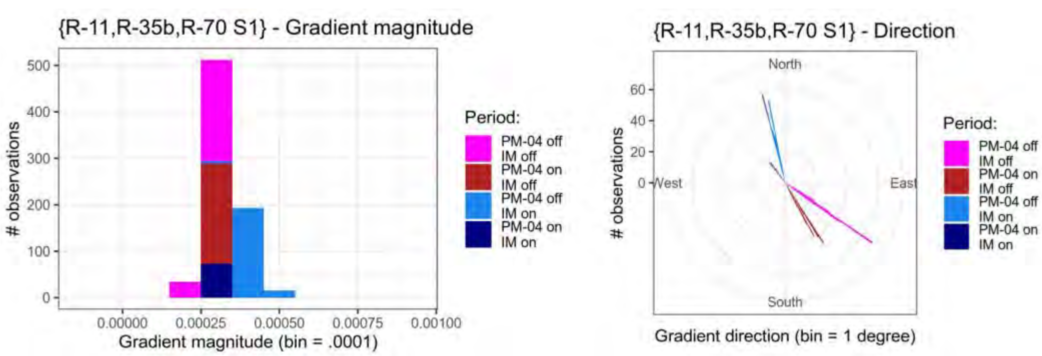

Figure 16. Example of gradient magnitude and direction plots for well screen triplets.

Changes in gradient as a response to sustained operation of PM-04 are quantified as follows: the IM system pumping is held constant (either on or off), and the difference in estimated gradients between PM-04 on and off periods reflect the impact of PM-04. Similarly, changes in gradient as a response to sustained operation of the full IM system are quantified as follows: PM-04 pumping is held constant (either on or off), and the difference in estimated gradients between the IM on and off periods reflect the impact of the IM. In each case, this provides two independent measures of change. The extent of change in gradient magnitude and direction resulting from PM-04 pumping is then compared to the extent of change to impacts observed from sustained operation of the IM, using a simple ratio.

To calculate this ratio, the mean gradient magnitude from each of the four periods is estimated, and gradients are compared between the periods (Figure 17). The difference in magnitude and azimuth are provided, along with a relative percent change. The change in magnitude between the impacts of IM and PM-04 are provided as a ratio.

- Ratio 1 compares the influences of PM-04 and the IM. The magnitude of change induced by PM-04 is assessed when the IM is off, and similarly, the magnitude of change induced by the IM is assessed when PM-04 is off.
- Ratio 2 compares the influences of PM-04 and the IM. The magnitude of change induced by PM-04 is assessed when the IM is operating, and similarly, the magnitude of change induced by the IM is assessed when PM-04 is pumping.

While Figure 17 uses vertical gradient magnitude as an example, ratios for magnitude and azimuth of lateral gradients are calculated in the same manner. Note: there is a “divide by zero” risk, e.g., if PM-04 has no quantifiable impact, which is addressed in Section 3.2.5.

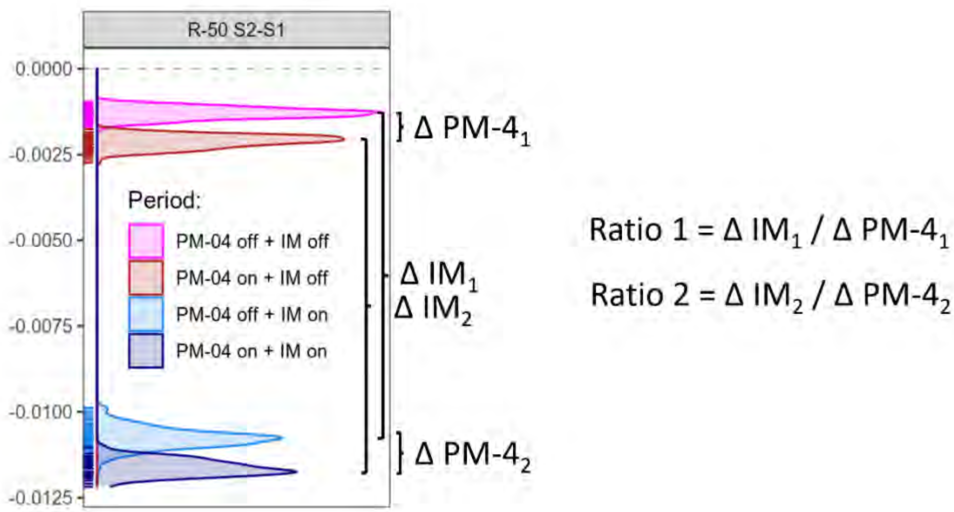

Figure 17. Visual depiction of how changes in gradient magnitude are compared between periods, and a ratio is calculated to compare the impact from PM-04 vs the IM.

A ratio of 1.5 means that the effect of IM is 50% or more compared to PM-04, and 2/3 is selected as it represents the reciprocal (e.g., 1/1.5) when PM-04 is estimated to have 50% or more impact compared to the IM. If ratios 1 and 2 result in different conclusions, then the result is categorized as “Inconclusive.”

Summarizing:

Both |ratios| > 1.5 = IM dominates

Both |ratios| < 2/3 = PM-04 dominates

2/3 > |Both ratios| < 1.5 = Similar impact

Ratio1 category ≠ Ratio2 category = Inconclusive

The four classifications are assigned colors (shown in Figure 18), and are used in later sections of this Appendix to highlight the rows of ratio results in Table 3, Table 4, Table 6, and the spatial plots in Figure 21, Figure 26, and Figure 30.

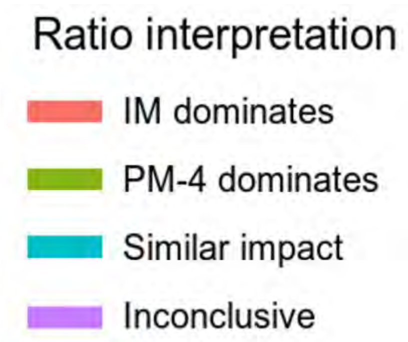

Figure 18. Colors used to describe ratio conclusions.

3.2.5 Statistical Tests for Shift in Gradient

Shifts in gradient magnitude and direction are quantified using the difference in mean values between time periods. The point estimates can be useful and intuitive, but they are also important to understand whether the differences between PM-04 and IM pumping are statistically significant. The effects of PM-04 and IM pumping need to be large enough, and to be based on enough data, to allow a determination of whether their impacts are statistically different from noise during periods of no pumping.

Gradient magnitude and direction is modeled as a linear function of the effects of PM-04, IM, and the interaction of PM-04 and IM operating simultaneously. The model is fit separately for each well triplet. The fitted linear-regression model gives estimates of pumping effects. Importantly, it also provides a p-value for each estimated effect, which helps determine whether the effect is statistically significant. For this analysis, a p-value threshold of 0.01 is used; for values greater than 0.01, the effect is not considered statistically significant.

For all triplets, the estimated effect of the IM is statistically significant. However, there are two well triplets where the effect of PM-04 is not statistically significant with respect to magnitude of lateral gradient, and four triplets where the effect of PM-04 is not statistically significant with respect to direction. When the IM has a significant effect and PM-04 does not, the IM has an infinitely large effect compared to no effect from PM-04. In such cases, the calculated ratio is not meaningful. An asterisk (*) is used to indicate where the shift in gradient magnitude or azimuth from PM-04 pumping is not significant, and therefore the calculated ratio is not meaningful.

3.3 Results

3.3.1 Vertical Gradients

The estimated vertical gradients for dual-screen wells in the vicinity of the Cr plume are provided as density plots in Figure 19; the median gradient for each period is plotted as a vector in Figure 20, with the direction indicating the sign (down = negative, up = positive). Baseline vertical gradients are plotted in pink in the density and vector plots, indicating slightly negative (downward) gradients are present in all wells, except R-61 and R-70. For these two wells, water level elevations measured in the lower screen during baseline conditions are slightly higher than those measured in the shallower screen, indicating slight upward vertical gradients are present at these locations. The slight but consistently upward gradient measured at R-70 during the baseline period is surprising given the postulated Cr-free recharge zone in the area (*Chromium Model: Calibrated with Uncertainty through 2022*, *(Neptune 2023a)*).

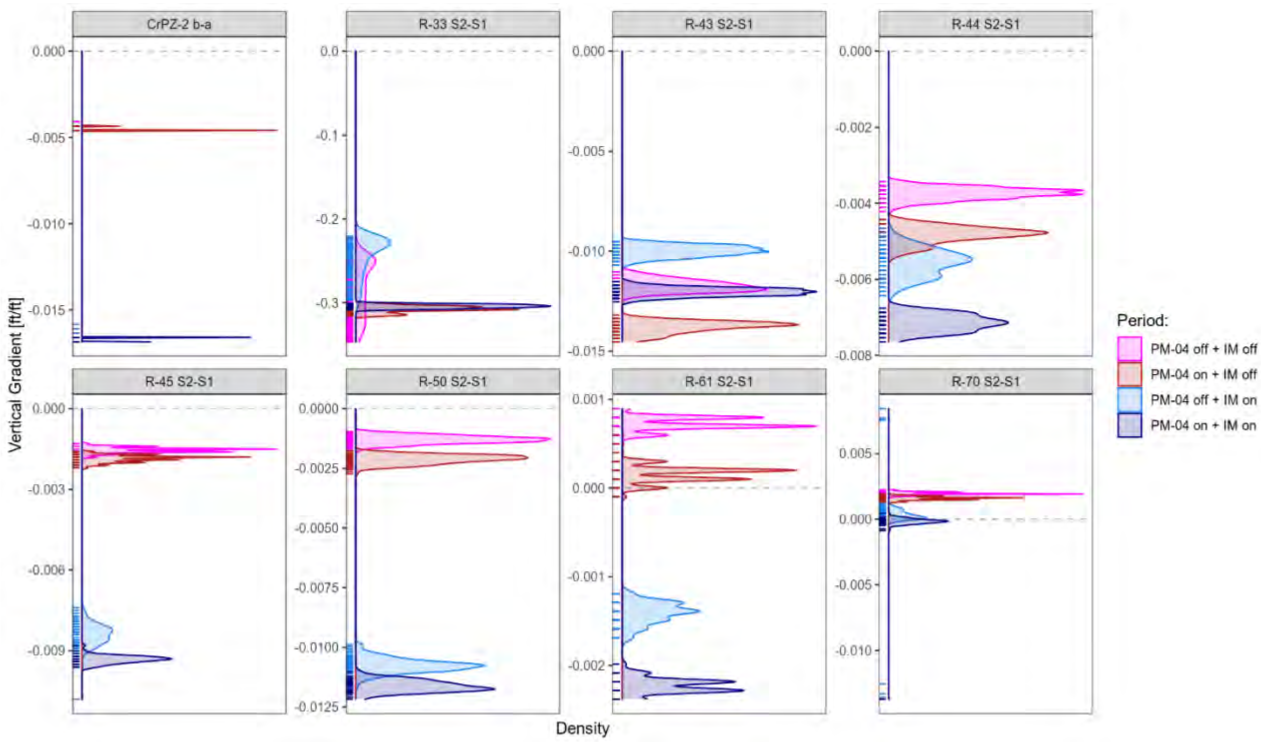

Figure 19. Vertical gradients for dual screened wells, shown as density plots.

When PM-04 turns on, but the IM remains off (PM-04 on + IM off; plotted in red in the density and vector plots), downward vertical gradients generally increase (become more negative) relative to baseline conditions. This agrees with the conclusions of McLin (2005, 2006) that sustained supply-well pumping would result in increased vertical gradients in the leaky portion of the aquifer system. Gradients during the PM-04 on + IM off period are compared to baseline in Table 3, where the differences in median value are provided along with the percent relative change. The largest changes from baseline are seen at R-50 and R-61; a 60% increase in the downward gradient magnitude is observed at R-50, and a nearly 80% reduction in upward vertical gradient magnitude at R-61, effectively neutralizing any vertical gradient altogether at this location. The remaining wells in the Cr plume show modest increases (more negative) in gradient magnitude, approximately 10-30%, resulting from PM-04 pumping.

The impacts of the IM on vertical gradients are also seen in Figure 19 and Figure 20, plotted in light and dark blue colors. The median vertical gradient for the four periods are plotted as vectors in Figure 20, with the direction indicating the sign (down = negative, up = positive). Baseline conditions (PM-04 off + IM off) are shown in pink; the three pumping periods shown in red and light/dark blue indicate the influence of PM-04 and IM pumping on vertical gradients in the aquifer.

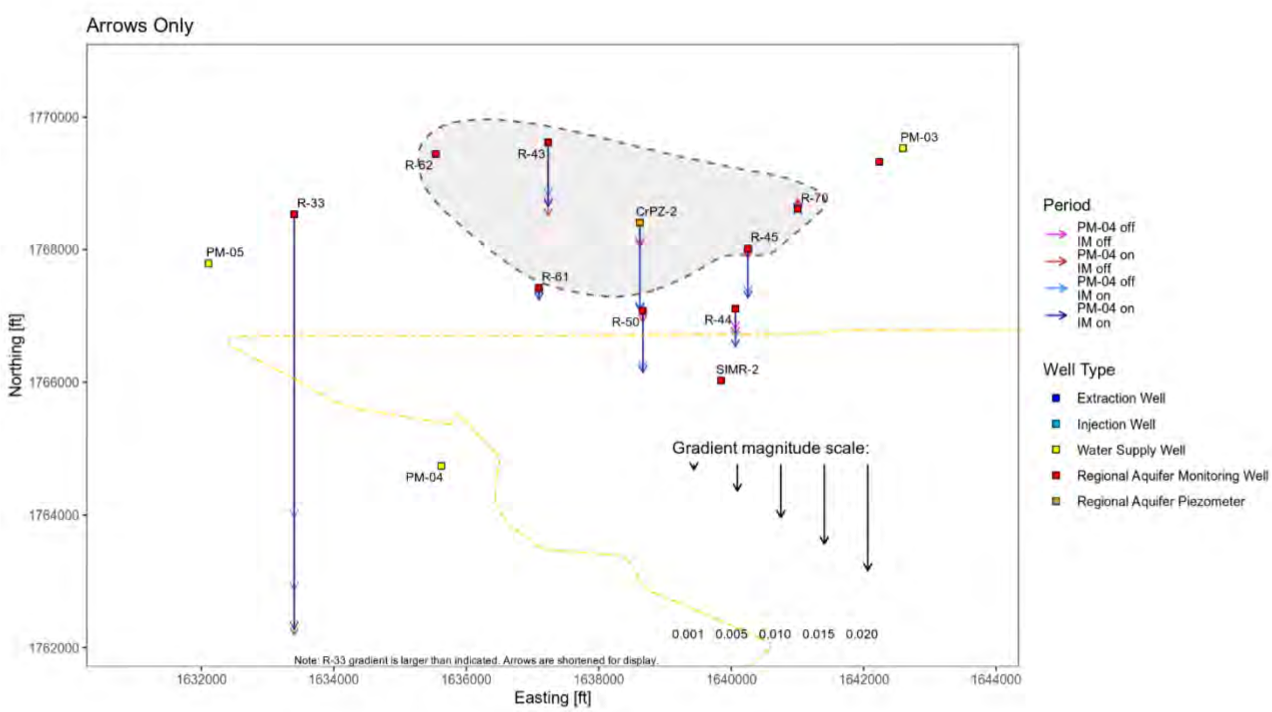

Figure 20. The median vertical gradient for the four periods.

The magnitude of change induced by the IM is shown by 1) the shift in magnitude between the pink and light blue density plots, and 2) the shift between the red and dark blue density plots. The shifts in magnitude because of the IM are much larger than the impacts due to PM-04 pumping, which are shown by the differences in magnitude between the pink and red shades, and differences between the light and dark shades of blue. The magnitude in change from the IM is compared and quantified to that from PM-04 in Table 3; results are provided at the bottom of the table as ratios, which are also plotted spatially in Figure 21.

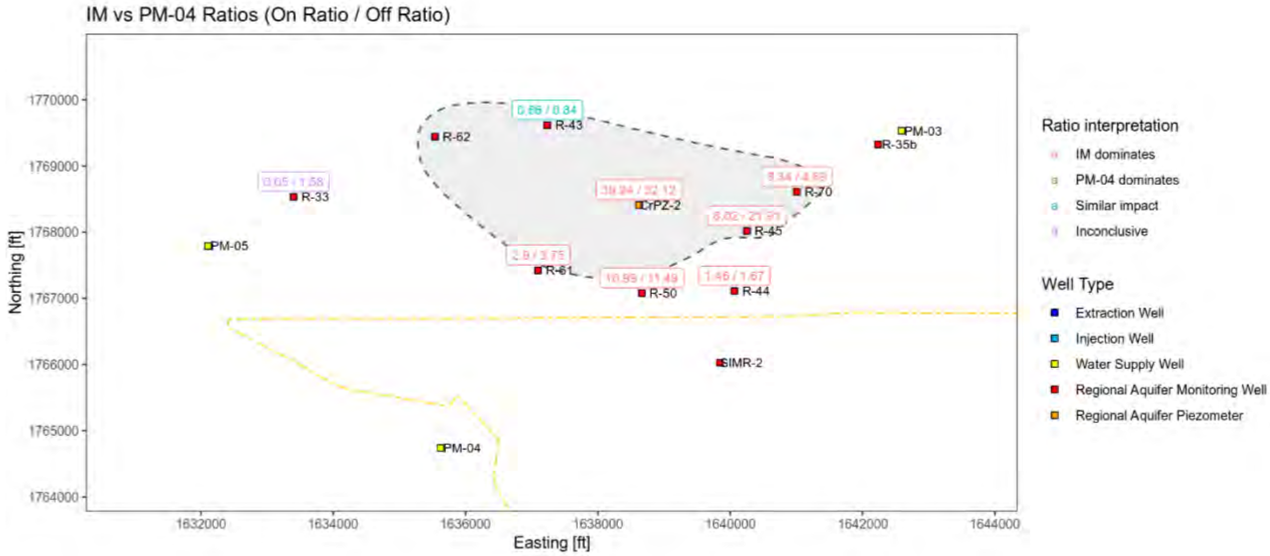

Figure 21. Ratios of IM vs. PM-04 impacts on vertical gradients are plotted spatially. Within the Cr plume, the IM creates 3x-30x more change in vertical gradient compared to that from PM-04. The exception is R-43 (and possibly R-44) which show a similar magnitude impact on vertical gradients from PM-04 and IM pumping.

In wells CrPZ-2, R-45, R-50, R-61, and R-70, the IM has a much greater impact on vertical gradients than PM-04, with ratios ranging from approximately 3 to 40, indicating that the magnitude of change in vertical gradient as a result of IM operations is 3x to 40x greater than the change induced by sustained PM-04 pumping. At regional wells R-43 (located far upgradient from the IM system) and R-44 (located downgradient), impacts from IM operations on vertical gradients appear less strong, suggesting that the observed increases in downward vertical gradients from extraction and injection wells is local, and becomes muted with distance. The impacts of PM-04 pumping at R-44 are also larger than those measured at wells R-45/50/61, leading to an overall low ratio at this well. As such, PM-04 and the IM system appear to have similar magnitude impact on vertical gradients at these distances upgradient (R-43) and downgradient (R-44) of the IM.

R-33 is located far upgradient of the Cr plume and shows a strong influence from PM-04 when the IM is fully operational. However, during baseline conditions and during the PM-04 off + IM on period, the range of estimated gradient values is quite wide (Figure 22), indicating that stresses to the aquifer from sources other than PM-04 and the IM system are the dominant mechanisms controlling water levels at this location. Nearby supply wells PM-05 and O-4 are relatively close to R-33, and their pumping was not controlled in this study. Additionally, the unusually strong and sustained vertical gradient magnitude measured at R-33 suggests that localized recharge may be occurring and impacting vertical gradients at this location.

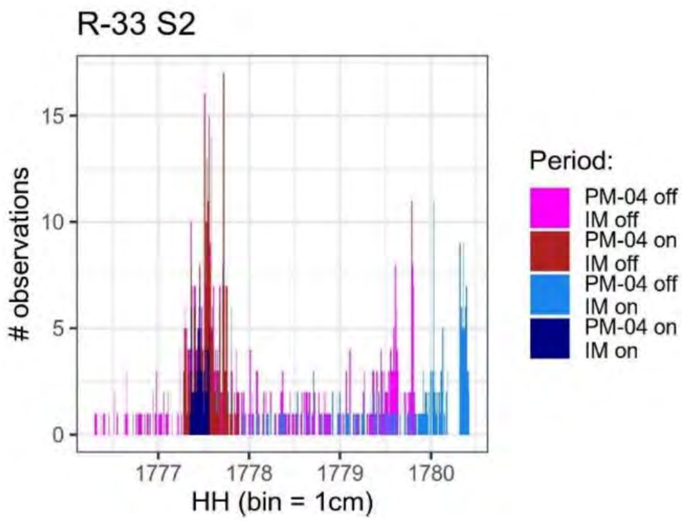

Figure 22. Water levels is observed at R-33 S2 during periods when PM-04 is off, suggesting neither PM-04 nor the IM are the dominant mechanisms controlling water levels at this screen.

Table 3. The impact of IM pumping on vertical gradients in the Cr plume are compared to impacts from PM-04 pumping using vertical well screen pairs. The magnitude in change from each is compared as a ratio, provided in the last rows of the table. Figure 18 provides a legend for the coloring used to classify each ratio result.

	Screen Pair:	CrPZ-2 b-a	R-33 S2-S1	R-43 S2-S1	R-44 S2-S1	R-45 S2-S1	R-50 S2-S1	R-61 S2-S1	R-70 S2-S1
IM off	**PM-04 off**	-4.17E-03	-2.82E-01	-1.17E-02	-3.74E-03	-1.54E-03	-1.29E-03	7.23E-04	1.94E-03
	PM-04 on	-4.55E-03	-3.08E-01	-1.38E-02	-4.83E-03	-1.85E-03	-2.12E-03	1.55E-04	1.59E-03
	Difference	-3.79E-04	-2.52E-02	-2.07E-03	-1.09E-03	-3.13E-04	-8.24E-04	-5.68E-04	-3.51E-04
	% change	**-9.08%**	**-8.93%**	**-17.63%**	**-29.13%**	**-20.29%**	**-63.67%**	**78.60%**	**18.07%**
IM on	**PM-04 off**	-1.63E-02	-2.43E-01	-9.99E-03	-5.56E-03	-8.39E-03	-1.08E-02	-1.41E-03	2.95E-04
	PM-04 on	-1.66E-02	-3.04E-01	-1.20E-02	-7.15E-03	-9.32E-03	-1.16E-02	-2.23E-03	-2.61E-04
	Difference	-3.03E-04	-6.16E-02	-2.05E-03	-1.59E-03	-9.32E-04	-8.65E-04	-8.22E-04	-5.55E-04
	% change	**-1.85%**	**-25.40%**	**-20.53%**	**-28.56%**	**-11.10%**	**-8.04%**	**-58.32%**	**188.38%**
PM-04 off	**IM off**	-4.17E-03	-2.82E-01	-1.17E-02	-3.74E-03	-1.54E-03	-1.29E-03	7.23E-04	1.94E-03
	full IM on	-1.63E-02	-2.43E-01	-9.99E-03	-5.56E-03	-8.39E-03	-1.08E-02	-1.41E-03	2.95E-04
	Difference	-1.22E-02	3.98E-02	1.74E-03	-1.82E-03	-6.85E-03	-9.47E-03	-2.13E-03	-1.65E-03
	% change	**-291.74%**	**14.08%**	**14.85%**	**-48.60%**	**-444.43%**	**-731.76%**	**294.91%**	**84.83%**
PM-04 on	**IM off**	-4.55E-03	-3.08E-01	-1.38E-02	-4.83E-03	-1.85E-03	-2.12E-03	1.55E-04	1.59E-03
	full IM on	-1.66E-02	-3.04E-01	-1.20E-02	-7.15E-03	-9.32E-03	-1.16E-02	-2.23E-03	-2.61E-04
	Difference	-1.21E-02	3.35E-03	1.76E-03	-2.32E-03	-7.47E-03	-9.51E-03	-2.38E-03	-1.85E-03
	% change	**-265.78%**	**1.09%**	**12.75%**	**-47.95%**	**-402.85%**	**-449.02%**	**1541.82%**	**116.36%**
Ratio 1	(*while PM-04 off*) **IM difference** / **PM difference** (*while IM off*)	32.121	-1.578	-0.843	1.668	21.906	11.492	3.752	4.694
Ratio 2	(*while PM-04 on*) **IM difference** / **PM difference** (*while IM on*)	39.939	-0.054	-0.858	1.459	8.017	10.995	2.903	3.337

3.3.2 Shallow Lateral Gradients

Baseline lateral gradients in shallow well-screen triplets are shown in Figure 23. Though the figures appear to show only one arrow, in fact, the hourly calculated gradients have been plotted on top of each other, indicating very little variability across the baseline period in most well triplets. Vector lengths are shown in $\log_{10}$ scale due to the large range of values. The larger gradients (10^{-2} ft/ft) in the west dissipate substantially in the area of the Cr plume, where lateral gradient estimates are on the order of 10^{-3} ft/ft. Standard deviations in water levels are generally $\leq$ 0.1 ft during the baseline period, resulting in estimates of gradient magnitude and direction that are very stable.

To condense the results section, only the mean gradient is plotted in Figure 24 through Figure 26 to show the shifts in gradient between periods. Histogram plots of lateral gradient magnitude and direction for all well triplets are included in .

The three-point method assumes that a planar surface exists between the three well screens used to define a triplet, and represents an average hydraulic gradient magnitude and direction within the triplet. It is not recommended to use this method when other stresses are occurring inside of this assumed planar surface, such as sources of recharge or extraction/injection from wells (EPA 2014). Therefore, gradients are not calculated in triplets containing extraction or injection wells during periods when the IM is operational. This means that, for those triplets, the impacts of the IM cannot be compared to PM-04. When sources or sinks are “just outside” a well triplet, this also has the potential to affect the planar assumption within the triplet. Given the limited amount of wells available, an attempt was made to include as many triplets as possible; therefore, only triplets that explicitly contained an extraction or injection well inside of its boundary were excluded in this analysis.

The mean gradient from the baseline is compared to the median gradient from the PM-04 on + IM off period in Figure 24. The change in gradient magnitude and azimuth between the two periods for each triplet are provided in Table 4 and Table 5. PM-04 pumping has a small, but measurable, impact on shallow lateral gradients throughout the Cr plume when the IM is not operational, though its impact is variable and lacking any clear spatial trends. The spatial variability suggests that highly heterogeneous aquifer properties exist within the leaky layer, and that these may play a bigger role than distance from PM-04 in determining where stresses from deep within the aquifer are able to affect water levels at the water table surface.

The impacts of the IM on shallow lateral hydraulic gradients are visually compared to impacts from PM-04 in Figure 25, where the median gradient from each period is plotted. The estimated differences and calculated ratios are provided in Table 5, and ratio results are plotted spatially in Figure 26. For triplets located within the estimated Cr plume extent, IM pumping has a much greater impact on lateral gradients compared to PM-04. In most cases, the IM appears to cause large systematic shifts in hydraulic gradients; increases in magnitude are observed, and large changes in direction towards the extraction wells suggest a high level of hydraulic control. At distances closer to the CrIN and CrEX wells (where triplets have been excluded from analysis) hydraulic control is even stronger.

Immediately downgradient of the Cr plume and to the east of the injection wells, the IM also shows greater influence on gradients than PM-04, but to a lesser extent than within the plume. The ratio results are mixed in the northeast of the plume. The triplet {R-11, R-70 screen 1, and R-35b} indicates that the IM produces a large shift in hydraulic gradient direction, but not overall magnitude; however, the complete reversal of direction suggests that CrEX-5 has a strong influence over local flow direction, impacting water levels in R-11 and R-70 screen 1. Triplets to the south of R-70, {R-45 screen 1, R-70 screen 1, R-13} and {R-45 screen 1, R-44 screen 1, R-13}, also show strong shifts in direction, but only minor changes in magnitude. Changes in direction are generally away from the injection wells, suggesting that some water-table mounding is occurring downgradient of injection. Triplet {R-70 screen 1, R-35b, R-13}, to the east of R-70, indicates little influence from either the IM or PM-04, with estimated gradients very similar between all four periods.

To the southeast of the Cr plume, the ratio results suggest that PM-04 has a larger impact on shallow lateral gradients than does the IM. Looking at Figure 24 and Table 5, PM-04 pumping shifts the gradient direction about 5 degrees, with little change in magnitude. While the ratio results from the triplet containing R-1 in the far west suggest that the IM has a larger impact compared to PM-04, the estimated gradient magnitude and direction for all four periods are nearly identical (Figure 25 and Table 5). The reality is that neither PM-04 nor the IM appear to have any meaningful impact on gradients in this triplet.

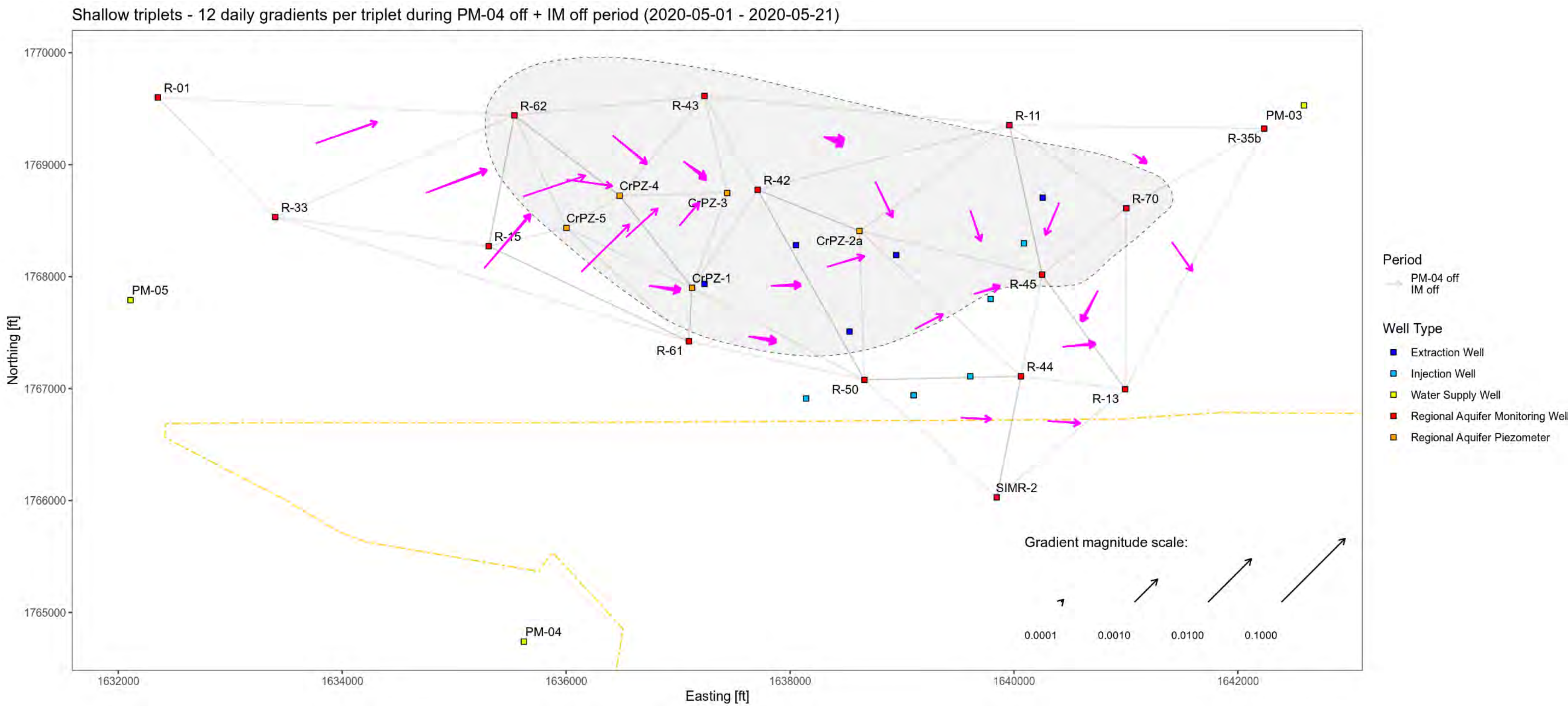

Figure 23. Baseline lateral gradients in shallow triplets indicate overall west to east flow at the water table of the regional aquifer. Magnitudes in the west are approximately 10^{-3}, which decrease to approximately 10^{-2} in most areas of the Cr plume. Each hourly calculated gradient is plotted on top of one another, indicating very little variability across the baseline period in most well triplets.

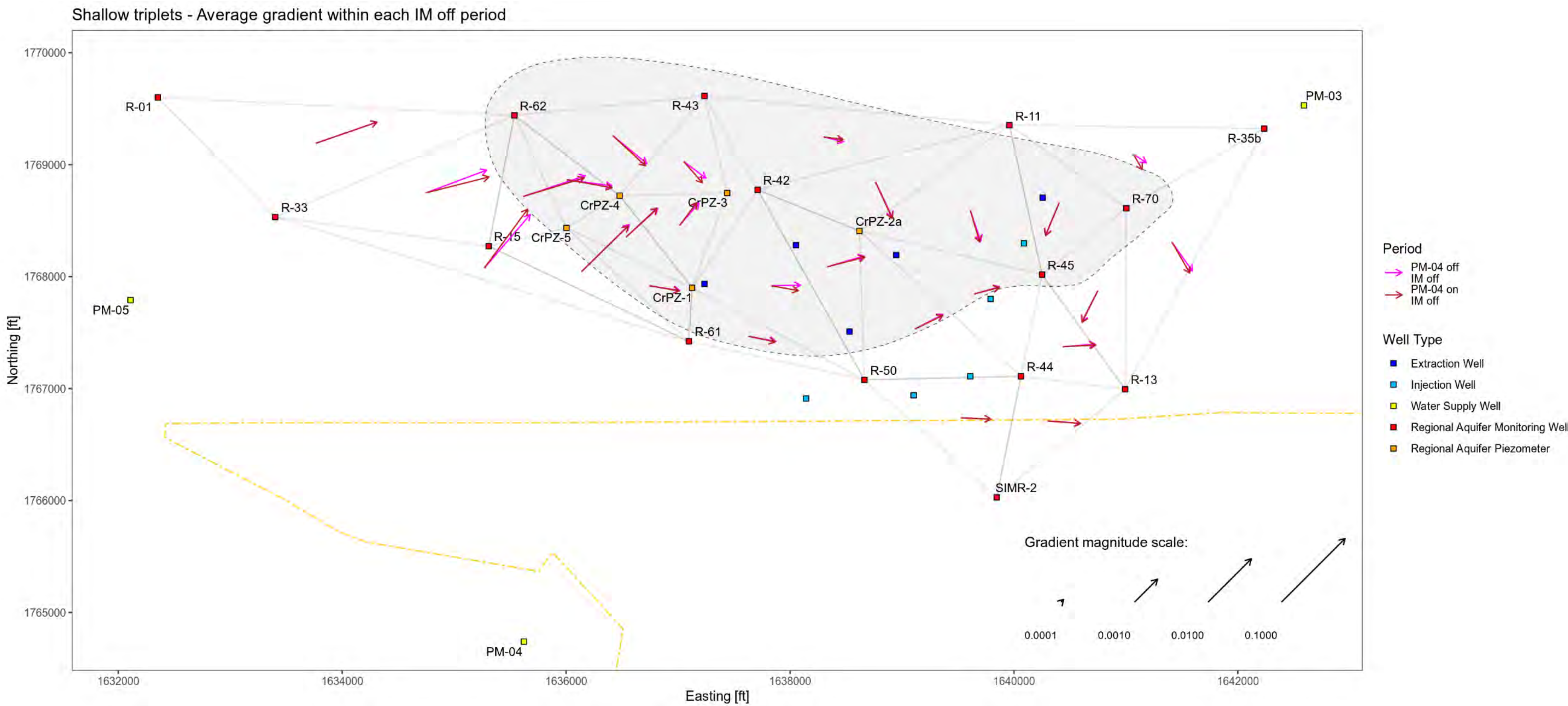

Figure 24. The mean gradient during baseline conditions (PM-04 off + IM off) is compared to the PM-04 on + IM off period for shallow triplets. Small differences in magnitude and direction indicate PM-04 has small but measurable impacts on lateral gradients in the Cr plume when the IM is not operational.

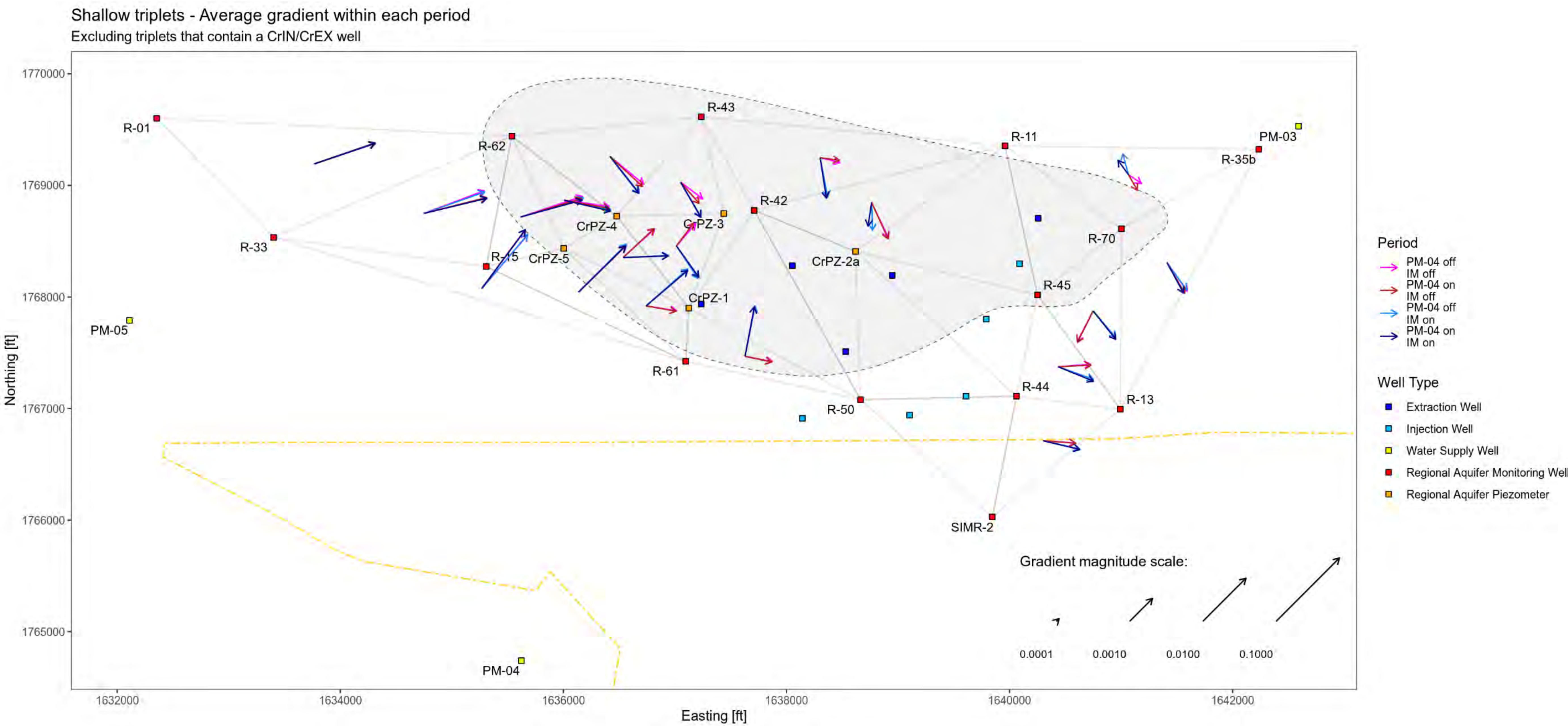

Figure 25. The mean gradient during baseline conditions (PM-04 off + IM off) is compared to the three pumping periods for shallow triplets. Small differences in magnitude and direction between the pink and red vectors, and between the light and blue vectors, indicate that pumping from PM-04 has small but measurable impact on lateral gradients in the Cr plume, regardless of the state of the IM. However, the overall difference between the red and blue vectors, a shift in gradients as result of the IM system being operated, show a clear increase in magnitude and shift in direction towards the extraction wells. Within the Cr plume extent, extraction and injection from IM operations overwhelm lateral hydraulic gradients indicating strong hydraulic control.

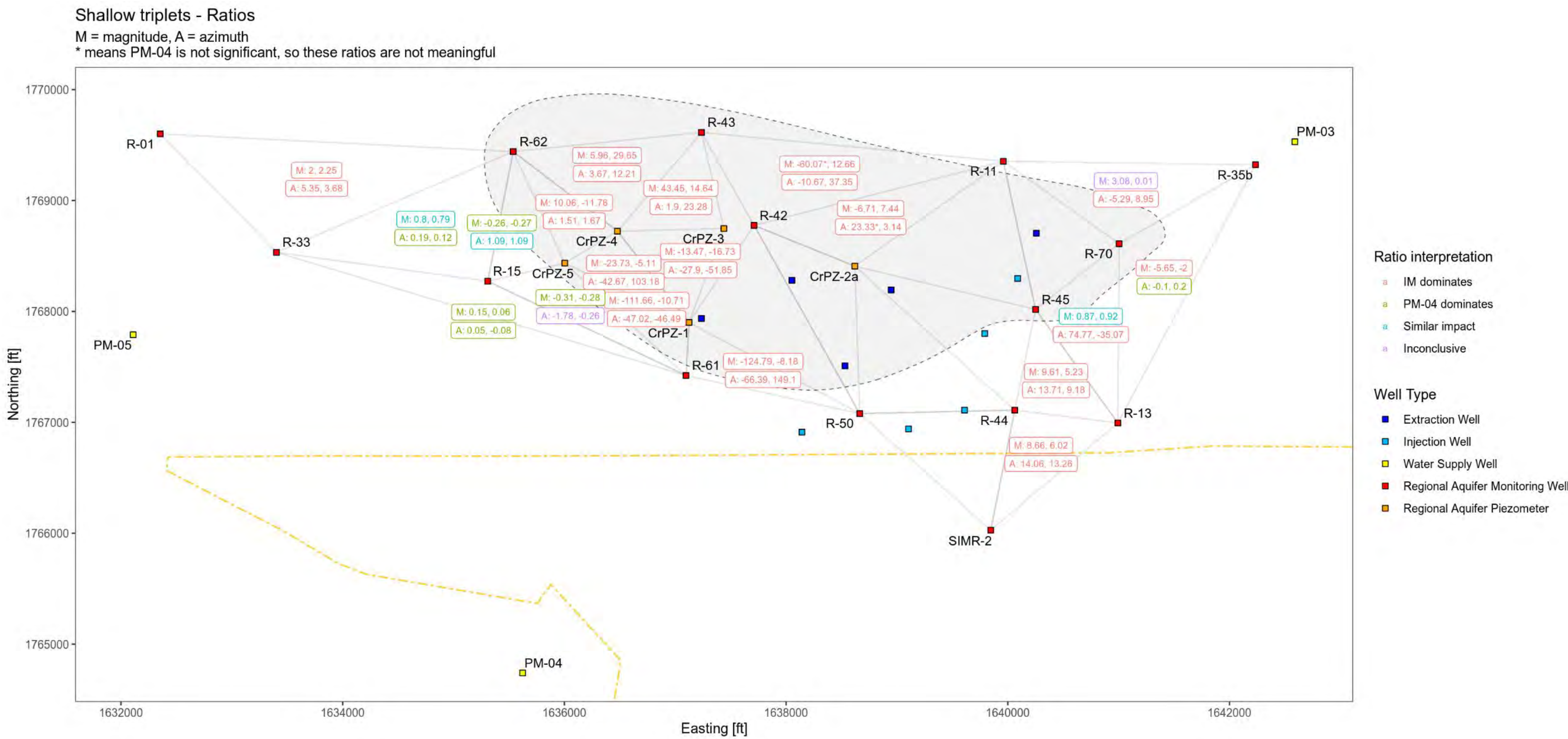

Figure 26. Ratios of IM vs. PM-04 impacts on shallow lateral gradients are plotted for each triplet. Within the Cr plume, the IM pumping results in changes in gradient magnitude and direction that are at least 50% larger compared to changes induced from PM-04 pumping, and generally 10x greater or more. Ratios are not calculated for shallow triplets that contain an extraction or injection well per EPA guidance (EPA 2014). An asterisk (*) is used to indicate where for two ratios, the shift in gradient magnitude or azimuth from PM-04 pumping is not statistically significant, and therefore the calculated ratio is not meaningful.

Table 4. Estimated influence of IM pumping compared to PM-04 pumping on lateral hydraulic gradient magnitude and azimuth in shallow triplets. Gradients and ratios are not calculated for triplets that contain an extraction or injection well. Baseline conditions (PM-04 off + IM off) are shown in the top line of the magnitude and azimuth results, shaded in darker grey. Figure 18 provides a legend for the coloring used to classify each ratio result. An asterisk (*) is used to indicate where for two ratios, the shift in gradient magnitude or azimuth from PM-04 pumping is not statistically significant, and therefore the calculated ratio is not meaningful.

	triplet:	CrPZ-1 R-61 S1 R-50 S1	CrPZ-3 CrPZ-1 CrPZ-4	CrPZ-3 R-43 S1 CrPZ-4	CrPZ-5 CrPZ-4 CrPZ-1	CrPZ-5 R-61 S1 CrPZ-1	R-01 R-33 S1 R-62	R-11 R-35b R-70 S1	R-13 R-35b R-70 S1	R-13 R-45 S1 R-70 S1	R-15 CrPZ-5 R-61 S1	R-15 R-62 CrPZ-5	R-33 S1 R-61 S1 R-15	R-33 S1 R-62 R-15	R-42 CrPZ-2a R-11	R-42 R-43 S1 R-11	R-43 S1 CrPZ-4 R-62	R-44 S1 R-45 S1 R-13	R-62 CrPZ-5 CrPZ-4	SIMR-2 R-44 S1 R-13
	type	magnitude	magnitude	magnitude	magnitude	magnitude	magnitude	magnitude	magnitude	magnitude	magnitude	magnitude	magnitude	magnitude	magnitude	magnitude	magnitude	magnitude	magnitude	magnitude
IM off	**PM-04 off**	6.80E-04	7.90E-04	6.70E-04	2.23E-03	8.90E-04	1.30E-02	2.60E-04	1.26E-03	1.15E-03	1.61E-02	1.38E-02	2.11E-02	1.30E-02	1.67E-03	3.70E-04	2.46E-03	9.90E-04	2.82E-03	9.70E-04
	PM-04 on	6.50E-04	7.20E-04	7.00E-04	2.20E-03	8.40E-04	1.31E-02	3.10E-04	1.28E-03	1.23E-03	1.40E-02	1.20E-02	2.57E-02	1.32E-02	1.82E-03	3.50E-04	2.57E-03	1.04E-03	2.88E-03	1.03E-03
	difference	-3.00E-05	-7.00E-05	3.00E-05	-3.00E-05	-5.00E-05	9.00E-05	5.00E-05	2.00E-05	8.00E-05	-2.11E-03	-1.79E-03	4.55E-03	2.30E-04	1.50E-04	-2.00E-05	1.10E-04	5.00E-05	6.00E-05	6.00E-05
	% change	**-4.41%**	**-8.86%**	**4.48%**	**-1.35%**	**-5.62%**	**0.69%**	**19.23%**	**1.59%**	**6.96%**	**-13.07%**	**-12.94%**	**21.54%**	**1.77%**	**8.98%**	**-5.41%**	**4.47%**	**5.05%**	**2.13%**	**6.19%**
IM on	**PM-04 off**	4.57E-03	1.66E-03	1.81E-03	2.83E-03	6.42E-03	1.32E-02	4.20E-04	1.14E-03	1.22E-03	1.68E-02	1.43E-02	2.18E-02	1.32E-02	6.70E-04	1.83E-03	3.13E-03	1.48E-03	3.38E-03	1.45E-03
	PM-04 on	4.15E-03	1.61E-03	1.89E-03	2.73E-03	5.94E-03	1.33E-02	3.10E-04	1.19E-03	1.34E-03	1.46E-02	1.25E-02	2.59E-02	1.34E-02	4.90E-04	1.96E-03	3.15E-03	1.58E-03	3.34E-03	1.53E-03
	difference	-4.20E-04	-5.00E-05	8.00E-05	-1.00E-04	-4.80E-04	7.00E-05	-1.10E-04	5.00E-05	1.20E-04	-2.16E-03	-1.77E-03	4.11E-03	2.30E-04	-1.80E-04	1.30E-04	2.00E-05	1.00E-04	-4.00E-05	8.00E-05
	% change	**-9.19%**	**-3.01%**	**4.42%**	**-3.53%**	**-7.48%**	**0.53%**	**-26.19%**	**4.39%**	**9.84%**	**-12.86%**	**-12.39%**	**18.86%**	**1.74%**	**-26.87%**	**7.10%**	**0.64%**	**6.76%**	**-1.18%**	**5.52%**
PM-04 off	**IM off**	6.80E-04	7.90E-04	6.70E-04	2.23E-03	8.90E-04	1.30E-02	2.60E-04	1.26E-03	1.15E-03	1.61E-02	1.38E-02	2.11E-02	1.30E-02	1.67E-03	3.70E-04	2.46E-03	9.90E-04	2.82E-03	9.70E-04
	IM on	4.57E-03	1.66E-03	1.81E-03	2.83E-03	6.42E-03	1.32E-02	4.20E-04	1.14E-03	1.22E-03	1.68E-02	1.43E-02	2.18E-02	1.32E-02	6.70E-04	1.83E-03	3.13E-03	1.48E-03	3.38E-03	1.45E-03
	difference	3.89E-03	8.70E-04	1.14E-03	6.00E-04	5.53E-03	1.80E-04	1.60E-04	-1.20E-04	7.00E-05	6.60E-04	4.60E-04	6.70E-04	1.90E-04	-1.00E-03	1.46E-03	6.70E-04	4.90E-04	5.60E-04	4.80E-04
	% change	**572.06%**	**110.13%**	**170.15%**	**26.91%**	**621.35%**	**1.38%**	**61.54%**	**-9.52%**	**6.09%**	**4.09%**	**3.33%**	**3.17%**	**1.46%**	**-59.88%**	**394.59%**	**27.24%**	**49.49%**	**19.86%**	**49.48%**
PM-04 on	**IM off**	6.50E-04	7.20E-04	7.00E-04	2.20E-03	8.40E-04	1.31E-02	3.10E-04	1.28E-03	1.23E-03	1.40E-02	1.20E-02	2.57E-02	1.32E-02	1.82E-03	3.50E-04	2.57E-03	1.04E-03	2.88E-03	1.03E-03
	IM on	4.15E-03	1.61E-03	1.89E-03	2.73E-03	5.94E-03	1.33E-02	3.10E-04	1.19E-03	1.34E-03	1.46E-02	1.25E-02	2.59E-02	1.34E-02	4.90E-04	1.96E-03	3.15E-03	1.58E-03	3.34E-03	1.53E-03
	difference	3.50E-03	8.90E-04	1.19E-03	5.30E-04	5.10E-03	1.60E-04	0.00E+00	-9.00E-05	1.10E-04	6.10E-04	4.80E-04	2.30E-04	1.90E-04	-1.33E-03	1.61E-03	5.80E-04	5.40E-04	4.60E-04	5.00E-04
	% change	**538.46%**	**123.61%**	**170.00%**	**24.09%**	**607.14%**	**1.22%**	**0.00%**	**-7.03%**	**8.94%**	**4.35%**	**3.99%**	**0.90%**	**1.44%**	**-73.08%**	**460.00%**	**22.57%**	**51.92%**	**15.97%**	**48.54%**
	Ratio 1	-124.79	-13.47	43.45	-23.73	-111.66	2	3.08	-5.65	0.87	-0.31	-0.26	0.15	0.8	-6.71	-60.07*	5.96	9.61	10.06	8.66
	Ratio 2	-8.18	-16.73	14.64	-5.11	-10.71	2.25	0.01	-2	0.92	-0.28	-0.27	0.06	0.79	7.44	12.66	29.65	5.23	-11.76	6.02
	type	azimuth	azimuth	azimuth	azimuth	azimuth	azimuth	azimuth	azimuth	azimuth	azimuth	azimuth	azimuth	azimuth	azimuth	azimuth	azimuth	azimuth	azimuth	azimuth
IM off	**PM-04 off**	100.63	40.6	126.92	47.91	98.97	70.87	123.86	144.8	207.43	45.42	71.51	40.57	69.4	154.39	103.93	129.46	85.41	97.88	93.84
	PM-04 on	101.98	36.8	138.82	46.98	100.04	70.95	150.13	149.99	206.52	45.68	73.06	36.34	75.79	155.41	97.81	132.68	87.16	100.18	94.47
	difference	1.35	-3.80	11.90	-0.93	1.07	0.08	26.27	5.19	-0.91	0.26	1.55	-4.23	6.39	1.02	-6.12	3.22	1.75	2.30	0.63
	% change	**1.34%**	**-9.36%**	**9.38%**	**-1.94%**	**1.08%**	**0.11%**	**21.21%**	**3.58%**	**-0.44%**	**0.57%**	**2.17%**	**-10.43%**	**9.21%**	**0.66%**	**-5.89%**	**2.49%**	**2.05%**	**2.35%**	**0.67%**
IM on	**PM-04 off**	11.25	146.56	149.54	87.52	48.44	71.31	-15.18	144.25	139.52	44.95	73.19	40.36	70.62	178.02	169.25	141.25	109.45	101.36	102.63
	PM-04 on	10.64	144.49	150.02	87.92	49.53	71.44	-35.97	151.44	141.37	45.53	74.61	36.63	76.51	188.58	171.22	142.01	112.17	103.13	103.3
	difference	-0.61	-2.07	0.48	0.40	1.09	0.13	-20.79	7.19	1.85	0.58	1.42	-3.73	5.89	10.56	1.97	0.76	2.72	1.77	0.67
	% change	**-5.42%**	**-1.41%**	**0.32%**	**0.46%**	**2.25%**	**0.18%**	**136.96%**	**4.98%**	**1.33%**	**1.29%**	**1.94%**	**-9.24%**	**8.34%**	**5.93%**	**1.16%**	**0.54%**	**2.49%**	**1.75%**	**0.65%**
PM-04 off	**IM off**	100.63	40.6	126.92	47.91	98.97	70.87	123.86	144.8	207.43	45.42	71.51	40.57	69.4	154.39	103.93	129.46	85.41	97.88	93.84
	IM on	11.25	146.56	149.54	87.52	48.44	71.31	-15.18	144.25	139.52	44.95	73.19	40.36	70.62	178.02	169.25	141.25	109.45	101.36	102.63
	difference	-89.38	105.96	22.62	39.61	-50.53	0.44	-139.04	-0.55	-67.91	-0.47	1.68	-0.21	1.22	23.63	65.32	11.79	24.04	3.48	8.79
	% change	**-88.82%**	**260.99%**	**17.82%**	**82.68%**	**-51.06%**	**0.62%**	**-112.26%**	**-0.38%**	**-32.74%**	**-1.03%**	**2.35%**	**-0.52%**	**1.76%**	**15.31%**	**62.85%**	**9.11%**	**28.15%**	**3.56%**	**9.37%**
PM-04 on	**IM off**	101.98	36.8	138.82	46.98	100.04	70.95	150.13	149.99	206.52	45.68	73.06	36.34	75.79	155.41	97.81	132.68	87.16	100.18	94.47
	IM on	10.64	144.49	150.02	87.92	49.53	71.44	-35.97	151.44	141.37	45.53	74.61	36.63	76.51	188.58	171.22	142.01	112.17	103.13	103.3
	difference	-91.34	107.69	11.20	40.94	-50.51	0.49	-186.10	1.45	-65.15	-0.15	1.55	0.29	0.72	33.17	73.41	9.33	25.01	2.95	8.83
	% change	**-89.57%**	**292.64%**	**8.07%**	**87.14%**	**-50.49%**	**0.69%**	**-123.96%**	**0.97%**	**-31.55%**	**-0.33%**	**2.12%**	**0.80%**	**0.95%**	**21.34%**	**75.05%**	**7.03%**	**28.69%**	**2.94%**	**9.35%**
	Ratio 1	-66.39	-27.9	1.9	-42.67	-47.02	5.35	-5.29	-0.1	74.77	-1.78	1.09	0.05	0.19	23.33*	-10.67	3.67	13.71	1.51	14.06
	Ratio 2	149.1	-51.85	23.28	103.18	-46.49	3.68	8.95	0.2	-35.07	-0.26	1.09	-0.08	0.12	3.14	37.35	12.21	9.18	1.67	13.26

Table 5. Estimated influence of PM-04 pumping on baseline gradients in shallow triplets that contain an extraction or injection well. Baseline conditions (PM-04 off + IM off) are shown in the top line of the magnitude and azimuth results, shaded in darker grey.

	triplet:	CrPZ-1 R-50 S1 R-42	CrPZ-2a R-11 R-45 S1	CrPZ-2a R-42 R-50 S1	CrPZ-2a R-44 S1 R-45 S1	CrPZ-2a R-44 S1 R-50 S1	R-45 S1 R-11 R-70 S1	R-50 S1 R-44 S1 SIMR-2
	type	magnitude	magnitude	magnitude	magnitude	magnitude	magnitude	magnitude
IM off	**PM-04 off**	7.50E-04	9.80E-04	1.58E-03	6.00E-04	9.10E-04	1.20E-03	8.20E-04
	PM-04 on	6.60E-04	1.05E-03	1.65E-03	5.90E-04	8.80E-04	1.27E-03	8.00E-04
	difference	-9.00E-05	7.00E-05	7.00E-05	-1.00E-05	-3.00E-05	7.00E-05	-2.00E-05
	% change	**-12.00%**	**7.14%**	**4.43%**	**-1.67%**	**-3.30%**	**5.83%**	**-2.44%**
IM on	**PM-04 off**	--	--	--	--	--	--	--
	PM-04 on	--	--	--	--	--	--	--
	difference	--	--	--	--	--	--	--
	% change	--	--	--	--	--	--	--
PM-04 off	**IM off**	--	--	--	--	--	--	--
	IM on	--	--	--	--	--	--	--
	difference	--	--	--	--	--	--	--
	% change	--	--	--	--	--	--	--
PM-04 on	**IM off**	--	--	--	--	--	--	--
	IM on	--	--	--	--	--	--	--
	difference	--	--	--	--	--	--	--
	% change	--	--	--	--	--	--	--
	Ratio 1	--	--	--	--	--	--	--
	Ratio 2	--	--	--	--	--	--	--
	type	azimuth	azimuth	azimuth	azimuth	azimuth	azimuth	azimuth
IM off	**PM-04 off**	88.75	161.25	73.54	74.13	62.45	203.04	92.46
	PM-04 on	100.12	163.47	75.35	75.49	63.75	202.74	92.51
	difference	11.37	2.22	1.81	1.36	1.30	-0.30	0.05
	% change	**12.81%**	**1.38%**	**2.46%**	**1.83%**	**2.08%**	**-0.15%**	**0.05%**
IM on	**PM-04 off**	--	--	--	--	--	--	--
	PM-04 on	--	--	--	--	--	--	--
	difference	--	--	--	--	--	--	--
	% change	--	--	--	--	--	--	--
PM-04 off	**IM off**	--	--	--	--	--	--	--
	IM on	--	--	--	--	--	--	--
	difference	--	--	--	--	--	--	--
	% change	--	--	--	--	--	--	--
PM-04 on	**IM off**	--	--	--	--	--	--	--
	IM on	--	--	--	--	--	--	--
	difference	--	--	--	--	--	--	--
	% change	--	--	--	--	--	--	--
	Ratio 1	--	--	--	--	--	--	--
	Ratio 2	--	--	--	--	--	--	--

3.3.3 Deep Lateral Gradients

The baseline gradients at depth are shown in Figure 27, where the hourly calculated gradients are plotted on top of one another. Vector lengths are again shown in $\log_{10}$ scale. Standard deviations of water levels in all wells during the baseline period (Table 1) are generally ≤ 0.1 ft, except R-33 screen 2 that has a standard deviation of 3.56 ft. While marginally larger gradients are estimated in west compared to the east, the contrast is not nearly as strong as that seen at the water table.

The majority of estimated gradients within the Cr plume appear highly regular; all triplets (except the triplet that contains R-33 screen 2) have a standard deviation in azimuth of about 1 degree or less. The triplet containing R-33 screen 2 shows a high amount of variability in direction during the selected baseline period, indicating that other pumping stresses are likely impacting R-33 screen 2's water level, such as PM-05 or O-4.

Impacts of PM-04 pumping on baseline gradients are shown in Figure 28. Changes in lateral gradient magnitude and direction due to PM-04 pumping when the IM is not operational are apparent, but the magnitude of change is small. A spatial pattern does appear to exist in the deep triplets, where all triplets in the southern portion of the Cr plume appear to shift slightly to the south a few degrees in response to PM-04.

As discussed in the previous section, the three-point method is not recommended when other stresses are occurring inside a well-screen triplet. Therefore, deep lateral gradients are not calculated for triplets during periods when the IM is operational, and for those triplets the impacts of the IM cannot be compared to PM-04.

After removing triplets containing active pumping, only three deep triplets are available for analysis, the results of which are shown in Figure 29, Figure 30, and Table 6. The results indicate that the IM has a moderate impact on deep lateral hydraulic gradients east of the injection wells, however PM-04 appears to have a larger impact on flow direction compared to the IM in the triplet east of R-44 and R-45. Results for the triplet containing R-33 screen 2 in the west show inconclusive results, which is not surprising given the high variability of water levels observed in this screen. Overall, water level data at depth is limited in the Cr plume, and is insufficient to make any general conclusions about the impacts of IM and PM-04 pumping at this depth.

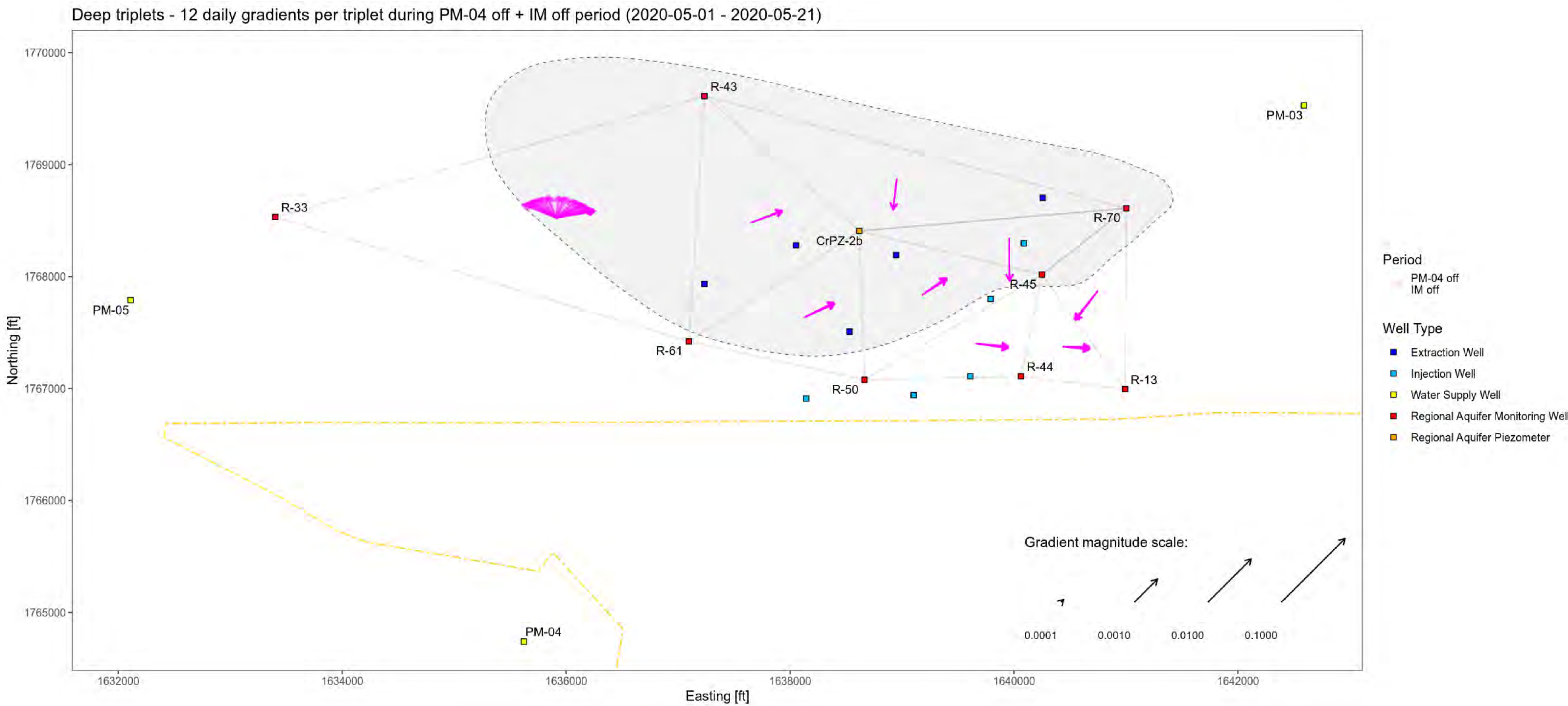

Figure 27. Baseline lateral gradients in deep triplets indicate overall west to east flow at depth in the regional aquifer. Magnitudes at depth are more similar from west to east at approximately 10^{-2} in most areas. Each hourly calculated gradient is plotted on top of one another, indicating very little variability across the baseline period in most well triplets except the triplet in the far west that includes R-33 S2. This screen shows a high variability during the baseline periods (sd = 3.56 ft) indicating stresses other than those from PM-04 and the IM are impacting water levels at this location, such as nearby supply wells PM-05 and O-4. Additionally, the large vertical gradient measured at this location indicates strong localized recharge in the area.

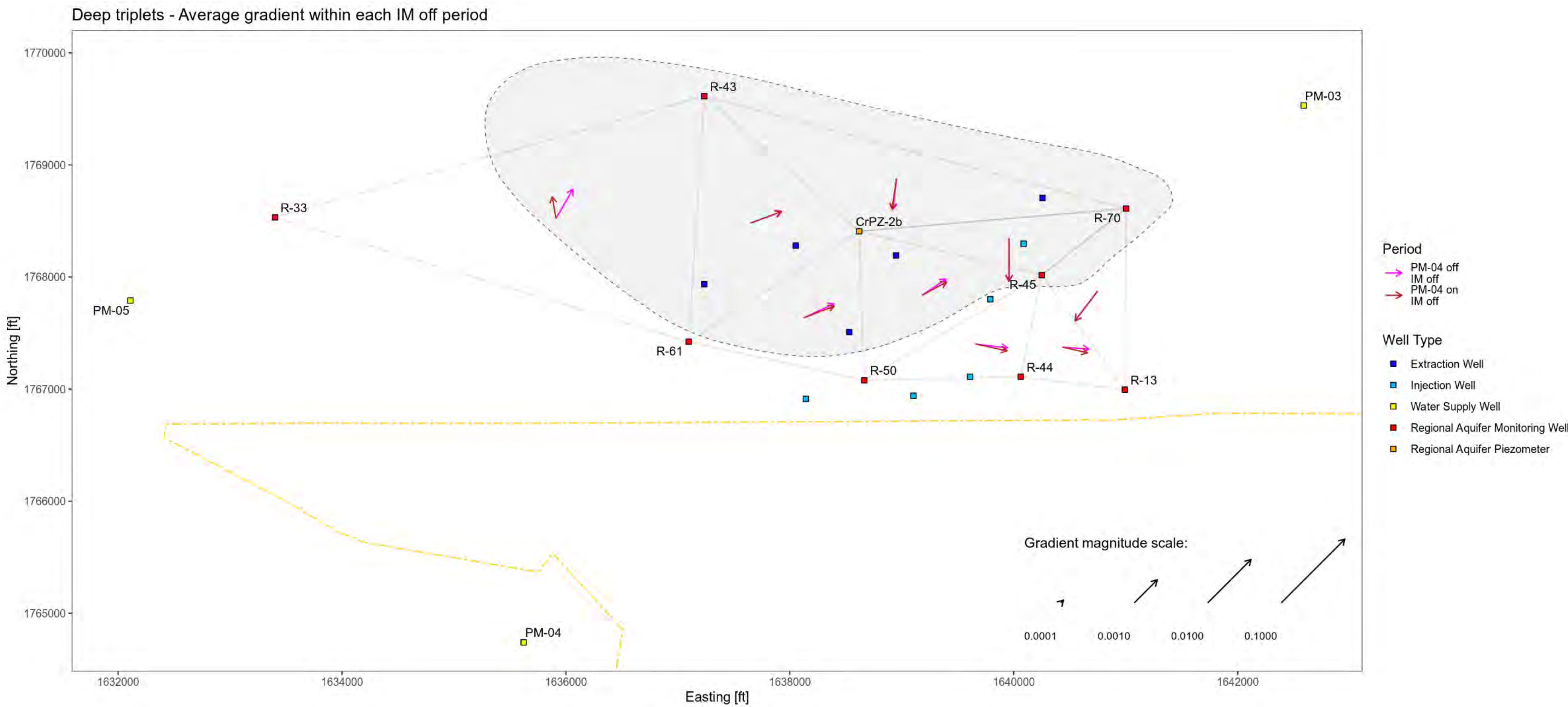

Figure 28. The mean gradient during baseline conditions (PM-04 off + IM off) is compared to the PM-04 on + IM off period for deep triplets. Small differences in magnitude and direction indicate PM-04 has a small but measurable impact on lateral gradients in the Cr plume when the IM is not operational. The apparent shift in gradient in the triplet to the west containing R-33 S2 is small in the context of the range of estimated gradients during both of these periods. When variability is this high, any estimated shift in the mean not meaningful; results are provided for completeness only.

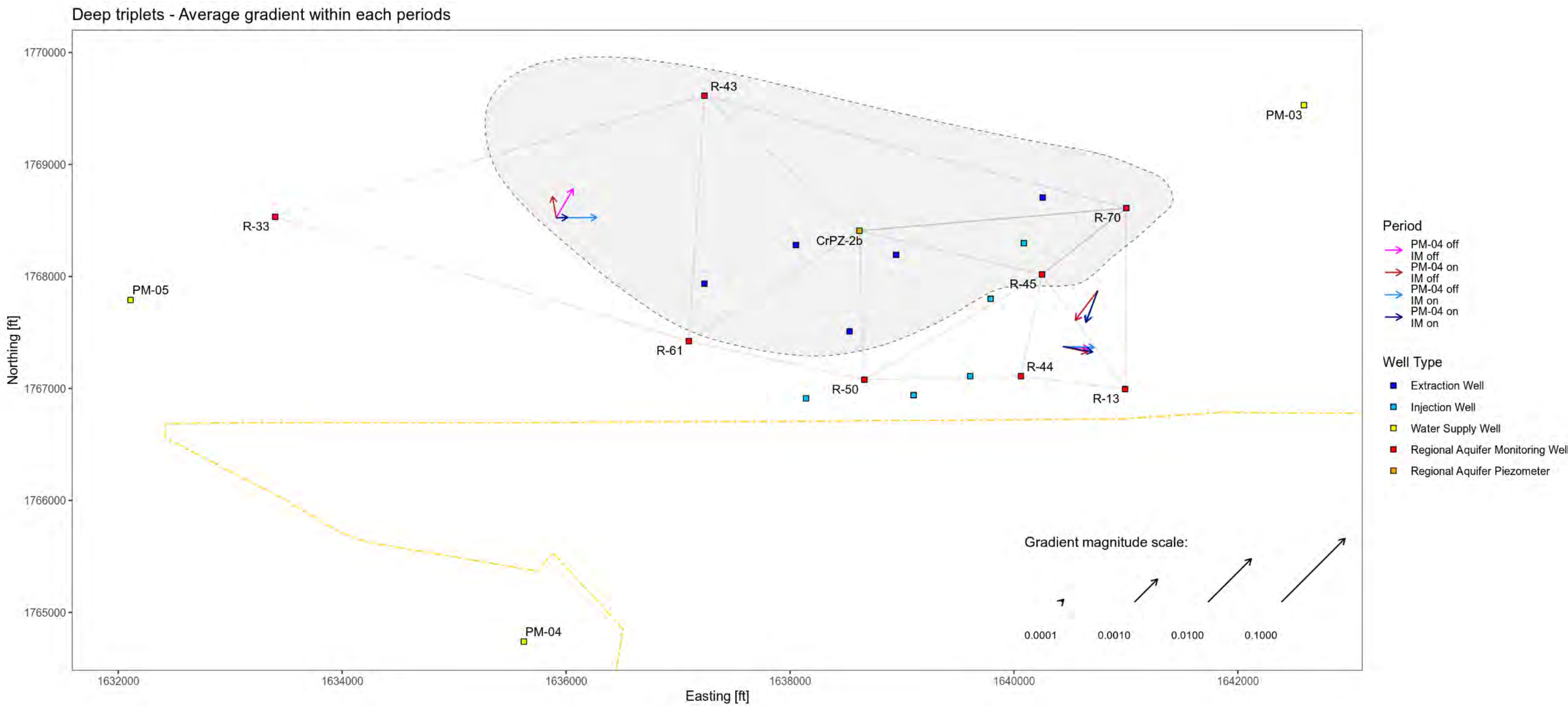

Figure 29. The mean gradient during baseline conditions (PM-04 off + IM off) is compared to the three pumping periods for shallow triplets. Gradients are not calculated for deep triplets that contain an extraction or injection well, leaving only three triplets. The IM appears to have a moderate impact on deep lateral hydraulic gradients east of the injection wells, however PM-04 appears to have an impact on flow direction in the triplet east of R-44 and R-45. Data is limited at this depth, and comparisons of the impacts of IM and PM-04 pumping are not sufficient to make any general conclusions.

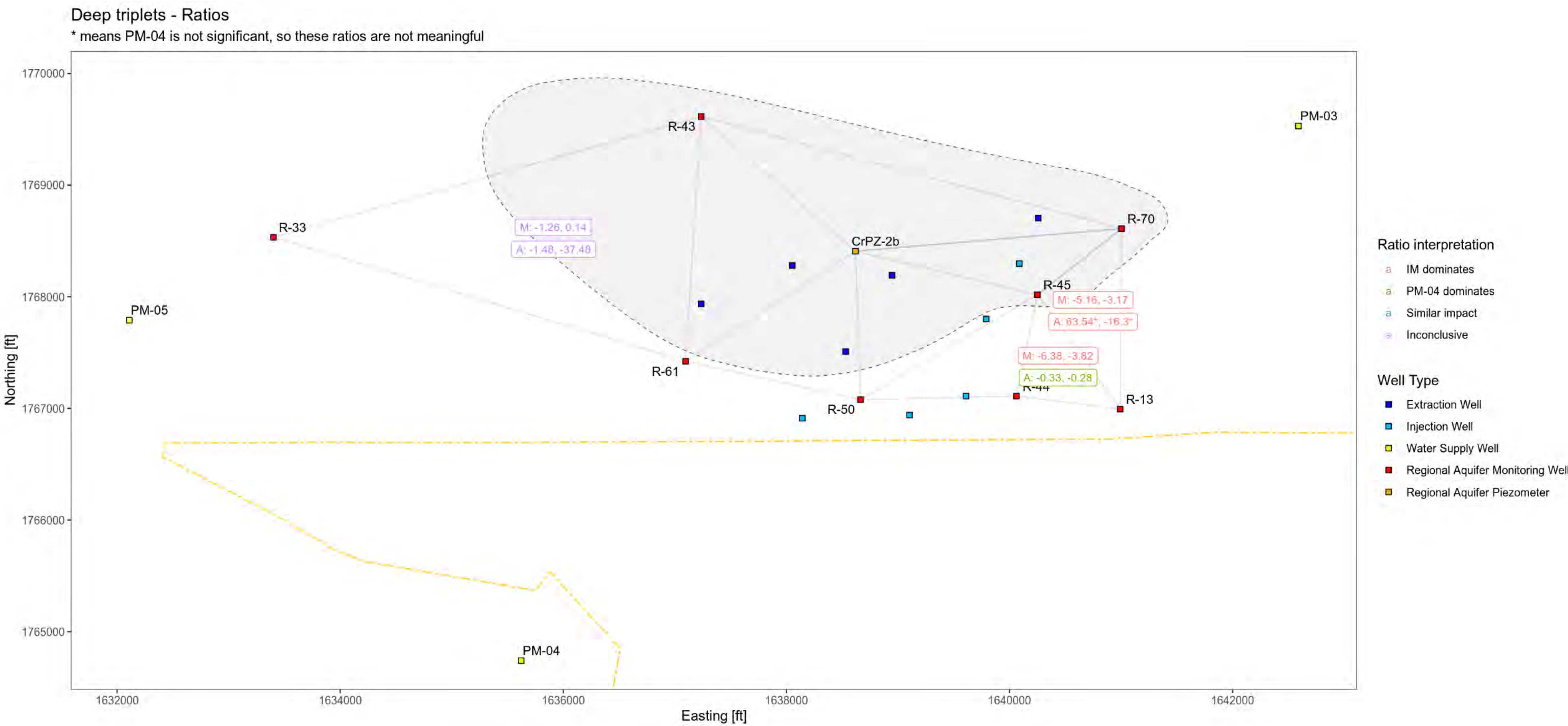

Figure 30. Ratios of IM vs. PM-04 impacts on deep lateral gradients are plotted for each triplet. Ratios are not calculated for deep triplets that contain an extraction or injection well, leaving only three triplets. The IM appears to have a moderate impact on deep lateral hydraulic gradients east of the injection wells, however PM-04 has a larger impact on flow direction compared to the IM in the triplet east of R-44 and R-45. Data is limited at this depth, and comparisons of the impacts of IM and PM-04 pumping are not sufficient to make any general conclusions. An asterisk (*) is used to indicate where for two ratios, the shift in gradient magnitude or azimuth from PM-04 pumping is not statistically significant, and therefore the calculated ratio is not meaningful.

Table 6. Estimated influence of IM pumping to PM-04 pumping on hydraulic gradient magnitude and azimuth in deep triplets. Gradients and ratios are not calculated for triplets that contain an extraction or injection well. Baseline conditions (PM-04 off + IM off) are shown in the top line of the magnitude and azimuth results, shaded in darker grey. An asterisk (*) is used to indicate where for two ratios, the shift in gradient magnitude or azimuth from PM-04 pumping is not statistically significant, and therefore the calculated ratio is not meaningful.

	Triplet	R-33 S2 R-43 S2 R-61 S2	R-45 S2 R-44 S2 R-13	R-45 S2 R-70 S2 R-13	R-50 S2 R-43 S2 R-61 S2	R-45 S2 R-44 S2 R-50 S2	R-45 S2 R-70 S2 R-13	R-43 S2 CrPZ-2b R-61 S2	R-43 S2 CrPZ-2b R-70 S2	R-50 S2 CrPZ-2b R-45 S2
	type	gradient	gradient	gradient	gradient	gradient	gradient	gradient	gradient	gradient
IM off	**PM-04 off**	1.08E-03	6.10E-04	1.39E-03	1.05E-03	8.80E-04	7.70E-04	1.03E-03	9.70E-04	2.19E-03
	PM-04 on	4.20E-04	5.60E-04	1.47E-03	9.70E-04	8.60E-04	7.10E-04	9.70E-04	9.70E-04	2.29E-03
	difference	-6.60E-04	-5.00E-05	8.00E-05	-8.00E-05	-2.00E-05	-6.00E-05	-6.00E-05	0.00E+00	1.00E-04
	% change	**-61.11%**	**-8.20%**	**5.76%**	**-7.62%**	**-2.27%**	**-7.79%**	**-5.83%**	**0.00%**	**4.57%**
IM on	**PM-04 off**	1.91E-03	9.10E-04	1.00E-03	--	--	--	--	--	--
	PM-04 on	1.80E-04	8.40E-04	1.11E-03	--	--	--	--	--	--
	difference	-1.73E-03	-7.00E-05	1.10E-04	--	--	--	--	--	--
	% change	**-90.58%**	**-7.69%**	**11.00%**	--	--	--	--	--	--
PM-04 off	**IM off**	1.08E-03	6.10E-04	1.39E-03	--	--	--	--	--	--
	IM on	1.91E-03	9.10E-04	1.00E-03	--	--	--	--	--	--
	difference	8.30E-04	3.00E-04	-3.90E-04	--	--	--	--	--	--
	% change	**76.85%**	**49.18%**	**-28.06%**	--	--	--	--	--	--
PM-04 on	**IM off**	4.20E-04	5.60E-04	1.47E-03	--	--	--	--	--	--
	IM on	1.80E-04	8.40E-04	1.11E-03	--	--	--	--	--	--
	difference	-2.40E-04	2.80E-04	-3.60E-04	--	--	--	--	--	--
	% change	**-57.14%**	**50.00%**	**-24.49%**	--	--	--	--	--	--
	Ratio 1	-1.26	-6.38	-5.16	--	--	--	--	--	--
	Ratio 2	0.14	-3.82	-3.17	--	--	--	--	--	--
	type	azimuth	azimuth	azimuth	azimuth	azimuth	azimuth	azimuth	azimuth	azimuth
IM off	**PM-04 off**	30.26	94.17	217.57	69.53	186.68	55.95	64.8	96.94	179.78
	PM-04 on	-9.88	102.61	217.29	69.56	188.52	61.46	68.96	102.23	180.15
	difference	-40.14	8.44	-0.28	0.03	1.84	5.51	4.16	5.29	0.37
	% change	**-132.65%**	**8.96%**	**-0.13%**	**0.04%**	**0.99%**	**9.85%**	**6.42%**	**5.46%**	**0.21%**
IM on	**PM-04 off**	89.48	91.41	199.8						
	PM-04 on	86.9	100.13	200.81						
	difference	-2.58	8.72	1.01						
	% change	**-2.88%**	**9.54%**	**0.51%**						
PM-04 off	**IM off**	30.26	94.17	217.57						
	IM on	89.48	91.41	199.8						
	difference	59.22	-2.76	-17.77						
	% change	**195.70%**	**-2.93%**	**-8.17%**						
PM-04 on	**IM off**	-9.88	102.61	217.29						
	IM on	86.9	100.13	200.81						
	difference	96.78	-2.48	-16.48						
	% change	**-979.55%**	**-2.42%**	**-7.58%**						
	Ratio 1	-1.48	-0.33	63.54*	--	--	--	--	--	--
	Ratio 2	-37.48	-0.28	-16.3*	--	--	--	--	--	--

3.4 Discussion and Conclusions

Shifts in hydraulic gradients due to pumping stresses from PM-04 and the IM network are spatially variable. The greatest shifts in lateral gradients due to IM operations are seen in areas upgradient of the IM, largely to the west and northwest of the extraction and injection wells. In areas downgradient of the Cr plume, the IM shows less impact on hydraulic gradients, though ratios still suggest the IM still has a 5–10 times greater impact on magnitude and direction compared to that from PM-04 pumping in this region.

Vertical gradient results are similar. Most dual-screened wells within the Cr plume show a larger shift in gradient resulting from IM operations, compared to that from sustained PM-04 pumping. In most wells, the result of IM operations and PM-04 pumping both cause a downward shift in vertical gradient, though the impact from the IM is 3–30 times stronger than the impact from PM-04. Downward gradients form PM-04 pumping are likely the result of a drop in water levels within the productive portion of the regional aquifer, resulting in vertical gradients produced in the upper semi-confining, leaky portion of the aquifer system. Localized downward gradients produced by the IM are the result of combined extraction and injection.

The largest impacts on vertical gradients are seen at wells R-45, R-50 and R-61, which is not surprising given their close proximity to injection wells. The impacts observed at R-43, R-44, and R-70 are much more muted, suggesting that the production of vertical gradients is limited in extent.

Although PM-04 does show an influence on hydraulic gradients within the Cr plume, the magnitude of impact is minor compared to the change induced from a localized extraction, treatment, and injection system. All other supply wells are likely to have a smaller influence compared to PM-04, due to their intermittent operations and lower pumping rates. While PM-04 does produce measurable impacts, sustained operation of the IM extraction and injection system within the Cr plume produces stronger shifts in hydraulic gradients.

The assumption that LAC supply wells have a negligible impact on hydraulic gradients local to the Cr plume in the presence of a pump and treat system is supported by the hydraulic analyses presented here.

The results show that, in the Cr plume area, impacts on lateral and vertical hydraulic gradients from supply-well pumping are small compared to impacts from extraction and injection wells, and IM operations dominate groundwater hydraulics near the Cr plume. This result aligns with the overall conclusions of a capture zone analysis (Neptune 2023b) finding that substantial capture of the Cr plume is taking place within the current configuration of the IM system.

Overall, the two questions posed in the Introduction to this data-based study of hydraulic gradients have been answered. The analysis concluded the following:

- During periods when IM operations are off, ambient hydraulic gradients show a dominant east-to-southeast orientation.

- Small, but quantifiable, impacts on hydraulic gradients from pumping of county supply well PM-04 are observed in the Cr plume.
- The operation of extraction and injection wells as part of the IM operation results in large, systematic changes in hydraulic gradients within the vicinity of the Cr plume. Hydraulic gradients appear stronger in magnitude upgradient of the IM as a result of operations, with a shift in direction generally toward the extraction wells.
- Changes in hydraulic gradients resulting from IM operations are least 50% greater than those due to pumping of PM-04 in all areas of the chromium plume; the gradients for triplets close to the extraction and injection wells indicate impacts from the IM that are at least 10 times greater. Therefore, any impact that the nearby supply wells may have on hydraulic gradients in the regional aquifer is negligible in the near-term context of Cr plume fate and transport.
- Vertical gradient changes due to the onset of IM operations were apparent at all dual-screened well pairs in the Cr plume (R-43, R-44, R-45, R-50, and R-61). Small ambient downward vertical gradients were observed at most wells when IM operations were off. Most well pairs show a small (about 0.01–0.001 ft/ft), but systematic, increase in the downward gradient because of IM operations.

4.0 References

Birdsell, K., et al., 2005. *Los Alamos National Laboratory's Hydrogeologic Studies of the Pajarito Plateau: A Synthesis of Hydrogeologic Workplan Activities (1998–2004),* LA-14263-MS, Los Alamos National Laboratory, Los Alamos NM, December 2005

Broxton, D.E., and D.T. Vaniman, 2005. Geologic framework of a groundwater system on the margin of a rift basin, Pajarito Plateau, North-Central New Mexico, *Vadose Zone Journal* 4 (3) 522 doi: 10.2136/vzj2004.0073

Collins, K.A., et al., 2005. *Los Alamos National Laboratory's Hydrogeologic Studies of the Pajarito Plateau: A Synthesis of Hydrogeologic Workplan Activities (1998–2004),* LA-14263-MS, Los Alamos National Laboratory, Los Alamos NM, December 2005

Cook, R.D., 1977. Detection of Influential Observation in Linear Regression, *Technometrics* 19 (1) 15–18

DBS&A, 2006. *Long-Range Water Supply Plan, Los Alamos County,* prepared for Los Alamos County Water Utility, Daniel B. Stephens & Associates Inc., Albuquerque NM, August 2006

EPA, 2008. *A Systematic Approach for Evaluation of Capture Zones at Pump and Treat Systems,* EPA/600/R-08/003, United States Environmental Protection Agency, Office of Research and Development, National Risk Management Research Laboratory, Cincinnati OH, January 2008

EPA, 2014. *3PE: A Tool for Estimating Groundwater Flow Vectors,* EPA 600/R-14/273, United States Environmental Protection Agency, Washington DC, September 2014

Fetter, C.W., 1994. *Applied Hydrogeology, Third Edition*, Macmillan College Publishing Company, New York NY

Heath, R.C., 1983. *Basic Ground-Water Hydrology, U.S. Geological Survey Water-Supply Paper 2220,* U.S. Geological Survey (USGS), Reston VA, 1983

Kleinfelder, 2005. *Final Well R-26 Completion Report, Los Alamos National Laboratory, Los Alamos, New Mexico, Project No. 37151, Rev. 1,* prepared for the United States Department of Energy and the National Nuclear Security Administration through the United States Army Corps of Engineers Sacramento District, Kleinfelder, Albuquerque NM, January 2005

Koch, R.J., and S. Schmeer, 2010. *Groundwater Level Status Report for 2009, Los Alamos National Laboratory,* LA-14416-PR, Los Alamos National Laboratory, Los Alamos NM, March 2010

LANL, 2015. *Interim Measures Work Plan for Chromium Plume Control,* LA-UR-15-23126, EP2015-0089, Los Alamos National Laboratory, Los Alamos NM, May 2015

LANL, 2018. *Compendium of Technical Reports Related to the Deep Groundwater Investigation for the RDX Project at Los Alamos National Laboratory,* LA-UR-18-21326, EP2018-0006, Los Alamos National Laboratory, Los Alamos NM, March 2018

McLin, S.G., 2005. *Analyses of the PM-2 Aquifer Test Using Multiple Observation Wells,* LA-14225-MS, Los Alamos National Laboratory, Los Alamos NM, July 2005

McLin, S.G., 2006. *Analyses of the PM-4 Aquifer Test Using Multiple Observation Wells,* LA-14252-MS, Los Alamos National Laboratory, Los Alamos NM, January 2006

N3B, 2019. *Investigation Report for Royal Demolition Explosive in Deep Groundwater,* EM2019-0235, prepared for U.S. Department of Energy Environmental Management Los Alamos Field Office (EM-LA), Newport News Nuclear BWXT-Los Alamos, LLC (N3B), Los Alamos NM, August 2019

N3B, 2021. *Assessment Report for the Evaluation of Conditions in the Regional Aquifer Around Well R-70,* EM2021-0321, Newport News Nuclear BWXT-Los Alamos, LLC (N3B), Los Alamos NM, June 2021

Neptune, 2023a. *Chromium Model: Calibrated with Uncertainty through 2022,* EMID-702781, prepared by Neptune and Company Inc. for the U.S. Department of Energy Environmental Management Los Alamos Field Office, Neptune and Company Inc., Los Alamos NM, February 17, 2023

Neptune, 2023b. *Chromium Interim Measure Capture Zone Analysis,* EMID-702782, prepared by Neptune and Company Inc. for the U.S. Department of Energy Environmental Management Los Alamos Field Office, Neptune and Company Inc., Los Alamos NM, January 31, 2023

Purtymun, W.D., 1975. *Geohydrology of the Pajarito Plateau with Reference to Quality of Water, 1949–1972,* ERID-0011787, Los Alamos Scientific Laboratory, Los Alamos NM, December 1975

Purtymun, W.D., 1995. *Geologic and Hydrologic Records of Observation Wells, Test Holes, Test Wells, Supply Wells, Springs, and Surface Water Stations in the Los Alamos Area,* LA-12883-MS, Los Alamos National Laboratory, Los Alamos NM, January 1995

Purtymun, W.D., et al., 1980. *Geohydrology of White Rock Canyon of the Rio Grande from Otowi to Frijoles Canyon,* LA-8635-MS, ERID 0006048, Los Alamos Scientific Laboratory, Los Alamos NM, December 1980

Toll, N.J., and T.C. Rasmussen, 2007. Removal of Barometric Pressure Effects and Earth Tides from Observed Water Levels, *Ground Water* 45 (1) 101–105

Vesselinov, V.V., 2005. *An Alternative Conceptual Model of Groundwater Flow and Transport in Saturated Zone Beneath the Pajarito Plateau,* LA-UR-05-6741, Los Alamos National Laboratory, Los Alamos NM, 2005

Hydraulic Analysis of the Pajarito Plateau: Appendix A

Time Series Plots, Trend Results, and Correlation Results

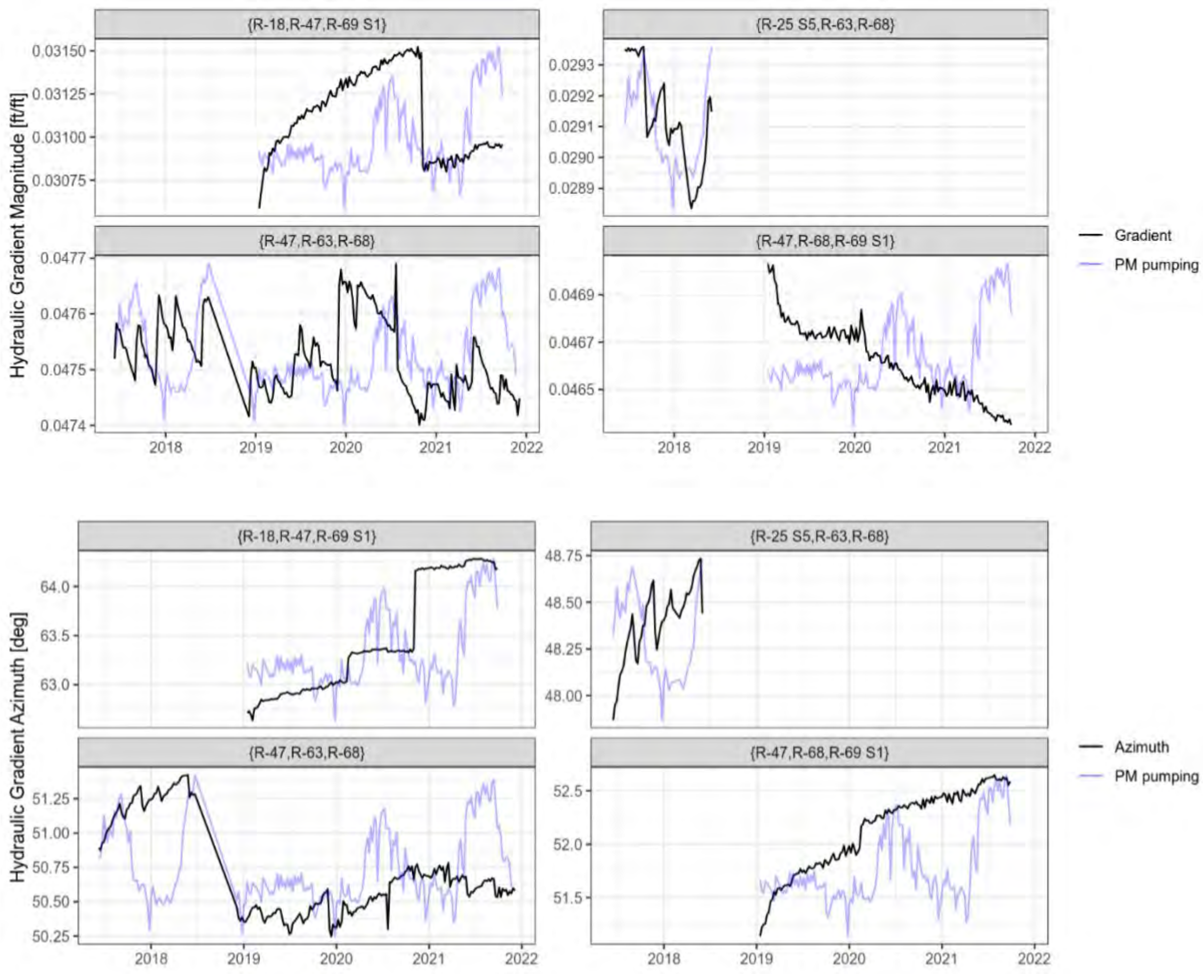

Figure 1. Gradient magnitude (top) and azimuth (bottom), shown in black, with supply well pumping (PM-2 + PM-4 + PM-5), shown in blue, through time for RRM target triples.

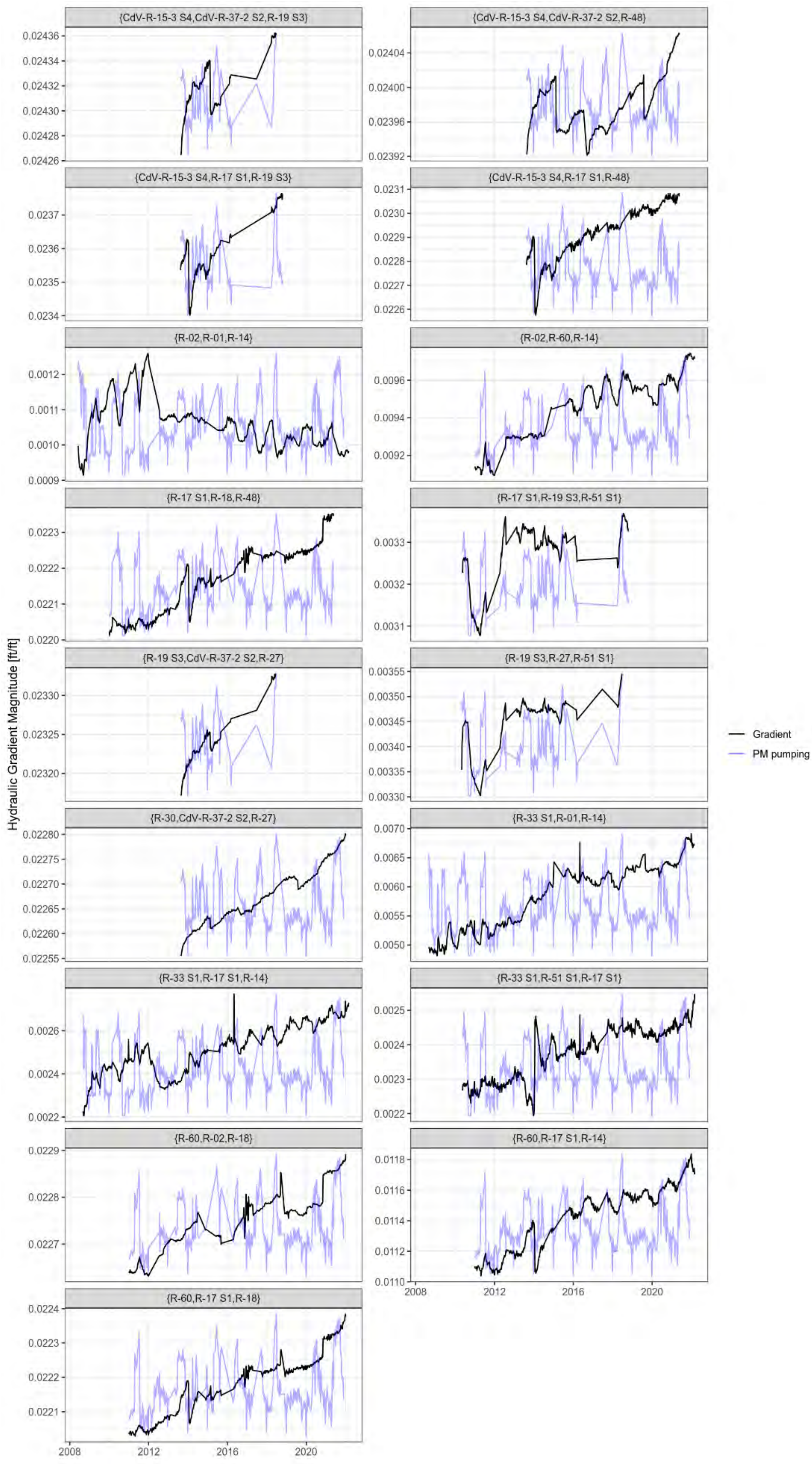

Figure 2. Gradient magnitude, shown in black, with supply well pumping (PM-2 + PM-4 + PM-5), shown in blue, through time for water table triples.

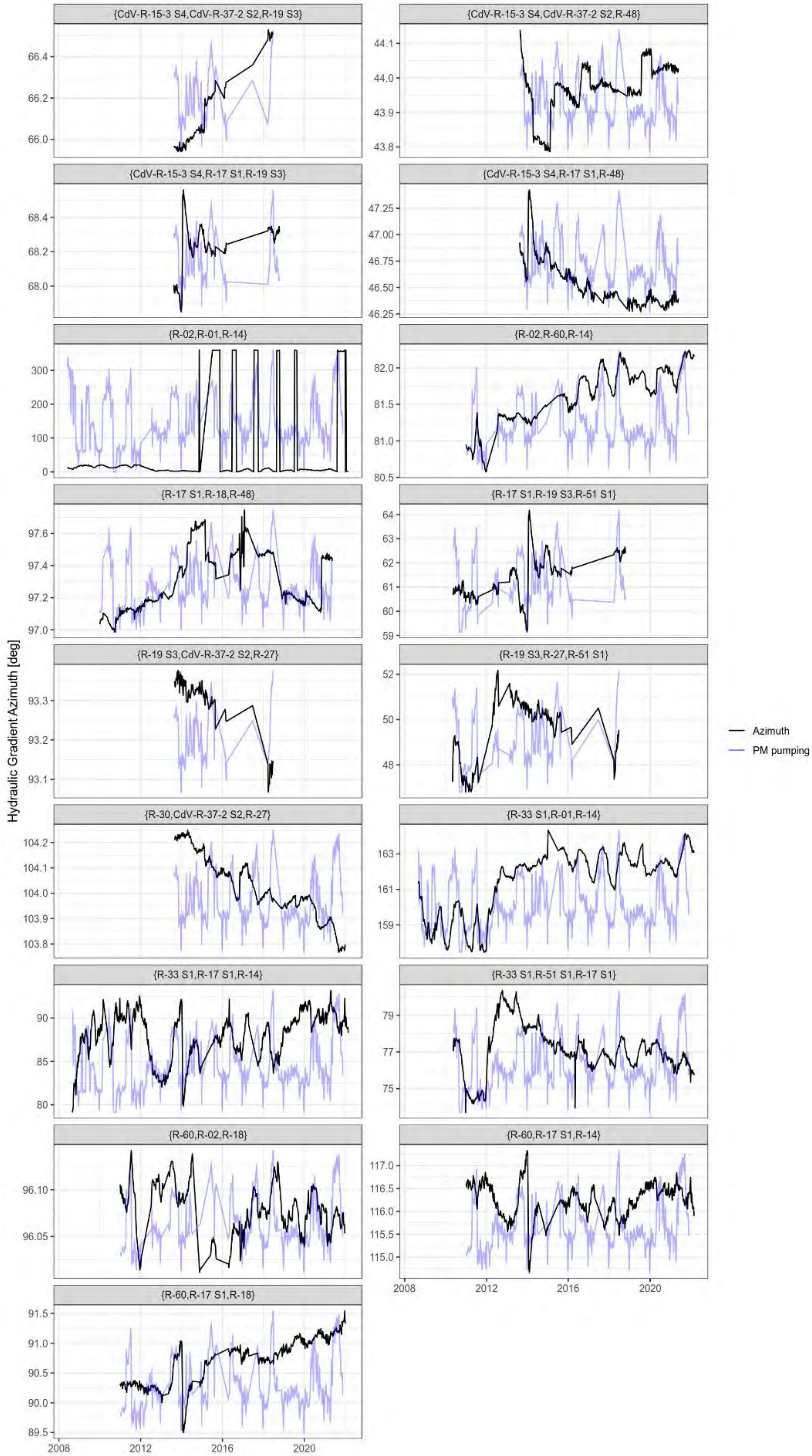

Figure 3. Gradient azimuth, shown in black, with supply well pumping (PM-2 + PM-4 + PM-5), shown in blue, through time for water table triples.

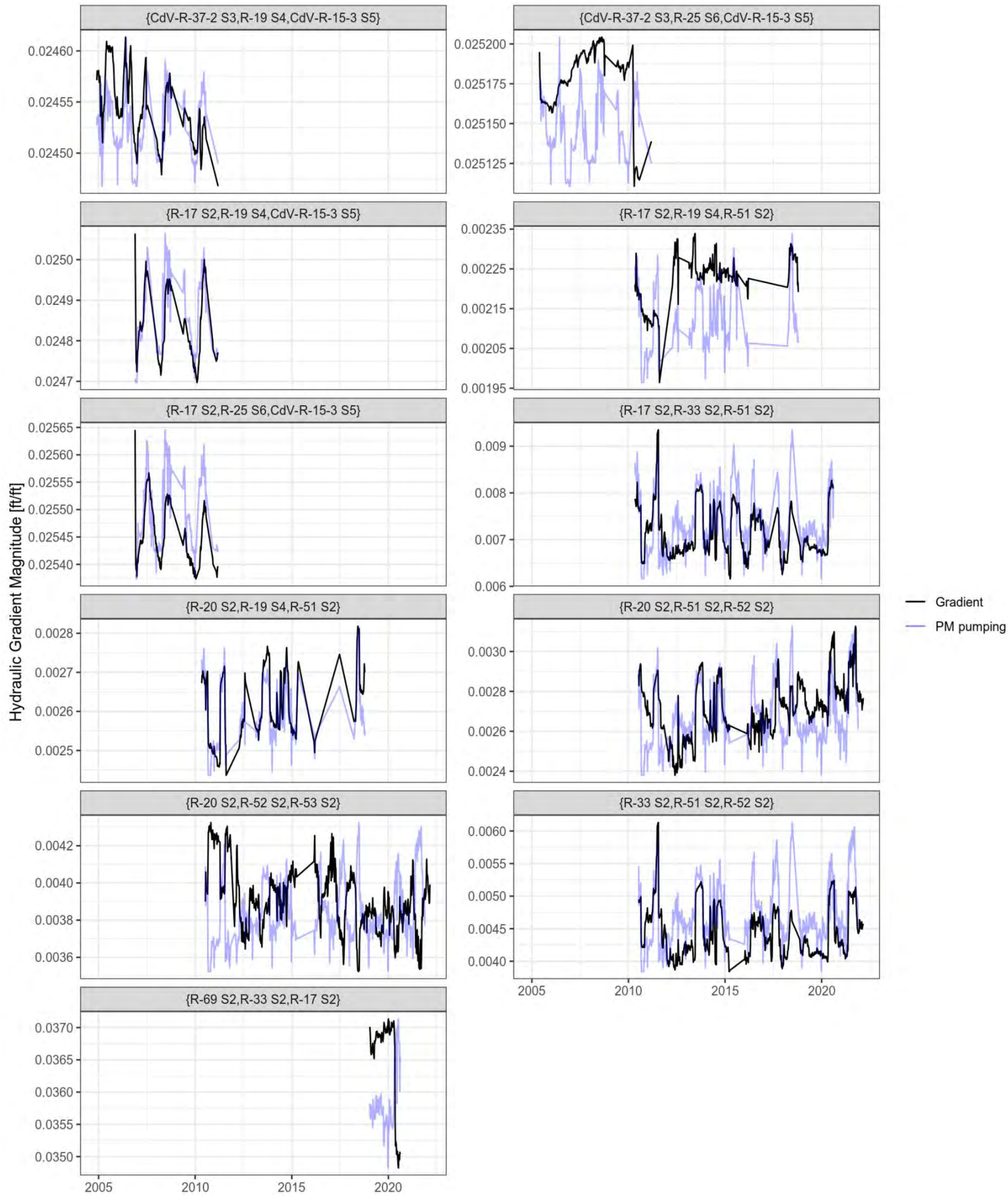

Figure 4. Gradient magnitude, shown in black, with supply well pumping (PM-2 + PM-4 + PM-5), shown in blue, through time for mid-depth triples.

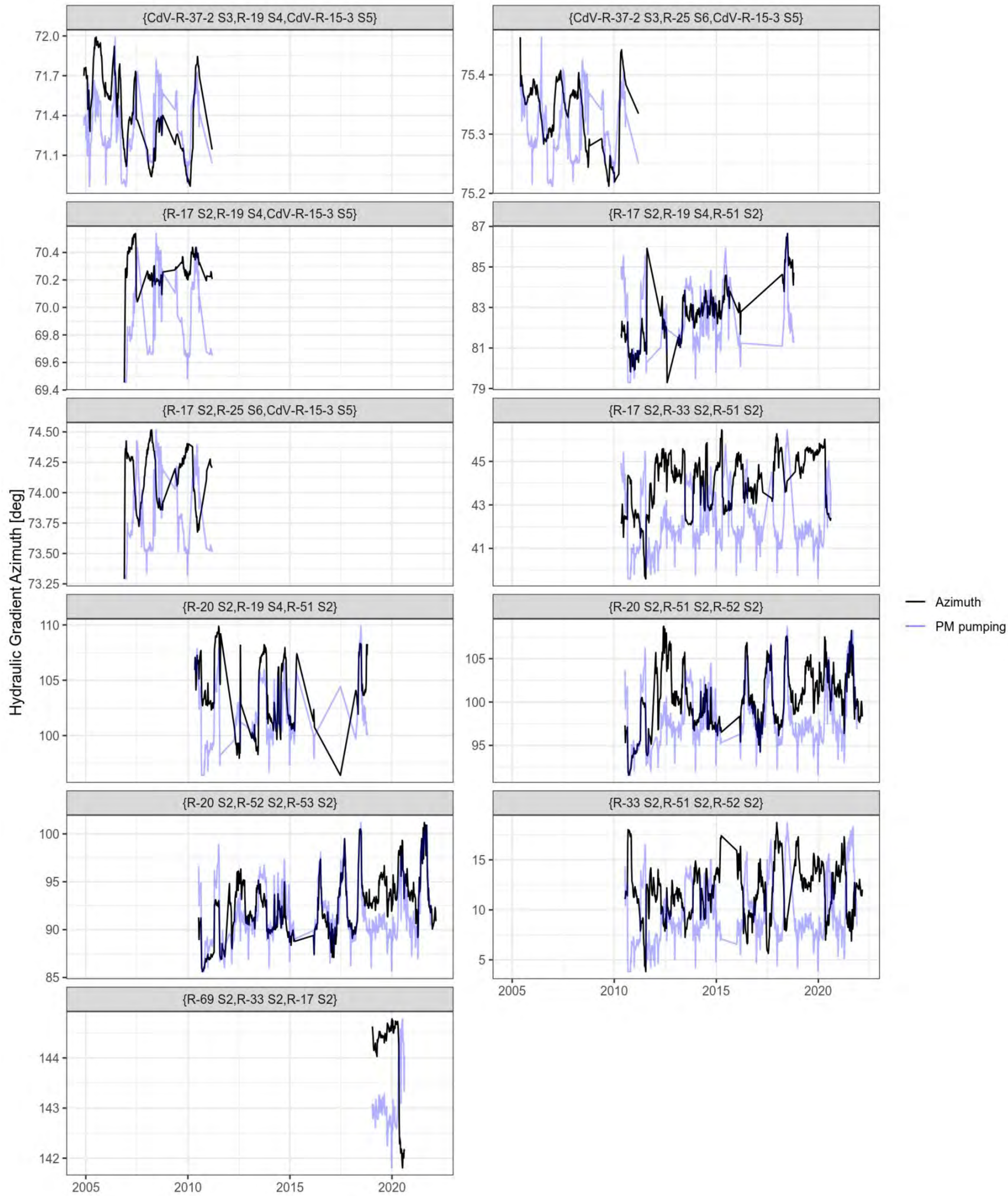

Figure 5. Gradient magnitude (left) and azimuth (right), shown in black, with supply well pumping (PM-2 + PM-4 + PM-5), shown in blue, through time for mid-depth triples.

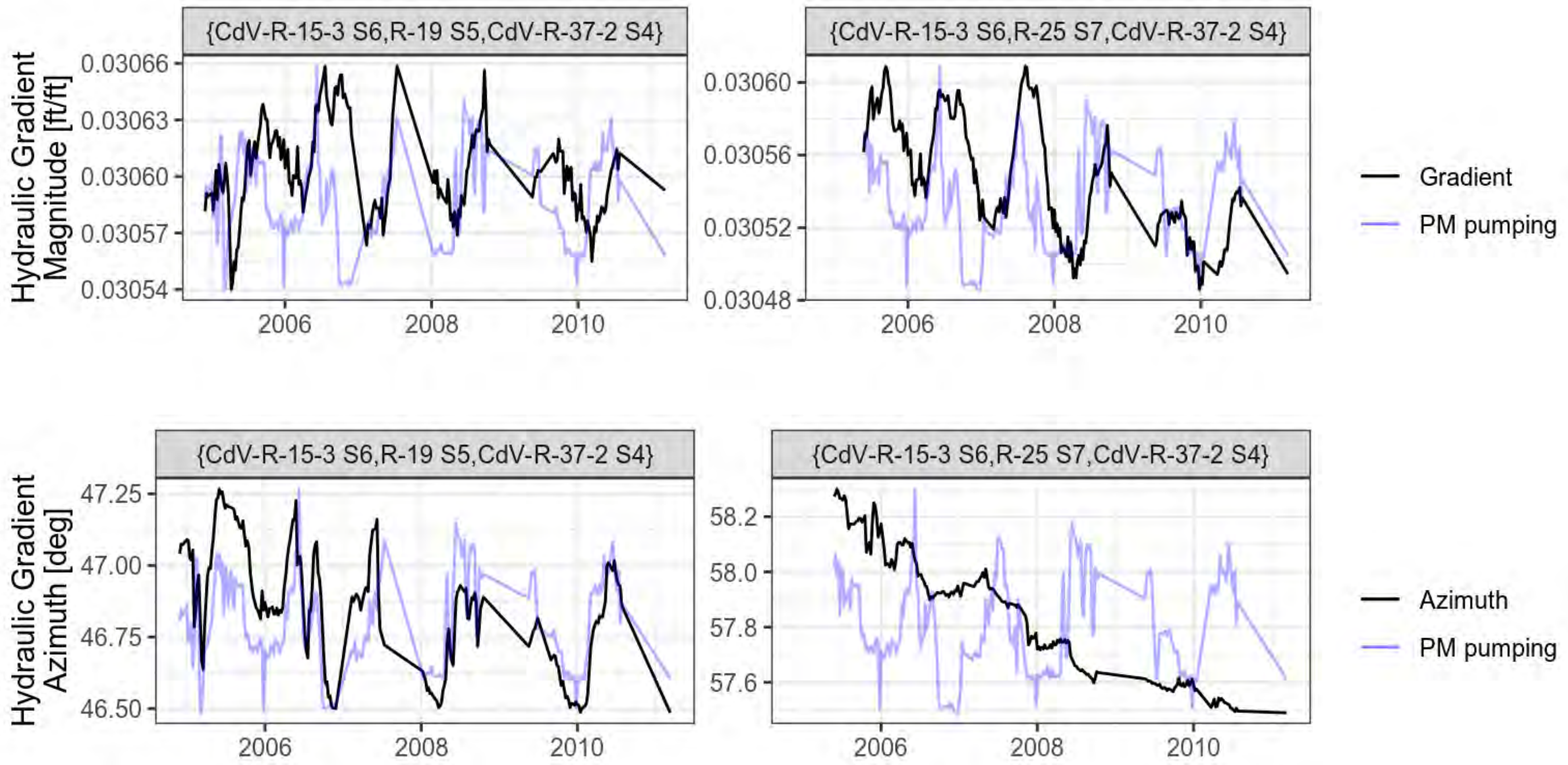

Figure 6. Gradient magnitude (top) and azimuth (bottom), shown in black, with supply well pumping (PM-2 + PM-4 + PM-5), shown in blue, through time for deep triples.

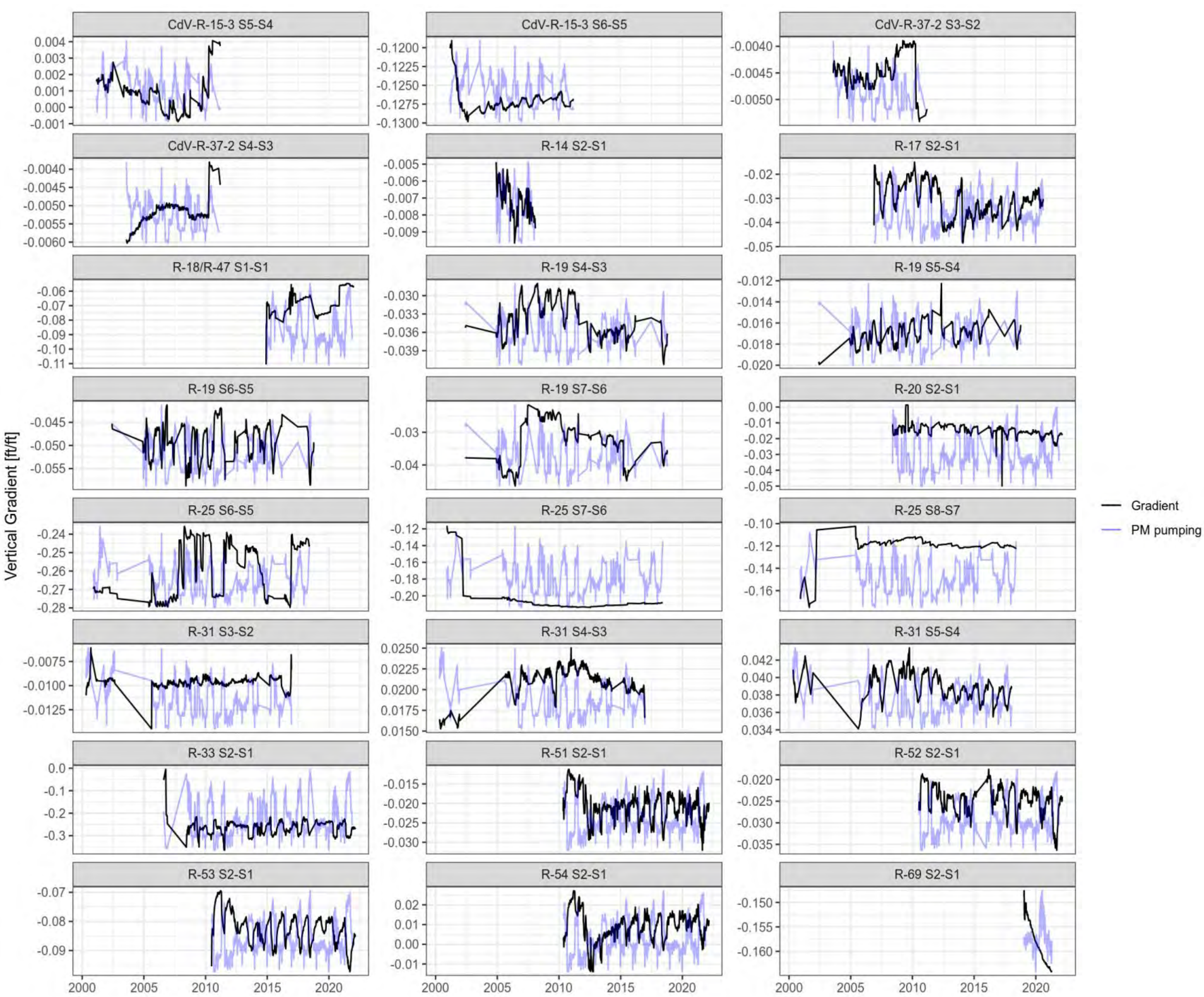

Figure 7. Vertical gradient magnitude through time with supply well pumping (PM-2 + PM-4 + PM-5).

Table 1. Results of Mann-Kendall test for trend, estimated linear change based on Sen's method, and correlation to supply well pumping (PM-2 + PM-4 + PM-5) for hydraulic gradient magnitude (above) and azimuth (below) of RRM gradient target triples.

	Mann-Kendall			Sen's Slope (yr^{-1})			supply well pumping	
triple	statistic	*p*-value	n	estimate	Low	high	correlation	*p*-value
R-18, R-47, R-69 S1	2.10E+00[1]	3.55E-02	144	2.32e-06	1.5e-07	3.85e-06	1.02E-01	2.24E-01
R-25 S5, R-63, R-68	-4.92E+00	8.87E-07	48	-9.28e-06	-1.12e-05	-5.98e-06	5.49E-01	5.42E-05
R-47, R-63, R-68	-5.82E+00	5.91E-09	216	-3.89e-07	-5.07e-07	-2.69e-07	-5.93E-02	3.88E-01
R-47, R-68, R-69 S1	-1.52E+01	3.28E-52	144	-3.41e-06	-3.56e-06	-3.28e-06	-5.02E-01	1.53E-10

[1] Results that are not statistically significant (p>0.001) are highlighted in red.

	Mann-Kendall			Sen's Slope (yr^{-1})			Supply Well Pumping	
triple	statistic	*p*-value	n	estimate	Low	high	correlatio	*p*-value
R-18, R-47, R-69 S1	1.58E+01	3.52E-	144	1.12e-02	9.51e-03	1.23e-	4.46E-01	2.18E-08
R-25 S5, R-63, R-68	7.08E+00	1.40E-	48	1.32e-02	1.07e-02	1.58e-	-2.48E-01[1]	8.91E-02
R-47, R-63, R-68	-1.46E+00	1.45E-	216	-1.13e-03	-2.24e-03	3.37e-	2.32E-01	6.16E-04
R-47, R-68, R-69 S1	1.65E+01	1.94E-	144	8.4e-03	8.04e-03	8.79e-	4.53E-01	1.21E-08

[1] Results that are not statistically significant (p>0.001) are highlighted in red.

Table 2. Results of Mann-Kendall test for trend, estimated linear change based on Sen's method, and correlation to supply well pumping (PM-2 + PM-4 + PM-5) for hydraulic gradient magnitude (above) and azimuth (below) of water table well screen triples.

	Mann-Kendall			Sen's Slope (yr^{-1})			Supply Well	
Triple	**statistic**	***p*-value**	**n**	**estimat**	**low**	**high**	**correlatio**	***p*-**
CdV-R-15-3 S4, CdV-R-37-2 S2, R-	7.92E+0	2.41E-	123	4.94E-	4.23E-07	5.43E-	-8.11E-	3.73E-
CdV-R-15-3 S4, CdV-R-37-2 S2, R-	1.18E+0	2.33E-	382	1.83E-	1.54E-07	2.10E-	-1.60E-01	1.66E-
CdV-R-15-3 S4, R-17 S1, R-19 S3	1.06E+0	4.99E-	140	2.03E-	1.57E-06	2.37E-	1.21E-01	1.53E-
CdV-R-15-3 S4, R-17 S1, R-48	2.41E+0	7.69E-	368	9.64E-	9.35E-07	9.93E-	-1.74E-01	8.26E-
R-02, R-01, R-14	-	2.78E-	671	-2.01E-	-2.17E-	-1.85E-	-3.97E-01	3.30E-
R-02, R-60, R-14	2.42E+0	6.64E-	517	9.69E-	9.20E-07	1.01E-	3.42E-01	2.99E-
R-17 S1, R-18, R-48	2.90E+0	7.58E-	508	5.94E-	5.79E-07	6.09E-	1.48E-01	7.91E-
R-17 S1, R-19 S3, R-51 S1	6.74E+0	1.55E-	242	3.73E-	2.71E-07	5.17E-	2.99E-01	2.09E-
R-19 S3, CdV-R-37-2 S2, R-27	1.34E+0	9.32E-	121	7.92E-	7.20E-07	8.74E-	1.67E-01	6.64E-
R-19 S3, R-27, R-51 S1	1.02E+0	2.01E-	226	3.20E-	2.40E-07	4.20E-	3.93E-01	8.71E-
R-30, CdV-R-37-2 S2, R-27	2.80E+0	3.57E-	413	4.62E-	4.50E-07	4.74E-	5.55E-03	9.11E-
R-33 S1, R-01, R-14	3.21E+0	2.91E-	690	2.56E-	2.50E-06	2.62E-	2.36E-01	5.29E-
R-33 S1, R-17 S1, R-14	2.78E+0	1.35E-	657	5.31E-	5.08E-07	5.55E-	3.02E-02	4.45E-
R-33 S1, R-51 S1, R-17 S1	2.55E+0	1.41E-	602	3.79E-	3.68E-07	3.92E-	1.48E-01	3.05E-
R-60, R-02, R-18	2.45E+0	1.19E-	463	4.37E-	4.21E-07	4.51E-	1.96E-01	2.50E-
R-60, R-17 S1, R-14	2.77E+0	3.09E-	526	1.28E-	1.24E-06	1.32E-	2.91E-01	2.00E-
R-60, R-17 S1, R-18	2.93E+0	8.87E-	493	6.13E-	5.93E-07	6.31E-	2.31E-01	2.64E-

[1] Results that are not statistically significant (p>0.001) are highlighted in red.

	Mann-Kendall			Sen's Slope (yr^{-1})			Supply Well	
Triple	**statistic**	***p*-value**	**n**	**estimat**	**low**	**high**	**correlatio**	***p*-**
CdV-R-15-3 S4, CdV-R-37-2 S2, R-	1.42E+0	1.69E-	123	3.62E-	3.24E-03	3.93E-	2.90E-01[1]	1.15E-
CdV-R-15-3 S4, CdV-R-37-2 S2, R-	9.89E+0	4.78E-	382	2.98E-	2.46E-04	3.46E-	-2.53E-02	6.21E-
CdV-R-15-3 S4, R-17 S1, R-19 S3	4.46E+0	8.10E-	140	1.28E-	7.44E-04	1.93E-	-1.19E-01	1.61E-
CdV-R-15-3 S4, R-17 S1, R-48	-	4.41E-	368	-1.57E-	-1.68E-	-1.48E-	1.55E-01	2.90E-
R-02, R-01, R-14	-	3.89E-	671	-1.13E-	-1.47E-	-7.78E-	-3.87E-01	6.56E-
R-02, R-60, R-14	2.24E+0	2.51E-	517	2.11E-	2.01E-03	2.23E-	3.78E-01	1.69E-
R-17 S1, R-18, R-48	1.07E+0	1.59E-	508	6.32E-	4.34E-04	7.50E-	2.36E-01	7.03E-
R-17 S1, R-19 S3, R-51 S1	9.93E+0	2.97E-	242	7.39E-	6.45E-03	8.30E-	7.16E-02	2.67E-
R-19 S3, CdV-R-37-2 S2, R-27	-	2.37E-	121	-9.04E-	-1.08E-	-7.68E-	-2.86E-01	1.47E-
R-19 S3, R-27, R-51 S1	1.83E-	8.55E-	226	4.57E-	-3.67E-	4.94E-	1.65E-01	1.32E-
R-30, CdV-R-37-2 S2, R-27	-	1.65E-	413	-9.77E-	-1.01E-	-9.45E-	-7.72E-02	1.20E-
R-33 S1, R-01, R-14	2.00E+0	3.94E-	690	5.99E-	5.48E-03	6.50E-	4.30E-01	9.32E-
R-33 S1, R-17 S1, R-14	8.24E+0	1.70E-	657	4.64E-	3.51E-03	5.79E-	-2.43E-01	4.18E-
R-33 S1, R-51 S1, R-17 S1	-	5.00E-	602	-2.73E-	-3.26E-	-2.19E-	2.71E-01	2.17E-
R-60, R-02, R-18	-	6.38E-	463	-5.56E-	-7.22E-	-3.85E-	1.76E-01	1.51E-
R-60, R-17 S1, R-14	1.86E+0	6.35E-	526	2.13E-	-1.11E-	4.64E-	-2.04E-01	3.31E-
R-60, R-17 S1, R-18	2.26E+0	7.98E-	493	2.22E-	2.12E-03	2.32E-	1.84E-01	4.54E-

[1] Results that are not statistically significant (p>0.001) are highlighted in red.

Table 3. Results of Mann-Kendall test for trend, estimated linear change based on Sen's method, and correlation to supply well pumping (PM-2 + PM-4 + PM-5) for hydraulic gradient magnitude (above) and azimuth (below) of mid-depth well screen triples.

triple	Mann-Kendall statistic	*p*-value	n	Sen's Slope (yr^{-1}) estimate	low	high	Supply Well correlatio	*p*-value
CdV-R-37-2 S3, R-19 S4, CdV-R-15-3	-8.60E+00	7.90E-	220	-3.10E-	-3.73E-	-2.48E-	6.07E-01	1.43E-
CdV-R-37-2 S3, R-25 S6, CdV-R-15-3	6.55E+00	5.93E-	224	1.43E-07	1.15E-07	1.70E-07	-2.54E-03[1]	9.70E-
R-17 S2, R-19 S4, CdV-R-15-3 S5	-7.32E-01	4.64E-	125	-1.60E-	-6.00E-	2.39E-07	7.67E-01	1.66E-
R-17 S2, R-19 S4, R-51 S2	5.84E+00	5.30E-	244	3.64E-07	2.59E-07	4.67E-07	2.44E-01	1.15E-
R-17 S2, R-25 S6, CdV-R-15-3 S5	-3.87E+00	1.08E-	153	-3.58E-	-5.28E-	-1.87E-	6.98E-01	1.24E-
R-17 S2, R-33 S2, R-51 S2	-2.80E+00	5.10E-	504	-3.94E-	-6.97E-	-1.12E-	6.87E-01	9.86E-
R-20 S2, R-19 S4, R-51 S2	4.11E+00	3.99E-	225	4.03E-07	2.14E-07	5.67E-07	8.50E-01	4.38E-
R-20 S2, R-51 S2, R-52 S2	1.04E+01	3.06E-	560	4.09E-07	3.42E-07	4.73E-07	2.99E-01	9.42E-
R-20 S2, R-52 S2, R-53 S2	-9.49E+00	2.36E-	560	-4.46E-	-5.36E-	-3.52E-	-6.00E-01	1.26E-
R-33 S2, R-51 S2, R-52 S2	-1.82E-01	8.56E-	558	-1.82E-	-2.10E-	1.64E-07	5.35E-01	1.54E-
R-69 S2, R-33 S2, R-17 S2	4.14E-01	6.79E-	85	6.13E-07	-3.23E-	2.86E-06	-7.20E-01	8.08E-

[1] Results that are not statistically significant (p>0.001) are highlighted in red.

triple	Mann-Kendall statistic	*p*-value	n	Sen's Slope (yr^{-1}) estimate	low	high	Supply Well correlatio	*p*-value
CdV-R-37-2 S3, R-19 S4, CdV-R-15-3	-9.34+00	1.00E-20	220	-3.25E-	-3.82E-	-2.72E-	5.58E-01	2.04E-
CdV-R-37-2 S3, R-25 S6, CdV-R-15-3	-5.34+00	9.49E-08	224	-3.98E-	-5.35E-	-2.47E-	1.12E-01[1]	9.53E-
R-17 S2, R-19 S4, CdV-R-15-3 S5	3.56+01	7.22E-01	125	9.05E-05	-4.48E-	6.59E-04	1.17E-01	1.94E-
R-17 S2, R-19 S4, R-51 S2	1.48+01	1.52E-49	244	1.63E-02	1.47E-02	1.78E-02	4.04E-01	5.21E-
R-17 S2, R-25 S6, CdV-R-15-3 S5	-1.11+00	2.69E-01	153	-4.32E-	-1.21E-	3.77E-04	-7.11E-01	7.62E-
R-17 S2, R-33 S2, R-51 S2	1.06+01	4.89E-26	504	3.89E-03	3.20E-03	4.62E-03	-4.03E-01	4.47E-
R-20 S2, R-19 S4, R-51 S2	-6.1-01	5.42E-01	225	-2.33E-	-1.03E-	4.85E-03	5.22E-01	3.91E-
R-20 S2, R-51 S2, R-52 S2	8.86+00	7.67E-19	560	8.39E-03	6.62E-03	1.01E-02	5.34E-01	1.67E-
R-20 S2, R-52 S2, R-53 S2	1.19+01	1.51E-32	560	9.87E-03	8.39E-03	1.14E-02	6.45E-01	1.43E-
R-33 S2, R-51 S2, R-52 S2	4.43+00	9.58E-06	558	3.08E-03	1.73E-03	4.44E-03	-7.03E-01	2.44E-
R-69 S2, R-33 S2, R-17 S2	7.17-01	4.73E-01	85	1.36E-03	-3.88E-	4.20E-03	-7.37E-01	8.70E-

[1] Results that are not statistically significant (p>0.001) are highlighted in red.

Table 4. Results of Mann-Kendall test for trend, estimated linear change based on Sen's method, and correlation to supply well pumping (PM-2 + PM-4 + PM-5) for hydraulic gradient magnitude (above) and azimuth (below) of deep well screen triples.

triple	Mann-Kendall statistic	*p*-value	n	Sen's Slope (yr^{-1}) estimate	low	high	Supply Well Pumping correlation	*p*-value
CdV-R-37-2 S3, R-19 S4, CdV-R-15-3	1.70E+0	8.92E-	212	-4.74E-	-1.00E-	7.30E-09	9.91E-02[1]	1.50E-01
CdV-R-37-2 S3, R-25 S6, CdV-R-15-3	-	7.84E-	224	-3.40E-	-3.89E-	-2.91E-	3.04E-01	3.60E-06

[1] Results that are not statistically significant (p>0.001) are highlighted in red.

triple	Mann-Kendall statistic	*p*-value	n	Sen's Slope (yr^{-1}) estimate	low	high	Supply Well Pumping correlation	*p*-value
CdV-R-37-2 S3, R-19 S4, CdV-R-15-3	-	5.97E-	212	-1.95E-	-2.42E-	-1.49E-03	6.35E-01	2.36E-25
CdV-R-37-2 S3, R-25 S6, CdV-R-15-3	-	1.63E-	224	-3.37E-	-3.47E-	-3.25E-03	-2.13E-02[1]	7.51E-01

[1] Results that are not statistically significant (p>0.001) are highlighted in red.

Table 5. Results of Mann-Kendall test for trend, estimated linear change based on Sen's method, and correlation to supply well pumping (PM-2 + PM-4 + PM-5) for vertical hydraulic gradient well screen pairs.

	Mann-Kendall			Sen's Slope (yr^{-1})			Supply Well Pumping	
triple	statistic	*p*-value	n	estimate	low	high	correlation	*p*-value
CdV-R-15-3 S5-S4	-9.21E+00	3.40E-20	380	-4.41E-	-5.18E-	-3.52E-	2.18E-01	1.82E-05
CdV-R-15-3 S6-S5	9.46E+00	3.07E-21	397	3.99E-06	3.33E-06	4.63E-06	-3.62E-01	9.43E-14
CdV-R-37-2 S3-S2	7.14E+00	9.54E-13	369	1.35E-06	1.06E-06	1.62E-06	-1.32E-01[1]	1.13E-02
CdV-R-37-2 S4-S3	1.04E+01	1.50E-25	369	1.79E-06	1.52E-06	2.13E-06	-1.61E-01	1.91E-03
R-14 S2-S1	-7.84E+00	4.43E-15	150	-1.27E-	-1.54E-	-9.88E-	-8.59E-02	2.96E-01
R-17 S2-S1	-8.07E+00	6.85E-16	677	-1.29E-	-1.55E-	-1.03E-	-4.73E-01	4.16E-39
R-47/R-18 S1-S1	9.59E+00	8.44E-22	325	5.00E-05	4.26E-05	5.90E-05	1.84E-01	9.89E-04
R-19 S4-S3	-6.87E+00	6.27E-12	488	-7.47E-	-9.50E-	-5.49E-	-5.31E-01	6.47E-37
R-19 S5-S4	7.42E+00	1.18E-13	479	2.45E-06	1.83E-06	3.08E-06	-6.55E-01	5.63E-60
R-19 S6-S5	5.21E-01	6.02E-01	479	6.26E-07	-1.78E-	2.97E-06	-7.01E-01	4.79E-72
R-19 S7-S6	-3.03E+00	2.45E-03	463	-1.34E-	-2.01E-	-4.52E-	-3.14E-01	4.86E-12
R-20 S2-S1	-1.54E+01	1.53E-53	671	-9.38E-	-1.04E-	-8.37E-	-6.62E-01	3.51E-84
R-25 S6-S5	7.74E+00	1.03E-14	583	3.09E-05	2.18E-05	4.04E-05	-9.71E-02	1.90E-02
R-25 S7-S6	-8.91E+00	4.91E-19	590	-9.96E-	-1.19E-	-7.60E-	1.27E-01	1.95E-03
R-25 S8-S7	-6.28E+00	3.31E-10	586	-5.93E-	-7.34E-	-4.34E-	-8.11E-02	4.97E-02
R-31 S3-S2	7.06E+00	1.69E-12	603	6.62E-07	4.85E-07	8.43E-07	-4.36E-02	2.85E-01
R-31 S4-S3	-1.73E+00	8.38E-02	510	-1.06E-	-2.10E-	1.55E-07	-4.81E-01	6.59E-31
R-31 S5-S4	-1.15E+01	8.10E-31	613	-4.51E-	-5.17E-	-3.85E-	-5.96E-01	2.75E-60
R-33 S2-S1	2.52E+00	1.18E-02	716	1.27E-05	2.93E-06	2.20E-05	-7.52E-01	7.53E-129
R-51 S2-S1	-5.58E+00	2.43E-08	627	-4.99E-	-6.77E-	-3.21E-	-6.34E-01	2.86E-70
R-52 S2-S1	-6.26E+00	3.76E-10	579	-5.41E-	-6.93E-	-3.80E-	-8.45E-01	3.66E-155
R-53 S2-S1	-9.79E+00	1.29E-22	619	-1.20E-	-1.44E-	-9.73E-	-8.01E-01	1.39E-136
R-54 S2-S1	3.65E+00	2.60E-04	624	7.01E-06	3.28E-06	1.04E-05	-5.75E-01	6.40E-55
R-69 S2-S1	-1.58E+01	4.71E-56	121	-1.14E-	-1.20E-	-1.10E-	-1.07E-01	2.42E-01
CdV-R-15-3 S5-S4	-9.21E+00	3.40E-20	380	-4.41E-	-5.18E-	-3.52E-	2.18E-01	1.82E-05

[1] Results that are not statistically significant (p>0.001) are highlighted in red.

Hydraulic Analysis of the Pajarito Plateau: Appendix B

Histogram Plots of Water Levels and Lateral Gradient Magnitudes/Azimuths

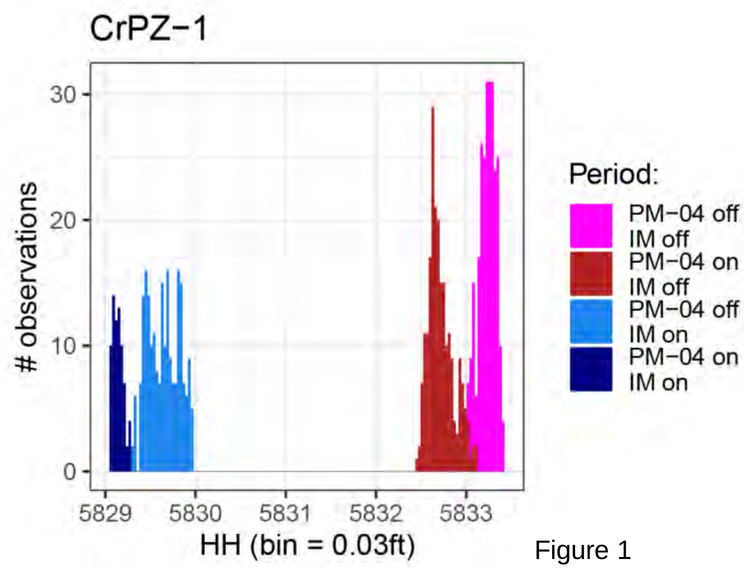

Figure 1

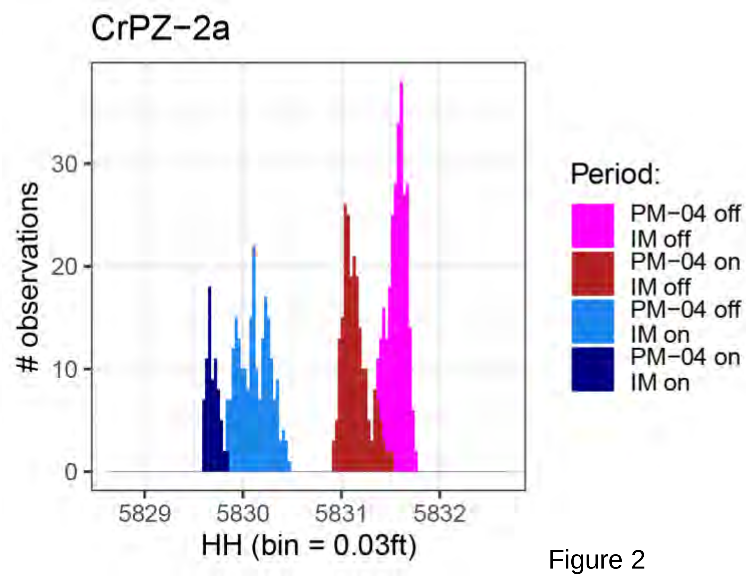

Figure 2

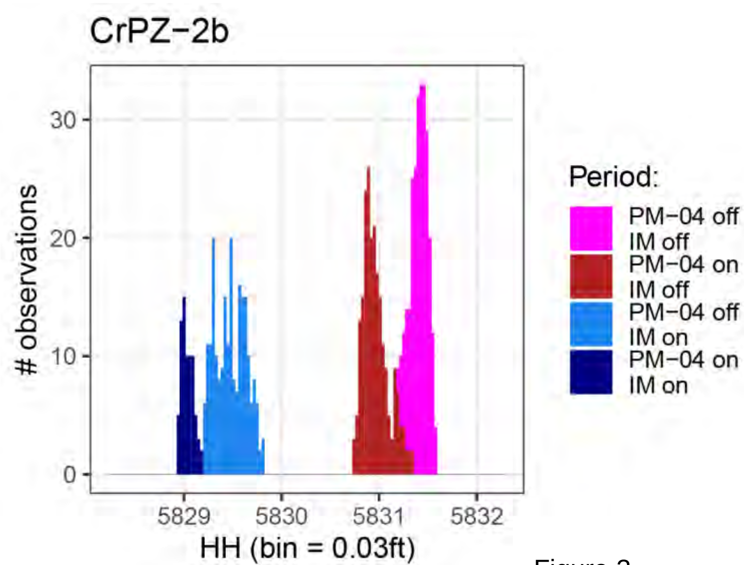

Figure 3

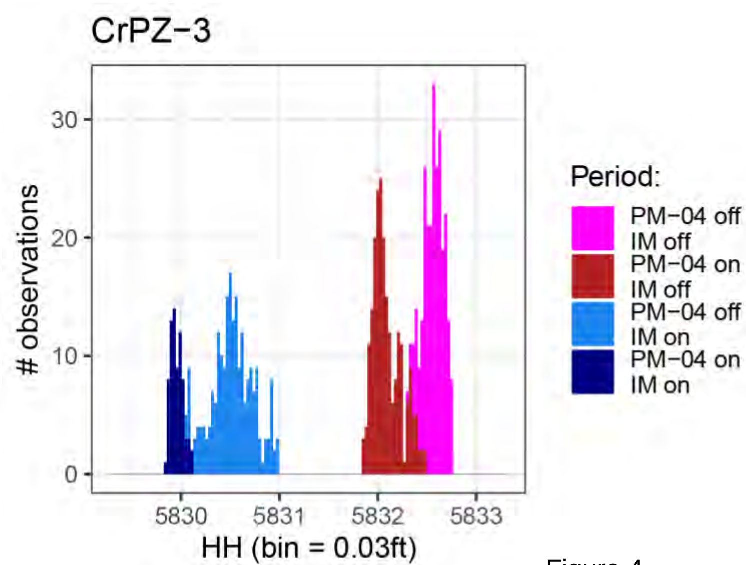

Figure 4

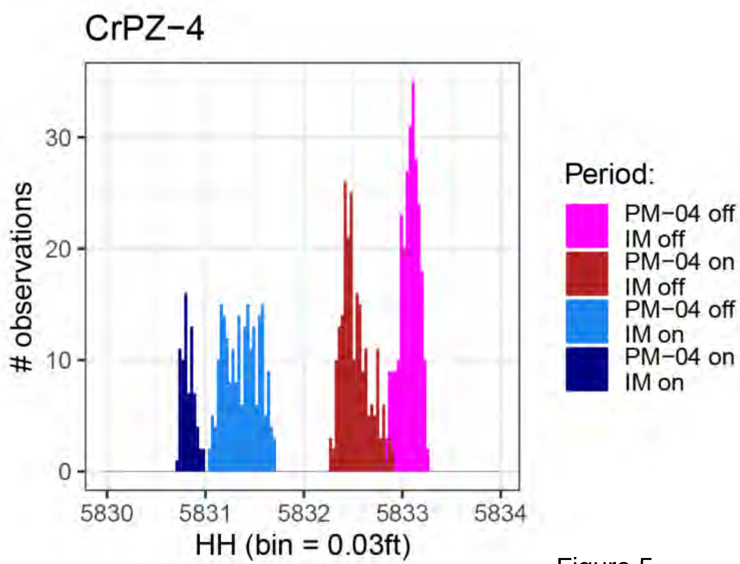

Figure 5

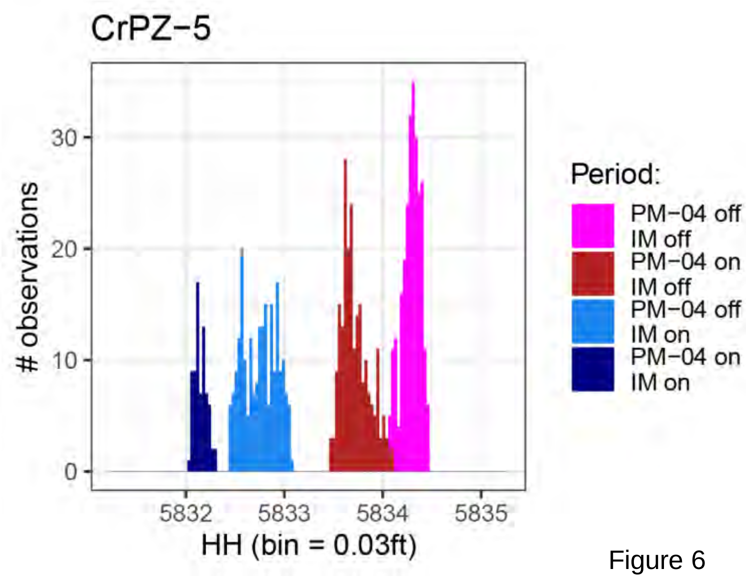

Figure 6

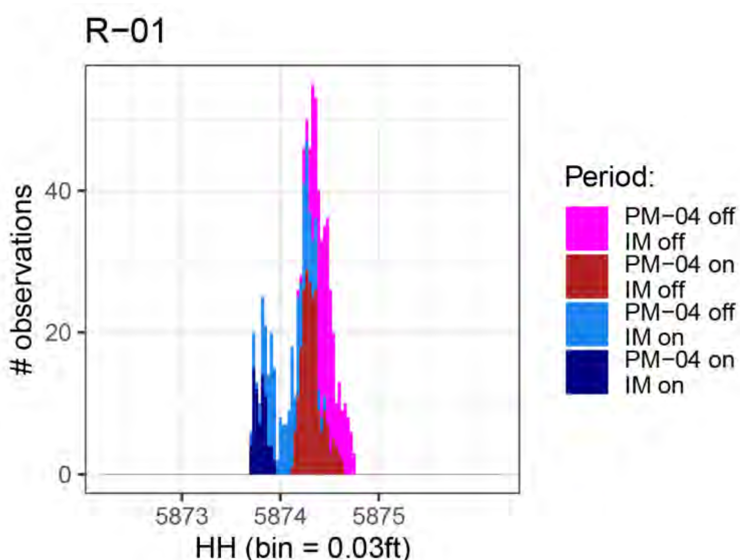

Figure 7

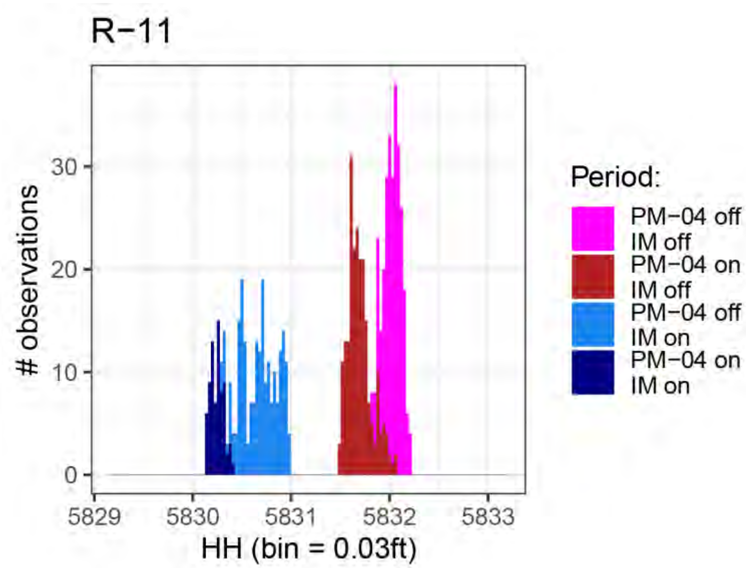

Figure 8

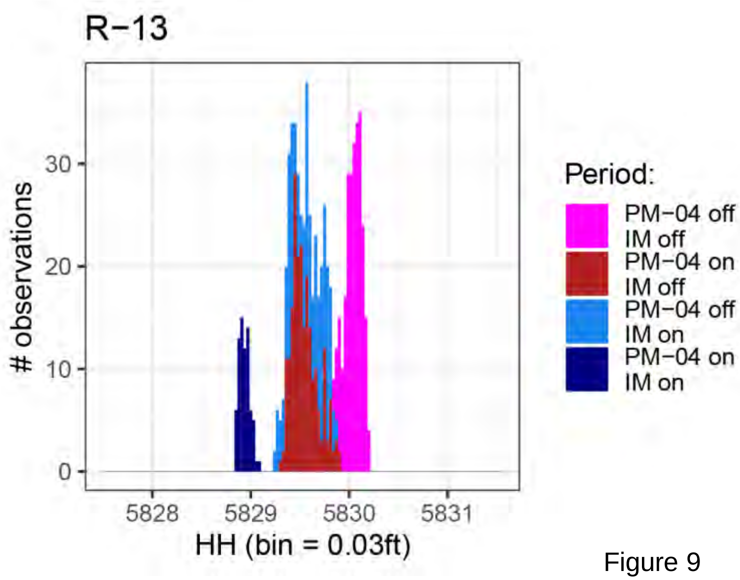

Figure 9

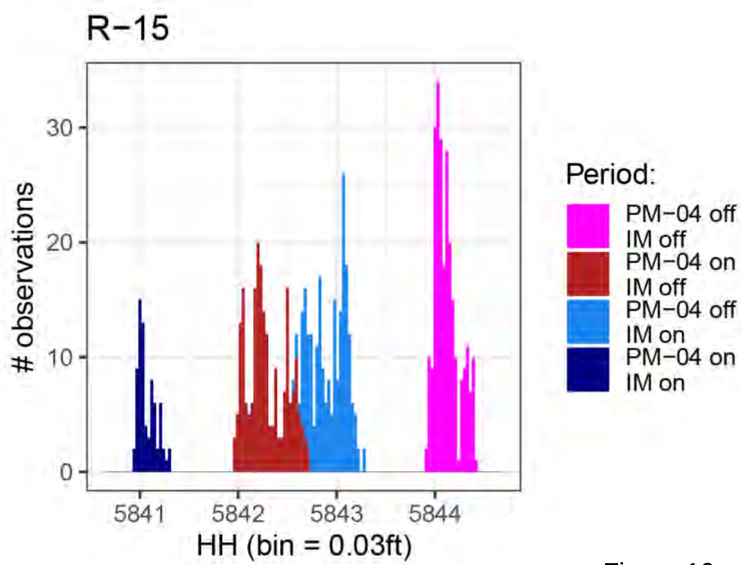

Figure 10

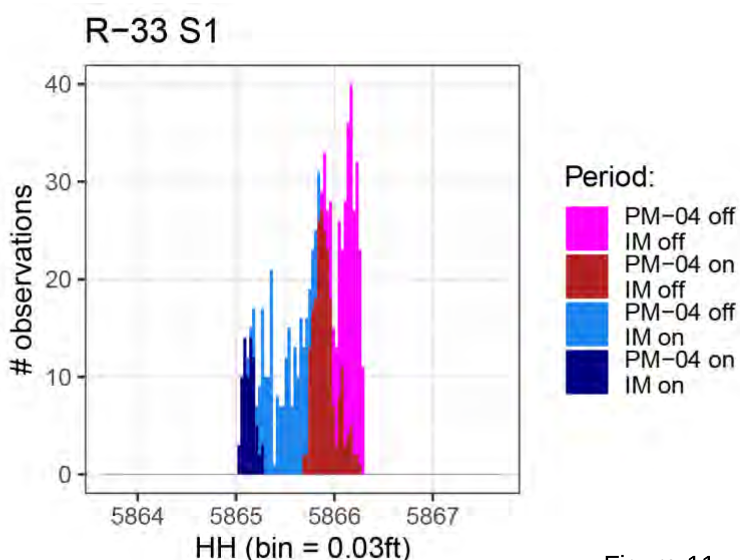

Figure 11

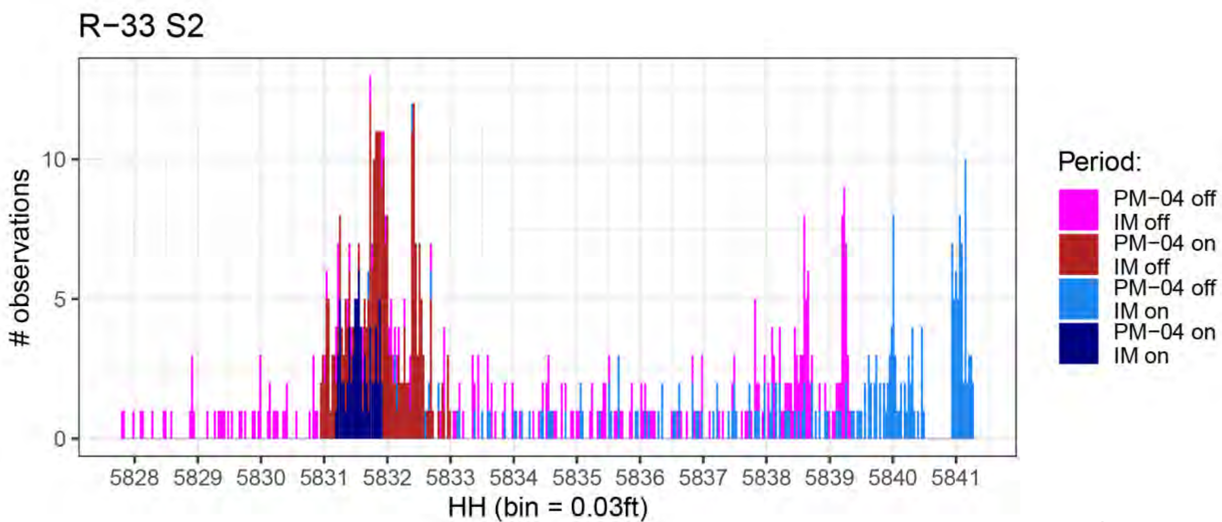

Figure 12

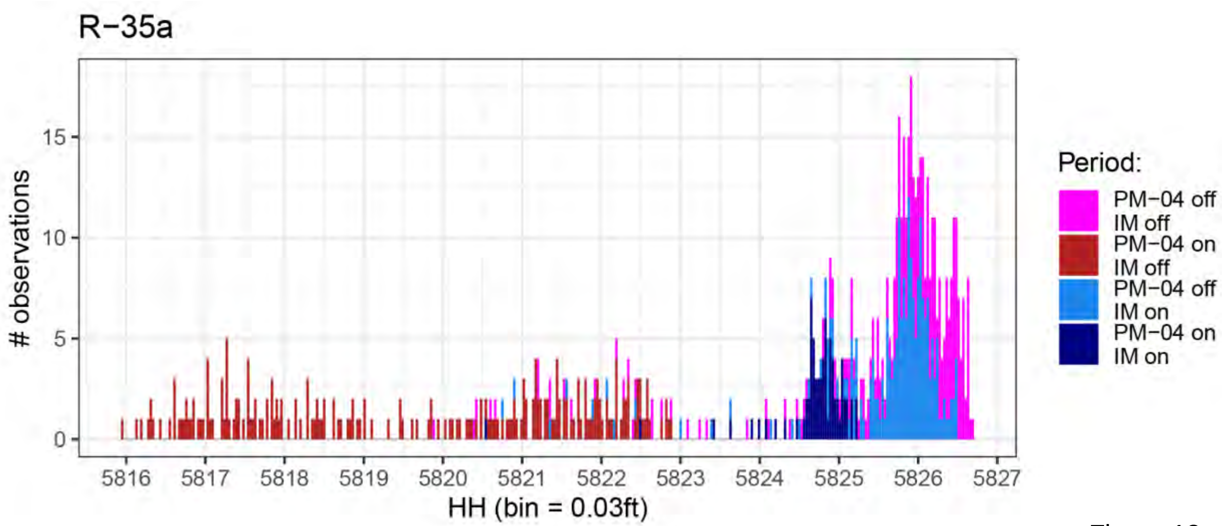

Figure 13

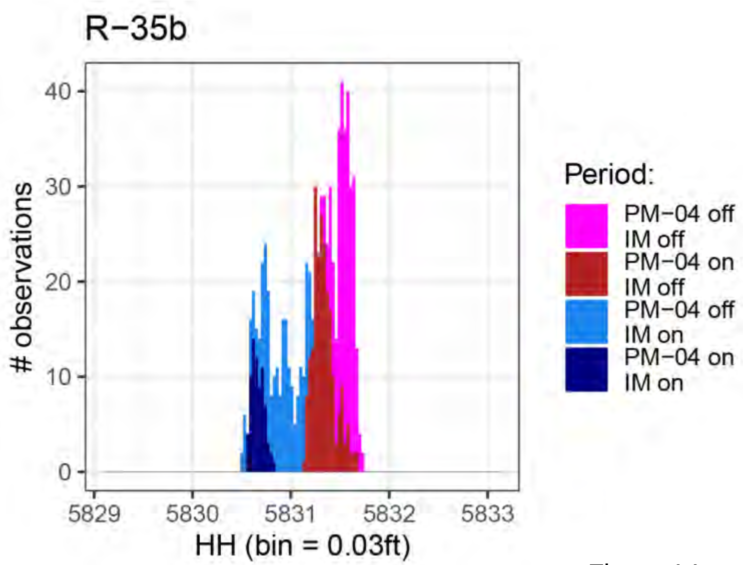

Figure 14

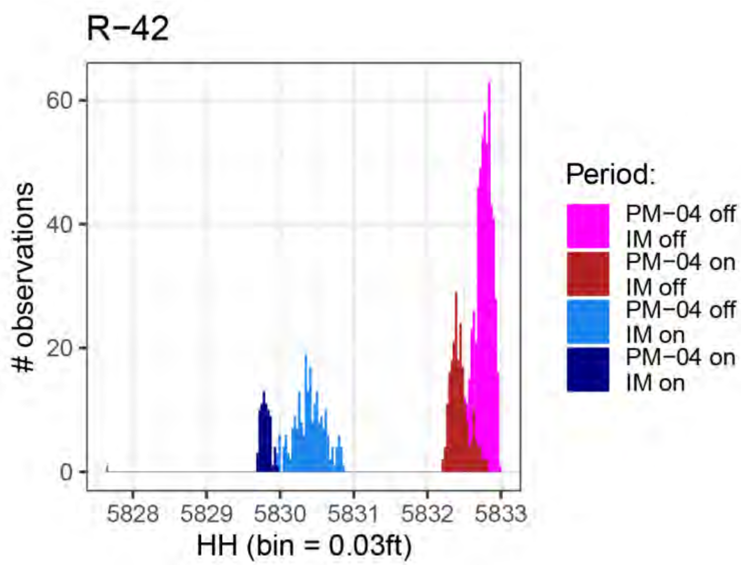

Figure 15

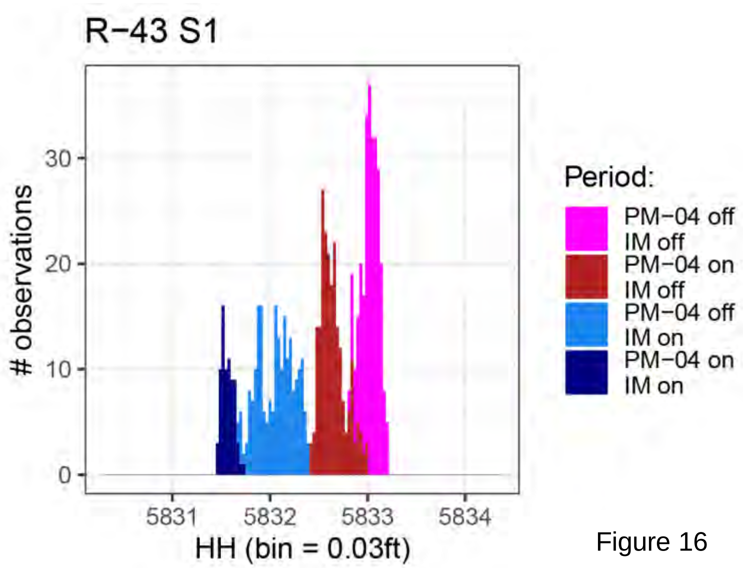

Figure 16

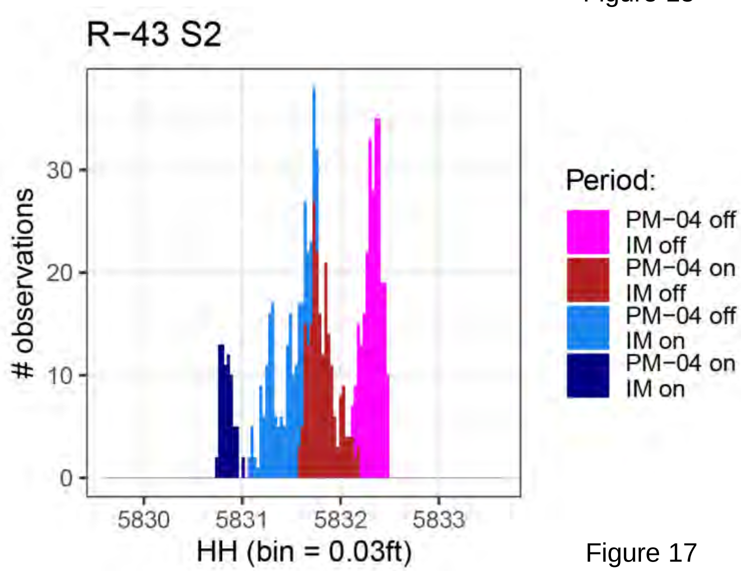

Figure 17

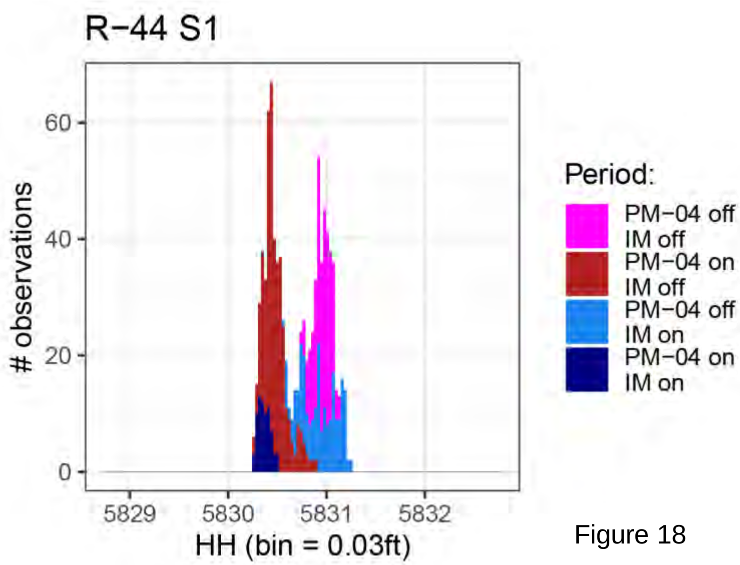

Figure 18

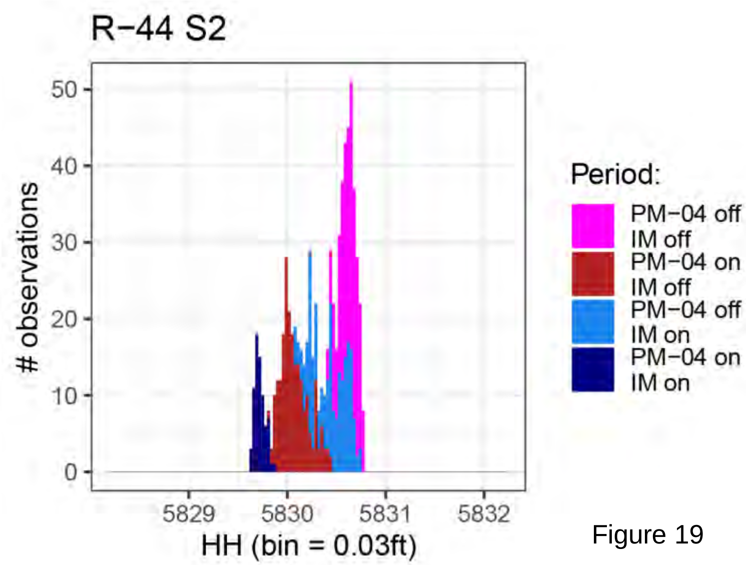

Figure 19

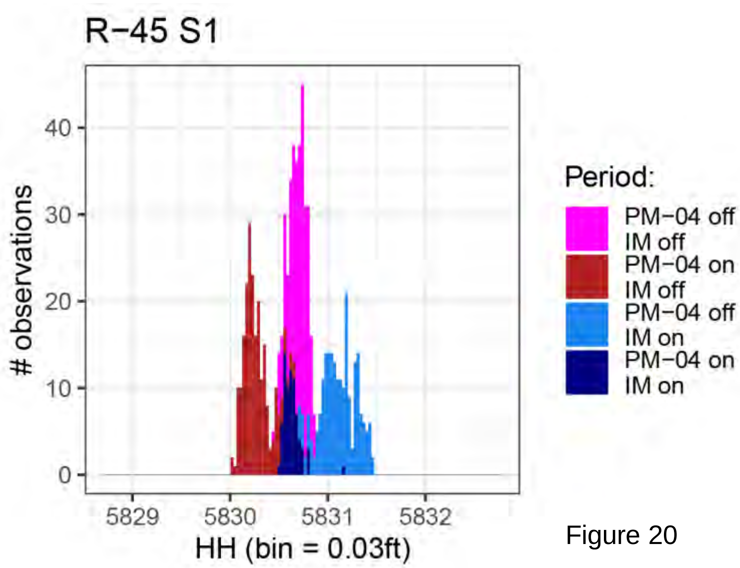

Figure 20

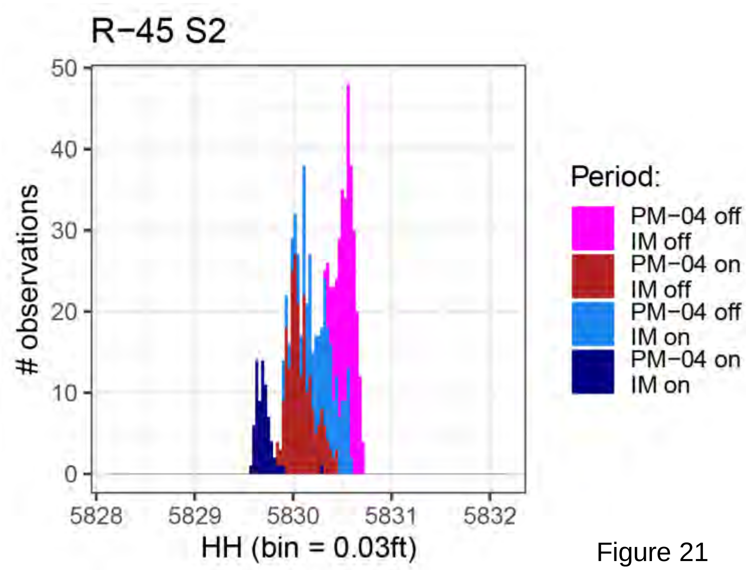

Figure 21

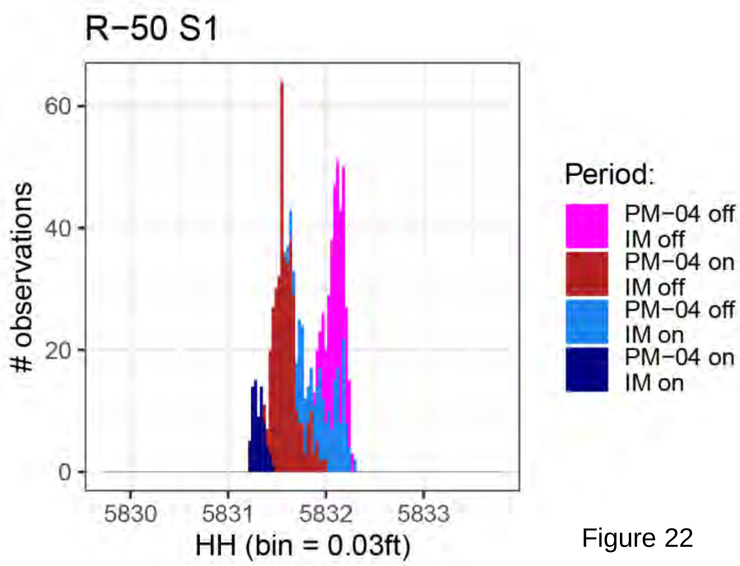

Figure 22

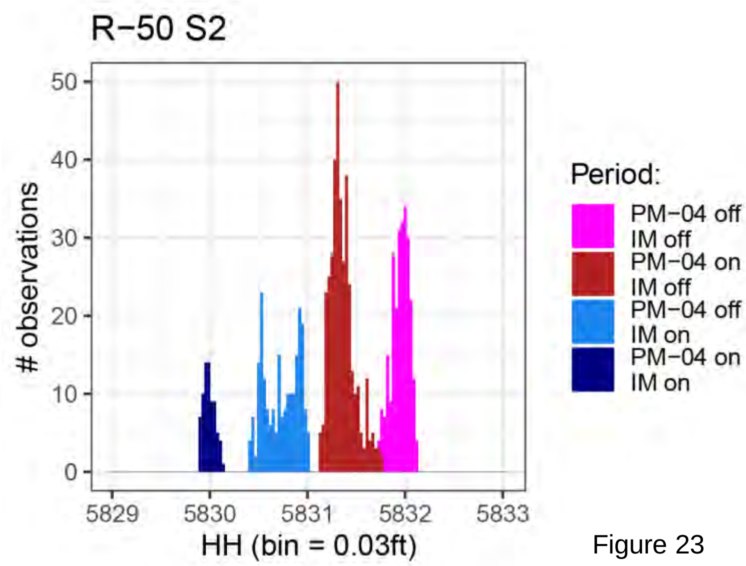

Figure 23

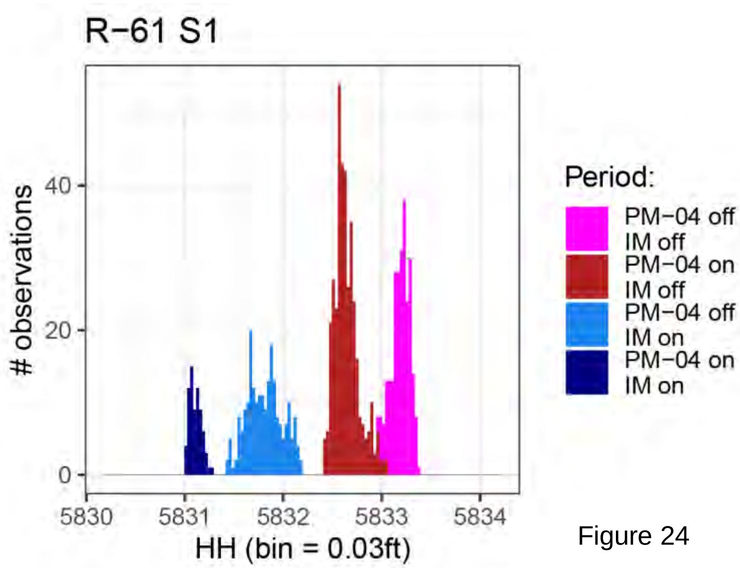

Figure 24

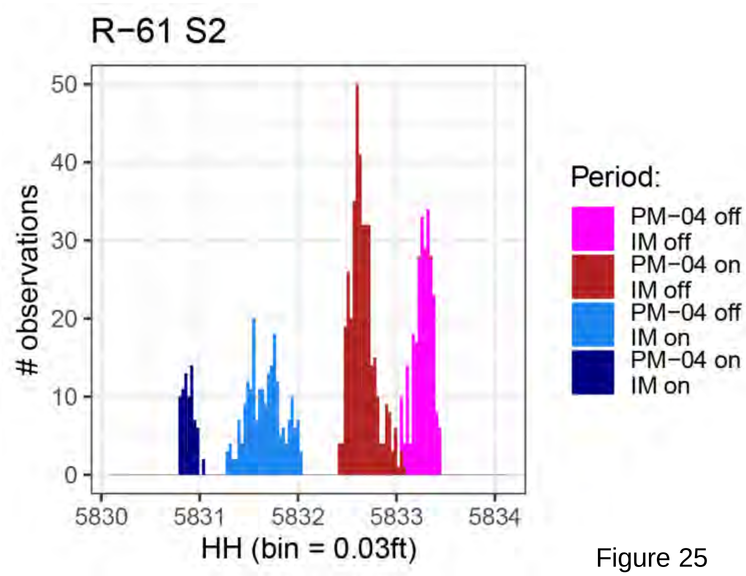

Figure 25

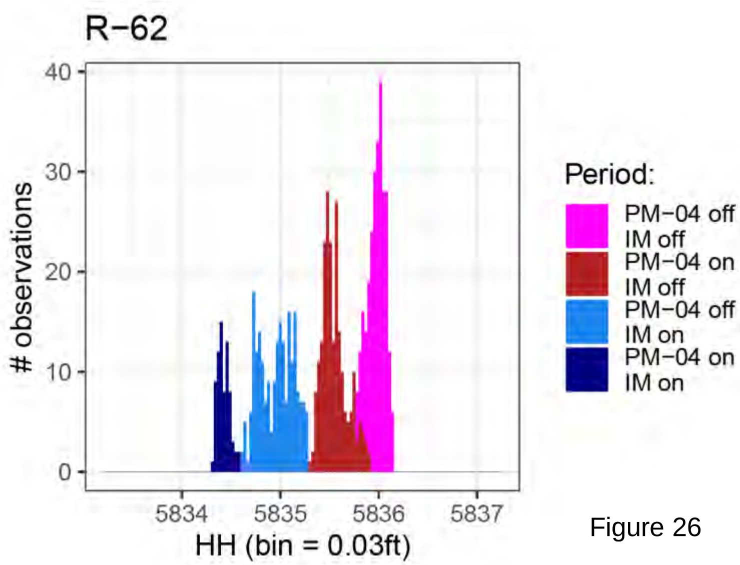

Figure 26

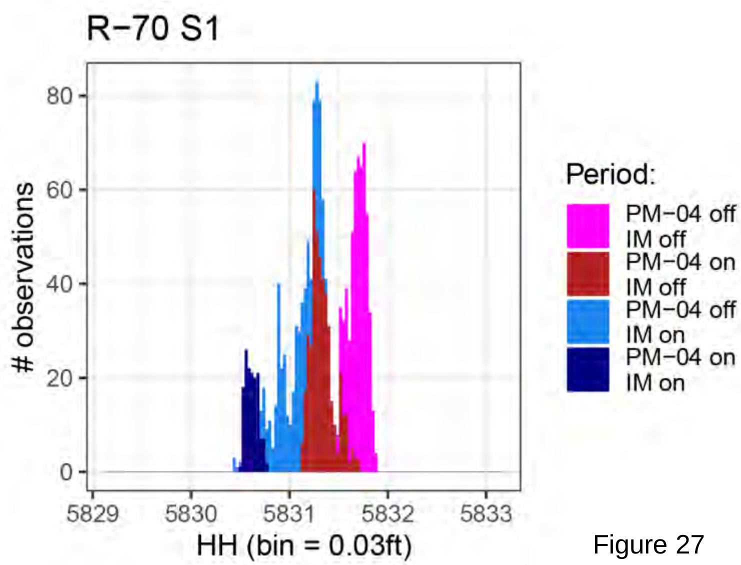

Figure 27

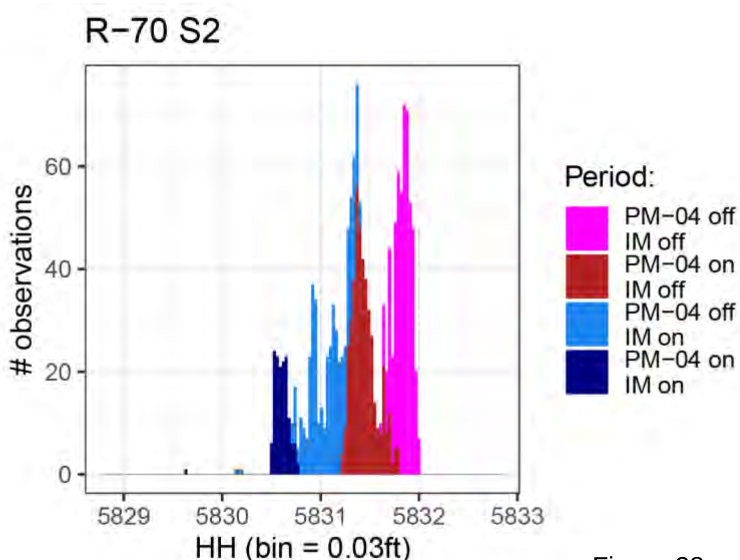

Figure 28

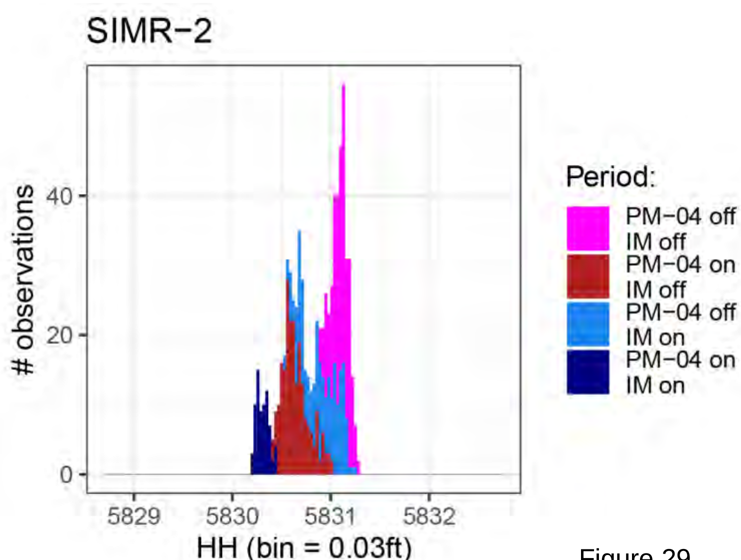

Figure 29

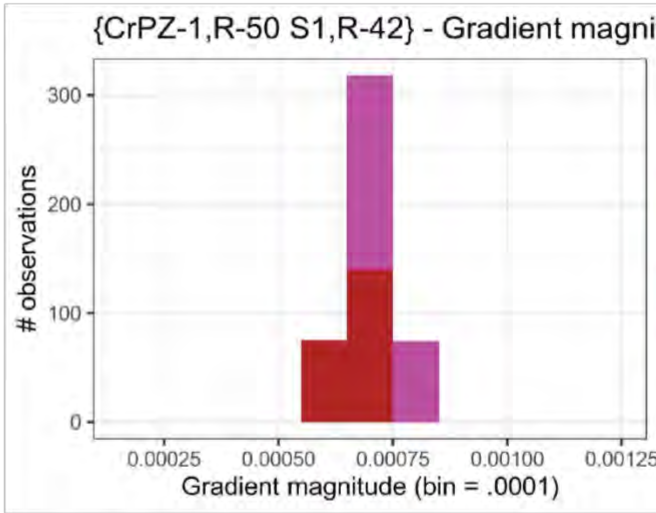

Figure 30

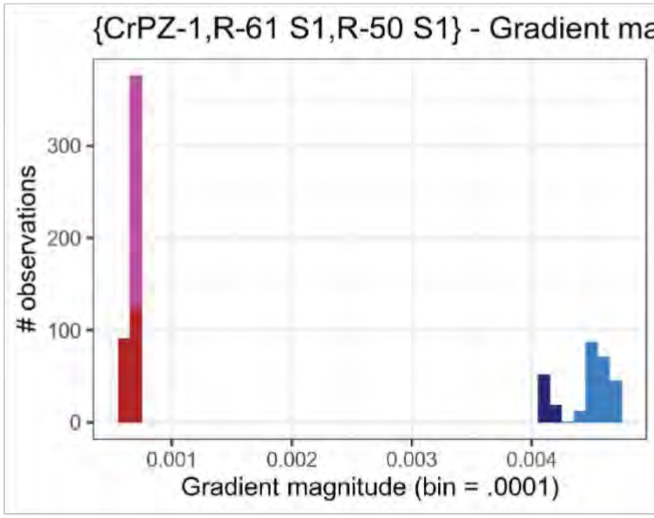

Figure 31

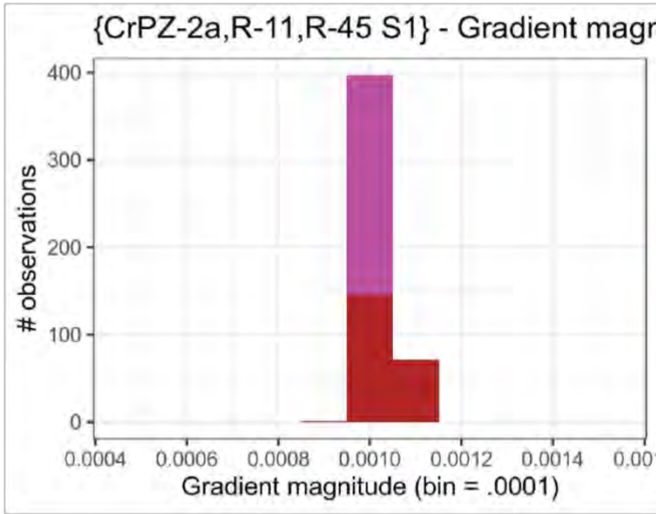

Figure 32

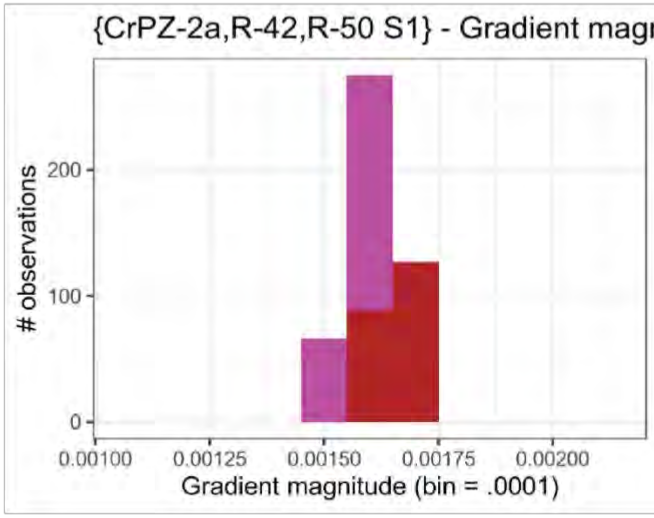

Figure 33

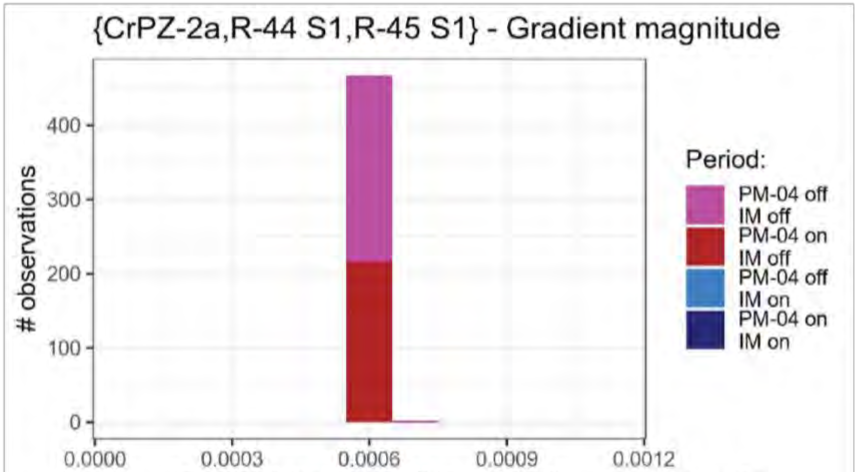

Figure 34

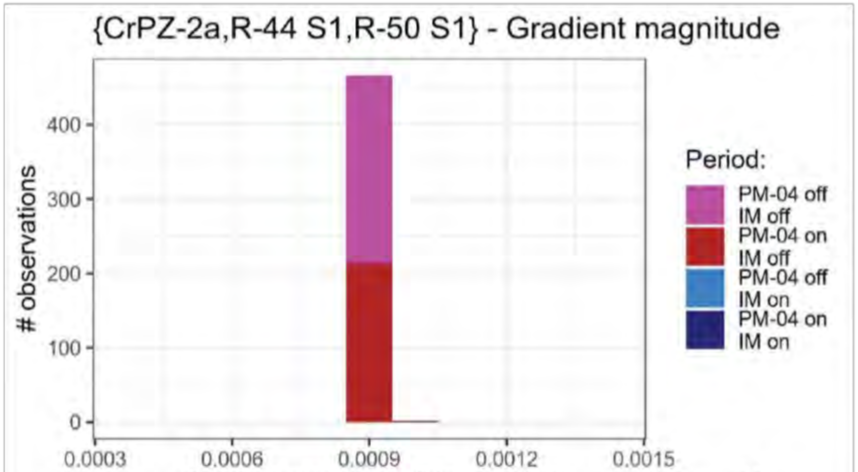

Figure 35

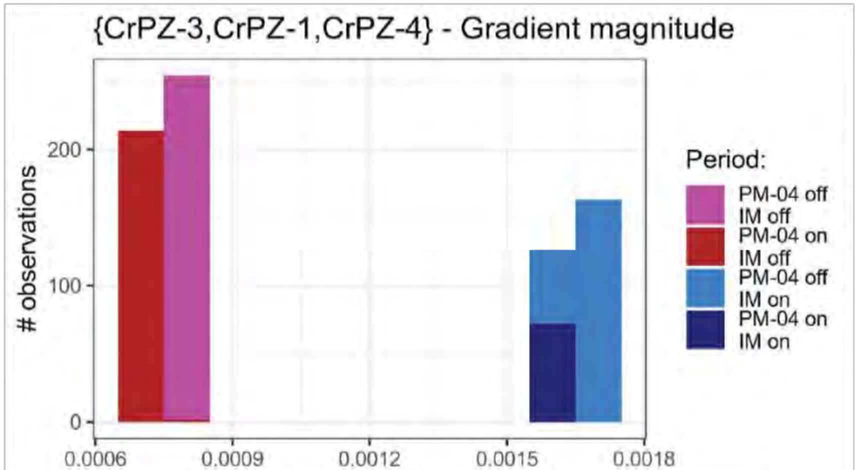

Figure 36

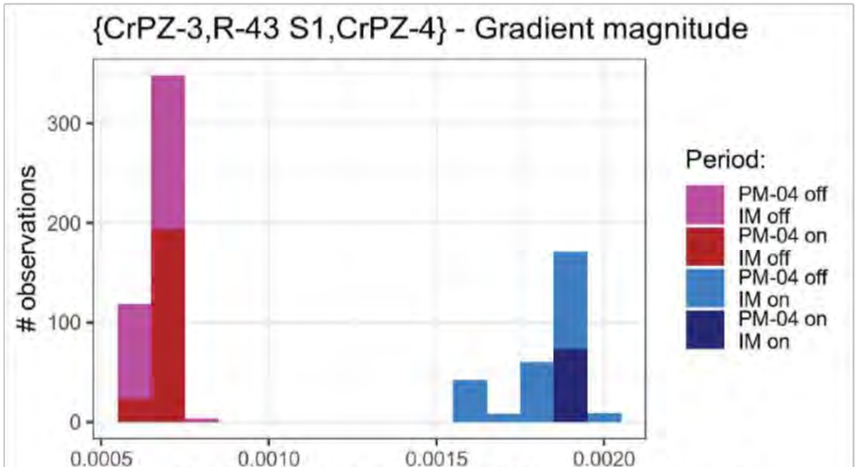

Figure 37

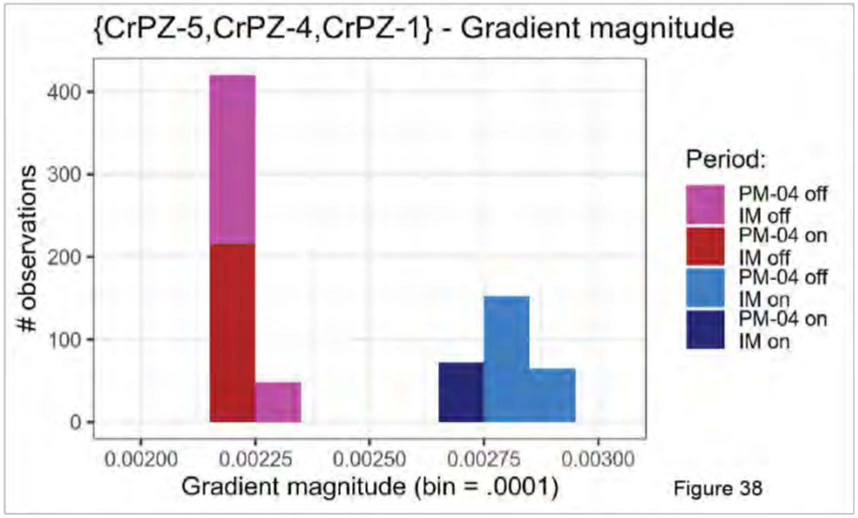

Figure 38

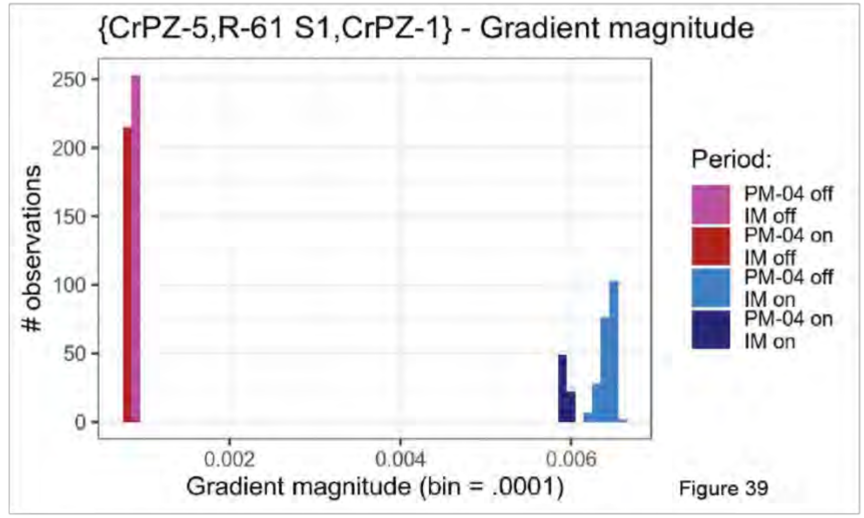

Figure 39

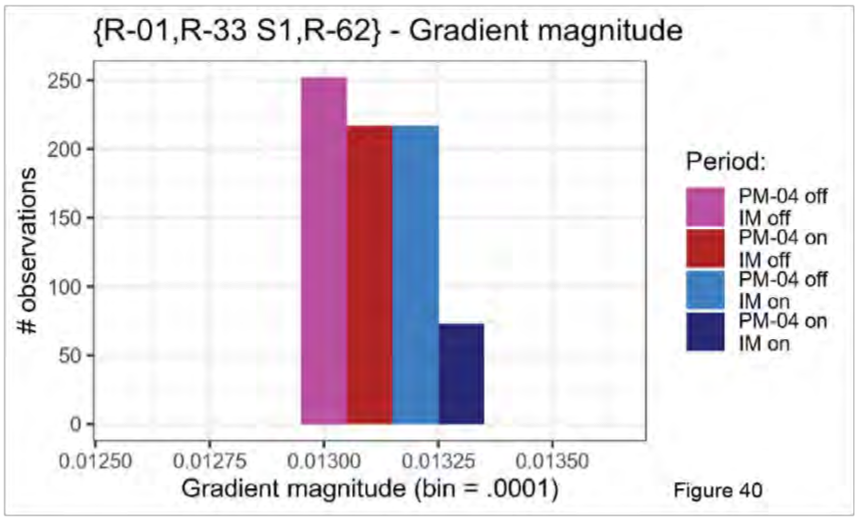

Figure 40

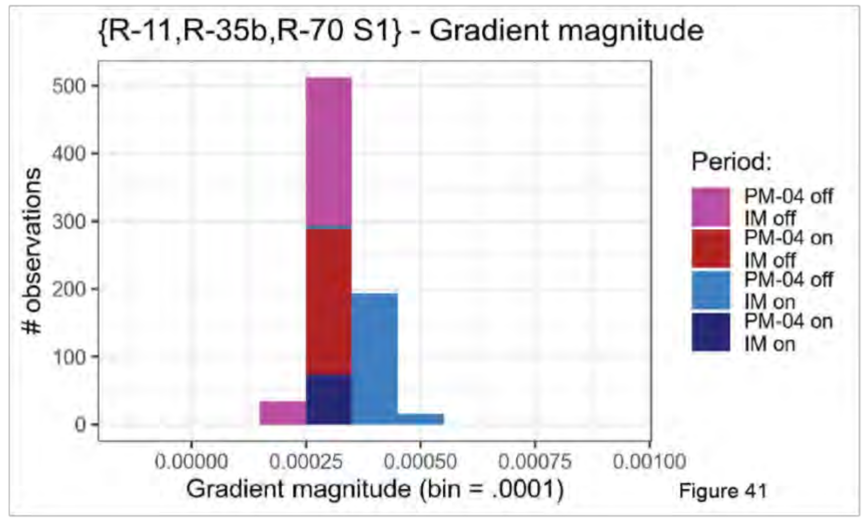

Figure 41

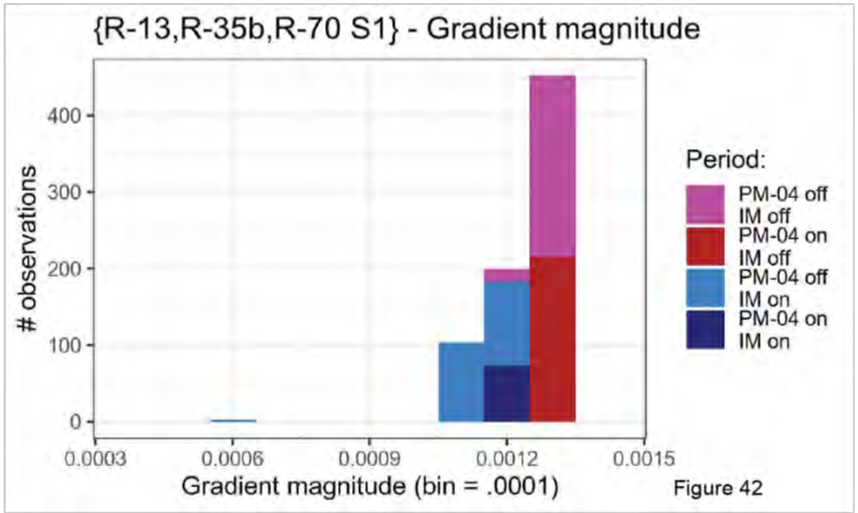

Figure 42

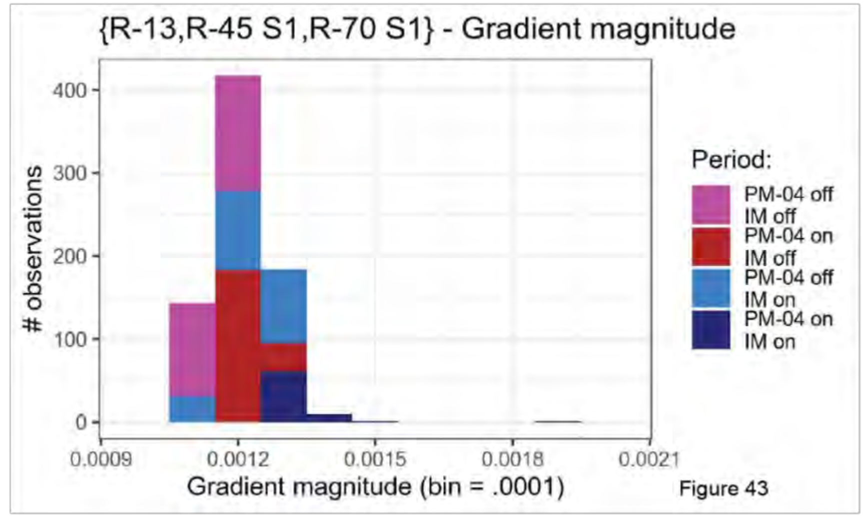

Figure 43

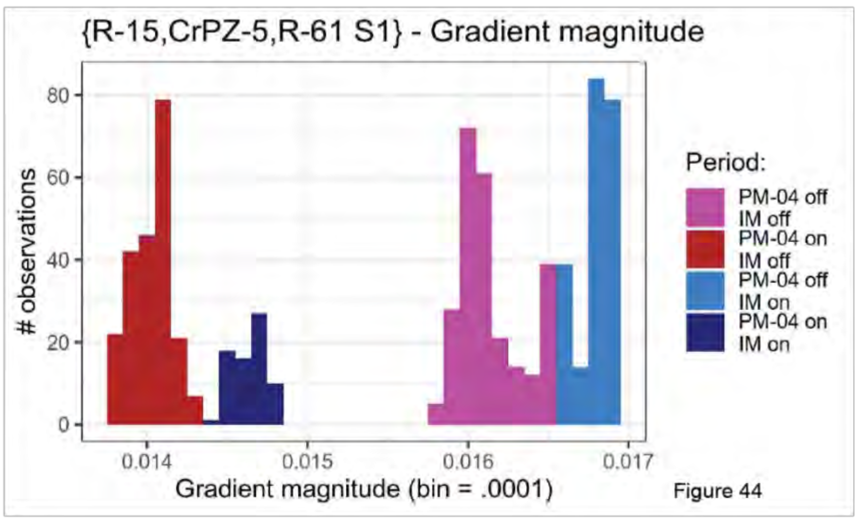

Figure 44

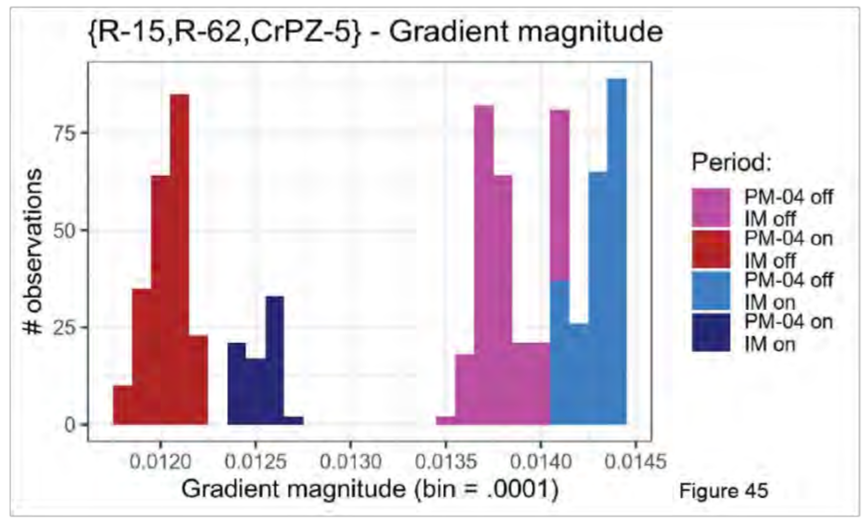

Figure 45

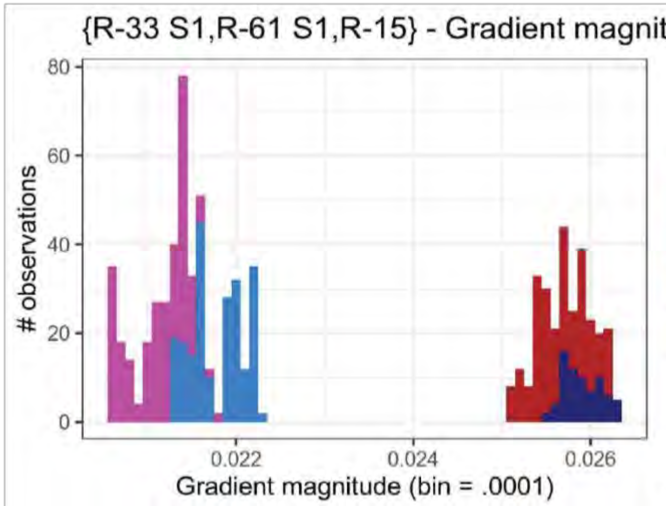

Figure 46

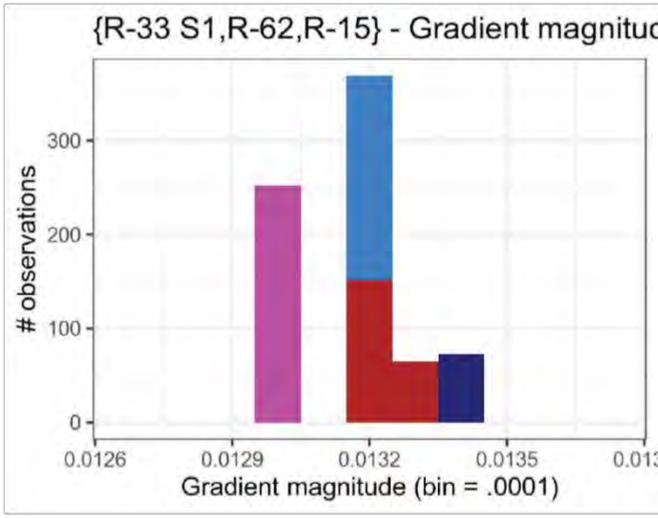

Figure 47

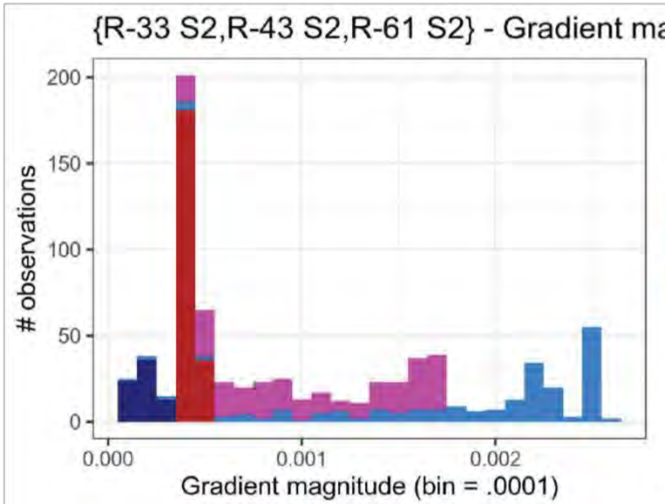

Figure 48

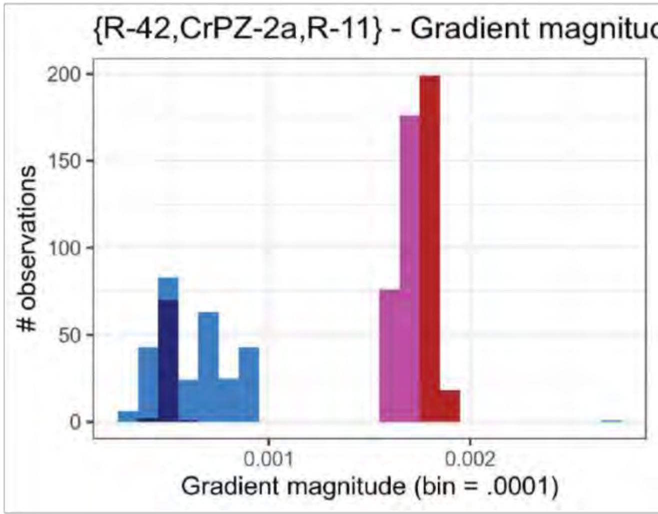

Figure 49

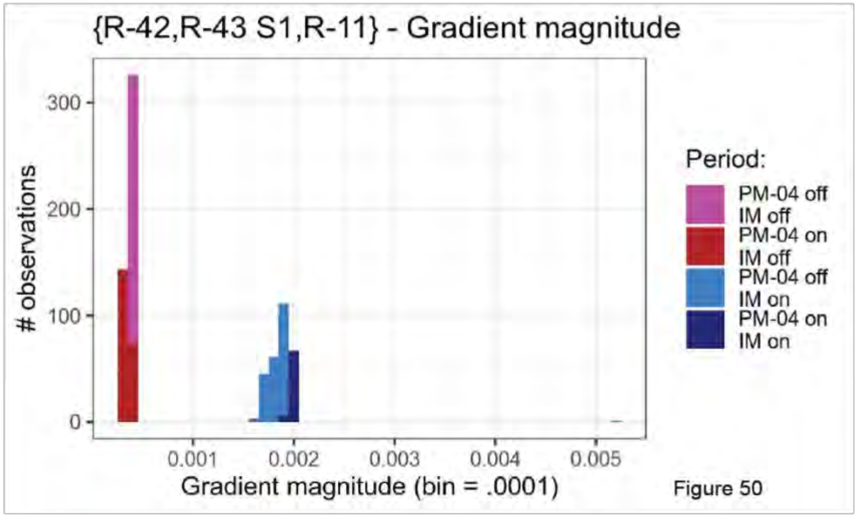

Figure 50

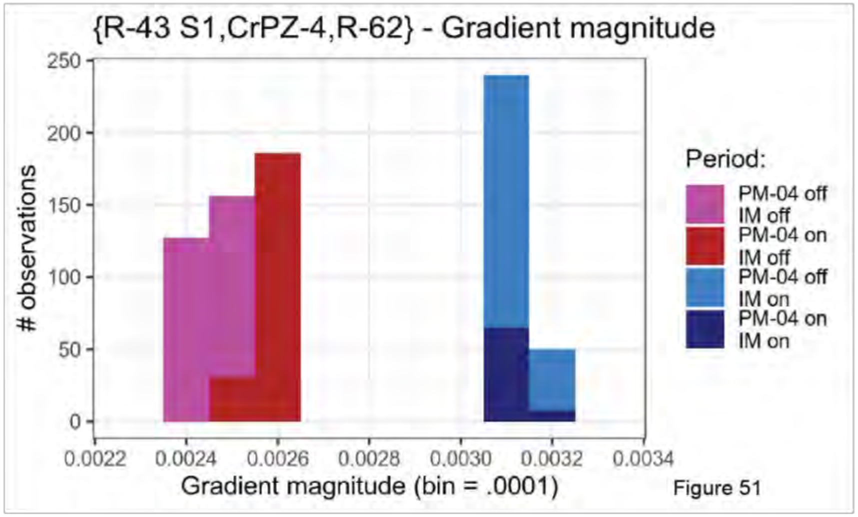

Figure 51

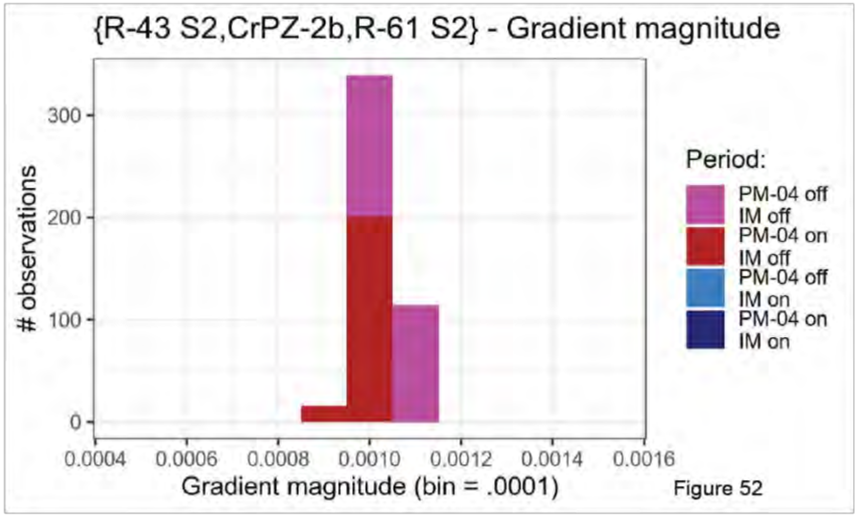

Figure 52

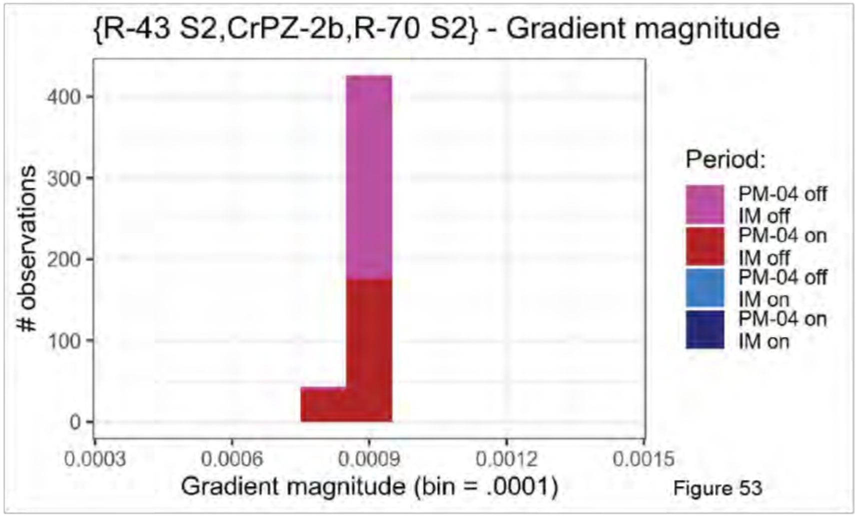

Figure 53

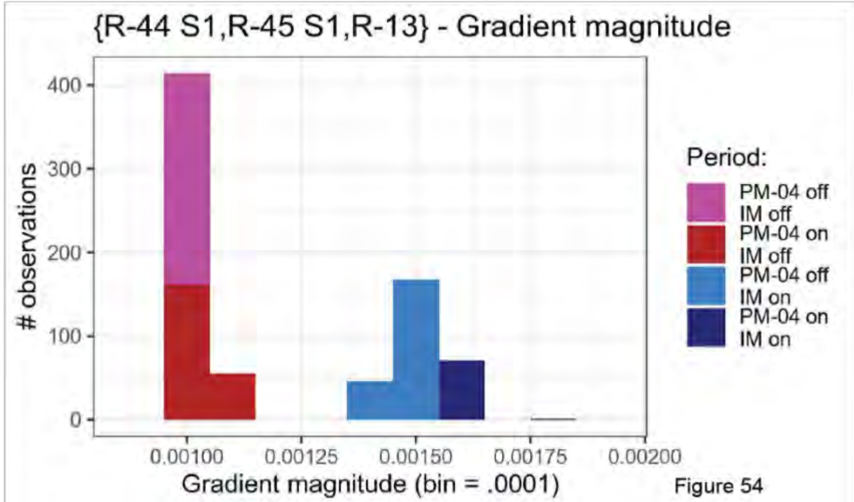

Figure 54

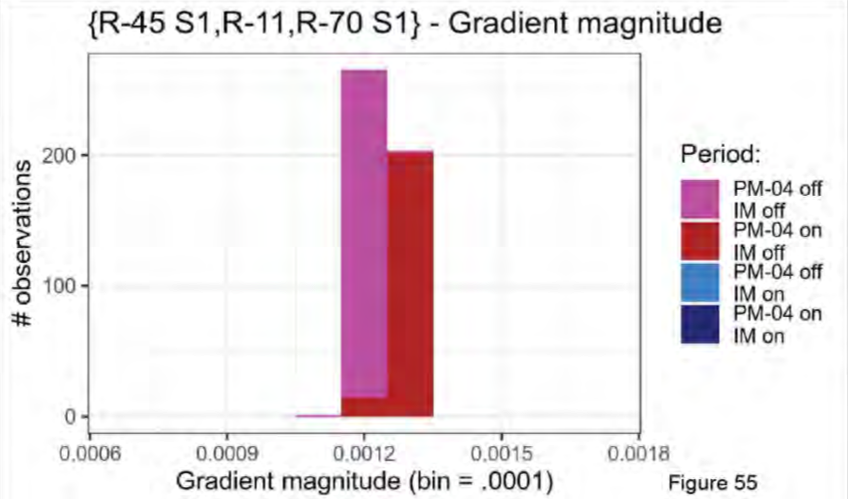

Figure 55

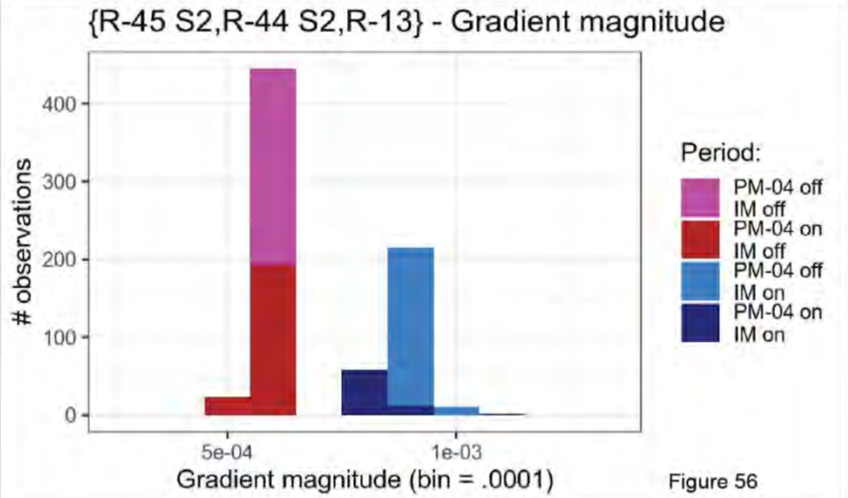

Figure 56

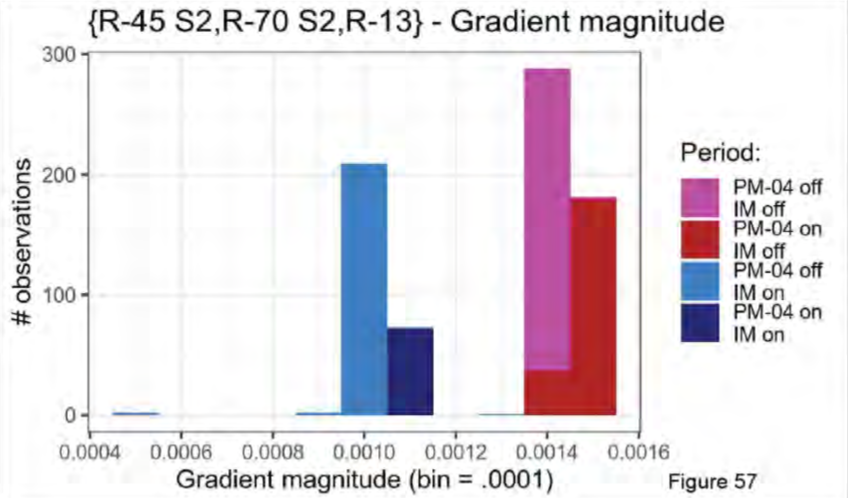

Figure 57

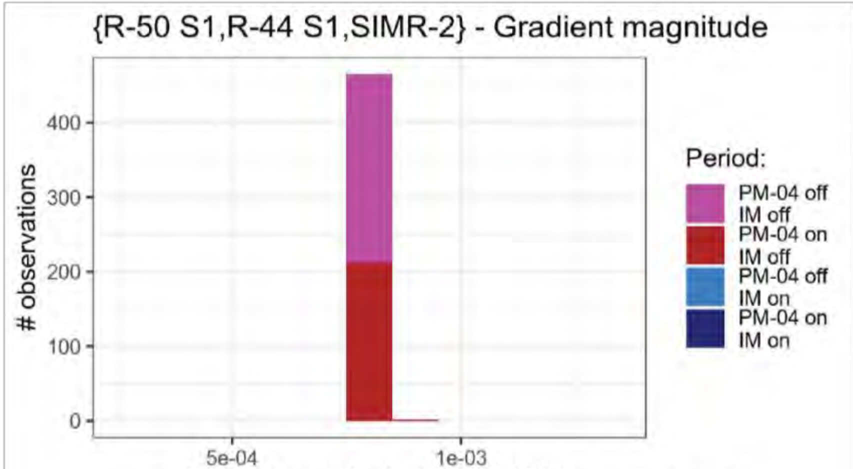

Figure 58

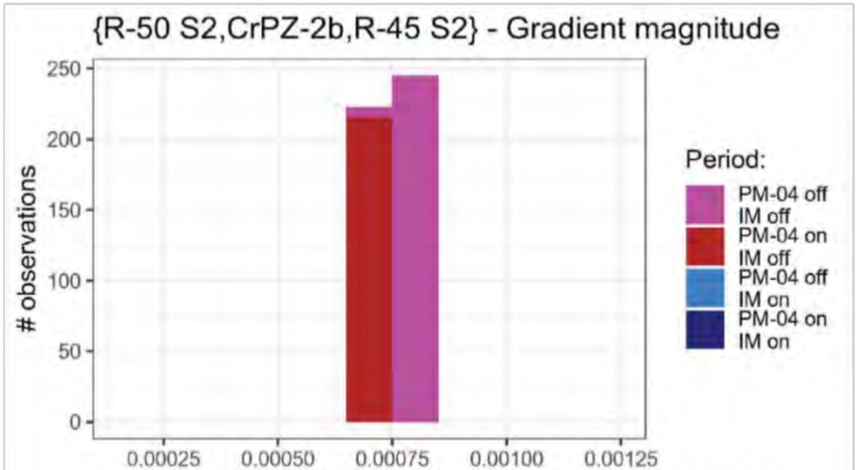

Figure 59

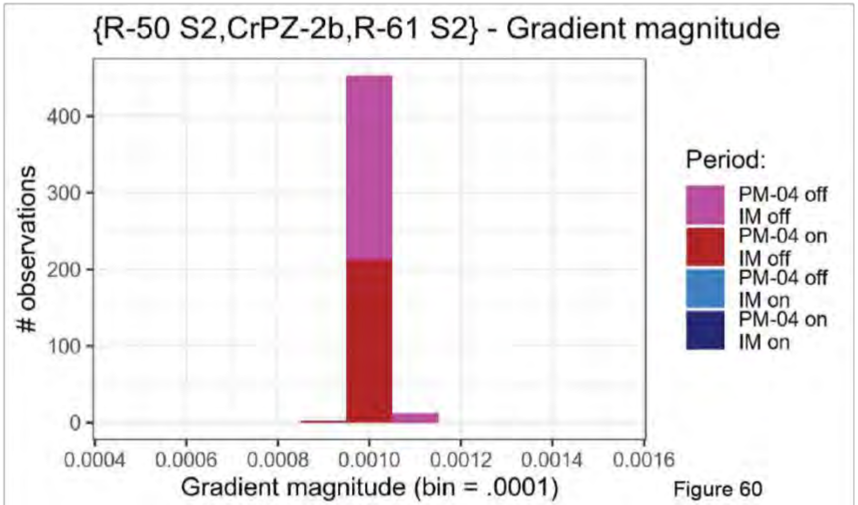

Figure 60

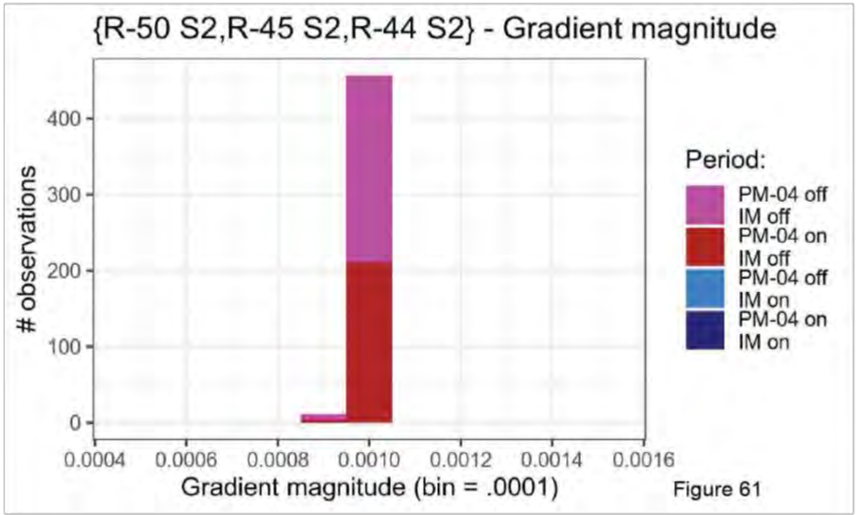

Figure 61

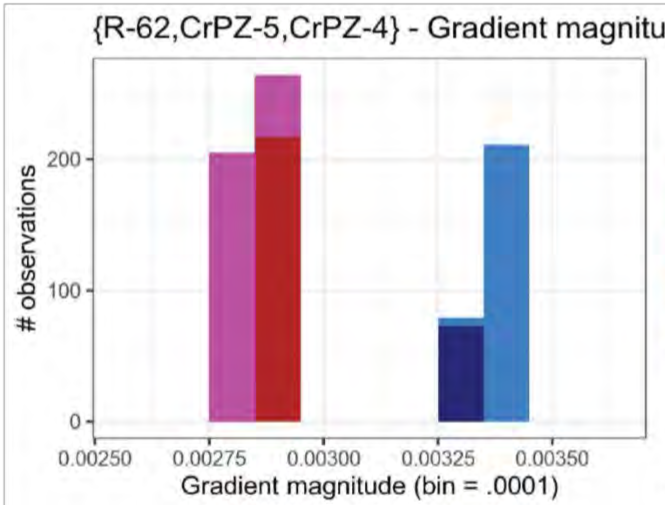

Figure 62

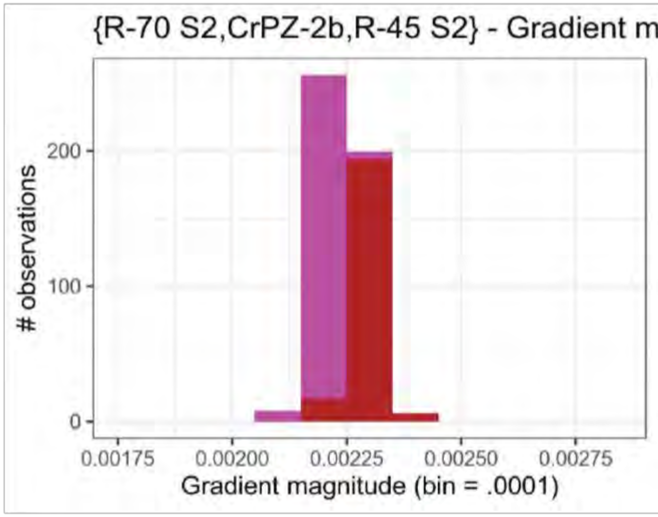

Figure 63

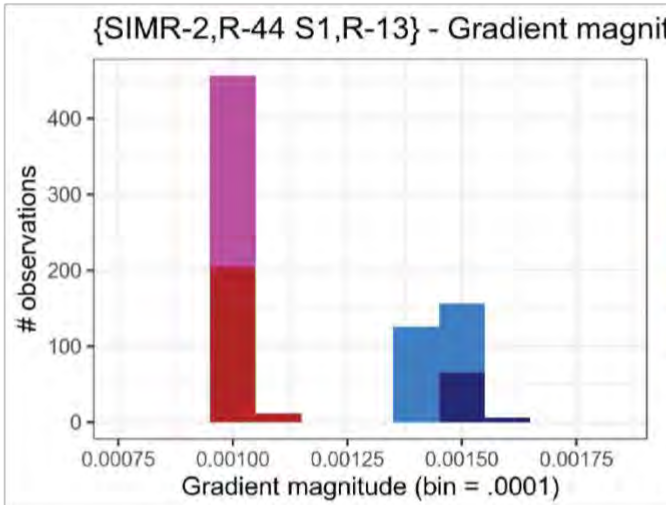

Figure 64

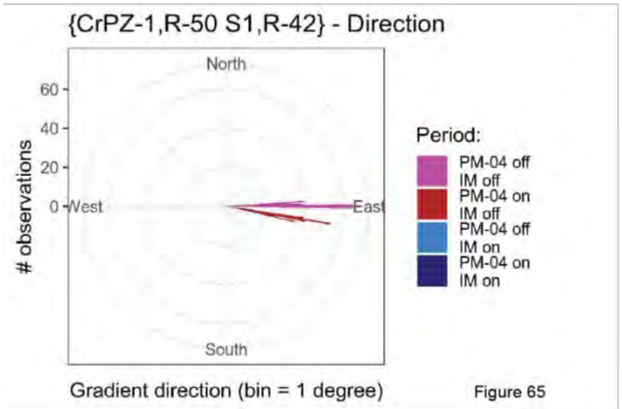

Figure 65

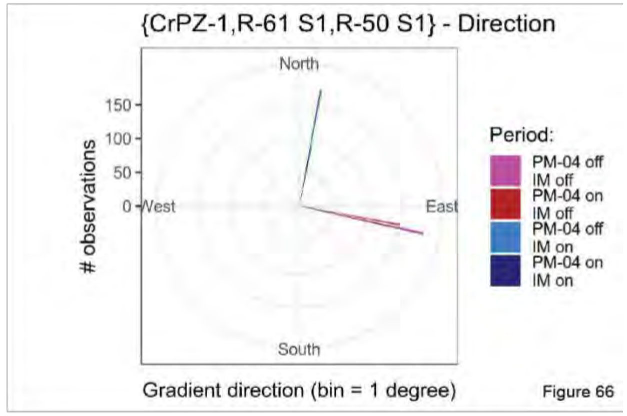

Figure 66

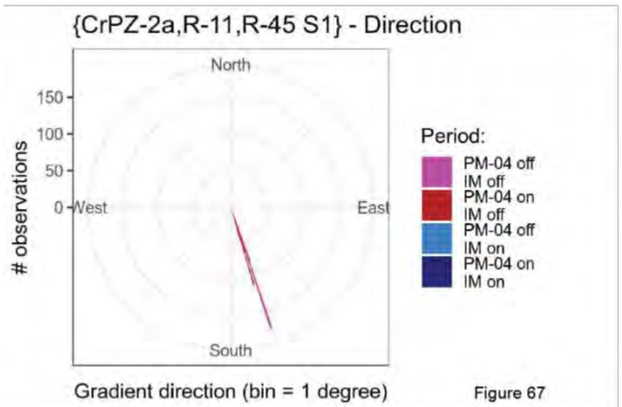

Figure 67

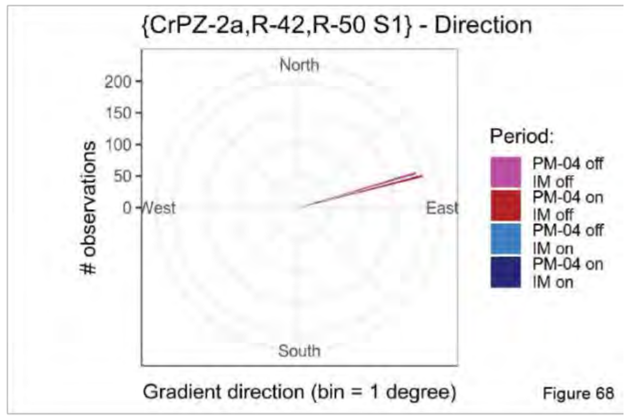

Figure 68

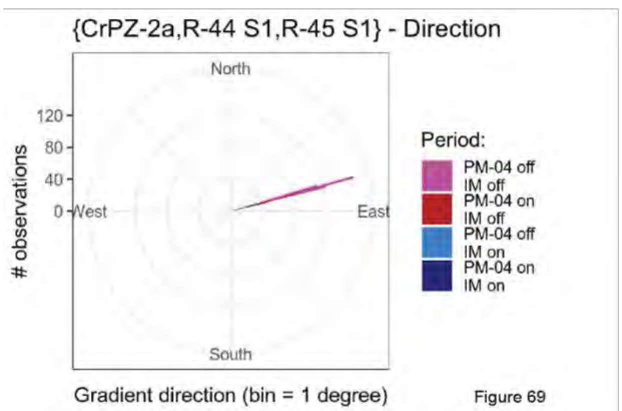

Figure 69

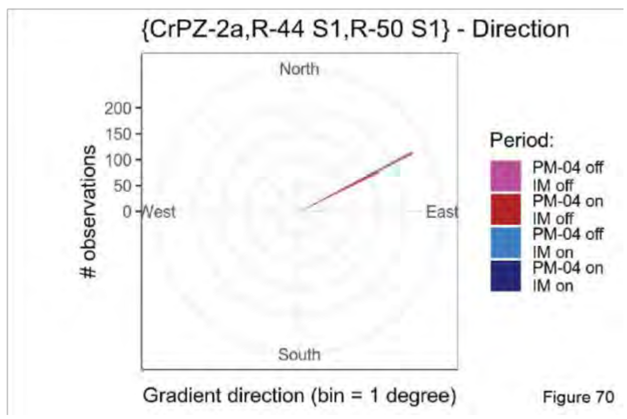

Figure 70

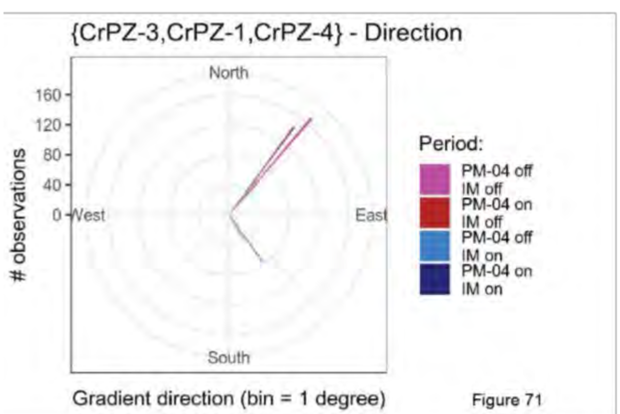

Figure 71

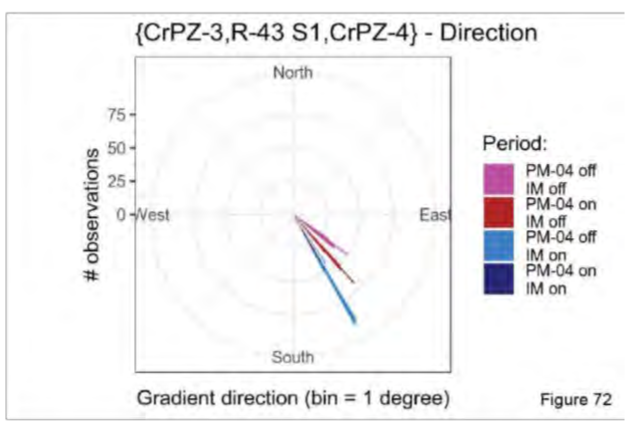

Figure 72

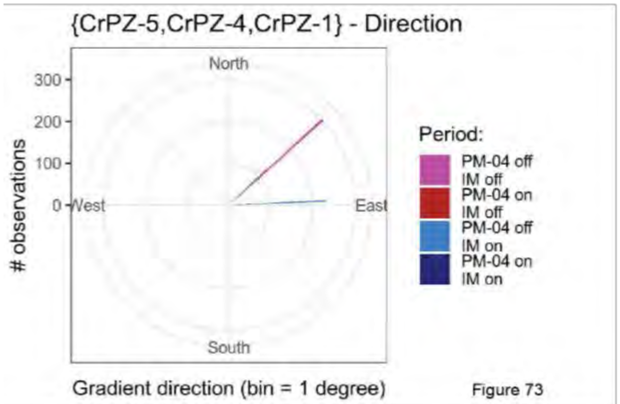

Figure 73

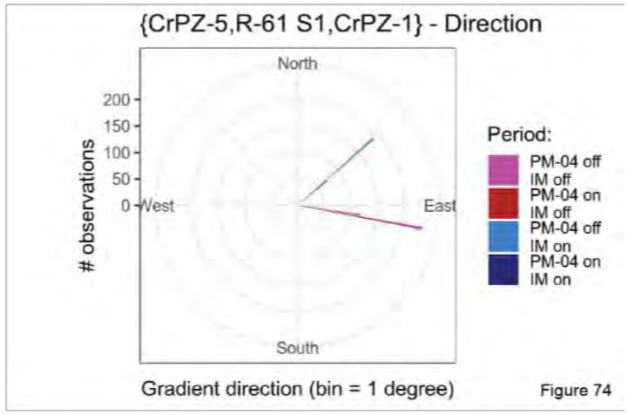

Figure 74

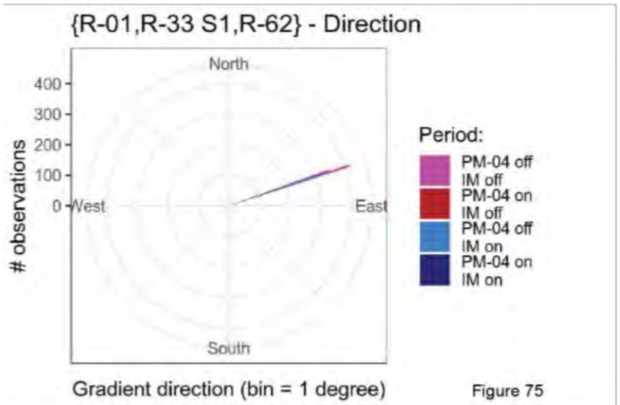

Figure 75

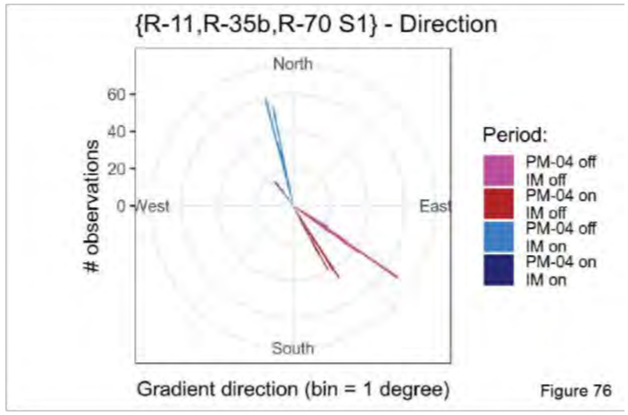

Figure 76

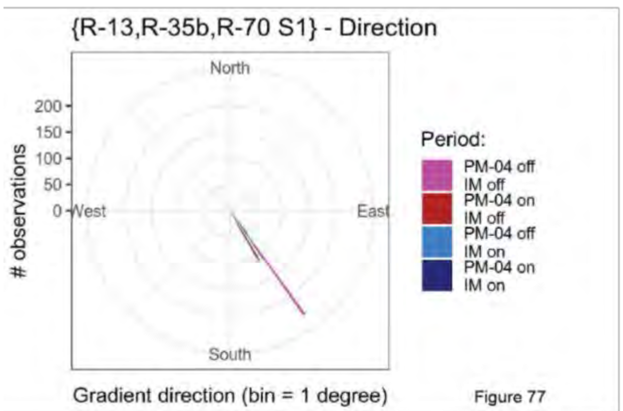

Figure 77

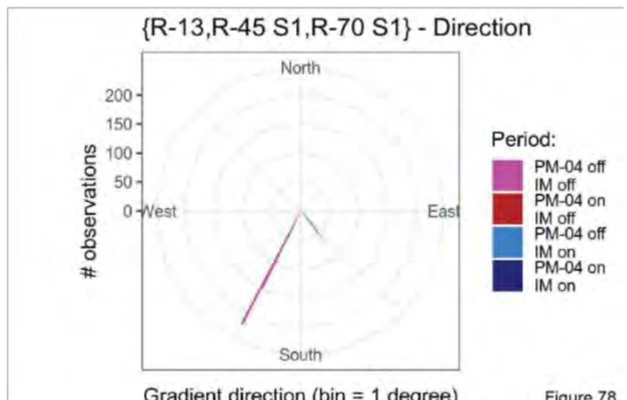

Figure 78

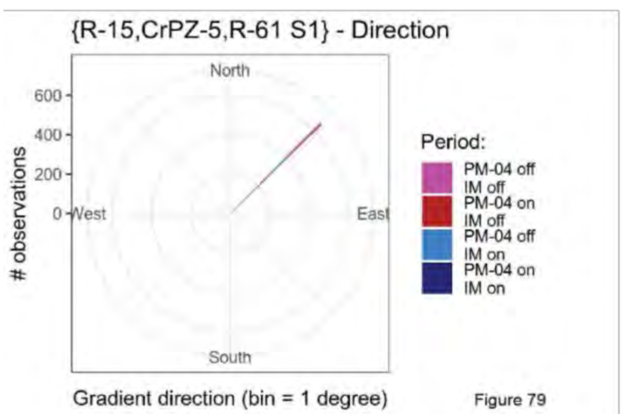

Figure 79

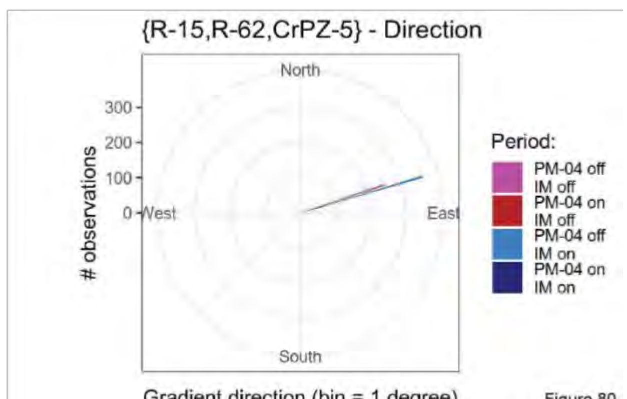

Figure 80

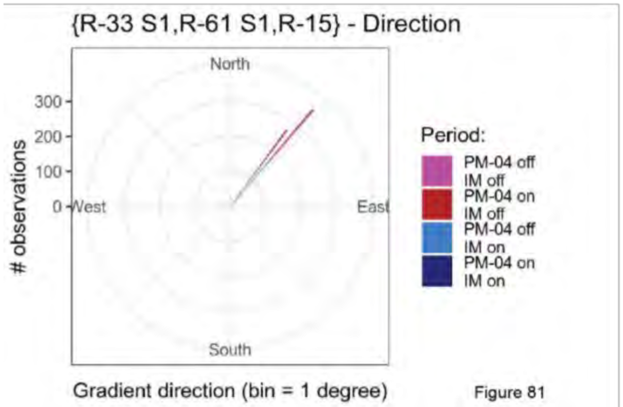

Figure 81

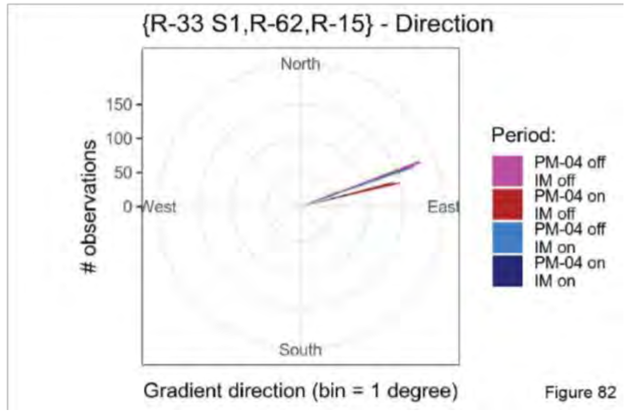

Figure 82

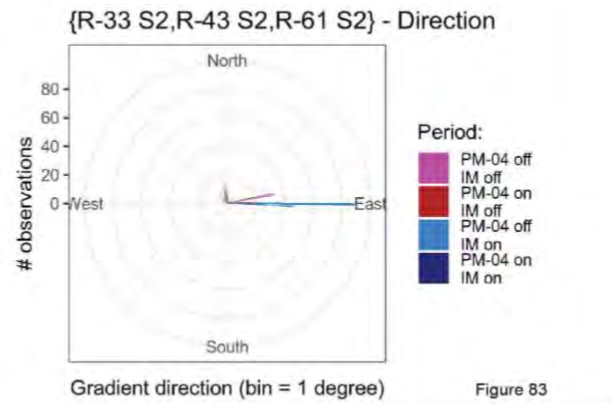

Figure 83

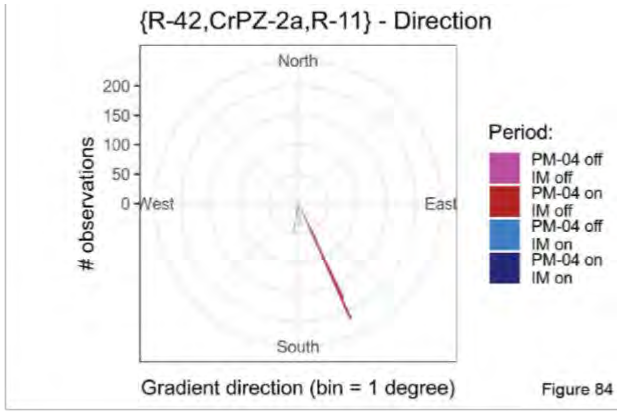

Figure 84

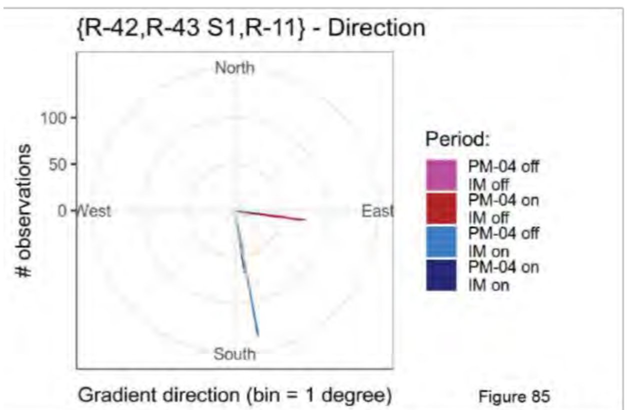

Figure 85

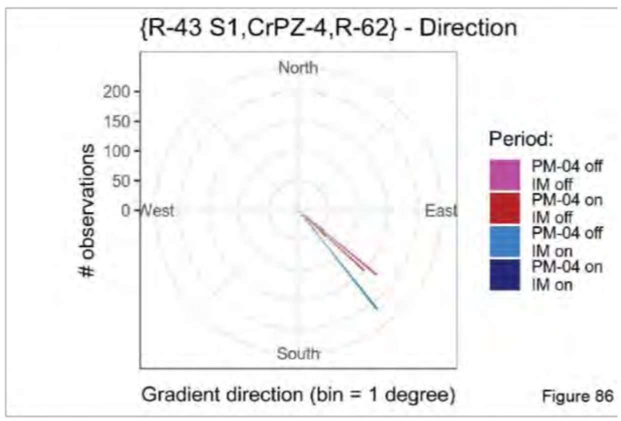

Figure 86

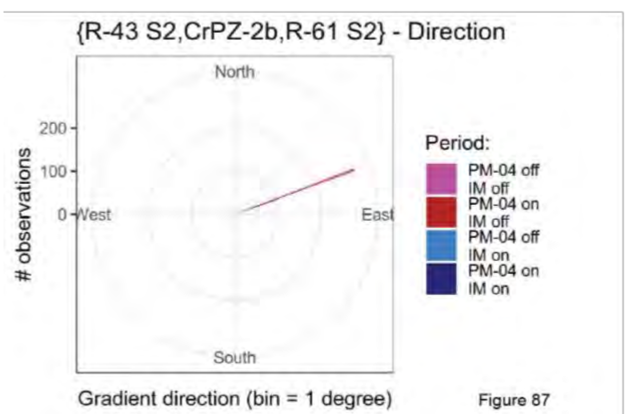

Figure 87

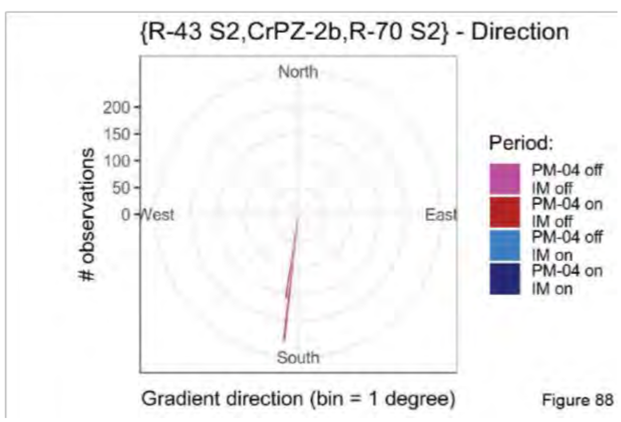

Figure 88

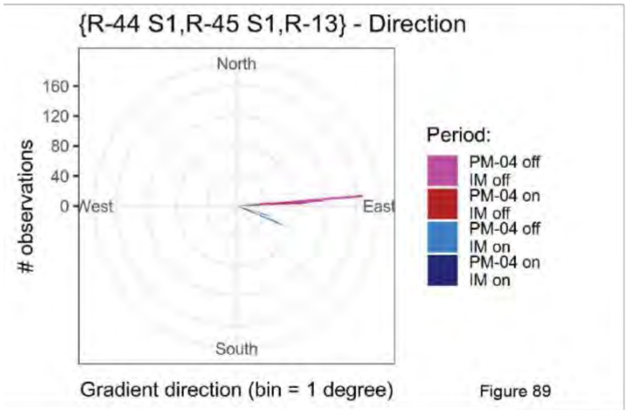

Figure 89

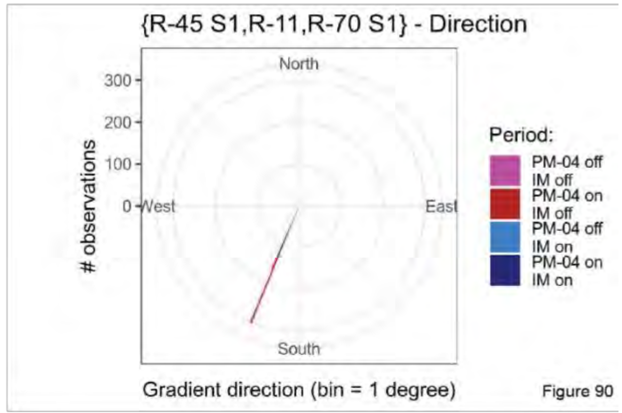

Figure 90

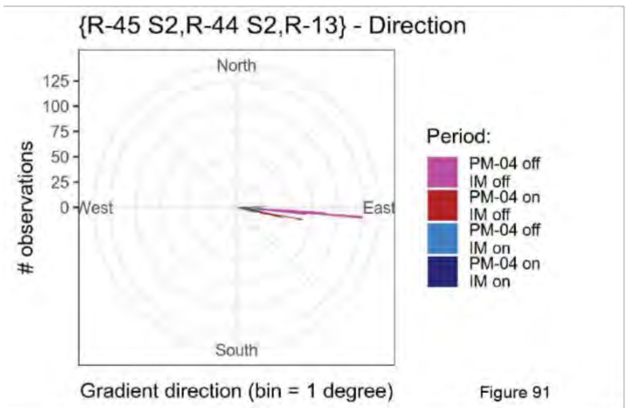

Figure 91

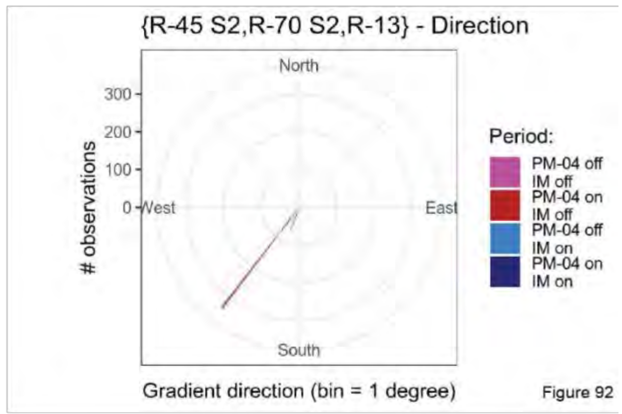

Figure 92

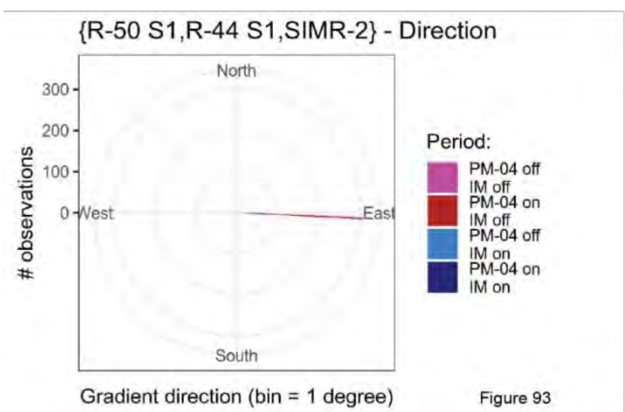

Figure 93

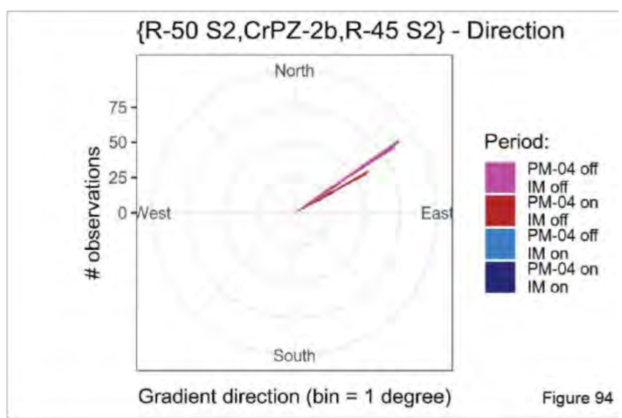

Figure 94

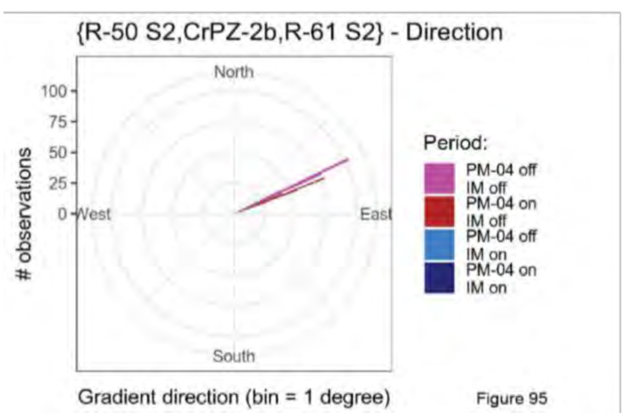

Figure 95

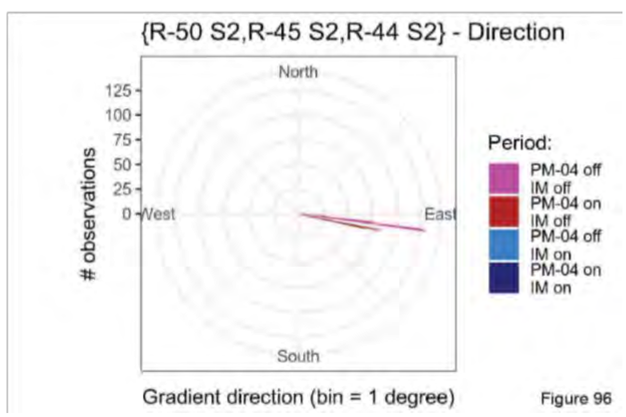

Figure 96

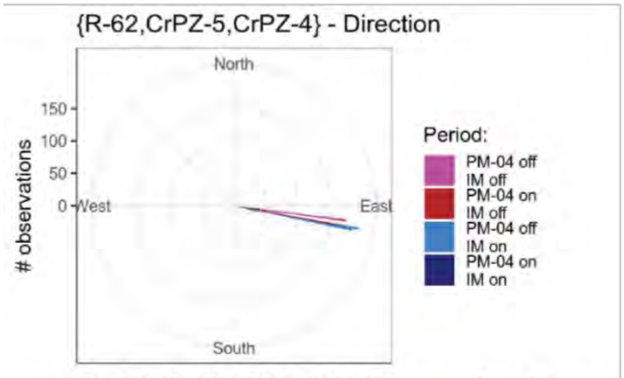

Figure 97

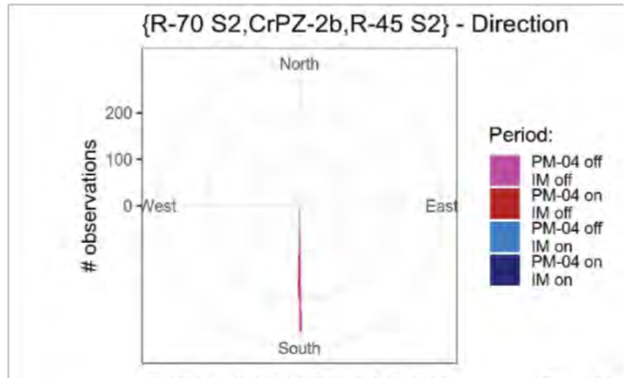

Figure 98

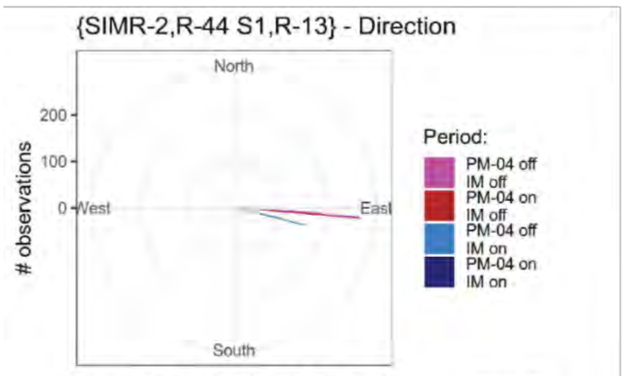

Figure 99

Enclosure 3

Chromium Model: Calibrated with Uncertainty through 2022

Neptune and Company, Inc.
1505 15th St.
Suite B
Los Alamos, New Mexico 87544
720-746-1803
www.neptuneinc.org

16 June 2023

To: Cheryl L. Rodriguez
DOE EM-LA

Please find attached to this letter a copy of the *Chromium Interim Measure Capture Zone Analysis* report for enclosure to the *Annual Progress Report on Chromium Plume Control Interim Measure Performance, April 2022 through March 2023*.

Sincerely,
Lauren Foster

Neptune and Company

Chromium Model: Calibrated with Uncertainty through 2022

16 June 2023

NEPTUNE AND COMPANY, INC.
1505 15th St. Suite B, Los Alamos, NM 87544

EXECUTIVE SUMMARY

This report documents the model structure, parameterization, and calibration of a numerical fate and transport model for a hexavalent chromium (Cr^{6+}, referred to as chromium in this document) plume in the regional aquifer below Los Alamos National Laboratory (LANL). The Chromium Model (abbreviated as CM in this document) is designed as a tool to support optimization of the existing Interim Measures (IM) network of extraction and injection wells, improve understanding of the plume, and provide quantitative metrics for uncertainty to aid in identifying new well locations.

The CM is calibrated to available chromium concentration and head data from wells in the regional aquifer and is validated using drawdown responses throughout the aquifer between different pumping and response wells. Since the purpose of the model is to support IM operations, calibration targets that represent responses to the chromium extraction (CrEX) and chromium injection (CrIN) wells are prioritized. The model is calibrated using data from well completions through October 2022.

The calibration reproduces concentration trends at 40 well screens over 20 years of data along with other datasets (drawdown responses to pumping, water levels, and hydraulic gradients). These data include an inverted concentration gradient at CrEX-4 and R-70 where higher concentrations are present deeper in the aquifer, strong responses to the IM network implementation (R-50, R-45, and R-44, CrPZ-1), and accurate transport estimates throughout the site at different orders of magnitude. Head conditions, flow gradients, and drawdown responses are closely matched and the flow field is further validated using nearly 500 pump/response well pairs throughout the plume region. Selected results are shown in Figure 1 for a small subset with wells of interest; full calibration results can be found in Figure 18 through Figure 24. Uncertainty is estimated between and outside of target datapoints using Bayesian methods and Markov Chain Monte Carlo (MCMC) simulations. This uncertainty can be used to optimize future well placements, interrogate the conceptual site model (CSM), and inform focus points for future study.

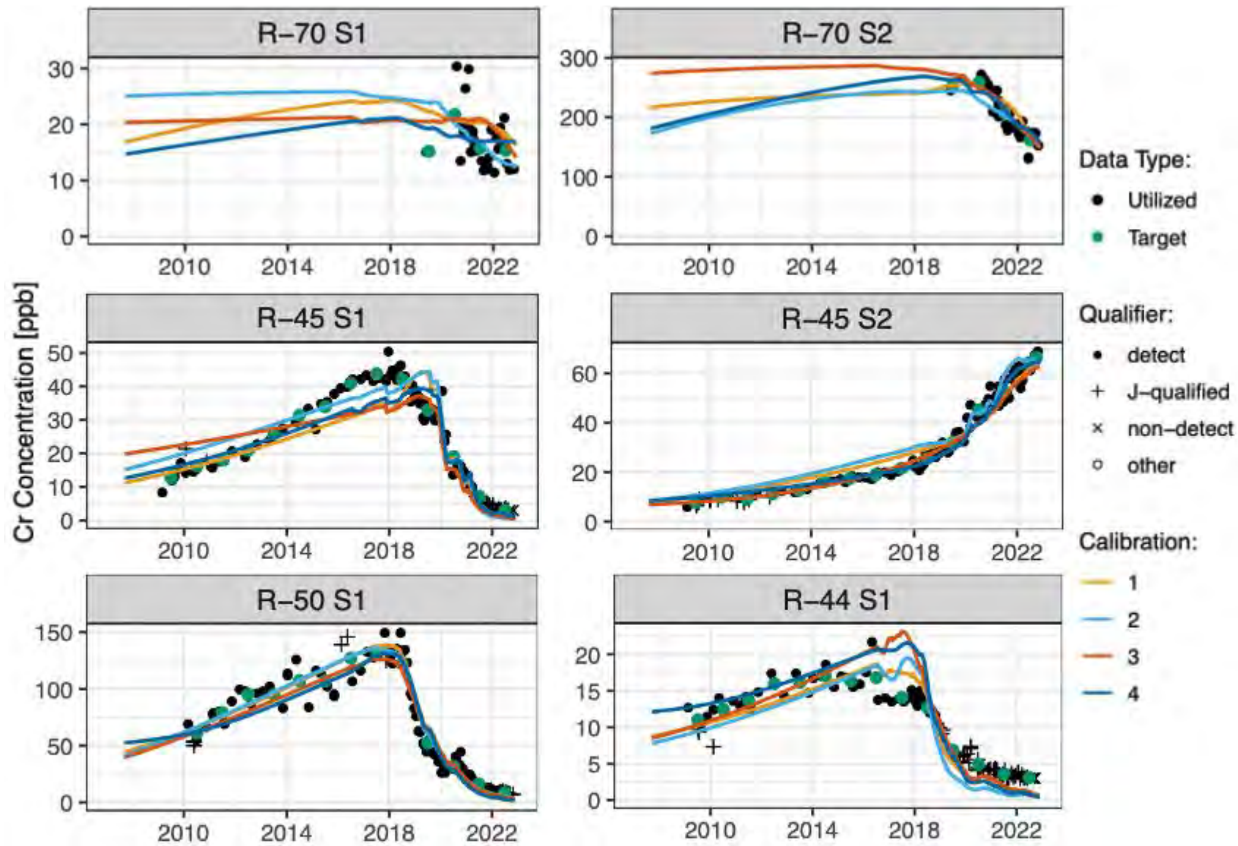

Figure 1. Selected calibration results. Full results for all wells presented in Section 3.1.

CONTENTS

FIGURES

TABLES

ACRONYMS AND ABBREVIATIONS

amsl	above mean sea level
CM	Chromium Model
CrEX	chromium extraction well
CrIN	chromium injection well
CSM	conceptual site model
EPA	(United States) Environmental Protection Agency
FEHM	Finite Element Heat and Mass (flow and transfer code)
IM	Interim Measures
LANL	Los Alamos National Laboratory
LM	Levenberg-Marquardt (algorithm)
MADS	Model Analysis and Decision Support (software)
MCMC	Markov Chain Monte Carlo
OF	objective function
ppb	parts per billion
SCADA	Supervisory Control and Data Acquisition
TA	Technical Area
VZ	vadose zone

1.0 Introduction

This report presents the Chromium Model (CM), a calibrated numerical groundwater model of the hexavalent chromium ([Cr(VI)], referred to as chromium in this document) plume at Los Alamos National Laboratory (LANL, or the Laboratory). The CM was built to improve understanding of chromium plume migration, to evaluate capture and flood zones of the existing interim measure (IM) wells, and to optimize IM operations. This report discusses the model structure, input parameters and data, target data, and calibration approach; it also presents results of a Bayesian uncertainty analysis.

1.1 Background

A plume of chromium in excess of the 50 ppb New Mexico groundwater standard was detected in the regional aquifer below LANL property in multiple monitoring wells since elevated chromium concentrations were initially identified in 2005. Comprehensive investigations of the plume have been ongoing since 2005 (Heikoop et al. 2014; LANL 2008, 2015, 2018a, 2018b, 2018d; N3B 2021b; Vesselinov et al. 2013). Historically, the highest measured concentration is approximately 1200 ppb. Figure 2 shows a plan view map of the chromium project area, including monitoring wells and IM injection and extraction wells. The main source of chromium is effluent from a LANL power plant, which was released into Sandia Canyon between 1956 and 1972.

1.2 Conceptual Site Model

1.2.1 Geologic Context

The regional aquifer at the chromium plume site intersects several geologic strata that define the hydrogeologic conceptual framework used in the CM (Figure 3). The Puye formation (Tpf), Puye pumiceous subunit (Tpf(p)), Miocene pumiceous unit (Tjfp), and Miocene riverine deposits of the upper Santa Fe Group (Tcar) are the primary geologic units of interest. The Tpf is an approximately 200–300-ft-thick alluvial fan deposit comprised of poorly-sorted muddy, sandy gravel and coarse sand, interbedded with thin ash and pumice deposits; the Tpf(p) subunit contains relatively higher fractions of pumiceous material than the Tpf. The Tcar consists of Miocene axial river deposits (mud, silt, sand, gravel, and cobbles) from the ancestral Rio Grande. Further lithologic characteristics of these units are described in (Broxton and Vaniman 2005; LANL 2016, 2018b; N3B 2021b). To date, no strong evidence suggests that chromium migration is substantially impacted by geologic unit boundaries between the Tpf, Tpf(p), and Tjfp (N3B 2021, 701506), and chromium easily migrates across these strata boundaries.

Less is known about the effect of the Tcar boundary. Few wells are screened in the Tcar in the chromium plume area, but R-43 screen 1, which straddles the Tjfp and Tcar at ~900 ft bgs, has exhibited elevated concentrations of chromium, increasing from background levels before 2010 to above 200 ppb around 2019. R-43 screen 2, screened entirely within the Tcar, has seen concentrations rise from below background to above 40 ppb in that same period. Two cross-sections of the geology, both including R-43 and running west to east and north to south, are provided in Figure 3.

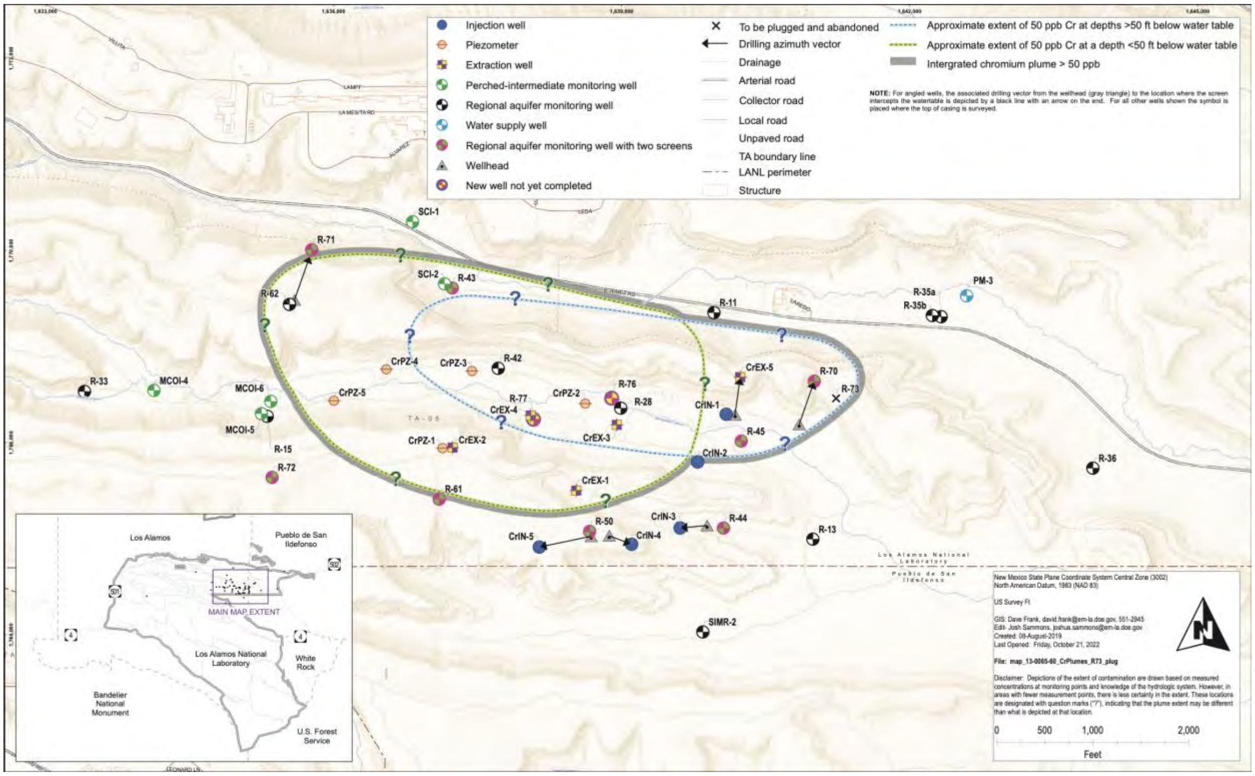

Figure 2. Chromium plume site location and area discussed in this report.

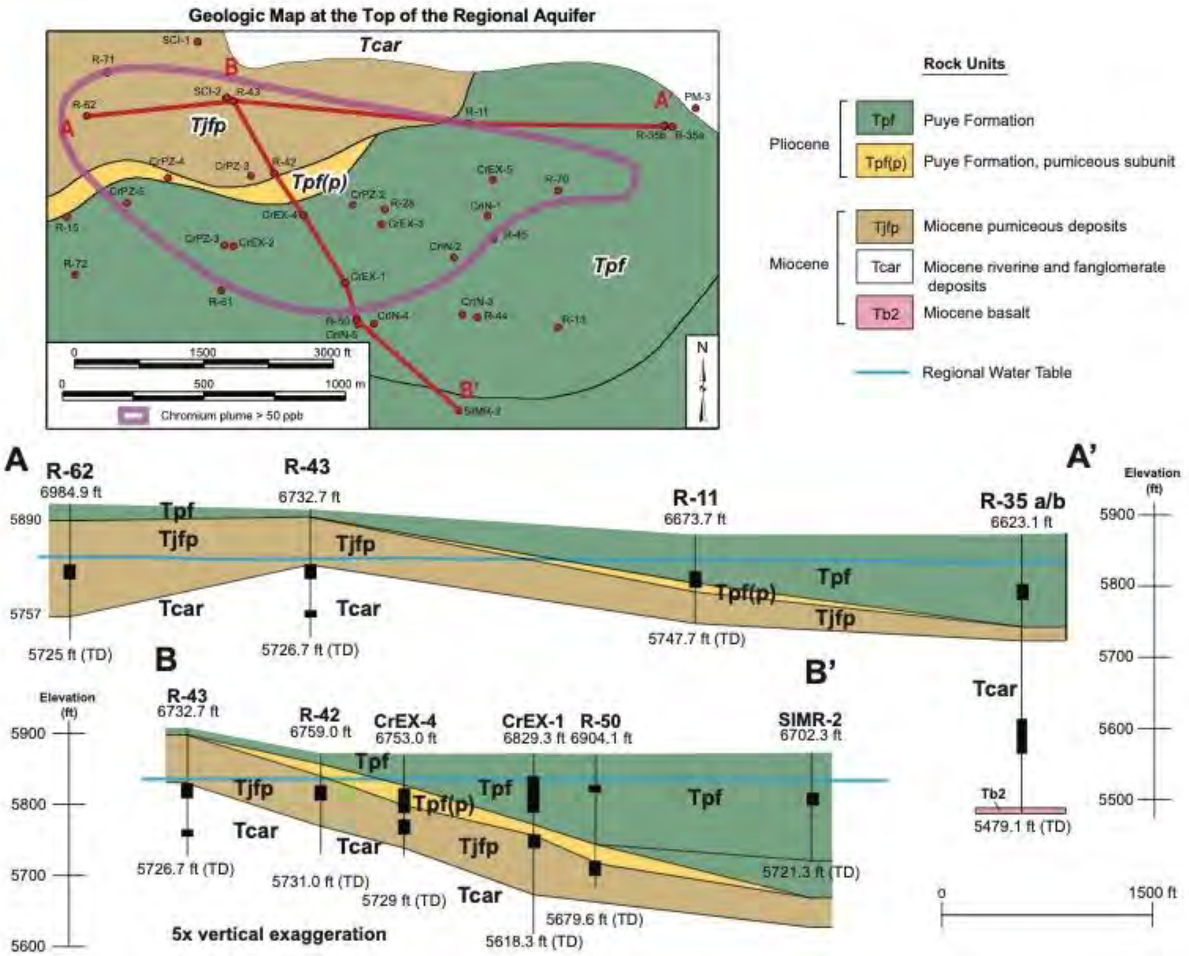

Figure 3. Geologic map at the top of the regional aquifer and geologic cross-sections for portions of the regional aquifer in the chromium plume at LANL.

1.2.2 Hydrologic Context

A complex migration pathway through the vadose zone (VZ) resulted in the current plume location in the regional aquifer to the east (downgradient) and south (beneath Mortandad Canyon) of the primary release location in Sandia Canyon. At the top of the regional aquifer, several “hydraulic windows” or drip points from the VZ are estimated to be located in the central plume area (LANL 2018b); these windows carry chromium and other comingled contaminants. Chromium is thought to migrate from the chromium-contaminated hydraulic windows at the water table, which are of uncertain location but are thought to include the central plume area around R-42 and other upgradient locations. Dual-screened monitoring well data prior to the completion of R-70 suggested the plume existed only in the upper 50–70 ft of the aquifer. However, the discovery of higher concentrations of chromium in R-70 screen 2 compared to screen 1 has resulted in the conceptualization of separate deep and shallow plume extents shown in Figure 2.

Most observations of the chromium plume, including observations in dual-screened downgradient wells, support the hypothesis that the plume moved primarily laterally under ambient conditions with the highest concentrations near the surface. More recent data in the northern portion of the plume at dual-screened wells CrEX-4 and R-70 show inverted gradients, with higher concentrations at the deeper screens (N3B 2019), as well as compelling geochemical evidence that recharge water at R-70 screen 1 may have a different, more northerly source term than at R-70 screen 2. This discovery has resulted in the conceptualization of the deep and shallow plume extents shown in Figure 2, and two deep wells (R-76 and R-77) are proposed to confirm the depth of the plume in this area. Well R-70 also has a negligible to slightly upward vertical hydraulic gradient under ambient conditions. The discovery of high chromium concentrations at R-70 screen 2 resulted in a re-evaluation of the conceptual site model (CSM) in this area to explain the inverted chromium gradient behavior (N3B 2021b). A non-chromium contaminated source of recharge has been hypothesized to exist along the north/northeast side of the plume that links the geochemically similar water at R-11 to R-70 screen 2 and R-45 screen 2 (N3B 2021, 701506). This recharge source is represented in the numerical model.

The IM well network was planned and developed with the objectives of:

(1) maintaining the 50-ppb downgradient plume edge within the laboratory boundary, and
(2) hydraulically controlling plume migration in the eastern downgradient portion of the plume (LANL 2018a).

The network currently includes five injection and five extraction wells (Figure 2). An ion-exchange system treats the extracted water and supplies the injection wells. After R-70 was drilled and deep contamination was found at R-70 screen 2, an injection well previously named CrIN-6 was converted to perform extraction and was renamed CrEX-5. This decision was informed by modeling analyses that indicated better conformance with IM objectives in that configuration (LANL 2018d).

Results from pumping tests, including at the deep-screened municipal water-supply wells, support a hydrogeologic CSM that describes the top of the water table as predominantly phreatic (unconfined), with increasingly confined/leaky-confined behavior as depth increases (Collins et al. 2005; Neptune 2023a). Some of the deeper confined behavior may be attributed to specific, spatially correlated units such as deeper Miocene basalts (Tb2) (McLin 2006; N3B 2021b), while closer to the surface, locally confined conditions may be caused by the observed strong anisotropy and non-continuous layering (LANL 2012; N3B 2021b). The overall hydraulic gradient at the site is generally from west to east or slightly southeast. The chromium plume area water table is 10–100 times flatter than regions immediately upgradient and downgradient.

Pumping at municipal water-supply wells (PM wells) occurs around the site. PM-3 is slightly north and immediately east of the site (Figure 2). Wells PM-2 and PM-5 are to the west of the site, and PM-4 is to the southwest of the site; they all fall outside the region shown in Figure 2. The municipal wells have long screens that are much deeper than those in the monitoring wells and chromium-plume wells; Figure 4 shows well screens in cross-section from PM-4 to PM-3, including monitoring well screens for R-50, R-45, and R-70. Chromium-area monitoring wells respond to pumping at PM-2, PM-4, and PM-5 to varying degrees (LANL 2018d), though the magnitude of these responses is much lower than responses to IM pumping (Neptune 2023a). More strikingly, the signal from PM-3 pumping is not observed in chromium plume-area shallow monitoring wells despite PM-3's closer distance (LANL 2018d; N3B 2021b). At sentinel well

R-35, no response is observed in the shallower screen (R-35b). The deeper screen (R-35a), which is much deeper than other dual-screened wells near the chromium plume, shows the only response to pumping (Figure 2, Figure 4). The impact of IM operation on hydraulic heads in monitoring wells is substantially greater than the impact of municipal water-supply pumping, including PM-4 (Neptune 2023a).

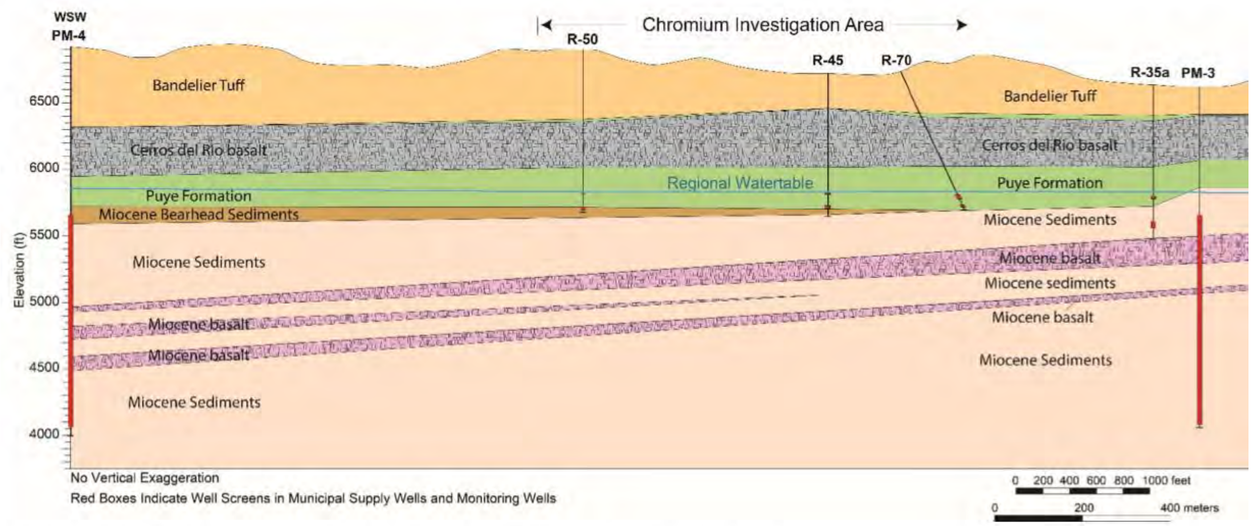

Figure 4.1-8 West-southwest/east-northeast regional geologic cross-section

Figure 4. Regional geologic cross-section, reproduced and cropped from (N3B 2021b)

1.2.3 Hydraulic Gradients Study Summary

A separate study, using hydraulic head data to explore pumping responses in the chromium plume region, has been conducted to explore the impacts of IM extraction and injection operations on hydraulic gradients in the chromium plume. The results of this analysis are used as one of many lines of evidence to determine the capture and flood zones from the IM system (Neptune 2023b) as well as to inform model assumptions about water-supply (PM) wells described in this document. While some PM wells have been shown to impact water levels in some monitoring wells within the chromium plume (McLin 2005, 2006), the prevailing hypothesis is that local extraction and injection from the IM overwhelms any potential impacts from the deeper, longer screened, and more distant supply wells. This analysis interrogates this assumption by assessing the impact on flow gradients in the chromium plume area from IM operations and PM operations.

The study is summarized here and described in detail in “Hydraulic Gradients Across the Pajarito Plateau” (Neptune 2023a). The periods when the IM is in full operation, and when it is completely shut down, are sub-categorized into periods when supply well PM-4 is on and when it is off; hydraulic gradients calculated from head measurements (both laterally and vertically) are analyzed within each of these four refined periods. PM-4 is used to quantify the maximum impact from a water supply well for two reasons:

(1) it has been observed to have the largest impact on water levels in the chromium plume (compared to other supply wells), and
(2) its largely seasonal use allows for separation of pumping vs. non-pumping timeframes to quantify the change.

This allows for an estimate of the magnitude of change in hydraulic gradients resulting from PM-4 pumping compared to that during IM operations.

In the chromium plume area, impacts on lateral and vertical hydraulic gradients are shown to be 3–30 times stronger from IM operations than from water-supply well pumping. Given that IM operations dominate groundwater hydraulics in the vicinity of the chromium plume, supply-well pumping has not yet been incorporated into the CM.

Overall, the hydraulic analyses study concludes:

1. The operation of extraction and injection wells as part of the IM operation is observed to result in large systematic changes on hydraulic gradients within the vicinity of the chromium plume.
2. Small, but quantifiable, impacts on hydraulic gradients from county supply well pumping are observed in some monitoring wells in the chromium plume.
3. The shift in lateral and vertical hydraulic gradients in the chromium plume due to IM operations is between 3–30 times larger than the impacts from PM-4 within the vicinity of the chromium plume. Therefore, any impact the nearby supply wells may have on hydraulic gradients in the regional aquifer is small in the context of the chromium plume fate and transport on short (decadal) time scales.
4. Since the impacts of IM operations dominate hydraulic gradients local to the chromium plume, it is concluded that the model framework, without the inclusion of supply well pumping, is sufficient to optimize the IM system for the chromium plume in the regional aquifer.

2.0 Methods, Analysis, and Discussion

2.1 Approach to Modeling

Figure 5 shows a conceptualization of the modeling approach. First, a decision context must be identified to inform appropriate assumptions and other critical numerical modeling decisions. In the case of this iteration of the CM, the purposes of the model are to evaluate the chromium plume migration and to support IM operations and associated decision-making (LANL 2015). To this end, the model is used for a capture and flood zone analysis (Neptune 2023b). Additionally, the model can be used to identify modifications to the IM operations or network and to optimize the performance of the system. These efforts contribute to plume understanding and support data-gap analyses to optimize future well locations. The calibrated model can also be used to explore mechanistic drivers of observations at the site through numerical experiments.

The next step is to integrate all the lines of evidence, or sources of information, that are available into the model structure, input parameterization, and calibration. Site-specific data are used when available to inform input parameterization or decisions about model structure. The conceptual site model (CSM) helps inform model assumptions, boundary conditions, and parameterization.

The numerical CM is built using the Finite Element Heat and Mass transfer code (FEHM) (Zyvoloski 2007) and is calibrated using the Model Analysis and Decision Support (MADS) software, available at https://mads.lanl.gov/. FEHM transport calculations have been benchmarked against MODFLOW and FEHM is shown to be equal in accuracy and provide improved numerical stability relative to MODFLOW (Keating and Zyvoloski 2009).

Finally, the results of the model calculations are subjected to sensitivity analysis, expert review, and validation to verify and adjust the analyses as required. As the arrows in Figure 5 indicate, this approach to modeling is iterative, and previous steps are returned to as needed or required.

The following sections describe each of the steps shown in Figure 5 in more detail.

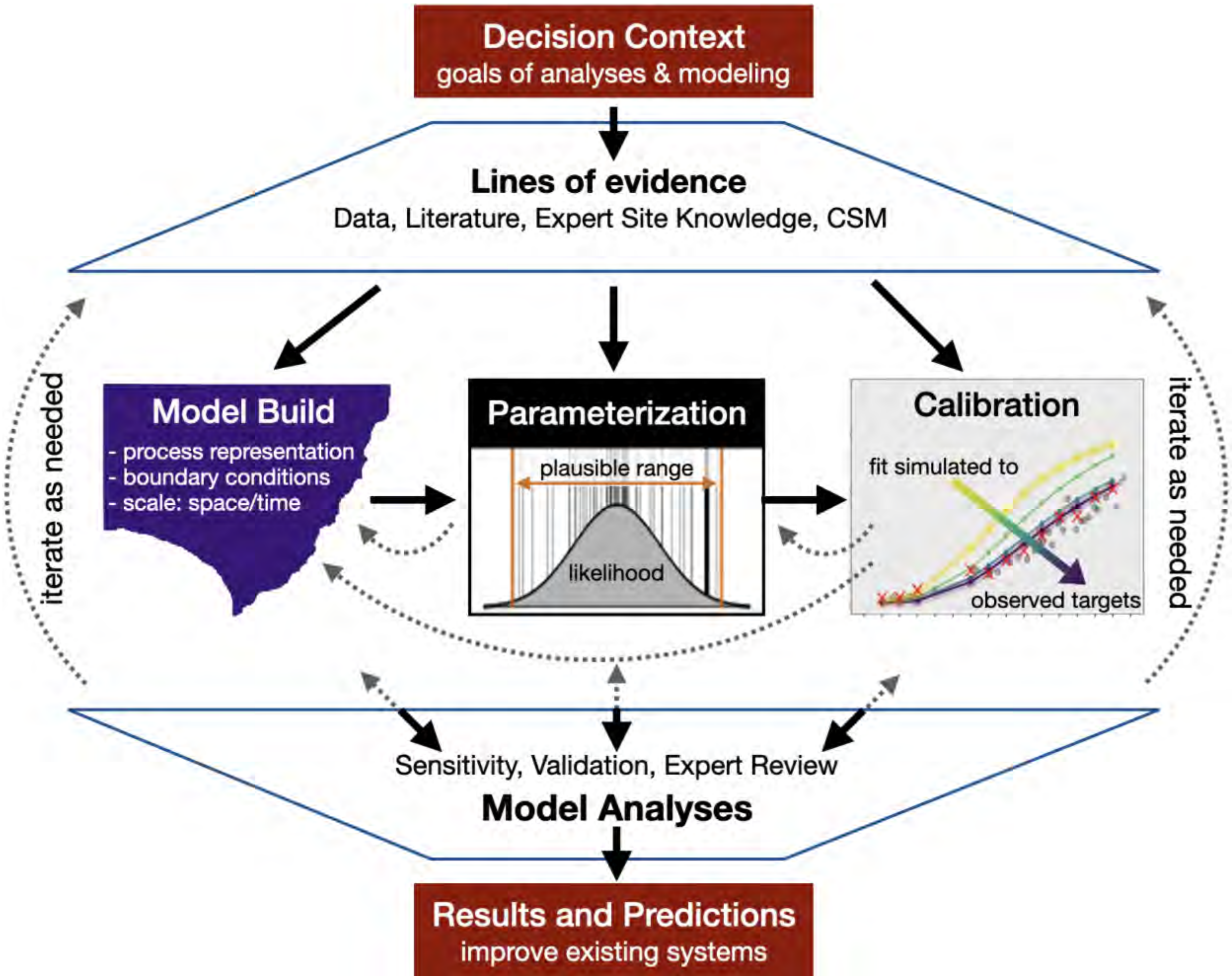

Figure 5. Conceptualization of modeling framework shows how lines of evidence are applied to the building, parameterization, and calibration of the model. Analyses of the model provide more information that often prompts iterative steps to improve earlier steps in the modeling workflow.

2.2 Model Domain and Grid

The upper surface of the CM is the regional aquifer water table, which is approximately 300–400 m (~1000 ft) below the land surface. Water table elevations range from 1920 m above mean sea level (m amsl) (6300 ft amsl) near the western edge of the domain, which approaches the mountain block, to 1616 m (5300 ft) amsl near the Rio Grande, whose *x* and *y* coordinates define the eastern model boundary. The model is designed to represent the regional aquifer and covers an area of 221 km^2 (85 mi^2) horizontally extending from the water table down to 1000 m (3280 ft) amsl in the vertical direction. While the plume covers only a small portion of the regional aquifer, a large domain size with successive levels of refinement is used to provide detailed characterization in the plume region and to avoid boundary effects in flow and transport modeling. Including the entire regional aquifer in the model allows for selection of physically significant boundaries (such as the Rio Grande to the east), and the use of selective refinement minimizes the computational burdens associated with a large domain on a regular grid.

The model is discretized into an unstructured tetrahedral mesh whose surface is aligned with the regional water table using the LANL LaGriT mesh generator, available at https://lagrit.lanl.gov/ (Gable et al. 1996). Two levels of refinement are used in areas of interest, which increases lateral resolution from 125 m to 62.5 m and 31.25 m (410 ft to 205 ft and 102.5 ft) respectively. The z direction is variably refined, ranging from 6–24 m (20–79 ft) in thickness, with higher resolution at the top of the regional aquifer. The grid is connected according to Delaunay criteria and is quality tested both in terms of Voronoi volumes and negative coefficients (Figure 6).

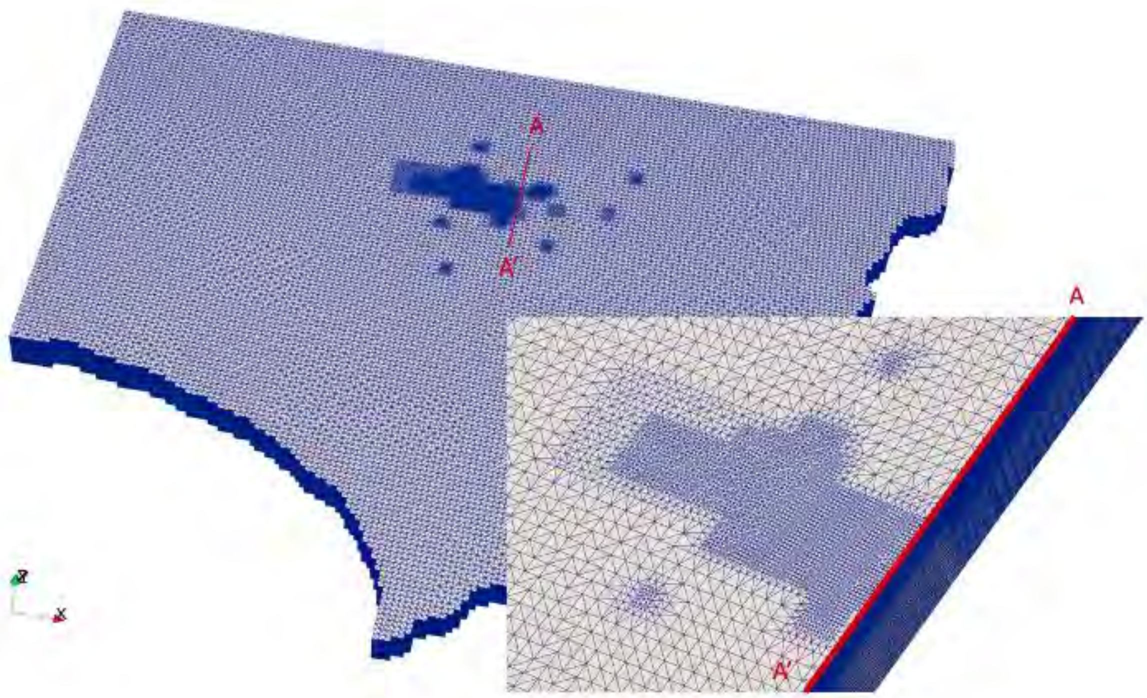

Figure 6: CM variably refined mesh with cross-section showing vertical refinement.

2.3 Model Operation, Initial, and Boundary Conditions

The FEHM code (Zyvoloski 2007) is used to simulate flow and transport in the CM. The model represents the regional aquifer and is saturated at every node. Most boundary conditions, like other model parameters, use input distributions that limit parameters to plausible values. The main flow gradient in the model is developed by assigning constant head conditions to the western (mountain block) and eastern (Rio Grande) boundaries. No-flow boundaries are set approximately parallel to regional flow (north and south model edges) and at the base of the model, which is sufficiently deep (400–600 m or 1312–1968 ft) so that it does not interfere with plume transport behavior. On the surface of the CM, elliptical hydraulic windows representing preferential recharge from the VZ, both chromium-contaminated and chromium-free, are applied. More detail, including figures, on parameterization for all boundary conditions is described in Section 2.4.

The initial condition is established by running the model until the hydraulic heads reach a steady state that are calibrated against measurements in February 2014 (see Section 2.5). Then, the transient portion of the simulation begins, starting in the year 1964 and running through the calibration period (i.e., until the end of 2022). The transient simulation includes all IM pumping and chromium transport. Time series of chromium concentrations and head responses are output for every well within the domain during this transient portion of the simulation.

IM activity is a boundary condition in the model at the nodes, representing extraction and injection well screens. Actual IM pumping can be variable on a sub-minute basis, so smoothing on the pumping rates is performed to prevent the model timesteps from being intractably small due to pumping changes. Extraction and injection flow rates are obtained from the well completion reports or reported by LANL’s Supervisory Control and Data Acquisition (SCADA) system. Pseudocode for the smoothing and filtering applied to pumping events is as follows:

1. If two pumping events are separated by at least 12 hours, they are defined as two unique pumping events; otherwise, both events are considered part of the same pumping event. Iterate through all pumping events in the database, and assign a unique pumping event identifier based on the above rule.
2. For each pumping event defined in step 1, compute the event’s duration by taking the difference between the earliest start time and the latest end time. Remove all pumping events that are less than 4 days in duration.
3. For each pumping event remaining after the screening in step 2, compute a weighted average flow rate where the weights equal the duration of each unique flow rate contained within the event.

Figure 7 shows actual IM flow rates (represented by black lines), as reported by LANL’s SCADA system, versus smoothed flow rates computed by the process described above (represented by red lines), for the first quarter of 2020. This comparison indicates that the pumping implemented in the model is a reasonable approximation of the actual pumping that occurred.

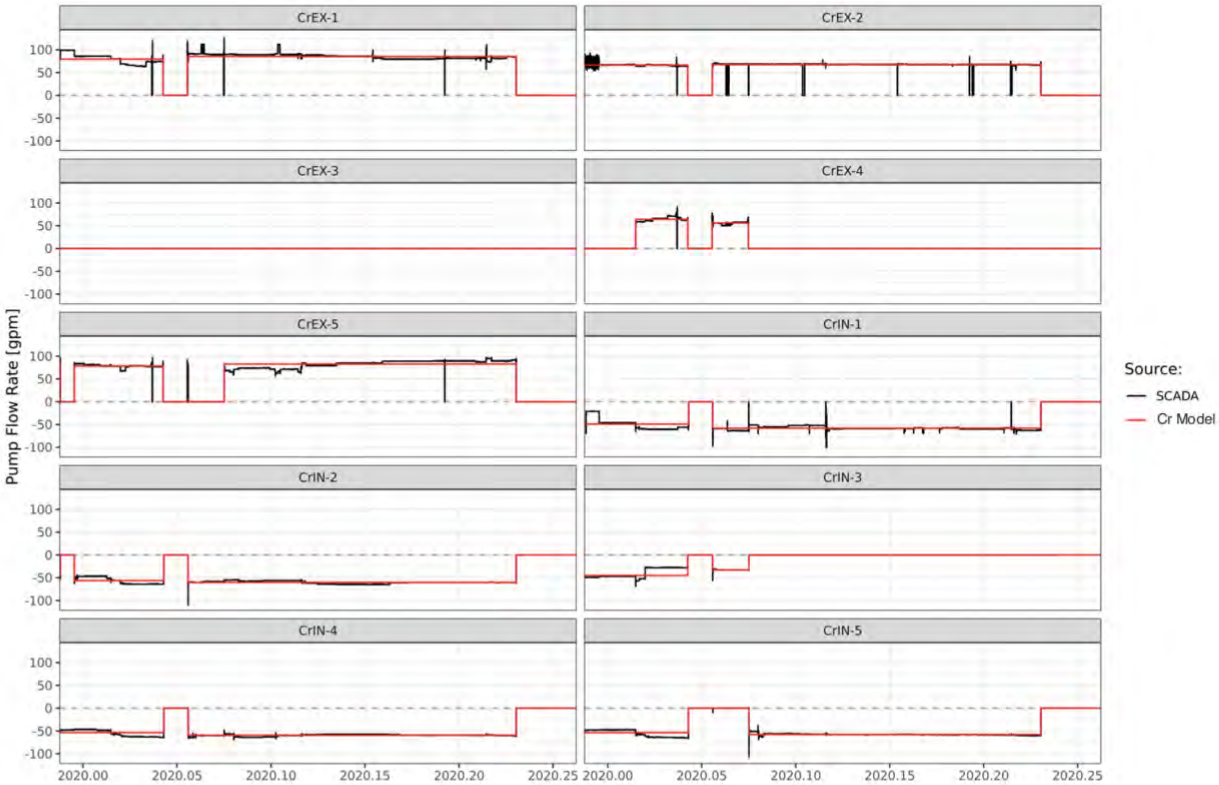

Figure 7. Comparison of actual (SCADA) and smoothed (CM) pumping rates during the first quarter of 2020. Positive and negative flow rates correspond to extraction and injection, respectively.

2.4 Input Parameter Distribution Development

All input parameters to the CM are described using distributions that inform the range and likelihood of plausible values given existing site data. The model has 416 parameters, but several parameters are represented by the same input distribution. Table 1 lists the distributions used in the CM, along with the parameter, model key, median, and the 1st and 99th percentiles of the distribution, which are used to set the bounds on how far the parameter can be moved by the Levenberg-Marquardt (LM) algorithm during the calibration process. Distributions are developed using a rigorous process of gathering all available sources of information, including data, published literature values, and, where data are not available, elicitation of possible values from site experts. Sources of information for each distribution are also listed in Table 1.

Table 1. Prior distributions for input parameters.

Material Properties Parameters

Parameter	Model Notation	Median	1st, 99th %	Unit	Sources of Information
Hydraulic Conductivity(1)	-	-	-	-	-
Puye Formation (pilot points)	(kx, ky)(pp#)	12	0.2, 685	ft/d	Well Data, Literature
Anchor points(6)	(kx, ky)(ap#)	0.8 - 161	x 10^{-1}, x 10^{1}	ft/d	Well Data, Literature
Specific Storage	-	-	-	-	-
Shallow (unconfined to semi-confined)(3)	s(pp#)	$10^{-3.7}$	$10^{-7.5}$, $10^{-0.7}$	1/m	Well Data, Literature
Deep (confined to semi-confined)	s(pp#)	$10^{-5.9}$	$10^{-7.6}$, $10^{-4.2}$	1/m	Well Data, Literature
Dispersivity(1)	-	-	-	-	-
Longitudinal	disp_long	17.5	5.1, 60.1	m	Literature
Transverse Horizontal	disp_trans_hor	4.4	1.1, 17.3	m	Literature
Transverse Vertical	disp_trans_vert	0.2	0.1, 0.8	m	Literature
Other	-	-	-	-	-
Krige Scale(3)	krige_range(K,S)	2264	410, 4204	m	Literature, Modeling
Krige Anisotrophy Ratio(5)	krige_v(K,S)_semiaxis	0.27	0.01, 0.8	-	Literature, Modeling
Advective porosity(5)	adv_por	0.15	0.04, 0.35	-	Well Data, Literature

Boundary Condition Parameters

Long name	Parameter name	Median	1st, 99th %	Unit	Sources of Information
Primary window centroid coordinates(3)	s2(x,y)0	(499284, 539141)	x(498979,499589) y(538986,539295)	State Plane NAD83	CSM, Modeling, Geochemistry
Secondary window centroid coordinates(3)	s1(x,y)0	(499106, 538984)	x(498832,499380) y(538830,539139)	State Plane NAD83	CSM, Modeling, Geochemistry
Northwest window centroid coordinates(3)	s3(x,y)0	(498506, 539359)	x(498285,498727) y(539160,539558)	State Plane NAD83	CSM, Modeling, Geochemistry
Southwest window centroid coordinates(3)	s4(x,y)0	(498631, 538953)	x(498410,498852) y(538798,539108)	State Plane NAD83	CSM, Modeling, Geochemistry
Primary/secondary window elipse radii(3)	s(1-2)r(x,y)	138	49, 226	m	CSM, Modeling, Geochemistry
Northwest window elipse radii(3)	s3r(x,y)	288	29, 589	m	CSM, Modeling, Geochemistry
Southwest window elipse radii(3)	s4r(x,y)	188	35, 347	m	CSM, Modeling, Geochemistry
Primary window Cr concentration(4)	s2c	1408	239, 4353	ppb	CSM, Modeling
Other window Cr concentration(4)	s(1,3,4)c	597	83, 1995	ppb	CSM, Modeling
Hydraulic window recharge rate(3)	infils(1-5)	201	10, 500	mm/yr	CSM, Modeling
Preferential recharge centroid coordinates(3)	s5(x,y)0	(499850, 539281)	x(499585,500115) y(539149,539414)	State Plane NAD83	CSM, Modeling, Geochemistry
Preferential recharge window x radius(3)	s5rx	700	276, 1124	m	CSM, Modeling, Geochemistry, Data
Preferential recharge window y radius(3)	s5ry	350	138, 562	m	CSM, Modeling, Geochemistry, Data
Primary/secondary window arrival time	t0s(1-2)	1975	1964, 2005	year	CSM, Modeling
Northwest/sourthwest window arrival time	t0s(3-4)	2000	1990, 2009	year	CSM, Modeling
Window eccentricity (tilt)(3)	s(1-5)corr	0	-1, 1	-	CSM, Modeling
Eastern constant head(2)	easthead	1745	1715, 1775	m	Data, Literature, Modeling
Western constant head(2)	westhead	1830	1800, 1860	m	Data, Literature, Modeling

NOTE: Parameter distributions are normal unless marked superscripts: (1) lognormal, (2) uniform, (3) truncnormal, (4) gamma, (5) beta, (6) anchor points range: median +/- one order of magnitude

Modelers and statisticians work together to make decisions regarding the relevance and usage of data. Combining subject matter modeling expertise and statistical expertise ensures that the distribution adequately represents, but does not overstate, parameter uncertainty. Extensive discussion of the distribution development approach is described in "Scaling Input Distributions for Probabilistic Models" (Black et al. 2019).

Parameters for some material and transport properties are assigned on a node-by-node basis, while others are homogeneous throughout the domain. Material properties and transport parameters include advective porosity, dispersivity, lateral and vertical hydraulic conductivity (***K***), specific storage (S_s), and kriging parameters that are used to interpolate ***K*** and S_s.

Boundary condition parameters include constant head on the east and west faces and hydraulic window characteristics such as recharge rate and window location, shape, and size. The CM domain begins at the top of the regional aquifer, where chromium-contaminated water enters the water table. These pathways are referred to as hydraulic windows. Their footprints on the regional aquifer are referred to as the sources of chromium at the water table. The five hydraulic windows in the CM are represented as ellipses. The parameterization of the ellipses is controlled by the center coordinates and *x* and *y* radii, as shown in Figure 8.

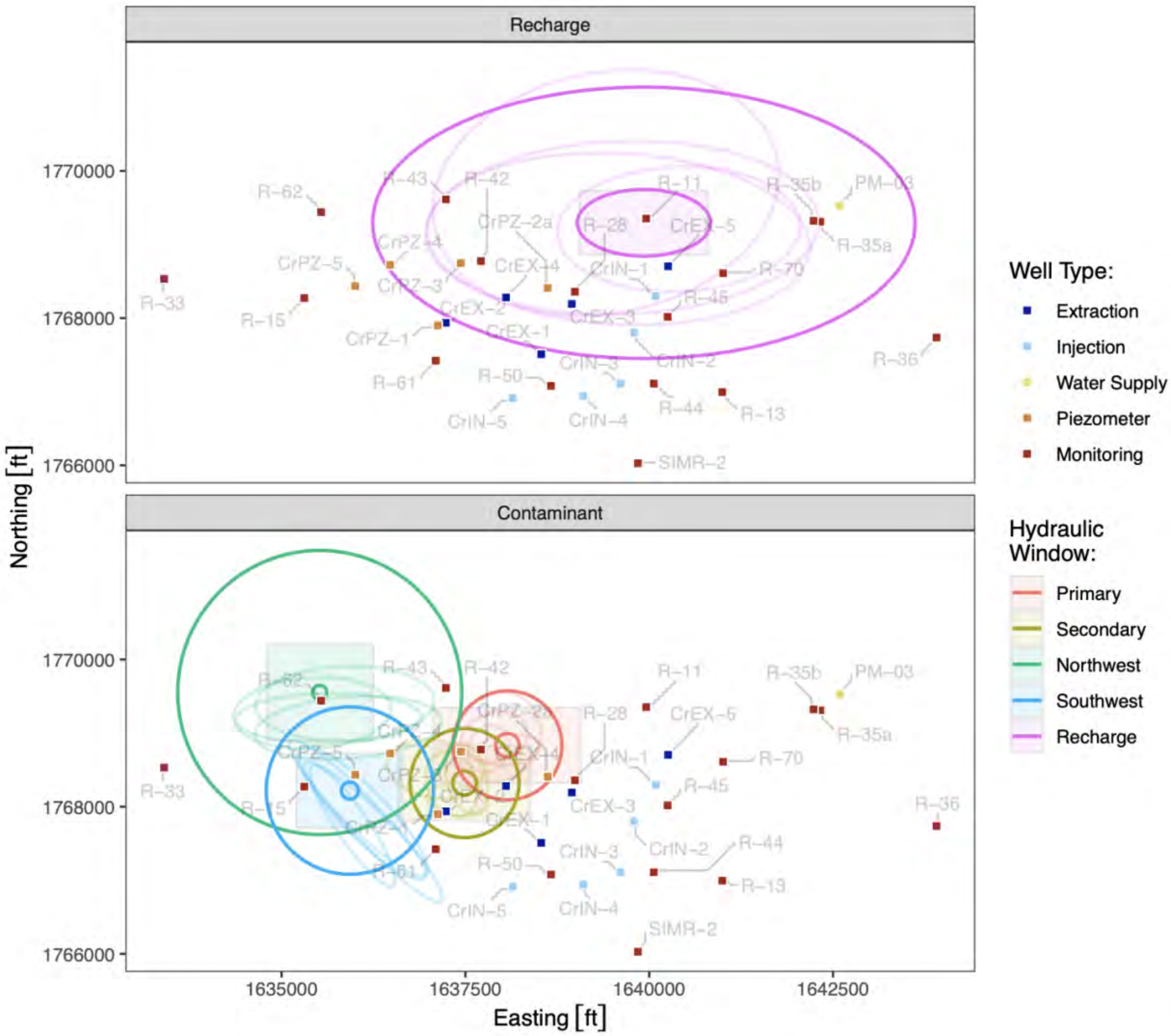

Figure 8. Chromium-free recharge (top) and chromium-contaminated (bottom) hydraulic window location distributions for spatial input parameters. The shaded rectangle shows the range of allowed center coordinate locations, and the darker ellipses show the allowed range of *x* and *y* radii. Example calibrated hydraulic windows are shown for each source as transparent ellipses.

A zone of preferential chromium-free recharge in the northeastern portion of the domain is indicated by a blind source separation study (LANL 2018b), which suggests that the chemistry at

R-11 reflects a nitrate-contaminated but chromium-free source of recharge from Sandia Canyon that post-dates the chromium-releases. Other wells near R-11 have a chemical makeup that suggests that a portion of their water is derived from a similar source of recharge, including R-43 screen 1 and screen 2, and to lesser extents R-35b and R-45 screen 2. This suggests a relatively large but diffuse source of chromium-free recharge. Additionally, vertical differences in chromium concentrations in the plume further justify the presence of a chromium-free source of recharge in this region of the plume. Samples taken from R-70 and CrEX-4 both indicate higher concentrations of chromium at depth. Additionally, CrPZ-2 has relatively low observed concentrations of chromium, and its screen is closer to the water table compared to surrounding wells like R-42, CrEX-4, and R-28. This preferential recharge source has a larger distribution for radii in the x direction owing to the general west to east direction of Sandia Canyon.

The primary and secondary windows together comprise the main flux of chromium from the VZ into the regional aquifer. R-42 has the highest observed concentration of chromium detected in a well in the chromium plume, therefore the primary source is most likely near, and upgradient of, R-42. There is insufficient geochemical evidence to distinguish the presence of two unique sources in this region. However, the difference in concentrations between the northern and southern regions of the plume requires the presence of two distinct sources to match historical concentration trends. The secondary source is placed to the south of the primary, where generally lower concentrations (<200 ppb) have been observed in downgradient wells (CrIN-4, CrIN-5, R-50, R-44, R-45) compared to monitoring wells in the north where concentrations above 200 ppb have been observed (R-28, CrEX-4, CrEX-5, R-70).

Monitoring wells R-62 and R-43 have both shown increasing trends since completion. These trends begin at similar times and are at lower concentrations than the plume centroid. Their location upgradient of the primary and secondary sources likely indicates a unique window close to the two wells. While most wells do not see meaningful fluctuation in concentrations of chromium with duration of purge time, R-62 is unique in that concentrations increase during longer-duration purges. R-62 is pumped each year with an extended purge time, and much higher concentrations are observed when this extended pumping is conducted. This suggests that a northwestern source is very near R-62. A unique geochemical signature of perchlorate contamination is located in the southwestern portion of the plume (LANL 2018b). The perchlorate, along with the groundwater flow direction (which is primarily west to east but has a northward component), indicate a separate window of chromium arriving from the VZ and contributing to the regional aquifer plume. This source is identified as recharge downstream from the outfall from the TA-50 radioactive liquid waste treatment facility, where releases of chromium and perchlorate are known to have occurred. Geochemical evidence and proximity suggest that the southwest source contributes to concentrations observed in R-15, CrPZ-4, CrPZ-5, and R-61.

Material property parameters include hydraulic conductivity, specific storage, dispersivity, and kriging parameters. Given the heterogeneity of the Puye Formation, and the sensitivity of flow and transport to local hydraulic conductivity, a heterogeneous $\boldsymbol{K}$ field is generated on a node-by-node basis using the pilot point approach (Doherty 2003). This approach samples from narrower distributions at well locations that are informed by hydraulic conductivity estimates derived from aquifer tests at that particular location (referred to as "anchor points") and from wider distributions derived from all relevant site data at locations between the well anchor points (referred to as "pilot points") (Figure 9 and Figure 10).

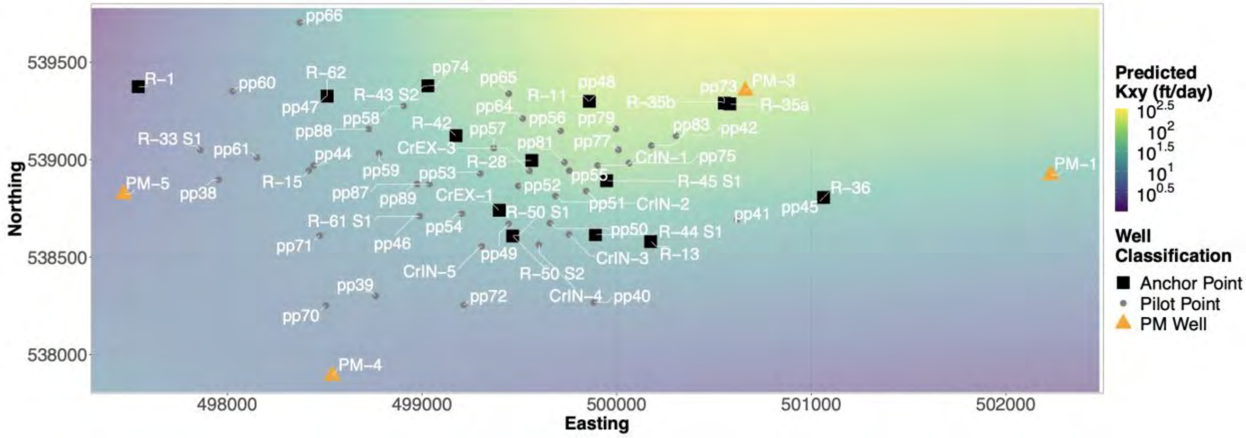

Figure 9. Map of anchor and pilot points used in the CM. The underlying *K* field is created using a spatial model of the central value of each anchor point in the domain (though this plot is in plan view, there are pilot and anchor points at depth and the kriged field is 3-dimensional).

For each simulation, the values drawn at anchor and pilot points are then kriged to form a heterogeneous ***K*** field that honors both the available estimates, their spatial locations, and the associated uncertainty. The kriging model uses a spherical variogram with a calibrated range parameter. A scaling factor applied to the range parameter in the *z* direction (i.e., anisotropy) is utilized to allow for the layering behavior present from the alluvial deposition of the sedimentary geologic units at the chromium site—i.e., more correlation in the lateral directions than the vertical direction. *K* and specific storage fields are kriged independently. Distributions for specific storage and the kriging parameters are shown in **Error! Reference source not found.**.

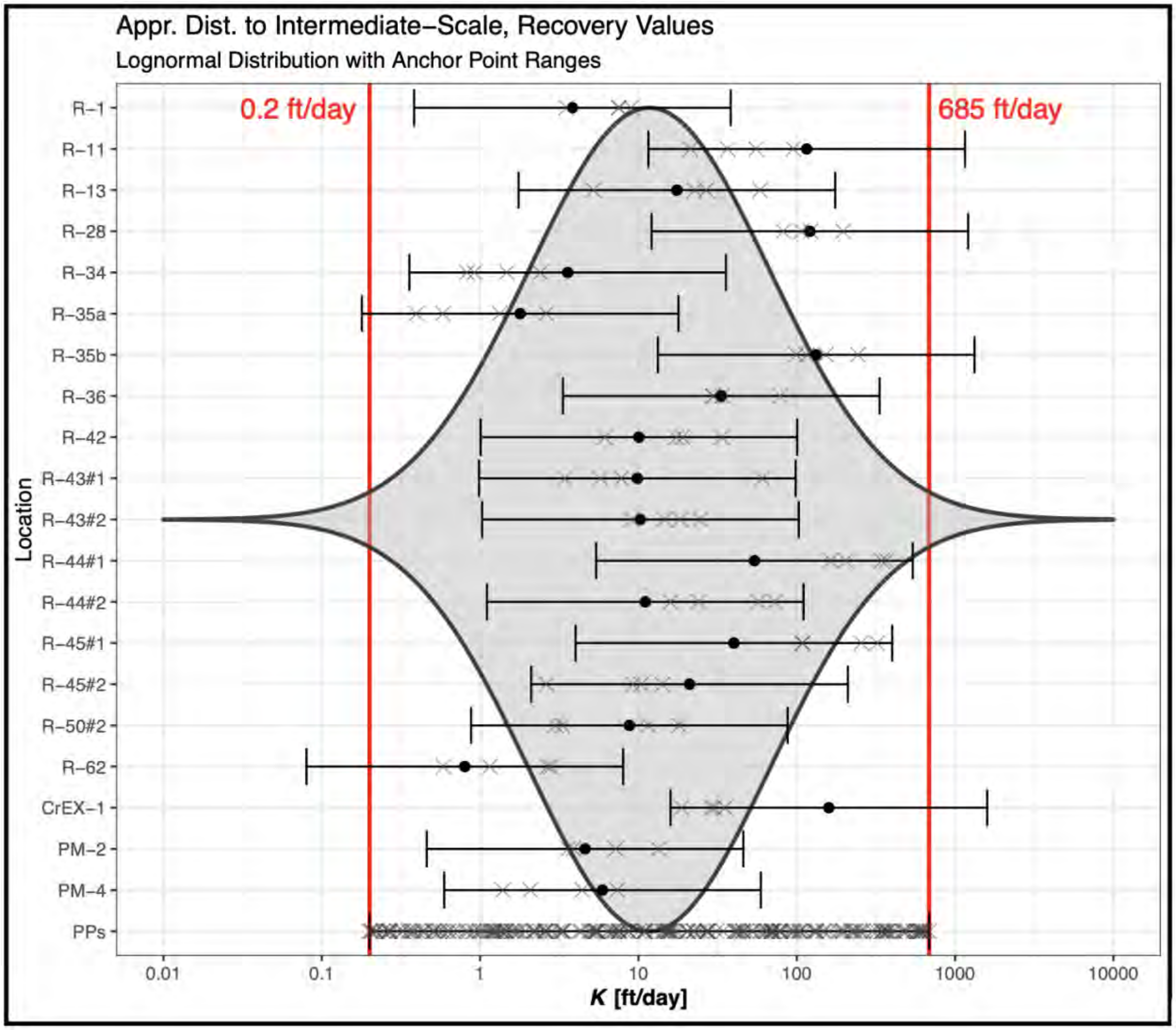

Figure 10. Anchor point hydraulic conductivity distributions at well locations (horizontal bars), which combine to form the overall distribution that informs pilot points with no spatially explicit data (bottom bar and shaded gray violin plot). The 1st and 99th percentiles, used to limit the calibration movement, are shown as red lines. Final initialization points of the top four calibrations are shown as grey x's for all anchor and pilot points.

Figure 11 shows parameter distributions that are not shown in other figures.

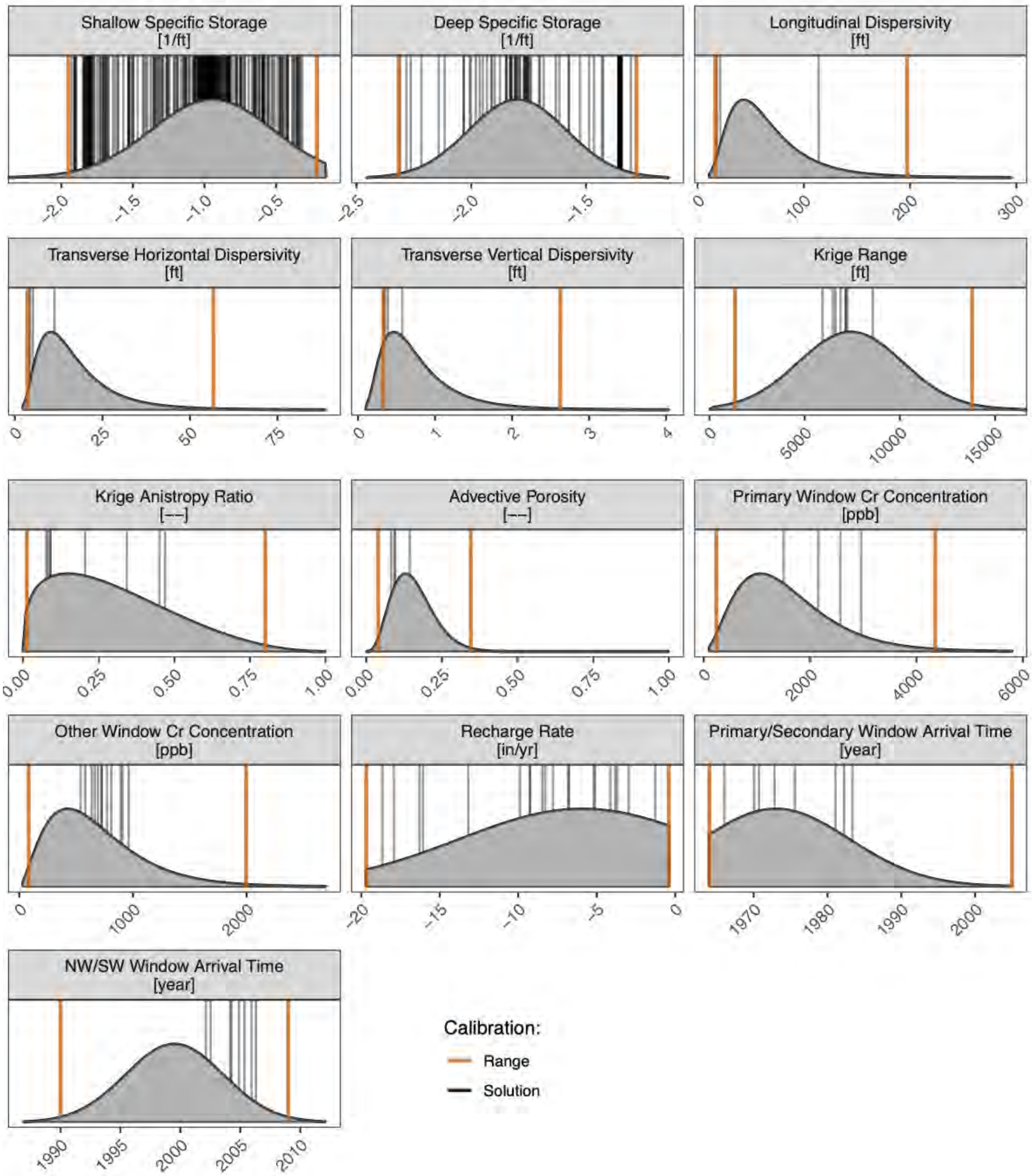

Figure 11: Parameter distributions not shown in other figures. The 1st and 99th percentiles are indicated by orange vertical lines and constrain the range of the LM calibration. Final values for four top calibrations are shown as grey lines behind the distribution. NOTE: uniform distributions are listed in Table 1 but not shown, as they simply run from a minimum to a maximum value.

2.5 Calibration

Model development and calibration is an iterative process targeted at evolving the CSM and its implementation in the CM. The process includes both qualitative and quantitative components that span lines of evidence based on subject matter expert knowledge, monitoring data, laboratory experiments, and geophysical data. The CM integrates these lines of evidence by providing a quantitative calibration of the conceptual model to data (Figure 5) and estimating the uncertainty associated with input parameters. Calibration is a learning process that employs several qualitative and quantitative approaches. Typically, a classical calibration fits a nonlinear regression model to target data. This section provides an overview of target datasets and a brief discussion of the tools used in calibration and uncertainty quantification, including the LM algorithm and Markov Chain Monte Carlo (MCMC) sampler.

2.5.1 Target Development

The objective function (OF) drives the calibration by measuring how well the model matches observed datasets. It is composed of target variables that relate model results to observed data. The main form of data available for the CM is from monitoring wells at the LANL site. Water level data and chemical data with concentrations of chromium are available for screened intervals in these wells or boreholes drilled on the Pajarito Plateau. The data from these wells is available publicly on the Intellus website (https://intellusnm.com).

Target development takes place alongside distribution development in an iterative process. The spatial and temporal scales of targets are important to represent the observed data at a similar scale to the model for a successful calibration. Currently, the CM uses 416 targets that can be classified into four groups:

1. Chromium concentrations at individual well screens. For each observed year with a full year of data (through 2021), the yearly average is used (356 targets); for partial years (2022) a smoothing approach is used to estimate the target at particular dates (31 targets).
2. Hydraulic head gradients between wells of interest (6 targets magnitude, 6 targets direction).
3. Hydraulic head measurements within each well screen for February 2014 (18 targets).
4. Hydraulic head drawdown responses measured in monitoring wells during specific IM operations at CrIN and CrEX wells (13 targets slope, 13 targets intercept).

Each of these groups of targets can be weighted differently to define an OF that is most appropriate for the calibration. For example, if the hydraulic head targets better support the CSM than the concentration targets, weights for concentration data can be increased relative to the hydraulic head targets. These are called the “group weights.” Within each group, individual targets (certain wells, or certain times) can also be weighted differently. These are called the “preference weights.” The weights and the targets are also standardized, so that different units of measurement or scales of data do not have a different impact on the OF. This is called the “meaningful difference” between targets. The OF therefore is a grouped, weighted average of residuals that measure how closely the simulation matches the observed data.

Final weighting schemes are identified to prioritize data points that have a larger influence on maintaining the CSM, encouraging important physical behaviors, and matching responses to well pumping. Target priorities in descending order are approximately:

1. Concentrations in the following wells are the highest priority:
    a. R-35a, R-35b, SIMR-2 because they are sentinel wells (currently at background levels).
    b. R-70 screen 2 so that the inverted gradient and deeper plume is represented (N3B 2021a).
    c. R-45 screen 2 to represent concentration increases beginning in 2018, possibly as the result of IM operations.
2. Concentrations in the following wells are important because they are critical to the CSM:
    a. R-70 screen 1
    b. CrEX-4 screen 1 and screen 2
    c. R-45 screen 2 prior to IM operation (pre-2018)
3. Concentrations in the following wells prioritize the response to the IM operations:
    a. Between 2018–2021: R-50 screen 1, R-45 screen 1, R-44 screen 1.
    b. CrEX-1, CrEX-2, CrEX-3, CrEX-4, and CrEX-5
    c. CrPZ-1 2017 and 2019 responses to CrEX-2 pumping.
4. Concentrations in:
    a. All CrIN wells pre-IM responses. (Note: injection causes concentration estimates to be unreliable since injection water, which is even lower in chromium than the background, is added into the aquifer.) Complex concentration recovery patterns in response to changing pumping rates are evaluated qualitatively as validation points during the calibration process.
    b. R-28 and R-42 are important because they represent the likely centroid of the plume with the highest observed chromium.
    c. Pre-2018 (prior to IM implementation): R-50 screen 1, R-45 screen 1, R-44 screen 1.
    d. CrPZ-2a is important to the CSM because of low chromium near the plume centroid at the surface, which helps the model reproduce the observed inverted concentration gradients at CrEX-4 and R-70.
5. Drawdown responses to IM pumping.
6. Wells that do not significantly impact the CSM individually but constrain the overall behavior: R-36, R-11, R-13, R-15, R-44 screen 2, R-50 screen 2, R-61 screen 1, R-62.
7. Water level gradients.
8. Steady-state water levels and upgradient wells observed at background levels of chromium: R-33.

Chromium Concentration and Trend Targets

Concentration data were obtained from the publicly available Intellus database (https://intellusnm.com). The data include sample results through October 2022. Data filtering is conducted to confirm that every included point is a valid measurement. The data filtering process includes removing:

- all samples from well purging,

- samples that were lower quality in lab analysis,
- samples that may have been compromised by amendments or other chemicals (for example, hammer-oil contamination occurred in early R-61 screen 2 data),
- injection well data during operations, and
- extreme outliers (for example, the second data point collected at R-70 screen 1).

For chromium concentrations, targets are developed by averaging all results for a given year at each well with detectable levels of chromium. If *only* chromium non-detections and/or concentrations below background are observed at a given well, a calibration target of 5 ppb is used for each year to match the background level of chromium specified in the model (5 ppb). Wells in the background group are R-13, R-35a, R-35b, R-36, R-50 screen 2, and SIMR-2. All other wells use the yearly average of the sample results to define the calibration target for that year; results from both detected and non-detected samples are used in calculating the average. If no samples were collected in a given year, no calibration target is developed for that year. Not every well screen has chromium data available for all intended sampling events for 2022. Since most wells have an incomplete dataset for 2022, a smoothing approach is used to estimate concentration targets with the partial dataset available in 2022. All chromium concentration-based calibration targets are shown in Figure 12 and Figure 13.

In 2017, chromium concentrations were measured in packed-off screen 1 and screen 2 at CrEX-4, as well as together as one composite screen. Later, all data from 2019 to the present were collected as a composite screen. Because the initial data in the separate screens provided additional information about the vertical distribution of chromium in this part of the plume, the separate CrEX-4 screen 1 and screen 2 targets are retained for 2017, and all other targets from 2017–2021 are treated as CrEX-4 as a single composite screen.

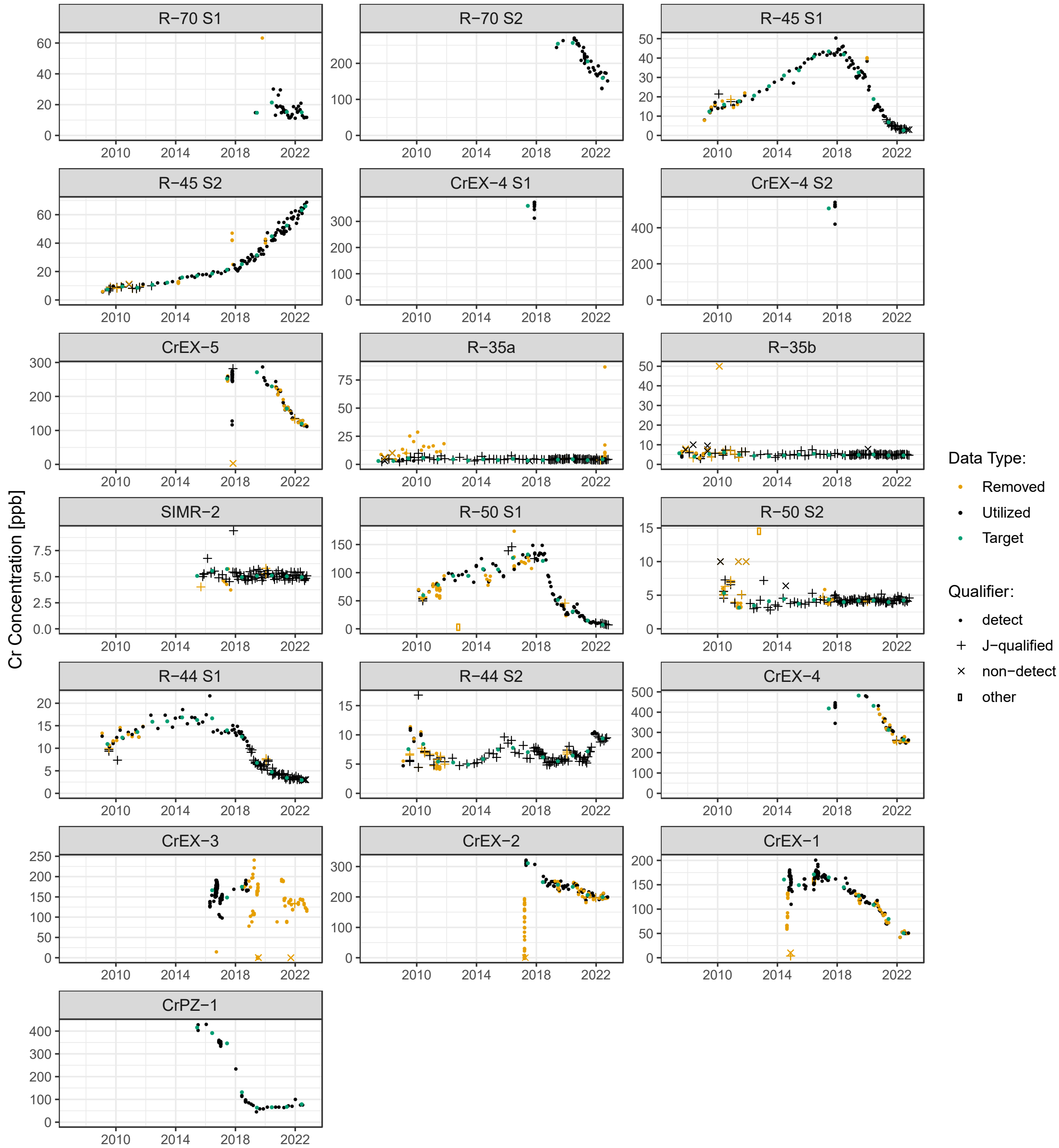

Figure 12. Yearly averaged chromium raw data and concentration targets (green) derived from raw data (black) at monitoring wells that receive top priorities in the OF weighting scheme. These include sentinel wells, CSM-critical wells, extraction infrastructure wells, and wells that show a clear response to IM operations.

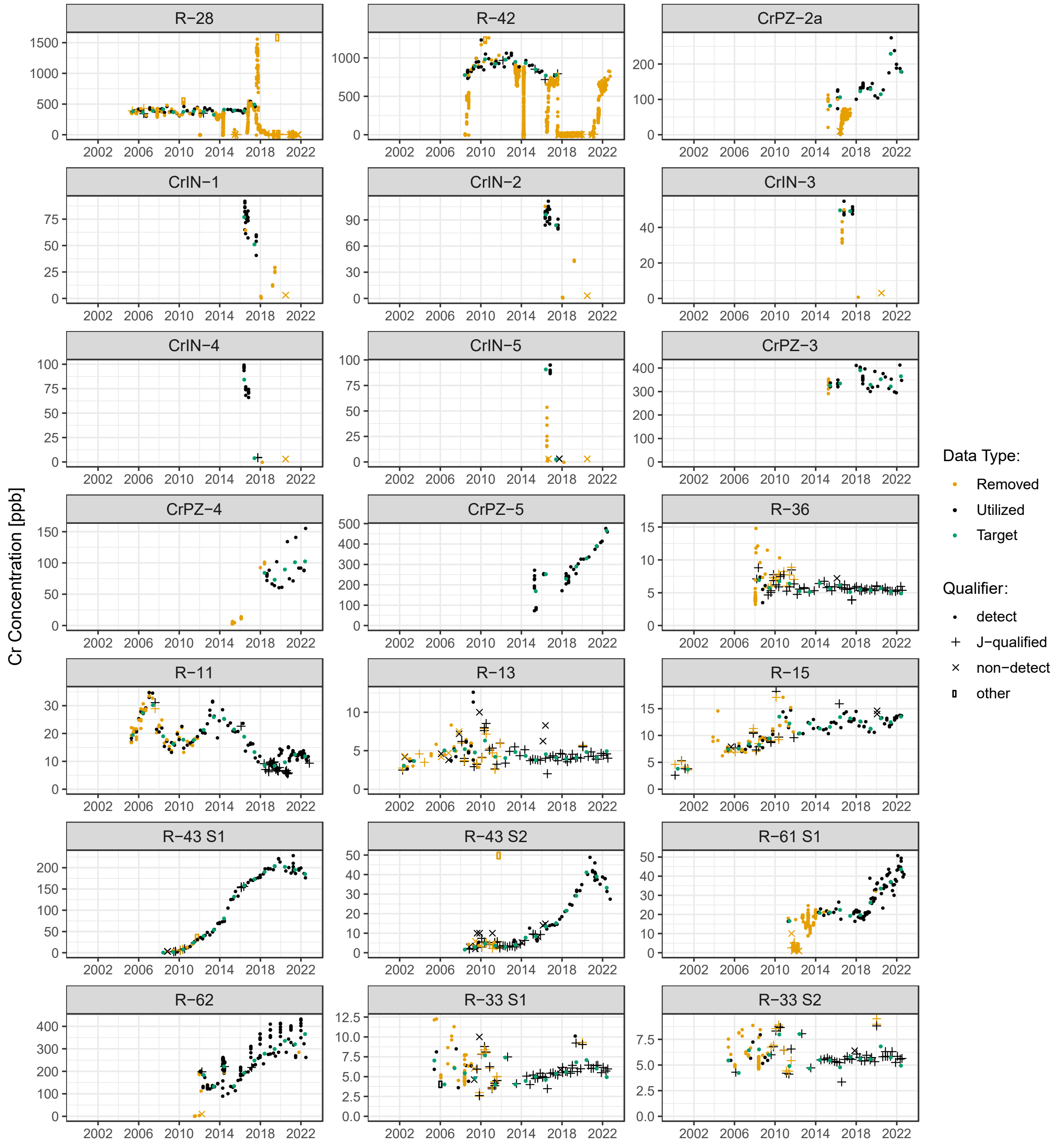

Figure 13. Yearly averaged chromium concentration targets (green) derived from raw data (black) at remaining monitoring wells throughout the domain.

Hydraulic Head and Hydraulic Gradient Targets

Hydraulic head targets were derived for monitoring well screens located within and near the chromium plume. These wells include R-11, R-13, R-15, R-28, R-33 screen 1, R-35b, R-36, R-42, R-43 screen 1 and screen 2, R-44 screen 1 and screen 2, R-45 screen 1 and screen 2, R-50 screen 1 and screen 2, R-61 screen 1, and R-62. Each target represents the average head (shown in m amsl) observed within the well screen during February 2014. High-temporal resolution head data obtained from Intellus were aggregated to a monthly average target value by iteratively averaging values using the following successive temporal windows:

(1) 2-hour interval within a calendar day,
(2) calendar day,
(3) month of February.

For instances of wells without head values during the period of interest, values were imputed via regression analysis using nearby wells with a long period of record (N3B 2022a, 2022b).

Additionally, lateral hydraulic gradients were derived using the hydraulic head target values for a subset of well screens located within the core of the plume. Hydraulic gradients are computed for specified triplets of well screens using the three-point method detailed in (Heath 1983). Target values for a given triplet consist of both a gradient magnitude and azimuth, each of which are weighted independently within the OF. The hydraulic gradient targets serve to provide an additional constraint on the hydraulic head target values to ensure that the flow gradients local to the plume are honored. Using seven monitoring locations that cover the overall plume area (R-43 screen 1, R-11, R-28, R-45 screen 1, R-61 screen 1, R-50 screen 1, and R-13), six hydraulic gradients were computed, resulting in twelve total targets (magnitude and gradients are shown alongside model results in Figure 22).

Drawdown Responses to IM Pumping

Drawdown targets were developed for pairs of a pumping well and nearby wells with an observed water level response to help calibrate the heterogeneous *K* and *S* field. Capturing this kind of hydrologic response in modeling is suggested in EPA (2008). Drawdown targets were developed for extraction events at three infrastructure wells: CrEX-1, CrEX-5, and CrIN-2 (during a pump test in which it was extracting). To isolate the effect of extraction at each well, opportunistic periods in the record were identified when no other infrastructure wells were operating. Drawdowns were observed for 13 targets:

1. CrEX-1 pumping from 07/06/2016 – 07/21/2016 leads to drawdown targets in:
    a. CrEX-3
    b. R-28
    c. R-44 screen 1
    d. R-44 screen 2
    e. R-50 screen 1
    f. R-50 screen 2
2. CrEX-5 pumping from 11/02/2017 – 11/07/2017 leads to drawdown targets in:
    a. CrEX-3
    b. R-11
    c. R-45 screen 1
    d. R-45 screen 2
3. CrIN-2 pumping from 06/01/2016 – 06/02/2016 leads to drawdown targets in:
    a. R-44 screen 1
    b. R-44 screen 2

c. R-45 screen 1

Pumping event start and end times are determined by examining a pumping well water-level values for initial drawdown and recovery. Water level values within each response well are barometrically corrected using either regression deconvolution (Toll and Rasmussen 2007) or a basic correction algorithm (which simply converts barometric pressure to feet of water, subtracts from the water level, and normalizes). Barometric corrections are made using publicly available tidal data and barometric pressures from LANL's TA-54 weather station. In some instances, barometric correction resulted in a noisier time series and therefore was not utilized. In many cases it was necessary to also detrend the water levels from the background decline in the aquifer. To do this, a linear regression was applied from the time prior to the pumping event and the time after the assumed recovery occurred to account for background water level decline. This is illustrated in Figure 14, where a red line is fit to the data included only in the grey shaded regions, which represent time before the CrIN-2 pumping and after the recovery. The red line from Figure 14 represents background decline, which is subtracted from the computed drawdown to isolate the effect of drawdown from the pumping well (Figure 15).

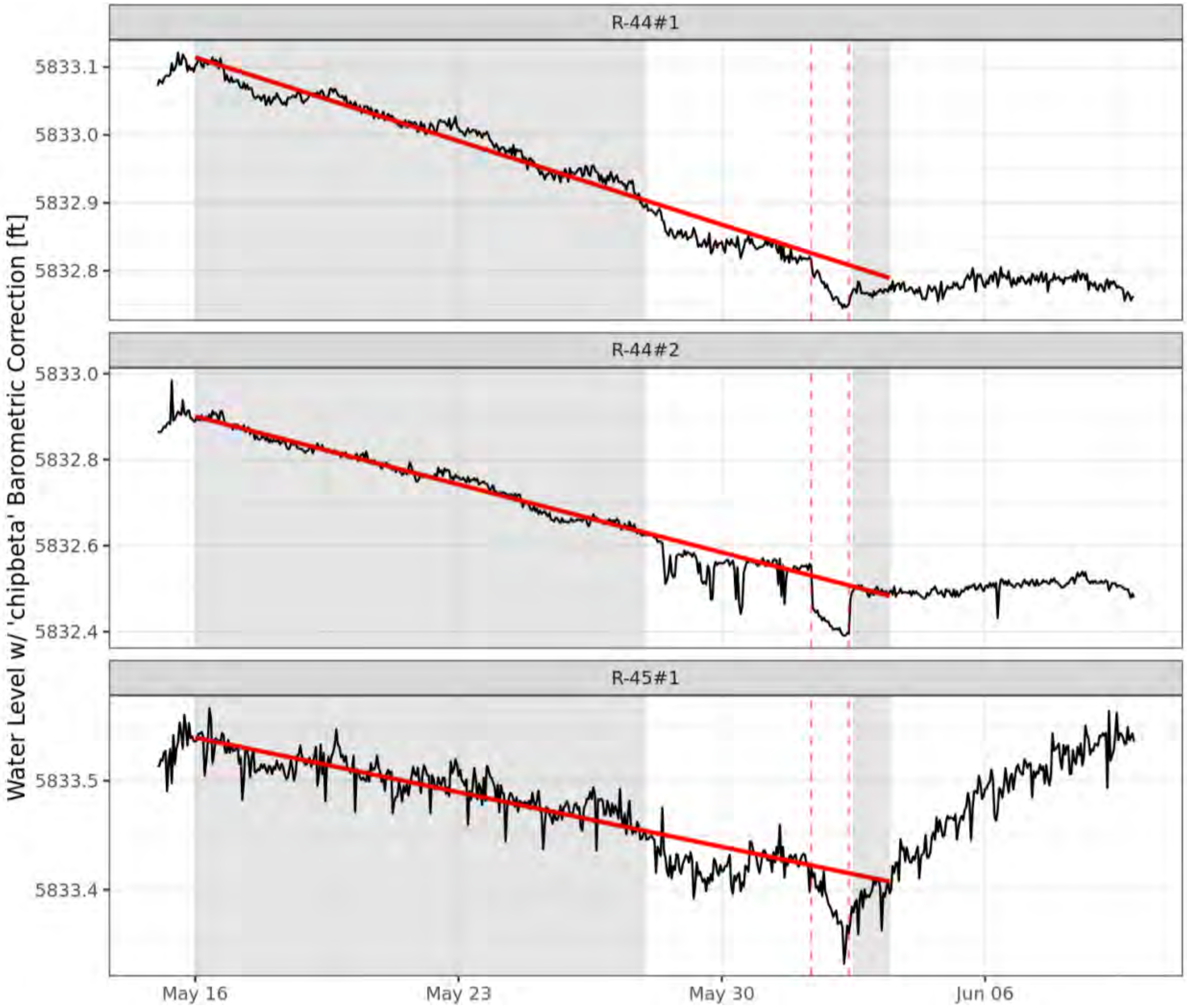

Figure 14. Barometrically corrected water levels before, during, and after the CrIN-2 drawdown event (black) and the fitted line for background decline (red). Note that the line is fitted to the data in the shaded grey regions which represent time before the CrIN-2 pumping and after the recovery.

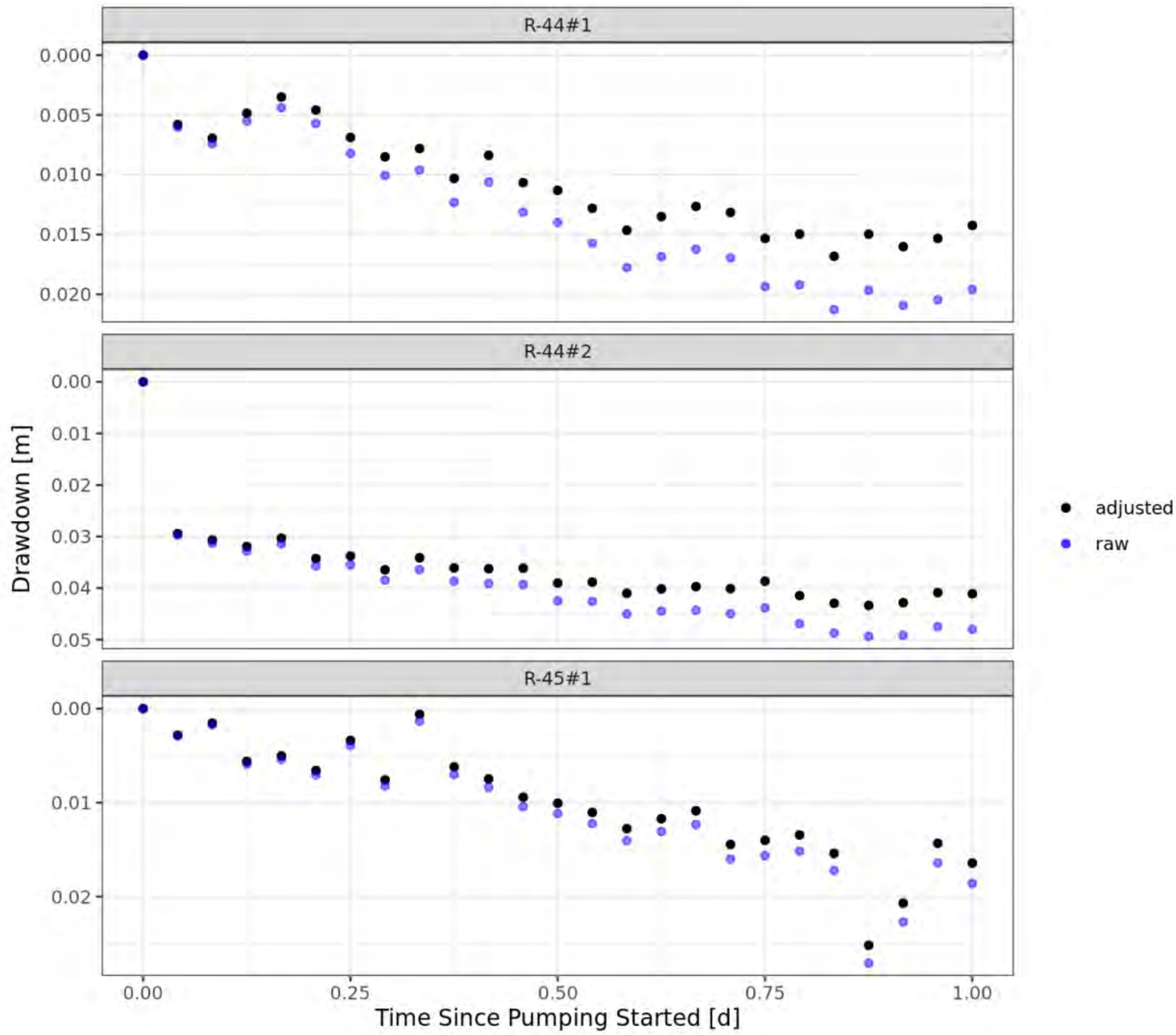

Figure 15. Drawdown data during the CrIN-2 pumping event. The adjusted data subtracts the background decline and is used for target development.

The drawdown targets for a given response well consist of a slope and an intercept, obtained from a regression of drawdown versus the logarithm of time since pumping began, similar to the Cooper and Jacob late-time approximation of the Theis equation. To determine the starting point of the late-time approximation, a range of times is specified such that the drawdown curve is approximately linear when plotted as the logarithm of time versus drawdown. A grid search is then used to determine the time that maximizes the fitted linear model's R-squared value. The fitted drawdown line for R-44 screen 2 is shown as a red line in Figure 16. Note that Figure 16 uses linear time to be intuitive to the reader, but the target slope and intercept are applied to drawdown versus the logarithm of time.

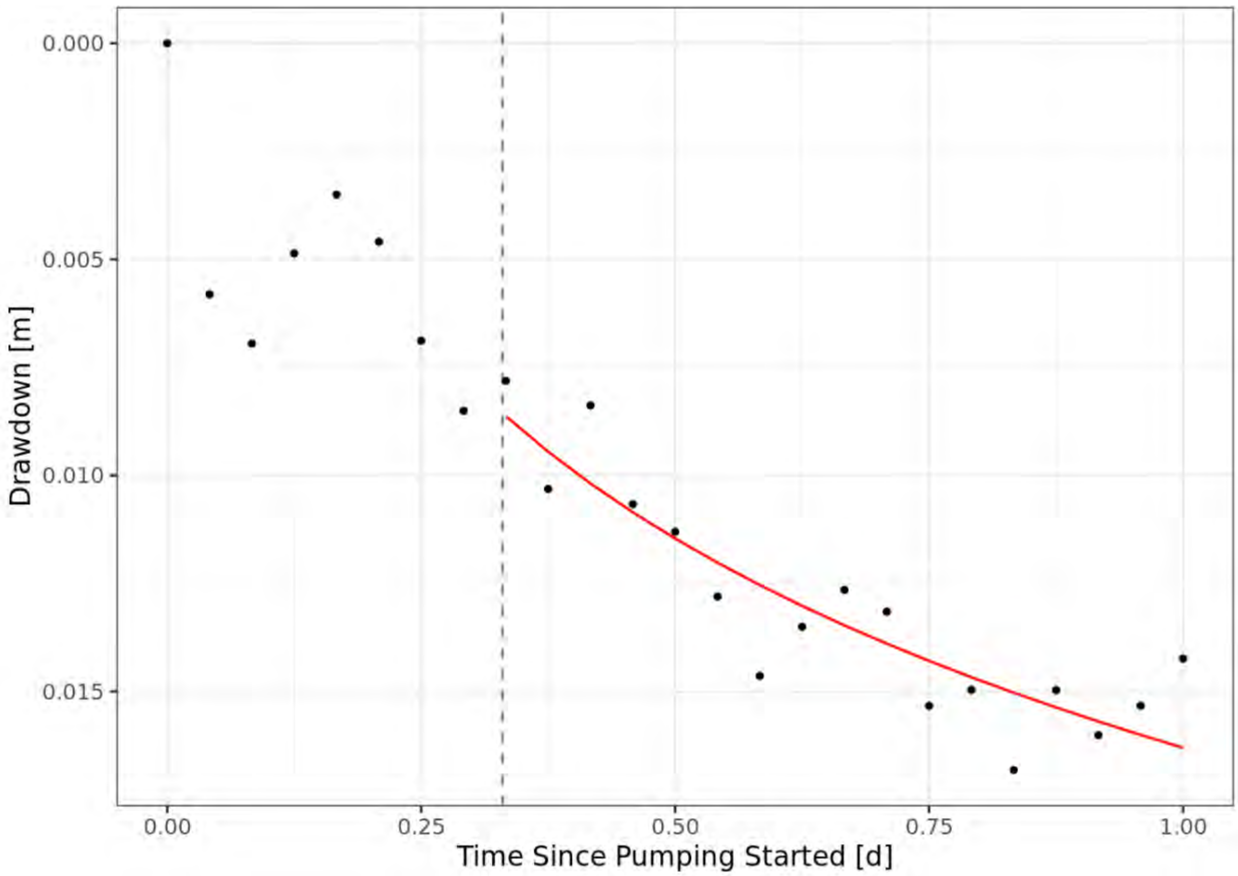

Figure 16. Drawdown target shown in red for R-44 screen 2 response to CrIN-2 pumping event.

2.5.2 Method and Uncertainty Quantification

A classical calibration involves identifying a deterministic model with one set of input parameters that minimizes the error between observations (target data) and the predictions of the simulation (CM). Achieving a well-calibrated model in the 400+ dimensional parameter space used in the physically-based CM is challenging, and the following method is used to identify promising local minima with which to initialize an LM algorithm for fine-tuning.

First, a grid search is conducted using tens of thousands of draws across the full extent of parameter space, as defined by the distributions described in Section 2.4. A higher density of runs is used in regions of higher parameter likelihoods. Next, these 30,000–50,000 runs are filtered to 10–20 top parameter sets by identifying the best matches to target datasets. These 10–20 top runs are then explored closely through a combination of vetting parameter sets with the CSM and hand-tuning of highly sensitive parameters. Lastly, the remaining top parameter sets are used to initialize an LM algorithm to further minimize the error between model and observed target data. This process facilitates selection of parameter sets that are conceptually meaningful, in agreement with available data, and have been closely examined by subject-matter experts for hydrologic reasonability and conformance with the CSM. Results from this effort are used to initialize a sampler to quantify uncertainty, as described below.

A Bayesian approach is taken to quantifying uncertainty. Uncertainty in parameters related to hydraulic conductivities, specific storages, boundary conditions, and rates of recharge from hydraulic windows are addressed from a conceptual model perspective by including multiple calibration endpoints. That is, these parameters are optimized through the iterative process described in the preceding paragraph, and multiple conceptualizations of these parameters are identified that all meet the criteria of a well-calibrated model (e.g., parameters are physically realistic, simulated values compare closely to observed data, and the CSM is honored). Ultimately, four distinct parameter sets are identified that meet these criteria, representing four discrete deterministic solutions that match the described targets. These four models represent a range of hydraulic properties that impact chromium migration in the regional aquifer.

Uncertainty in transport parameters—dispersivity, source concentration, advective porosity, and time of chromium arrival—are estimated using the MCMC sampler. Contaminant transport is most heavily influenced by these parameters, and quantitative estimates of their uncertainty are important to predictive modeling of plume transport and migration into the future. Uncertainty in these parameters is characterized with continuous prior-probability distributions to form a joint posterior distribution for the parameters. Uncertainty in the flow field parameters (hydraulic conductivities, specific storages, boundary conditions, and rates of recharge from hydraulic windows) are characterized by the discrete parameter sets described by the four models.

Ultimately, the calibration and uncertainty quantification process involves a variety of tools and numerical techniques to arrive at results that characterize uncertainty through a statistical model but also provide the necessary prior constraints to ensure physical accuracy.

2.6 Validation

The models are validated by a comparison of observed and simulated well responses. Relationships, between pumping wells and monitoring wells, as measured by head changes, were compared across the site using as many pumping events as possible. 86% of 484 well pair events analyzed are well matched in the model (see Figure 17), indicating that the model reproduces observed connections between wells effectively even in areas without drawdown targets guiding the calibration (refer to Figure 23, below). The validation method is described below.

Extraction and injection events used in validation are identified using the following criteria:

1. Pumping rate threshold: The well turns completely off or on.
2. Minimum time threshold: The pumping rate remains constant for at least two days.
3. Maximum time threshold: If the pumping rate continues for longer than seven days, only the first seven days are retained as part of the event.

For each identified pumping event, monitoring well responses are measured as the change in head over the timeframe of the event, divided by the standard deviation, in both the data and model. Monitoring well responses are then compared to the changes in pumping rate over the same period. A Huber regression, a method that is less sensitive to outliers than traditional least-squares regression (Huber 1973), is performed across all identified events for each pair of pumping and monitoring wells to determine whether the monitoring well consistently responds to the pumping well across many events, for both the data and the model.

The results of the regression analysis are shown graphically in Figure 17. Observed responses are defined using the significance of the Huber regression slope for the field data (x-axis in Figure 17; $p<0.01$ represents a significant connection between wells in a pair). The degree to which the model matches the observed connection is quantified using the significance of the data-model difference slope (y-axis in Figure 17; $p>0.01$ represents a match between the model and data). The validation points can be quantified as shown in Figure 17. The top left and top right quadrants represent accurate lack of connections (76%) or accurate connections (10%), respectively, in the model. The bottom right represents data where the model overstates (4%) or understates (1.5%) an observed connection, while the bottom left represents well pairs where connections are observed in the model but not in the data (8.5%). These results demonstrate that the flow field, as described by well relationships across the site, are very well represented in the model.

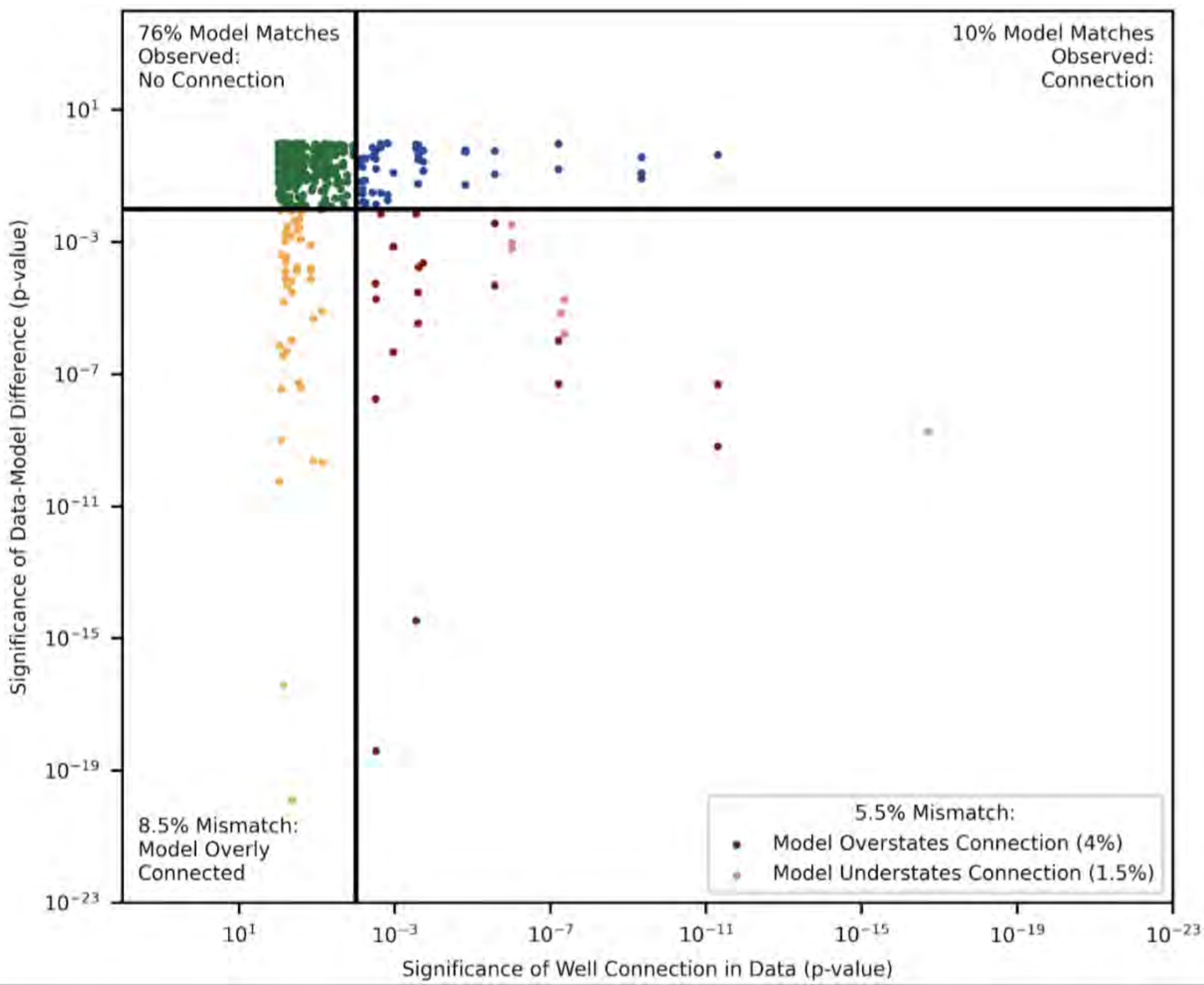

Figure 17. Monitored responses to pumping wells across the site are matched in the CM in 86% of cases validating the flow field in the model. Significance threshold for p-values is marked with a vertical and horizontal line at 0.01.

3.0 Results

3.1 LM Calibration Results

The LM calibration is measured by the minimum of the OF, which is in turn a metric of how well the simulation matches the observed target data, given the weighting scheme described in the calibration methods. Many different starting points are selected based on the best forward runs available, including some manually-calibrated starting locations. The LM calibration gradually improves the matches to data through iterations of runs. Four local minima, representing unique source configurations and flow pathways, were identified. All are consistent with the CSM, and all closely match target datasets. The calibrations of the CM model are randomly numbered 1 to 4; the numbers do not reflect confidence in the model. These four solutions form the initialization state for the MCMC sampler, as described in Section 3.2.

3.1.1 Chromium Concentrations

The main priority for the simulation is matching concentrations of chromium in the regional aquifer. Figure 18 and Figure 19 show the results of the four LM calibrations plotted against data. Raw data are plotted in black and target data points are plotted in green. The OF compares simulated results only to target data, not to raw data or validation data.

Figure 18 shows wells from the top three priority categories (see Section 2.5.1 for more information on prioritization). The four calibrated models show close agreement with all wells that receive highest priorities in the OF weighting scheme, including sentinel wells, CSM-critical wells, extraction infrastructure wells, and wells that show a clear response to IM operations.

The chromium concentrations at the sentinel wells R-35a, R-35b, and SIMR-2 are between 2.5 and 10 ppb. Background concentrations of chromium in the regional aquifer are somewhere between 3 and 10 ppb, i.e., there is naturally occurring chromium in the aquifer at low levels in this range. In the model, background concentration is set to 5 ppb; results at 5 ppb indicate that no chromium from the plume sources (hydraulic windows) has arrived at that location in the model. All simulations show exactly 5 ppb at all three sentinel wells, indicating consistency with observed background at these wells.

R-70 screen 2 is prioritized because of the very high concentrations (near 270 ppb) observed upon installation, followed by a decrease after the conversion of CrIN-6 to CrEX-5 (LANL 2018c). All four calibrations match this initial signal, as well as the decrease after extraction began at CrEX-5. R-70 screen 1 has concentration an order of magnitude lower than screen 2 (~20 ppb instead of ~200 ppb) with all measured concentrations falling between 10–30 ppb. All four models are above the single datapoint collected in 2019 (which is also a model target) and all four are then effective at following the noisy downward trend observed in 2020 and 2021. The main inverted gradient is matched at these two different orders of magnitude between R-70 screen 1 and screen 2.

CrEX-4 is the other well at the site with higher concentrations at depth, though the difference in screens (~350 ppb in the upper screen and ~450 ppb in the lower screen) is much smaller than the inversion at R-70. It is much further upgradient than R-70, and the only data from two screens available is from 2018. After this date, CrEX-4 was converted to a single-screened well for the purposes of larger extraction. This later CrEX-4 data is shown on a separate plot and is discussed with the other CrEX wells below. The model matches both of these targets well.

R-45 screen 2 is another well screen that is prioritized, since concentrations have recently (near the end of 2021) gone above the 50 ppb threshold used to delineate the plume. All four models predict the early increasing trend from 2010–2019 and the increase in slope that occurs in 2020.

R-50 screen 1, R-45 screen 1, and R-44 screen 1 all show a similar response to the implementation of full operations of the IM network in 2018, with increasing trends prior to initiation and sharply decreasing trends afterwards. These wells also represent responses across different orders of magnitudes, with R-50 screen 1 data peak at 150 ppb, R-45 screen 1 data peak around 50 ppb, and R-44 screen 1 data peak just over 20 ppb, all in 2018. All three wells decrease to or near background concentrations quickly over the years from 2018 (when the IM is fully initiated) to 2022. The models are effective in matching these strong responses, including the three different magnitudes of IM-induced rise and fall in concentrations.

The calibrations match the decreasing trends at extraction wells (CrEX-5, CrEX-4, CrEX-2, and CrEX-1). CrEX-3 data after 2018 was excluded from target development until the potential impacts of biofouling from amendments nearby can be determined. CrPZ-1 is also included on the first panel of plots because of the sharp decrease from over 300 ppb to below 100 ppb in a very short space of time, due to the initiation of pumping at nearby CrEX-2. All four calibrations capture this trend at CrPZ-1 and provide a good fit to the data. However, none of the four models match the early, more gentle decreasing trend observed in 2015–2017. This is likely due to some natural process—perhaps an influx of cleaner water, or shifting concentrations in the source of chromium—that is not built into the model. Without data to inform a conceptualization of this gradual reduction, no structure is included in the model. A similar lack of structure is shown at R-11, which is discussed below.

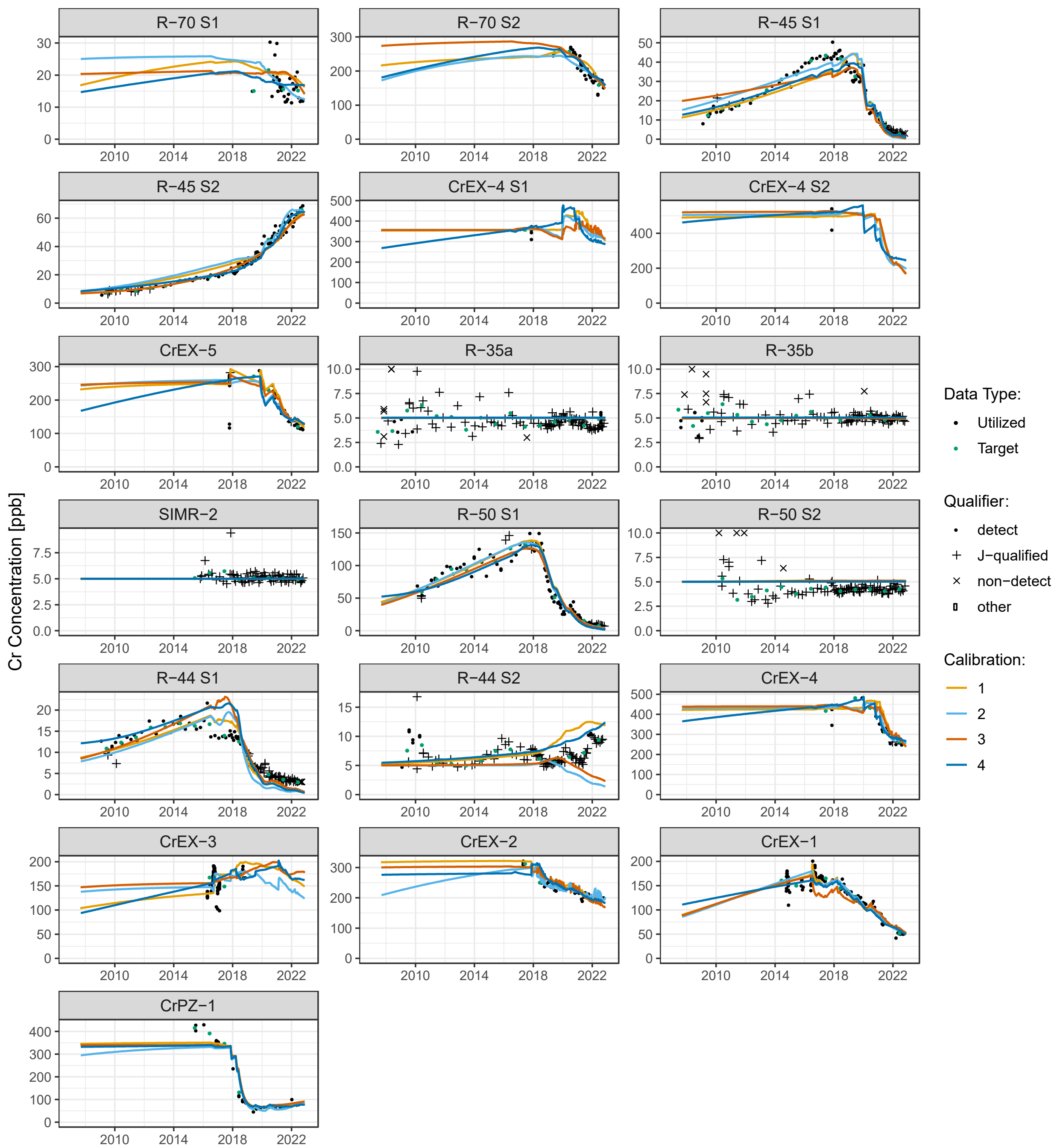

Figure 18. Four calibrated models show close agreement with all wells that receive highest priorities in the OF weighting scheme. These include sentinel wells, CSM-critical wells, extraction infrastructure wells, and wells that show a clear response to IM operations.

Figure 19 shows the remaining wells used as targets in the chromium plume and surrounding area. R-28 and R-42 are important to match because they are the highest chromium concentrations observed in the plume, and therefore are most likely to represent the centroid of mass. Data at R-28 and R-42 after 2018 are excluded due to amendment testing in these wells

(LANL 2017; N3B 2022b). All four models match the order of magnitude of chromium concentration correctly at these two wells, though they do not show the oscillation observed in the concentration data. At R-28, these data are likely just noise, though at R-42 it appears that there is possibly a real, albeit small, trend upward followed by a downward trend. The final rise in 2017 at R-28 looks like it may be a signal, and all four models show an increase at this time, driven by IM operations. The magnitude of this increase and the data since 2018 and 2022 are uncertain, and there is significant variability represented across the four calibrations.

CrPZ-2a, which is located laterally between R-28 and R-42, has much lower observed concentrations than either of those wells. CrPZ-2a is at shallower depths than the screens at R-28 or R-42. The inclusion of CrPz-2a helps match the conceptualization of the inverted concentration gradient observed at CrEX-4 and R-70. Like other inverted concentration gradient locations, the models accurately represent the lower concentrations at CrPZ-2a.

During injection well operation, concentration data obtained at injection well screens are not indicative of true concentrations, so the CrIN wells only have targets pre-injection. These data are well matched. All other background wells—R-36, R-13, and both screens of R-33—have concentrations of 5 ppb, indicating that no added chromium is reaching those locations where no chromium beyond background has been observed. Upward trends at R-15 and R-61 are represented in all four models. R-43 screen 1 and screen 2 both show increasing trends, followed by stabilization and eventual decreasing trends. The four models match the increasing trend; however, they underestimate speed of data plateau and turnover.

The clear, oscillating trend at R-11 at low chromium concentrations is not captured by the models. The current hypothesis for this is that oscillations are due to a recharge signal, which is part of the evidence for a clean source of recharge driving the inverted concentration gradient observed at CrEX-4 and R-70. The time-varying recharge source is not temporally discretized to a high degree of refinement. However, the overall magnitude of the data is matched at R-11.

Overall, the four models simulate concentration data that match the magnitude of concentrations and their trends measured in 40 monitoring wells over a 20-year period.

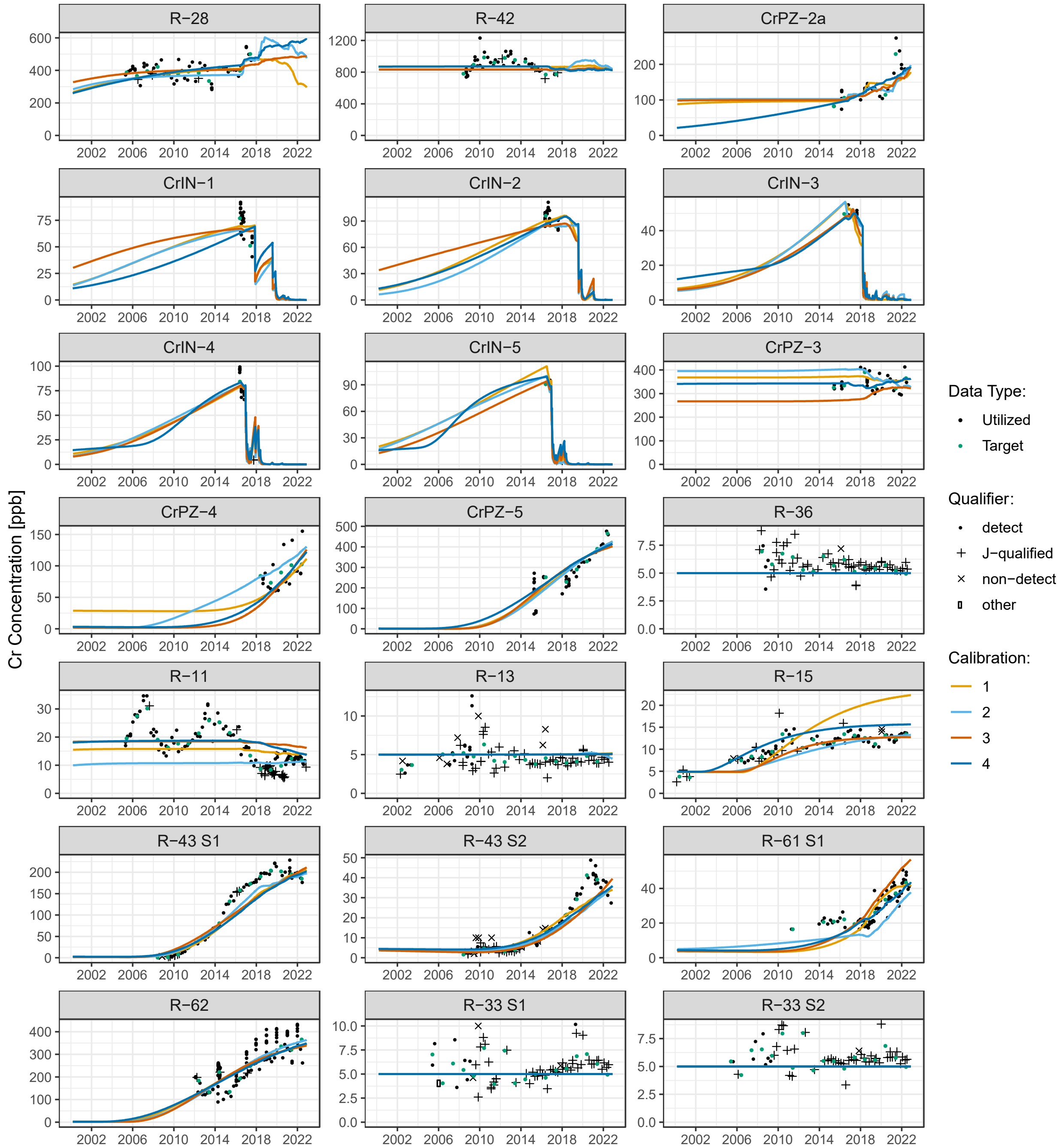

Figure 19. Four calibrated model results show close agreement with remaining wells in the modeling domain.

3.1.2 Hydraulic Head

Water levels in the LM calibrations (18 observations across four calibrations) also match closely with simulated values, falling within 1 ft of target data throughout the domain, and with the vast majority falling within 6 inches of the target data (Figure 20 – Figure 21). Figure 20 shows the head targets as a green cross within a circle, ordered by x-coordinate (i.e., from west to east).

Head targets are shown generally to decrease from the western side of the domain to the east, with the exception of R-35b and R-36 shown increasing to the east of the plume. Note that this figure excludes the much higher head condition at R-33 and R-36, which makes it easier to identify the nuances in the flat chromium plume region by compressing the y-axis to a narrower range. The calibration results are difficult to discern on this scale because many points overlap.

R-43 screen 2 is overpredicted by all four calibrations, though matches to R-43 screen 1 are very close, indicating that the water table surface is well estimated by the model, but the slight downward vertical gradient at this location is not represented in the model. Though all four calibrations match the direction of the downward gradient (between -0.01 and -0.02), the magnitude is not reached due to the higher estimated heads at the lower R-43 screen. Figure 21 depicts the calibrated water table contours in plan view for each of the calibrations. The cross-section shows both the screen length and screen depth, and the circle represents the exact location of the model node used to estimate head residuals within the well screen.

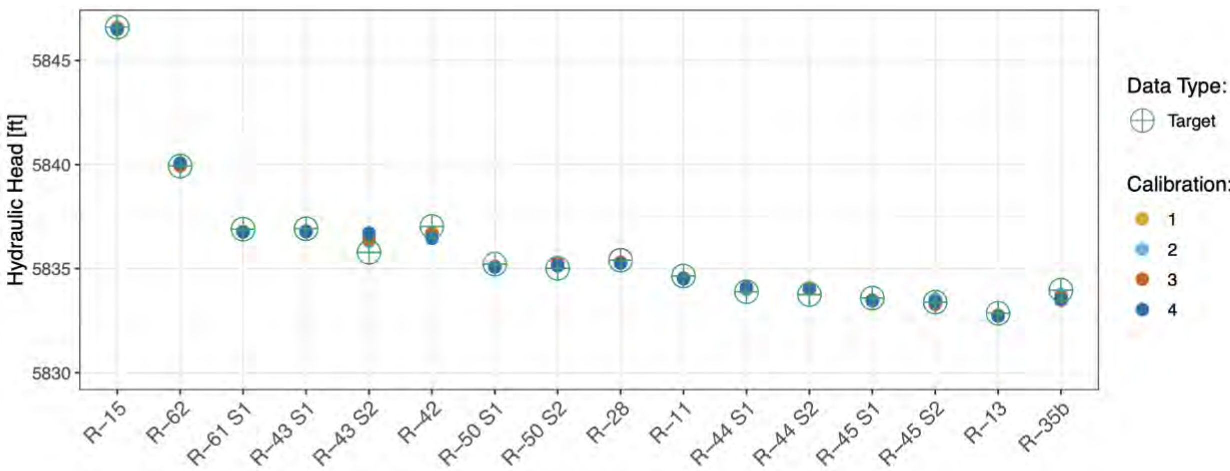

Figure 20. Head targets and calibration results plotted for each well, ordered according to their x-coordinate (i.e., from west to east).

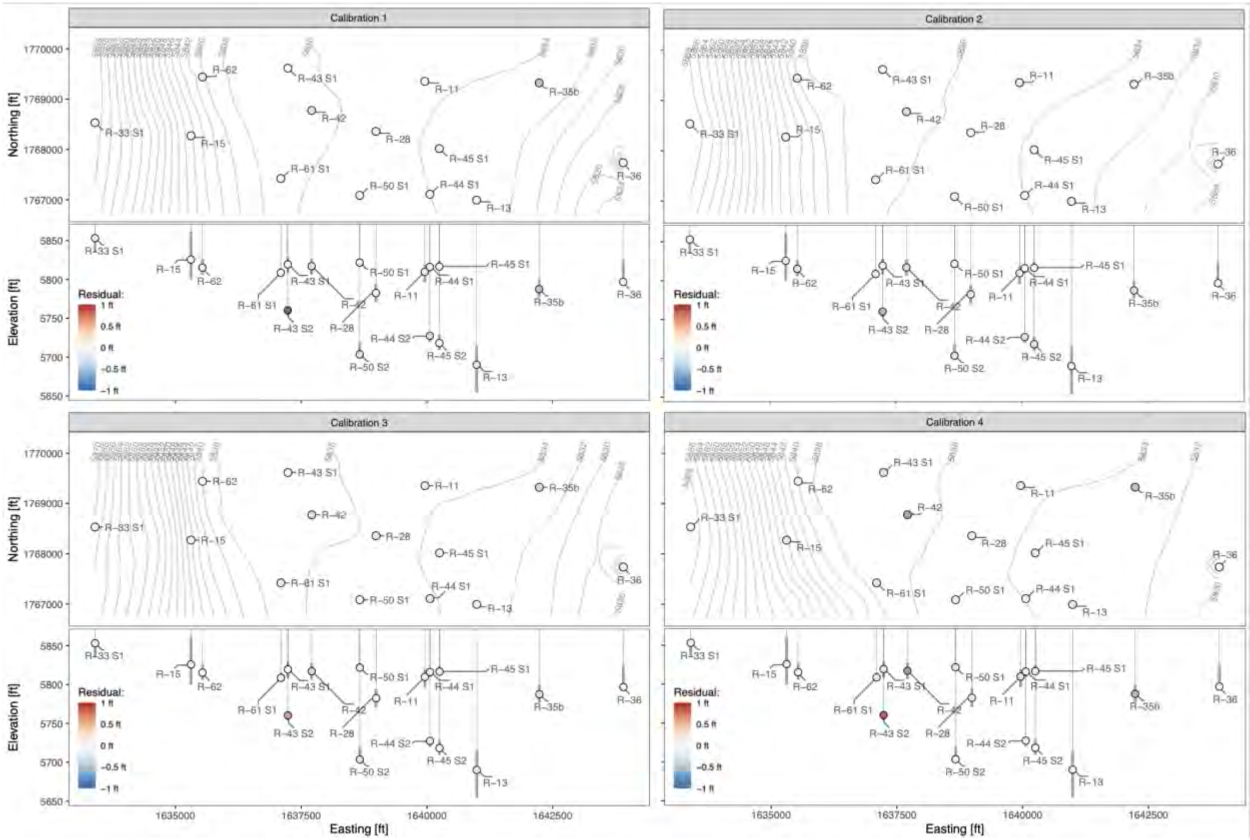

Figure 21. Four calibrated models show close agreement to head data with every residual less than 1 ft as shown by the shading of head measurements in circles. Each calibration shows a plan view of the modeled water-table contours with the upper well screens shown as circles (top) and a cross-section of depth vs. x-coordinate with all well screens as grey bars and the model node for each screen as a circle (bottom).

In addition to the water levels, the hydraulic gradient is also an important target. Gradient targets are helpful to simulate regional flow. Gradients are calculated using sets of three wells and six gradients are used as targets for the CM. Figure 22 shows the hydraulic gradient targets (as black arrows) and the four calibrated LM model results. The simulation gradients are plotted as black arrows and are difficult to see below the target arrows because the results match both magnitude and direction of measured data.

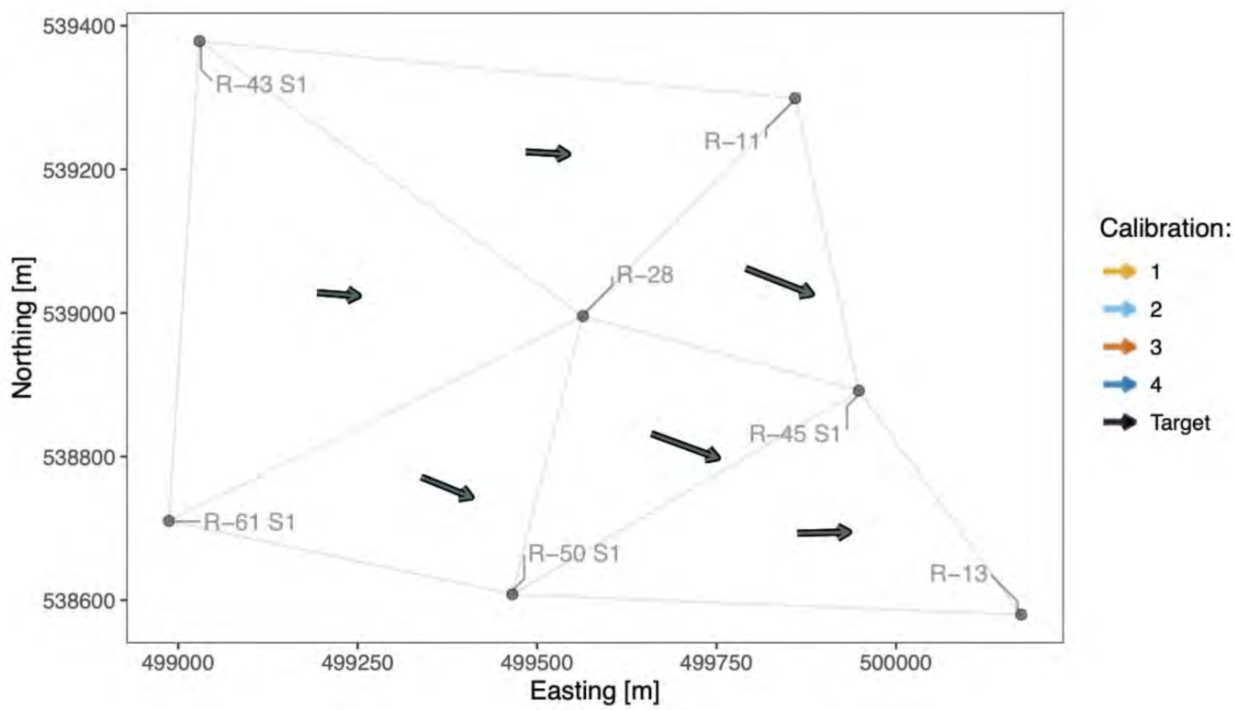

Figure 22. LM calibration results (arrows colored by calibration number) match hydraulic gradient targets (black arrows) almost perfectly in both magnitude and direction. Due to the near-perfect match, many of the underlying arrows are not visible.

Drawdown targets for the three isolated pumping events identified in the pumping record are shown for each response well in Figure 23 as heavier solid lines colored by screen number. Calibration matches are shown as thinner lines, with different calibrations shown as different line types. Most responses at the site are small, with observed drawdown being less than 3 in. in all cases except for the response at R-50 screen 2 during the CrEX-1 pumping event, which was nearly 0.5 ft of drawdown. Matches to the slope of drawdowns are generally closer than the intercept matches, though the overall behavior is matched as seen in the differentiation of multi-screened responses. A notable exception to this differentiation is in Calibration 2, which (though it has the best head residuals) is not effective at differentiating the multi-screened responses in R-44 and R-45, though it does differentiate the strongest observed response between R-50 screen 1 and screen 2.

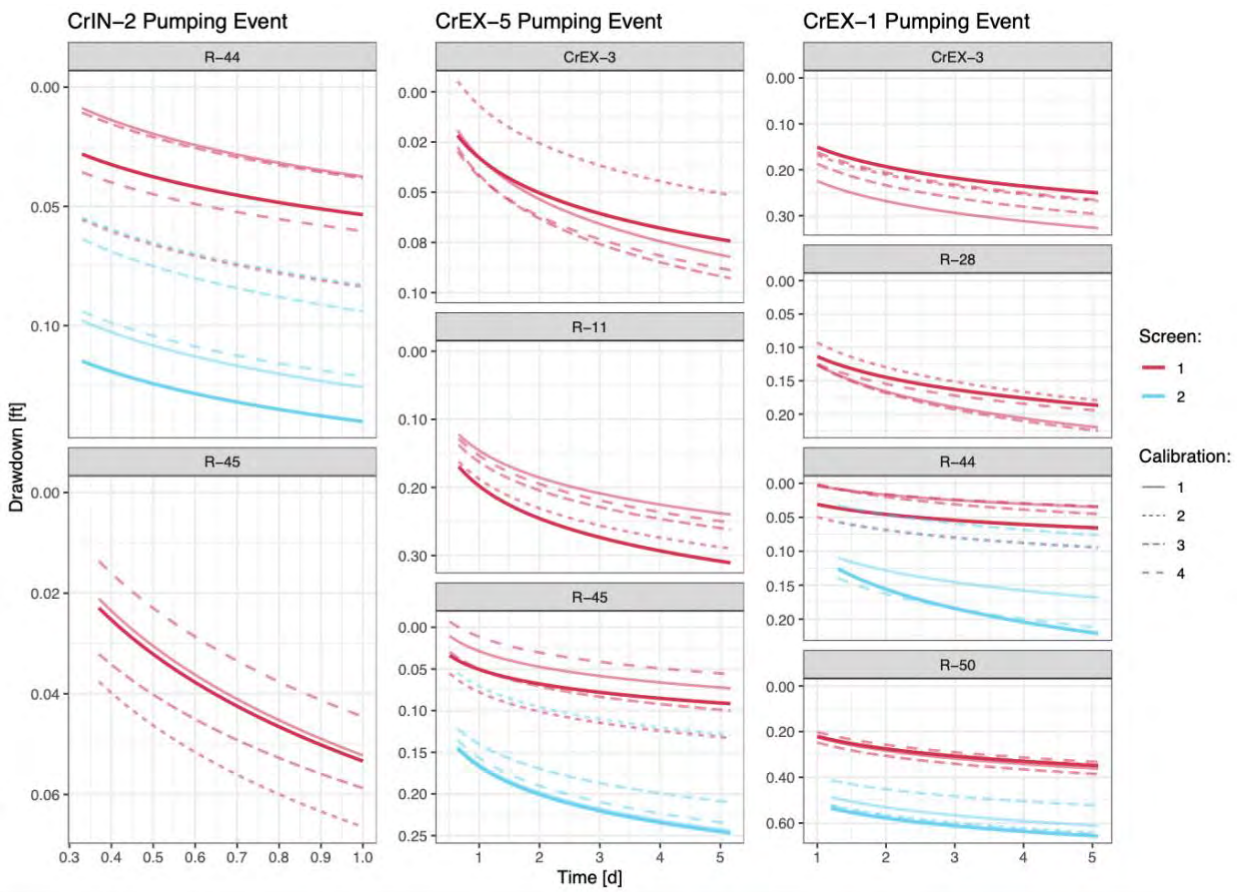

Figure 23. Drawdown responses at monitoring locations to the CrIN-2, CrEX-5, and CrEX-1 pumping events. Observations are plotted as heavy solid lines for each screen and calibration results are plotted thinner with designated line types.

3.1.3 Final source locations

Another important metric that can be used to understand and analyze the LM results involves the source locations in the context of the CSM. Figure 24 shows the final locations in each of the four calibrations of the five hydraulic windows for the LM calibrations (as also shown in Figure 8 under the distributions). The sources have the degrees of freedom to be a wide variety of elliptical shapes, so it is worth noting that the southwest and northwest sources, in all four calibrations, both seem to fit a particular elliptical shape.

The southwest source is the most dramatic, having a long and narrow shape and consistent tilt around 45 degrees to the west. This is likely due to it being responsible for a variety of wells with complex responses at different orders of magnitude.

R-15, CrPZ-4, CrPZ-5, and R-61 (listed from west to east) all have complex, increasing trends at different magnitudes. CrPZ-4 is further from the source but has higher observed chromium than CrPZ-5. To match this variability in observed data, in a flow field constrained by the hydraulic gradients, head conditions, and IM pumping, this window is seemingly forced into this long and narrow shape. Similarly, the consistent elliptical shape of the northwest source is likely driven by the calibration attempting to match the distinct increasing trends at R-62 and R-43 screen 1 and screen 2. It demonstrates more variability, likely because matching three wells with distinct trends is easier, and therefore more flexible, than matching the four wells in the southwest. Both the northwest and southwest sources have arrival times between 2002 and 2006, much later than the primary and secondary sources near the plume centroid.

By contrast, the clean recharge source has a great deal of variability across calibrations, suggesting that there is not enough data to constrain any of the parameters that define it. It ranges from being over much of the plume centroid to being smaller and to the northwest of the centroid. There is also quite a bit of variability in the primary and secondary sources. In calibration 1, they overlap and the recharge source sits over portions of both, likely producing a more cohesive plume with variability in magnitude of concentrations. Calibrations 2 and 3 do not overlap, but the recharge source is over both the primary and secondary windows. In Calibration 4, the primary, secondary, and recharge sources are completely distinct, likely leading to more variability in plume concentrations and potentially even regions of the plume with gaps (i.e., regions with more distinct subplumes than one larger plume). This variability indicates that there is more uncertainty in this region, and many possible parameterizations of sources are possible to match the target datasets.

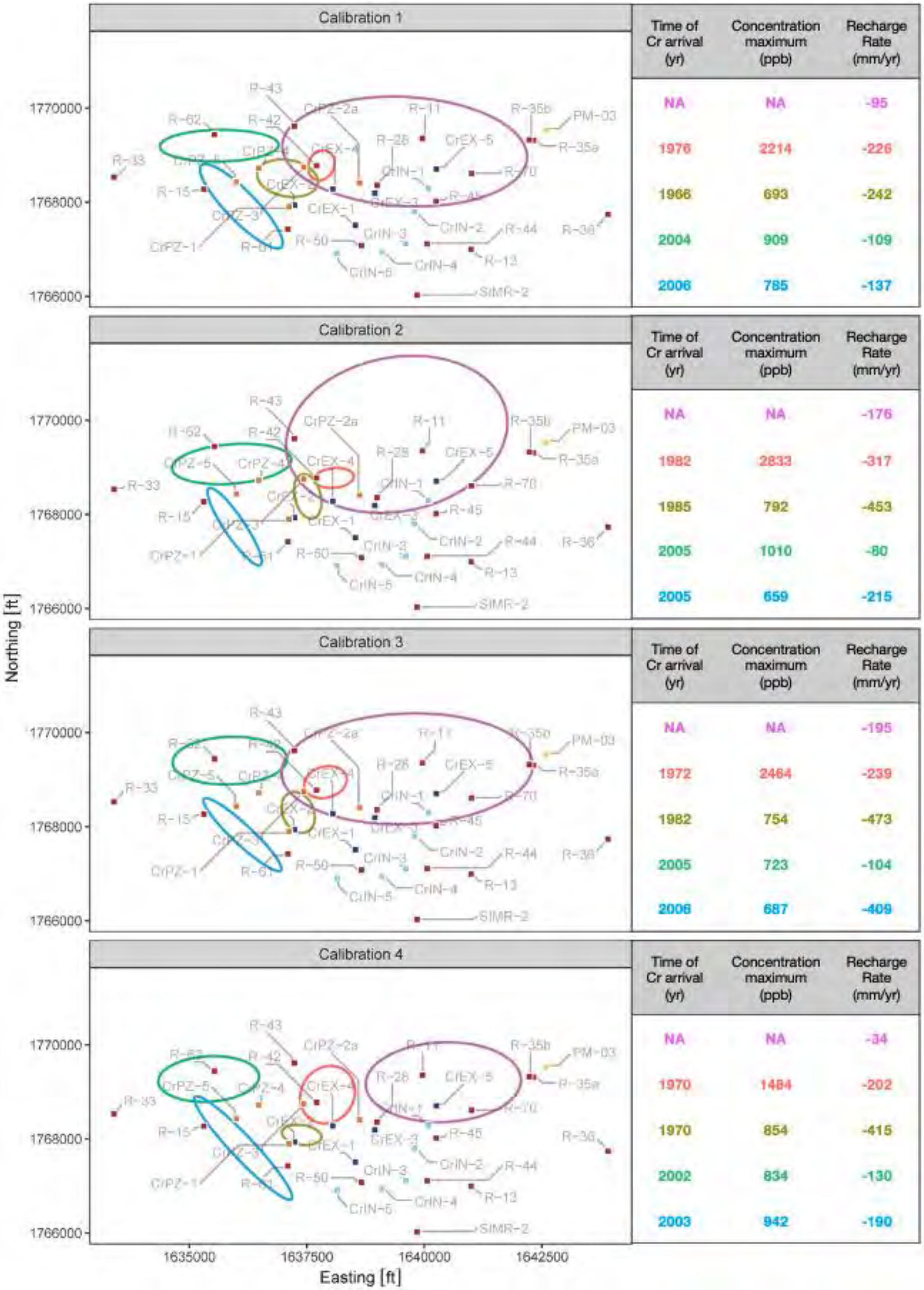

Figure 24. Input parameterizations of the hydraulic windows for the top four calibrations shown with the well locations.

3.2 MCMC Calibration Results

The MCMC approach is employed to quantify uncertainty for future predictions of contaminant locations and concentrations. The MCMC sampler is implemented using an affine-invariant ensemble method, which has been shown to work well when parameters are on very different scales; it can also be significantly faster than other MCMC methods. The MCMC sampler is initialized using the top four LM calibration results presented in the previous section and is run with an ensemble of 60 walkers and 70 iterations, with the first 10 iterations discarded as burn-in. With nine parameters varied within each ensemble, this is well within the recommended rule of thumb of twice the number of walkers as parameters and is shown to be sufficient for convergence (Goodman and Weare 2010).

For each of the four calibration endpoints, one of the 60 walkers is initialized at the LM calibration result, and the remaining walkers are initialized by a draw from a generalized beta distribution defined by a sigma parameter of 0.01, a mean equal to the LM calibration result, and a minimum and maximum defined by the 1st and 99th percentiles of the corresponding prior distribution. In each step of the algorithm, an affine transformation is applied with a tuning parameter, a, and the walker movement takes place in the transformed space. The a parameter provides control over the region of the multi-dimensional parameter space that is explored and thus allows tuning of the walker proposal acceptance rate. After analyzing the movement of the walkers when $a = 2$ is used, this parameterization is found to be appropriate following Foreman-Mackey et al. (2013a); (Foreman-Mackey et al. 2013b). The proposed set of parameter values for an individual walker depends both on the previous parameter set for that walker, and on the position of the other walkers in the ensemble.

The movement of each walker with each iteration was evaluated to ensure convergence. The algorithm had an overall acceptance rate of 36.6%, indicating that the walker moved to the proposed set in 36.6% of all iterations. If the proposed parameter set is rejected, the walker stays in place. Higher posterior density is indicated by parameter sets where the walker remains stuck for multiple iterations. Though the algorithm allows a walker to move from higher to lower likelihood (likelihood that the simulation matches available data), it is much more likely to move towards higher likelihood. This method leads to posterior distributions with higher density in regions that tend to increase the likelihood function, and lower density in regions where results are still possible but less likely. The method gives more weight to parameter sets that are most consistent with observed data but does not exclude the possibility of parameter sets that could, but are less likely to, produce observed chromium concentrations and other model targets.

Marginal posterior distributions for all nine parameters varied in the MCMC sampler are displayed in Figure 25.

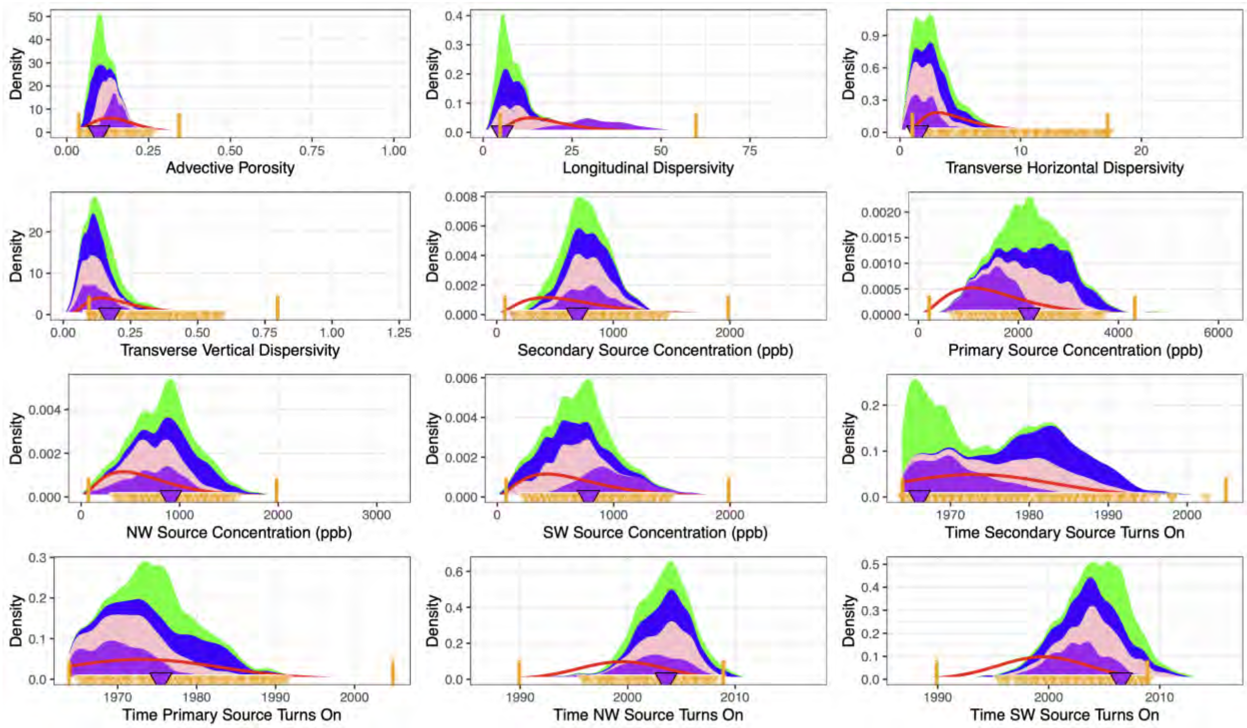

Figure 25. Posterior parameter distributions for the nine parameters varied continuously in the MCMC for each of the four LM endpoints. As an example, the purple triangle represents the initialization point from calibration 1 and the orange triangles represent the initial values of the other walkers in calibration 1's ensemble. The green density plot shows the parameter density for calibration 1, blue shows calibration 2, pink shows calibration 3, and purple shows calibration 4.

Posterior predictive distributions are developed by processing MCMC results into a unique chain of parameter sets for predictive modeling. The chain includes 5804 unique parameter sets that include both the conceptual uncertainty from the four LM calibrations and quantitative uncertainty from the MCMC sampler. Predictive forward runs can then be launched from each unique set, and these predictive forwards will be weighted by the frequency of occurrence of the parameter set from which they were derived, such that predictive runs with better matches to the data occur more frequently in any set of predictive forwards. Predictive forward modeling can help decision makers compare future scenarios or estimate future plume movement under different conditions. These runs are much more useful when they explicitly include uncertainty estimates derived from the posterior parameter distributions shown in Figure 25.

4.0 Conclusions

The chromium site is complex, and the calibrated CM matches observed targets using four distinct parameter sets. This includes concentrations at wells of interest, hydraulic head data, and drawdown responses to infrastructure pumping within the plume. The model also does well against validation data, despite not using these data explicitly in the calibration process. Uncertainty is thoroughly explored using Bayesian methods that include multiple deterministic endpoints defining the flow field, with explicit quantification of uncertainty using an MCMC sampler for all transport parameters. Overall, flow and transport are well parameterized, using plausible values for inputs that are consistent with the CSM, and the model is well suited to be used as a tool to inform decision-making through scenario experiments, capture zone analysis, or optimization of pump and treat systems.

5.0 References

Black, P., et al., 2019. Scaling Input Distributions for Probabilistic Models-19472, *Waste Management 2019 Conference, March 3–7, 2019*, March 3–7, 2019, Phoenix, Arizona

Broxton, D.E., and D.T. Vaniman, 2005. Geologic Framework of a Groundwater System on the Margin of a Rift Basin, Pajarito Plateau, North-Central New Mexico, *Vadose Zone Journal* 4 (3) 522–550

Collins, K.A., et al., 2005. *Los Alamos National Laboratory's Hydrogeologic Studies of the Pajarito Plateau: A Synthesis of Hydrogeologic Workplan Activities (1998–2004),* Los Alamos, New Mexico, December 2005

Doherty, J., 2003. Ground Water Model Calibration Using Pilot Points and Regularization, *Ground Water* 41 (2) 170-177

EPA, 2008. *A Systematic Approach for Evaluation of Capture Zones at Pump and Treat Systems,* EPA/600/R-08/003, United States Environmental Protection Agency, Office of Research and Development, National Risk Management Research Laboratory, Cincinnati OH, January 2008

Foreman-Mackey, D., et al., 2013a. emcee: The MCMC Hammer, *Publications of the Astronomical Society of the Pacific* 125 (925) 306–312

Foreman-Mackey, D., et al., 2013b. emcee: The MCMC Hammer, *Publications of the Astonomical Society of the Pacific* 125 (925) 306-312

Gable, C.W., et al., 1996. *Numerical Grid Generation in Computational Fluid Dynamics and Related Fields*, *Geological Applications of Automatic Grid Generation Tools for Finite Elements Applied to Porous Flow Modeling*, Mississippi State University Press, Jackson, Mississippi

Goodman, J., and J. Weare, 2010. Ensemble Samplers with Affine Invariance, *Communications in Applied Mathematics and Computational Science* 5 (1) 65-80

Heath, R.C., 1983. *Basic Ground-Water Hydrology*, In *prepared in cooperation with the North Carolina Department of Natural Resources and Community Development*, Reston, Virginia

Heikoop, J.M., et al., 2014. Isotopic Evidence for Reduction of Anthropogenic Hexavalent Chromium in Los Alamos National Laboratory Groundwater, *Chemical Geology* 3731–9

Huber, P.J., 1973. Robust Regression: Asymptotics, Conjectures and Monte Carlo, *The Annals of Statistics* 1 (5) 799–821

Keating, E., and G. Zyvoloski, 2009. A Stable and Efficient Numerical Algorithm for Unconfined Aquifer Analysis, *Ground Water* 47 (4) 569–579

LANL, 2008. *Fate and Transport Investigations Update for Chromium Contamination from Sandia Canyon,* LA-UR-08-4702, Los Alamos, New Mexico, July 2008

LANL, 2012. *Phase II Investigation Report for Sandia Canyon,* LA-UR-12-24593, Los Alamos, New Mexico, September 2012

LANL, 2015. *Interim Measures Work Plan for Chromium Plume Control,* LA-UR-15-23126, Los Alamos, New Mexico, May 2015

LANL, 2016. *Groundwater Background Investigation Report, Revision 5,* LA-UR-16-27907, Los Alamos, New Mexico, October 27, 2016

LANL, 2017. *Pilot-Scale Amendments Testing Work Plan for Chromium in Groundwater beneath Mortandad Canyon,* LA-UR-17-25406, EP2017-0091, Los Alamos National Laboratory, Los Alamos NM, July 2017

LANL, 2018a. *Chromium Plume Control Interim Measure Performance Monitoring Work Plan,* LA-UR-18-23082, Los Alamos, New Mexico, April 2018

LANL, 2018b. *Compendium of Technical Reports Conducted Under the Work Plan for Chromium Plume Center Characterization,* LA-UR-18-21450, Los Alamos, New Mexico, March 2018

LANL, 2018c. *Evaluation of Chromium Plume Control Interim Measure Operational Alternatives for Injection Well CrIN-6,* LA-UR-18-23385, EP2018-0060, Los Alamos National Laboratory, Los Alamos NM, April 2018

LANL, 2018d. *Evaluation of Chromium Plume Control Interim Measure Operational Alternatives for Injection Well CrIN-6,* LA-UR-18-23385, Los Alamos, New Mexico, April 2018

McLin, S., 2005. *Analyses of the PM-2 Aquifer Test Using Multiple Observation Wells,* Los Alamos, New Mexico, July 2005

McLin, S., 2006. *Analyses of the PM-4 Aquifer Test Using Multiple Observation Wells,* Los Alamos, New Mexico, January 2006

N3B, 2019. *Semiannual Progress Report on Chromium Plume Control Interim Measure Performance, January through June 2019*, Los Alamos, New Mexico

N3B, 2021a. *Assessment Report for the Evaluation of Conditions in the Regional Aquifer Around Well R-70,* EM2021-0321, Newport News Nuclear BWXT-Los Alamos, LLC (N3B), Los Alamos NM, June 2021

N3B, 2021b. *Assessment Report for the Evaluation of Conditions in the Regional Aquifer Around Well R-70*, Los Alamos, New Mexico

N3B, 2022a. *Fate and Transport Modeling and Risk Assessment Report for RDX Contamination in Deep Groundwater Revision 1,* EM2022-0581, Newport News Nuclear BWXT-Los Alamos, LLC (N3B), Los Alamos NM, September 2022

N3B, 2022b. *Fate and Transport Modeling and Risk Assessment Report for RDX Contamination in Deep Groundwater, Revision 1*, Los Alamos, New Mexico

Neptune, 2023a. *Hydraulic Analysis of the Pajarito Plateau,* EMID-702780, prepared by Neptune and Company Inc. for the U.S. Department of Energy Environmental Management Los Alamos Field Office, Neptune and Company Inc., Los Alamos NM, April 28, 2023

Neptune, 2023b. *Chromium Interim Measure Capture Zone Analysis,* EMID-702782, prepared by Neptune and Company Inc. for the U.S. Department of Energy Environmental Management Los Alamos Field Office, Neptune and Company Inc., Los Alamos NM, January 31, 2023

Toll, N.J., and T.C. Rasmussen, 2007. Removal of Barometric Pressure Effects and Earth Tides from Observed Water Levels, *Ground Water* 45 (1) 101–105

Vesselinov, V.V., et al., 2013. Data and Model-Driven Decision Support for Environmental Management of a Chromium Plume at Los Alamos National Laboratory—13264, *WM2013 Conference, February 24–28, 2013*, Phoenix AZ

Zyvoloski, G., 2007. *FEHM: A Control Volume Finite Element Code for Simulating Subsurface Multi-Phase Multi-Fluid Heat and Mass Transfer,* LA-UR-07-3359, Los Alamos, New Mexico, May 18, 2007

Enclosure 4

Chromium Interim Measure Capture Zone Analysis

Neptune and Company, Inc.
1505 15th St.
Suite B
Los Alamos, New Mexico 87544
720-746-1803
www.neptuneinc.org

16 June 2023

To: Cheryl L. Rodriguez
DOE EM-LA

Please find attached to this letter a copy of the *Chromium Model: Calibrated with Uncertainty through 2022* report for enclosure to the *Annual Progress Report on Chromium Plume Control Interim Measure Performance, April 2022 through March 2023*.

Sincerely,
Lauren Foster

Neptune and Company

Chromium Interim Measure Capture Zone Analysis

16 June 2023

NEPTUNE AND COMPANY, INC.
1505 15th St. Suite B, Los Alamos, NM 87544

EXECUTIVE SUMMARY

Capture and flood zone analyses have been used to determine the interim measures (IM) system impact on the potentiometric surface and chromium plume capture at chromium project area at Los Alamos National Laboratory (LANL or the Laboratory). Multiple lines of evidence based on site data, analytical calculations, and numerical modeling are combined to evaluate system behavior and uncertainty in capture and flood zone estimates for the entire IM system. Note, the analysis presented here is across the full system, which was designed to operate with all wells simultaneously. It is not a well-by-well analysis of hypothetical capture or flood zones for each individual IM well, but an analysis of the IM system as a whole.

Figure 37, replicated in this summary, shows the mean estimated capture zones from four methodologies, two methods based on data only and two methods are based on the chromium model, indicating agreement between lines of evidence and providing confidence in estimated capture. The range of uncertainty for each methods is not included because it obscures the differences between methods, which largely agree with each other, however, it should be noted that all results were explored with uncertainty and only the mean result is shown here.

The target capture zone is achieved for all methods at the southern and southeastern downgradient portions of the plume. This target capture is defined as meeting the IM objectives, which are (a) protection of the southern LANL boundary with the Pueblo de San Ildefonso and maintaining the 50-ppb contour north of that boundary and (b) hydraulic control of the eastern front of the plume (LANL 2015b). While the data-based methods indicate complete capture for the entire chromium plume, a region of concern in the northeastern portion of the plume (near CrEX-5 and R-70) is identified using the particle-tracking and solute transport modeling methodologies. In half of the simulations uncaptured chromium is identified to the north of R-70. This area is identified as a critical data-gap given this uncertainty, and it requires more information to determine whether capture in the northeast portion of the plume near R-70 and CrEX-5 is sufficient or not. This analysis recommends continued IM operation, additional attention to data gaps in the northeast, and continued monitoring in the south and at R-45 S2 to confirm continued IM performance.

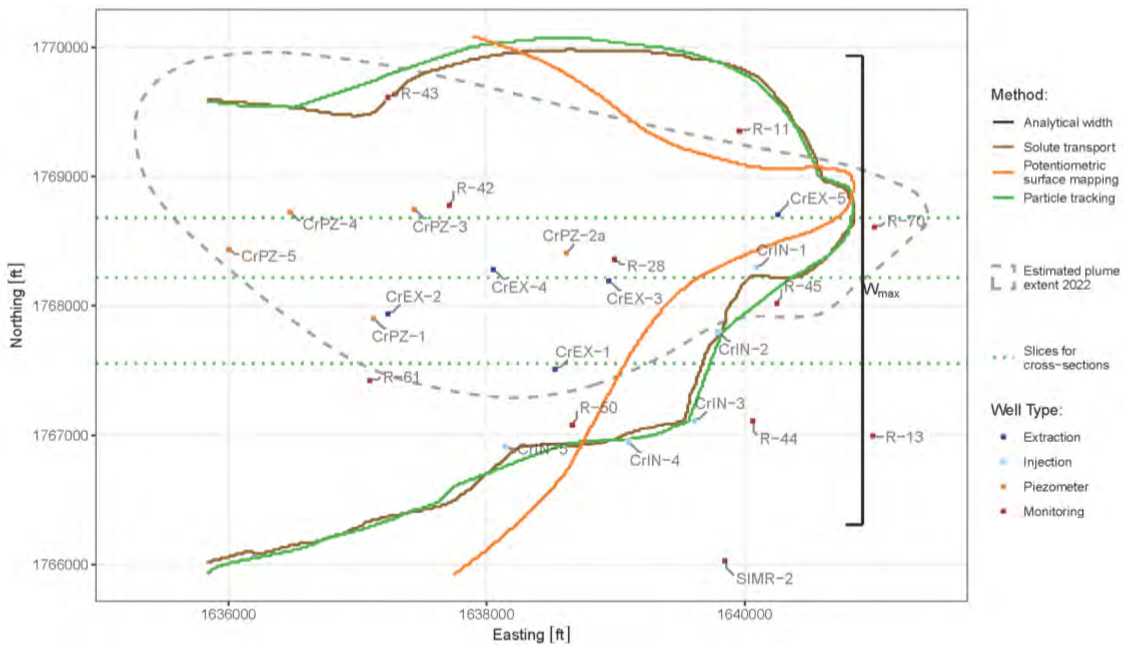

Figure 37 (from main report). Capture zone of the IM during full operation, estimated by multiple methods.

CONTENTS

FIGURES

TABLES

ACRONYMS AND ABBREVIATIONS

amsl	above mean sea level
CM	chromium Model
CrEX	chromium extraction well
CrIN	chromium injection well
CSM	conceptual site model
EPA	(United States) Environmental Protection Agency
FEHM	Finite Element Heat and Mass (flow and transfer code)
IM	Interim Measures
LANL	Los Alamos National Laboratory
LM	Levenberg-Marquardt (algorithm)
MADS	Model Analysis and Decision Support (software)
MCMC	Markov Chain Monte Carlo
OF	objective function
ppb	parts per billion
SCADA	Supervisory Control and Data Acquisition
TA	Technical Area
VZ	vadose zone

1.0 Introduction

This report presents capture and flood zone analyses that were conducted to evaluate the effectiveness and performance of the hexavalent chromium (Cr^{6+}, represented as chromium in this document) plume interim measure (IM) at Los Alamos National Laboratory (LANL). Figure 1 shows the approximate plume area, monitoring wells, and IM injection and extraction wells.

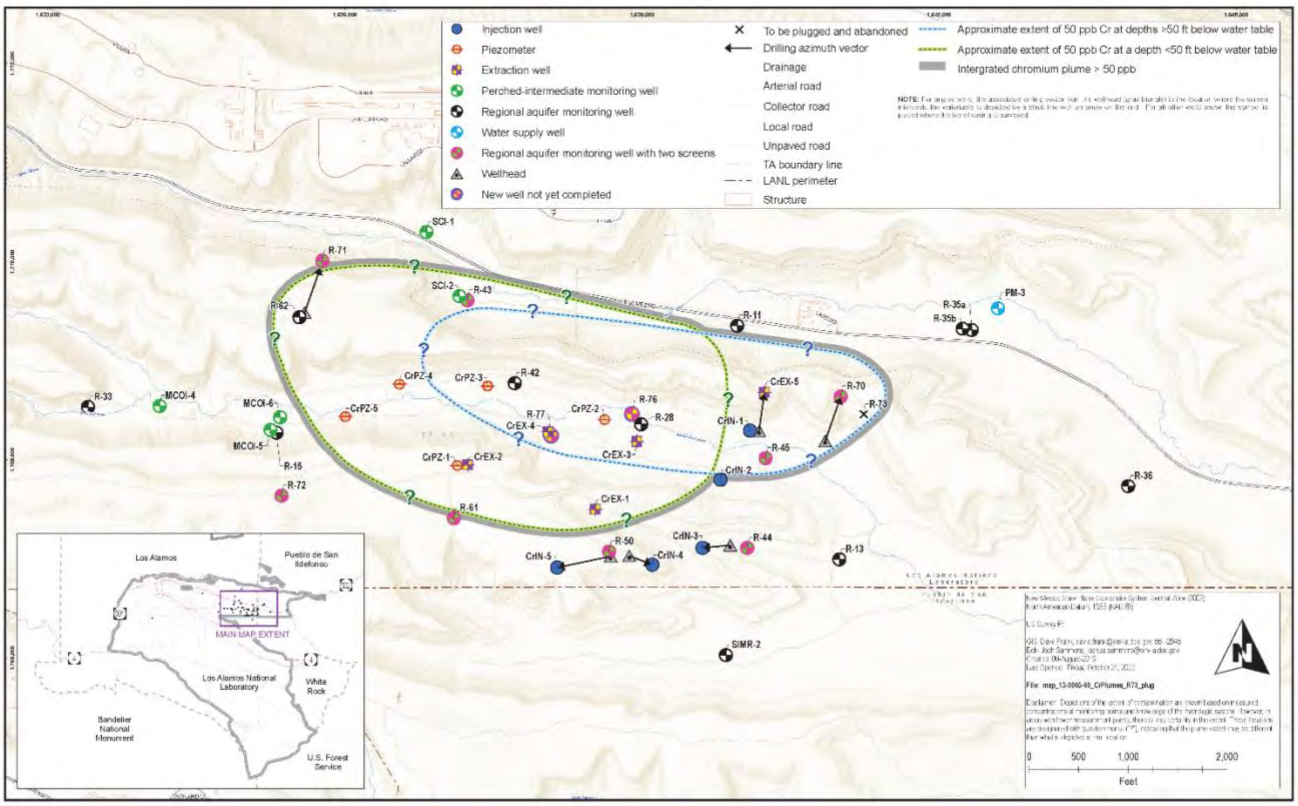

Figure 1: Chromium plume site location and area discussed in this report.

Methods for the systematic evaluation of pump and treat systems using multiple lines of evidence are given in EPA (2008). The process is described therein as iterative, since additional data and information to inform analyses become available as the system operates. Identifying data gaps and installing additional monitoring wells is part of the iterative process.

The six steps to capture zone analysis given in EPA (2008) are:

1. Review site data, the conceptual site model (CSM), and remedy objectives
2. Define the target capture zone
3. Water level data analysis
4. Analytical and numerical models
5. Evaluate concentration trends
6. Interpret capture based on steps 1-5, assess uncertainties and data gaps.

The EPA guidelines emphasize the need for multiple converging lines of evidence, because "each of these techniques is subject to limitations, and, in most cases, no single line of evidence will conclusively differentiate between successful and failed capture" (p.4). The use of multiple techniques aids in increasing confidence in the conclusions of the capture zone analysis.

1.1 Site Data

At the chromium project area, a network of 28 monitoring well screens (22 wells) and 10 infrastructure wells (five extraction "CrEX" and five injection "CrIN" wells) provide concentration and water-level data. Information collected from the well network is essential to understand nature and extent of the chromium plume and to inform the CSM. Wells shown in Figure 1 provide geologic information (from borehole stratigraphy and some geophysics), aquifer properties estimated from pumping tests, hydraulic head collected with automated pressure transducers, and groundwater analytical data from environmental sampling. Barometric pressure, temperature, and other environmental data are collected at several weather stations around the site.

1.2 Conceptual Site Model

The chromium plume area CSM has been developed over years of observations and investigations at the site, e.g., (Heikoop et al. 2014; LANL 2008, 2009a, 2012, 2015b, 2018a, 2018b, 2018c; N3B 2021a). A longer explanation of the CSM as it affects the model construction is provided in the model documentation (Neptune 2023a).

After discovery of the plume at R-28 in 2005, and identification of the likely chromium plume location in subsequent years as more monitoring locations were established, a workplan to install an IM pump and treat system was published in 2015 (LANL 2015b). This work plan proposed six injection locations and four extraction locations to create hydraulic control at the leading edge of the plume and prevent further migration. CrEX-5 (northeast region of the plume in Figure 1) was originally designed as an injection well, CrIN-6, but the first samples near the end of 2017 identified concentrations of chromium at ~250 ppb and the well was converted into an extraction well. This decision was informed by modeling analyses that indicated better conformance with IM objectives in that configuration (LANL 2018c). The full IM system (5 extraction wells and 5 injection wells) began operating near capacity in November 2019. Besides typical variability in equipment and operations, the IM system was run continuously until October 2022 with one extended shutdown from April to July, 2020 as a result of the pandemic.

The overall hydraulic gradient at the site is generally from west to east or slightly southeast. The chromium plume area water table is 10-100 times flatter than the region immediately upgradient (west) and downgradient (east) of the plume. Sitewide water table maps are presented in (LANL 2008, 2012, 2017; N3B 2020b) and local chromium plume area maps and hydraulic gradients are discussed extensively (Neptune 2023b).

In terms of geology, the shallow portion of the regional aquifer at the chromium plume lies mostly within the Puye (Tpf) and pumiceous Puye (Tpf(p)), however a few monitoring wells penetrate below these and into the upper portions of the underlying Miocene sediments (also known as the upper Santa Fe sediments, or Tcar), where pumiceous Miocene sediments (Tjfp) are also found. While the Puye Formation is over a thousand feet thick in the western portion of the aquifer (LANL 2018, 602963), near the chromium plume it is only a few hundred feet thick. Few wells have been constructed into the Tcar, due to chromium contamination being historically thought to be largely restricted to the first 100-150 ft of the water table surface, within the Puye formation.

1.3 Interim Measures Objectives

The Interim Measures Work Plan for Chromium Plume Control (LANL 2015b) (IM Work Plan) was developed to outline the steps taken to “control chromium migration in groundwater while long-term corrective action remedies are being evaluated” (p.1). The objectives and associated metrics of the IM Work Plan are:

1. To achieve and maintain the 50 part per billion (ppb) downgradient plume edge within the laboratory boundary; metric: reduction of chromium at R-50 to under 50 ppb within 3 years.
2. Hydraulically control plume migration in the eastern, downgradient portion of the plume.
3. Utilize information obtained from the IM to refine the hydrogeologic understanding of the site (i.e., investigation through remediation).

The objectives note that “pumping conducted for hydraulic control will also incidentally reduce the mass of chromium within the regional aquifer, but mass removal is not specifically an objective of this IM” (p.1). The process is intended to include “adaptive management of the extraction and injection system as necessary” (LANL 2018b), p.1. As additional data became available in the eastern part of the plume at proposed injection well CrIN-6, an evaluation was performed to also consider protection of water-supply well PM-3 in addition to the objectives above (LANL 2018c). The results of that evaluation resulted in changing CrIN-6 to extraction well CrEX-5.

1.4 Target Capture Zone

EPA (2008) defines a CZ as “the three-dimensional region that contributes the groundwater extracted by one or more wells or drains.” The CZ is distinct from the well’s zone of influence (ZOI), defined by the cone of depression or extent of drawdown. Figure 2 (from EPA (2008)) shows the distinction between the two for a simplified system. Note that conceptualizing a capture zone as a well-defined region of space implies a steady-state flow field, as a changing flow field (due to, for example, increasing pumping rates) would have a time-dependent capture zone.

Hydraulic analysis of the ZOI and drawdown response to pumping are crucial to understand the effects of IM operation with respect to gradient directions, changes, and impacts on the flow system. However, because ZOI and drawdown pumping response is not directly equivalent to contaminant capture and containment (i.e., impact on transport), the capture zone analysis here is conducted in three dimensions to fully evaluate the system performance.

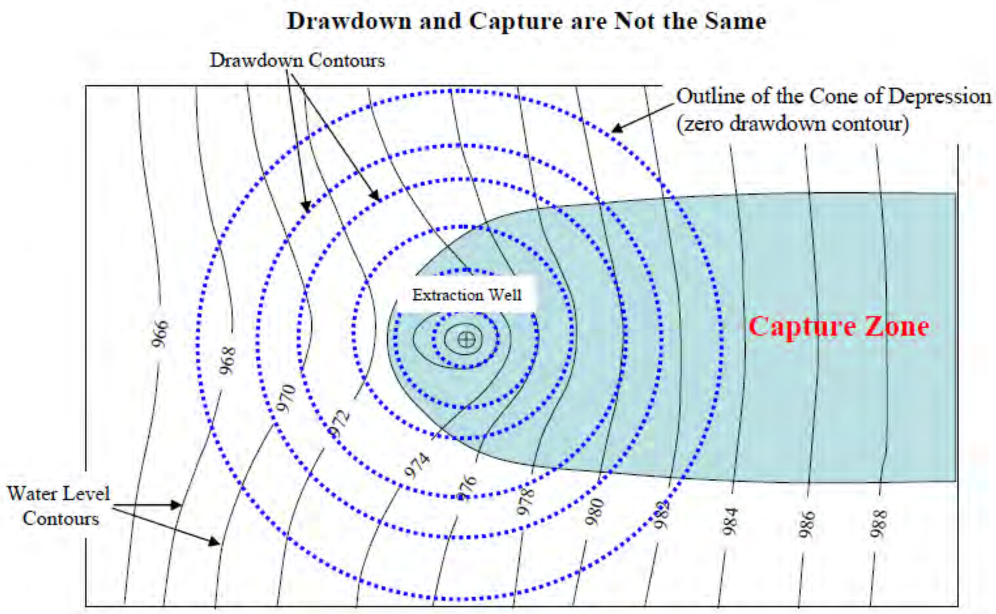

Figure 2. Comparison of the zone of hydraulic influence (ZOI) caused by drawdown at a pumping well, and its capture zone (CZ) for contaminant containment. From EPA (2008), Figure 6.

The target capture zone is defined by EPA (2008) as "the three-dimensional zone of ground water that must be captured by the remedy extraction wells for the hydraulic containment portion of the remedy to be considered successful. This will depend on the site-specific remedy objectives (Step 1)" (p.6). The IM objectives outlined in Section 1.3 specified (a) protection of the southern LANL boundary with the Pueblo de San Ildefonso and maintaining the 50-ppb contour north of that boundary and (b) hydraulic control of the eastern front of the plume. All references to success or failure relative to the "target capture zone" in this document refer specifically to those objectives. The objectives of the IM did not include a particular spatial goal or "target capture zone" for those regions with chromium concentrations less than 50 ppb, other than to keep them within the LANL boundary. However, the results presented here can be used to help understand how much change or optimization of the IM would be required to meet future of the management goals.

2.0 Water-Level Data Analysis

This section presents methods used for hydraulic data analysis as described in EPA (2008). Following the guidelines in that document, hydraulic head measurements under both ambient and IM pumping conditions are used to:

- Generate water level/piezometric head maps to evaluate flow directions (Section 2.1)
- Evaluate gradients based on well screen pairs (vertical gradients) and triples (horizontal gradients) (Section 2.2)

This section focuses on describing the methods used with examples to demonstrate all aspects of the analysis. A synthesis of all lines of evidence, including those discussed in this section, is presented in Section 5.0.

2.1 Potentiometric Surface Mapping

Water level head (or potentiometric surface) mapping is one tool for evaluating pumping well capture zones at the water table. The steps to this analysis include (1) data selection, (2) contouring of the head measurements, (3) drawing flow lines perpendicular to contours, and (4) finding the envelope for which flow lines terminate at the extraction wells, i.e., the capture zone. Velocities interpreted from gradients and groundwater table maps are discussed in Section 3.3.

In the first step, data is selected for the analysis and the time(s) of interest are identified relative to activities at the site. The most appropriate application of either synoptic measurements (water-levels measured as close as possible to the same moment in time) or averaging periods is decided. Synoptic maps represent single moments in time and have the benefit of identifying transient effects that might not be represented in an average depiction of water-levels, such as changes in pumping, recharge, and barometric pressure. However, there is inherent variability in water-level measurements, such as small fluctuations in transducer outputs that may affect the interpretation of water-table maps in relatively flat areas of the potentiometric surface, such as the chromium project area. Synoptic measurements are typically easy to apply at the chromium site due to the high frequency of automated water level data collection (generally every 1-2 hours or more frequent). Conversely, averaging over an appropriate time period (e.g., over a time when pumping is consistent) has the benefits of smoothing spurious water-level measurements that may occur at synoptic times, as well as effects from variability in pumping rates at IM wells or activities at monitoring wells (such as sampling for chemical concentrations). For wells that respond to barometric pumping with similar barometric efficiency, averaging across barometric fluctuations has the same effect of barometric pressure on synoptic maps: i.e., the absolute water levels may be higher or lower than the actual barometrically corrected values, but relative relationships on the water table maps are maintained as the barometric fluctuations impact water levels equally. This is generally the case based on the construction of the chromium area wells, which are generally observed to have high barometric efficiencies of 90-100%, e.g., (LANL 2009b), and the style of their pressure transducers which are vented or “gauge” type (LANL 2015a).

Synoptic times corresponding to ambient conditions as well as IM pumping conditions were selected for the chromium project area capture zone analysis. Table 1 gives the times selected for synoptic water table mapping, the rationale for the time selected, and the associated IM pumping conditions. Figure 3 shows IM pumping from January 1, 2020 to November 8, 2021, with the selected synoptic map times marked, as well as several monitoring well hydrographs from locations near the IM wells. The baseline map date of 5/1/20 was selected because it represents an approximate baseline equilibrium after the shut-down of the IM on 3/23/20. The Full IM date of 6/15/21 was selected because it represents the longest period of time (at the time of this analysis) in which all 10 infrastructure wells had been in consistent operation. The 11/1/21 date, which was during a period of when 8 out of 10 IM wells were in operation (all but CrEX-1 and CrIN-3), was selected for comparison to the Full IM.

Data selection also includes the identification of appropriate wells for the maps. Water level data from the 10 IM wells themselves may not be used because they are reflective of within-borehole conditions and may not represent aquifer conditions immediately outside the borehole. Table 2 shows the categorization of monitoring screens into shallow well screens and deeper well screens. These are interpolated independently for water table maps to compare hydraulic head response to the IM at two depth intervals.

For the well screens listed in Table 2, at the synoptic times listed in Table 1, there were no deviations from the 1:00 AM synoptic times except for 1:01 AM measurements at R-70 S1, R-70 S2 (all dates), and R-42 (5/1/20). All data were obtained from the Intellus database (https://www.intellusnm.com/index.cfm).

Table 1.
Times selected for synoptic water-table maps, and IM well pumping rates (gpm)

Date	Reason	EX-1	EX-2	EX-3	EX-4	EX-5	IN-1	IN-2	IN-3	IN-4	IN-5	Total (EX)	Total (IN)
5/1/2020 1:00 AM	Baseline map	0	0	0	0	0	0	0	0	0	0	0	0
6/15/21 1:00 AM	Full IM Operational	66	61	22	57	70	-65	-64	-31	-55	-57	276	-272
11/1/21 1:00 AM	Full IM except CrEX-1 and CrIN-3	0	68	12	55	71	-53	-53	0	-50	-51	206	-207

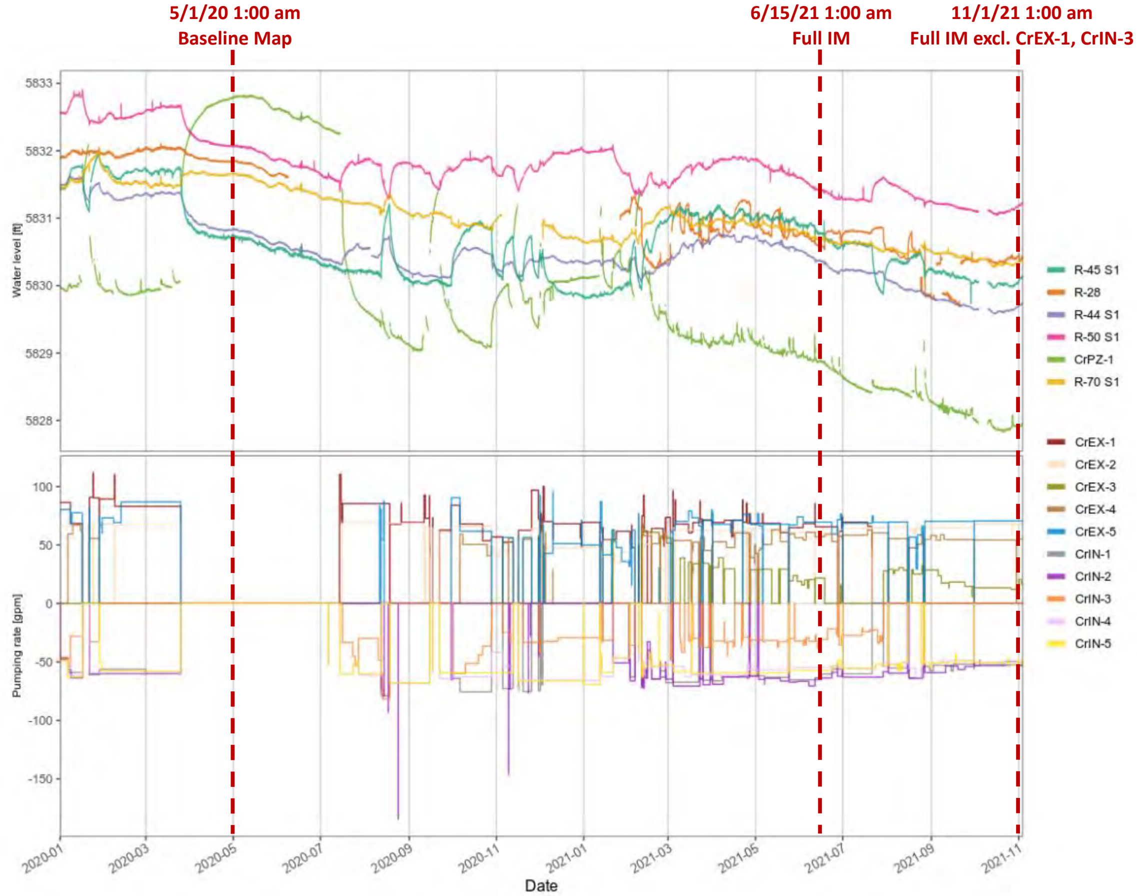

Figure 3. Times selected for synoptic water table maps to compare the effects of the IM between a baseline (no pumping) and full or nearly full IM operation. Top panel: water levels at select wells affected by IM pumping. Bottom panel: IM pumping and injection. Extraction is positive; injection is negative.

Table 2.
Well locations used for water-table maps

Shallow Screens	Comments	Deep Screens	Comments
CrPZ-1		CrPZ-2b	Shallower than other S2's
CrPZ-2a		R-13	Crosses Tpf/Tpf(p)/Tjfp
CrPZ-3		R-33 S2	Excluded when PM-4 is pumping
CrPZ-4		R-43 S2	Entirely in Tcar
CrPZ-5		R-44 S2	
SIMR-2		R-50 S2	
R-1		R-61 S2	
R-11		R-70 S2	
R-13	Deeper than other shallow screens; crosses Tpf/Tpf(p)/Tjfp		
R-15	Longer than most shallow screens, crosses Tpf/Tpf(p)/Tjfp		
R-28			
R-33 S1			
R-35b			
R-42	In Tjfp		
R-43 S1	Straddles Tjfp/Tcar, mostly in Tcar		
R-44 S1			
R-45 S1			
R-50 S1			
R-61 S1			
R-62	In Tjfp		
R-70 S1			

R-36 was excluded from consideration in the hydraulic head maps due to uncertainty associated with mounding at this location, discussed in (LANL 2009a). R-35a was also excluded because its screen is located in a different hydrostratigraphic regime and, unlike all other chromium plume area monitoring wells, is strongly impacted by PM-3 pumping. As described in LANL (2008), R-9 and R-12 (located in the Miocene basalt and possibly representative of a deep compartmentalized zone), and R-4 and R-24 are also excluded due to their locations in different hydrostratigraphic regimes. Data from R-33 S2 is useful for constraining the deep map's western edge, but it is strongly affected by PM-4 pumping at a magnitude much greater than the immediate chromium site area wells (~7 ft of drawdown during PM-4 pumping), so data from R-33 S2 is not used while PM-4 is active. Future wells can be added to the chromium area water level maps after installation is complete and transducer measurements are available.

Contouring water level data may be done using manual, hand-drawn methods or automated interpolation tools. Both methods have been applied at the chromium site, with hand-drawn methods aided by automated calculations of gradient vectors using the three point method (Heath 1983). EPA (2008) notes, "There are many different approaches to contouring measured water levels. The interpolation or mapping approach is probably most common. Some prefer contouring by hand, while others prefer using computer-based contouring algorithms… In either case, vastly different (yet reasonable) interpretations of flow direction and capture may be inferred from the same water level data, based on the interpolations (between data points) and extrapolations (beyond data points) associated with the evaluation. Whether contouring is performed by hand or is computer-based, the results should be evaluated for hydrogeologic reasonableness" (p. 13). It is also noted that advantages to hand-contouring are the inherent inclusion of professional judgement, while disadvantages include lack of reproducibility and time-consuming map preparation. This makes it more difficult to generate many maps for evaluating differences (subtraction maps), where differences may be due to hydrologist interpretation rather than the data. On the other hand, computer-based contouring is reproducible and faster, making difference or comparison maps easier to generate and interpret. EPA (2008) notes that control points or "pseudo-data points" may be used to incorporate professional judgement, just as in hand drawn mapping. Storing control point information digitally can preserve reproducibility thus combining the benefits of hand-drawn and automated methods.

Automated contouring algorithms typically contain multiple parameters for smoothing that need to be selected and different algorithms can produce different results. Some advanced methods for automated contouring include Bayesian techniques for including prior information (e.g., Carson et al. (2020), as well as conditioning based on model results or physical principles such as groundwater flow direction (e.g., Rivest et al. (2008).

The maps in this analysis were hand-contoured to assure the reasonableness of the potentiometric surface and incorporate expert opinion.

2.1.1 Shallow Potentiometric Contours

The three-point solution method (EPA 2014) combined with hand-contouring was used on monitoring well triplets across the area, as shown in Figure 4 for a time in which the IM had been operating at capacity for a significant period of time (June 15, 2021, 1:00 am; see Table 1 and Figure 3). In this method, gradient vectors are calculated for each triplet using the method of Heath (1983); markers are provided as guidelines along the sides of the triangles using an assumption of equally spaced contours; and then a hydrologist provides a hand-drawn interpretation using the markers and gradient vectors as guides (generally perpendicular to contours).

The three-point method is performed under the assumption of planar (horizontal) flow, which does not occur near active extraction and injection wells (EPA 2014). When an active IM well is located near a well triplet composed of nearby monitoring wells, the gradient vector derived at that location is not reliable. Therefore, gradient vectors in Figure 4 from triplets surrounding pumping and injection are not shown.

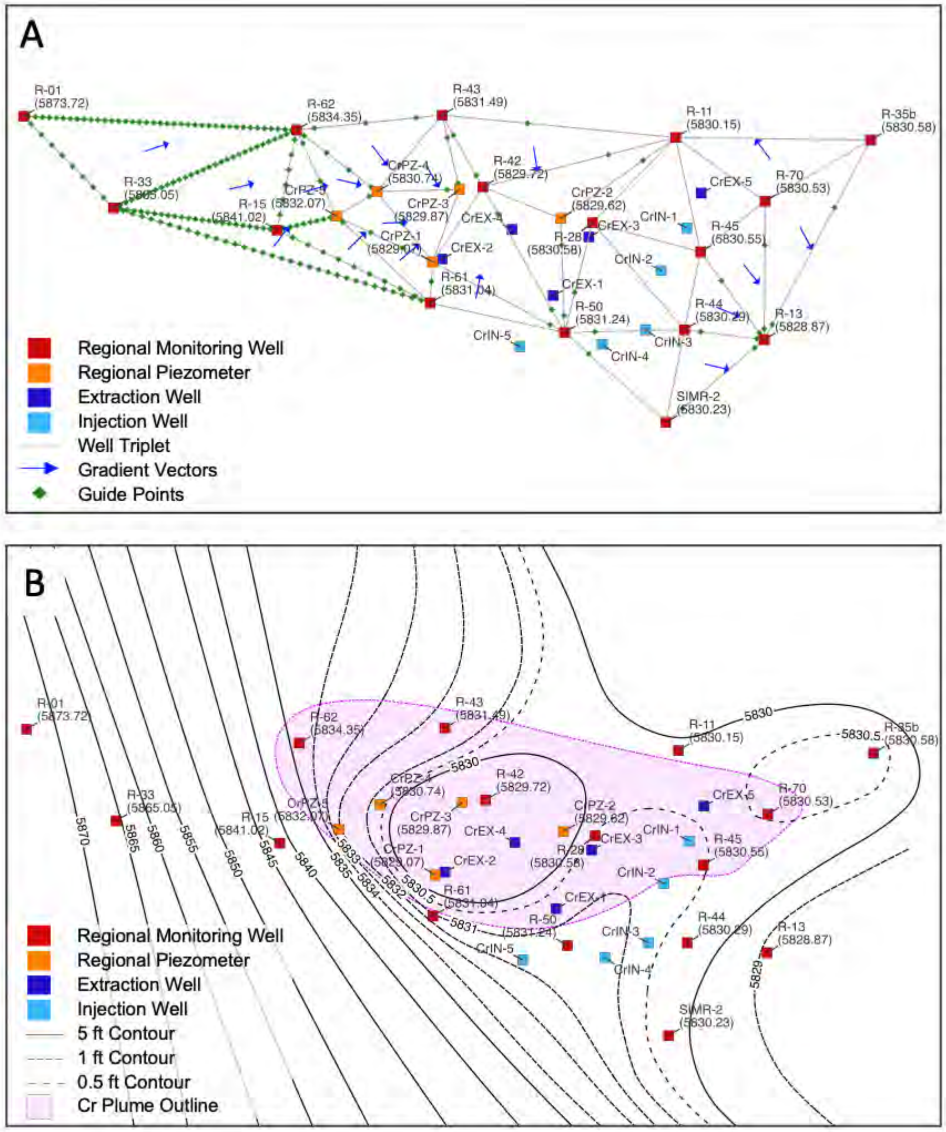

IM Well	Pumping Rate
CrEX-1	66 gpm
CrEX-2	61 gpm
CrEX-3	22 gpm
CrEX-4	57 gpm
CrEX-5	70 gpm
CrIN-1	-65 gpm
CrIN-2	-64 gpm
CrIN-3	-31 gpm
CrIN-4	-55 gpm
CrIN-5	-57 gpm

Figure 4. A) Water table mapping method using three-point gradient vectors (EPA 2014), and midline markers as guide points (green dots). The map for June 15, 2021 1:00 AM includes full IM operation (pumping and injection at all CrIN/CrEX wells) at the indicated rates. Note that gradient vectors calculated during pumping and injection violate the assumptions of the three-point method (EPA 2014). B) Water level contours for June 15, 2021 at 1:00 AM based on the three-point method, with the outline of the chromium Plume shown (pink)

A 0.5 ft contour is added to this map. While the data are sparse in the eastern area, the 0.5 ft contour has been interpreted to disconnect the higher values seen in the R-35b/R-70 area from the rest of the ridge to the southwest. As discussed below, the baseline map includes a slight mound/ridge connecting R-70 and R-35b (in the absence of IM activity), which has been previously noted in the context of mounding at R-35b (LANL 2009a). Hydrographs indicate that CrEX-5 causes drawdown at surrounding monitoring wells R-70 S1, R-45 S1, and R-11 (see (N3B 2021b). Therefore, the ridge in the 0.5 ft contour is more plausible than a fully connected 5830.5 ft contour around R-35b.

CrEX-1 and CrEX-3 are outside the apparent integrated cone of depression created by the extraction wells. CrEX-1 is located near the CrIN injection front and the nearest shallow screen monitoring well (R-50 S1), which shows a rise in water levels due to injection. It is uncertain exactly where the 5830 and 5830.5 ft contours fall relative to CrEX-1, but it is likely that the cone of depression is contiguous to the location of CrEX-1. Due to a relatively high water level at R-28, CrEX-3 is outside the integrated cone of depression. It has previously been observed that R-28, under baseline conditions, has higher water levels than upgradient well CrPZ-2, creating uncertainty in the reliability of measured water levels at R-28 and CrPZ-2. Although R-28 has been impacted by amendment injections, its data are included in the interpretation of the water table based on expert judgment, recognizing that its exclusion would significantly change the interpreted location of the integrated cone of depression.

To interpret capture around pumping wells vectors are drawn perpendicular to the derived head contours. Figure 5 shows the flow net built by evaluating the underlying water level map. A capture zone can be inferred by the vectors that point towards the cone of depression and/or extraction wells.

IM Well	Pumping Rate
CrEX-1	66 gpm
CrEX-2	61 gpm
CrEX-3	22 gpm
CrEX-4	57 gpm
CrEX-5	70 gpm
CrIN-1	-65 gpm
CrIN-2	-64 gpm
CrIN-3	-31 gpm
CrIN-4	-55 gpm
CrIN-5	-57 gpm

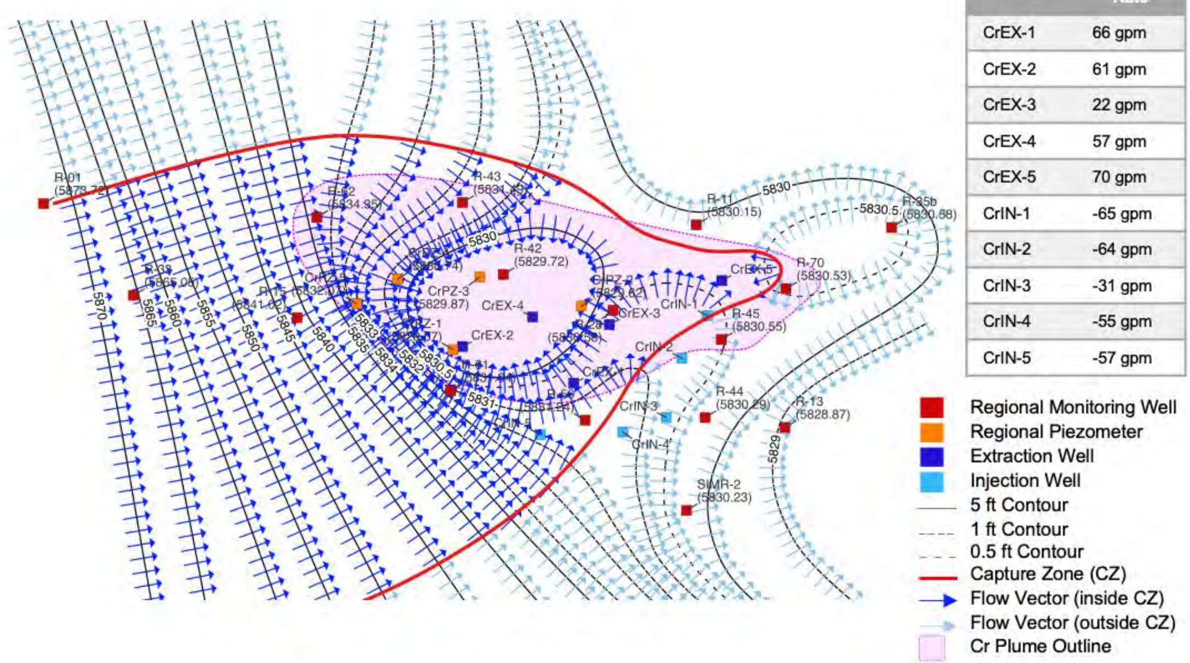

Figure 5. Capture zone interpretation based on vectors perpendicular to the water-table contours shown in Figure 4. The map for June 15, 2021 1:00 AM includes full IM operation (pumping and injection at all CrIN/CrEX wells) at the indicated rates.

Interpreting capture from water table/hydraulic gradient maps must be done with caution (EPA 2008). For example, the assumption that flow lines are perpendicular to water level contours is invalidated by anisotropy. Additionally, the hand-drawn maps themselves are an interpretive product, as described above, and therefore conclusions drawn from them are at least partially based on a subjective interpretation of the data, especially in a region with sparse data and flat gradients. When using synoptic snapshots in time, transient influences and temporal variability in water-level measurements need to be considered in a more holistic interpretation of the IM system capture zone. The effects of temporal variability on gradients formed using the three-point method are explored in Section 2.2.

Figure 6 shows a water table map for an active period of the IM (11/1/21 at 1:00 am) where only CrEX-1 and CrIN-3 were not operational (see Table 1 and Figure 3). In this map, the central cone of depression appears somewhat smaller, and the ridge effect is still pronounced, even without CrIN-3 injection. Figure 7 shows the capture zone interpreted from flow vectors perpendicular to the contours for the same water-level contour map.

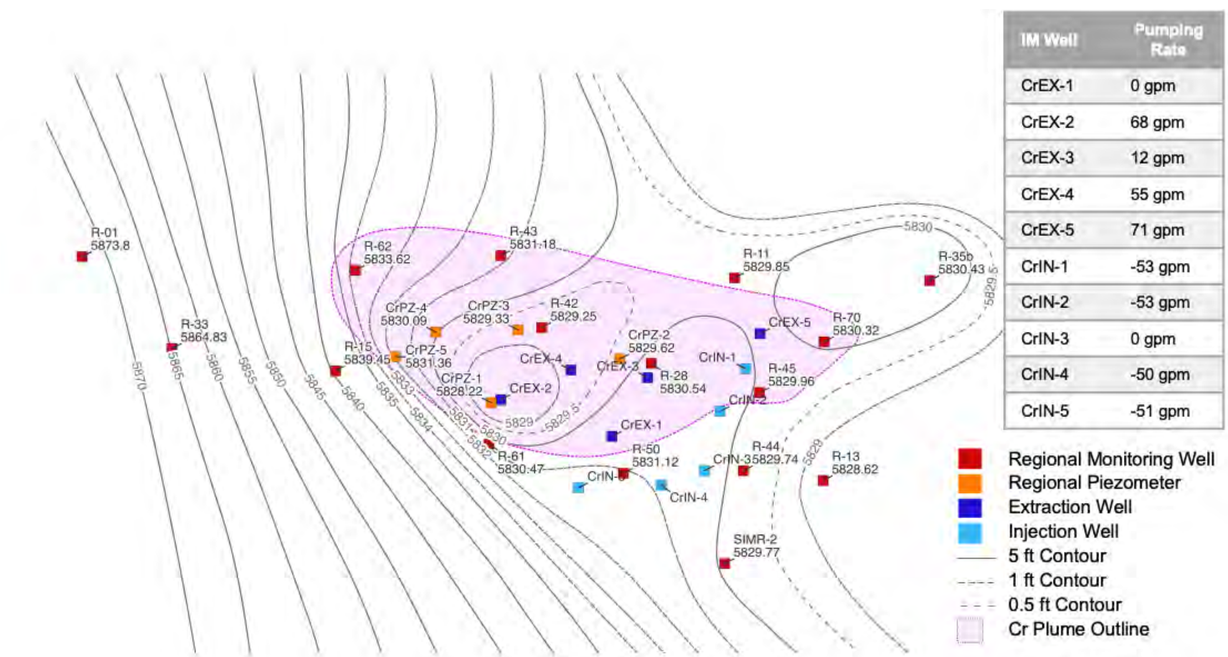

Figure 6. Water table map for November 1, 2021 1:00 am, which includes nearly full IM operation (with the exception of CrEX-1 and CrIN-3).

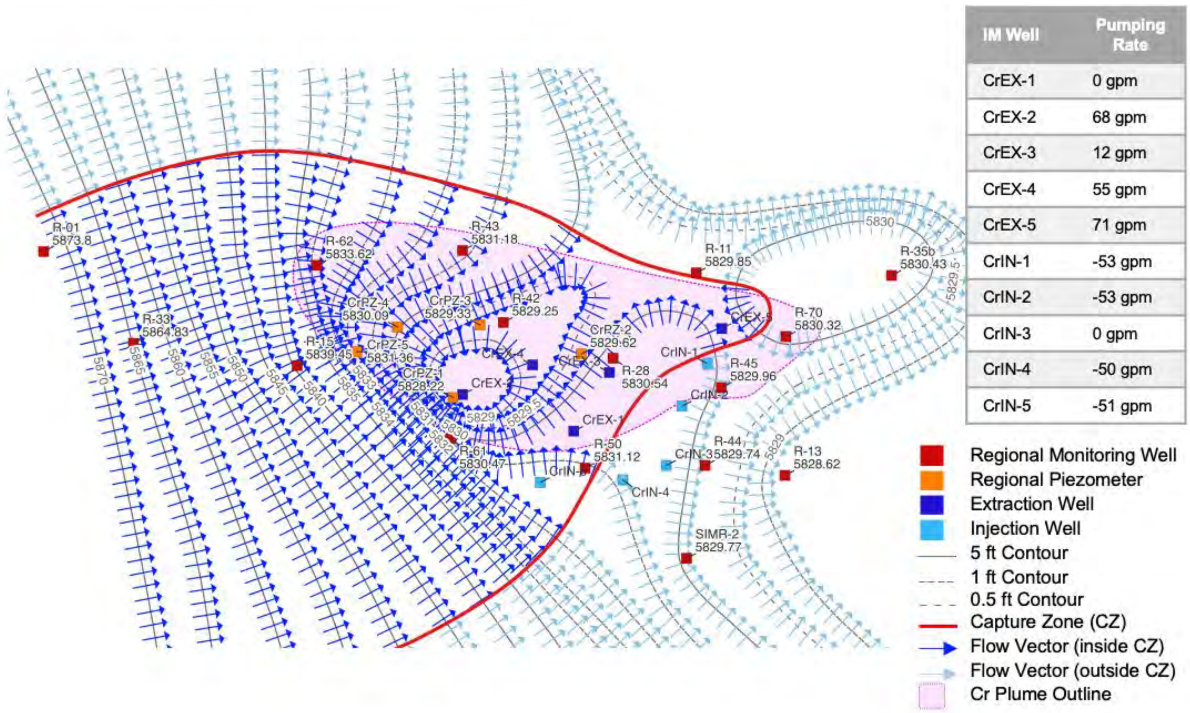

Figure 7. Capture zone interpretation based on vectors perpendicular to the water-table contours shown in Figure 6.

Figure 8 shows the water-table map for a "baseline" period of no IM extraction or injection. The time selected was May 1, 2020 at 1:00 AM during a several months-long shutdown in IM activity. Differences in gradient vectors between pre-IM baseline, shutdown baseline, and during different phases of the IM are discussed in further detail in Section 2.2. A full analysis and comparison of IM impacts on hydraulic head is provided in Section 5.0.

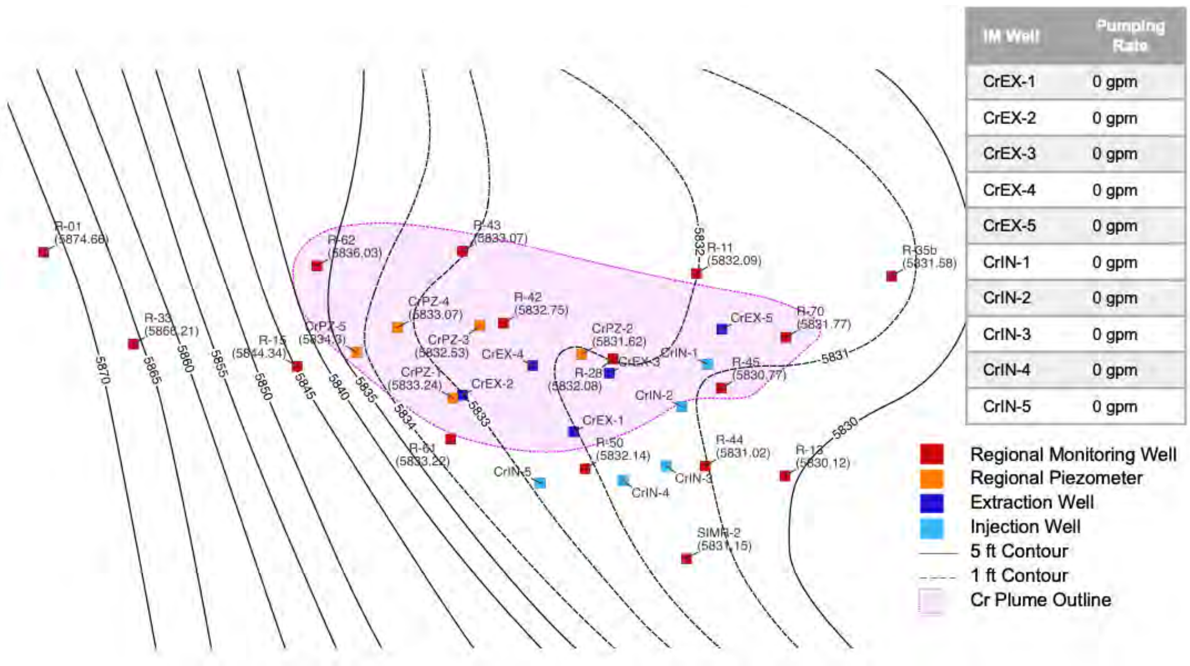

Figure 8. Water table map for May 1, 2020 1:00 am, which represents ambient ("baseline") conditions.

2.1.2 Deep Potentiometric Contours

Maps of hydraulic head using the deeper screens, >50 ft below the water table, can be used to identify IM impacts at depth. Although the number of deep screens (8 at depth compared to 21 at the water table screens, see Table 2) is limited, a clear influence of the IM is observed relative to the baseline, no IM activity on 5/1/20, (Figure 9) to IM activity on 6/15/21 and 11/1/21 (Figure 10 and Figure 11). The full IM map on 6/15/21 is further limited by the exclusion of R-33 S2 data due to the influence of PM-4 pumping (Figure 10), as described above.

The deep maps all show a gradient that is generally towards the southeast, similar to the baseline shallow map (Figure 8). Further comparisons between shallow and deep maps during all conditions of pumping are provided in Section 5.0.

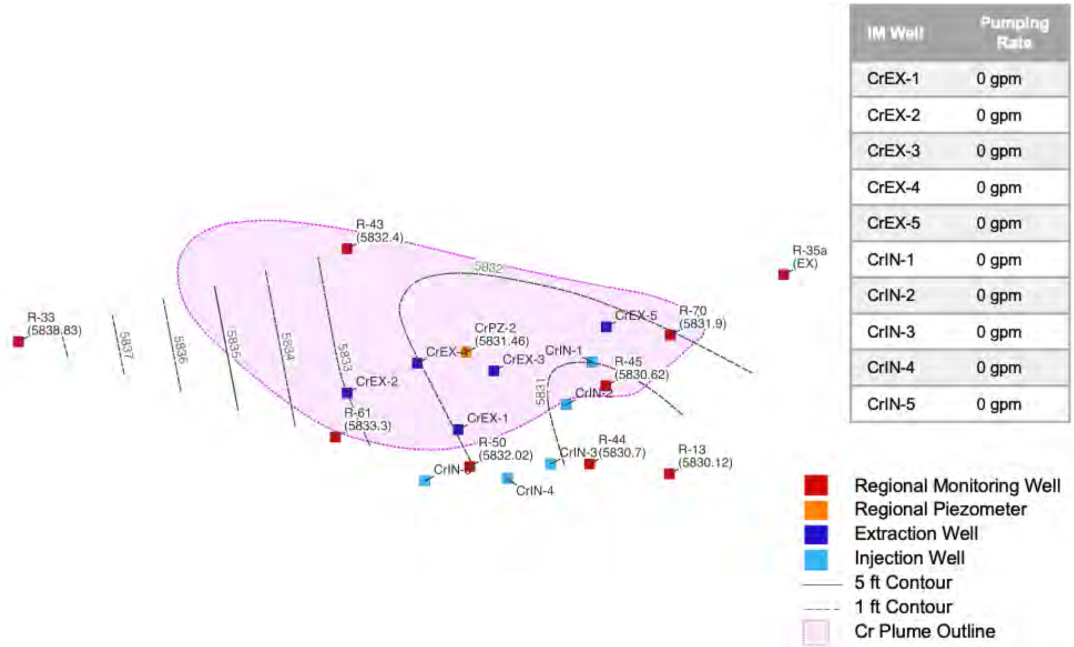

IM Well	Pumping Rate
CrEX-1	0 gpm
CrEX-2	0 gpm
CrEX-3	0 gpm
CrEX-4	0 gpm
CrEX-5	0 gpm
CrIN-1	0 gpm
CrIN-2	0 gpm
CrIN-3	0 gpm
CrIN-4	0 gpm
CrIN-5	0 gpm

Figure 9. Deep-screen hydraulic head map for May 1, 2020 1:00 am, which represents ambient ("baseline") conditions.

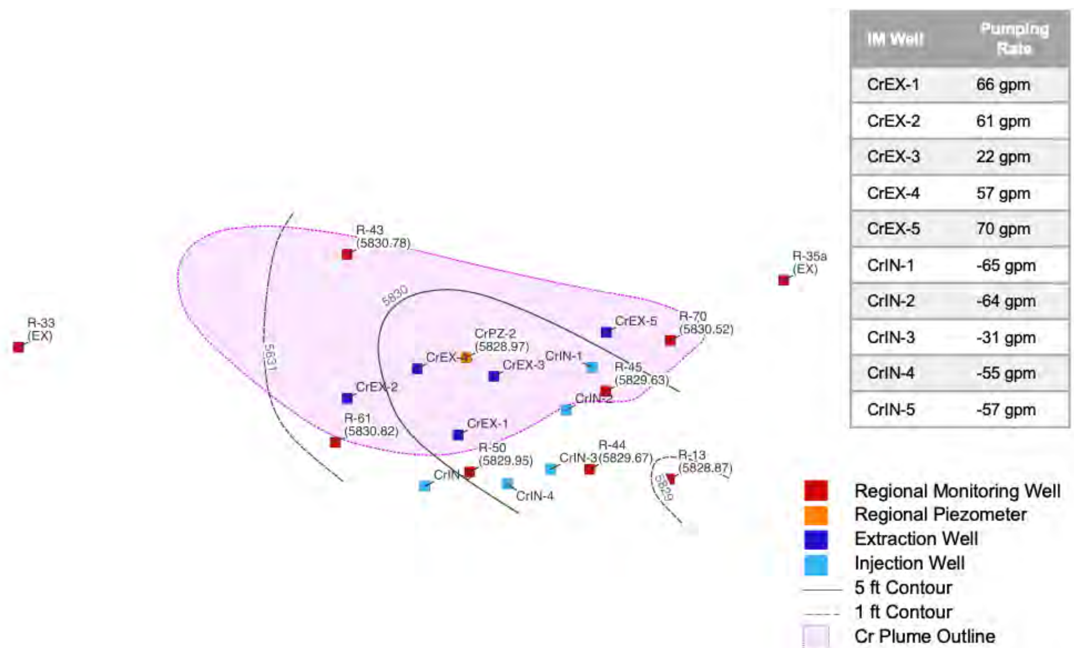

IM Well	Pumping Rate
CrEX-1	66 gpm
CrEX-2	61 gpm
CrEX-3	22 gpm
CrEX-4	57 gpm
CrEX-5	70 gpm
CrIN-1	-65 gpm
CrIN-2	-64 gpm
CrIN-3	-31 gpm
CrIN-4	-55 gpm
CrIN-5	-57 gpm

Figure 10. Deep-screen hydraulic head map for June 15, 2021 1:00 a.m., which includes full IM operation (pumping and injection at all CrIN/CrEX wells).

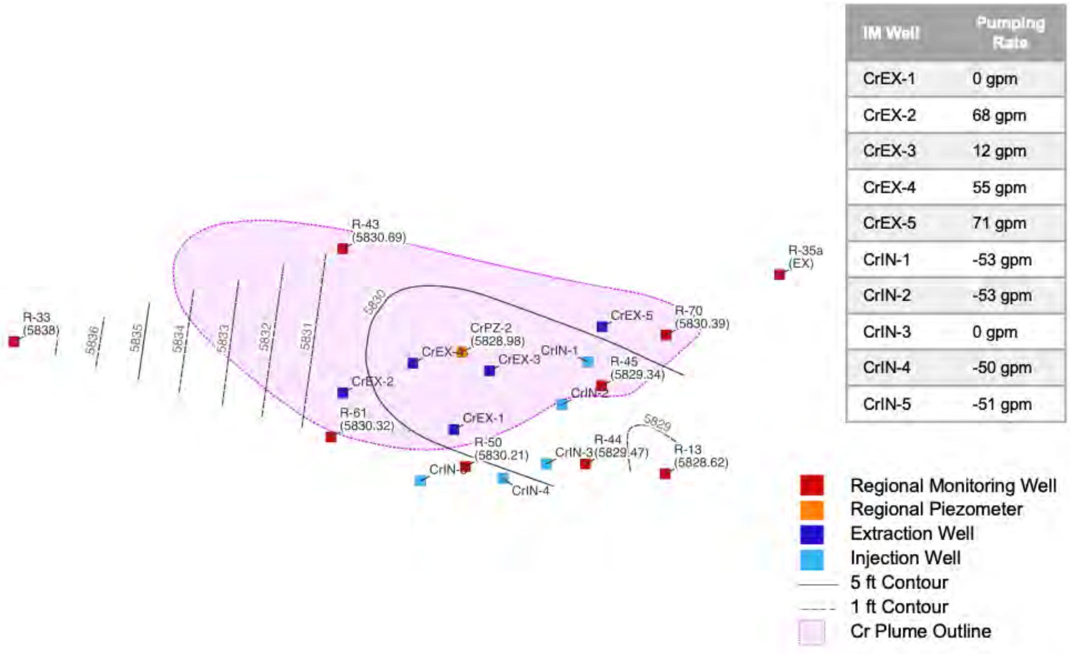

Figure 11. Deep-screen hydraulic head map for November 1, 2021 1:00 am, which includes nearly full IM operation (with the exception of CrEX-1 and CrIN-3).

2.2 Hydraulic Data Analysis

The purpose of the IM was to establish hydraulic control of the chromium plume (Section 1.3). Hence, a complete analysis of hydraulic gradients was performed and is documented in a separate report (Neptune 2023b). Given the importance of the hydraulic gradient analysis for identifying the influence of IM operations on the chromium site, results from this document are summarized here.

The analyses presented in (Neptune 2023b) are used to estimate hydraulic gradients within the vicinity of the chromium plume. Gradient control points are described in EPA (2008) as a way to demonstrate inward flow relative to a boundary, such as a property boundary or a target capture zone. The gradients are calculated between pairs of wells on either side of the boundary, or, in a more complex example in EPA (2008), as triples calculated using the three-point method described above (p. B2-14 to 17). The density of wells in the chromium plume does not permit the types of well pair analyses suggested by EPA (2008), as wells are sparse and located several hundred feet apart (Figure 1). The analysis uses the three-point method to explore the impacts of IM pumping quantitatively, comparing the magnitude and direction of gradients during periods when the IM is fully operational, to periods when the IM is completely off. The analysis also uses well screen pairs at dual-screened wells to look at pumping impacts on vertical gradients. Statistical tests are used to determine where significant differences in magnitude and direction exist between IM operational periods and baseline periods (no IM operations).

Additionally, the impact from sustained pumping at nearby PM-4 (considered to have the largest potential impact on water levels and hydraulic gradients in the chromium plume) on baseline conditions is assessed and compared to the magnitude of that from the IM. Overall, shifts in gradient magnitude and direction as a result of PM-4 are small relative to the influence of the IM system. Local to the IM capture zone and chromium plume, as well as immediately downgradient, IM pumping overwhelms impacts from PM-4 except at monitoring well R-33.

While the full analysis is provided in (Neptune 2023b), the key conclusions are summarized below:

- During periods when IM operations are off, ambient hydraulic gradients show a dominant east to southeast orientation.
- Small, but quantifiable, impacts on hydraulic gradients from county supply well PM-4 pumping are observed in the chromium plume.
- The operation of extraction and injection wells as part of the IM operation is observed to result in large, systematic changes on hydraulic gradients within the vicinity of the chromium plume. Hydraulic gradients appear stronger in magnitude upgradient of the IM as a result of operations, with a shift in direction generally toward the extraction wells.
- Changes in hydraulic gradients as the result of IM operations are least 50% greater compared to that from PM-4 in all areas of the chromium plume; hydraulic gradients close to the extraction and injection wells indicate impacts from the IM are at least 10 times greater.
- Vertical gradient changes due to the onset of IM operations were apparent at all dual-screened well pairs in the chromium plume (R-43, R-44, R-45, R-50, and R-61). Small ambient downward vertical gradients were observed at most wells during periods when IM operations were off. Most well pairs show a small but systematic increase, on the order of 0.01 - 0.001 ft/ft, in the downward gradient as a result of IM operations.

3.0 Calculations

Step 4 of capture zone analysis in EPA (2008) is to perform analytical and numerical calculations. The analytical estimates pertaining to capture are described in Section 3.1. Numerical modeling results using the calibrated chromium model (CM) are presented in Section 3.2.

3.1 Analytical Methods

Analytical methods are generally considered simplified estimates because the assumptions are not met, to varying degrees depending on the site (EPA 2008). Nonetheless, they are simple to perform, and provide a check on more complex analyses. Assumptions of analytical methods typically include a homogeneous, isotropic aquifer, an infinite aquifer of uniform thickness, and extraction wells that fully penetrate the aquifer. The aquifer is also assumed to be of infinite areal extent. Although this latter assumption is valid at the chromium project area (since it is far from aquifer boundaries), the assumptions of homogeneity, isotropy, and uniform thickness are challenged at the chromium site. The aquifer is hundreds to thousands of feet thick (a thickness of approximately 850 ft has been estimated at PM-2, PM-4, and PM-5 locations (McLin 2006)), whereas the extraction wells and chromium plume are located in the upper 150 ft of the aquifer. For calculations that require an aquifer thickness when a well is partially penetrating, the screen length or 1.5 times screen length can be used in place of the aquifer thickness when appropriate (LANL 2012; McLin 2006). However, in analytical calculations of the CZ at the chromium project area, the substitution of the screen length resulted in unreasonably large CZ estimates, so a full penetration assumption was used here.

3.1.1 Estimated Flow Rate Calculation

This calculation estimates the flow rate Q at an extraction well that would be required to capture a plume or plume portion of width w. It does not allow for an understanding of vertical capture if the well partially penetrates the plume. The assumptions above are required along with steady-state flow, negligible vertical gradient, and recharge accounted for in the regional hydraulic gradient with no additional sources of water (EPA 2008).

The estimated required flow rate to capture a plume of width w is given by (EPA 2008):

$$Q = K \cdot b \cdot w \cdot i \cdot f, \tag{1}$$

where

Q is the extraction rate [$ft^3\ d^{-1}$],
K is hydraulic conductivity [$ft\ d^{-1}$],
b is saturated thickness [ft],
w is plume width [ft],
i is regional hydraulic gradient [–], and
f is a factor used to account for other contributions to the pumping well (EPA 2008).

Values used in the above calculation are shown in Table 3. A factor of 1 is used because contributions to CrEX-1 from other sources are expected to be negligible. The resulting flow rate is Q = 28.5 gpm. Raising and lowering all the parameters (except screen length) by a factor of 50% changes the value to 144 gpm and 1.8 gpm, respectively. Given the extreme assumptions required for this calculation, particularly with respect to the partial penetration of the well, and uncertainty in the inputs, these results should only be considered as a point of discussion. Note that assuming the screen length is the aquifer thickness leads to a much smaller estimated gpm.

Table 3.
Estimated Flow Rate Calculation

Parameter	Value	Value +50%	Value -50%	Source
K, ft/d	11.7	17.55	5.85	Mean of distribution developed for Puye formation
b, ft	850	-	-	850 ft (McLin 2006)
w, ft	750	1125	375	See Figure 12
i, -	0.000737	0.001105	0.0003683	Gradient estimate at CrEX-1 location based on baseline map, see Figure 8
f, -	1	1.5	0.5	(EPA 2008)
Q, ft^3/d	5494	27,816	343	-

Q, gpm	28.5	144	1.8	-

3.1.2 Estimated Width

An analytical estimate of maximum capture zone width, w_{max}, given the simplifying assumptions above, is included below:

$$w_{max} = {}^{Q}/_{Kbi} \tag{2}$$

Terms used in the equation for capture zone width are included in Table 4. The capture zone width at the well itself is half the maximum width at an infinite distance upgradient (EPA 2008). For a flow rate of 65 gpm, and other parameters defined in Table 3, w_{max} = 1708 ft, and w_{well} (width of the capture zone at the well) = 854 ft (Figure 12). Using the screen length as a substitution for aquifer thickness resulted in an unreasonably large estimate of the CZ at Q = 65 gpm.

For sites with multiple extraction wells, a rough estimate of capture zone width may be made by locating one hypothetical "equivalent well" at the center of the region of extraction wells. For a total pumping rate of 276 gpm during full IM operations (Table 1), the estimated maximum capture zone width is 7252 ft, or 3626 ft at a point at the center of the extraction well field.

An estimated width assuming unconfined conditions can be calculated using the method of Grubb (1993), which uses the concept of discharge potentials and takes as inputs the hydraulic head at a location upgradient and downgradient of the pumping well during a period without pumping. Table 4 gives the input parameters used to calculate w_{max} using this method, with the same violations in assumptions associated with partial penetration and unknown effective aquifer thickness. R-61 S1 and R-44 S1 (Figure 1) are used as the upgradient and downgradient wells from CrEX-1, respectively. The estimated w_{max} using this method is only slightly smaller (1681 ft) than w_{max} = 1708, calculated by the simpler method above. All plots shown that include the analytical width estimate use the confined equation given in EPA 2008.

Table 4.
Estimated Width Calculation for Unconfined Conditions

Parameter	Value	Source
K, ft/d	11.7	Mean of distribution developed for Puye formation
Elevation of bottom of aquifer, ft	4970	McLin (2006)
h_1, ft	5833.22	Head at R-61 S1 measured on 5/1/20 at 1:00 am
h_2, ft	5831.02	Head at R-44 S1 measured on 5/1/20 at 1:00 am
L, ft	2982	Distance between R-61 and R-44
Q, ft^3/d	12512	65 gpm in ft^3/d
w_{max}, ft	1681	Grubb (1993)

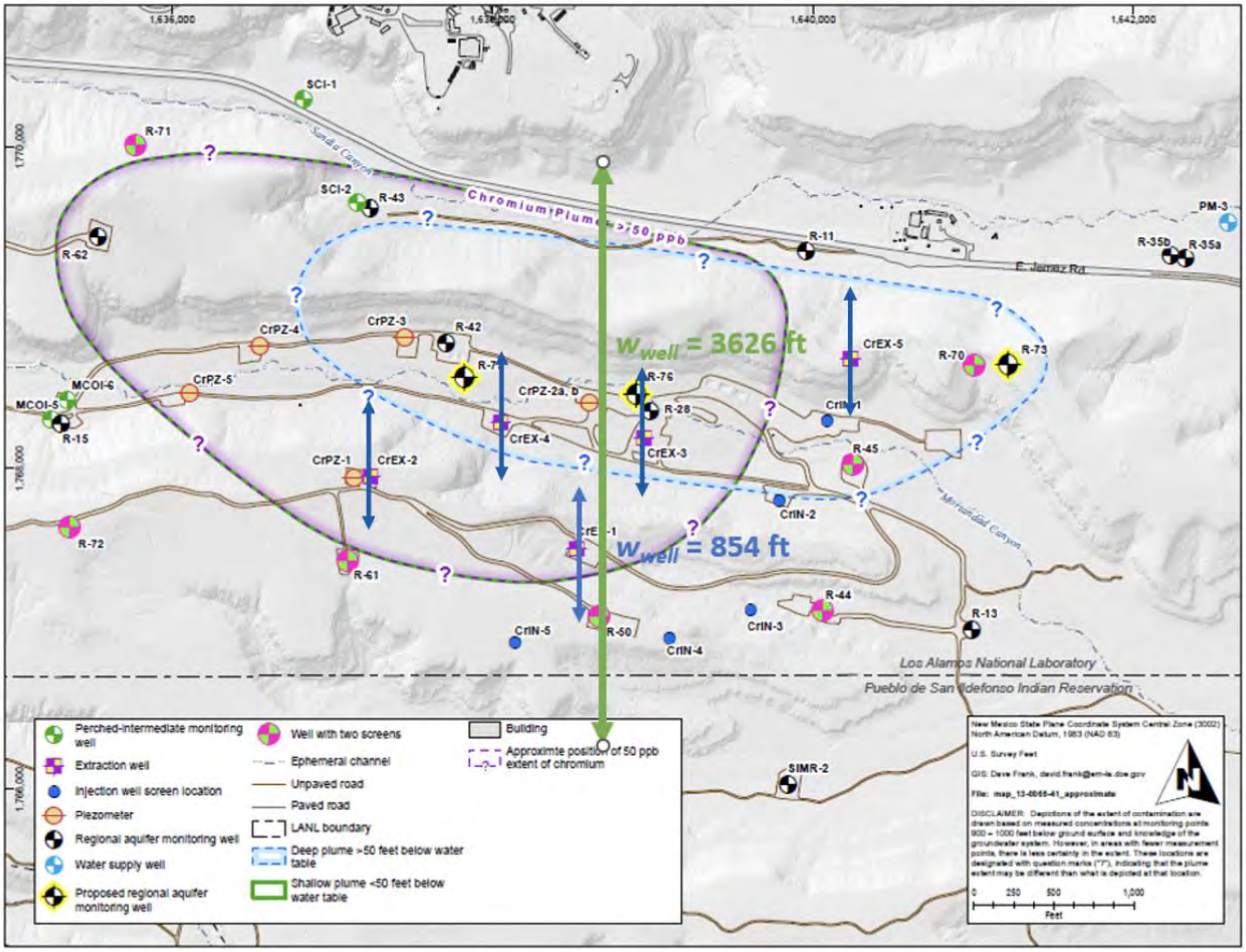

Figure 12. Estimated capture widths for individual wells and for the entire IM system using the analytical methods described above and parameters shown in Table 4.

3.2 Numerical Methods

Numerical modeling plays a key role in capture and flood zone analyses. EPA (2008) states, "Although ground-water model results are subject to uncertainty… EPA encourages the use of ground-water modeling at more complex sites as a tool for evaluating and improving the site conceptual model, predicting capture zones, and evaluating alternate remediation scenarios" (p.24). Hence, numerical modeling is used as a complement to the analytical approaches. As described below, the numerical model incorporates a wide array of site knowledge beyond what can be represented in an analytical estimate.

3.2.1 Modeling Tools

A numerical model of the chromium plume area has been built using the code, Finite Element Heat and Mass Transfer (FEHM) (https://fehm.lanl.gov/). FEHM can account for complexities associated with partially penetrating wells, aquifer heterogeneity, and complex boundary conditions. The FEHM code has been validated against analytical methods (Dash et al. 2015) and benchmarked with other common numerical codes, including MODFLOW and TOUGH2 (Keating and Zyvoloski 2009).

Among the numerical modeling tools used to evaluate the IM's effectiveness are (a) concentration-based analyses that use FEHM's *trac* module, and (b) particle-based tracking simulations using FEHM's *sptr* module (Zyvoloski et al. 1997, 1999), which have been used at other DOE and non-DOE sites (Arnold et al. 2003; Kelkar et al. 2010).

Some of the model structures present in the CM impact capture zones causing them to vary substantially from the theoretical capture zone depicted in Figure 2. In any numerical model of a capture zone, the capture zone of an extraction well will extend toward boundary condition(s) that can supply water to the extraction nodes in sufficient quantity to satisfy the specified extraction flux of the well. In this model, there are both specified flux and specified head boundary conditions (Neptune 2023a). The injection wells of the IM system are in close proximity to the extraction wells, and therefore can supply water to meet the extraction demand. This design creates a dipole-like effect of the coupled injection and extraction, which increases the capture zone of the extraction wells, extending them further downgradient. Additionally, there are five regions of specified infiltration described below in Section 3.2.2 on the top surface of the model that also contribute water to the extraction wells. While these five infiltration areas are sufficient to calibrate the model to water level and concentration targets, it is very likely that similar infiltration sources occur elsewhere in the vicinity; while these areas would be difficult to assess and parameterize, their inclusion in the model could materially impact capture zones of the extraction wellfield. The highly heterogeneous conductivity field of the model calibrations also impacts the capture zones, as water is more readily available to the extraction wells if it is connected to a given location with a high-conductivity pathway.

3.2.2 Chromium Hydraulic Windows

The CM domain begins at the top of the regional aquifer, where water and chromium enter the water table. These pathways are referred to as hydraulic windows. Their footprints on the regional aquifer are referred to as the sources of chromium at the water table. The five hydraulic windows in the CM are represented as ellipses, although one in the northeast acts as a source of clean, uncontaminated recharge. The parameterization of the ellipses is controlled by the center coordinates and *x* and *y* radii as shown in Figure 13. The evidence constraining these locations is described in more detail in (Neptune 2023a).

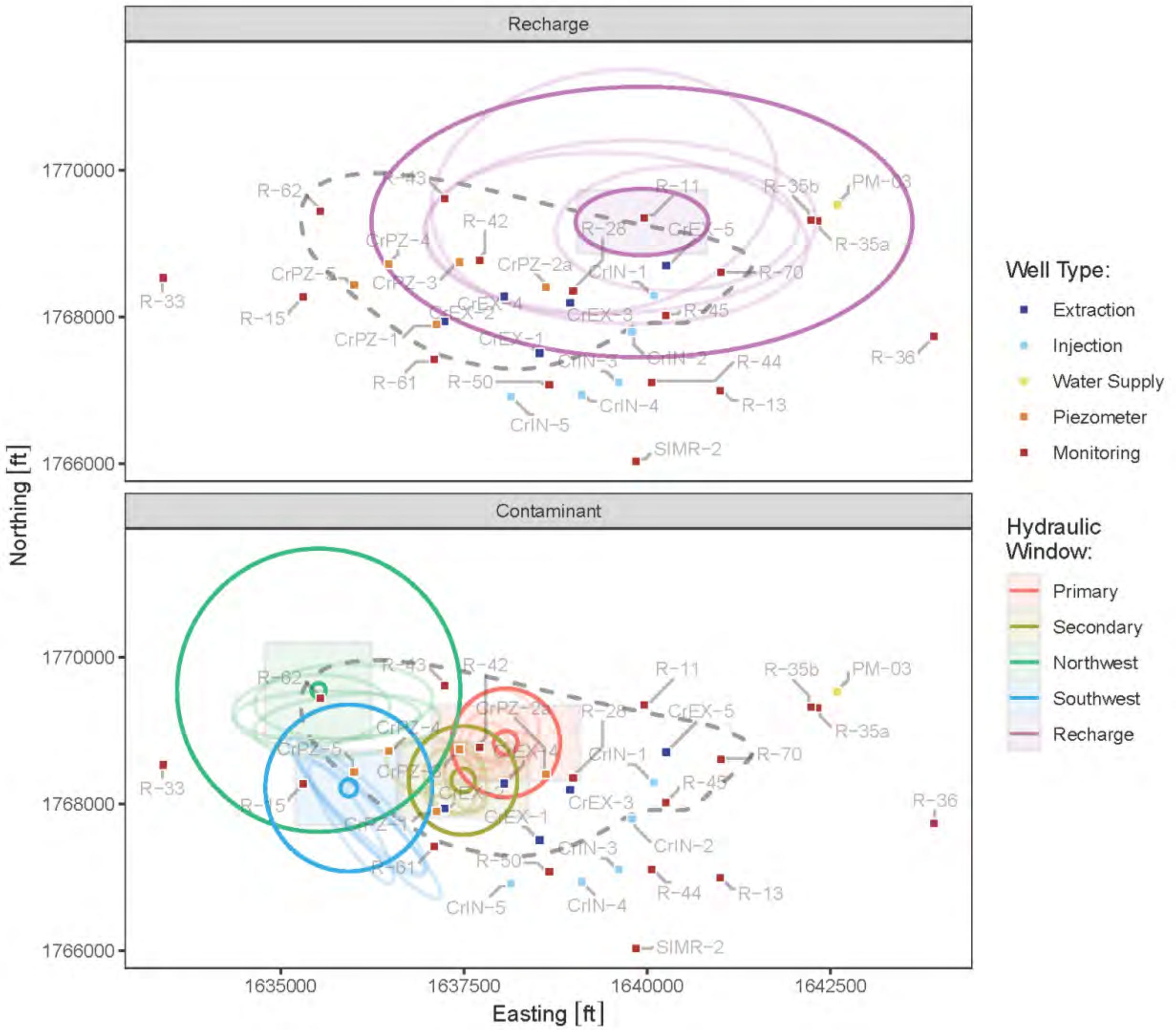

Figure 13: Chromium free recharge (top), and chromium contaminated (bottom) hydraulic window location distributions for spatial input parameters. The shaded rectangle shows the range of allowed center coordinate locations, and the darker ellipses show the allowed range of x and y radii. Example calibrated hydraulic windows are shown for each source as transparent ellipses. Estimated chromium plume is outlined in dashed gray.

3.2.3 Four Calibrations

The CM is calibrated to hydraulic head data, flow gradients, drawdown responses to pumping, and concentrations at 40 wells over the 20-year period of record (through Oct. 22, 2022). The flow and transport calibration process led to four calibrations that all match available data using different:

- Chromium source areal extents, recharge rates, and concentrations
- Hydraulic flow parameter fields (including hydraulic conductivity and specific storage)

These four calibrations represent a range of possible solutions based on the calibration targets and allow for more thorough explorations of uncertainty in estimated capture. Because several distinct chromium source configurations (shown in Figure 13) and hydraulic flow parameter fields lead to a good match to data, any single deterministic calibration is “non-unique” and must be considered alongside other calibrations to understand where the capture zone has been delineated with the greatest confidence. All calibrations represent a single conceptual model (described in Section 1.2 and (Neptune 2023a). These are arbitrarily named Calibration 1, 2, 3, and 4 in the sections below and are not indicative of ranking. The capture zone results show the final calibrated location of the four chromium hydraulic windows in the model for reference.

EPA (2008) also notes: “Ideally, the calibrated numerical model should be subsequently ‘verified’ by simulating drawdown responses to different pumping conditions and comparing those predicted responses to field measurements. This instills confidence that the model provides a reasonable interpretation of the physical system.” All four models demonstrate accurate responses to drawdown and mounding simulated in both upper and lower screens throughout the aquifer. Additionally, the model is validated against almost 500 pumping-response pairs. Key differences between the calibrations and in the capture and flood zones are discussed in Section 5.0. Full details of the model build and calibration are documented in (Neptune 2023a).

3.2.4 Steady-state Assumption

All the numerical modeling analyses use pumping and injection rates based on a single configuration termed the Future Pumping Scenario (FPS) operating at a total of 285 gpm (see Table 5). Although alternative extraction and injection rates are possible, the predominant historical rates were used to initiate the analysis. Other configurations could be explored in future work as different operating scenarios are identified.

Table 5.
Future Pumping Scenario (FPS)

Well	Pumping Rate (gpm)
CrEX-1	75
CrEX-2	65
CrEX-3	30
CrEX-4	50
CrEX-5	65
Total Extraction	285
CrIN-1	60
CrIN-2	60
CrIN-3	45
CrIN-4	60
CrIN-5	60
Total Injection	285

Similar to the analytical solutions, capture zone estimates with a numerical model also require a steady-state assumption. In other words, the numerical modeling methods presented in this document delineate the capture zones after they have achieved complete development and reached their maximum extent, in keeping with the conceptualization of a capture zone presented in EPA (2008) and described in Section 1.4. In contrast, a transient analysis could describe the evolution of the capture zone that results from a changing flow field (e.g., growth of the capture zone during the initial phase of IM well operations); this type of analysis is beyond the scope of this document and may be considered for future work.

Steady-state equilibrium between chromium sources to the model and IM pumping rates is achieved using a hypothetical scenario in which the both the IM operation and the calibrated chromium sources are run continuously for long enough to reach a steady state. These simulations turn on both constant IM pumping and chromium source inputs to the regional aquifer at simulation start and run for 150 years until an equilibrium between source arrival and IM extraction is reached. These results serve as the initial condition of an equilibrated flow field used in all modeling analyses of capture and flood zone.

3.2.5 Solute Transport Analysis

The solute transport analysis comprises traditional concentration-based forward modeling and estimates the down-gradient concentrations associated with potential uncaptured pathways that could result from the model's calibrated source locations and injection rates.

Portions of the plume reach steady state, indicating that the plume is contained and no longer expanding. Those portions that continue to expand slowly downgradient of the IM wells indicate potential uncaptured pathways. The assumption of continuing chromium sources represents an unrealistic pessimistic scenario since total chromium inventory would likely be exhausted before reaching a steady-state (equilibrium) condition.

The results are shown in Figure 14, presented as 50 ppb chromium concentration contours at depths 0 to 118 ft below the water table. The 50 ppb chromium contour does not extend south or east through the arc of CrIN wells in any of the four calibrations. However, all four calibrations predict that chromium concentrations can exceed 50 ppb east of CrEX-5. The extent and orientation of the 50 ppb contour vary from calibration to calibration due to the differences in chromium source areal extents, recharge rates, and concentrations, as well as differences in the hydraulic flow parameter fields (Section 3.2.3). In some calibrations (e.g., Calibrations 1 and 4), the 50 ppb contour only extends about 600 ft east of CrEX-5, whereas in other calibrations (e.g., Calibration 3) it extends more than 1600 ft east of CrEX-5 at 79 ft depth and 2600 ft east of CrEX-5 at 98 ft and 118 ft depths.

The 50 ppb contour at depths 0 – 118 ft does not encompass CrEX-1 in any calibration in steady-state simulations because CrEX-2, -3, and -4 have reduced downgradient chromium concentrations below 50 ppb and effectively prevented the plume from migrating to CrEX-1.

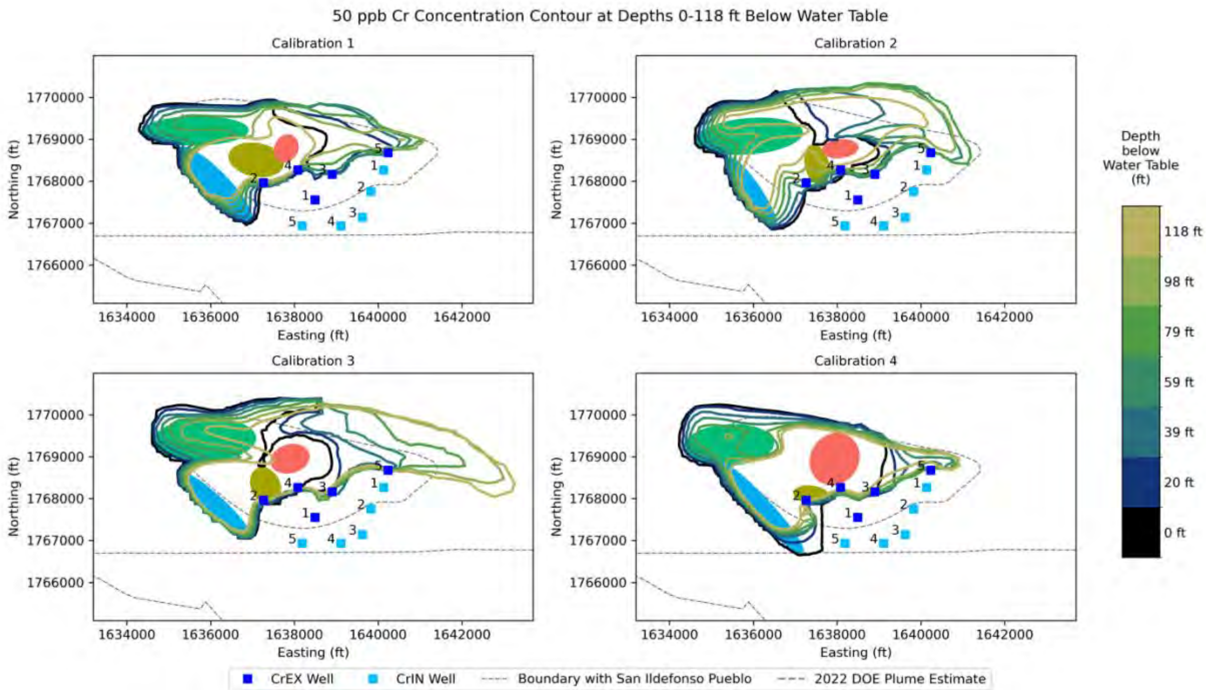

Figure 14. Plan view depiction of the solute tracer results from the top 4 calibrations run to steady-state presented as 50 ppb chromium concentration contours at various depths below the water table. Chromium sources to the model are shown as colored ellipses.

3.2.5.1 Node-by-node Solute Capture Analysis

A set of nearly 3000 simulations are run using the initial condition described in Section 3.2.4 to evaluate the capture zone of the IM by initiating a solute concentration at a single water table node per simulation, and identifying regions where most of the solute is captured by the IM wells. This is similar in intent to the particle tracking analysis described below, in which particles are initiated from a large block of upgradient water table locations to delineate the capture zone. This analysis uses an initial solute concentration in lieu of particles, and, therefore, includes processes like dispersion that are employed in the model calibration, whereas the particle tracking analyses presented below require only hydraulic head information to determine the flow field and particle trajectories.

This transport simulation is run for 50,000 days (137 years). The percent of the initial mass that exits the system through the IM is calculated at the end of the simulations. Capture is defined for each initializing node if most of the initial unit concentration is removed from the domain by the IM system. This simulation is repeated for each of the 2734 nodes at the top of the model domain in the region shown in Figure 15. By performing these simulations for all nodes at the water table around the IM area, an estimate of the capture zone for the IM is derived. Note that each of these node-by-node simulations represents a hypothetical scenario; there is no chromium present above background concentrations at all locations within the bounding area.

Figure 15 shows the percent captured after 137 years in Calibrations 1–4 for nodes at the surface. The red contour bounds the region where a majority (>50%) of the initial mass was extracted by the IM system. These results, and comparisons with the other methods, are discussed with the results obtained by other methods in Section 5.0.

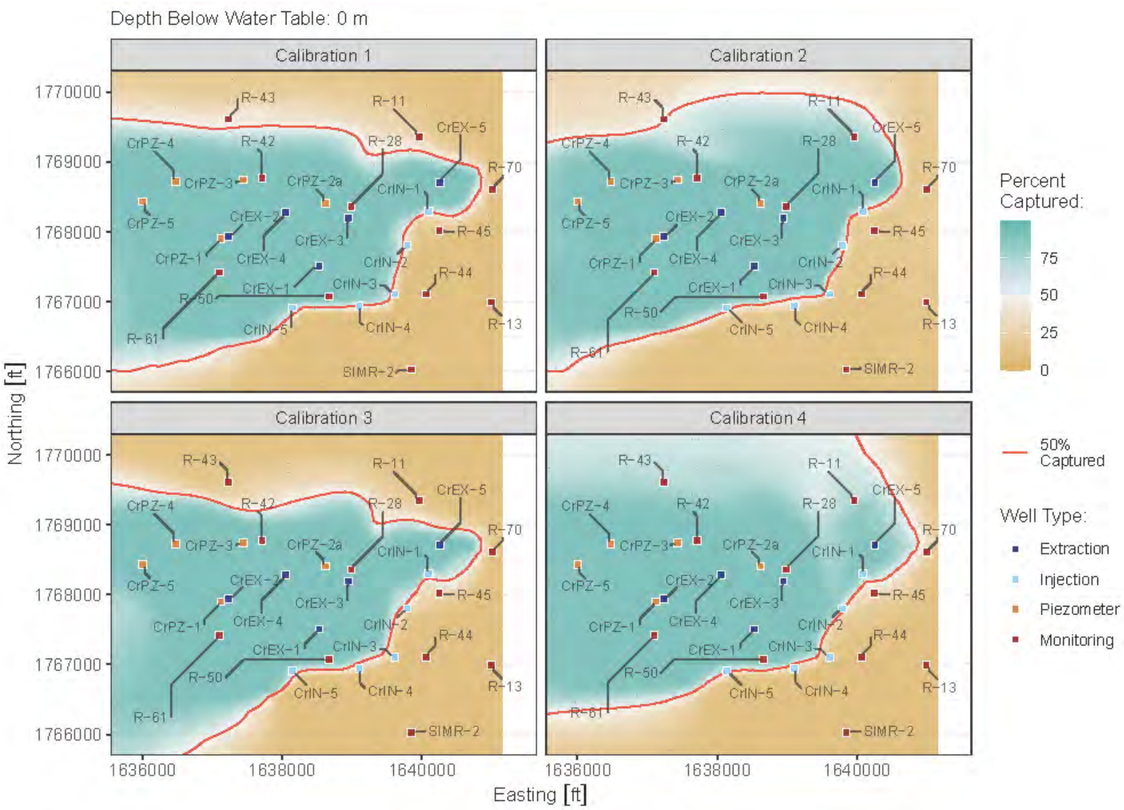

Figure 15. Capture zone of the IM system in terms of percent of particles captured after 137 years of continuous operation at the Future Pumping Scenario (FPS) rates in Table 5, at 0 m below the water table.

3.2.5.2 Node-by-node Solute Flood Zone Analysis

A set of simulations were executed to evaluate the IM flood zones at injection wells using the initial condition described in Section 3.2.5. The domain is initialized with a uniform solute concentration (100 ppb) throughout, and incoming water in all flow boundaries is also set to an input concentration of 100 ppb. CrIN well injection water is set to an input concentration of 0 ppb. The contrast of the injection concentration of 0 ppb and the initial ambient concentration of 100 ppb allows for discerning the spatial extent of the injection well impact (flood zone) as a numerical analogue of a tracer test.

Figure 16 shows the results of these four simulations. Areas with concentrations less than 100 ppb are impacted by the 0 ppb injectate. The area of impact extends to the line of extraction wells, suggesting that in the IM injection water eventually reaches the extraction wells. Detection of CrIN-4 injectate at CrEX-1 has already been documented in a field-based tracer experiment

(Reimus et al. 2021). Reimus (2021) notes that this tracer flow direction is contrary to the natural gradient in the absence of IM pumping, suggesting hydraulic control created by the injection and extraction well combination in the chromium plume area.

Additional discussion of these results is provided in Section 5.2.

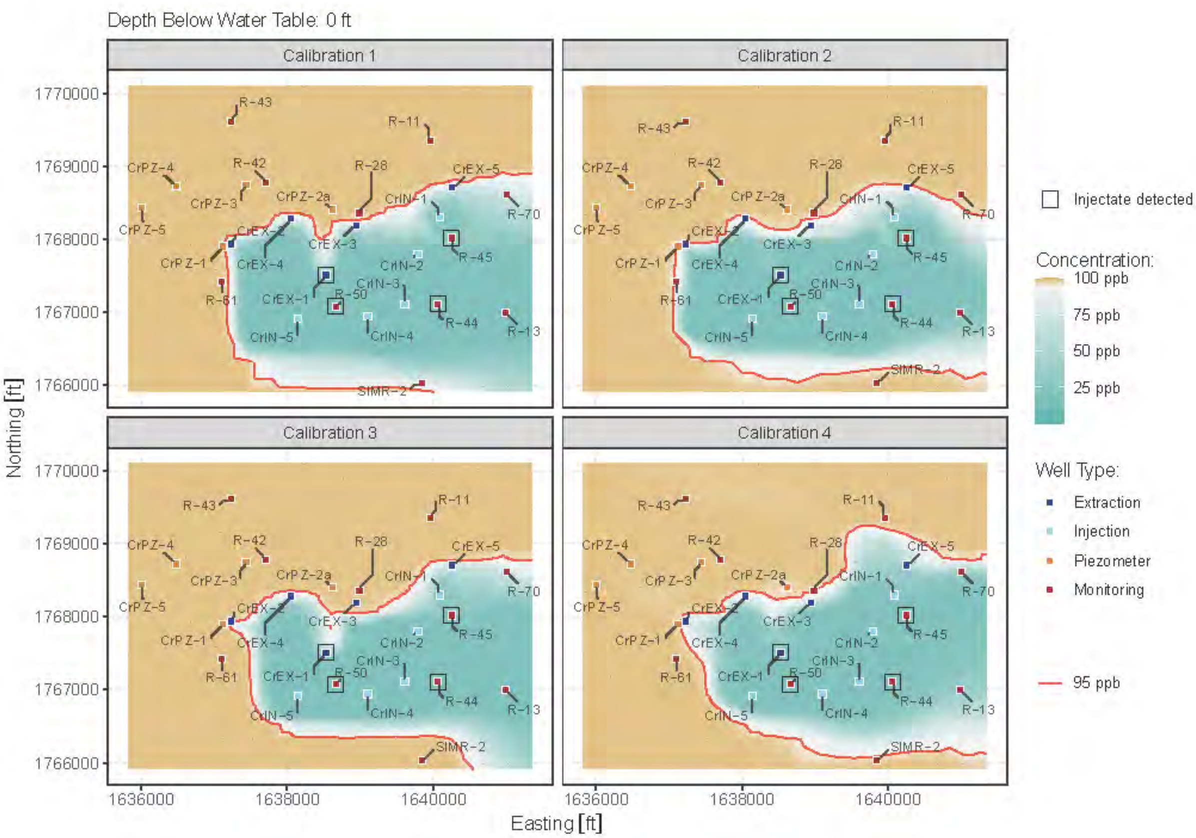

Figure 16. Flood zones for Calibrations 1–4 based on initializing concentrations at 100 ppb everywhere and injecting 0 ppb water at the injection wells. Wells in which injectate has been detected in reality are boxed.

3.2.6 Particle Tracking Analysis

Particle tracking is performed using the CM in the configuration described in Section 3.2.4 to analyze historical or expected flow paths of particles. The capture zone is defined by particle paths that terminate at an extraction well. An estimate of the spatial extent of the capture zone can be obtained by initiating particles at a variety of upgradient locations and distinguishing which are captured and which continue traveling downgradient past the wellfield. Flood zones of injection wells can be mapped in a similar, but inverse, fashion by initiating particles near the injection well and tracking their paths away from the injection well screens. Capture and flood zone particle tracking for the IM is performed using *sptr*[1], a module in FEHM (Zyvoloski et al. 1997).

Similar to the node-by-node capture and flood zone analyses presented in Section 3.2.5, particle tracking is performed within the three-dimensional groundwater flow and transport model. Whereas the node-by-node analysis simulates dispersion, dispersivities have been set to zero in the *sptr* particle tracking analysis to identify the smallest potential extent of the capture zones.

To provide the most complete mapping of capture and flood zones, each of these following types of analysis are discussed below:

1. Capture of infiltration to the water table: forward tracking of particles initialized in a large area upgradient of and in the vicinity of the IM at depths near the water table. These results are more directly comparable to the potentiometric surface mapping method (see next analysis for particles released at depth); particles terminating at CrEX wells define the capture zone
2. Three-dimensional capture zone: particles initialized in a three-dimensional grid covering the IM and vicinity to define capture at depth; these results include plots of capture well by well
3. Flood zone delineation: Particles initialized at the CrIN wells to delineate the impact of injection water
4. Analysis of particles initialized at chromium hydraulic windows: forward tracking of particles initialized at chromium source locations

3.2.6.1 Capture Zone: Infiltration at the Water Table

This scenario delineates the IM system capture zone for water and chromium arriving at the water table by initiating particles in a rectangular grid at the water table over the area of interest. See Section 3.2.6.2 for an analysis of particles released at depth. Particles were initialized with 10 m spacing just below the water table over a large area upgradient and in the vicinity of the IM wells (the same extent as shown in Figure 15 and used in the solute simulations described in Section 3.2.5.1) and tracked forward in time. Path lines that terminate at CrEX wells define the capture zone. Particle tracking was performed for each of the four model calibrations.

---

[1] The *sptr* tool was closely reviewed to determine its compatibility with the unstructured mesh used in the CM, including analysis of the source code and existing literature, along with discussions with developers. The CM uses an unstructured tetrahedral mesh with octree refinement in the vicinity of the plume. In finite element schemes, heads are solved at the nodes and the velocity is constant within each element. However, as particle tracking requires a zero-divergence flux field but the velocity field varies discretely, an interpolation method is needed to honor zero flux-divergence ($\boldsymbol{\nabla^2 v} = 0$). The *sptr* tool uses the Pollock (1994) method in areas without octree refinement to interpolate velocities onto a Voronoi polygon, whereas the code uses a least squares algorithm in areas of octree-refinement (where nodes generally have more than six neighbors) to interpolate velocities onto a Voronoi polygon. Based on our detailed assessment, we are confident in the ability of the code to accurately represent particle transport within areas of uniform mesh refinement; results along boundaries between areas of grid refinement are generally more uncertain.

A bounding polygon for the captured particle paths is constructed and is shown in blue in Figure 17. The resulting capture zones are presented along with chromium hydraulic windows that represent chromium sources at the water table in the numerical model (Neptune 2023a).

In general, the southern and eastern extents of the capture zones for all model calibrations are similar and bounded by the injection wells. This comports with the understanding that the injection wells provide hydraulic control by creating locally high water levels. This directs water away from the injection wells in all directions, including north and west toward the extraction wells, against the natural hydraulic gradient, as shown in Figure 8. This effectively increases the downgradient reach of the extraction wellfield and contains the contaminated area on the southern and eastern sides.

The northern extents of the shallow capture zones in the four calibrations exhibit more variability due to differences in the flow regime north of the extraction wells, which is in turn determined by the hydraulic conductivity field and the recharge rates associated with the chromium source locations (Section 3.2.3). Specifically, the groundwater flow direction north of CrEX-5 in Calibration 4 has a significant north-to-south component because *y*-direction hydraulic conductivity is greater in Calibration 4 than in the other calibrations, which causes the capture zone of CrEX-5 to be more extensive in the north in that calibration compared with the other three. These differences suggest that the northern extent of the capture zone is more uncertain than the southern and eastern extents and would benefit from additional observations.

Whereas Figure 17 presents capture zones derived from a two-dimensional grid of particles launched near the water table, Section 3.2.6.2 examines capture zones delineated using a three-dimensional grid of particles. The blue region represents the bounding shape for the particle paths.

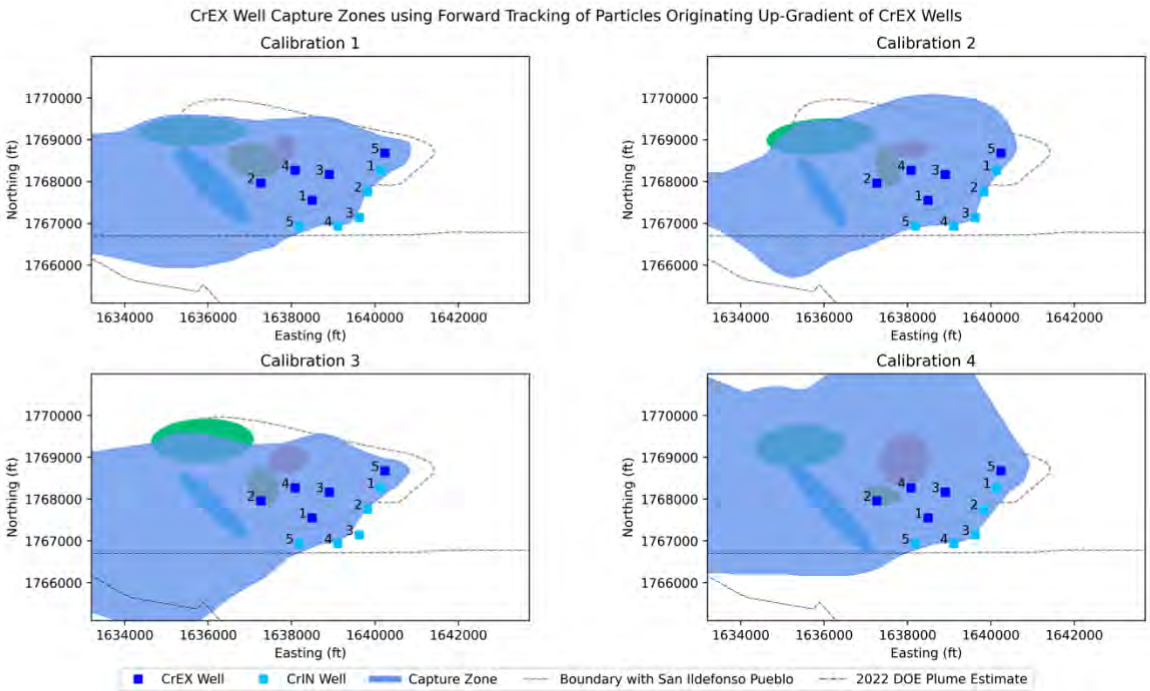

Figure 17. Capture zones derived from forward tracking of particles initialized at the water table over a large upgradient area for Calibrations 1-4.

3.2.6.2 Capture Zones: Three-dimensional Particle Releases

Capture zones are evaluated in three dimensions by initiating a vertical stack of particles at each location in a 20 m by 20 m (65 ft) grid. Note: the model is built using standard SI units (meters) and the ensuing description uses those units to be consistent with the modeling methodology despite most results presented in this document having been converted to feet. Each stack consists of 12 particles spaced 10 m (32 ft) apart; the total depth between the top and bottom particles is 110 m (360 ft), with the top particle positioned just below the water table at every lateral location. A total of 165,600 particles are evaluated for a travel time of 30 years. Because particles are only allowed to travel 30 years, additional caution should be applied when interpreting capture from far upgradient locations when compared to locations near the IM system. The figures below color the particle initiation points by their eventual capture fate. This allows for identifying if a particle is captured and by which extraction well.

An angled overview of the well-by-well capture for Calibration 1 is shown in Figure 18. Similar overviews for Calibrations 2, 3 and 4 are shown in Figure 19, Figure 20, and Figure 21. The angle of each three-dimensional image in this section is indicated by the orientation of the coordinate axes shown in the bottom left of the figure, where the positive x-axis points east, the positive y-axis points north, and the positive z-axis points upward. The IM well locations (both CrIN and CrEX wells) are shown for further orientation. The long cylinder extending upward from each IM well location represents the vertical extent of the well casing to scale, while the radius of the casing is exaggerated for visibility in the figures. The well screens, shown as cylinders of larger radius at the bottom of the casing, are similarly accurate in the vertical dimension but exaggerated in the radial direction for visibility. More detailed section views for each calibration are presented below.

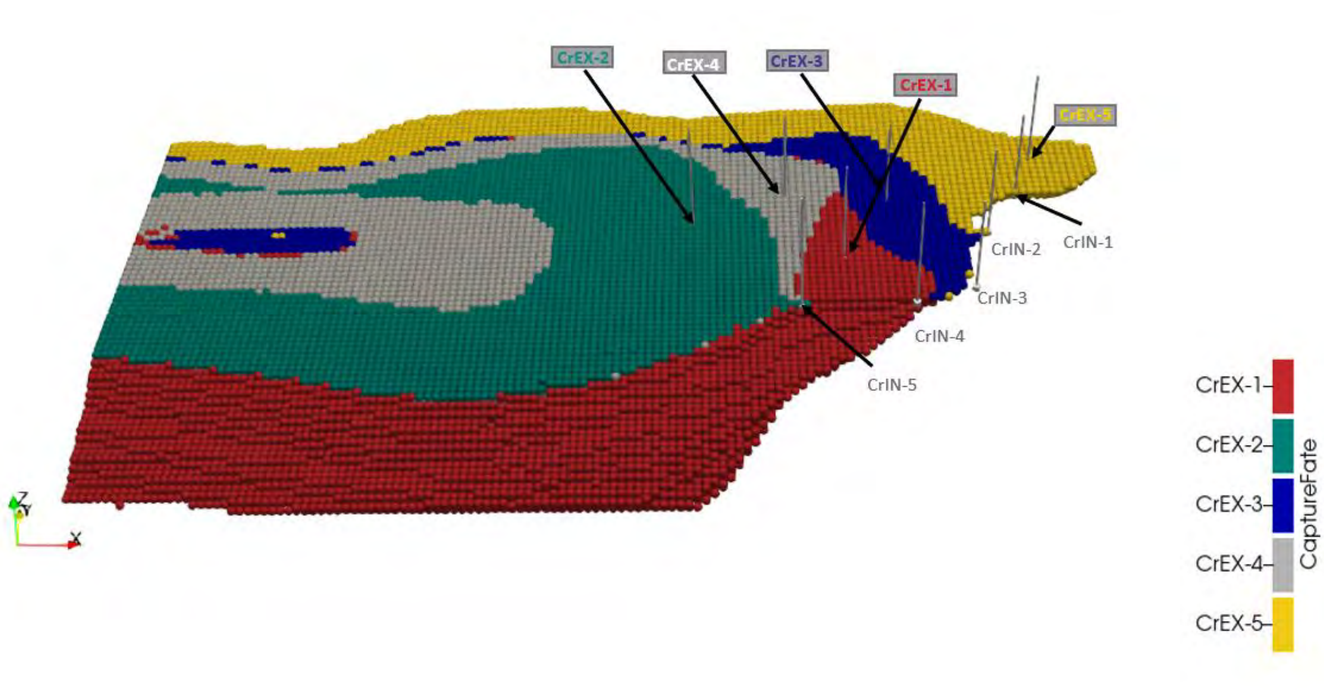

Figure 18: Angled overview (48 degrees off vertical) of the 3D capture zone for Calibration 1. Lateral particle spacing is 20 m (65.6 ft).

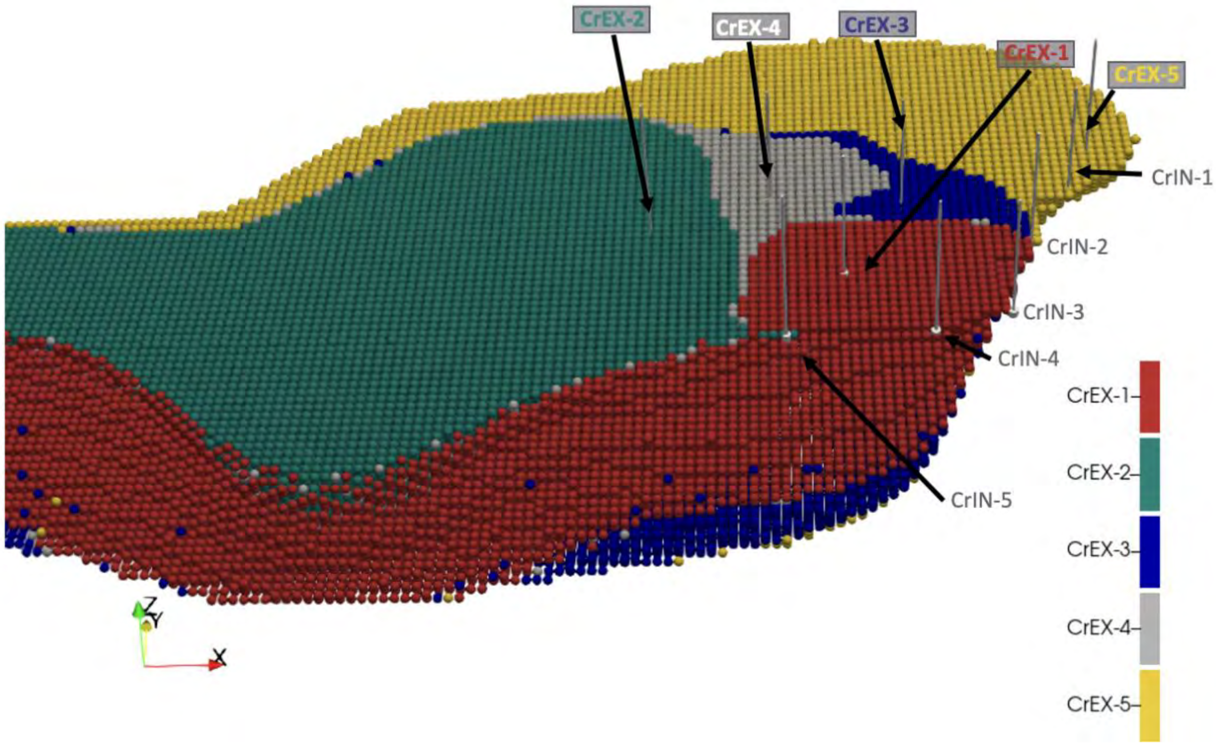

Figure 19: Angled overview (48 degrees off vertical) of the 3D capture zone for Calibration 2. Lateral particle spacing is 20 m (65.6 ft).

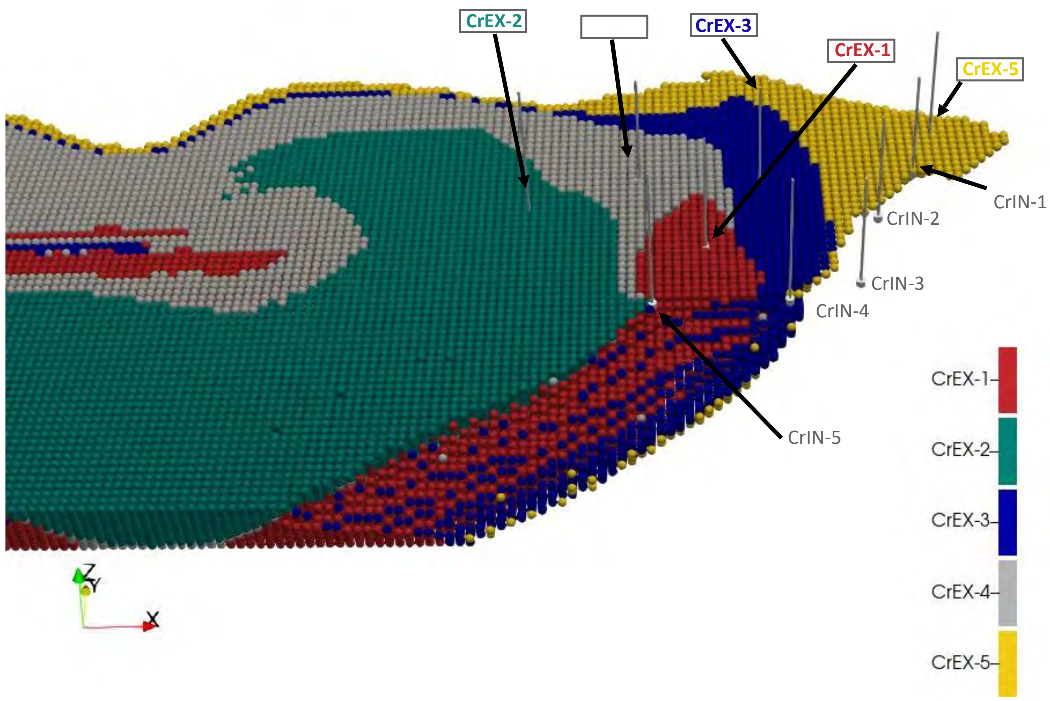

Figure 20: Angled overview (48 degrees off vertical) of the 3D capture zone for Calibration 3. Lateral particle spacing is 20 m (65.6 ft).

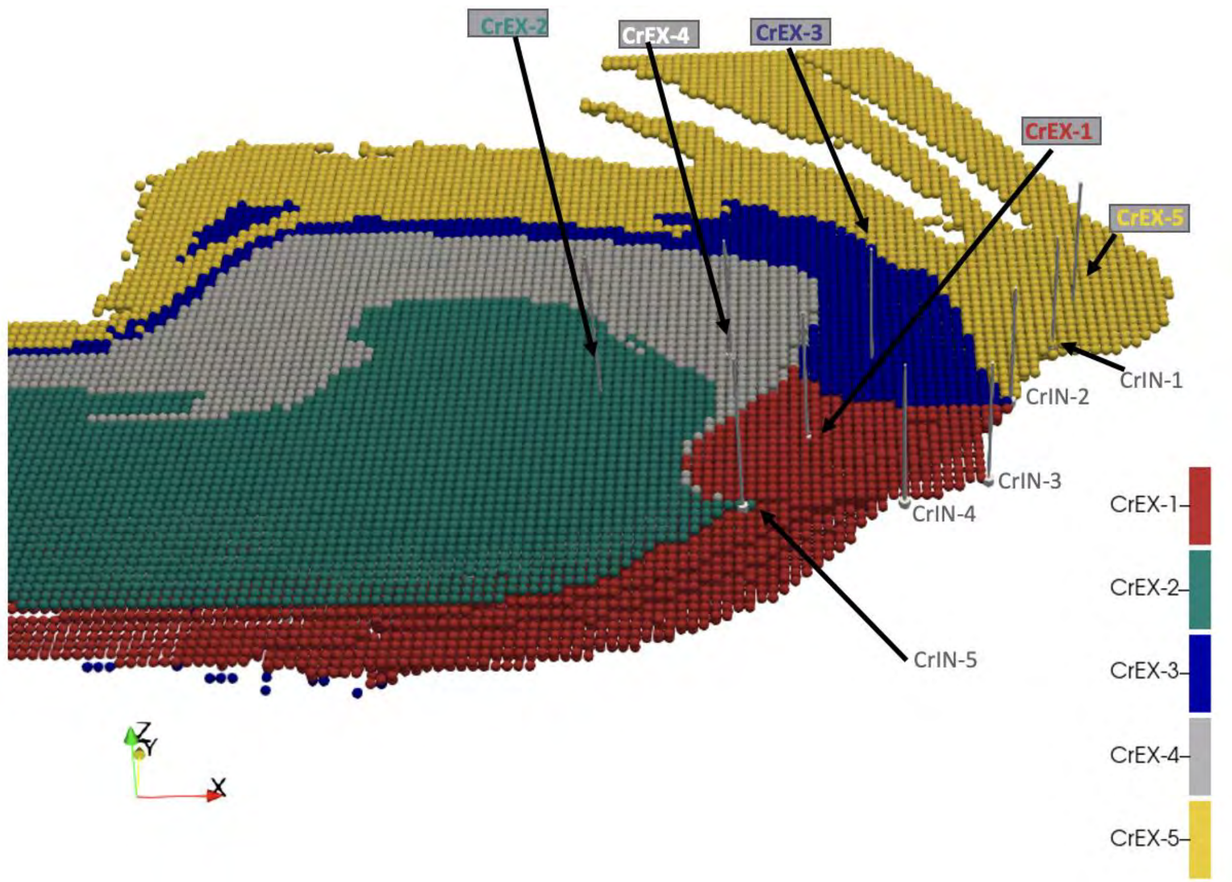

Figure 21: Angled overview (48 degrees off vertical) of the 3D capture zone for Calibration 4. Lateral particle spacing is 20 m (65.6 ft).

Some observations common to each of the four calibrations can be made based on the overview figures. First, shallow capture upgradient of the IM wells is dominated by CrEX-2 and CrEX-4 in all calibrations. This is expected given that these are the most upgradient extraction wells. As can be seen in the cross-sections below, the downgradient extraction wells' capture zones extend to greater depths. Additionally, while the capture zone of the IM system at shallow depth is roughly bounded by the injection wells in the southern extremes (e.g., Figure 17), the 3D simulations reveal that, at depth, the IM capture zone includes the area around and south of CrIN-4 and CrIN-5. This is indicative of south-to-north flow at moderate depths (~25 m to 100 m) in the region south of the IM system. In Calibration 4, shown in Figure 21Figure 21, the shallow capture zone of CrEX-5 is notable for its northern extent at low depths. As noted above, this is in part due to the southern component of the flow velocity in the area north of CrEX-5. Some gaps in the CrEX-5 capture zone of Calibration 4 are also observed. Possible explanations include high heterogeneity in the 3D conductivity, as well as non-uniform spatial discretization in this area. As noted above, there is increased uncertainty in areas of non-uniform discretization. In all calibrations, the northern region of the shallow capture zone is attributed to extraction by CrEX-5.

Cross-sections of the 3D capture zones for each of the four calibrations are presented in Figure 22, Figure 23, Figure 24, and Figure 25, respectively. As noted above, the lateral spacing of particles is 20 m, while the vertical spacing is 10 m.

Sections A and B show that the capture zones of the extraction wells obey the pattern described above, in which the most upgradient extraction wells dominate capture in the shallows, while the downgradient extraction wells capture water from increasing depth. The capture zone of the IM extends to at least 110 m below the water table, which is as deep as was evaluated in these simulations, though the locations of deepest capture vary by calibration.

Sections C and D indicate that, in all calibrations, the IM system pulls water from the south at depth (below CrIN-5) to the north toward the extraction wells. Capture in this southern area is attributed to a combination CrEX-1, CrEX-3, and CrEX-4, with the relative contributions varying by calibration. Section D for all calibrations shows that the capture zone at the water table is bounded by CrIN-5. This is generally true for all of the CrIN wells, with the exception of CrIN-1, which is close enough to CrEX-5 that some particles initiated east of CrIN-1 can still be captured.

Additional assessment of the depth of capture, including quantitative estimates of the capture depths though various areas of the plume, is presented in Section 5.0.

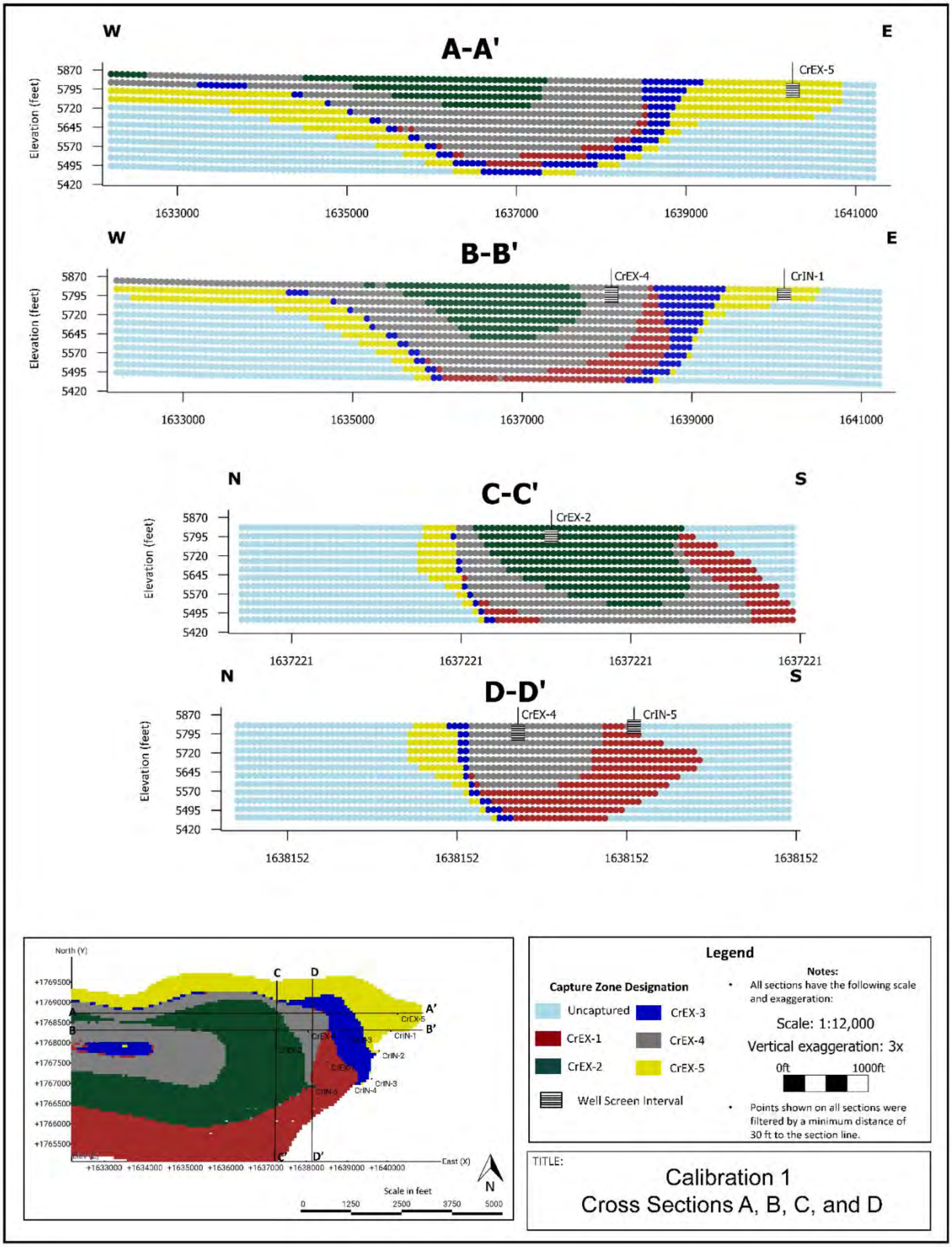

Figure 22: Section views of the 3D particle tracking results (Calibration 1).

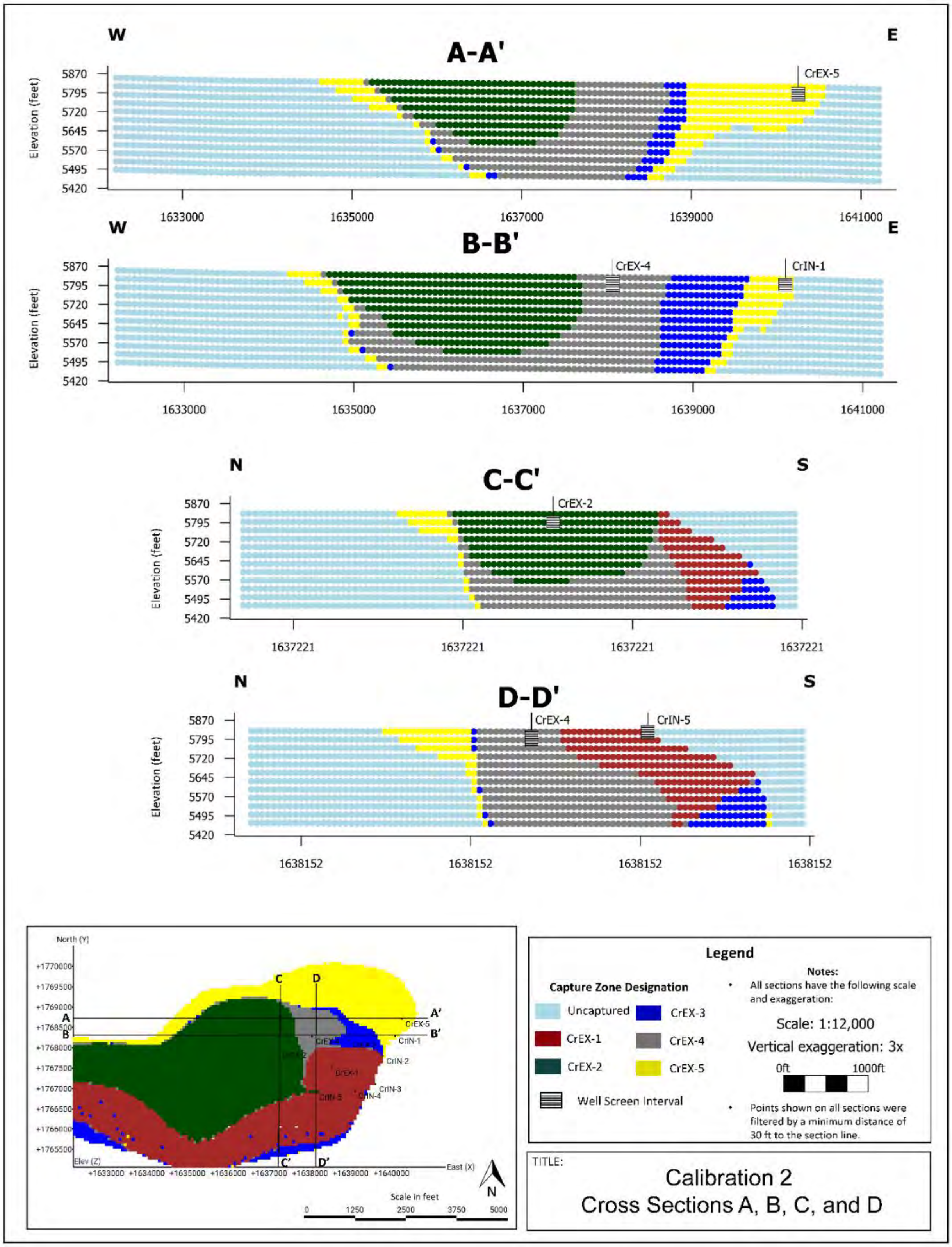

Figure 23: Section views of the 3D particle tracking results (Calibration 2).

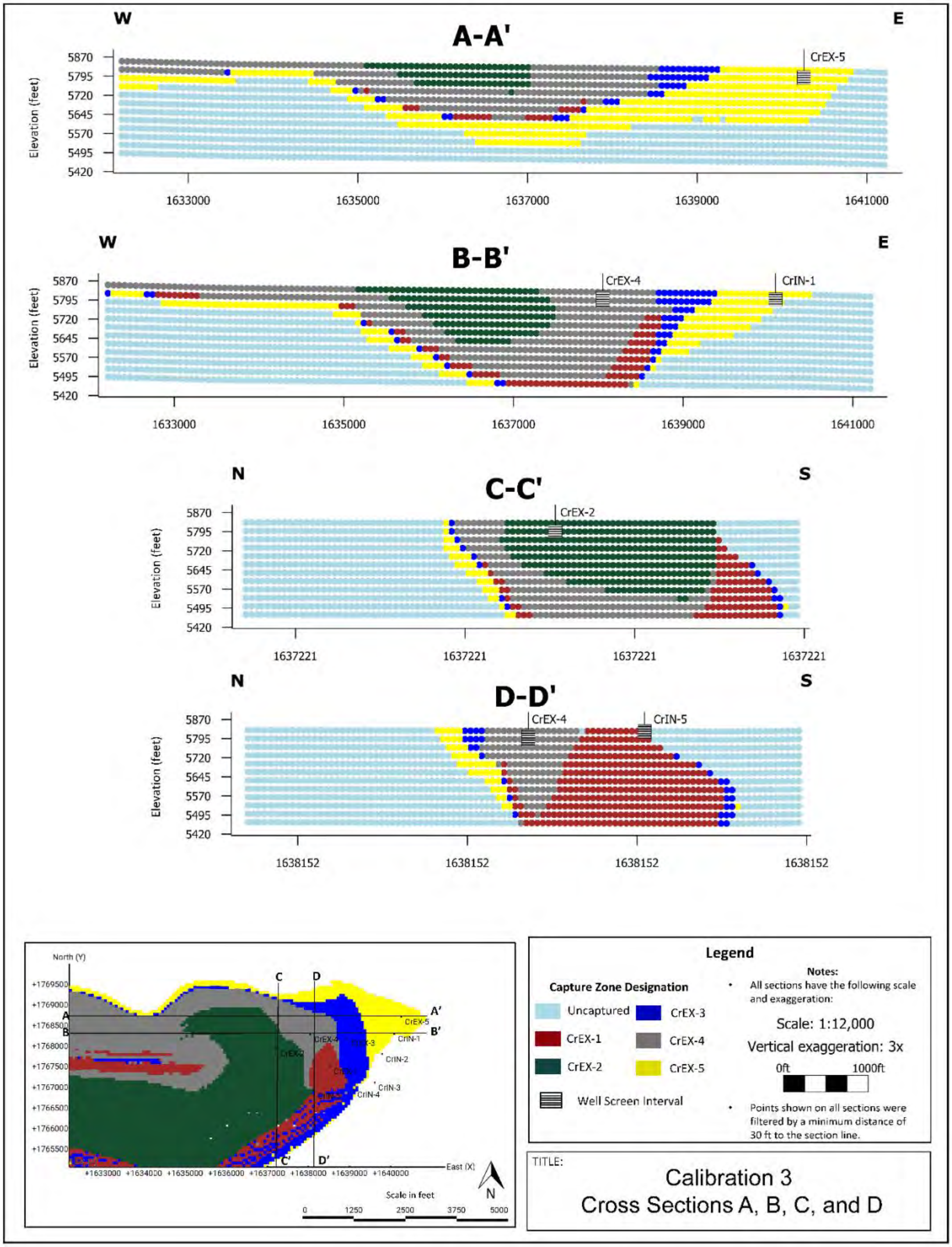

Figure 24: Section views of the 3D particle tracking results (Calibration 3).

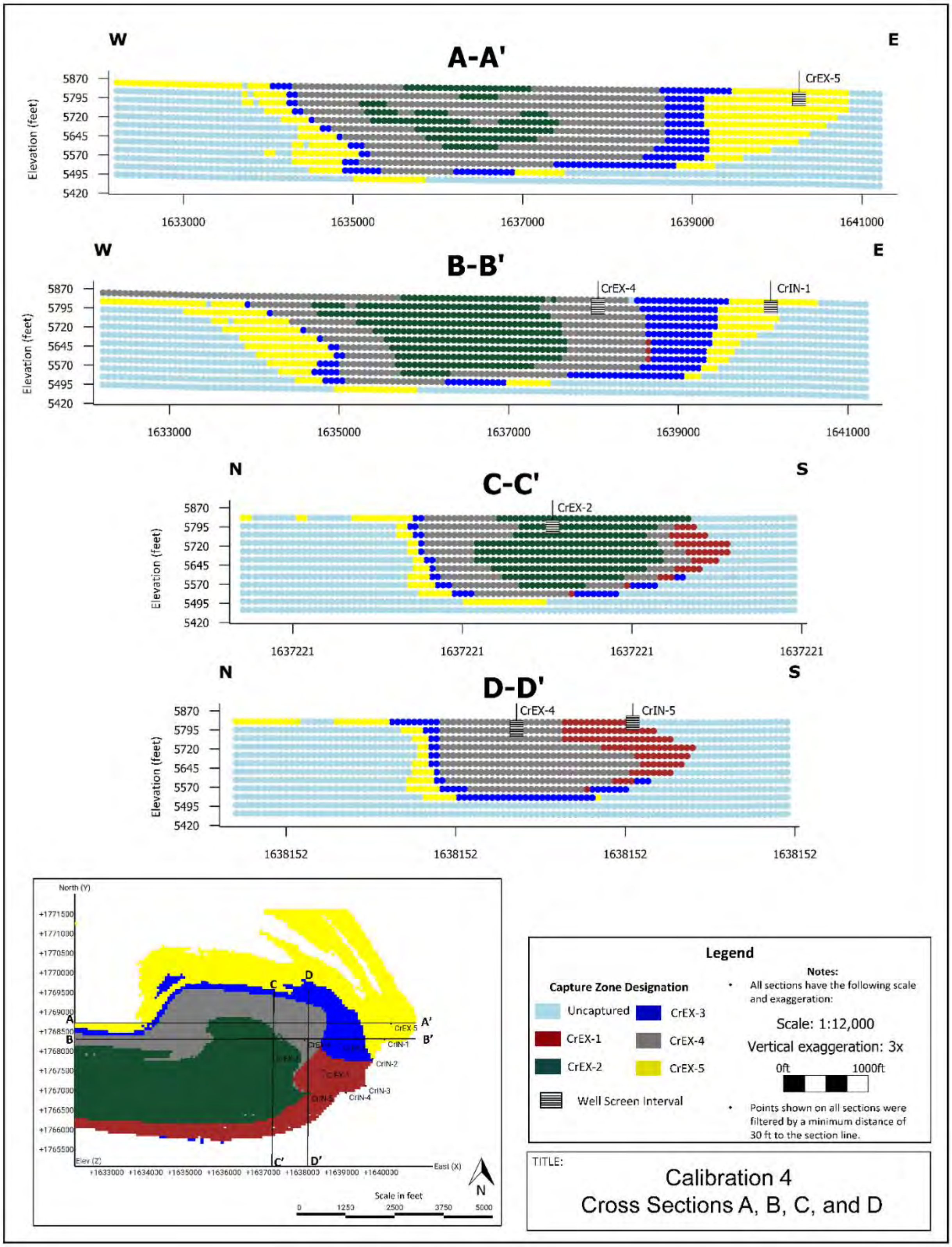

Figure 25: Section views of the 3D particle tracking results (Calibration 4).

3.2.6.3 Flood Zones Using Forward Particle Tracking

Flood zones can also be estimated using forward particle tracking. This analysis initiates particles at the injection wells and tracks their paths forward to determine the locations that are impacted by injection of clean water. As with all the particle tracking analyses presented in this document, these simulations use a steady-state flow field (see Section 3.2.4).

Figure 26 shows the resulting flood zone for each of the four model calibrations. Flood zones derived from particle tracking generally show that the particles released at the injection wells arrive at the extraction wells, and flood zones extend downgradient southeast of the CrIN wells in a narrow band that varies between around 300 ft and 1600 ft in width. Flood zones are generally similar across calibrations because the underlying flow fields are relatively similar to the southeast of the IM, where there are relatively few calibration targets (hydraulic heads, concentrations) and few observations of hydraulic flow properties.

These are compared with flood zones derived from other methods in Section 5.0.

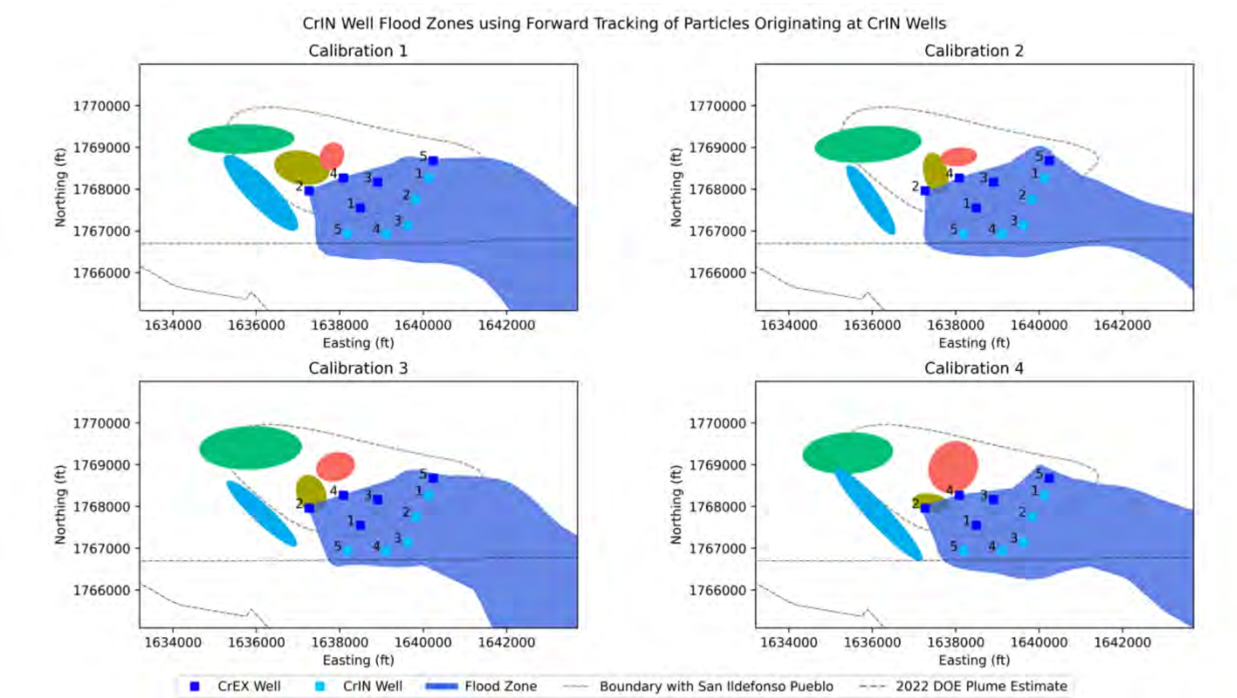

Figure 26. Flood zones derived from forward tracking of particles initialized at CrIN wells using steady-state simulations in which all IM wells are active at FPS rates (Table 5), for Calibrations 1-4.

3.2.6.4 Analysis of Particles Initiated from the Calibrated Chromium Source Areas

The capture zones in Figure 17 do not completely encompass the chromium hydraulic windows in Calibrations 2 and 3. Accordingly, the fate of chromium sources was investigated at these locations. The chromium source areas, depicted with uncertainty in Figure 13 and in their final calibrated locations in Figure 27, are discussed in detail in (Neptune 2023a).

For this analysis, particles are initialized with 5 m lateral spacing at the chromium source areas at the water table (Figure 27) and tracked forward in time using steady-state simulations in which all IM wells are active at FPS pumping rates (Table 5). In contrast to the analyses presented in Sections 3.2.6.1 and 3.2.6.2, which use 10 m and 20 m lateral particle spacing, respectively, over a very large area, 5 m lateral spacing is employed here to enable high-resolution visualization of uncaptured pathways over a relatively smaller area. Visualizing particle paths initiated from source areas provides insight into the potential flow paths of contamination from the sources to the extraction wells or downgradient beyond the IM.

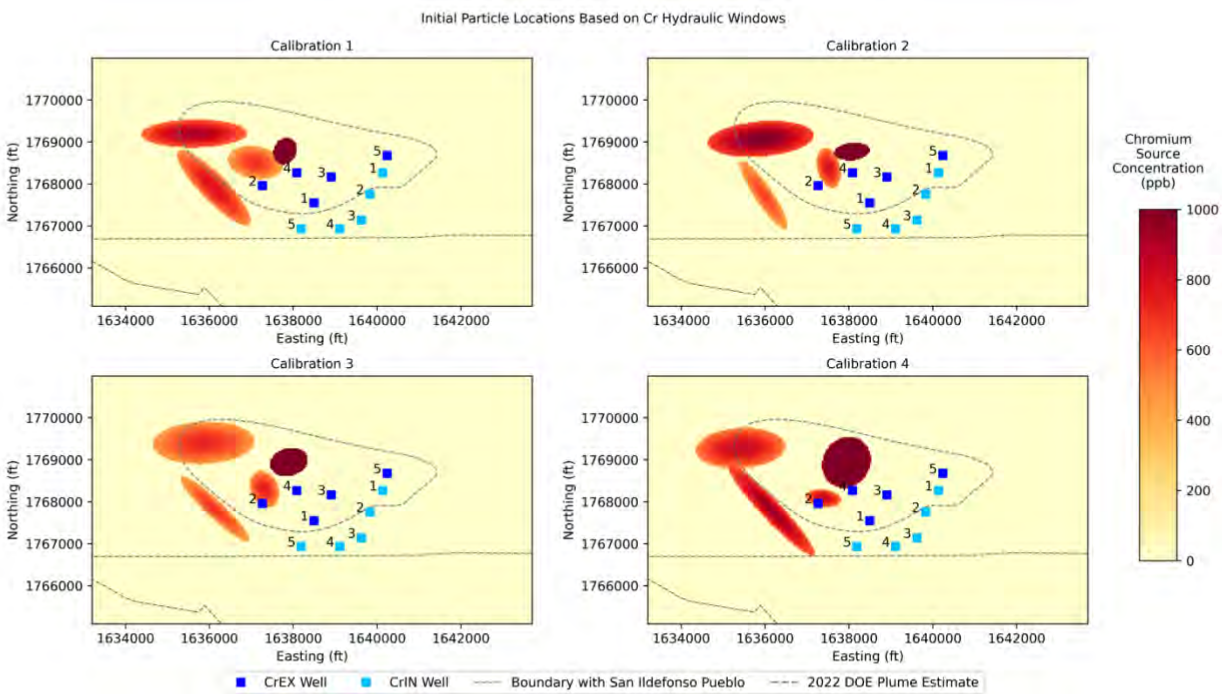

Figure 27. Chromium source areas used to derive initial particle locations.

Path lines that terminate at CrEX wells (i.e., captured particles) are shown in Figure 28. Note that this figure does not depict the entire capture zone of particles initiated at the water table as in Figure 17, because particles were only initiated in the chromium source areas. Figure 28 shows that there are no uncaptured particles from the chromium source areas in Calibrations 1 and 4, whereas Calibrations 2 and 3 show some particles originating from the northern part of the source areas are not captured by IM operations.

All four calibrations suggest connected particle pathways from the chromium source areas to extraction wells CrEX-2, CrEX-3, CrEX-4, and CrEX-5. CrEX-1 appears to be connected to the chromium sources areas in only Calibration 1. At the southern extreme of the source areas, all four model calibrations show a similar pattern of northeasterly flow toward the IM extraction wellfield. The three-dimensional particle tracking presented in Section 3.2.6.2 corroborates this idea, suggesting that the IM extraction well capture zones extend south below CrIN-5 at depth (i.e., flow is this area is generally northerly and from deep to shallow toward the extraction wells). The potentiometric surface maps presented in Section 2.1 also suggest south-to-north flow in the vicinity of CrIN-5. Due to this northerly flow, the model suggests that the southern chromium source area is within the capture zone of the IM in all four model calibrations.

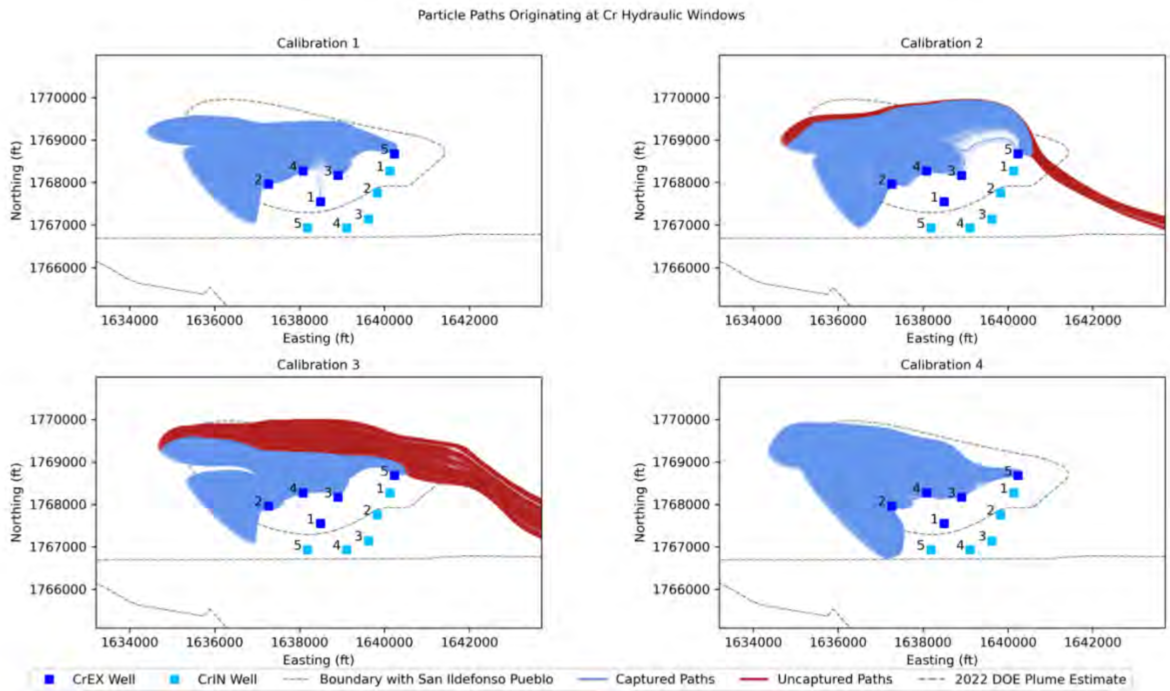

Figure 28. Particle paths derived from forward tracking of particles initialized at chromium source areas, for Calibrations 1-4.

Uncaptured particle paths from the source areas are depicted in Figure 29, with the concentrations predicted by the steady-state analysis from Section 3.2.5 and the depths relative to the water table mapped onto the particle paths. Only Calibrations 2 and 3 are presented in Figure 29 because Calibrations 1 and 4 do not feature uncaptured particles (Figure 28).

The particle tracking analysis coupled with the steady-state solute transport analysis (Section 3.2.5) provides unique insights into the downgradient concentrations associated with uncaptured flow paths. Figure 29 shows the steady-state concentrations predicted by the analysis described in Section 3.2.5 mapped onto the uncaptured particle paths; concentrations along particle paths less than 50 ppb are depicted in gray. Concentrations associated with uncaptured particles paths in Calibration 2 originate from the large chromium source area in the northwest and are reduced to below 50 ppb immediately downgradient of CrEX-5. In Calibration 3, particle paths initiated from a both the larger chromium source to the northwest and a portion of the high-concentration "primary" chromium source located just north of CrEX-4 are uncaptured. The input concentrations in the latter source range from about 2500 ppb at the center to around 1500 ppb at the edges; mixing with the clean water source (described above, and not shown in figures), diluting the input concentration to a range from about 800 ppb to 1350 ppb. Figure 29 shows that concentrations associated with uncaptured pathways in Calibration 3 are greater than 200 ppb immediately downgradient of CrEX-5 and diminish to below 50 ppb about 2500 ft east of CrEX-5. These concentrations east of CrEX-5 occur at about 100 – 130 ft below the water table.

Figure 29 shows that uncaptured particles originating at the chromium source areas remain near the water table before moving to greater depths. The uncaptured particles in Calibration 2 remain at relatively shallow depths, less than 70 ft below the water table, while traversing the IM wellfield, and those in Calibration 3 move relatively deeper to depths of around 100-130 ft below the water table. In both calibrations, uncaptured particles move to depths exceeding 160 ft below the water table when they are about 3000 ft east of CrEX-5, near the eastern edge of the extent of Figure 29. One factor responsible for the downward trajectory of these particles is the clean water source mentioned above, which provides widespread downward pressure in the eastern plume area; the infiltration rate associated with this source is strongest in Calibration 3 compared to the other calibrations, and the area of the uncontaminated source mixes with the contaminated source.

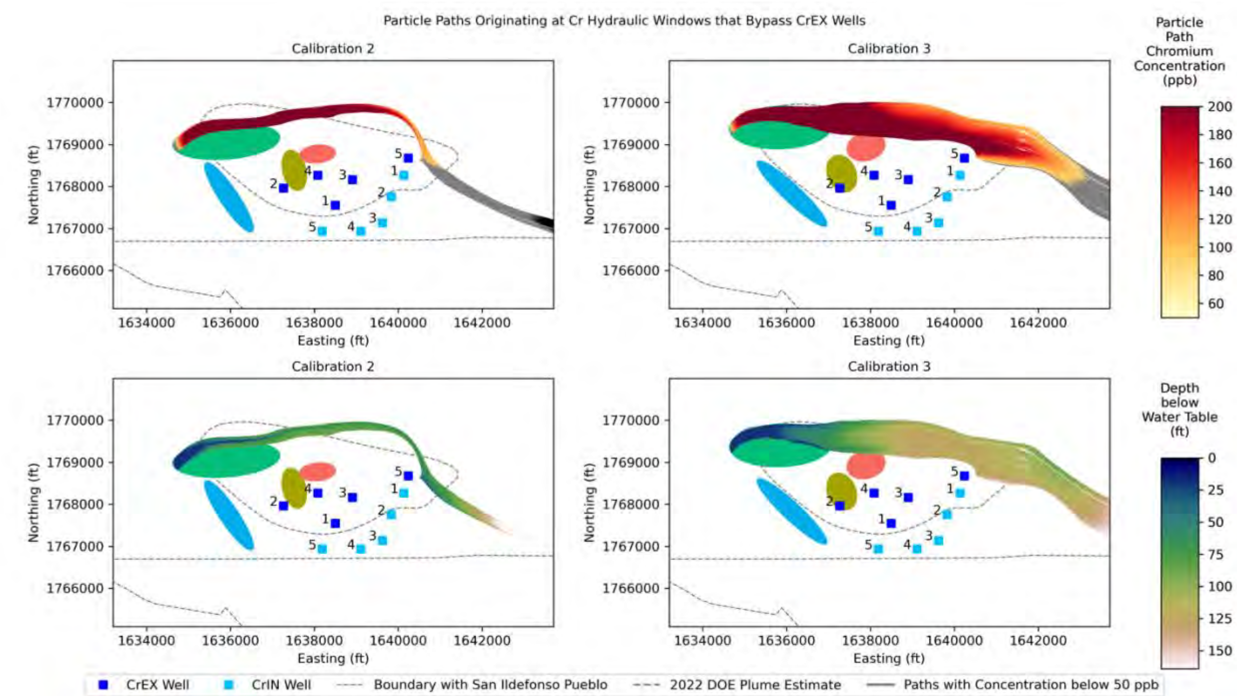

Figure 29. Paths colored by concentration (top row, yellow-red scale) and depth below water table (bottom row, blue-green-brown scale) for particles originating at chromium source locations that are not captured by CrEX wells, for Calibrations 2 and 3 (note that in Calibrations 1 and 4 all chromium source particles are captured).

3.3 Velocity Estimates

3.3.1 Velocities Using Potentiometric Surface Mapping

Average linear groundwater flow velocity was estimated at several locations during various conditions of IM operation or quiescence using Eq. (3). Figure 30 shows the locations used: (A) upgradient of the IM at CrPZ-4, (B) in the central plume area at CrPZ-2, and (C) downgradient at R-45. Point (B) also has a corresponding deep location, based on deep water table maps presented in Section 2.1.2 (deep maps at points A and C are too uncertain to use for velocity estimates). The approach is described in detail here; calculated velocities, along with the variable parameters used to demonstrate uncertainty in the estimates, are presented in Table 6..

$$v = \frac{K}{n_e}\frac{dh}{dl}, \tag{3}$$

where

K is hydraulic conductivity [ft d^{-1}],
n_e is effective (advective) porosity [–], and
dh/dl is the local hydraulic gradient [–].

Velocity estimates are subject to considerable uncertainty in all of the parameters in Eq. (3): the hydraulic gradient (estimated from maps shown in Section 2.1), the effective or advective porosity n_e, and hydraulic conductivity K. The hydraulic gradient is especially uncertain because the method is only valid when flow is assumed to be horizontal rather than three-dimensional. Estimates of the hydraulic gradient in Table 6 used the hydraulic gradients shown as green arrows in Figure 30.

Because K is known to be variable around the site due to the heterogeneity of the sediments comprising the aquifer, for the central value in the velocity estimates K is approximated by using pumping test results from the closest wells around the location. For point A, the average K is estimated using wells R-62, R-15, R-61, and R-42. For point B, the R-28 average K value is used, and for point C, the R-45 S1 average K value is used. These values are also given in Table 6. For uncertainty in K, the 1st and 99th percentiles of the K distribution for the Puye developed for the CM are used to calculate minimum and maximum velocity range estimates in Table 6 (Neptune 2023a).

For effective porosity, the distribution development for values at the site described in (N3B 2022) was used. The mean, 1st, and 99th percentiles of the total porosity distribution were multiplied by the mean fractional advective porosity value to generate a minimum, central, and maximum effective porosity value to inform the estimates in Table 6. Additional evaluation of the velocity estimates, comparison to literature values and model-derived velocities is provided in Section 5.0.

Estimated velocites using potentiometric surface mapping range six orders of mangitude, from 9E-05 to 3.3E01 ft/day, with the ceneter of the estimated ranges along with the closest K estimates generally falling between 10^{-2} to 1 ft/day. Estimated velocities from potentiometric surface mapping are discussed compared in further detail in Section 5.3 (Table 6).

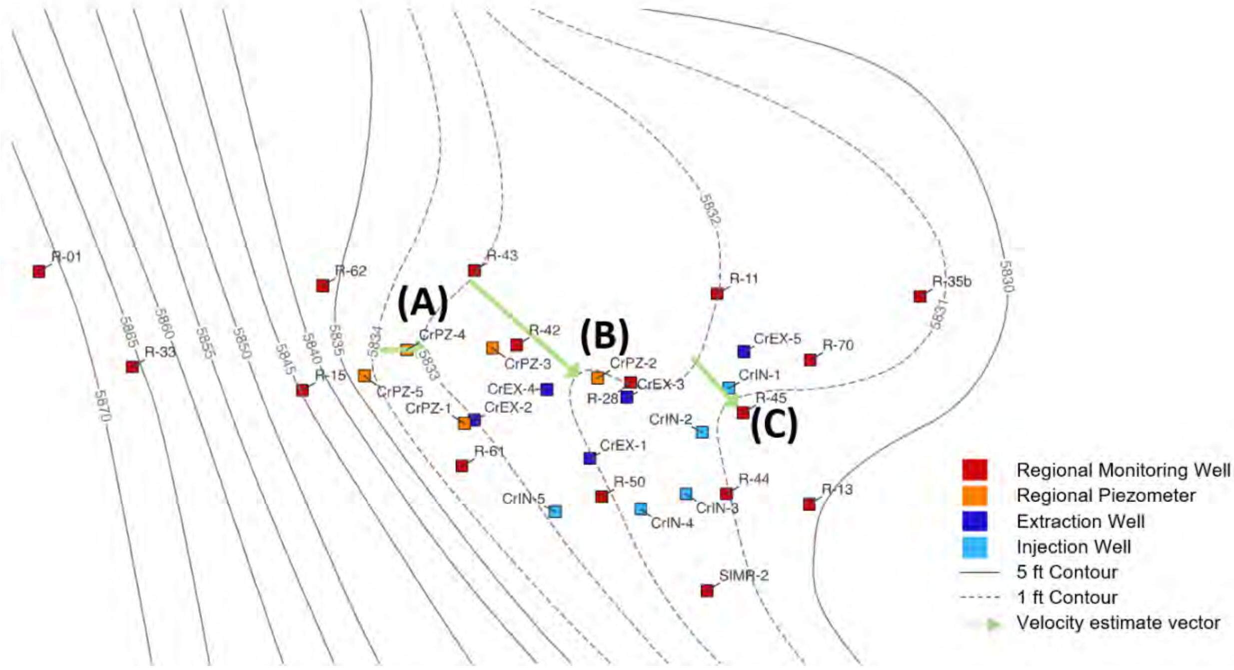

Figure 30. **Locations used for velocity estimates. Green arrows show the locations of gradients used to estimate velocities.**

Table 6.
Hydraulic Gradient and Groundwater Flow Velocity Estimates

Date	IM Status	Loc.	Hydraulic gradient[1] (ft/ft)	Closest *K* estimate[2] (ft/d)	*K* range, 1/99th percent[3]	n_e range, 1/99th percent[4]	Velocity, closest *K* (ft/d)	Velocity range[5] (ft/d)	
5/1/2020	OFF	A	2E-03	3.42	(0.2, 685)	(0.06, 0.26)	0.036	1E-03	19
5/1/2020	OFF	B	6E-04	144	(0.2, 685)	(0.06, 0.26)	0.562	5E-04	6.9
5/1/2020	OFF	C	1E-03	42.5	(0.2, 685)	(0.06, 0.26)	0.364	1E-03	15
6/15/2021	Full	A	3E-03	3.42	(0.2, 685)	(0.06, 0.26)	0.062	2E-03	32
6/15/2021	Full	B	3E-03	144	(0.2, 685)	(0.06, 0.26)	2.588	2E-03	32
6/15/2021	Full	C	1E-04	42.5	(0.2, 685)	(0.06, 0.26)	0.029	9E-05	1.2
11/1/2021	CrEX-1 Off	A	2E-03	3.42	(0.2, 685)	(0.06, 0.26)	0.042	2E-03	22
11/1/2021	CrEX-1 Off	B	3E-03	144	(0.2, 685)	(0.06, 0.26)	2.684	2E-03	33
11/1/2021	CrEX-1 Off	C	1E-04	42.5	(0.2, 685)	(0.06, 0.26)	0.026	8E-05	1.1

1. Estimated from water table maps.
2. Mean hydraulic conductivity based on pumping tests at nearby wells.
3. (Neptune 2023a) – hydraulic conductivity development.
4. Porosity and advective porosity estimates from N3B (2020a).
5. Uncertainty in velocity with variable *K* and total porosity; hydraulic gradient and advective porosity fraction fixed.

3.3.2 Velocities Using Model Results

To compare model-generated velocities with map-based velocities the same A, B, and C locations used for the map-based estimates (Figure 30) are estimated for the same conditions of IM operations. The results are presented in Table 7. The velocity is calculated to be consistent with data-based estimates in Equation (3) when the IM is off and fully on, and results are presented as an average and for each of the four calibrated models. These velocity estimates compare in magnitude with the values calculated from field data in Table 6. A summary and comparison of all estimated velocities is provided in Section 5.3.

Estimated velocites using model results range two orders of mangitude, from 0.21 to 5.4 ft/day. Estimated velocities from model results are discussed compared in further detail in Section 5.3 (Table 6).

Table 7.
Average Linear Groundwater Flow Velocity from Calibrated Model

IM Status	Loc.	Velocity Cal 1 (ft/d)	Velocity Cal 2 (ft/d)	Velocity Cal 3 (ft/d)	Velocity Cal 4 (ft/d)	Average Velocity[1] (ft/d)
OFF	A	0.26	0.20	0.24	0.13	0.21
OFF	B	0.12	0.45	0.28	0.02	0.22
OFF	C (R-45 S1)	1.70	2.11	3.22	0.80	1.96
OFF	C (R-45 S2)	0.48	0.83	0.71	0.28	0.57
Full	A	0.31	0.26	0.30	0.16	0.26
Full	B	0.12	0.61	0.56	0.01	0.32
Full	C (R-45 S1)	4.93	5.88	7.20	3.64	5.41
Full	C (R-45 S2)	0.99	1.76	1.21	0.49	1.11

1. Averaged across the four calibrations.

4.0 Concentration Monitoring Data Trend Analysis

Step 5 of the workflow in EPA (2008) is to evaluate downgradient monitoring well concentration trends to confirm the results derived in other steps of the process. “Sentinel wells” are downgradient wells not currently impacted above background concentrations and “downgradient performance monitoring wells” are wells which are currently impacted outside of and downgradient of the target capture zone. Sentinel wells at the chromium project area include R-35a, R-35b, R-13, and SIMR-2 (Figure 1). Downgradient performance monitoring wells include R-44, R-45, R-50, and R-70 (both screens at all locations). R-50 is upgradient of many CrIN wells but is included as a downgradient performance monitoring well because it is a target for clean-up with specific metrics (LANL 2015b)Section 1.3).

Figure 31 and Figure 32 depict chromium concentrations at sentinel and downgradient performance monitoring wells. The details about data filtering are presented in Neptune (2023a), and the resulting exclusions and removals are clearly indicated in the figures.

To date, the sentinel wells remain unimpacted by Cr.

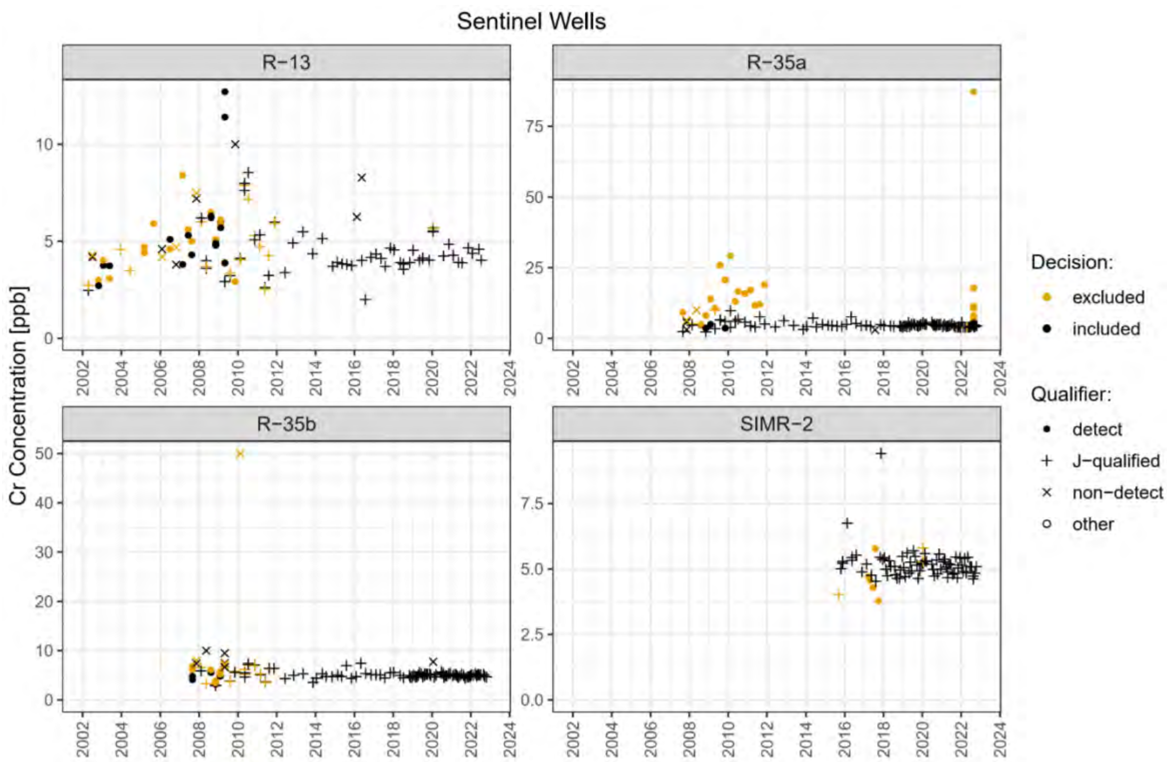

Figure 31. Chromium concentrations at sentinel wells R-13, R-35a, R-35b, and SIMR-2. Data filtering for inclusion and exclusion is described in Neptune (2023a).

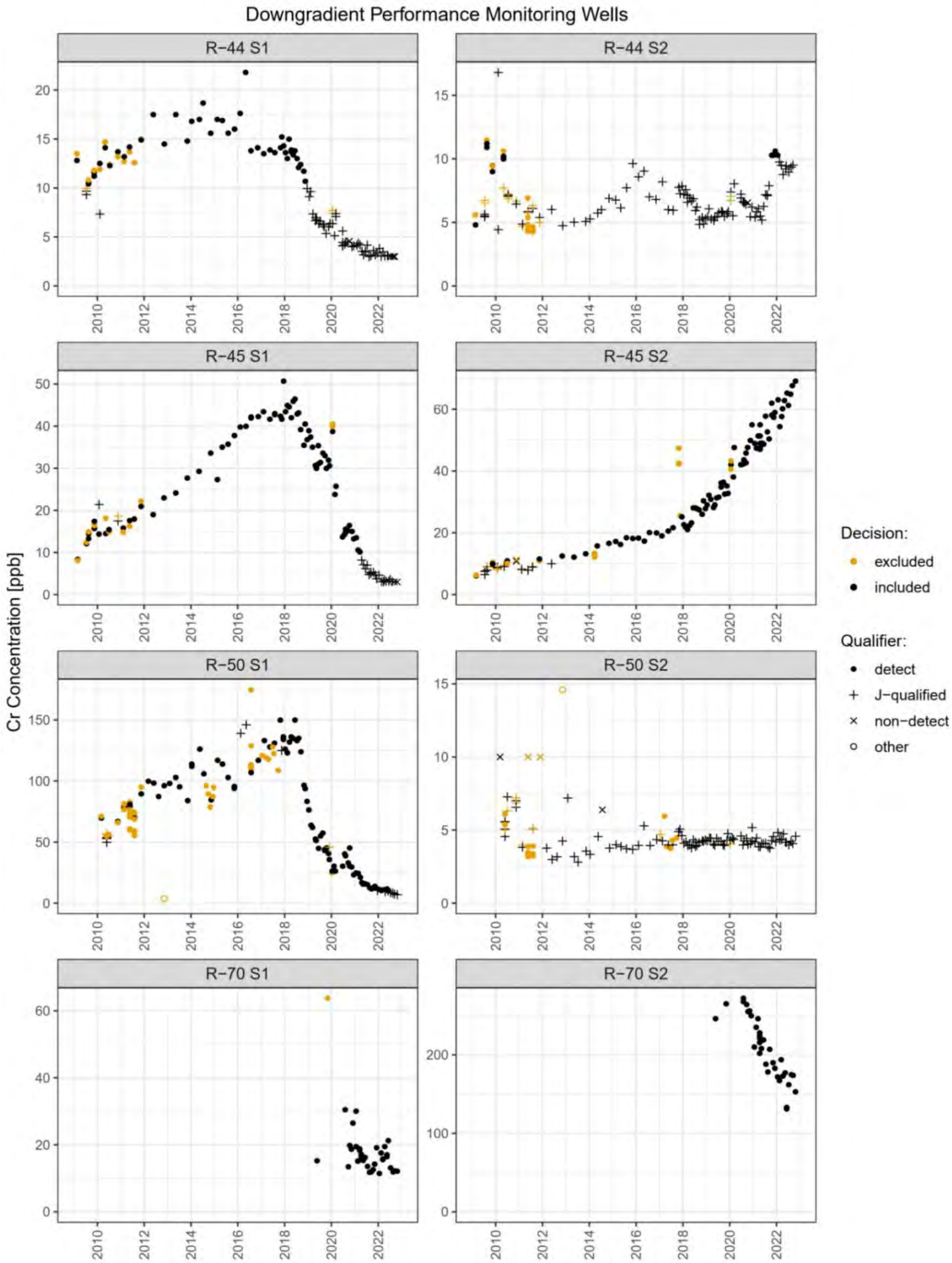

Figure 32. Chromium concentrations at downgradient performance monitoring wells R-44, R-45, R-50, and R-70. Data filtering is described in (Neptune 2023a).

The downgradient performance monitoring wells show various behaviors related to their locations adjacent to the plume. Additional analytes, including chloride (Cl^-) and sulfate (SO_4^{2-}) are present in the water that is re-injected at the CrIN wells in concentrations above background, and can be used as tracers of injected water. R-44 S1 appeared to be leveling off prior to full initiation of the IM in mid-2018, although activities at the site in 2016-2017 may have contributed to the drop seen in 2016. In Figure 33, at R-44 S1 Cr, Cl^-, and SO_4^{2-} concentrations are shown along with pumping rates at IM wells. The drop in 2016 (point A in Figure 33) is aligns with pumping tests at *extraction* at injection wells, including extraction from nearby CrINs 2 and 3, but it is unclear if those activities are related to the change in concentrations. Once the southern/central area IM operation (CrEX-1, CrEX-2, and CrEX-3; CrIN-3, CrIN-4, CrIN-5) begins in full in 2018 (point B), rises in Cl^- and SO_4^{2-} indicate the arrival of injection water at R-44 S1, and concentrations drop to below background levels. (Note that chromium concentrations in injection water are below background concentrations (~5-9 ppb) in the aquifer.)

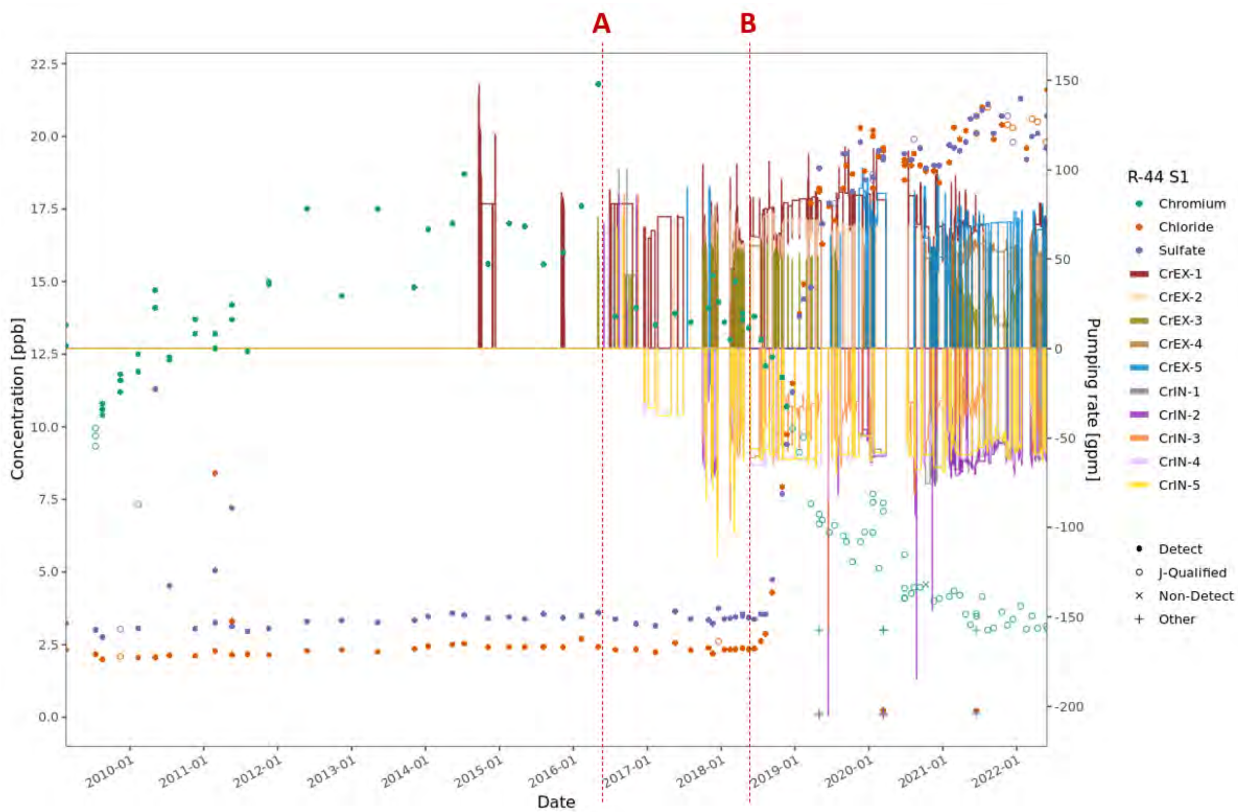

Figure 33. Cr, Cl^-, and SO_4^{2-} concentrations at R-44 S1 versus IM pumping (positive) and injection (negative) rates. A decline in chromium concentrations at point A is congruous in time with IM testing (extraction, including testing at the newly-installed injection wells). Shortly after the full southern area IM begins in 2018 (point B), a rise in chloride and sulfate concentrations indicates the arrival of injectate at R-44 S1.

R-44 S2 is considered a performance monitoring well, although concentrations remain close to background. Some variability is seen in its trend, including a recent slight rise in concentrations.

It does not appear that chloride and sulfate are increasing in R-44 S2, which is also consistent with tracer test results (Reimus et al. 2021). In those experiments, the tracer Na 1,3,6-NDS, injected into CrIN-3 in 2018, arrived at R-44 S1 a few months later but was not observed at R-44 S2, suggesting that injected water does not reach this depth.

As at R-44 S1, R-45 S1 shows a slight leveling off before the IM begins in full, around 2017-2018, with uncertain connection to the IM's initial testing activity (Figure 34). Consistent with the IM beginning regular operation in mid-2018 (point A in Figure 34), chromium concentrations at R-45 S1start to drop. R-45 S2 shows an increasing rate of chromium concentration concurrent with the IM, though small increases in concentrations have been observed since 2011, prior to the start of any IM activities. Cl^-, and SO_4^{2-} begin to rise at R-45 S2 and to decline at R-45 S1 in 2018 (Figure 34). On the other hand, both Cl^-, and SO_4^{2-} rise sharply at R-45 S1 in late 2019 after eastern area IM operations (CrEX-5; CrINs 1 and 2) began in full (point B), and continue to rise at R-45 S2. Given capture zone results (Sections 2.0-3.0), R-45 S2's rise in chromium concentration is most likely associated with portions of the plume that existed in the immediate upgradient area of R-45 prior to IM initiation instead of continuous chromium migration beyond the IM.

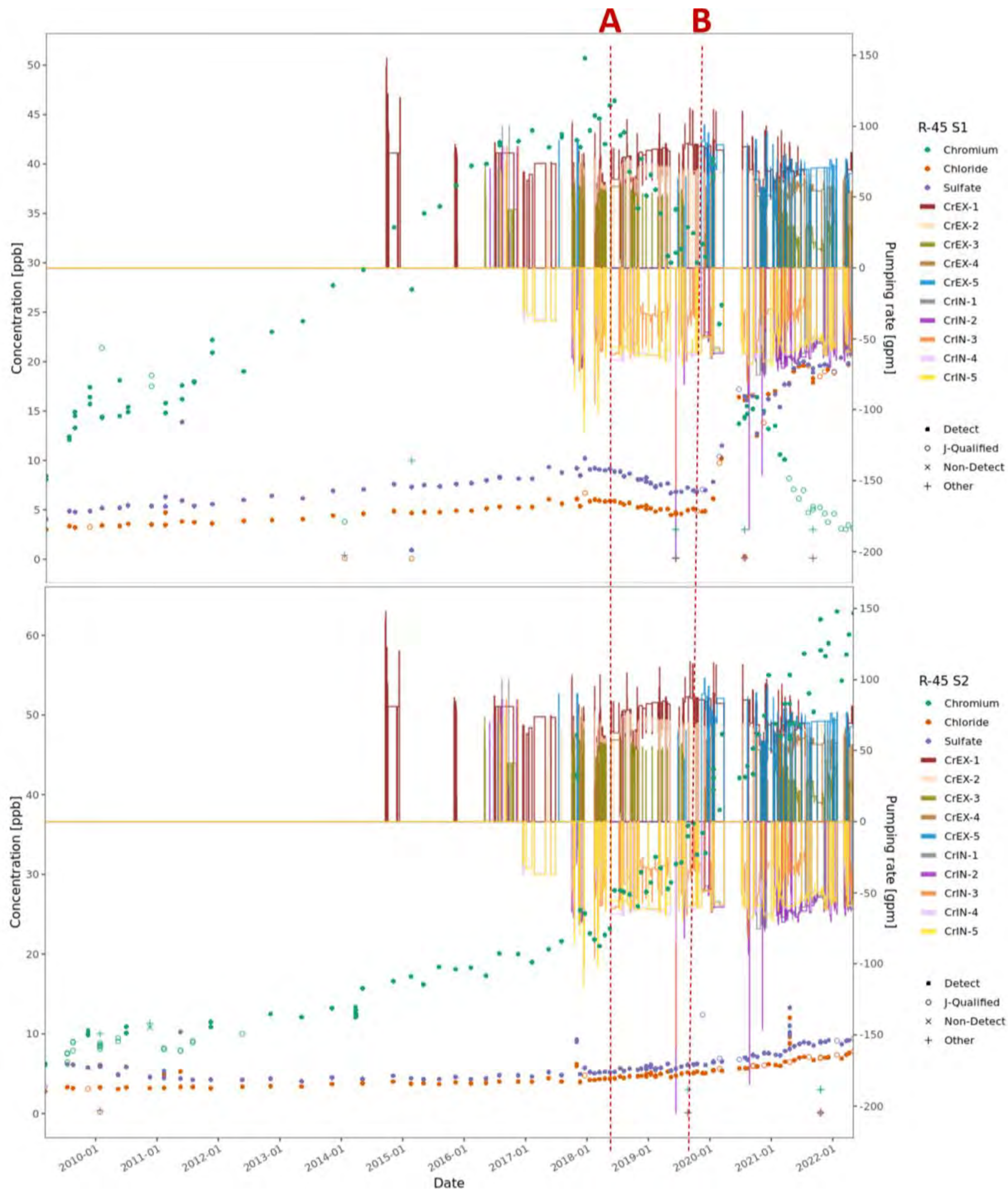

Figure 34. Cr, Cl$^-$, and SO_4^{2-} concentrations at R-45 S1 and S2 versus IM pumping (positive) and injection (negative) rates. R-45 S1, like R-44 S1, shows a chromium concentrations leveling off before the southern area IM begins in full at point A. Shortly after the eastern area IM begins in 2019 (point B), a rise in chloride and sulfate concentrations indicates the arrival of injectate at R-45 S1. At R-45 S2, an increase in the rate of chromium concentration rise is congruous with the southern area IM at point A, and chloride and sulfate concentrations begin to rise as well.

Figure 35 shows Cr, Cl^-, and SO_4^{2-} concentrations at R-50 S1 and S2. At point A, when southern area IM operation begins in full, a steep decline in chromium concentrations followed by a rise in chloride and sulfate at R-50 S1 clearly suggests the causal impact of the IM. At point B, an apparent rebound in chromium concentrations following a pause in the IM further corroborates the direct impact of the IM at this location. Although R-50 S2 is considered a performance monitoring well, rather than a sentinel well, chromium concentrations remain below background with no detectable trends.

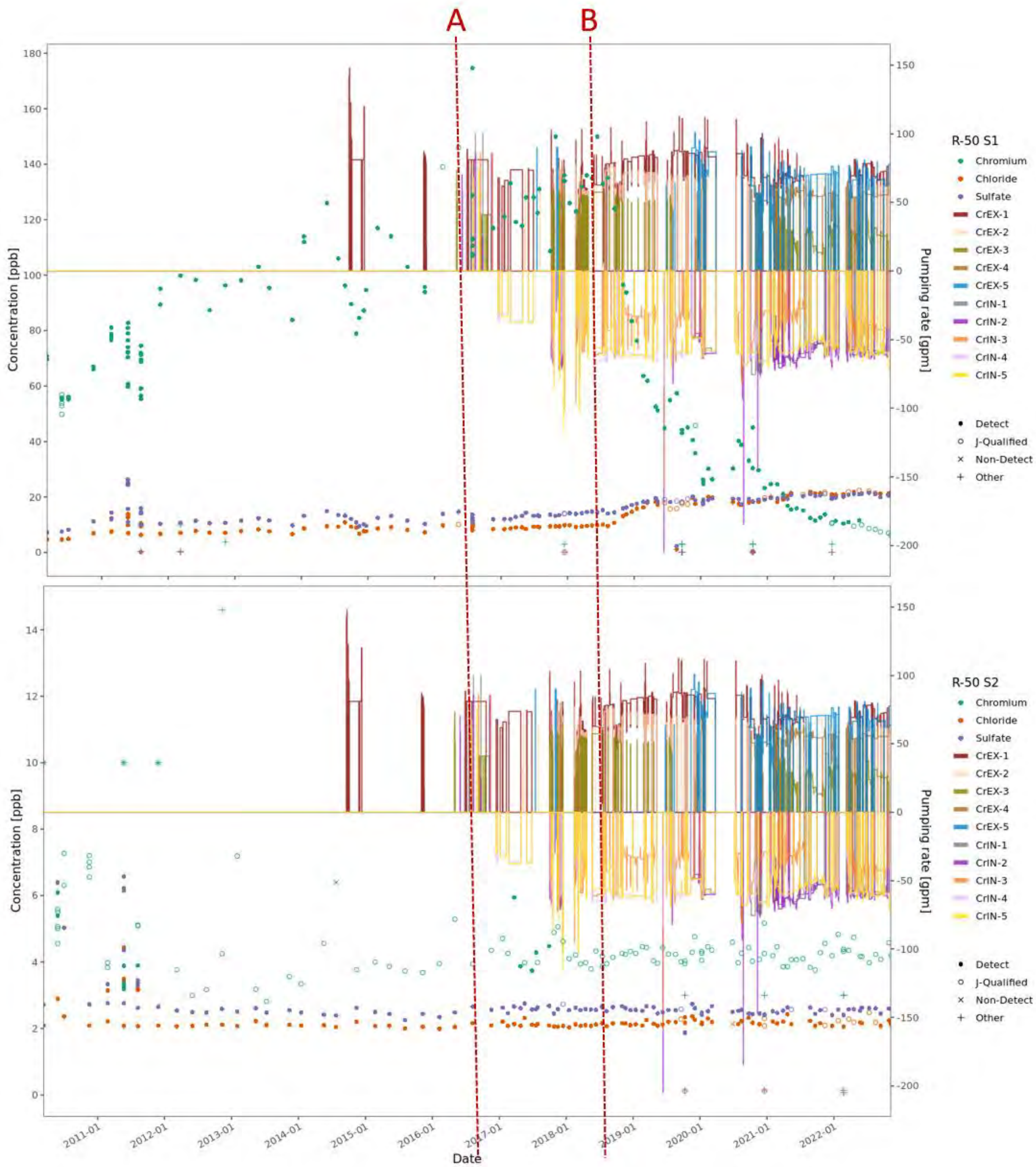

Figure 35. Cr, chloride, and sulfate concentrations at R-50 S1 and S2 versus IM pumping (positive) and injection (negative) rates. At point A, southern area IM operation begins in full; a steep decline in chromium concentrations occurs at S2, followed by a rise in chloride and sulfate. At point B, there is an apparent rebound in chromium concentrations at S2 following a pause in the IM. Chromium concentrations in S2 remain below background with no detectable trends in chloride and sulfate.

R-70 is a newer monitoring well with a limited period of record. R-70 is downgradient of CrEX-5 and recent analytical data indicates that it contains higher chromium concentrations at S2 than at S1. Figure 36 shows R-70 S1 and S2 chromium concentrations plotted with extraction and injection rates. Cl^-, and SO_4^{2-} are not shown in Figure 32 as it is inferred that neither appear to be increasing during IM operations. However, additional future analytical data will confirm if clean injected water reaches this location as eventually predicted by some flood zone analyses (Section 5.2). R-70 S1 concentrations remain consistently low throughout eastern area IM operations, which begin in late 2019 (point A in Figure 36). At R-70 S2, decreasing chromium concentrations appear to be congruent with eastern area IM operations. After a pause in IM operations at point B, chromium concentrations may temporarily rebound before returning to a decline in early 2022. If this is causal to eastern area IM operation, it suggests that R-70 S2 is within the zone of hydraulic influence of CrEX-5 or is impacted by the effects the nearby injection wells.

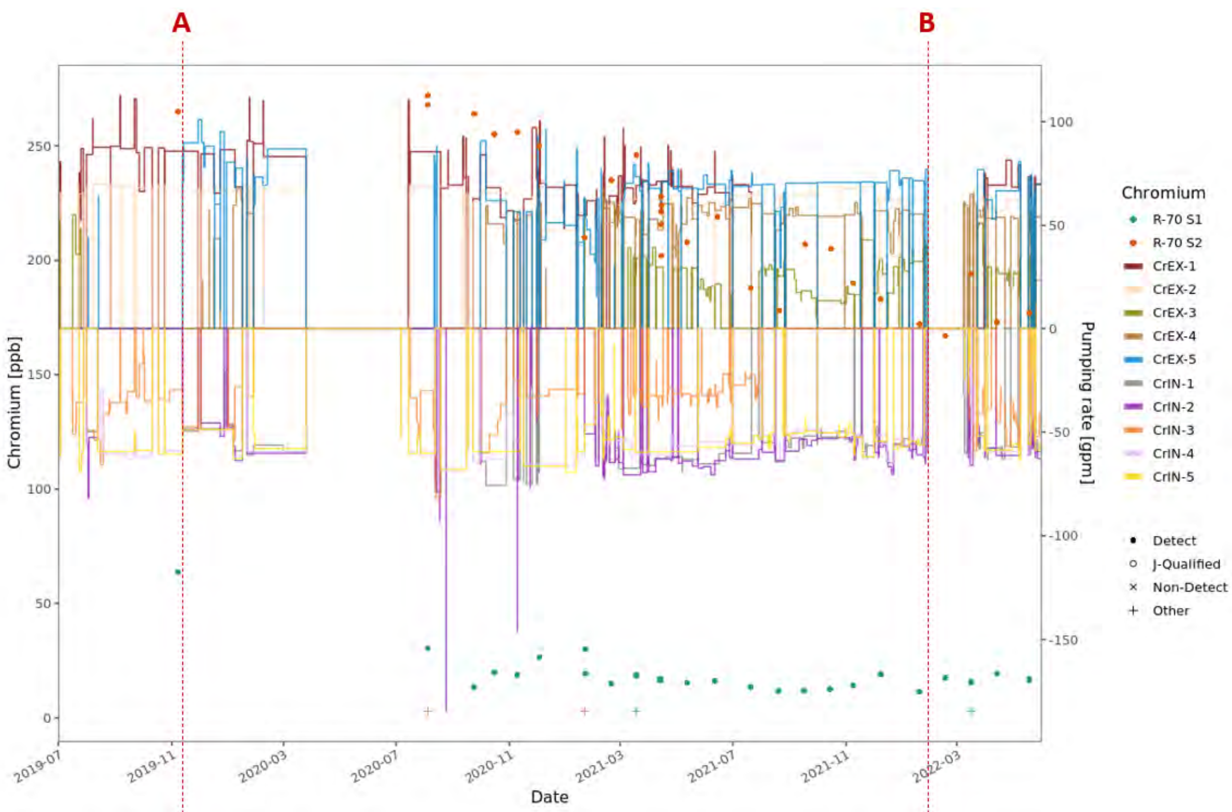

Figure 36. Chromium concentrations at R-70 S1 and R-70 S2 versus IM pumping (positive) and injection (negative) rates. Without much R-70 data before the eastern area IM begins in 2019, it is difficult to discern from the data alone what the trend is before the nearby wells begin pumping, but a decline is observed in R-70 S2. During a brief pause in the IM at point B, a possible rebound in R-70 S2 concentrations may have occurred for one sampling event while the IM starts up again.

In order to fill apparent data gaps, additional monitoring locations are also planned around the site, including downgradient of the plume. This will help with the iterative process of recalibrating the numerical model, updating the site CSM, and ultimately understanding the capture and flood zones to prepare for designing and evaluating a final remedy.

5.0 Discussion

In this Discussion section (Step 6 of EPA (2008)), capture and flood zones are evaluated by combining all lines of evidence presented in Section 2, 3 and 4. Each method has inherent uncertainty, and more confidence can be placed on estimated capture that is corroborated across lines of evidence.

Additionally, while not identified by the EPA (2008) workflow, velocities (computed both from data and the model) are estimated for key points of interest around the site (Section 3.3). The final steps of the EPA workflow include assessing uncertainty, which is done in Section 5.4.

The process of capture and flood zone evaluation presented in EPA (2008) is intended to be iterative. As the interim measure remediation proceeds, valuable new data are collected that will help inform and refine these results.

5.1 Capture Zones

The extent of the capture zone of the IM has been estimated quantitatively using several methods. The capture zone extent determined by each of these methods is shown in Figure 37. Each curve on Figure 37 represents the average capture zone for that method; for example, the orange curve is the averaged capture zone across the two water level maps presented above, while the green curve represents the shallow capture zone, calculated using particle tracking, averaged across the four model calibrations.

The smallest capture zone is estimated by potentiometric surface mapping (orange). The analytical width estimate (black) agrees favorably with the other estimates, despite the major assumptions and simplifications inherent in the method.

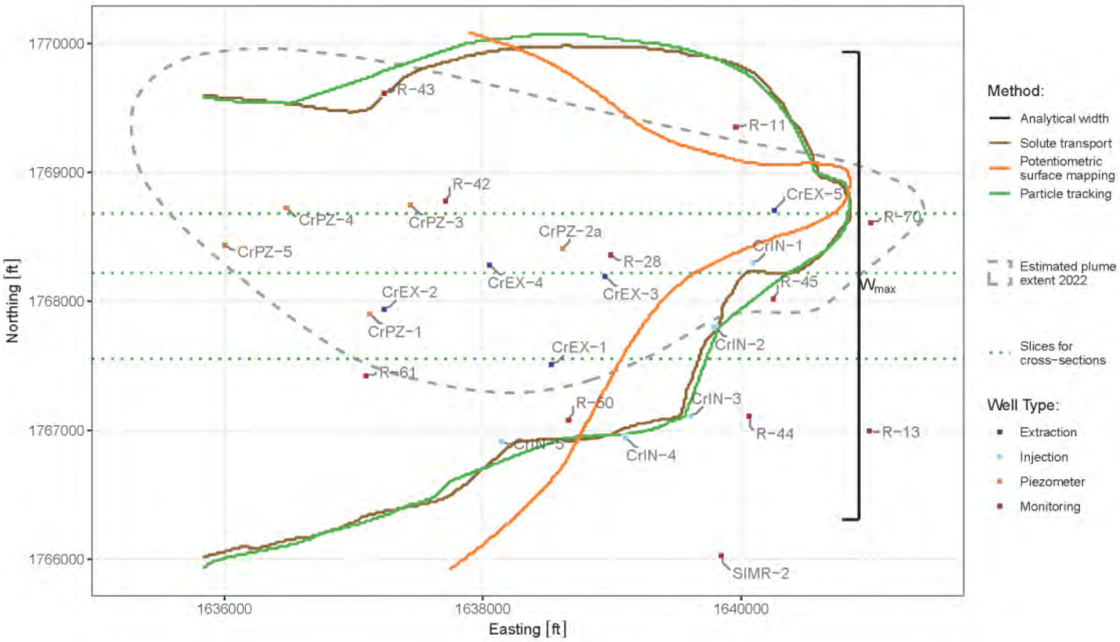

Figure 37. Capture zone of the IM during typical full operation, estimated by multiple methods.

The estimated plume extent as of 2022 is also shown in the Figure 37. The plume estimated footprint extends downgradient further than the estimated capture zones, suggesting that there is some contamination that is beyond the reach of the IM extraction wells. This part of the estimated plume is relatively deep below the water table (~50 ft or more) based on the data at R-70 S2. In the area near CrEX-5, the 3D particle tracking indicates that the capture zone footprint becomes smaller at depth; Figure 38 (top panel) shows the estimated depth profile for the capture zone in the west-east section intersecting CrEX-5, averaged across the four calibrations, for the 3D particle tracking simulations. The lower panels of Figure 38 show similar slices west-east slices of the 3D particle tracking results through the center of the plume near CrEX-4 (center panel), and the southern part of the plume area through CrEX-1 (lower panel). As noted above, capture was only evaluated to a depth of approximately 110 m below the water table, so the total depth of the capture zones shown should not be overinterpreted; the leading edge of the capture (downgradient, or right side of Figure 38) is accurate based on the simulations and of greater interest with respect to depth of capture near the edge of the capture zone.

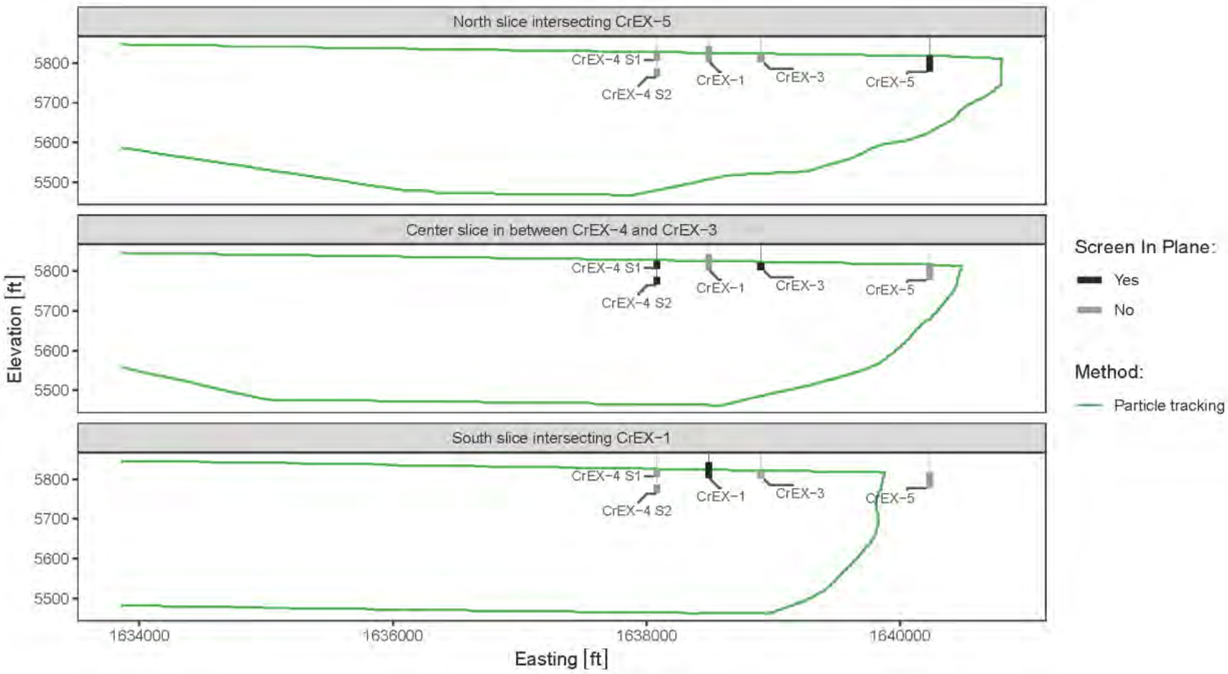

Figure 38. Capture zone of the IM in cross-section view along three East-West sections (top), estimated using 3D particle tracking (Section 3.2.6.2).

The composite results shown in Figure 37 suggest that the objectives of the IM system and target capture (Section 1.4) are met in most simulations across most methods. Capture zone analyses indicate consistent capture at the southern and southeastern edges of the plume. Model results suggest a potential pathway for chromium in concentrations exceeding 50 ppb to bypass the IM to the north of CrEX-5, though all model results suggest that dispersion and dilution reduce the plume footprint in this downgradient region considerably over time and space.

Finally, observations of chromium concentrations in sentinel wells and downgradient performance monitoring wells, presented in Section 4.0, show that all sentinel wells remain at background levels of chromium (Figure 31). Concentration decreases at performance monitoring wells R-44, R-45, R-50, and R-70 indicate that these wells are part of the integrated capture zone created by the IM.

5.2 Flood Zones

The extent of the flood zone of the IM is also estimated using several methods and is shown in Figure 39. Additionally, tracer study results are shown with squares in locations where injected tracers have been identified in other monitoring wells.

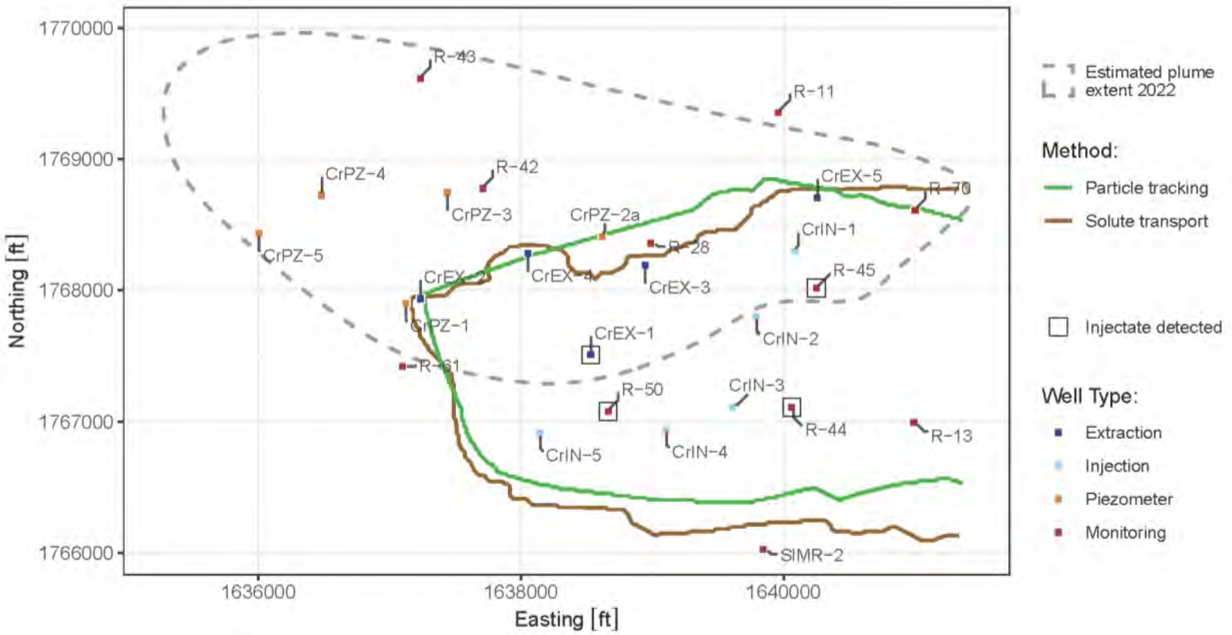

Figure 39. Flood zone of the IM during typical full operation, estimated by three numerical methods. At well locations where tracers have been detected a box is used to denote tracer arrival.

The three regions defined by the methods 1-3 above show good agreement with one another. All show that the flood zone of the injection wells extends to the extraction wells, and that the injection water flows downgradient.

Another way to examine flood zones is with geochemical tracer experiments, both planned and opportunistic (Reimus et al. 2021). Opportunistic tracers include Cl^- and SO_4^{2-}, both of which are elevated in the injectate at the CrIN wells, as described in Section 4.0. Rising Cl^- and SO_4^{2-} at a monitoring well suggests that it is likely within the flood zone of the injection wells.

Figure 40 shows Cl^- and SO_4^{2-} concentrations for eastern and some southern area wells (R-70, CrEX-5, R-45, R-44, and R-13) along with extraction and injection rates. Some wells have a clear signal of injection water. Observed signals of breakthrough likely correspond to either the onset of southern area IM operations in R-44 S1, or eastern area operations, like R-45 S1. CrEX-5 and R-70 S2 appear to have elevated levels of Cl^- and SO_4^{2-} from the beginning of their periods of record, and so their response to injection is unclear. For the other deep screens, R-44 S2 shows little sign of injectate (except possible sulfate), while R-45 S2 demonstrates a clear rise in both Cl^- and SO_4^{2-}. R-13 shows no increase in Cl^- or SO_4^{2-}.

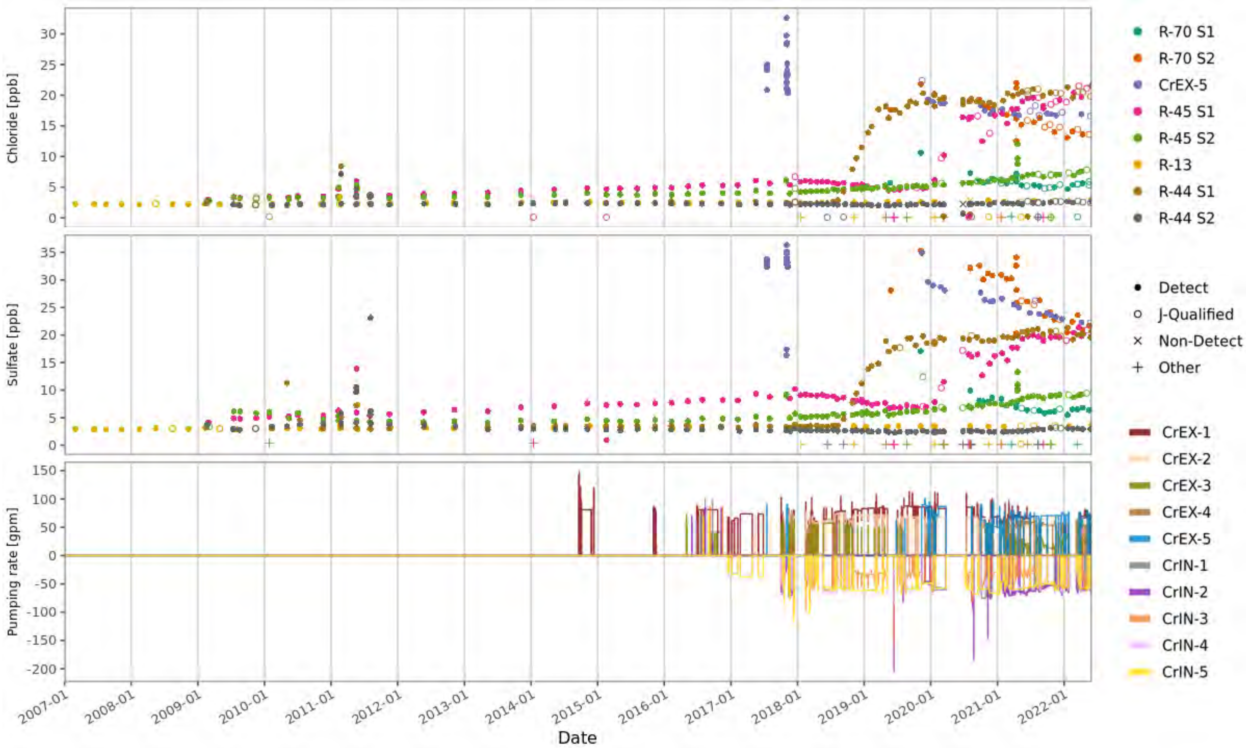

Figure 40. Top panel: Cl^- concentrations at R-13, R-44, R-45, R-70, and CrEX-5. Middle panel: SO_4^{2-} concentrations. Bottom panel: IM pumping (positive) and injection (negative) rates.

Figure 41 shows Cl^- and SO_4^{2-} concentrations at southern and central area wells. Most central area wells show elevated Cl^- and SO_4^{2-}, likely as a result of injected water migrating towards the center of the capture zone as a result of the IM system. R-50 S1 shows a clear rise in Cl^- and SO_4^{2-}, likely associated with the onset of consistent IM operations in the south.

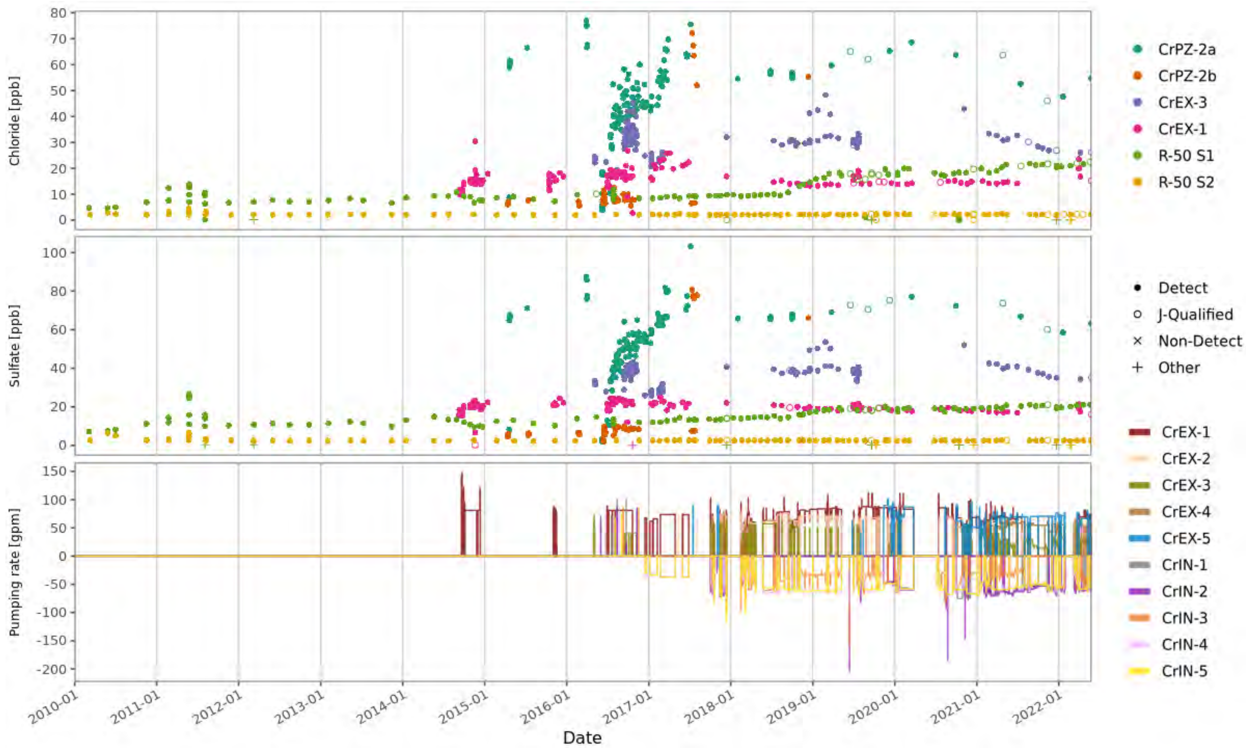

Figure 41. Top panel: Cl^- concentrations at CrPZ-2a, CrPZ-2b, CrEX-1, CrEX-3, R-50 S1, and R-50 S2. Middle panel: SO_4^{2-} concentrations. Bottom panel: IM pumping (positive) and injection (negative) rates.

Opportunistic injectate chemical tracer results are similar to modeled results shown in Figure 39. Near the edges of the predicted flood zones it is important to remember that numerical analyses depict long-term steady-state operations over many years, so there is a temporal component to the extent of the flood zone.

In addition to the opportunistic tracers, planned tracer tests were performed using disodium naphthalene disulfonate (NDS) tracers in the injection wells; multiple tests were conducted in 2017 and 2018 at CrINs 3, 4, and 5 (Reimus et al. 2021). The results indicated that even under the influence of injection, there was no detection of CrIN tracers in deeper screens of monitoring wells. The tracers injected in CrIN-4 (Na 1,5-NDS and Na 2,6-NDS) were detected in R-50 S1 (and CrEX-1, in the case of Na 1,5-NDS). The tracer in CrIN-3 (Na 1,3,6-NDS) was clearly detected in R-44 S1 a few months after it was deployed. No tracers from CrIN-5 were definitively detected in any monitoring well locations.

5.3 Velocities at Key Locations

Velocities in the chromium plume are compared at the three key locations depicted in Figure 30. Points A and B are upgradient of the IM, and point C is located downgradient of the IM. The ambient velocities estimated based on the water table maps and site data (Table 6) and the model (Table 7) are compared side-by-side for the same locations and times in Table 8.

For the IM "off" status, modeled velocities at points A and C (0.26 ft/d and 5.41 ft/d, respectively) are faster (by approximately one order of magnitude) than the field data estimates based on the hydraulic conductivity data from the well closest to the point. However, the modeled velocities remain well within the ranges of estimated velocities when uncertainty in hydraulic conductivity and porosity is accounted for (0.0013 to 19 ft/d for location A, and 0.0011 to 15 ft/d for location C). For the IM "full" status, the field data and modeled estimates both find that velocities decrease at point C when the IM is operational. The modeled velocity at location C is approximately a third, and the velocity based on the closest K is approximately a tenth, of velocities during the IM "off" status. However, for points A and B, the model-based estimates show a small decrease in velocity magnitude when the IM is on, whereas the data-based estimates show increases in velocity as a results of larger hydraulic gradients estimated at those points from a potentiometric surface (Section 3.3.1).

Modeled velocities compare favorably with literature estimates at the central plume location, including ones based on similar methods (LANL 2012) and on experiments using tracers and borehole dilution tests (Reimus et al. 2021). These other methods focused on the central plume area during ambient (non-pumping) conditions, similar to location B in Figure 30 during IM status "off" (5/1/20 in Table 6). Table 9 summarizes velocity estimates from prior work around the site.

While there is general agreement between data-based, model-based, and tracer/dilution test derived velocities, the uncertainty in aquifer properties combined with a relatively flat water table results in a range of magnitude estimates that span several orders of magnitude. The wide range of estimated velocities highlights how uncertain these calculations are for the chromium plume.

Table 8.
Velocity Estimates from Field Data and Model

		Data calculations			Model estimates
IM Status	Location	Velocity range[2] (ft/d)		Velocity, closest[1] *K* (ft/d)	Velocity average (ft/d)
OFF	A	0.0013	19	0.04	0.26
OFF	B	0.0005	6.9	0.56	0.32
OFF	C	0.0011	15	0.36	5.41
Full	A	0.0022	32	0.06	0.21
Full	B	0.0022	32	2.59	0.22
Full	C	8.51198E-05	1.2	0.03	1.96
CrEX-1 Off	A	0.0015	22	0.04	-
CrEX-1 Off	B	0.0023	33	2.68	-
CrEX-1 Off	C	7.68049E-05	1.1	0.03	-

1. Mean hydraulic conductivity based on pumping tests at nearby wells.
2. Uncertainty in velocity with variable *K* and total porosity; hydraulic gradient and advective porosity fraction fixed.

Table 9.
Velocity Estimates from Prior Analyses

Location	IM status	Type of Analysis	Estimated Velocity, ft/d	Reference
R-42 area	Ambient	Tracer test	0.427	Reimus et al. 2021
R-42 area	Ambient	Borehole dilution test	0.459	Reimus et al. 2021
R-28 area	Ambient	Tracer test	3.937	Reimus et al. 2021
R-28 area	Ambient	Borehole dilution test	3.609	Reimus et al. 2021
R-50 S1 area	Ambient	Borehole dilution test	0.820	Reimus et al. 2021
CrPZ-2 to CrEX-3	Mostly Ambient	Cross-hole tracer test	3.281	Reimus et al. 2021
R-43 S1	Ambient	Borehole dilution test	6.562	Reimus et al. 2021
CrPZ-3	Ambient	Borehole dilution test	0.197	Reimus et al. 2021
R-62	Ambient	Borehole dilution test	0.262	Reimus et al. 2021
CrPZ-1	Ambient	Borehole dilution test	0.853	Reimus et al. 2021
CrPZ-2a	Ambient	Borehole dilution test	0.115	Reimus et al. 2021
CrPZ-2b	Ambient	Borehole dilution test	0.082	Reimus et al. 2021
Chromium plume area	Ambient	Data using Eq. (1)	0.36 - 0.45	LANL 2012, Table J-3.0-1
Chromium plume area, full range	Ambient	Data using Eq. (1)	0.009 - 5.4	LANL 2012, Table J-3.0-1

In general, past and present velocity estimates in the chromium plume area yield the following results:

- Ambient velocities are higher upgradient and downgradient of the plume, due to larger hydraulic gradients (points A and C compared to point B).
- *Within* the plume area, velocities are thought to vary and are faster in the R-28 area (near point B) (Reimus et al. 2021). (R-43 S1 also displays apparently high velocities, see Table 9.)
- During pumping, from the data-based estimates with gradients estimated over a larger cross-section of contours, velocity magnitudes appear to increase upgradient (A) and in the central plume area (B), and decrease at the point C downgradient location. However, at the exact point locations selected for model output, the modeled velocities decrease at A and B as well.

5.4 Conclusions

All estimates presented here for full IM capture and flood zone extent have inherent uncertainty, and corroboration across these multiple methodologies instills higher confidence in the results. For example, regarding uncertainty associated with standard methods presented here as outlined in EPA (2008):

- **Capture zone by water table map**: "Multiple interpretations of water level contours and associated flow directions are possible for one data set by using a different contouring algorithm (or by having a different hydrogeologist contour the data manually). The potential for alternate interpretations of water level contours should be considered when evaluating capture based on the contours" (p.11).

- **Streamlines and particle tracking**: "Particle tracking based on simulation of heads can provide a precise delineation of both horizontal and vertical hydraulic capture (not accounting for dispersion). Precision, however, should not be confused with accuracy. The capture zone indicated by the particle tracking is only as accurate as the underlying head predictions from the simulation model, which are subject to many types of uncertainty (e.g., parameter values, boundary conditions)" (p.23).
- **Concentration monitoring data trend analysis**: "However, since the actual extent of the capture zone is not generally known, the concentration trend at [a downgradient monitoring well] could be erroneously interpreted as failed capture (because concentrations downgradient of the extraction well remain above background). Interpretation of capture based on concentration trends at monitoring wells located downgradient of the Target Capture Zone is complicated by several other factors: there may be limited concentration data…interpretations of concentration data related to capture may take years because ground-water flow velocities (and associated concentration changes) are generally quite slow…" (p.25).

For particle tracking, EPA (2008) recommends that the most reliable approach is "tracking particles forward in space and time from a large variety of starting points (horizontally and vertically) and determining which of those particles reach each extraction location" (p.24). This is the primary approach described in Section 3.2.6. As EPA (2008) notes, however, parameter uncertainty can never be completely eliminated; however, the four models bracket uncertainty in parameter space. Vesselinov (2007) notes that, for model-based transient capture zone analyses, uncertainties in the source terms can have important impacts on capture zone estimates. The chromium source area parameters, which differ between the four model calibrations, are considered some of the more sensitive and uncertain parameters. Differences between the calibrations are not only due to the different source characteristics but also different underlying flow fields and heterogeneous conductivity fields. Spatially varying parameters like conductivity are calibrated primarily in the immediate area of the plume where observation data (head and concentration, primarily) are available. Therefore, particle tracking results are increasingly uncertain at points far from the calibration targets. Model discretization can also impact the particle tracking results. As mentioned previously, particle tracking results near regions of non-uniform spatial discretization should be interpreted cautiously.

Estimates of capture zones based on flow direction inferred from water level mapping are subject to the uncertainty of human interpretation (in the case of hand-drawn maps), contouring algorithm and smoothing parameters (in the case of automated interpolations), and data reliability. Additionally, the approach to capture zones described in Section 2.1.1, where vectors or streamlines are assumed perpendicular to hydraulic head contours, has additional uncertainty caused by the hydraulic conductivity field. In an anisotropic medium, if the principal directions of the permeability tensor and hydraulic gradients are not aligned, then flow vectors are not coincident to the hydraulic head gradients (Fetter 1994).

Using multiple methodologies and accounting for parameter uncertainty builds confidence in the reliability of results presented here. Final determinations of capture are described method by method in Table 10. In general, all methods show full capture of chromium from the IM network at the southern and southeastern portions of the plume, and the particle tracking and solute transport methods indicate uncertainty and potential for uncaptured regions north of and at depth near CrEX-5. This region in the northeast portion of the plume needs additional data, especially to the north of R-70, and more study to optimize extraction and injection such that capture can be more assured. All capture zone methodologies suggest that the IM is completing full capture of the plume on the southern and southeastern downgradient portions of the plume, which is an important result in the context of future optimization.

Table 10.
Results of the Capture Zone Evaluation

Type of Analysis	Line of Evidence	Is Capture Sufficient (Are IM Objectives Met?)	Comments
Water Level Data	Potentiometric surface maps	Yes	The capture zone area estimated by streamlines perpendicular to contours is wide enough to encompass the target capture zone in the central and southern areas. The hydraulic control created by injection wells along the southern boundary is evident when comparing water table maps with and without IM operation.
	Water level gradient (shallow)	Yes	Analysis of the hydraulic gradients suggests the IM has hydraulic control upgradient of the IM and along the southern boundary of the plume. The IM has at least a 50% larger impact on hydraulic gradients within the chromium plume, and in many areas >10x the impact. In the northeast, downgradient of CrEX-5, a probable reversal in flow direction is observed, consistent with the results of other analyses. Observed gradient changes are consistent with the expected behavior during IM operations. Pumping from IM and PM-4 operations both result in small increases in downward gradients in the chromium plume.
Analytical Calculation	Estimated flow rate calculations	Yes	The calculation suggests that IM pumping rates are sufficient to encompass the target capture area.

Type of Analysis	Line of Evidence	Is Capture Sufficient (Are IM Objectives Met?)	Comments
	Capture zone width calculations	Yes	The capture zone estimated by an analytical method suggests that the IM system's capture zone is sufficiently large to meet IM objectives. As with all simple analytical techniques employed in complicated settings, this calculation is highly uncertain.
Numerical Modeling	Streamline method	Yes	Streamline analysis of the four model calibrations suggests that the capture zone of the IM is sufficient to encompass the known plume area, with some uncaptured chromium source areas in the northwestern portion of the plume (Calibration 3).
	Particle tracking method	Areas of concern	Particle tracking suggests that the IM system is sufficiently large to meet IM objectives in the south and southeastern portions of the site. Uncaptured pathways are identified in the northern portion of the plume, starting northwest of CrEX-5 and going past R-70 in the northeast, especially at depth, in half of the simulations modeled. This indicates uncertainty in the extent of the chromium plume and the extent of capture in this region.
	Solute transport method	Areas of concern	The node-by-node solute transport analysis results in a capture zone that is sufficiently large to cover the majority of the plume, particularly in the south and southeastern portions. However, the northern portion of the plume falls outside of the capture zone in some simulations, which could lead to uncaptured pathways in the north, similar to the particle tracking method result.

Type of Analysis	Line of Evidence	Is Capture Sufficient (Are IM Objectives Met?)	Comments
Monitoring Well Data	Concentration trends at downgradient performance monitoring wells	Yes	At R-45 S2, an increasing trend is observed. At this location all capture methods estimate that R-45 S2 is within the capture zone, suggesting that this rise is related to temporary movement of the existing plume and not indicative of failed capture. Chromium concentration data from all other downgradient performance monitoring wells – R-44 (S1/S2), R-45 S1, R-50 (S1/S2) and R-70 (S1/S2) – do not show concerning trends, although the record at R-70 is comparatively short and will be monitored carefully due to high concentrations at depth.
	Concentration trends at sentinel wells	Yes	Sentinel wells R-35a, R-35b, R-13, and SIMR-2 remain at background levels for Cr

6.0 References

Arnold, B.W., et al., 2003. Radionuclide Transport Simulation and Uncertainty Analyses with the Saturated-Zone Site-Scale Model at Yucca Mountain, Nevada, *Journal of Contaminant Hydrology* 2003 (62–63) 401–419 doi: 10.1016/S0169-7722(02)00158-4

Carson, J., et al., 2020. Bayesian Approach to Estimation of Water Table Elevations Using Historical Rasters as Prior Information – 20430, proceedings of the *Waste Management Symposia 2020, March 8–12*, Phoenix AZ, 2020

Dash, Z.V., et al., 2015. *Software Validation Report for the FEHM Application Version 3.1–3.X,* LA-UR-15-27776, Los Alamos National Laboratory, Los Alamos NM, December 2015

EPA, 2008. *A Systematic Approach for Evaluation of Capture Zones at Pump and Treat Systems,* EPA/600/R-08/003, United States Environmental Protection Agency, Office of Research and Development, National Risk Management Research Laboratory, Cincinnati OH, January 2008

EPA, 2014. *3PE: A Tool for Estimating Groundwater Flow Vectors,* EPA 600/R-14/273, United States Environmental Protection Agency, Washington DC, September 2014

Fetter, C.W., 1994. *Applied Hydrogeology, Third Edition*, Macmillan College Publishing Company, New York NY

Grubb, S., 1993. Analytical Model for Estimation of Steady-State Capture Zones of Pumping Wells in Confined and Unconfined Aquifers, *Ground Water* 31 (1) 27–32

Heath, R.C., 1983. *Basic Ground-Water Hydrology, U.S. Geological Survey Water-Supply Paper 2220,* U.S. Geological Survey (USGS), Reston VA, 1983

Heikoop, J.M., et al., 2014. Isotopic Evidence for Reduction of Anthropogenic Hexavalent Chromium in Los Alamos National Laboratory Groundwater, *Chemical Geology* 373 (2014) 1–9

Keating, E., and G. Zyvoloski, 2009. A Stable and Efficient Numerical Algorithm for Unconfined Aquifer Analysis, *Ground Water* 47 (4) 569–579

Kelkar, S., et al., 2010. Modeling Solute Transport through Saturated Zone Ground Water at 10 km Scale: Example from the Yucca Mountain License Application, *Journal of Contaminant Hydrology* 2010 (117) 7–25 doi: 10.1016/j.jconhyd.2010.05.003

LANL, 2008. *Fate and Transport Investigations Update for Chromium Contamination from Sandia Canyon,* LA-UR-08-4702, EP2008-0374, Los Alamos National Laboratory, Los Alamos NM, July 2008

LANL, 2009a. *Investigation Report for Sandia Canyon,* LA-UR-09-6450, EP2009-0516, Los Alamos National Laboratory, Los Alamos NM, October 2009

LANL, 2009b. *Completion Report for Regional Aquifer Well R-44,* LA-UR-09-3066, EP2009-0254, Los Alamos National Laboratory, Los Alamos NM, May 2009

LANL, 2012. *Phase II Investigation Report for Sandia Canyon,* LA-UR-12-24593, EP2012-0195, ERID-228624, Los Alamos National Laboratory, Los Alamos NM, September 2012

LANL, 2015a. *Groundwater-Level Data Processing, Review, and Validation,* ER-SOP-20231, R0, Los Alamos National Laboratory, Los Alamos NM, April 2015

LANL, 2015b. *Interim Measures Work Plan for Chromium Plume Control,* LA-UR-15-23126, EP2015-0089, Los Alamos National Laboratory, Los Alamos NM, May 2015

LANL, 2017. *Interim Facility-Wide Groundwater Monitoring Plan for the 2018 Monitoring Year, October 2017–September 2018,* LA-UR-17-24070, EP2017-0068, Los Alamos National Laboratory, Los Alamos, NM, May 2017

LANL, 2018a. *Compendium of Technical Reports Conducted Under the Work Plan for Chromium Plume Center Characterization,* LA-UR-18-21450, EP2018-0026, Los Alamos National Laboratory, Los Alamos NM, March 2018

LANL, 2018b. *Chromium Plume Control Interim Measure Performance Monitoring Work Plan,* LA-UR-18-23082, EP2018-0055, Los Alamos National Laboratory, Los Alamos NM, April 2018

LANL, 2018c. *Evaluation of Chromium Plume Control Interim Measure Operational Alternatives for Injection Well CrIN-6,* LA-UR-18-23385, EP2018-0060, Los Alamos National Laboratory, Los Alamos NM, April 2018

McLin, S.G., 2006. *Analyses of the PM-4 Aquifer Test Using Multiple Observation Wells,* LA-14252-MS, Los Alamos National Laboratory, Los Alamos NM, January 2006

N3B, 2020a. *Fate and Transport Modeling and Risk Assessment Report for RDX Contamination in Deep Groundwater,* EM2020-0135, Newport News Nuclear BWXT-Los Alamos, LLC (N3B), Los Alamos NM, May 2020

N3B, 2020b. *Interim Facility-Wide Groundwater Monitoring Plan for the 2021 Monitoring Year, October 2020–September 2021,* EM2020-0113, Newport News Nuclear BWXT-Los Alamos, LLC (N3B), Los Alamos NM, May 2020

N3B, 2021a. *Assessment Report for the Evaluation of Conditions in the Regional Aquifer Around Well R-70,* EM2021-0321, Newport News Nuclear BWXT-Los Alamos, LLC (N3B), Los Alamos NM, June 2021

N3B, 2021b. *Semiannual Progress Report on Chromium Plume Control Interim Measure Performance, July through December 2020,* EM2021-0110, Newport News Nuclear BWXT-Los Alamos, LLC (N3B), Los Alamos NM, March 2021

N3B, 2022. *Fate and Transport Modeling and Risk Assessment Report for RDX Contamination in Deep Groundwater Revision 1,* EM2022-0581, Newport News Nuclear BWXT-Los Alamos, LLC (N3B), Los Alamos NM, September 2022

Neptune, 2023a. *Chromium Model: Calibrated with Uncertainty through 2022,* EMID-702781, prepared by Neptune and Company Inc. for the U.S. Department of Energy Environmental Management Los Alamos Field Office, Neptune and Company Inc., Los Alamos NM, February 17, 2023

Neptune, 2023b. *Hydraulic Analysis of the Pajarito Plateau,* EMID-702780, prepared by Neptune and Company Inc. for the U.S. Department of Energy Environmental

Management Los Alamos Field Office, Neptune and Company Inc., Los Alamos NM, April 28, 2023

Pollock, D.W., 1994. *User's Guide for MODPATH/MODPATH-PLOT, Version 3: A Particle Tracking Post-Processing Package for MODFLOW, the U. S. Geological Survey Finite-Difference Ground-Water Flow Model,* U. S. Geological Survey Open-File Report 94-464, United States Geological Survey (USGS), Reston VA, September 1994

Reimus, P., et al., 2021. Using Tracers and Opportunistic Geochemical Signatures to Inform Modeling of Cr(VI) Migration at LANL – 21081, proceedings of the *Waste Management Symposia 2021, March 7–11*, Phoenix AZ, 2021

Rivest, M., et al., 2008. Hydraulic Head Field Estimation Using Kriging with an External Drift: A Way to Consider Conceptual Model Information, *Journal of Hydrology* 2008 (361) 349–361 doi: 10.1016/j.jhydrol.2008.08.006

Vesselinov, V.V., 2007. Uncertainties in Transient Capture-Zone Estimates of Groundwater Supply Wells, *Journal of Contemporary Water Research & Education* 2007 (137) 1–7

Zyvoloski, G.A., et al., 1997. *User's Manual for the FEHM Application—A Finite-Element Heat-and Mass-Transfer Code,* LA-13306-M, Los Alamos National Laboratory, Los Alamos NM, July 1997

Zyvoloski, G.A., et al., 1999. *Models and Methods Summary for the FEHM Application,* FEHM MMS, SC-194, Los Alamos National Laboratory, Los Alamos NM, July 1999